NUTRIENT USE-EFFICIENCY IN PLANTS: AN INTEGRATIVE APPROACH

EDITED BY: Guillermo Esteban Santa María, Francisco Rubio and Manuel Nieves-Cordones

PUBLISHED IN: Frontiers in Plant Science

frontiers Research Topics

frontiers

ISSN 1664-8714
ISBN 978-2-88966-446-7
DOI 10.3389/978-2-88966-446-7

About Frontiers

Frontiers is more than just an open-access publisher of scholarly articles: it is a pioneering approach to the world of academia, radically improving the way scholarly research is managed. The grand vision of Frontiers is a world where all people have an equal opportunity to seek, share and generate knowledge. Frontiers provides immediate and permanent online open access to all its publications, but this alone is not enough to realize our grand goals.

Frontiers Journal Series

The Frontiers Journal Series is a multi-tier and interdisciplinary set of open-access, online journals, promising a paradigm shift from the current review, selection and dissemination processes in academic publishing. All Frontiers journals are driven by researchers for researchers; therefore, they constitute a service to the scholarly community. At the same time, the Frontiers Journal Series operates on a revolutionary invention, the tiered publishing system, initially addressing specific communities of scholars, and gradually climbing up to broader public understanding, thus serving the interests of the lay society, too.

Dedication to Quality

Each Frontiers article is a landmark of the highest quality, thanks to genuinely collaborative interactions between authors and review editors, who include some of the world's best academicians. Research must be certified by peers before entering a stream of knowledge that may eventually reach the public - and shape society; therefore, Frontiers only applies the most rigorous and unbiased reviews.
Frontiers revolutionizes research publishing by freely delivering the most outstanding research, evaluated with no bias from both the academic and social point of view. By applying the most advanced information technologies, Frontiers is catapulting scholarly publishing into a new generation.

What are Frontiers Research Topics?

Frontiers Research Topics are very popular trademarks of the Frontiers Journals Series: they are collections of at least ten articles, all centered on a particular subject. With their unique mix of varied contributions from Original Research to Review Articles, Frontiers Research Topics unify the most influential researchers, the latest key findings and historical advances in a hot research area! Find out more on how to host your own Frontiers Research Topic or contribute to one as an author by contacting the Frontiers Editorial Office: frontiersin.org/about/contact

NUTRIENT USE-EFFICIENCY IN PLANTS: AN INTEGRATIVE APPROACH

Topic Editors:
Guillermo Esteban Santa María, National University of General San Martín, Argentina
Francisco Rubio, Spanish National Research Council, Spain
Manuel Nieves-Cordones, Spanish National Research Council, Spain

Citation: Santa-María, G. E., Rubio, F., Nieves-Cordones, M., eds. (2021). Nutrient Use-Efficiency in Plants: An Integrative Approach. Lausanne: Frontiers Media SA. doi: 10.3389/978-2-88966-446-7

Table of Contents

frontiers in Plant Science

EDITORIAL
published: 15 December 2020
doi: 10.3389/fpls.2020.623976

Editorial: Nutrient Use-Efficiency in Plants: An Integrative Approach

Manuel Nieves-Cordones[1], *Francisco Rubio*[1] *and Guillermo E. Santa-María*[2]*

[1] *Departamento de Nutrición Vegetal, Centro de Edafología y Biología Aplicada del Segura-CSIC, Murcia, Spain,* [2] *Instituto Tecnol?gico Chascomús (INTECH), Consejo Nacional de Investigaciones Científicas y Técnicas, Universidad Nacional de San Martín, Buenos Aires, Argentina*

Keywords: nutrient use efficiency, plant, uptake, mobilization, abiotic stress, fertilizer

Editorial on the Research Topic

Nutrient Use-Efficiency in Plants: An Integrative Approach

Modern agriculture faces major issues resulting from the need to ensure crop production for a growing population while also minimizing the environmental impact of agricultural practices as well as the cost associated with them, all of which can be worsened by the high incidence of abiotic stresses imposed by climate change. The agricultural use of land for crop production leads to the continuous extraction of soil nutrients. In the absence of adequate nutrient replenishment, a subsequent decrease of soil nutrient availability may occur, exerting a negative effect on yield. Yield limitation could also occur as a consequence of there being intrinsically low levels of nutrients in soils. Strategies to overcome low nutrient availability in soils mainly rely on the use of fertilizers and crop breeding. According to the Food and Agricultural Organization (FAO, 2019), approximately 109 Mt of nitrogen (N), 45 Mt of phosphorus (P), and 38 Mt of potassium (K^+) were used during 2017. Some of the fertilizers applied are based on the use of rock reservoirs that constitute a non-renewable resource. In addition, the use of fertilizers can result in collateral problems, as they can harm ecosystems, with additional costs to agricultural practices. This is a major drawback for low input agriculture as practiced in some regions. In this complex context, ensuring sustainable agriculture requires the adoption of innovative strategies that involve new concepts in the management of agroecosystems, including the use of bio-fertilizers, and the genetic improvement of crops and pastures. One promising goal is to develop crops with high nutrient use efficiency and high resilience to environmental constraints.

Nutrient use efficiency is typically divided into two interactive components: the efficiency of nutrient acquisition (i.e., the amount of nutrient taken up by plants in relation to nutrient supply) and the efficiency of nutrient utilization, which informs the biomass produced by the unit of nutrient incorporated by plants. The existence of relevant constraints in improving these components while maintaining food quality has been highlighted (Barraclough et al., 2010). Further knowledge of the genetic basis, as well as the physiological and molecular mechanisms that determine these efficiencies in plants, may allow for the design of original approaches to addressing these constraints. This Research Topic from Frontiers in Plant Science includes contributions made by several authors from different countries to help to illuminate some of the specific aspects involved in nutrient use efficiency in plants.

N, P, and K^+ constitute the most common nutrients in fertilizers. To optimize and reduce the applications of fertilizers, we require more insight into how these nutrients are taken up and utilized by plants. With respect to N, four research articles cover aspects related to N use efficiency (NUE) at different levels. Two of them deal with grain yield. Paponov et al. compared two maize varieties with contrasting NUEs. The authors found evidence suggesting that kernel set was differentially regulated in these genotypes, and propose that they play a major role in sink restriction. In turn,

OPEN ACCESS

Edited by:
Jan Kofod Schjoerring, University of Copenhagen, Denmark

Reviewed by:
Gerd Patrick Bienert, Technical University of Munich, Germany

***Correspondence:**
Guillermo E. Santa-María
gsantama@intech.gov.ar

Specialty section:
This article was submitted to Plant Nutrition, a section of the journal Frontiers in Plant Science

Received: *30 October 2020*
Accepted: *23 November 2020*
Published: *15 December 2020*

Citation:
Nieves-Cordones M, Rubio F and Santa-María GE (2020) Editorial: Nutrient Use-Efficiency in Plants: An Integrative Approach. Front. Plant Sci. 11:623976. doi: 10.3389/fpls.2020.623976

Fan et al. evaluated the consequences of manipulating a component of the autophagy machinery, OsATG8b. Autophagy constitutes a relevant process in nutrient use-efficiency at the reproductive stage. Increased expression of *OsATG8b* increased yield, grain quality, and higher transfer of N to the seeds.

A different way of improving NUE in plants could be based on chloride (Cl^-) supply, as shown by Rosales et al.. Taking into account the fact that, as is the case for nitrate (NO_3^-), Cl^- fulfills osmotic functions in the vacuole, the authors showed that Cl^- enables a higher amount of NO_3^- to be available for assimilation. Indeed, high Cl^- supply specifically increased N Utilization Efficiency (NUtE) with little or no effect on N uptake. The positive effects of Cl^- supply on NUE were also observed in most of the plant species examined. Concerning NO_3^- and Cl^- nutrition, Rubio et al. address the impact of high carbon dioxide (CO_2) and high bicarbonate (HCO_3^-) on cytosolic NO_3^- and Cl^- pools in leaves of *Posidonia oceanica* by using ion-sensitive microelectrodes. Importantly, the current rise in atmospheric CO_2 levels may affect nutrient accumulation by crops (Loladze, 2014). Elevated CO_2 results in higher levels of HCO_3^- in seawater, which is used by aquatic plants as a carbon source for photosynthesis. The studies on *Posidonia* by Rubio et al. showed that the high cytosolic HCO_3^- together with a concomitant increase in cytosolic pH, activated S-type anion channels which allowed NO_3^- and Cl^- efflux from leaf cells. Thus, the effect of high atmospheric CO_2 on NO_3^- and Cl^- retention in *Posidonia* deserves further investigation, particularly regarding how it could affect NUE.

The efficient use of nutrients by plants requires tight regulation of the systems involved in their homeostasis. Increasing evidence points to a co-regulation among the homeostasis of different nutrients. Raddatz et al. examined the interactions between K^+ and NO_3^- nutrition. In addition to describing uptake and distribution systems, the authors highlighted how these processes were co-regulated. Important components of this co-regulation are the CIPK23/CBL complex—which post-translationally regulates both K^+ and NO_3^- transporters by their phosphorylation—and the existence of transporters, such as NRT1.5, with the ability to transport both macronutrients. In addition, the interactions of sodium (Na^+) with K^+ and NO_3^- nutrition were also covered because of the important effects exerted by the former on the nutrition of the others. In turn, the review by Villette et al. was centered on the transport systems that regulate the K^+ concentration of grapevine berries, which is critical for the optimal quality of fruits and wine properties. Special attention was given to the detrimental effects that climate change will have on these parameters. In particular, high temperatures lead to an increase in K^+ and sugar accumulation in berries, which results in a lower quality of wine.

Two papers cover P use efficiency (PUE) at different levels. Galatro et al. present a review article about the role of nitric oxide (NO) under P-deficient conditions. NO is a signaling molecule associated with N metabolism. The authors gave an update on the acclimation responses to low P and the NO signaling pathways in plants. The authors stated that there is a potential to improve P-deficiency responses in plants by understanding the contribution of NO on this topic. A second review on P, by Powers and Thavarajah, deals with the PUE of field pea. This leguminous crop has high protein/micronutrient content but it is not widely cultivated. Due to this high content, field pea could be used to replenish N levels in soils after culture rotation. However, it has a high P demand. The authors hypothesize that diversity may exist among field pea varieties regarding PUE and encourage further exploration of its natural diversity to enable potential cultivation.

Regarding magnesium (Mg^{2+}) nutrition, Ogura et al. described Mg^{2+} deficiency and its effects on the retranslocation of other mineral nutrients within the plant as well as changes in sucrose partitioning, photosynthesis, and biomass production. These observations were in agreement with the described crosstalk in the nutrition of different nutrients (Amtmann and Blatt, 2009; Kellermeier et al., 2014). A second contribution on Mg^{2+} by Wang et al., consists of a meta-analysis from 99 field research articles to determine the effect of Mg^{2+} fertilization on crop yield and other agronomic parameters.

Regarding micronutrients, Alejandro et al. contribute a comprehensive review of the systems involved in manganese (Mn) uptake and compartmentalization. Most of the proteins that transport Mn are not specific for the metal and can transport other divalent cations. Thus, diverse families of transporters are involved in the Mn homeostatic network. Dimkpa et al. present an original research paper on an alternative and more-efficient approach to zinc (Zn) fertilization which enhances Zn uptake under drought stress in wheat plants. By supplying Zn as nano-particles, increases in plant performance and Zn accumulation were achieved.

Avoiding high levels of toxic elements is critical in modern agriculture. Adams et al. contribute an original research paper showing that sulfur supply alleviated aerial chlorosis and growth retardation caused by cesium (Cs^+) stress without reducing Cs^+ accumulation in Arabidopsis plants. Their findings indicate that exposure to Cs^+ increased glutathione accumulation, a process that can be promoted by the exogenous application of sulfur-containing compounds.

The regulation of the transport proteins is a key process of nutrient homeostasis. A review by Saito and Uozumi examines how plants control the uptake and balance of nutrients by Calcium-regulated phosphorylation, a mechanism emerging as pivotal for the regulation of transport systems. The review is focused on CPK and CBL-CIPK systems, the latter also highlighted by Raddatz et al.. These regulatory systems are crucial for maintaining important physiological processes such as intracellular osmolality, cell expansion and movement, salt stress tolerance, the control of ammonium (NH_4^+) uptake, regulation of metal ions uptake, and toxins.

Lastly, Dreyer and Michard offer an original research article that challenges the classical concept of high- and low-affinity uptake systems. The authors propose that the affinity concept based on enzyme kinetics did not have proper scientific grounds. Using a simulation-based approach, the authors showed that affinities for substrate transport may be an artifact of data display,

or that the transport affinities originated from the voltage- and pH-dependency of the H^+-ATPase. Thus, the classification of transporters based on these studies is misleading thermodynamically.

Collectively, the contributions to this Research Topic provide very interesting and relevant information on the homeostasis of mineral nutrients in plants and its effects on dry matter production and grain quality. The articles cover important aspects such as the systems involved in nutrient acquisition and utilization, the components involved in their regulation, and the existence of common regulatory pieces that support the observed cross-talk in the homeostasis of different nutrients. The information gathered in this Research Topic could be used to develop tools for improving the nutrient use efficiency of plants, aiming at generating crops better suited for future agriculture.

AUTHOR CONTRIBUTIONS

The editorial was written, corrected, and accepted by all authors.

ACKNOWLEDGMENTS

We thank the authors, reviewers, and Frontiers editorial staff for their valuable contributions to this Research Topic. We acknowledge the financial support provided by ANPCYT (PICT 2018-2109), Ministerio de Ciencia (PID2019-106649RB-I00), and Fundación Séneca (20806/PI/18). MN-C was the recipient of a Ramón y Cajal Fellowship (RyC-2017-21924). This Research Topic of Frontiers in Plant Science is dedicated to the memory of our dear colleague Professor Marcela Simontacchi (1965-2020), who was an author and reviewer for this issue.

REFERENCES

Amtmann, A., and Blatt, M. R. (2009). Regulation of macronutrient transport. *New Phytol.* 181, 35–52. doi: 10.1111/j.1469-8137.2008.02666.x

Barraclough, P. B., Howarth, J. R., Jones, J., Lopez-Bellido, R., Parmar, S., Shepherd, C. E., et al. (2010). Nitrogen efficiency of wheat: genotypic and environmental variation and prospects for improvement. *Eur. J. Agron.* 33, 1–11. doi: 10.1016/j.eja.2010.01.005

FAO (2019). *World Food and Agriculture – Statistical Pocketbook 2019*. Rome. Available online at: http://www.fao.org/3/ca6463en/ca6463en.pdf

Kellermeier, F., Armengaud, P., Seditas, T. J., Danku, J., Salt, D. E., and Amtmann, A. (2014). Analysis of the root system architecture of arabidopsis provides a quantitative readout of crosstalk between nutritional signals. *Plant Cell* 26, 1480–1496. doi: 10.1105/tpc.113.122101

Loladze, I. (2014). Hidden shift of the ionome of plants exposed to elevated CO(2) depletes minerals at the base of human nutrition. *Elife* 3:e02245. doi: 10.7554/eLife.02245.017

Conflict of Interest: The authors declare that the research was conducted in the absence of any commercial or financial relationships that could be construed as a potential conflict of interest.

frontiers in Plant Science

REVIEW
published: 15 November 2019
doi: 10.3389/fpls.2019.01489

Checking Agriculture's Pulse: Field Pea (*Pisum Sativum* L.), Sustainability, and Phosphorus Use Efficiency

*Sarah E. Powers and Dil Thavarajah**

Plant and Environmental Sciences, 270 Poole Agricultural Center, Clemson University, Clemson, SC, United States

Investigations regarding the incorporation of better sustainable production strategies into current agricultural-food systems are necessary to grow crops that reduce negative impacts on the environment yet will meet the production and nutritional demand of 10 billion people by 2050. The introduction of organic, alternative staple food crops, such as nutrient-dense field pea (*Pisum sativum* L.), to the everyday diet, may alleviate micronutrient malnutrition and incorporate more sustainable agriculture practices globally. Varieties are grown in organic systems currently yield less than conventionally produced foods, with less bioavailable nutrients, due to poor soil nutrient content. One of the most limiting nutrients for field pea is phosphorus (P) because this legume crop requires significant inputs for nodule formation. Therefore, P use efficiency (PUE) should be a breeding target for sustainable agriculture and biofortification efforts; the important role of the soil microbiome in nutrient acquisition should also be examined. The objectives of this review are to highlight the benefits of field pea for organic agriculture and human health, and discuss nutritional breeding strategies to increase field pea production in organic systems. Field pea and other pulse crops are underrepresented in agricultural research, yet are important crops for a sustainable future and better food systems. Furthermore, because field pea is consumed globally by both developed and at-risk populations, research efforts could help increase global health overall and combat micronutrient malnutrition.

Keywords: field pea, organic farming, phosphorus, pulse crop physiology, biofortification

OPEN ACCESS

Edited by:
Manuel Nieves-Cordones, Spanish National Research Council, Spain

Reviewed by:
Petr Smýkal, Palacký University, Czechia
Zivko S. Jovanovic, University of Belgrade, Serbia
Beata Gabrys, University of Zielona Góra, Poland

****Correspondence:***
Dil Thavarajah
dthavar@clemson.edu

Specialty section:
This article was submitted to Plant Nutrition, a section of the journal Frontiers in Plant Science

Received: *02 July 2019*
Accepted: *28 October 2019*
Published: *15 November 2019*

Citation:
Powers SE and Thavarajah D (2019) Checking Agriculture's Pulse: Field Pea (Pisum Sativum L.), Sustainability, and Phosphorus Use Efficiency. Front. Plant Sci. 10:1489. doi: 10.3389/fpls.2019.01489

INTRODUCTION

The Green Revolution is indisputably one of the most critical feats in recent agricultural history, but what has it cost our soils, crops, and environment as a whole? One result of the focus on mass production in monocultural systems for prolonged periods is the over-application of fertilizers and pesticides, which is a prevalent issue associated with conventional farming methods (Ponisio et al., 2015). As a result, soil fertility and microbial biodiversity have decreased while rates of environmental pollution and greenhouse gas emissions continue to increase (Reganold et al., 1987; Amundson et al., 2015; Reganold and Wachter, 2016; Peoples et al., 2019). Organic agriculture offers a potential solution to these problems, as organic production relies on environmentally friendly practices to increase soil fertility. However, current varieties bred for conventional systems do not perform as

well in organic soils, resulting in reduced yield and nutritional quality. The agriculture industry as a whole has also begun to deplete the natural mineral deposits on which crops depend, such as phosphate rock, which is a nonrenewable resource (van de Wiel et al., 2016). Organic and conventional agriculture both use phosphorus rock for around 90% of the phosphorus (P) found in fertilizers, feed, and other food additives; however, most P is subsequently lost from the food system due to mining and field practices (Cordell and White, 2014; Amundson et al., 2015). The P that is applied as a fertilizer is also often mismanaged; specifically, it is over-applied to fields, leading to a build-up of the element in the soil where it is inaccessible to plants due to its immobile nature and affinity to form insoluble complexes with other minerals (Vance et al., 2003; MacDonald et al., 2011). Experts cannot seem to agree on when phosphorus reserves will run out, with estimates between the years 2030 and 2100 (van de Wiel et al., 2016); regardless, agriculture must still address its current P problem for future crop production.

Phosphorus is vital to agriculture because it is required by all plants, being involved in seed germination, root growth, structure development, and numerous metabolic processes such as photosynthesis and nutrient formation (van de Wiel et al., 2016). Therefore, when P is limited in soils it negatively affects not only plant growth and yield but also the nutrient concentration and bioavailability in food crops, leading to micronutrient deficiencies or "hidden hunger" (Assuero et al., 2004; Welch and Graham, 2004; Rehman et al., 2018). Potential solutions to hidden hunger include: 1) biofortification to increase bioavailable micronutrients in staple crops through agronomic, plant breeding, and biotechnology efforts (Welch and Graham, 2004) and 2) diversifying staple crops to include cheaper, environmentally sustainable, and more nutrient-dense foods, such as field pea (*Pisum sativum L.*) and other pulse crops (Foyer et al., 2016).

Field pea is a member of the Leguminosae family, along with faba bean (*Vicia faba*), grass pea (*Lathyrus sativus*), white lupin (*Lupinus albus*), lentils (*Lenis culinaris*), mung bean (*Vigna radiata*), soybean (*Glycine max*), cow pea (*Vigna ungulicata*), and common bean (*Phaseolus vulgaris*) among others (Foyer et al., 2016). Additionally, Leguminosae consists of the subfamily Papilionideae which splits into two distinct clades of cultivated legumes: 1) Hologalegina, evolving 50 million years ago and 2) Phaseoloid, evolving 45 million years ago (Foyer et al., 2016). These clades evolved separately, as Hologalegina is comprised of all cool season legumes, such as field pea, lentil, faba bean, and grass pea, while Phaseoloids consists of warm-season legumes (pigeon pea, soybean, common bean, mung bean, and cowpea) (Foyer et al., 2016). Cool season legumes are critical to sustainable agriculture, as they are planted during winter, complementing the growing season of cereals, and providing essential nitrogen and other nutrients back to the soil.

Field pea is a critical economic and nutritive crop and is often called "poor man's meat" due to its high protein, vitamin and mineral, and prebiotic carbohydrate content yet affordability for poorer consumers (Amarakoon et al., 2012). More specifically, field pea is naturally rich in iron and zinc and thus, could address two of the most common micronutrient deficiencies in the world (Amarakoon et al., 2012). Despite the potential for the higher consumption of field pea to help alleviate hidden hunger, little advancement has been made to increase production and yields have lagged behind those of cereals (Amarakoon et al., 2012). One of the main issues with field pea, and legumes, in general, is that they require much more P input than other crops due to their nodules, which require P for energy transformation (Vance et al., 2003); this presents an issue for sustainable agriculture.

Field Pea Benefits Agriculture

Field pea is one of the oldest domesticated pulse crops, appearing in the Mediterranean between 7000 and 6000 BC and persisting in current agriculture (Helback and Hopf, 1959). Pulse crops are a category of legumes, with seeds specifically harvested at full maturity (FAO, 1994). Pulses are very beneficial to agriculture systems, achieving large success in sustainable agriculture systems through intercropping and crop rotations with cereals. Pulses are able to break disease and weed cycles associated with cereals, while replenishing nitrogen (N) in the soil through their ability to fix N from the atmosphere through their nodules and symbioses with rhizobia. Globally, 21 Mt of nitrogen is fixed by legumes, with 5–7 Mt returned to the soil by pulses, specifically, which saves U.S. farmers $8-12 billion in total (Foyer et al., 2016). In Australia, farmers reported a 30% increase in wheat after adding a legume rotation compared to monocropped wheat (Stagnari et al., 2017). Studies from Denmark also report nitrogen uptake of various crops increases between 23–59% after rotations with field pea and lupin (Stagnari et al., 2017). As N is another of the most limiting nutrients for cereal and crop production, this legume-mediated increase in nitrogen use efficiency offers a sustainable and cost-effective alternative to high input fertilizer regiments. Pulses also foster other beneficial properties for soil health, such as increased biodiversity, soil organic carbon (SOC) levels, and soil water retention, while decreasing greenhouse gas emissions (GHG) (Foyer et al., 2016; Stagnari et al., 2017; Peoples et al., 2019). Field pea has the most positive effect on SOC by improving humus levels and supplying organic C as a result of bacterial nitrogen fixation (Stagnari et al., 2017).

In 2017, a total of 8,141,031 hectares of field pea were harvested globally (**Figure 1**), with the top producers consisting of Canada, Russia, China, India, and the United States (FAOSTAT, 2019); however, this is only a minimal fraction compared to cereal production. Cultivated land acreage for field pea and other pulses has been in steady decline over the past 30 years (Stagnari et al., 2017). Average yields have increased about 70–84% since 1974 for staple legumes, such as soybean, lentil, chickpea, and groundnut; in contrast, yields for field pea have increased but resulted in no net production gains due to decreasing land acreage (Foyer et al., 2016). The minimal expansion of pulses in agriculture is due to smaller and unpredictable yields, caused by susceptibility to environmental factors, and has resulted in a less-developed global market with decreased profits, disincentivizing farmers from using pulses for income while policymakers focus more attention and resources on cereals in developing countries (Foyer et al., 2016; Stagnari et al., 2017). These practices have compromised human nutrition, as cereals have less protein

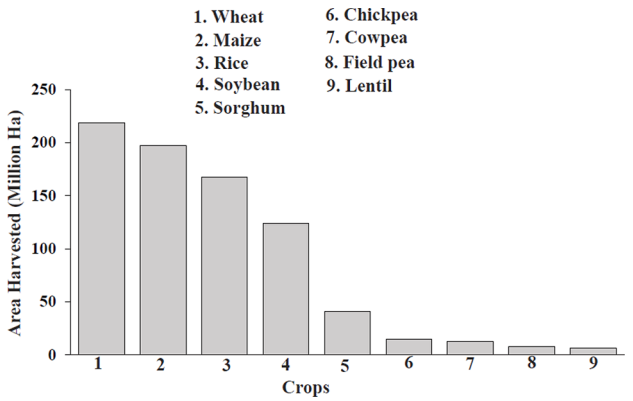

FIGURE 1 | Comparison of area harvested for cereals and field pea in 2017 (FAOSTAT, 2019). The numbers above each bar represent the individual harvest totals of each crop.

than field pea and pulse crops as well as inadequate levels of micronutrients, contributing to hidden hunger (Pingali, 2012). Pulses are also good sources of prebiotic carbohydrates (essential for gut health), fiber, minerals, vitamins, carotenoids, and polyphenols, allowing them to address health problems such as malnutrition, prenatal care, cardiovascular disease, diabetes, cancer, obesity, and gastrointestinal (GI)-related issues that plague both developing and developed nations (Welch, 2002; Foyer et al., 2016).

An additional hindrance to legume production is the high phosphorus requirement for nodule formation and function. Intensive mineral P fertilization has caused P surpluses in the soil of many countries, but deficits still exist in parts of Africa, the Northern U.S., South America, Eastern Europe, and Asia, likely due to multiple cycles of mono-crop farming or limited access to mineral fertilizers (MacDonald et al., 2011). Many resource-poor farmers practice subsistence agriculture, which utilizes organic principles such as no pesticides, chemical fertilizers, or industrial equipment. The soils they farm are generally poorer in nutrients, resulting in poorer yields and possibly poorer nutritional quality of the crop. For pulses such as field pea to be effective in combating hidden hunger, breeding efforts should be conducted to prepare varieties for these limiting environments. In addition, more specific breeding efforts should also focus on breeding field pea varieties solely for the organic environment to resolve the yield and nutritional discrepancies between conventional and organic agriculture.

Organic Soil Vs. Conventional Soil

Organic agriculture is regarded as having healthier soils than conventional systems. Indeed, organic soil has higher soil organic matter, soil organic carbon, soil aggregate stability, and soil moisture content than conventional soils—all values that increase soil health and fertility (Schrama et al., 2018). Organic soils also have an increased level of biodiversity, as in a wider range of pollinators, insects, and earthworms, along with high microbial biomass and enzymatic activity (Hole et al., 2005). Despite healthier soils, limited herbicide and pesticide use along with additional weed pressure are limiting factors to productivity in organic agriculture. Additionally, N is a limiting nutrient in both conventional and organic production, but especially in organic systems that do not allow synthetic fertilizers as a source of N. Organic crops actually require twice as much N as conventional systems to achieve comparable yields (Seufert et al., 2012). Therefore, legumes are critical in organic systems, as they fix and efficiently use their own N, and supply it back to the soil from biomass after harvest at a rate of 40 million tons per year (Seufert et al., 2012; Udvardi and Poole, 2013).

Pulses face other nutrient constraints in organic agriculture due to their high P demand. Organic systems do not adequately replenish P supplies after harvest, leading to a deficit for the incoming crop (Oehl et al., 2002; Seufert et al., 2012). Additionally, sources of P for organic farming in the U.S. are restricted to FDA-approved manures and bone meal, as well as phosphate rock (Möller et al., 2018). For farmers that convert from conventional to organic management, decreases in available P in soils have been reported, meaning that the fertilizer is not adequate as a single source, and plants utilize P built up in the soil from previous fertilizer applications (Oehl et al., 2002). Overall, this means that organic agriculture is still dependent on nonrenewable sources of phosphorus, which decreases the sustainability of organic production.

One strategy to combat the negative impact of increased weed and disease pressure and nutrient limitations in organic environments is to identify breeding targets that fortify varieties to cope with these stressors. There are cereal organic breeding programs already underway (Wolfe et al., 2008; Jones et al., 2011). In field pea, genetic variation may also exist for phosphorus use efficiency (PUE), which would allow for the development of cultivars that are less dependent on P fertilizer input; this would benefit both conventional and organic growing systems. Additionally, PUE should be the main consideration for organic legumes, so that they can maintain nitrogen-fixing activity, yield stability, and adequate biomass under phosphorus-deficient conditions (van de Wiel et al., 2016). This will also prolong the period residual P can contribute to production, allowing it to be used more efficiently (van de Wiel et al., 2016). PUE is a complex trait, involving multiple pathways and gene networks, but can be broken into the ability of the plant roots to acquire P from the soil and the plant's ability to remobilize and allocate P to sustain productivity (van de Wiel et al., 2016). Unfortunately for field pea, there is a dearth of genomic information and resources regarding these processes, so more research should be conducted to identify these genomic regions as field pea becomes more popular in the health food market.

Phosphorus Physiology of Legumes

Phosphorus is only available to plants in its inorganic forms (Pi) as $H_2PO_4^-$ and HPO_4^{2-} which exist in very small concentrations in the soil (< 10 μm) (**Figure 2**) (Schachtman et al., 1998). Availability is also highly dependent on soil pH, as P forms insoluble complexes with Al and Fe under acidic conditions and Ca under alkaline conditions (Seufert et al., 2012). This presents

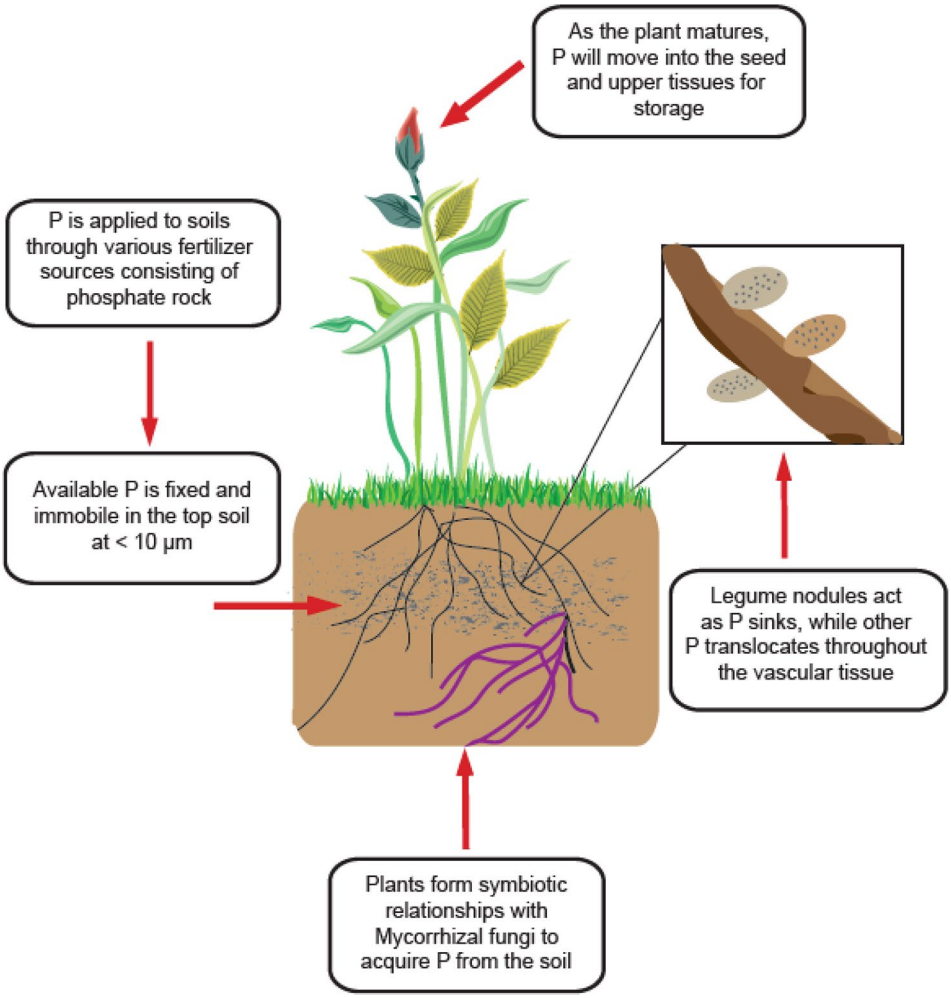

FIGURE 2 | General scheme of P acquisition and utilization of legume plants.

an issue for all forms of agriculture worldwide, as most soils are acidic (Reganold and Wachter, 2016; Slessarev et al., 2016). All plants have adopted mechanisms to combat the unavailable nature of P, such as altered root architecture, organic acid exudation, specialized transport systems, lipid remodelling, and symbiosis with arbuscular mycorrhizal fungi (AMF) (**Figure 2**) (Vance et al., 2003; Oehl et al., 2004). AMF are especially important in organic systems, where less is P available, and plants rely more heavily on these fungi to gather and supply P and other nutrients (Oehl et al., 2004). P is applied to soils from phosphate rock sources, and becomes immobile in the soil, with small concentrations accessible to the roots. Plants will form symbiotic relationships with Mycorrhizal fungi for greater P acquisition. For legumes specifically, high concentrations of P exist in the nodules to maintain nitrogen-fixing function. Due to stress or senescence, P is remobilized from younger tissues and moves into upper leaves and seeds for storage as phytic acid.

P uptake is regulated by high and low affinity transporters located throughout the vascular system of the plant. The root hair mediates the uptake of Pi from the soil, where it is transported across the root plasma membrane by a P-type H+-ATPase pump (Vance et al., 2003). From there, the Pi is transported into the nodules or upward into the shoot by the xylem where it goes to individual cells (Vance et al., 2003). The cytoplasm maintains a strict Pi concentration of around 5–10 mM (Schachtman et al., 1998); if no deficiency is detected, the Pi will be stored in the vacuole until P stress signals are detected or senescence begins. If Pi becomes limited throughout the plant, vacuolar Pi will efflux into the cell cytoplasm and be allocated to other vital tissues, such as legume nodules. Additionally, during senescence Pi is again effluxed from the vacuole, where it is transported from older leaves to younger leaves and seeds by the xylem and various transporters (Robinson et al., 2012; Yang et al., 2017; Xu et al., 2019). Once Pi reaches the seed, it is stored as phytic acid or phytate and utilized during seed germination to establish enough growth until the seedling can take up nutrients on its own (Robinson et al., 2012; Yang et al., 2017; Xu et al., 2019). Some crops have more phytic acid than others, with field pea containing a high amount. Phytic acid is an antinutrient, meaning it binds to other minerals and decreases bioavailability,

making crops high in phytic acid undesirable for animal and human consumption.

Adaptations for P limitation in legumes specifically involve preferential allocation of P to nodules to maintain N fixation, rhizosphere acidification through root exudation, formation of proteoid roots, and modified carbon metabolism and mycorrhizae formation to control for competition with nodule development (Vance et al., 2003). Therefore, legumes will suffer greatly if P is limited, as they will be unable to maintain nodule function and overall productivity due to decreased photosynthetic ability, tissue expansion, and flower formation (Sa and Israel, 1991; Vance et al., 2003; Sulieman and Tran, 2015). Most research on these processes has been conducted in soybean (*Glycine max*), so there is a need to investigate responses in field pea specifically. There is also a gap in the literature with respect to specific links between phosphorus deficiency and nutrient bioavailability. The nutritional value of organic crops compared to conventional crops is an additional gray area; however, it can be inferred that limited P not only affects human health through reduced yield, but could also decrease protein, carbohydrate, and lipid content due to P's involvement in plant metabolic activities.

P Efficiency and Plant-Soil-Microbe Interactions

As previously discussed, most vascular land plants have formed evolutionary beneficial relationships with AMF, but increasing evidence indicates the entire soil microbiome is a mediator for plant health. This relationship is caused by the secretion of photosynthates and carbon sources into the rhizosphere, acting as a tradeoff for various microbes (Bakker et al., 2018), which then provide the plant with various health benefits such as nutrient availability. The composition of soil microbiomes is largely dependent on the soil type and the environment, but plant genotype can also influence microbial populations depending on the type of root exudate and hormones it produces. For example, Arabidopsis accessions differ in their ability to colonize *Pseudomonas* bacteria, leading to some accessions being more disease resistant than others (Bakker et al., 2018). Additionally, salicylic acid exudation by Arabidopsis influences the composition of root microbiomes, again demonstrating the plant has some influence over the rhizosphere (Bakker et al., 2018).

The soil microbiome is implicated in P acquisition, and AMF and rhizobia interactions with legumes are well characterized. Legumes exude flavonoids into the rhizosphere that attract rhizobia to stimulate nodule formation as well as allow for AMF interaction; both lead to enhanced P availability for the legume (Jacoby et al., 2017). Another mechanism is the modification of root exudates under P limitation. Maize and rice alter their exudates to contain more carbohydrates and sugars to provide an energy source for AMF formation (Carvalhais et al., 2011). Increased sugar exudation has also been identified in *Pisum sativum,* which then increased the mineralization of insoluble P by microbial activity (Schilling et al., 1998).

A result of conventional farming is the notion that breeders have inadvertently selected for traits that weaken plant-microbe interactions due to intensive fertilizer and pesticide use (Bakker et al., 2018). Studies in barley, maize, and Arabidopsis indicate differences in rhizospheres between wild and domesticated material as well as natural variation among accessions (Bakker et al., 2018). More studies must be done to dissect the contribution of genetic variability to microbial communities, as these could be targets for organic plant breeding initiatives. The lack of efficient plant-soil-microbe interactions in conventionally bred crops could help explain reduced yields when these varieties are introduced to organic environments, where a stronger soil microbiome relationship would be beneficial due to the lack of fertilizers and pesticides (Jones et al., 2011; Bakker et al., 2018). Organic pulse breeding should focus on microbial interactions to improve P acquisition, and genomic studies should be performed in the diverse germplasm to discover any beneficial traits that may have been lost from modern day varieties over time.

Field Pea and Phosphorus Use Efficiency

PUE is defined as the total biomass per unit of P taken up and encompasses the plant's ability to acquire P from the soil then translocate, remobilize, and efficiently utilize it for various physiological processes (Shenoy and Kalagudi, 2005; Veneklaas et al., 2012). The overall goal of PUE breeding is to determine genomic regions that contribute to these processes and allow crops to grow and yield at optimal levels under low P conditions. Generally, a greater focus has been placed on improving P acquisition from the soil by identifying genes and processes associated with root systems architecture and rhizosphere modifications under P deficiency through quantitative trait loci (QTL), genome-wide association study (GWAS), and biotechnological methods (Rose and Wissuwa, 2012; Veneklaas et al., 2012; van de Wiel et al., 2016). While these aims would allow crops to scavenge residual P built up in the soil from the over-application of fertilizer, this strategy may deplete P from nutrient-poor soils and further upset the balance of fertilizer input to uptake, again leading to P depletion (van de Wiel et al., 2016). Remobilization of P from vegetative tissues is the main source of P for reproductive tissues, impacting yield and seed quality, so understanding and improving allocation efficiency is a necessary goal for crops with better PUE. Additionally, increased P acquisition for field pea may lead to a greater accumulation of phytate in seeds, thus decreasing the bioavailability of nutrients upon consumption. Therefore, in terms of field pea, a balance must be achieved between P acquisition and internal P utilization to avoid excess accumulation of phytate.

Several studies in grain crops have concerned PUE (Rose and Wissuwa, 2012), but none, as far as we are aware, have been conducted in field pea. Genetic variation is visible among pulse crop varieties, so field pea studies should not be ignored. A recent study in chickpea (*Cicer arietinum L.*) showed great variation among diverse germplasm and commercial varieties for various aspects of PUE, such as total biomass, photosynthetic rate, root structure, and root acquisition under limited P conditions (Pang et al., 2018). Several accessions from the diverse germplasm were shown to outperform commercial chickpea varieties in terms of these criteria, indicating genetic variation that may be exploited for PUE breeding purposes (Pang et al., 2018).

Another challenge for PUE in organic agriculture is that most studies are conducted in greenhouses or under conventional management, which differs significantly from organic practices (Rose and Wissuwa, 2012). Therefore, more PUE studies should be conducted with the field and growing environment in mind to generate more realistic results. Studies for PUE in field pea and other pulses should be increased in general and can be aided by recent genotypic data for the diverse field pea germplasm (Holdsworth et al., 2017). Breeding for PUE will significantly benefit organic agriculture as it is a P-limited environment, where the ratio of P input to P uptake is already off-balance and inadequate. Research concerning field pea PUE should be prioritized in biofortification programs, as adequate phosphorus utilization will aid in increasing the amount and bioavailability of nutrients.

Biofortification Potential of Legumes

As previously stated, agriculture not only faces the issue of yield deficits for a growing population but also increased incidences of hidden hunger as more people develop micronutrient deficiencies. A potential solution to overcome micronutrient deficiencies is to increase consumption of pulses, which contain superior protein, carbohydrate, fiber, and micronutrient content compared to cereals, as well as complementary amino acid profiles to those found in cereals (Rehman et al., 2018). Field pea is also attracting positive attention in health food markets, as they are rich in protein (23.5 g protein per 100 g) and a viable substitution to wheat and egg-based products. Protein extraction is reported to be most successful from field pea, and the protein structure of peas is the most similar to egg and stabilizes snacks and cereals most similarly to gluten when compared to other alternative protein sources. By increasing protein content of field pea, a more significant profit and expansion of the field pea market may take place, paving the way for more initiatives to support growers of field pea and other pulse crops. Another solution is to boost biofortification breeding efforts to increase nutritional value where legumes lack to supplement a low diversity diet due to climate change and crop availability.

However, an issue relating both biofortification and phosphorus use efficiency is the conversion of P to *myo*-inositol-1,2,3,4,5,6-hexa*kis*phosphate (InsP6), also known as phytic acid, which acts as an antinutritional factor by decreasing the bioavailability of nutrients in pulses when consumed (Rehman et al., 2018) (Raboy, 2003). As P is taken up by the roots from the soil, it is converted to glucose 6-phosphate (G6P) before entering the inositol phosphate pathway through the conversion of G6P to inositol 3-phosphate (Ins3P) by myo-inositol(3)P1 synthase (MIPS) (Raboy, 2003). From there, every carbon of the 6-carbon ring is phosphorylated until it becomes InsP6 or phytic acid (Raboy, 2003). Phytic acid is the primary storage form of P in seed and is often bound in phytate salts to Ca or Fe (Raboy, 2003). These structures cannot be broken down by humans as they lack the necessary enzymes (Raboy, 2003). As P is found throughout the plant and stored in various tissues during vegetative and reproductive growth, biofortification efforts should aim to understand the mobilization of P throughout the growing cycle. Additionally, more research should be dedicated to the speciation of P within the plant to identify genetic variation for P conversion and phytic acid content. These are concerns of both PUE and biofortification research as plants must efficiently take up P for growth, as well as convert P selectively for nutrient availability.

Several low phytic acid varieties have been developed in wheat, maize, barley, rice, and soybean through transgenic and biotechnological methods (Wilcox et al., 2000; Larson et al., 2000; Raboy et al., 2000; Guttieri et al., 2004; Rasmussen and Hatzack, 2004). Warkentin et al. developed low phytate field pea variety CDC Bronco *via* EMS to produce the desired mutation in MIPS to halt conversion to higher inositol phosphate molecules. Overall grain phytic acid is reduced, but there are reports of several agronomic issues, such as decreased stress tolerance, germination, growth, and seed weight, as the plant cannot store enough P to use during vegetative processes, in addition to reports of reduced protein content in winter wheat (Raboy et al., 1991; Oltmans et al., 2005; Bregitzer and Raboy, 2006; Warkentin et al., 2012; Rehman et al., 2018). While requiring less P overall, these lines are often stunted, with lower biomass and yield compared to commercial varieties, further illustrating the problem of less P uptake vs. high productivity (Raboy, 2009; Warkentin et al., 2012; Sparvoli and Cominelli, 2015). Additionally, for organic systems, transgenic and chemical mutants are not currently allowed, so they have no use in sustainable agriculture. Furthermore, transgenics and chemically modified seeds are not allowed in the food market, may be banned as in the EU, and consumer approval is generally considered negative or unclear (Lucht, 2015). A more conventional plant breeding approach could be more successful in terms of developing varieties with reduced phytic acid accumulation and positively impact biofortification.

Future Directions

Field pea is highly nutritious and beneficial to agriculture systems, along with other pulses. However field pea is especially advantageous in terms of protein content and extractability. This is the powerful avenue to expand field pea production as consumer interest in health foods, and meatless alternatives grow. Field pea could be biofortified for protein as well as micronutrient content, to increase marketability, as well as ability to fight hidden hunger. The adoption of organic principles is necessary, and organic agriculture should expand, as nonrenewable resources like P begin to deplete. Field pea and other pulses are critical to sustainable agriculture but will suffer from soil P deficiencies, affecting their beneficial status in organic systems and negatively affecting crops that depend on their nitrogen-fixing capabilities.

To adequately prepare and avoid the negative impacts of phosphorus deficiency, a thorough investigation of the genetic diversity of field pea in terms of phosphorus use efficiency is necessary. We hypothesize that there will be variation in the ability of different field pea accessions to acquire, mobilize, and store P under P deficient conditions. Phenotyping could reveal superior yield, nutritional value, and other important agronomic characteristics of some accessions and physiological and genetic analyses would aid in elucidating the biological mechanism. It is possible that there are accessions containing genes that can be incorporated into elite breeding lines to confer benefit in P deficient

environments. The investigation regarding natural genetic variation within the germplasm for differing rates of P speciation should also be considered. For example, one genotype may preferentially convert to Ins3P or other lower inositol phosphates over phytic acid, leading to increased Pi and nutrient bioavailability in the seed, and allowing for low phytic acid lines to be conventionally bred rather than mutagenized. This would increase field pea production sustainability and allow new varieties to be developed for consumer use. In terms of biofortification, identifying field pea genotypes with higher potential for micronutrient accumulation, especially under P and nutrient-deficient environments, will be critical, through the understanding of variation in acquisition and translocation of nutrients to the seed (Welch and Graham, 2004). The common bean core collection has demonstrated variation in Fe and Zn uptake, as well as elucidated a negative correlation between the two during breeding efforts, so these antagonistic relationships must also be discovered and considered (Welch and Graham, 2004).

Despite growing interest in field pea, at the time of this review, there is still no reference genome published, and when one is released, it will always be the first assembly, meaning it will likely need to undergo revisions as technology and genomic understanding of field pea and improve. A single core collection consisting of 431 pea accessions does exist and shows ample genetic variation between accessions, allowing for more genetic studies ((Holdsworth et al., 2017). By using GWAS and other omics methods, questions concerning organic and nutritional breeding may be answered. Additionally, more funding for field pea and pulse research is required, as it has been limited by unstable yields and forgotten by institutions, leading to little germplasm improvement. Government agencies must get involved to promote awareness and create funding opportunities to improve field pea and pulse germplasm, so that legume profitability may increase to better compete with cereals. This is a key measure to ensure people have access to a diverse nutritional diet to combat hidden hunger.

CONCLUSION

A primary focus of agriculture should be to increase sustainability and nutritional value to the human diet through the adoption of more organic practices; this includes diversification of staple crops to include more pulses such as field pea and decreased dependence on nonrenewable resources such as phosphorus. For these goals to be met, more organic-specific breeding initiatives should be undertaken, and more research should be conducted on field pea. The dearth of knowledge on pulses compared to cereals is detrimental to agricultural research and the human diet, so more genomic studies should be conducted to increase productivity and adoption of pulses. Research concerning PUE will benefit farmers and consumers of all types by decreasing reliance on fertilizers and maximizing productivity for already P-deficient soils. Because field pea is consumed globally by both developed and at-risk populations, these efforts could help increase global health overall and combat hidden hunger.

AUTHOR CONTRIBUTIONS

SP: drafted the manuscript and the doctoral student working on the project. DT: edited the draft and the project PI.

ACKNOWLEDGMENTS

Funding support for this project was provided by the Organic Agriculture Research and Extension Initiative (OREI) (award no. 2018-51300-28431/proposal no. 2018-02799) of the United States Department of Agriculture, National Institute of Food and Agriculture, and the USDA-NIFA National Needs Doctoral Fellowship.

REFERENCES

Amarakoon, D., Thavarajah, D., McPhee, K., and Thavarajah, P. (2012). Iron-, zinc-, and magnesium-rich field peas (Pisum sativum L.) with naturally low phytic acid: a potential food-based solution to global micronutrient malnutrition. *J. Food Compost. Anal.* 27 (1), 8–13. doi: 10.1016/J.JFCA.2012.05.007

Amundson, R., Berhe, A. A., Hopmans, J. W., Olson, C., Sztein, A. E., and Sparks, D. L. (2015). Soil and human security in the 21st century. *Science* 348 (6235), 1261071. doi: 10.1126/science.1261071

Assuero, S. G., Mollier, A., and Pellerin, S. (2004). The decrease in growth of phosphorus-deficient maize leaves is related to a lower cell production. *Plant Cell Environ.* 27 (7), 887–895. doi: 10.1111/j.1365-3040.2004.01194.x

Bakker, P. A. H. M., Pieterse, C. M. J., de Jonge, R., and Berendsen, R. L. (2018). The soil-borne legacy. *Cell* 172 (6), 1178–1180. doi: 10.1016/J.CELL.2018.02.024

Bregitzer, P., and Raboy, V. (2006). Effects of four independent low-phytate mutations on barley agronomic performance. *Crop Sci.* 46 (3), 1318. doi: 10.2135/cropsci2005.09-0301

Carvalhais, L. C., Dennis, P. G., Fedoseyenko, D., Hajirezaei, M.-R., Borriss, R., and von Wirén, N. (2011). Root exudation of sugars, amino acids, and organic acids by maize as affected by nitrogen, phosphorus, potassium, and iron deficiency. *J. Plant Nutr. Soil Sci.* 174 (1), 3–11. doi: 10.1002/jpln.201000085

Cordell, D., and White, S. (2014). Life's bottleneck: sustaining the world's phosphorus for a food secure future. *Annu. Rev. Environ. Resour.* 39 (1), 161–188. doi: 10.1146/annurev-environ-010213-113300

FAO. (1994). *Definition and Classification of Commodities. 4. Pulses and Derived Products*. Rome, Italy: Food and Agriculture Organization of the United Nations. http://www.fao.org/es/faodef/fdef04e.htm#4.02.

FAOSTAT. (2019) http://www.fao.org/faostat/en/#data/QC.

Foyer, C. H., Lam, H.-M., Nguyen, H. T., Siddique, K. H. M., Varshney, R. K., Colmer, T. D., et al. (2016). Neglecting legumes has compromised human health and sustainable food production. *Nat. Plants* 2 (8), 16112. doi: 10.1038/nplants.2016.112

Guttieri, M., Bowen, D., Dorsch, J. A., Raboy, V., and Souza, E. (2004). Identification and characterization of a low phytic acid wheat. *Crop Sci.* 44 (2), 418. doi: 10.2135/cropsci2004.4180

Helback, H., and Hopf, M. (1959). Domestication of Food Plants in the Old World: Joint efforts by botanists and archeologists illuminate the obscure history of plant domestication. *Science* 130 (3372), 365–372. doi: 10.1126/science.130.3372.365

Holdsworth, W. L., Gazave, E., Cheng, P., Myers, J. R., Gore, M. A., Coyne, C. J., et al. (2017). A community resource for exploring and utilizing genetic diversity in the USDA pea single plant plus collection. *Hortic. Res.* 4, 17017. doi: 10.1038/hortres.2017.17

Hole, D. G., Perkins, A. J., Wilson, J. D., Alexander, I. H., Grice, P. V., and Evans, A. D. (2005). Does organic farming benefit biodiversity?. *Biol. Conserv.* 122 (1), 113–130. doi: 10.1016/J.BIOCON.2004.07.018

Jacoby, R., Peukert, M., Succurro, A., Koprivova, A., and Kopriva, S. (2017). The role of soil microorganisms in plant mineral nutrition—current knowledge and future directions. *Front. In Plant Sci.* 8, 1617. doi: 10.3389/fpls.2017.01617

Jones, S. S., Murphy, K. M., Myers, J. R., and Messmer, M. M. (2011). The need to breed crop varieties suitable for organic farming, using wheat, tomato and broccoli as examples: A review. *NJAS - Wageningen J. Life Sci.* 58 (3–4), 193–205. doi: 10.1016/J.NJAS.2010.04.001

Larson, S. R., Rutger, J.N., Young, K.A. and Raboy, V., (2000). Isolation and genetic mapping of a non-lethal rice (Oryza sativa L.) low phytic acid 1 mutation. *Crop Science* 40 (5), 1397–1405.

Lucht, J. M. (2015). Public Acceptance of Plant Biotechnology and GM Crops. *Viruses* 7 (8), 4254–4281. doi: 10.3390/v7082819

Möller, K., Oberson, A., Bünemann, E. K., Cooper, J., Friedel, J. K., Glæsner, N., et al. (2018). "Improved phosphorus recycling in organic farming: Navigating between constraints" in *Advances in Agronomy*, vol. 147. (Elsevier: Amsterdam), 159–237. doi: 10.1016/bs.agron.2017.10.004

MacDonald, G. K., Bennett, E. M., Potter, P. A., and Ramankutty, N. (2011). Agronomic phosphorus imbalances across the world's croplands. *Proc. Natl. Acad. Sci. U.S.A.* 108 (7), 3086–3091. doi: 10.1073/pnas.1010808108

Oehl, F., Oberson, A., Tagmann, H. U., Besson, J. M., Dubois, D., Mäder, P., et al. (2002). Phosphorus budget and phosphorus availability in soils under organic and conventional farming. *Nutr. Cycl. In Agroecosys* 62 (1), 25–35. doi: 10.1023/A:1015195023724

Oehl, F., Sieverding, E., Mäder, P., Dubois, D., Ineichen, K., Boller, T., et al. (2004). Impact of long-term conventional and organic farming on the diversity of arbuscular mycorrhizal fungi. *Oecologia* 138 (4), 574–583. doi: 10.1007/s00442-003-1458-2

Oltmans, S. E., Fehr, W. R., Welke, G. A., Raboy, V., and Peterson, K. L. (2005). Agronomic and seed traits of soybean lines with low–phytate phosphorus. *Crop Sci.* 45 (2), 593. doi: 10.2135/cropsci2005.0593

Pang, J., Zhao, H., Bansal, R., Bohuon, E., Lambers, H., Ryan, M. H., et al. (2018). Leaf transpiration plays a role in phosphorus acquisition among a large set of chickpea genotypes. *Plant Cell Environ.* 41 (9), 2069–2079. doi: 10.1111/pce.13139

Peoples, M. B., Hauggaard-Nielsen, H., Huguenin-Elie, O., Jensen, E. S., Justes, E., and Williams, M. (2019). "The contributions of legumes to reducing the environmental risk of agricultural production" in *Agroecosystem Diversity: Reconciling Contemporary Agriculture and Environmental Quality*. Eds. Lemaire, P. C., De Faccio Carvalho, S., Kronberg, S., and Recous, G. (Amsterdam: Elsevier). doi: 10.1016/B978-0-12-811050-8.00008-X

Pingali, P. L. (2012). Green revolution: impacts, limits, and the path ahead. *Proc. Natl. Acad. Sci. U.S.A.* 109 (31), 12302–12308. doi: 10.1073/pnas.0912953109

Ponisio, L. C., M'gonigle, L. K., Mace, K. C., Palomino, J., de Valpine, P., and Kremen, C. (2015). Diversification practices reduce organic to conventional yield gap. *Proc. R. Soc. B: Biol. Sci.* 282 (1799), 20141396.

Raboy, V. (2009). Approaches and challenges to engineering seed phytate and total phosphorus. *Plant Sci.* 177 (4), 281–296. doi: 10.1016/j.plantsci.2009.06.012

Raboy, Victor, Noaman, M. M., Taylor, G. A., and Pickett, S. G. (1991). Grain phytic acid and protein are highly correlated in winter wheat. *Crop Sci.* 31 (3), 631. doi: 10.2135/cropsci1991.0011183X003100030017x

Raboy, V., Gerbasi, P. F., Young, K. A., Stoneberg, S. D., Pickett, S. G., Bauman, A. T., et al. (2000). Origin and seed phenotype of maize low phytic acid 1-1 and low phytic acid 2-1. *Plant Physiol.* 124 (1), 355–368. doi: 10.1104/pp.124.1.355

Raboy, V. (2003). myo-Inositol-1,2,3,4,5,6-hexakisphosphate. *Phytochemistry* 64 (6), 1033–1043. doi: 10.1016/S0031-9422(03)00446-1

Rasmussen, S. K., and Hatzack, F. (2004). Identification of two low-phytate barley (Hordeum Vulgare l.) grain mutants by TLC and genetic analysis. *Hereditas* 129 (2), 107–112. doi: 10.1111/j.1601-5223.1998.00107.x

Reganold, J. P., and Wachter, J. M. (2016). Organic agriculture in the twenty-first century. *Nat. Plants* 2 (2), 15221. doi: 10.1038/nplants.2015.221

Reganold, J. P., Elliott, L. F., and Unger, Y. L. (1987). Long-term effects of organic and conventional farming on soil erosion. *Nature* 330 (6146), 370–372. doi: 10.1038/330370a0

Rehman, H. M., Cooper, J. W., Lam, H.-M., and Yang, S. H. (2018). Legume biofortification is an underexploited strategy for combatting hidden hunger. *Plant Cell Environ.* 42 (1), 52–70. doi: 10.1111/pce.13368

Robinson, W. D., Carson, I., Ying, S., Ellis, K., and Plaxton, W. C. (2012). Eliminating the purple acid phosphatase AtPAP26 in Arabidopsis thaliana delays leaf senescence and impairs phosphorus remobilization. *New Phytol.* 196 (4), 1024–1029. doi: 10.1111/nph.12006

Rose, T. J., and Wissuwa, M. (2012). Rethinking internal phosphorus utilization efficiency: A new approach is needed to improve PUE in grain crops. *Adv. In Agron.* 116, 185–217. doi: 10.1016/B978-0-12-394277-7.00005-1

Sa, T.-M., and Israel, D. W. (1991). Energy status and functioning of phosphorus-deficient soybean nodules. *Plant Physiol.* 97, 928–935. doi: 10.1104/pp.97.3.928

Schachtman, D.P., Reid, R.J. and Ayling, S.M. (1998). Phosphorus uptake by plants: from soil to cell. *Plant Physiol.* 116 (2), 447–453. doi: 10.1104/pp.116.2.447

Schilling, G., Gransee, A., Deuhel, A., Ležoviž, G., and Ruppel, S. (1998). Phosphorus availability, root exudates, and microbial activity in the rhizosphere. *Z. Für Pflanzenernährung Und Bodenkunde* 161 (4), 465–478. doi: 10.1002/jpln.1998.3581610413

Schrama, M., de Haan, J. J., Kroonen, M., Verstegen, H., and van der Putten, W. H. (2018). Crop yield gap and stability in organic and conventional farming systems. *Agric. Ecosyst. Environ.* 256, 123–130. doi: 10.1016/J.AGEE.2017.12.023

Seufert, V., Ramankutty, N., and Foley, J. A. (2012). Comparing the yields of organic and conventional agriculture. *Nature* 485, 229–232. doi: 10.1038/nature11069

Shenoy, V. V., and Kalagudi, G. M. (2005). Enhancing plant phosphorus use efficiency for sustainable cropping. *Biotechnol. Adv.* 23 (7–8), 501–513. doi: 10.1016/j.biotechadv.2005.01.004

Slessarev, E. W., Lin, Y., Bingham, N. L., Johnson, J. E., Dai, Y., Schimel, J. P., et al. (2016). Water balance creates a threshold in soil pH at the global scale. *Nature* 540, 567–569. doi: 10.1038/nature20139

Sparvoli, F., and Cominelli, E. (2015). Seed biofortification and phytic acid reduction: a conflict of interest for the plant?. *Plants (Basel Switzerland)* 4 (4), 728–755. doi: 10.3390/plants4040728

Stagnari, F., Maggio, A., Galieni, A., and Pisante, M. (2017). Multiple benefits of legumes for agriculture sustainability: an overview. *Chem. Biol. Technol. In Agric.* 4 (2), 2. doi: 10.1186/s40538-016-0085-1

Sulieman, S., and Tran, L.-S. P. (2015). Phosphorus homeostasis in legume nodules as an adaptive strategy to phosphorus deficiency. *Plant Sci.* 239, 36–43. doi: 10.1016/j.plantsci.2015.06.018

Udvardi, M., and Poole, P.S. (2013). Transport and metabolism in legume-rhizobia symbioses. *Annu. Rev. Plant Biol.* 64, 781–805. doi: 10.1146/annurev-arplant-050312-120235

van de Wiel, C. C. M., van der Linden, C. G., and Scholten, O. E. (2016). Improving phosphorus use efficiency in agriculture: opportunities for breeding. *Euphytica* 207 (1), 1–22. doi: 10.1007/s10681-015-1572-3

Vance, C. P., Uhde-Stone, C., and Allan, D. L. (2003). Phosphorus acquisition and use: critical adaptations by plants for securing a nonrenewable resource. *New Phytol.* 157 (3), 423–447. doi: 10.1046/j.1469-8137.2003.00695.x

Veneklaas, E. J., Lambers, H., Bragg, J., Finnegan, P. M., Lovelock, C. E., Plaxton, W. C., et al. (2012). Opportunities for improving phosphorus-use efficiency in crop plants. *New Phytol.* 195 (2), 306–320. doi: 10.1111/j.1469-8137.2012.04190.x

Warkentin, T. D., Delgerjav, O., Arganosa, G., Rehman, A. U., Bett, K. E., Anbessa, Y., et al. (2012). Development and characterization of low-phytate pea. *Crop Sci.* 52 (1), 74–78. doi: 10.2135/cropsci2011.05.0285

Welch, R. M., and Graham, R. D. (2004). Breeding for micronutrients in staple food crops from a human nutrition perspective. *J. Exp. Bot.* 55 (396), 353–364. doi: 10.1093/jxb/erh064

Welch, R. M. (2002). The impact of mineral nutrients in food crops on global human health. *Plant Soil* 247 (1), 83–90. doi: 10.1023/A:1021140122921

Wilcox, J.R., Premachandra, G.S., Young, K.A., and Raboy, V. (2000). Isolation of high seed inorganic P, low-phytate soybean mutants. *Crop Sci.* 40 (6), 1601–1605. doi:10.2135/cropsci2000.4061601x

Wolfe, M. S., Baresel, J. P., Desclaux, D., Goldringer, I., Hoad, S., Kovacs, G., et al. (2008). Developments in breeding cereals for organic agriculture. *Euphytica* 163 (3), 323. doi: 10.1007/s10681-008-9690-9

Xu, L., Zhao, H., Wan, R., Liu, Y., Xu, Z., Tian, W., et al. (2019). Identification of vacuolar phosphate efflux transporters in land plants. *Nat. Plants* 5 (1), 84–94. doi: 10.1038/s41477-018-0334-3

Yang, S. Y., Huang, T. K., Kuo, H. F., and Chiou, T. J. (2017). Role of vacuoles in phosphorus storage and remobilization. *J. Exp. Bot.* 68 (12), 3045–3055. doi: 10.1093/jxb/erw481

Conflict of Interest: The authors declare that the research was conducted in the absence of any commercial or financial relationships that could be construed as a potential conflict of interest.

frontiers in Plant Science

ORIGINAL RESEARCH
published: 21 January 2020
doi: 10.3389/fpls.2019.01711

Glutathione and Its Biosynthetic Intermediates Alleviate Cesium Stress in Arabidopsis

Eri Adams[1], Takae Miyazaki[1], Shunsuke Watanabe[1], Naoko Ohkama-Ohtsu[2,3], Mitsunori Seo[1] and Ryoung Shin[1]**

[1] RIKEN Center for Sustainable Resource Science, Yokohama, Japan, [2] Institute of Agriculture, Tokyo University of Agriculture and Technology (TUAT), Fuchu, Japan, [3] Institute of Global Innovation Research, Tokyo University of Agriculture and Technology (TUAT), Fuchu, Japan

OPEN ACCESS

Edited by:
Francisco Rubio, Spanish National Research Council, Spain

Reviewed by:
Marcela Simontacchi, National Council for Scientific and Technical Research (CONICET), Argentina
Amna Mhamdi, Ghent University, Belgium

***Correspondence:**
Eri Adams
eri.adams@riken.jp
Ryoung Shin
ryoung.shin@riken.jp

Specialty section:
This article was submitted to Plant Nutrition, a section of the journal Frontiers in Plant Science

Received: *11 September 2019*
Accepted: *05 December 2019*
Published: *21 January 2020*

Citation:
Adams E, Miyazaki T, Watanabe S, Ohkama-Ohtsu N, Seo M and Shin R (2020) Glutathione and Its Biosynthetic Intermediates Alleviate Cesium Stress in Arabidopsis. Front. Plant Sci. 10:1711. doi: 10.3389/fpls.2019.01711

Phytoremediation is optimized when plants grow vigorously while accumulating the contaminant of interest. Here we show that sulphur supply alleviates aerial chlorosis and growth retardation caused by cesium stress without reducing cesium accumulation in *Arabidopsis thaliana*. This alleviation was not due to recovery of cesium-induced potassium decrease in plant tissues. Sulphur supply also alleviated sodium stress but not potassium deficiency stress. Cesium-induced root growth inhibition has previously been demonstrated as being mediated through jasmonate biosynthesis and signalling but it was found that sulphur supply did not decrease the levels of jasmonate accumulation or jasmonate-responsive transcripts. Instead, induction of a glutathione synthetase gene *GSH2* and reduction of a phytochelatin synthase gene *PCS1* as well as increased accumulation of glutathione and cysteine were observed in response to cesium. Exogenous application of glutathione or concomitant treatments of its biosynthetic intermediates indeed alleviated cesium stress. Interestingly, concomitant treatments of glutathione biosynthetic intermediates together with a glutathione biosynthesis inhibitor did not cancel the alleviatory effects against cesium suggesting the existence of a glutathione-independent pathway. Taken together, our findings demonstrate that plants exposed to cesium increase glutathione accumulation to alleviate the deleterious effects of cesium and that exogenous application of sulphur-containing compounds promotes this innate process.

Keywords: *Arabidopsis thaliana*, cesium, glutathione, jasmonates, potassium, phytoremediation, sodium, sulphur supply

Abbreviations: BSO, buthionine sulphoximine; Cys, cysteine; γ-Glu-Cys, γ-glutamylcysteine; Glu, glutamic acid; Gly, glycine; GSH, glutathione; JA, jasmonate/jasmonic acid; JA-Ile, jasmonyl-isoleucine; PC, phytochelatin; ROS, reactive oxygen species; Ser, serine.

INTRODUCTION

Plants readily absorb cesium when present in the soil mainly through the potassium uptake system in the roots. Potassium is an essential nutrient for plants, a lack of which causes severe growth retardation while cesium has no known beneficial role in plants and its accumulation in the plants inhibits growth. Due to the physicochemical similarities among the alkali metals, cesium and potassium share the same uptake system and cesium competes with potassium at the root surface and disrupts the physiological roles of potassium inside the plant cells (White and Broadley, 2000). We have recently shown that cesium selectively inhibits potassium intake through a potassium channel complex AKT1-KC1 and the inability of cesium-treated plants to accumulate potassium is the major cause of growth retardation in *Arabidopsis thaliana* (Adams et al., 2018). Plants exposed to cesium induce expression of a potassium transporter gene (*HAK5*), a potassium deficiency marker gene, and activate jasmonate (JA) biosynthesis and signalling (Adams et al., 2013). Cesium also inactivates proteins by interacting with potassium binding sites and changes a wide variety of gene expression and microRNA processing (Hampton et al., 2004; Sahr et al., 2005a; Sahr et al., 2005b; Jung et al., 2015). Although the natural occurrence of cesium in soils is relatively low, occasional inadvertent release of cesium, most likely radiocesium, through anthropogenic activities such as the nuclear power plant failure at Chernobyl and Fukushima can seriously contaminate soils. Radioactive cesium in the soil is not only harmful for the environment *per se*, but it can also enter and be concentrated in the human food chain *via* plants.

Phytoremediation is a biological remediation method to remove toxic compounds from contaminated land and is considered to be more cost-effective and environmentally-friendly than conventional physical and chemical remediation methods. As phytoremediation utilizes the ability of plants to absorb the metal of interests, it is non-destructive to the soil structure and is particularly preferred in farmland. Plants that accumulated the contaminant are harvested and subject to desiccation and combustion so that the volume of radioactive waste is dramatically reduced compared to the volume involved when physical removal of contaminated soil is deployed (Dushenkov, 2003). Ideal phytoremediation is enabled when plants 1) accumulate a large amount of the contaminant in the aerial parts and 2) maintain vigorous growth while accumulating the contaminant. For phytoremediation of cesium, a wide variety of plant species have been investigated in the search for a "hyperaccumulator" and biological or chemical factors which improve uptake ability of plants have been tested (Burger and Lichtscheidl, 2018). Our previous screening effort isolated a chemical compound, methyl cysteinate, which promotes cesium accumulation in plants (Adams et al., 2017). However, plants accumulating high levels of cesium suffer stunted growth. It has been known that a plentiful supply of potassium mitigates cesium-induced growth inhibition but only in exchange for reduced cesium accumulation (Zhu and Smolders, 2000). While the addition of potassium helps to protect agricultural crops from being contaminated with radiocesium, the addition of sulphur resulted in alleviation of growth inhibition by cesium without reduction of cesium accumulation in plants.

The involvement of sulphur metabolism in metal stress response has been well reported (Seth et al., 2012; Anjum et al., 2015). A sulphur-containing metabolite, glutathione (GSH), acts as a strong non-protein antioxidant that protects cells suffering from metal stress which causes oxidative damage (Noctor et al., 2011). GSH and downstream metabolites, phytochelatins (PCs), also function as metal chelators which then sequestrate the metal into vacuoles upon binding, a common detoxification strategy for heavy metals (Hasanuzzaman et al., 2017). Some examples of the interaction between metal stress and the sulphur metabolic pathway in plants are introduced here. Cadmium exposure in Arabidopsis induces expression of genes encoding sulphate transporter (SULTR), serine acetyltransferase (SERAT), γ-glutamylcysteine (γ-Glu-Cys) synthetase (GSH1), and GSH synthetase (GSH2) and in turn increases sulphate uptake and accumulation of cysteine (Cys) and PCs (Xiang and Oliver, 1998; Howarth et al., 2003; Yamaguchi et al., 2016; Ferri et al., 2017). Chromium has been shown to induce PC synthase genes (*PCS1* and *PCS2*) and increase hydrogen sulfide, Cys and GSH levels, while copper induces *GSH1* and *GSH2* in Arabidopsis (Xiang and Oliver, 1998; Fang et al., 2016). Proteomic analysis has revealed that GSH, PC and glucosinolate biosynthesis pathways are up-regulated during a response to lead in Arabidopsis (Zhu et al., 2016). Toxic levels of selenium have been demonstrated to induce a series of genes encoding SULTRs and sulphur metabolism enzymes in a selenium-resistant Arabidopsis accession Col-0 but not in a selenium-sensitive accession Ws-2 (Tamaoki et al., 2008). Meanwhile, a light metal, sodium, has also been shown to induce a range of *SULTR*s and sulphur metabolism genes in Arabidopsis (Cao et al., 2014). In mustard (*Brassica juncea*), sulphur supply has been indicated to alleviate sodium stress through increased GSH accumulation, promoted photosynthesis and reduced ethylene production (Fatma et al., 2014; Nazar et al., 2014).

In the present study, we demonstrated that sulphur supply alleviated the deleterious effects of cesium without reducing cesium accumulation in Arabidopsis. This alleviation was not due to increased potassium accumulation or reduced JA production. This alleviation was also not due to well-known metal detoxifying agents, PCs. Instead, we describe that GSH and its biosynthetic intermediates are important for retrieving growth in plants suffering from cesium stress.

MATERIAL AND METHODS

Plant Material and Growth Condition

The *A. thaliana* (L.) Heynh. accession Col-0 was used as a wild type. The mutant seeds *sultr1;1* (salk_093256c), *sultr1;2* (salk_122974), *sultr1;3* (salk_018910), *sultr2;1* (salk_109907c), *sultr2;2* (salk_111268c), *sultr3;1* (salk_127024c), *sultr3;2* (salk_023980c), *sultr3;3* (salk_000822c), *sultr3;4* (salk_100362), *sultr3;5* (salk_128559), *sultr4;1* (salk_103873c), *sultr4;2* (salk_103827c), and *cad1*-3 (CS68125) were obtained from the

ABRC (Arabidopsis Biological Resource Center, https://abrc.osu.edu/) and *aos* (CS6149) and *jar1*-1 (CS8072) were obtained from the NASC (Nottingham Arabidopsis Stock Centre, http://nasc.nott.ac.uk). Seeds were surface-sterilized with 70% (v/v) ethanol and 0.05% (v/v) Triton X-100 and sown on media containing 2 mM $Ca(NO_3)_2$, 0.5 mM phosphoric acid, 0.75 mM $MgSO_4$, 50 μM H_3BO_3, 10 μM $MnCl_2$, 2 μM $ZnSO_4$, 1.5 μM $CuSO_4$, 0.075 μM $NH_4Mo_7O_{24}$, and 74 μM Fe-EDTA, pH 5.8 with $Ca(OH)_2$, 1% (w/v) sucrose and 1% (w/v) of SeaKem agarose (Lonza) or agarose L03 (TaKaRa) supplemented with designated concentrations of KCl, CsCl and other chemicals. For sulphur supply, $CaSO_4$ was supplemented in addition to 0.75 mM $MgSO_4$ in the base media to add up to the indicated concentrations. After stratification for three to four days at 4°C, plants were placed in a growth cabinet at 22°C in a 16 h light/8 h dark photocycle with a light intensity of 70–90 μmol m^{-2} s^{-1}.

Phenotype Quantification

Aerial phenotype of cesium-treated plants was scored as follows: seedlings with fully expanded green aerial parts were given score 2, those with more than half the number of leaves (cotyledons plus true leaves) showing chlorosis were given score 0 and those with intermediate phenotype given score 1. Primary root lengths were measured on images using ImageJ (Schneider et al., 2012).

qRT-PCR Analysis

Seedlings grown for eight days on media containing 1.75, 0.5 or 0.01 mM KCl with or without 0.3 mM CsCl and additional $CaSO_4$ were divided into roots and shoots, flash-frozen in liquid N_2 and ground using a mixer mill. Total RNA was extracted, treated with DNaseI (Invitrogen) and synthesized into cDNA using SuperScript III (Invitrogen). Quantitative real-time reverse transcription-PCR (qRT-PCR) was performed using THUNDERBIRD SYBR qPCR mix (TOYOBO) and a Mx3000P qPCR system (Agilent Technologies). The amplification conditions were 95°C for 15 s and 60°C for 30 s. The cycle was repeated 40 times, preceded by 95°C for 1 min and followed by a dissociation programme to create melting curves. Three biological replicates each of which contains >30 seedlings were analyzed. The β-tubulin gene (*TUB2*, At5g62690) was used as a reference gene. The primer sequences for *HAK5*, *VSP2*, *PDF1.2*, *SULTR1;1*, *SULTR1;2*, *SULTR3;1*, *SULTR3;2*, *SULTR3;3*, *SULTR3;4,* and *SULTR3;5* are shown in the previous publications (Adams et al., 2013; Cao et al., 2014; Ferri et al., 2017). The rest of the primers used are listed in **Supplementary Table S1**.

Elemental Analysis

Whole seedlings were washed in Milli-Q water, dried on a paper towel, placed in a paper envelope and dried in an oven at 65°C for three to four days. Typically, 20 to 60 seedlings were pooled as one biological replicate and three biological replicates were analyzed. Approximately 2 mg of dried samples were extracted in 1 ml of 60% (v/v) HNO_3 at 125°C for 1 h, followed by 1 ml of 30% (v/v) H_2O_2 and diluted with Milli-Q water to get a total volume of 10 ml. For potassium and sodium analysis, samples were further diluted 10 and 100 times with 6% (v/v) HNO_3. For cesium analysis, 0.1% (w/v) KCl was added to each sample and standard solution to prevent ionisation of cesium, according to the manufacturer's instructions (PerkinElmer). Potassium, sodium, and cesium concentrations were measured on a flame atomic absorption spectrometer AAnalyst 200 (PerkinElmer). Concentrations were calculated against each standard curve.

Glutathione and Cysteine Quantification

Whole seedlings were harvested and fresh weights of approximately 20 to 40 seedlings were determined. Flash-frozen samples were ground using a mixer mill, extracted with 10 mM HCl and derivatized with monobromobimane as described previously (Minocha et al., 2008; Nishida et al., 2016), followed by HPLC (Shimadzu Corp.) with a Shim-pac FC-ODS column (150 × 4.6 mm, Shimadzu Corp.). The standard chemicals were purchased from Wako Pure Chemical Industries Ltd.

JA Quantification

Quantification of jasmonic acid (JA) and jasmonoyl–isoleucine (JA-Ile) were performed as described previously (Kanno et al., 2016). Briefly, whole seedlings grown in each condition were freeze-dried and then homogenized in the extraction solution [80% (v/v) acetonitrile containing 1% (v/v) acetic acid] with defined amounts of isotopically labelled JA (D_2-JA) and JA-Ile ($^{13}C_6$-JA-Ile) as internal standards. After incubation for 12 h at 4°C, the homogenate was centrifuged at 3,000 × g for 20 min. The supernatants were dried using nitrogen gas and dissolved with 1% (v/v) acetic acid solution. After purification of hormones by solid-phase extraction columns (Oasis WAX, Waters), extracts were dried using nitrogen gas and dissolved in 1% (v/v) acetic acid solution. Endogenous hormone levels were determined using a UPLC-MS/MS system consisting of a quadrupole/time-of-flight tandem mass spectrometer (Triple TOF 5600, AB SCIEX) and a Nexera UPLC system (Shimadzu Corp.) as described previously. To calculate plant hormone concentrations from the LC–MS–MS data, a software MultiQuant 2.0 (AB SCIEX) was used.

Statistical Analysis

All statistical analysis were performed using Prism (GraphPad Software). Green score was analyzed with Kruskal-Wallis test with Dunn's multiple comparison posttest using Prism (GraphPad Software) to determine the statistical significance. T-test was performed in order to determine the significant difference of *VSP2* and *PDF1.2* expression in Col-0 grown on media containing 1.75 mM K and 2 mM S compared to control condition (0.75 mM S). All other cases, one-way ANOVA tests with Bonferroni's or Dunnett's multiple comparison tests were used in order to determine the statistical significance.

RESULTS

Sulphur Supply Alleviates Cesium Stress in Plants

In order to assess the effects of nutrient supply on plants experiencing cesium stress, a plentiful supply of either potassium or sulphur in the form of sulphate was applied to Arabidopsis wild type (Col-0) seedlings. Metal stress usually causes uniform growth inhibition response but with cesium the response is often variable. At a sub-optimal potassium (0.5 mM KCl) with basal sulphur (0.75 mM $MgSO_4$) condition, seedlings supplied with cesium (0.3 mM CsCl) showed a characteristic mixed phenotype with some suffering aerial chlorosis and reduced root growth and others only minor growth retardation (**Figure 1A**). The similar phenotype was found in hydroponically grown seedlings. To highlight and quantify this distinctive aerial phenotype caused by cesium, green scoring was introduced and each seedling was given score 0–2 with score 0 being the severest cesium phenotype (see the *Material and Methods* section for the detailed scoring scale, **Figure 1B**). Increasing potassium concentrations to 5 or 10 mM totally cancelled the visible cesium phenotype (**Figures 1A, B**). Increasing the sulphur concentration to 2 mM dramatically improved the health and growth of plants exposed to cesium, however it did not alter cesium-induced *HAK5* expression ($P > 0.05$, **Figures 1A–C**). *HAK5* expression was not altered by sulphur supply in the absence of cesium either (0.77 times expression relative to the control, $P > 0.05$). Accordingly, potassium concentrations in the plants were not increased by sulphur supply in the presence or absence of cesium (**Figure 1D**). Moreover, sulphur supply did not alter cesium accumulation unlike potassium supply which resulted in a dose-dependent reduction of cesium concentrations in the plants (**Figure 1E**).

Sulphur Supply Alleviates Sodium Stress but Not Potassium Deficiency Response

Being an alkali metal, sodium is also known to compete with potassium and initiates a potassium deficiency response in plants. Increasing concentrations of sodium inhibited root growth in a dose-dependent manner but 2 mM sulphur supply mitigated this growth inhibition (**Figure 2A**). However, this growth mitigation was not due to altered potassium or sodium concentrations in the plants (**Figures 2B, C**). In contrast, 1–2 mM sulphur supply could not recover potassium deficiency phenotype or the reduced levels of potassium accumulation in plants (**Figures 2D, E**).

Sulphate Transporters Do Not Seem to be Involved in Cesium Stress Alleviation by Sulphur Supply

Sulphur-induced alleviation of cesium response in plants was not because sulphur could reverse a potassium accumulation loss that was caused by cesium or sodium. To test whether increased sulphur uptake and translocation in the cells are responsible for cesium stress alleviation, gene expression of *SULTR*s was analyzed. Expression of genes encoding high-affinity sulphate transporters, SULTR1;1 and SULTR1;2, or that of a gene encoding a low-affinity sulphate transporter, SULTR2;2 (Takahashi et al., 2000; Yoshimoto et al., 2002), was not altered in roots treated with cesium relative to those on the optimal potassium condition (1.75 mM KCl, **Figure 3A**). In contrast, expression of *SULTR3;5* responsible for the root-to-shoot sulphate transport (Kataoka et al., 2004a) was mildly induced in response to cesium. A complete expression pattern of all *SULTR*s in roots and shoots treated with cesium and sulphur supply in a sub-optimal potassium condition (0.5 mM KCl) is shown in **Supplementary Figure S1**.

To further investigate the role of SULTRs in cesium stress alleviation, insertional mutants of each *SULTR* were analyzed for cesium response and compared with the wild type. There was no statistical difference recognized in terms of green score and potassium accumulation between *sultr* mutants and the wild type (**Figures 3B, C**). Interestingly, *sultr1;3*, *sultr4;1,* and *sultr4;2* were shown to accumulate more cesium (**Figure 3D**). *sultr* mutants did not show altered phenotypic response to potassium deficiency relative to the wild type although *SULTR1;2*, *SULTR3;1,* and *SULTR3;5* were up-regulated in roots under potassium deficiency (**Supplementary Figure S1**).

GSH and Its Biosynthetic Intermediates, but Not PCs, Are Important for Cesium Stress Alleviation

Expression of sulphate metabolism genes was analyzed to understand which forms of sulphur-containing metabolites were important for cesium stress alleviation. Sulphate, once absorbed by plants, goes through a sequential assimilative reduction reaction and is synthesized into Cys. Serine acetyltransferase (SERAT) and *O*-acetlyserine(thiol)lyase (OASTL) are the two classes of proteins involved in Cys synthesis (Hatzfeld et al., 2000; Kawashima et al., 2005). *SERAT2;1*, a gene encoding one of three major SERATs (Kawashima et al., 2005), and *OASTLa*, a gene encoding a cytosolic form of OASTL (Jost et al., 2000), were not responsive to cesium in both roots and shoots (**Figure 4**). GSH is synthesized through a sequential addition of glutamic acid (Glu) and glycine (Gly) to Cys by the function of GSH1 and GSH2, respectively (May and Leaver, 1994; Ullmann et al., 1996) while PCs are synthesized from GSH by the action of PCS1 and PCS2 (Howden et al., 1995; Cazale and Clemens, 2001). Expression analysis revealed that *GSH2* was induced and *PCS1* was reduced in response to cesium in shoots and these alterations were more profound in shoots treated with cesium together with a supply of sulphur (**Figure 4**).

Next, internal levels of Cys, GSH and PCs were determined in the seedlings treated with cesium and sulphur supply. In consistency with *GSH2* expression (**Figure 4B**) and our previous results (Adams et al., 2017), cesium treatment increased both Cys and GSH but sulphur supply did not (**Figures 5A, B**). PC2 and PC3 levels were below detection limits in all the conditions tested. Exogenous application of GSH indeed alleviated aerial chlorosis caused by cesium to the degree equivalent to the sulphur supply (**Figures 5C, D**).

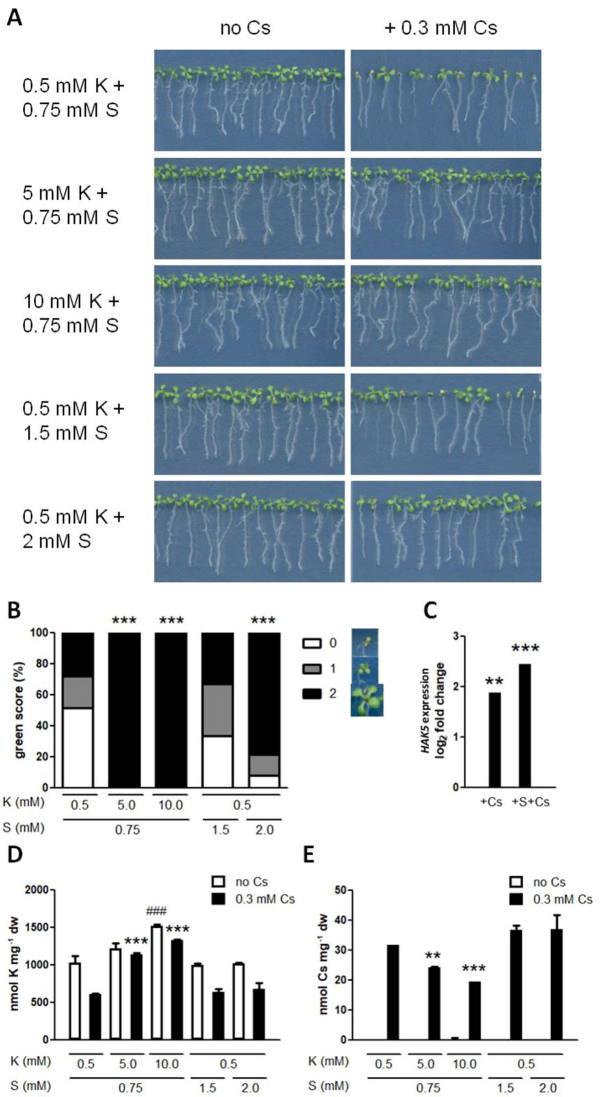

FIGURE 1 | Effects of potassium and sulphur supply on cesium stress. **(A)** Eight-day-old wild type (Col-0) seedlings germinated on media containing indicated concentrations of potassium (K) and sulphate (S) with or without cesium (Cs). **(B)** Percentile green scores for cesium-treated seedlings derived from **(A)**. Statistically significant differences relative to the control cesium condition (0.5 mM K + 0.75 mM S + 0.3 mM Cs) were determined by Kruskal-Wallis test with Dunn's multiple comparison posttest (n > 38, $P < 0.001$). Examples of a seedling with each score are provided next to the score legend. **(C)** Expression of *HAK5* in Col-0 grown on media containing 1.75 mM K and 0.3 mM Cs with or without 2 mM S for eight days. Values are $\log_2$ ratios relative to expression in the control seedlings grown in the absence of cesium (1.75 mM K + 0.75 mM S). Statistically significant differences were determined by one-way ANOVA with Bonferroni's multiple comparison posttest (n = 3, ** for $P < 0.01$, *** for $P < 0.001$). **(D)** K and **(E)** Cs concentrations in seedlings derived from **(A)**. Statistically significant differences were determined by one-way ANOVA with Bonferroni's multiple comparison posttest (n = 3, ### for $P < 0.001$ relative to the non-cesium control, ** for $P < 0.01$, *** for $P < 0.001$ relative to the cesium-treated control) and error bars represent the SE.

A mutant defective in PC synthesis, *cad1*-3 (Howden et al., 1995) showed a wild type-like response to cesium and this phenotype was also recovered to the same degree as the wild type by GSH treatment in excellent agreement with the *PCS* expression patterns and PC quantification results (**Figures 4B** and **5C**, **D**).

To further define the crucial sulphur-containing metabolites for cesium stress alleviation, the effects of 100 μM Glu, Cys or Gly on plant growth were investigated. Glu stunted primary root growth and increased secondary root structures both in the presence and absence of cesium (**Figure 6A**). Upon calculating green score, the percentage of the seedlings with score 0 decreased by treatment with any of these three amino acids and that with score 2 increased by Cys or Gly supplementation but these changes were not statistically significant relative to the non-amino acid supplemented control (**Figure 6B**). Next, concomitant treatments of Glu, Cys, Gly and γ-Glu-Cys were

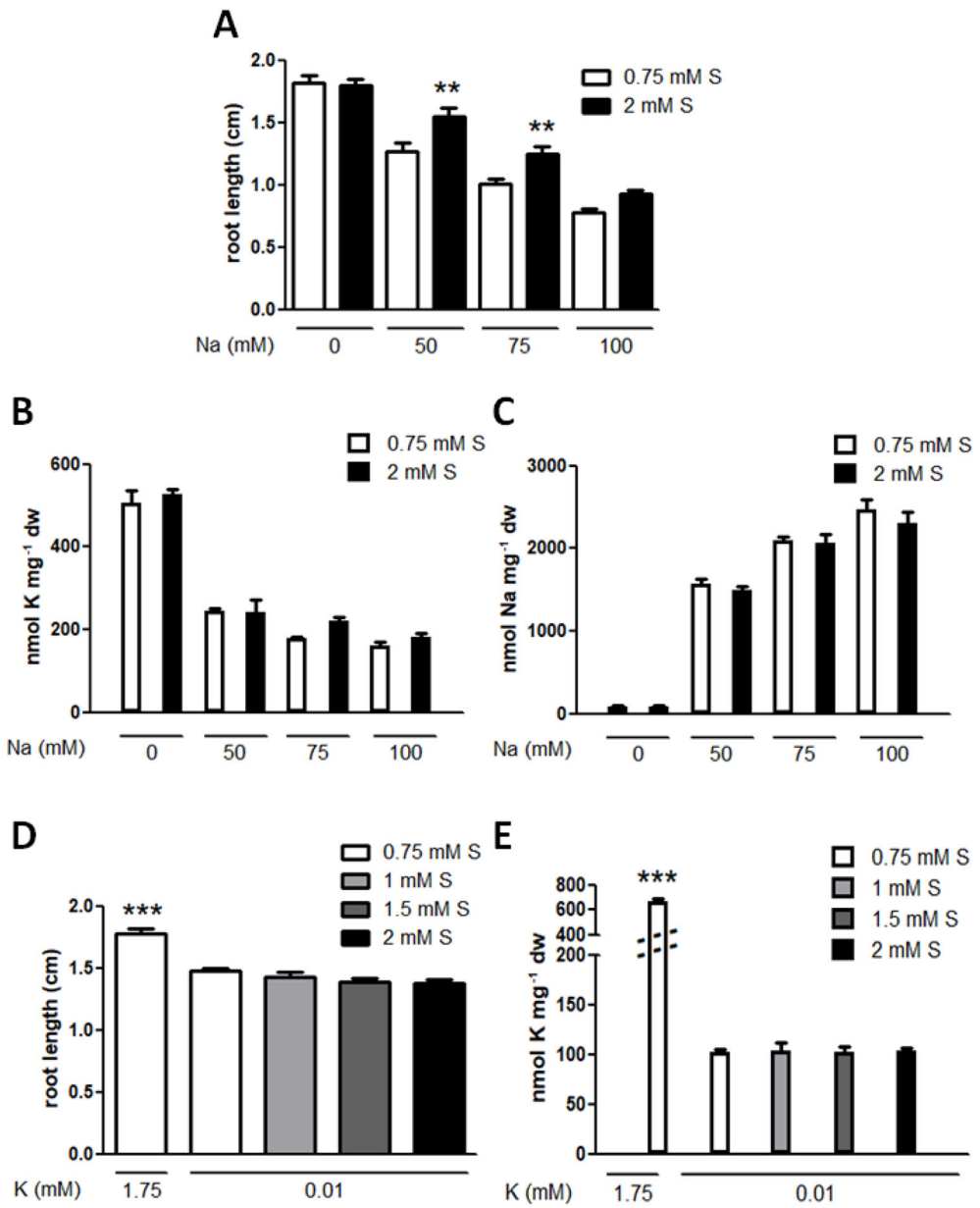

FIGURE 2 | Effects of sulphur supply on sodium stress and potassium deficiency response. **(A)** Root lengths of the wild type (Col-0) grown on media containing optimal potassium (1.75 mM K) and the indicated concentrations of sodium (Na) and sulphate (S) for eight days. Statistically significant differences between the basal (0.75 mM) and abundant (2 mM) S treatments at each Na concentration were determined by one-way ANOVA with Bonferroni's multiple comparison posttest and marked with asterisks (n > 30, $P < 0.01$). Error bars represent the SE. **(B)** K and **(C)** Na concentrations in seedlings derived from **(A)**. No statistical difference between the basal and abundant S treatments at each Na concentration was determined by one-way ANOVA with Bonferroni's multiple comparison posttest (n = 3) and error bars represent the SE. **(D)** Root lengths and **(E)** K concentrations of Col-0 grown in the optimal K condition or K deficiency (10 μM) with the indicated concentrations of S for eight days. A statistically significant difference relative to those treated with potassium deficiency and the basal S condition was determined by one-way ANOVA with Bonferroni's multiple comparison posttest and marked with asterisks (n > 32 for root lengths, n = 3 for K concentrations, $P < 0.001$). Error bars represent the SE.

tested. Applying Glu together with Cys dramatically recovered cesium phenotype (**Figures 6C, D**) to the same degree as with sulphur supply (**Figures 1A, B**). A single application of γ-Glu-Cys stunted plant growth in general in the absence of cesium while it strongly alleviated cesium-induced aerial chlorosis (**Figures 6C, D**). Concomitant application of Glu, Cys and Gly or γ-Glu-Cys and Gly also alleviated cesium stress. Interestingly, Glu- or γ-Glu-Cys-induced growth inhibition was somehow attenuated by addition of Gly. Buthionine sulphoximine (BSO) is a specific inhibitor of GSH1 (Griffith, 1982). Three hundred μM

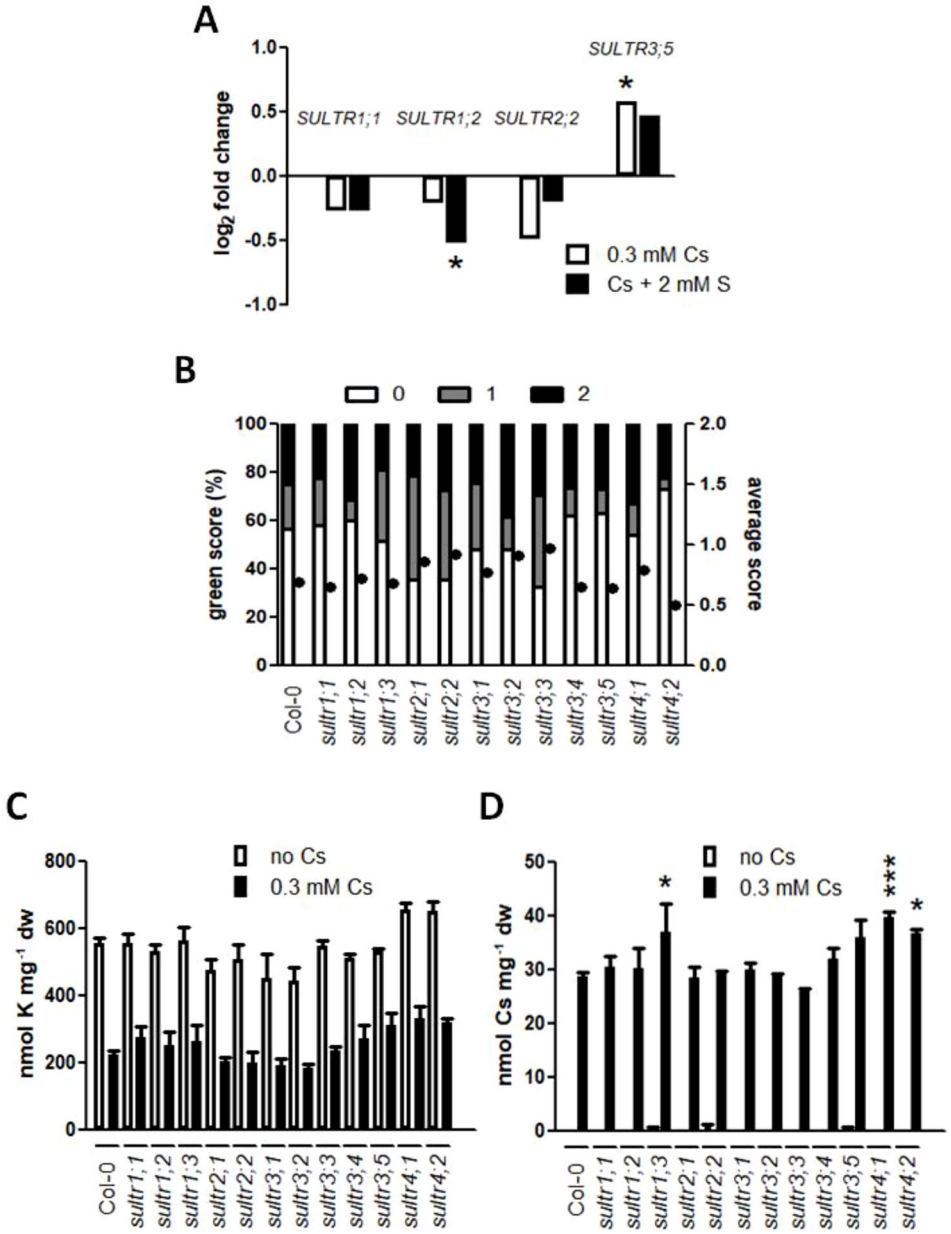

FIGURE 3 | Involvement of sulphate transporters (SULTRs) in cesium response. **(A)** Expression of *SULTR1;1*, *SULTR1;2*, *SULTR2;2* and *SULTR3;5* in the roots of the wild type (Col-0) grown on media containing 1.75 mM potassium (K) and 0.3 mM cesium (Cs) with or without 2 mM sulphate (S) for eight days. Values are $\log_2$ ratios relative to expression in the control seedlings grown in the absence of cesium (1.75 mM K + 0.75 mM S). Statistically significant differences were determined by one-way ANOVA with Bonferroni's multiple comparison posttest and marked with asterisks (n = 3, $P < 0.05$). **(B)** Percentile green scores (left axis) and average scores (right axis, closed circles) for *sultr* mutants treated with 0.5 mM K, 0.75 mM S and 0.3 mM Cs for eight days. No statistical difference relative to Col-0 was determined by Kruskal-Wallis test with Dunn's multiple comparison posttest (n > 60). **(C)** K and **(D)** Cs concentrations in seedlings derived from **(B)**. Statistically significant differences were determined by one-way ANOVA with Bonferroni's multiple comparison posttest (n = 3, * for $P < 0.05$, *** for $P < 0.001$ relative to Col-0) and error bars represent the SE.

of BSO treatment caused occasional stunting, partial loss of root gravitropism and aerial chlorosis independent of the effects caused by cesium (**Figure 6C**, indicated by red arrows) and the seedlings displaying these symptoms were excluded from green scoring. Moreover, the alleviation effects of concomitant treatments among Glu, Cys, γ-Glu-Cys, and Gly against cesium stress were not disrupted by the addition of BSO. Effectiveness of BSO was confirmed by measuring GSH levels in the seedlings treated with cesium and BSO (**Figure 5B**). Meanwhile, BSO treatment did not alter the internal Cys level (**Figure 5A**).

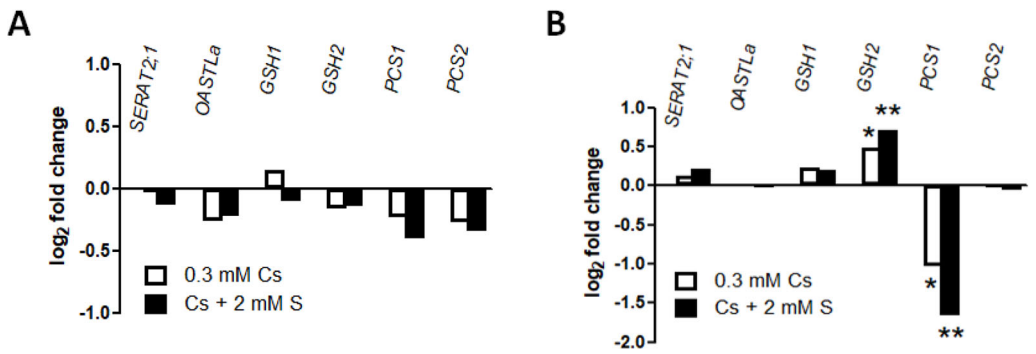

FIGURE 4 | Expression of sulphur metabolism genes in response to cesium. Gene expression in roots **(A)** and shoots **(B)** of the wild type (Col-0) grown on media containing 1.75 mM potassium (K) and 0.3 mM cesium (Cs) with or without 2 mM sulphate (S) for eight days. Values are $\log_2$ ratios relative to expression in the control seedlings grown in the absence of cesium (1.75 mM K + 0.75 mM S). Statistically significant differences were determined by one-way ANOVA with Bonferroni's multiple comparison posttest (n = 3, * for $P < 0.05$, ** for $P < 0.01$).

Sulphur-Induced Alleviation of Cesium Stress Is Independent of JA Biosynthesis and Signalling

JA-responsive genes, *VSP2* and *PDF1.2*, have previously been confirmed as being induced in response to cesium (Adams et al., 2013) and improved tolerance to alkaline stresses caused by JA has been linked to the ascorbate GSH cycle and glyoxylase metabolism (Mir et al., 2018). Cesium treatment with or without sulphur supply induced *VSP2* in shoots by 3.6 and 2.0 times, respectively, relative to the non-cesium control but the induction was not statistically significant for the concomitant treatment of cesium and sulphur supply (**Figure 7A**). This reduced level of *VSP2* during concomitant treatment could be due to the reduction of *VSP2* by sulphur supply alone (0.28 times) although it was not statistically significant (**Figure 7B**). On the other hand, *PDF1.2* was dramatically up-regulated in shoots treated with cesium alone or together with sulphur supply (333 and 576 times induction, respectively, **Figure 7A**). *PDF1.2* was found to be induced by 6.0 times in response to sulphur supply alone also (**Figure 7B**). There was no statistical difference between cesium treatments alone and together with sulphur supply for expression of both *VSP2* and *PDF1.2*. Consistently, internal concentrations of jasmonic acid and jasmonyl–isoleucine were markedly increased in response to cesium, and sulphur supply did not alter these levels (**Figures 7C, D**). The expression patterns of GSH metabolism-related genes, such as glyoxylase1 (At1g11840), glyoxylase4 (At1g15380), and glutathione-S-transferase24 (At1g17170) were analyzed in response to 0.3 mM cesium with or without 2 mM sulphur supply. However, expression of these genes was not altered by Cs treatment (**Supplementary Figure S2**). JA biosynthesis mutants defective in allene oxide synthase, *aos* (Park et al., 2002), and jasmonate-amido synthetase, *jar1*-1 (Staswick et al., 1992), were also analyzed for cesium response and recovery by GSH. Green scores for *aos* and *jar1*-1 treated with cesium in the absence of sulphur supply were comparable to those of the wild type. Recovery from the inhibitory effects of cesium was observed by addition of γ-Glu-Cys or GSH for both of the mutants, although the degree of recovery for *jar1*-1 by γ-Glu-Cys was somewhat compromised (**Figure 7E**).

DISCUSSION

Successful phytoremediation relies upon efficient absorption of the contaminant while at the same time maintaining vigorous plant growth, which means tolerance to the contaminant. Radiocesium contamination in soils poses a serious risk to humans and the environment but while potassium supply, a conventional method, is known to recover the healthy growth of the plants exposed to high concentrations of cesium, it causes a reduction in cesium accumulation in the plants, which is not helpful in terms of soil decontamination. Here we report that sulphur supply alleviates cesium-induced growth inhibition without compromising its accumulation in the plants. Increasing the basal level of sulphate (0.75 mM) up to 1.5 mM was not sufficient to reverse the cesium effects but up to 2 mM significantly recovered growth retardation caused by cesium (**Figure 1**). Increased potassium supply was demonstrated to confer "seeming" cesium tolerance by reducing cesium accumulation as well as reducing the degree of cesium-induced potassium loss, in turn resulting in lower cesium/potassium ratios. By contrast, with an abundant supply of sulphur, cesium and potassium concentrations were not altered, suggesting that sulphur supply enhanced "true" tolerance to cesium in the plants. This observation was reinforced by gene expression analysis of a potassium deficiency marker gene, *HAK5*, cesium-induce expression of which was not decreased by sulphur supply, indicating that the degree of potassium deficiency perceived by the plants was not eased. Similarly, sodium stress was alleviated by sulphur supply without altering sodium or potassium concentrations in the plants (**Figure 2**). Improved salt tolerance achieved by high levels of sulphur supplementation has previously been reported in soil-grown mustard but sodium accumulation was shown as being reduced by 100–200 mg sulphur kg^{-1} soil in these cases

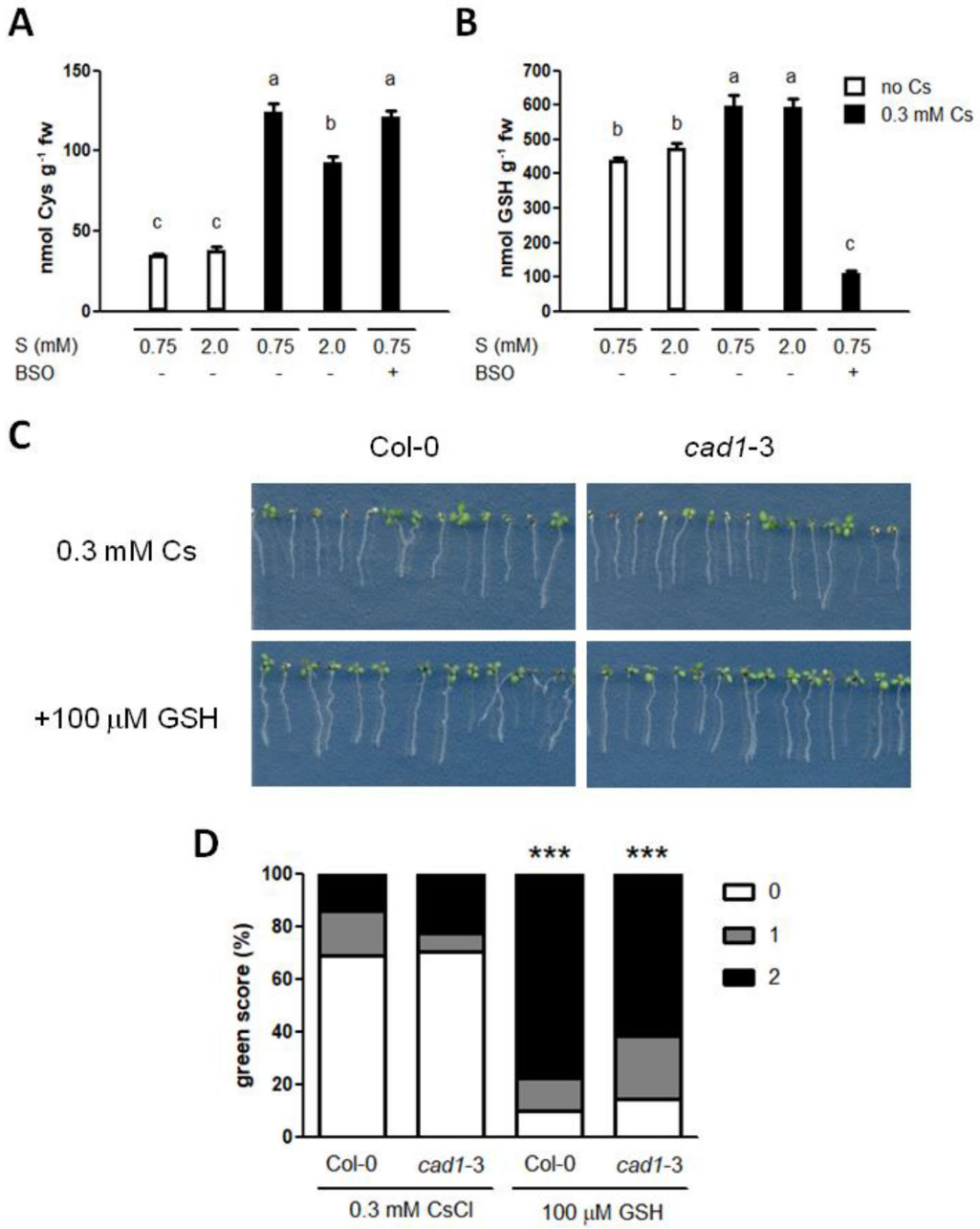

FIGURE 5 | Effects of glutathione on cesium stress. **(A)** Cysteine (Cys) and **(B)** Glutathione (GSH) levels in the wild type (Col-0) germinated and grown on media containing 0.5 mM potassium (K) with or without 0.3 mM cesium (Cs), 300 μM buthionine sulphoximine (BSO) and indicated concentrations of sulphate (S) for eight days. Alphabetical letters show statistical differences ($P < 0.01$) determined by one-way ANOVA with Bonferroni's multiple comparison posttest. **(C)** Eight-day-old Col-0 and *cad1*-3 seedlings germinated on media containing 0.5 mM K and 0.3 mM Cs with or without 100 μM GSH. **(D)** Percentile green scores for cesium-treated seedlings derived from **(C)**. Statistically significant differences relative to the control cesium condition for each line were determined by Kruskal-Wallis test with Dunn's multiple comparison posttest and marked with asterisks ($n > 40$, $P < 0.001$). No statistical difference was observed between Col-0 and *cad1*-3 of the same treatment.

(Fatma et al., 2014; Fatma et al., 2016). Both cesium and sodium are known to compete with potassium and to initiate a potassium deficiency response in plants, however, sulphur supply did not alleviate potassium deficiency stress. These results suggest that an addition of sulphur somehow helps plants acquire tolerance to the toxic metals but cannot reverse a lack of an essential nutrient.

Since sulphur supply-induced alleviation of cesium stress is not due to reduced levels of cesium or increased levels of

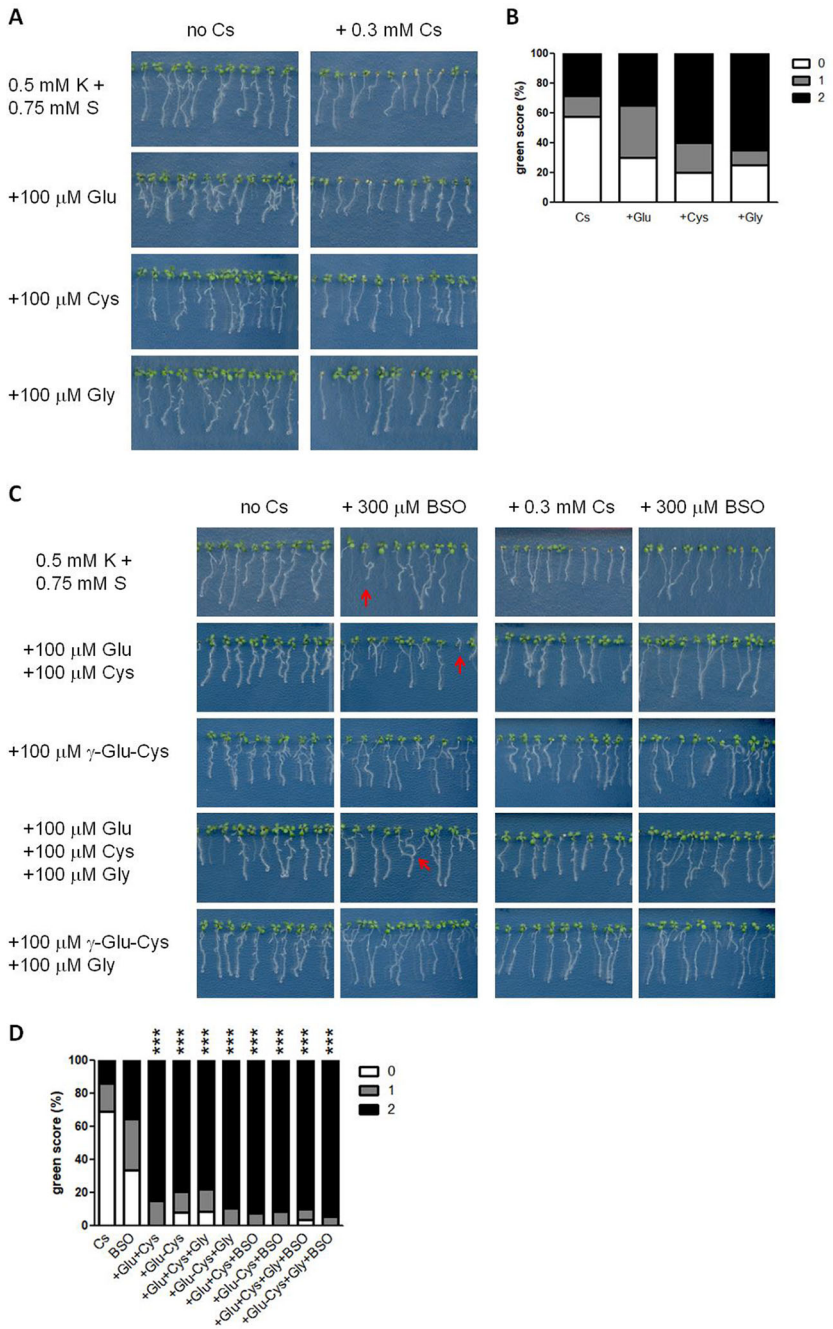

FIGURE 6 | Effects of glutathione biosynthetic intermediates on cesium stress. **(A)** Eight-day-old wild type (Col-0) seedlings germinated on media containing 0.5 mM potassium (K) with or without 0.3 mM cesium (Cs) and 100 μM glutamic acid (Glu), cysteine (Cys) or glycine (Gly). **(B)** Percentile green scores for cesium-treated seedlings derived from **(A)**. No statistical difference relative to the control cesium condition (0.5 mM K + 0.75 mM S + 0.3 mM Cs) was determined by Kruskal-Wallis test with Dunn's multiple comparison posttest ($n > 20$). **(C)** Eight-day-old Col-0 seedlings germinated on media containing 0.5 mM K and the indicated concentrations of Cs, Glu, Cys, Gly, γ-glutamylcysteine (γ-Glu-Cys) and buthionine sulphoximine (BSO). Red arrows indicate the distinct growth retardation phenotype the production of which is occasionally provoked by BSO treatment. **(D)** Percentile green scores for cesium-treated seedlings derived from **(C)**. Statistically significant differences relative to the control cesium condition were determined by Kruskal-Wallis test with Dunn's multiple comparison posttest and marked with asterisks ($n > 31$, $P < 0.001$).

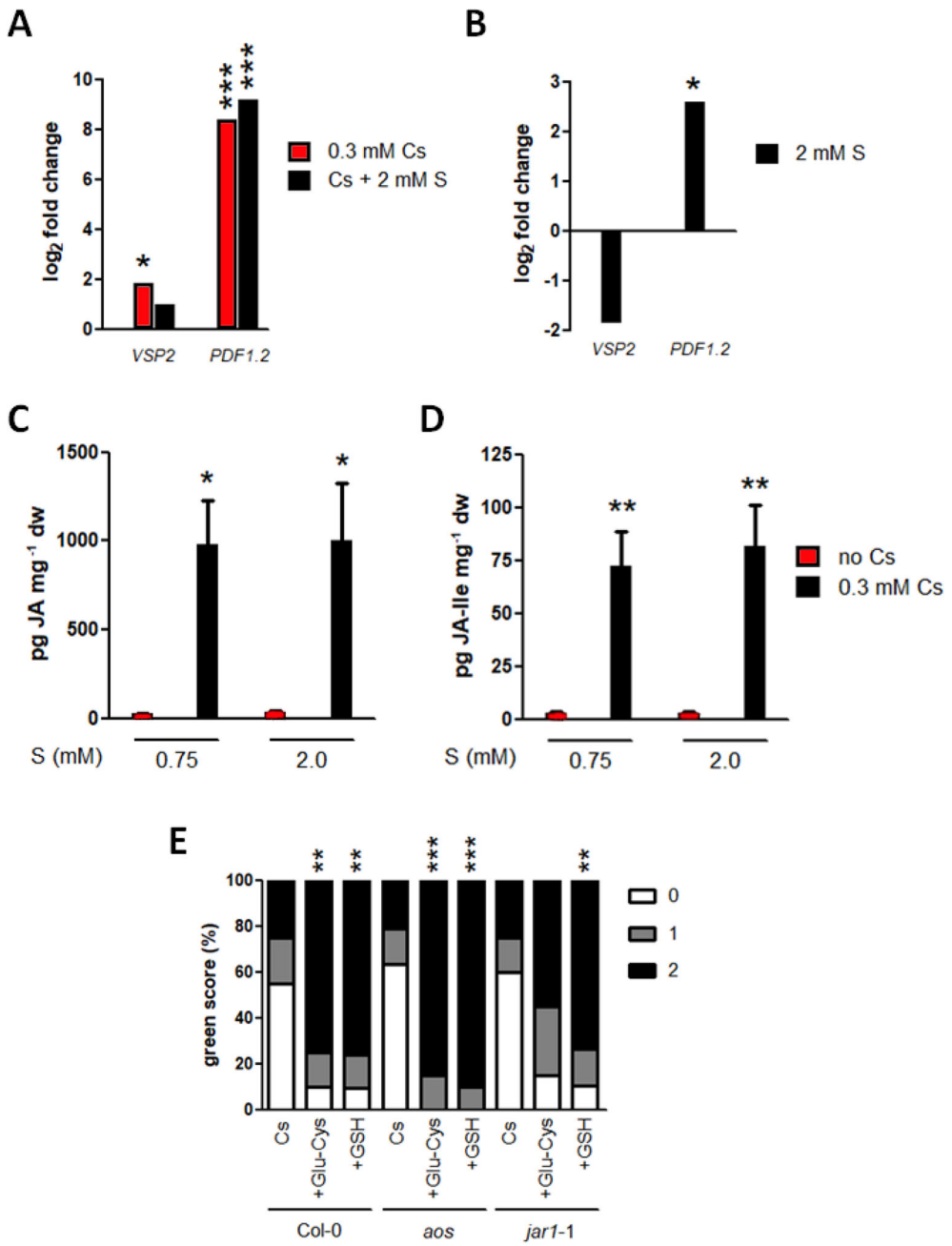

FIGURE 7 | Interaction of cesium stress alleviation by sulphur with jasmonate biosynthesis and signalling. **(A)** Expression of *VSP2* and *PDF1.2* in the wild type (Col-0) grown on media containing 1.75 mM potassium (K) and 0.3 mM cesium (Cs) with or without 2 mM sulphate (S) for eight days. Values are $\log_2$ ratios relative to expression in the control seedlings grown in the absence of cesium (1.75 mM K + 0.75 mM S). Statistically significant differences were determined by one-way ANOVA with Bonferroni's multiple comparison posttest (n = 3, * for $P < 0.05$, *** for $P < 0.001$). **(B)** Expression of *VSP2* and *PDF1.2* in Col-0 grown on media containing 1.75 mM K and 2 mM S for eight days. Values are $\log_2$ ratios relative to expression in the control seedlings grown in the basal S condition (0.75 mM). A statistically significant difference was determined by t-test and marked with an asterisk (n = 3, $P < 0.05$). **(C)** Jasmonic acid (JA) and **(D)** Jasmonyl-isoleucine (JA-Ile) concentrations in Col-0 grown on media containing 0.5 mM K with or without 0.3 mM Cs and 2 mM S for eight days. Statistically significant differences were determined by one-way ANOVA with Bonferroni's multiple comparison posttest (n = 6, * for $P < 0.05$, ** for $P < 0.01$ relative to the control seedlings grown in the basal S condition without Cs) and error bars represent the SE. **(E)** Percentile green scores for Col-0, *aos* and *jar1*-1 grown on media containing 0.5 mM K and 0.3 mM Cs with or without 100 μM γ-glutamylcysteine (γ-Glu-Cys) or glutathione (GSH) for eight days. Statistically significant differences relative to the control cesium condition (0.5 mM K + 0.75 mM S + 0.3 mM Cs) for each line were determined by Kruskal-Wallis test with Dunn's multiple comparison posttest (n > 19, ** for $P <$ 0.01, *** for $P < 0.001$). No statistical difference was observed between Col-0 and the mutants of the same treatment.

potassium, expression of *SULTRs* was tested. Expression of genes encoding high-affinity sulphate transporters in roots, SULTR1;1 and SUTLR1;2, is known to be induced by sulphate starvation (Takahashi et al., 2000; Yoshimoto et al., 2002). These transcripts have also been shown to be increased in response to cadmium and sodium stress (Cao et al., 2014; Yamaguchi et al., 2016; Ferri et al., 2017). However, *SULTR1;1* and *SULTR1;2* were not induced in response to cesium stress but *SULTR1;2* was rather reduced by cesium treatment in the presence of sulphur supply in the optimal potassium condition (**Figure 3**). A low-affinity sulphate transporter gene, *SULTR2;2*, known to be low sulphate-inducible (Takahashi et al., 2000) was also not up-regulated in response to cesium stress. Instead, *SULTR3;5* was mildly induced in response to cesium stress. SULTR3;5 has been reported as being responsible for root-to-shoot transport of sulphate only in the presence of a low-affinity sulphate transporter SULTR2;1 (Kataoka et al., 2004a), although our data indicated no altered expression for *SULTR2;1* in response to cesium (**Supplementary Figure S1**). Mutants for each of the *SULTR* genes were analyzed for cesium response but no phenotypic difference was observed relative to the wild type (**Figure 3**). There was a tendency for higher accumulation of potassium and cesium in *sultr4;1* and *sultr4;2* mutants although potassium accumulation was not statistically significant. SULTR4;1 and SULTR4;2 have been shown to facilitate sulphate efflux from the vacuoles to maintain optimal cellular concentrations of sulphate and the *sultr4;1 sultr4;2* double mutant demonstrates over-accumulation of sulphate in roots (Kataoka et al., 2004b). It is possible that this higher accumulation of sulphate in the mutants promoted higher accumulation of cesium and potassium in our system. Overall, SULTRs did not appear to participate much in cesium stress alleviation, unlike other metal stress response. By contrast, *SULTR1;2*, *SULTR3;1,* and *SULTR3;5* were found to be induced in response to potassium deficiency although none of the single mutants for these genes or any of the other *SULTR* genes showed altered response to potassium deficiency (**Supplementary Figure S1**). This transcriptional induction could be due to a general nutrient deficiency response where deficiency of a nutrient triggers transport/metabolism/signalling of another nutrient (Schachtman and Shin, 2007).

Our results highlight that SULTRs and altered sulphate uptake are unlikely to be involved in alleviation of cesium stress, suggesting that it is the downstream metabolic pathways that are important. Various sulphur metabolism genes have previously been indicated as being induced in response to heavy metal stress or sodium stress (Xiang and Oliver, 1998; Howarth et al., 2003; Tamaoki et al., 2008; Zhu et al., 2016), however, expression of *SERAT2;1*, *OASTLa* and *GSH1* was not altered either in roots or shoots in response to cesium stress (**Figure 4**). In contrast, expression of a GSH synthetase gene, *GSH2*, was mildly induced in response to cesium and concomitantly with sulphur supply suggesting an accumulation of GSH. PCs are a common detoxification agent for heavy metals and PC synthase genes, *PCS1* and *PCS2*, have been shown to be induced by chromium and lead (Fang et al., 2016; Zhu et al., 2016). Under cesium stress, however, these transcripts were not induced but *PCS1* was reduced in shoots with or without sulphur supply instead. Indeed, an increase of PC levels were not detected in response to cesium. This point was reinforced by observation of *cad1*-3 mutant carrying a point mutation in *PCS1* which makes plants sensitive to cadmium (Howden et al., 1995). The degree of cesium response in *cad1*-3 was comparable to that of the wild type (**Figure 5**), indicating that PCs are not important for alleviation of cesium stress. As GSH is the direct precursor of PCs and PCS1 is the major form of PC synthetase (Blum et al., 2010), our results further suggest increased accumulation of GSH in cesium-treated plants. An increase of GSH levels has been reported in plants exposed to sodium, cadmium, chromium and zinc (Nocito et al., 2006; Fatma et al., 2014; Nazar et al., 2014; Fang et al., 2016; Per et al., 2016). In agreement with our hypothesis, GSH levels were increased in the plants suffering from cesium stress and exogenous application of GSH to the cesium-exposed plants could alleviate the growth retardation effects of cesium to the same degree as with sulphur supply (**Figure 5**). Moreover, *cad1*-3 displayed a wild type-like response to GSH-induced alleviation of cesium effects, confirming that this alleviation event is dependent on GSH but independent of PCs. Consistently, treatments with concomitant supplementation of Glu and Cys together (or their synthetic product, γ-Glu-Cys) with or without Gly, which lead to GSH synthesis, could alleviate cesium stress to the level achieved through sulphur supply (**Figure 6**). Accumulation of γ-Glu-Cys has been demonstrated to inhibit plant growth in a JA-dependent manner (Wei et al., 2015) but this growth inhibition did not affect the alleviation effects of γ-Glu-Cys for cesium. An addition of Gly attenuated this growth inhibitory effects of γ-Glu-Cys possibly through pushing the reaction forward towards the direction of GSH synthesis so that γ-Glu-Cys was not accumulated. By contrast, the alleviation effects of single supplementation of Glu, Cys or Gly were observed but rather limited (**Figure 6**). To our surprise, and intriguingly in a way, inhibition of GSH synthesis did not cancel the alleviation effects of GSH precursors. As a mutation in *GSH2* causes seedling lethality (*gsh2*-T, according to the description provided by the ABRC), a specific inhibitor of the function of GSH1 (Griffith, 1982), BSO, was employed. BSO-treated plants cannot synthesize Glu and Cys into γ-Glu-Cys and decreased accumulation of GSH was observed in the seedlings treated with cesium and BSO (**Figure 5**). In theory, a concomitant treatment with Glu, Cys and BSO should not provide an alleviation effect if GSH was the sole alleviator of cesium stress, but this was not the case. Besides, BSO treatment alone somewhat alleviated cesium stress although it was not statistically significant. These findings strongly suggest that not only GSH but also GSH precursors, when concomitantly treated, have their own alleviatory function or feed into the pathways other than GSH synthesis which produce alleviatory effects against cesium stress. Our previous metabolic profiling has revealed a marked increase of Cys in both roots and shoots, as well as Glu and Gly to a lesser extent in shoots, in cesium-treated plants (Adams et al., 2017). Cys and its derivative, methyl cysteinate, were also demonstrated to be capable of chelating

with cesium and functioning as cesium accumulators in plants (Adams et al., 2017). A dramatic increase of Cys in response to cesium was confirmed in the current study but interestingly, BSO treatment did not further increase Cys (**Figure 5**), suggesting that accumulated Cys was quickly turned into other metabolites which might also have an alleviation effect. Together, it can be speculated that plants exposed to cesium accumulate GSH and its biosynthetic intermediates as a detoxification measure to protect the cells from the deleterious effects of cesium and exogenous application of sulphur-containing compounds can help the plants better perform this procedure.

We have previously shown that JA responsive genes, *VSP2* and *PDF1.2*, are induced in response to cesium stress and JA biosynthesis and signalling mutants, *aos* and *coi1*-16, display increased tolerance against cesium in terms of root growth inhibition (Adams et al., 2013). This indicates that cesium inhibits root growth through JA biosynthesis and signalling pathways. In order to test whether sulphur supply could turn down the JA pathways, JAs were quantified. Treatment with cesium dramatically increased JA and JA-Ile accumulation in the plants and consistently induced *VSP2* and *PDF1.2* expression (**Figure 7**). Sulphur supply neither decreased accumulation of JAs nor reduced expression of JA responsive genes, suggesting that sulphur supply does not alleviate cesium stress by reducing JA production. Interaction between JA pathways and sulphur metabolism has been documented in certain aspects: a positive regulator and a key transcription factor of JA signalling, MYC2, activates *GSH1 via* direct binding on its promoter (Yuan et al., 2017) and GSH is the key regulator of JA pathway (Mhamdi et al., 2010; Han et al., 2013). Exogenous application of JAs induces a series of sulphur metabolism genes including *GSH1* and *GSH2* and increases Cys and GSH levels in the plants (Jost et al., 2005; Sasaki-Sekimoto et al., 2005). Conversely, GSH application induces a wide variety of JA synthesis and signalling genes (Han et al., 2013; Hacham et al., 2014; Cheng et al., 2015). However, jasmonate biosynthesis mutants, *aos* and *jar1*-1, showed a wild type-like aerial phenotype to cesium and recovery from cesium stress by GSH and γ-Glu-Cys albeit to a lesser extent for *jar1*-1 by γ-Glu-Cys (**Figure 7**). These findings imply that cesium stress alleviation by GSH and its precursors does not rely on alteration in JA synthesis and, at the same time, is not disrupted by inability of JA synthesis.

Taken all together, GSH and its biosynthetic intermediates, but not PCs, have a capacity to mitigate cesium stress and this mitigation is independent of alteration in potassium/cesium accumulation. A predicted model is given in **Figure 8**. Plants exposed to cesium possibly promote root-to-shoot transport of sulphate by the function of SULTR3;5, accumulate Cys as well as Glu and Gly and increase GSH accumulation through induction of *GSH2* and reduction of *PCS1* in shoots to overcome cesium-induced aerial chlorosis and growth retardation. GSH biosynthetic intermediates also have alleviatory effects against cesium as they are or in as-yet-unknown pathways. It is well known that an increase of GSH helps to detoxify the reactive oxygen species (ROS) which were elevated by various abiotic stresses including alkaline metal stresses (Choe et al., 2013). It is possible that alleviation effects of cesium stress by GSH or Cys results from their thiol residues which have a potential to reduce ROS caused by Cs stress. However, our preliminary observation could not recognize ROS accumulation in response to cesium while ROS accumulation was clearly observed in the plants experiencing potassium deficiency (**Supplementary Figure S3**) as described before (Shin and Schachtman, 2004). As sulphur supply alleviates sodium stress but not potassium deficiency stress, this alleviation is not due to the recovery effects against a general nutrition deficiency by another nutrition supply but potentially due to the detoxification effects against xenobiotics. GSH is also known to conjugate with xenobiotics including toxic metals with the aid of GSH *S*-transferases (GSTs) and to sequestrate them into the vacuoles (Dixon et al., 2002; Hasanuzzaman et al., 2017). As GSTs constitute a large gene family in Arabidopsis, it is intriguing to investigate whether

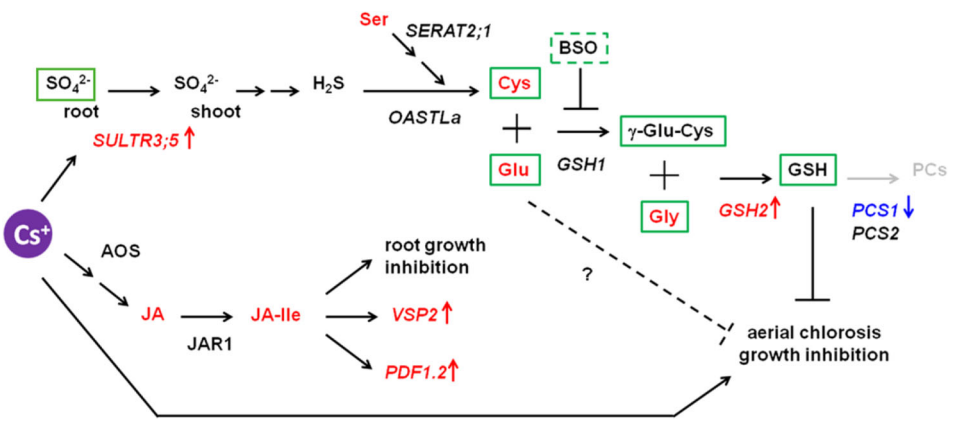

FIGURE 8 | Proposed model for interaction between cesium response and sulphur-mediated alleviation. The genes denoted in italics are the ones whose expression was investigated in this study. The transcripts and the metabolites indicated in red and blue were shown in this study or the previous study (Adams et al., 2017) to be increased or decreased, respectively, in response to cesium. The metabolites in green boxes are the ones with an ability to alleviate cesium-induced aerial chlorosis. The pathway in grey was proposed not to be involved.

cesium is conjugated with GSH and detoxified by one of the GSTs. It would also be interesting to reveal the mechanism by which GSH biosynthetic precursors alleviate cesium stress independently of GSH biosynthesis.

DATA AVAILABILITY STATEMENT

No datasets was generated or analyzed for this study.

AUTHOR CONTRIBUTIONS

EA, TM, SW and NO-O did experiments. EA, MS and RS designed the experiments. EA and RS wrote the manuscript.

ACKNOWLEDGMENTS

This work was supported by funding from RIKEN. We thank Ms. Yuri Kanno for technical assistance in hormone analysis. Many thanks also go to Dr. Michael Adams for comments and discussion on the paper.

SUPPLEMENTARY MATERIAL

The Supplementary Material for this article can be found online at: https://www.frontiersin.org/articles/10.3389/fpls.2019.01711/full#supplementary-material

REFERENCES

Adams, E., Abdollahi, P., and Shin, R. (2013). Cesium inhibits plant growth through jasmonate signaling in *Arabidopsis thaliana*. *Int. J. Mol. Sci.* 14, 4545–4559. doi: 10.3390/ijms14034545

Adams, E., Miyazaki, T., Hayaishi-Satoh, A., Han, M., Kusano, M., Khandelia, H., et al. (2017). A novel role for methyl cysteinate, a cysteine derivative, in cesium accumulation in *Arabidopsis thaliana*. *Sci. Rep.* 7, 43170. doi: 10.1038/srep43170

Adams, E., Miyazaki, T., Saito, S., Uozumi, N., and Shin, R. (2018). Cesium inhibits plant growth primarily through reduction of potassium influx and accumulation in Arabidopsis. *Plant Cell Physiol.* 60, 63–76. doi: 10.1093/pcp/pcy188.

Anjum, N. A., Gill, R., Kaushik, M., Hasanuzzaman, M., Pereira, E., Ahmad, I., et al. (2015). ATP-sulfurylase, sulfur-compounds, and plant stress tolerance. *Front. Plant Sci.* 6, 210. doi: 10.3389/fpls.2015.00210

Blum, R., Meyer, K. C., Wunschmann, J., Lendzian, K. J., and Grill, E. (2010). Cytosolic action of phytochelatin synthase. *Plant Physiol.* 153, 159–169. doi: 10.1104/pp.109.149922

Burger, A., and Lichtscheidl, I. (2018). Stable and radioactive cesium: a review about distribution in the environment, uptake and translocation in plants, plant reactions and plants' potential for bioremediation. *Sci. Total Environ.* 618, 1459–1485. doi: 10.1016/j.scitotenv.2017.09.298

Cao, M. J., Wang, Z., Zhao, Q., Mao, J. L., Speiser, A., Wirtz, M., et al. (2014). Sulfate availability affects ABA levels and germination response to ABA and salt stress in *Arabidopsis thaliana*. *Plant J.* 77, 604–615. doi: 10.1111/tpj.12407.

Cazale, A. C., and Clemens, S. (2001). *Arabidopsis thaliana* expresses a second functional phytochelatin synthase. *FEBS Lett.* 507, 215–219.

Cheng, M. C., Ko, K., Chang, W. L., Kuo, W. C., Chen, G. H., and Lin, T. P. (2015). Increased glutathione contributes to stress tolerance and global translational changes in Arabidopsis. *Plant J.* 83, 926–939. doi: 10.1111/tpj.12940.

Choe, Y.-H., Kim, Y.-S., Kim, I.-S., Bae, M.-J., Lee, E.-J., Kim, Y.-H., et al. (2013). Homologous expression of γ-glutamylcysteine synthetase increases grain yield and tolerance of transgenic rice plants to environmental stresses. *J. Plant Physiol.* 170, 610–618. doi: 10.1016/j.jplph.2012.12.002

Dixon, D. P., Lapthorn, A., and Edwards, R. (2002). Plant glutathione transferases. *Genome Biol.* 3, 3004.

Dushenkov, S. (2003). Trends in phytoremediation of radionuclides. *Plant Soil* 249, 167–175.

Fang, H., Liu, Z., Jin, Z., Zhang, L., Liu, D., and Pei, Y. (2016). An emphasis of hydrogen sulfide-cysteine cycle on enhancing the tolerance to chromium stress in *Arabidopsis*. *Environ. Pollut.* 213, 870–877. doi: 10.1016/j.envpol.2016.03.035

Fatma, M., Asgher, M., Masood, A., and Khan, N. A. (2014). Excess sulfur supplementation improves photosynthesis and growth in mustard under salt stress through increased production of glutathione. *Environ. Exp. Bot.* 107, 55–63.

Fatma, M., Masood, A., Per, T. S., and Khan, N. A. (2016). Nitric oxide alleviates salt stress inhibited photosynthetic performance by interacting with sulfur assimilation in mustard. *Front. Plant Sci.* 7, 521. doi: 10.3389/fpls.2016.00521

Ferri, A., Lancilli, C., Maghrebi, M., Lucchini, G., Sacchi, G. A., and Nocito, F. F. (2017). The sulfate supply maximizing Arabidopsis shoot growth is higher under long- than short-term exposure to cadmium. *Front. Plant Sci.* 8, 854. doi: 10.3389/fpls.2017.00854

Griffith, O. W. (1982). Mechanism of action, metabolism, and toxicity of buthionine sulfoximine and its higher homologs, potent inhibitors of glutathione synthesis. *J. Biol. Chem.* 257, 13704–13712.

Hacham, Y., Koussevitzky, S., Kirma, M., and Amir, R. (2014). Glutathione application affects the transcript profile of genes in *Arabidopsis* seedling. *J. Plant Physiol.* 171, 1444–1451. doi: 10.1016/j.jplph.2014.06.016

Hampton, C. R., Bowen, H. C., Broadley, M. R., Hammond, J. P., Mead, A., Payne, K. A., et al. (2004). Cesium toxicity in *Arabidopsis*. *Plant Physiol.* 136, 3824–3837.

Han, Y., Mhamdi, A., Chaouch, S., and Noctor, G. (2013). Regulation of basal and oxidative stress-triggered jasmonic acid-related gene expression by glutathione. *Plant Cell Environ.* 36, 1135–1146. doi: 10.1111/pce.12048

Hasanuzzaman, M., Nahar, K., Anee, T. I., and Fujita, M. (2017). Glutathione in plants: biosynthesis and physiological role in environmental stress tolerance. *Physiol. Mol. Biol. Plants* 23, 249–268. doi: 10.1007/s12298-017-0422-2

Hatzfeld, Y., Maruyama, A., Schmidt, A., Noji, M., Ishizawa, K., and Saito, K. (2000). β-Cyanoalanine synthase is a mitochondrial cysteine synthase-like protein in spinach and Arabidopsis. *Plant Physiol.* 123, 1163–1171.

Howarth, J. R., Dominguez-Solis, J. R., Gutierrez-Alcala, G., Wray, J. L., Romero, L. C., and Gotor, C. (2003). The serine acetyltransferase gene family in *Arabidopsis thaliana* and the regulation of its expression by cadmium. *Plant Mol. Biol.* 51, 589–598. doi: 10.1023/A:1022349623951

Howden, R., Goldsbrough, P. B., Andersen, C. R., and Cobbett, C. S. (1995). Cadmium-sensitive, *cad1* mutants of *Arabidopsis thaliana* are phytochelatin deficient. *Plant Physiol.* 107, 1059–1066.

Jost, R., Berkowitz, O., Wirtz, M., Hopkins, L., Hawkesford, M. J., and Hell, R. (2000). Genomic and functional characterization of the *oas* gene family encoding O-acetylserine (thiol) lyases, enzymes catalyzing the final step in cysteine biosynthesis in *Arabidopsis thaliana*. *Gene* 253, 237–247.

Jost, R., Altschmied, L., Bloem, E., Bogs, J., Gershenzon, J., Hahnel, U., et al. (2005). Expression profiling of metabolic genes in response to methyl jasmonate reveals regulation of genes of primary and secondary sulfur-related pathways in *Arabidopsis thaliana*. *Photosyn. Res.* 86, 491–508. doi: 10.1007/s11120-005-7386-8

Jung, I. L., Ryu, M., Cho, S. K., Shah, P., Lee, J. H., Bae, H., et al. (2015). Cesium toxicity alters microRNA processing and AGO1 expressions in *Arabidopsis thaliana*. *PloS One* 10, e0125514. doi: 10.1371/journal.pone.0125514

Kanno, Y., Oikawa, T., Chiba, Y., Ishimaru, Y., Shimizu, T., Sano, N., et al. (2016). AtSWEET13 and AtSWEET14 regulate gibberellin-mediated physiological processes. *Nat. Commun.* 7, 13245. doi: 10.1038/ncomms13245

Kataoka, T., Hayashi, N., Yamaya, T., and Takahashi, H. (2004a). Root-to-shoot transport of sulfate in Arabidopsis. Evidence for the role of SULTR3;5 as a component of low-affinity sulfate transport system in the root vasculature. *Plant Physiol.* 136, 4198–4204. doi: 10.1104/pp.104.045625

Kataoka, T., Watanabe-Takahashi, A., Hayashi, N., Ohnishi, M., Mimura, T., Buchner, P., et al. (2004b). Vacuolar sulfate transporters are essential determinants controlling internal distribution of sulfate in Arabidopsis. *Plant Cell.* 16, 2693–2704. doi: 10.1105/tpc.104.023960

Kawashima, C. G., Berkowitz, O., Hell, R., Noji, M., and Saito, K. (2005). Characterization and expression analysis of a serine acetyltransferase gene family involved in a key step of the sulfur assimilation pathway in *Arabidopsis*. *Plant Physiol.* 137, 220–230. doi: 10.1104/pp.104.045377

May, M. J., and Leaver, C. J. (1994). *Arabidopsis thaliana* γ-glutamylcysteine synthetase is structurally unrelated to mammalian, yeast, and *Escherichia coli* homologs. *Proc. Nat. Acad. Sci. U.S.A.* 91, 10059–10063.

Mhamdi, A., Hager, J., Chaouch, S., Queval, G., Han, Y., Taconnat, L., et al. (2010). Arabidopsis GLUTATIONE REDUCTASE1 plays a crucial role in leaf responses to intracellular hydorgen peroxide and in ensuring appropiate gene expression through both salicylic acid and jasmonic acid signaling pathways. *Plant Physiol.* 153, 1144–1160. doi: 10.1104/pp.110.153767

Minocha, R., Thangavel, P., Dhankher, O. P., and Long, S. (2008). Separation and quantification of monothiols and phytochelatins from a wide variety of cell cultures and tissues of trees and other plants using high performance liquid chromatography. *J. Chromatogr. A.* 1207, 72–83. doi: 10.1016/j.chroma.2008.08.023

Mir, M. A., John, R., Alyemeni, M. N., Alam, P., and Ahmad, P. (2018). Jasmonic acid ameliorates alkaline stress by improving gorwth peformance, ascorbate glutathione cycle and glyoxylase system in mainze seedlings. *Sci. Rep.* 8, 2831. doi: 10.1038/s41598-018-21097-3

Nazar, R., Khan, M. I., Iqbal, N., Masood, A., and Khan, N. A. (2014). Involvement of ethylene in reversal of salt-inhibited photosynthesis by sulfur in mustard. *Physiol. Plant* 152, 331–344. doi: 10.1111/ppl.12173

Nishida, S., Duan, G. L., Ohkama-Ohtsu, N., Uraguchi, S., and Fujiwara, T. (2016). Enhanced arsenic sensitivity with excess phytochelatin accumulation in shoots of a SULTR1;2 knockout mutant of *Arabidopsis thaliana* (L.) Heynh. *Soil Sci. Plant Nutr.* 62, 367–372. doi: 10.1080/00380768.2016.1150790

Nocito, F. F., Lancilli, C., Crema, B., Fourcroy, P., Davidian, J. C., and Sacchi, G. A. (2006). Heavy metal stress and sulfate uptake in maize roots. *Plant Physiol.* 141, 1138–1148. doi: 10.1104/pp.105.076240

Noctor, G., Queval, G., Mhamdi, A., Chaouch, S., and Flyer, C. H. (2011). "Glutathione," in *The Arabidopsis Book*, e0142. doi: 10.1199/tab0142

Park, J. H., Halitschke, R., Kim, H. B., Baldwin, I. T., Feldmann, K. A., and Feyereisen, R. (2002). A knock-out mutation in allene oxide synthase results in male sterility and defective wound signal transduction in *Arabidopsis* due to a block in jasmonic acid biosynthesis. *Plant J.* 31, 1–12.

Per, T. S., Khan, N. A., Masood, A., and Fatma, M. (2016). Methyl jasmonate alleviates cadmium-induced photosynthetic damages through increased S-assimilation and glutathione production in mustard. *Front. Plant Sci.* 7, 1933. doi: 10.3389/fpls.2016.01933

Sahr, T., Voigt, G., Paretzke, H. G., Schramel, P., and Ernst, D. (2005a). Caesium-affected gene expression in *Arabidopsis thaliana*. *New Phytol.* 165, 747–754. doi: 10.1111/j.1469-8137.2004.01282.x

Sahr, T., Voigt, G., Schimmack, W., Paretzke, H. G., and Ernst, D. (2005b). Low-level radiocaesium exposure alters gene expression in roots of Arabidopsis. *New Phytol.* 168, 141–148. doi: 10.1111/j.1469-8137.2005.01485.x

Sasaki-Sekimoto, Y., Taki, N., Obayashi, T., Aono, M., Matsumoto, F., Sakurai, N., et al. (2005). Coordinated activation of metabolic pathways for antioxidants and defence compounds by jasmonates and their roles in stress tolerance in *Arabidopsis*. *Plant J.* 44, 653–668.

Schachtman, D. P., and Shin, R. (2007). Nutrient sensing and signaling: NPKS. *Ann. Rev. Plant Biol.* 58, 47–69.

Schneider, C. A., Rasband, W. S., and Eliceiri, K. W. (2012). NIH Image to ImageJ: 25 years of image analysis. *Nat. Methods* 9, 671–675.

Seth, C. S., Remans, T., Keunen, E., Jozefczak, M., Gielen, H., Opdenakker, K., et al. (2012). Phytoextraction of toxic metals: a central role for glutathione. *Plant Cell Environ.* 35, 334–346. doi: 10.1111/j.1365-3040.2011.02338.x

Shin, R., and Schachtman, D. P. (2004). Hydrogen peroxide mediates plant root cell response to nutrient deprivation. *Proc. Nat. Acad. Sci. U.S.A.* 101, 8827–8832.

Staswick, P. E., Su, W. P., and Howell, S. H. (1992). Methyl jasmonate inhibition of root growth and induction of a leaf protein are decreased in an *Arabidopsis thaliana* mutant. *Proc. Nat. Acad. Sci. U.S.A.* 89, 6837–6840.

Takahashi, H., Watanabe-Takahashi, A., Smith, F. W., Blake-Kalff, M., Hawkesford, M. J., and Saito, K. (2000). The roles of three functional sulphate transporters involved in uptake and translocation of sulphate in *Arabidopsis thaliana*. *Plant J.* 23, 171–182.

Tamaoki, M., Freeman, J. L., and Pilon-Smits, E. A. (2008). Cooperative ethylene and jasmonic acid signaling regulates selenite resistance in *Arabidopsis*. *Plant Physiol.* 146, 1219–1230. doi: 10.1104/pp.107.110742

Ullmann, P., Gondet, L., Potier, S., and Bach, T. J. (1996). Cloning of *Arabidopsis thaliana* glutathione synthetase (GSH2) by functional complementation of a yeast *gsh2* mutant. *Eur. J. Biochem.* 236, 662–669.

Wei, H. H., Rowe, M., Riethoven, J. J. M., Grove, R., Adamec, J., Jikumaru, Y., et al. (2015). Overaccumulation of γ-glutamylcysteine in a jasmonate-hypersensitive *Arabidopsis* mutant causes jasmonate-dependent growth inhibition. *Plant Physiol.* 169, 1371–1381. doi: 10.1104/pp.15.00999

White, P. J., and Broadley, M. R. (2000). Mechanisms of caesium uptake by plants. *New Phytol.* 147, 241–256.

Xiang, C., and Oliver, D. J. (1998). Glutathione metabolic genes coordinately respond to heavy metals and jasmonic acid in Arabidopsis. *Plant Cell.* 10, 1539–1550.

Yamaguchi, C., Takimoto, Y., Ohkama-Ohtsu, N., Hokura, A., Shinano, T., Nakamura, T., et al. (2016). Effects of cadmium treatment on the uptake and translocation of sulfate in *Arabidopsis thaliana*. *Plant Cell Physiol.* 57, 2353–2366. doi: 10.1093/pcp/pcw156

Yoshimoto, N., Takahashi, H., Smith, F. W., Yamaya, T., and Saito, K. (2002). Two distinct high-affinity sulfate transporters with different inducibilities mediate uptake of sulfate in *Arabidopsis* roots. *Plant J.* 29, 465–473.

Yuan, L. B., Dai, Y. S., Xie, L. J., Yu, L. J., Zhou, Y., Lai, Y. X., et al. (2017). Jasmonate regulates plant responses to postsubmergence reoxygenation through transcriptional activation of antioxidant synthesis. *Plant Physiol.* 173, 1864–1880. doi: 10.1104/pp.16.01803

Zhu, Y. G., and Smolders, E. (2000). Plant uptake of radiocaesium: a review of mechanisms, regulation and application. *J. Exp. Bot.* 51, 1635–1645. doi: 10.1093/jexbot/51.351.1635

Zhu, F. Y., Chan, W. L., Chen, M. X., Kong, R. P., Cai, C., Wang, Q., et al. (2016). SWATH-MS quantitative proteomic investigation reveals a role of jasmonic acid during lead response in *Arabidopsis*. *J. Proteome Res.* 15, 3528–3539. doi: 10.1021/acs.jproteome.6b00258

Conflict of Interest: The authors declare that the research was conducted in the absence of any commercial or financial relationships that could be construed as a potential conflict of interest.

frontiers in Plant Science

SYSTEMATIC REVIEW
published: 24 January 2020
doi: 10.3389/fpls.2019.01727

Magnesium Fertilization Improves Crop Yield in Most Production Systems: A Meta-Analysis

Zheng Wang[1,2,3], *Mahmood Ul Hassan*[1], *Faisal Nadeem*[1], *Liangquan Wu*[3], *Fusuo Zhang*[1,2,3] *and Xuexian Li*[1,2*]

[1] Department of Plant Nutrition, The Key Plant-Soil Interaction Lab, MOE, China Agricultural University, Beijing, China, [2] National Academy of Agriculture Green Development, China Agricultural University, Beijing, China, [3] International Magnesium Institute, Fujian Agriculture and Forestry University, Fuzhou, China

OPEN ACCESS

Edited by:
Manuel Nieves-Cordones, Spanish National Research Council, Spain

Reviewed by:
Keitaro Tanoi, The University of Tokyo, Japan
Thomas David Alcock, University of Nottingham, United Kingdom

***Correspondence:**
Xuexian Li
steve@cau.edu.cn

Specialty section:
This article was submitted to Plant Nutrition, a section of the journal Frontiers in Plant Science

Received: *06 September 2019*
Accepted: *09 December 2019*
Published: *24 January 2020*

Citation:
Wang Z, Hassan MU, Nadeem F, Wu L, Zhang F and Li X (2020) Magnesium Fertilization Improves Crop Yield in Most Production Systems: A Meta-Analysis. Front. Plant Sci. 10:1727. doi: 10.3389/fpls.2019.01727

Magnesium deficiency is a frequently occurring limiting factor for crop production due to low levels of exchangeable Mg (ex-Mg) in acidic soil, which negatively affects sustainability of agriculture development. How Mg fertilization affects crop yield and subsequent physiological outcomes in different crop species, as well as agronomic efficiencies of Mg fertilizers, under varying soil conditions remain particular interesting questions to be addressed. A meta-analysis was performed with 570 paired observations retrieved from 99 field research articles to compare effects of Mg fertilization on crop production and corresponding agronomic efficiencies in different production systems under varying soil conditions. The mean value of yield increase and agronomic efficiency derived from Mg application was 8.5% and 34.4 kg kg^{-1} respectively, when combining all yield measurements together, regardless of the crop type, soil condition, and other factors. Under severe Mg deficiency (ex-Mg < 60 mg kg^{-1}), yield increased up to 9.4%, nearly two folds of yield gain (4.9%) in the soil containing more than 120 mg kg^{-1} ex-Mg. The effects of Mg fertilization on yield was 11.3% when soil pH was lower than 6.5. The agronomic efficiency of Mg fertilizers was negatively correlated with application levels of Mg, with 38.3 kg kg^{-1} at lower MgO levels (0–50 kg ha^{-1}) and 32.6 kg kg^{-1} at higher MgO levels (50–100 kg ha^{-1}). Clear interactions existed between soil ex-Mg, pH, and types and amount of Mg fertilizers in terms of crop yield increase. With Mg supplementation, Mg accumulation in the leaf tissues increased by 34.3% on average; and concentrations of sugar in edible organs were 5.5% higher compared to non-Mg supplemented treatments. Our analysis corroborated that Mg fertilization enhances crop performance by improving yield or resulting in favorable physiological outcomes, providing great potentials for integrated Mg management for higher crop yield and quality.

Keywords: magnesium, crop yield, agronomic efficiency, exchangeable Mg, pH, meta-analysis

INTRODUCTION

Magnesium (Mg) is an essential element for crops, animals, and humans, the deficiency of which affects photosynthesis and carbohydrate partitioning in crops (Nèjia et al., 2016), reduces sustainability of agricultural production and development, and causes long-term negative impacts on human and animal health (Robert and Helen, 2004; Jeroen et al., 2015). Unfortunately, obvious symptoms of Mg deficiency frequently occur in crops, especially at their critical developmental stage with rapid carbohydrate accumulation, grown in acidic soils widely distributed across the world (Cakmak et al., 1994; Nèjia et al., 2016). Edible agricultural products are the main source of Mg nutrition for humans and animals. Therefore, maintaining Mg contents of agricultural products within relatively sufficient range is very important for animal and human health.

In an agricultural production system, the availability of Mg to crops depends on various factors such as soil texture, cation exchangeable capacity (Hariadi and Shabala, 2004), site specific climatic and anthropogenic factors, agronomic management practices, as well as crop species itself (Scheffer and Schachtschabel, 2002; Mikkelsen, 2010). Crops absorb Mg from the soil mainly through their roots. Adequate soil Mg is a key to ensure robust crop growth and production. Absolute Mg deficiency in the soil dramatically reduces Mg absorption by crop roots, which is frequently a consequence of low Mg contents in source rocks (Papenfuß and Schlichting, 1979), Mg losses by mobilization and leaching in the soil (Schachtschabel, 1954), or Mg depletion due to intensive crop production (Pol and Traore, 1993). Additionally, cationic competition, resulting from long-term imbalanced soil fertilization, causes nutrient heterogeneity in soils. A good soil Mg condition is the pre-requisite to ensure Mg uptake by crop roots and enhance Mg utilization efficiency.

Soil acidity is another important factor determining crop productivity (Mohebbi and Mahler, 1989; Aggangan et al., 1996), closely associated with deficiency of potassium, calcium, magnesium, phosphorus, and zinc, while toxicity of aluminum and manganese (Guo et al., 2004; Zhu et al., 2004; Binh et al., 2018) antagonizes the availability of Mg (Wang et al., 2014). In addition, the highly mobile nature of Mg^{2+} ion makes it susceptible to leaching from the root zone by heavy rainfall (Schachtschabel, 1954; Grzebise, 2011; Gransee and Führs, 2013) especially in acidic soils, reducing nutrient utilization efficiencies and crop yield.

In recent decades, more emphasis has been given to nitrogen, phosphorus, and potassium fertilizers than Mg to obtain higher crop yield (Cakmak and Yazici, 2010). Soils undergoing intensive crop forage and harvest are not being replenished with Mg fertilizers, resulting in depletion of indigenous Mg from the soil and large-scale Mg deficiency. Nowadays, Mg deficiency has become a widespread problem severely reducing photosynthetic rates of crops especially grown in acidic soils (Fischer, 1997; Sun and Payn, 1999; Ridolfi and Garrec, 2000; Graeff et al., 2001; Hermans et al., 2004). Mg deficiency symptoms typically appear on older leaves (Bergmann, 1992). Chlorosis is a most obvious response of crops to Mg deficiency that foretells considerable yield reduction as a result of decreases in sugar transport from the source to sink organs and biomass accumulation in the root and reproductive tissues (Hermans et al., 2004; Cakmak and Yazici, 2010; Gransee and Führs, 2013). From a broader point of view, Mg fertilization improves tomato yield (7.7–17.9 t ha^{-1}) in South India (Kashinath et al., 2013), grain yield in barley (by 8.6%) in Iran (Mahdi et al., 2012), and hazel nut highest yield increase of 51% and total oil content increase of 4.8% in Turkey (Nedim and Daml, 2015), suggesting that Mg fertilization is an important measure to boost crop production. There is also substantial literature available on the importance of Mg for agricultural productivity, Mg deficiency in soils and crops, and Mg involvement in plant structure and physiological functions (Cakmak et al., 1994; Cakmak and Kirkby, 2008; Cakmak, 2013; Ceylan et al., 2016). However, it is imperative to better understand responses of crop yield to Mg-fertilization under different soil, cropping, and fertilization conditions in large-scale field experiments.

Until now, there has been no attempt made to systematically re-analyze effects of Mg fertilization on crop yield and agronomic efficiencies by summarizing the past experiments worldwide. Factors such as soil available Mg, soil pH, and rates and types of Mg fertilizers precondition yield responses to Mg application. In this study, a meta-analysis was conducted to (1) evaluate overall effects of Mg fertilizers on crop yield and corresponding agronomic efficiencies; (2) understand yield effects of Mg fertilization under different cropping and fertilization conditions; and (3) to estimate how exchangeable Mg and pH levels in the soil affects outcomes of Mg fertilization.

MATERIALS AND METHODS

Search Strategy and Data Extraction

To analyze the effect of Mg fertilizers on crop production in the field, a comprehensive literature search was performed using "Magnesium (Mg) fertiliz*," "Magnesium (Mg) fertilis*" in the article title and "crop yield*" as key terms on Web of Science (http://apps.webofknowledge.com/) and China National Knowledge Infrastructure (http://www.cnki.net/) electronic databases before November 2019. Data were extracted either directly from tables or indirectly from conversion of original figures in reported studies including crop yield, Mg and sugar concentrations responsive to Mg fertilization around the world (**Figure 1A**; most studies from China, much less from the other countries, and no reports found from Brazil). There were very few physiological and quality data available; hence, corresponding evaluation was not included in this study. Effects of Mg fertilization on yield followed the standard normal distribution (**Figure 1B**). The studies were selected according to the following four criteria: (1) studies containing

Abbreviations: N, nitrogen; P, phosphorus; K, potassium; Ca, calcium; Mg, magnesium; AE-Mg, agronomic efficiency of Mg fertilizers; ex-Mg, exchangeable magnesium.

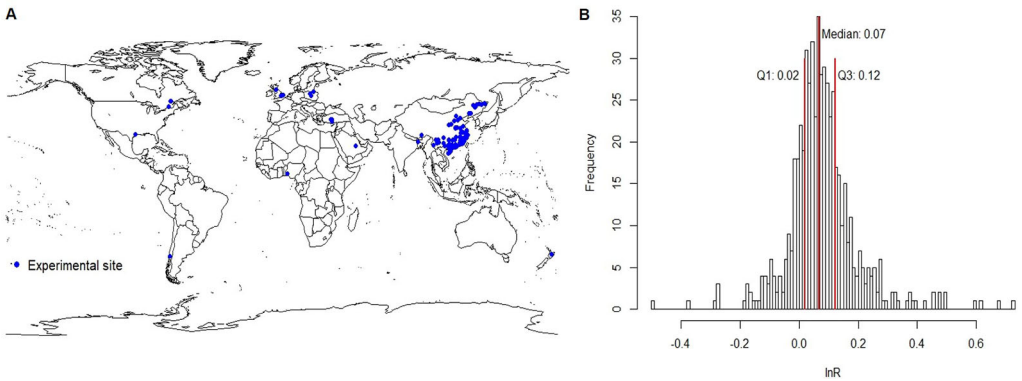

FIGURE 1 | The Map distribution of experimental sites **(A)** and frequency distribution of data indicating effects of Mg fertilization on crop yield **(B)** for our meta-analysis. The blue spots indicated local experimental sites of Mg fertilizers in the field **(A)**. The three red lines of Q1 (left), Median (middle), and Q3 (right) corresponded to data frequency 25%, 50%, and 75% **(B)**.

comparisons of magnesium fertilization and without magnesium fertilization (control), (2) representing field experiments, excluding pot experiment in the greenhouse, (3) with Mg fertilization in the soil, excluding foliar Mg application, (4) the study reporting types of crops, yield, the mean, and the number of paired observations (**Supplementary Figure S1**).

Data Sources

A total of 99 papers (see study list in **Supplementary Data Sheet S1**) with 570 pairwise comparisons qualified for our meta-analysis (396 from China and 174 from other countries). The field trials were reported in ten countries (Bangladesh, Canada, China, Chile, Iran, New Zealand, Nigeria, Poland, Turkey, and United Kingdom) (**Figure 1A**).

Effect Sizes and Their Modeling

Effects of Mg fertilization on crop yield were evaluated against corresponding control without Mg fertilization by the following equation:

$$lnR = ln(\frac{Xt}{Xc})$$

where *lnR* represented the natural log of the response ratio (the effect size), *Xt* represented the crop yield under Mg fertilization, and *Xc* represented the crop yield without Mg fertilization (Hedges et al., 1999; Verena et al., 2012). Given that more than 50% of case studies did not provide a measure of variance, case studies were weighted using numbers of study and experiment by mixed effects models in R. To interpret clearly, the effect on yield was expressed as the percentage change, which was calculated by (R−1) × 100%. A positive percentage change indicated an increase, whereas negative values indicated a decrease due to Mg fertilization. Mean percentage change was considered to be significantly different from zero if the 95% CI did not overlap with zero (Hedges et al., 1999).

Agronomic Efficiency of Mg fertilizers (AE-Mg) was calculated by the following equation:

$$AE - Mg = (Xt - Xc)/F_{Mg0}$$

where F_{MgO} represented amount (kg MgO ha^{-1}) of Mg fertilizers applied.

Statistical analysis was performed using mixed effects models in R (version 3.5.1) as follows: (1) the fixed effect, (2) the fixed effect and a random study effect, (3) the fixed effect and random effects of study and experiment nested in the study, and (4) the fixed effect and a unique experiment random effect. Appropriate random effects were identified by AIC (Akaike Information Criterion) and ANOVA analyses (R Stats Packages), with significant difference at $P < 0.05$ and $P < 0.01$ (SPSS 20.0).

Dataset Overview

The resulting dataset contained 570 case studies, covering more than 30 crops across ten countries (**Supplementary Data Sheet S1**). According to crop characteristics and their responses to Mg fertilization, related crops were analyzed in nine groups: cereals (rice, maize, wheat, barley), fruits (apple, banana, pineapple, orange, pomelo, litchi, watermelon, sugar cane), vegetables (cabbage, lettuce, pepper, tomato, cucumber), tubers (potato, sweet potato, cassava, carrot), oil crops (soybean, peanut, canola, sunflower), grasses, tobacco, tea, and other crops (sugar beet, onion, milk thistle, blueberry).

To better interpret the results, soils were empirically divided into acidic (<6.5), neutral (6.5–7.5), and alkaline (>7.5) or Mg deficient (<60 mg kg^{-1}), moderate (60—120 mg kg^{-1}), and relatively sufficient (>120 mg kg^{-1}) types, respectively, according to pH and exchangeable Mg levels in the soil.

Mg fertilizers were classified into two types: (1) slowly released (Mg-S) fertilizers including Mg oxide, Mg hydroxide, dolomite, Mg carbonate, and calcium-Mg phosphate, and (2) rapidly released (Mg-R) fertilizers including Mg sulfate, Mg chloride, and potassium Mg sulfate. Fertilization rates varied in a range of <50, 50–100, and >100 kg MgO ha^{-1}.

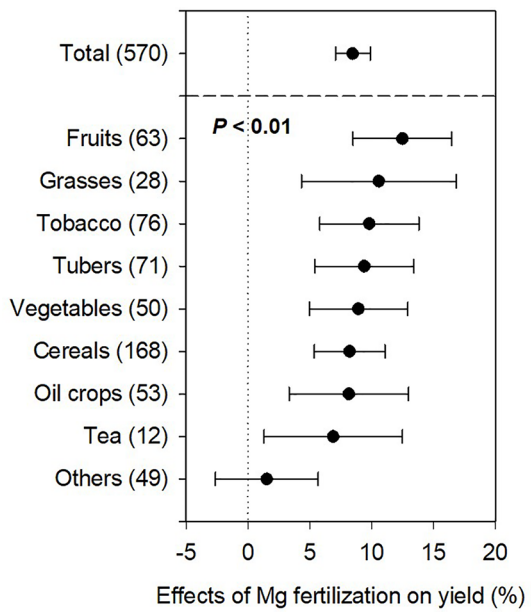

FIGURE 2 | Relative effects of Mg fertilization on crop yield. The data points were means ± 95% CI (confidence interval), and the number of experimental observations were indicated in parentheses. *P*, indicated the significant differences between crops.

RESULTS

Magnesium (Mg) Fertilization Enhanced Yield of Most Crops

Magnesium fertilizers generally promoted yield for most crops (**Supplementary Figure S2**) and yield increases varied depending on crop species, soil conditions, Mg fertilization rates, and other factors. The average yield increase in crop production was 8.5% according to our meta-analysis (**Figure 2**). Magnesium fertilization significantly enhanced production of fruits (12.5%), grasses (10.6%), tobacco (9.8%), tubers (9.4%), vegetables (8.9%), cereals (8.2%), oil crops (8.2%), and tea (6.9%), although non-significantly for the other crops (1.5%), compared to the non-Mg supplemented treatment at $P < 0.05$ (**Figure 2**). Moreover, average yield increases of fruit, grass, tobacco, tuber, and vegetable crops were higher than the overall average, while those of cereal, oil, tea, and other crops were lower (**Figure 2**). Crop responses to Mg differed due to soil and other related conditions. Meta-analysis revealed that Mg concentrations in leaves and sugar concentrations in crops tissues (tubers and beans) increased by 34.3% (**Figure 3A**) and 5.5% (**Figure 3B**) at $P < 0.01$, respectively, upon Mg fertilization.

Agronomic Efficiencies of Mg Fertilizers Were Positively Correlated to Yield Increases of Most Crops

The agronomic efficiency (AE) is an important parameter indicating relative fertilization efficiency in agricultural production. AE of Mg fertilizers was defined as the yield increase per unit of Mg fertilizers applied. On average, AE-Mg was 34.4 kg kg^{-1} when 541 cases (amount of Mg fertilization was not reported in 29 cases) were combined in this study (**Figure 4**). Similar to the effect of crop species on yield increases, the agronomic efficiencies of Mg fertilizers (AE-Mg) was also affected by crop species, though in a manner inconsistent with

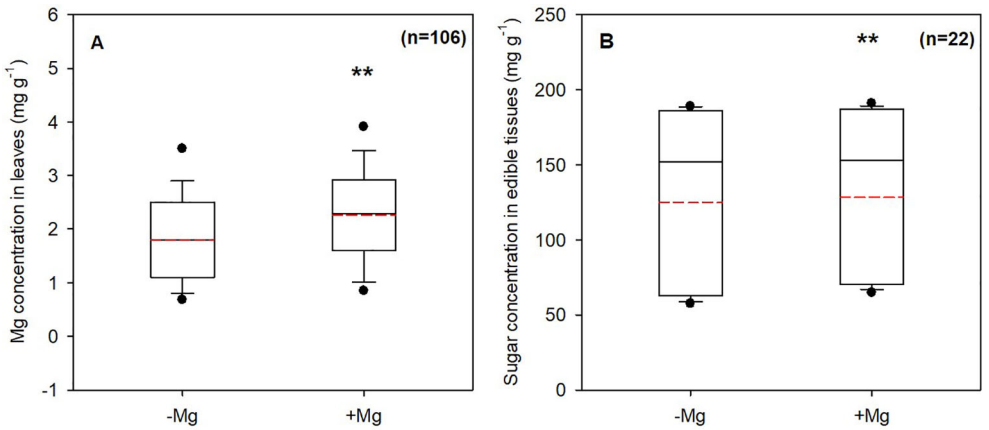

FIGURE 3 | Mg in leaves **(A)** and sugar in edible tissues **(B)** concentrations with Mg (+Mg) and without Mg (-Mg) supplementation. Solid black and dashed red lines indicated the median and mean, respectively. The box boundaries indicated the 75% and 25% quartiles; error bars indicated the 90th and 10th percentiles; and the black dots indicated the 95th and 5th percentiles. **, indicated highly significant differences between treatments ($P < 0.01$).

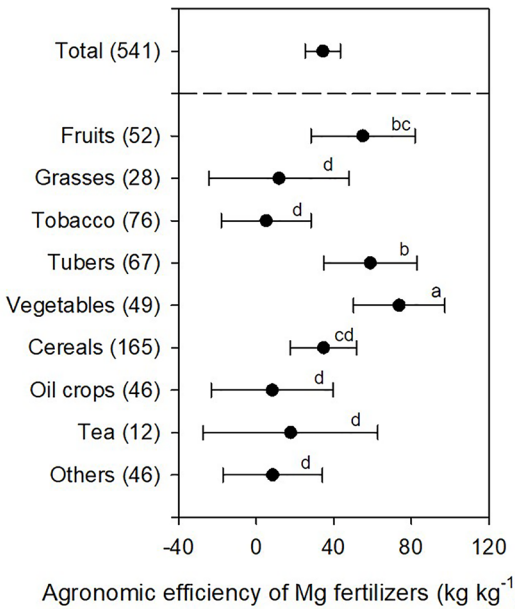

FIGURE 4 | The agronomic efficiency of Mg fertilizers (AE-Mg) in different crops. The data points were means ± 95% CI (confidence interval), and the number of experimental observations were indicated in parentheses. Small letters indicated the significant differences between different crops ($P < 0.05$).

the former effect. The AE-Mg of vegetable (73.7 kg kg^{-1}) was significantly higher than tuber (58.8 kg kg^{-1}), fruit (55.0 kg kg^{-1}), and cereal (34.7 kg kg^{-1}) crops at $P < 0.05$ (**Figure 4**). However, there was no significant difference in the AE-Mg between tea, grasses, oil, tobacco, and other crop experiments due to large variations (**Figure 4**).

AE-Mg calculation was based on fresh weights of harvested parts of different crops (except dry matter yield for grasses). Higher water content in the harvested organ tended to increase AE-Mg. Responses of crops to Mg (**Figure 5**) and the amount of Mg fertilizers applied (**Figure 6**) also affected the AE-Mg. Among four types of crops (vegetables, tubers, fruits, and cereals) responsive to Mg fertilization (**Figure 4**), yield increases in vegetables ($P < 0.05$) and fruits ($P < 0.01$) had significant correlation with Mg concentrations (**Figure 5B**).

Generally, the AE-Mg responded to Mg application when lower than 100 kg MgO ha^{-1} was applied (**Figure 6A**). Although there was no data for sugarcane (in the fruits group) and sugar beet (in the other crops group) under Mg fertilization lower than 50 kg MgO ha^{-1}, the AE-Mg in vegetable (90.8 kg kg^{-1}), tuber (68.0 kg kg^{-1}), and cereal (35.3 kg kg^{-1}) crops was responsive to Mg fertilization lower than 50 kg MgO ha^{-1} (**Figures 6B, C, E**); the AE-Mg in fruit (62.0 kg kg^{-1}) (**Figure 6D**) and other crops (9.6 kg kg^{-1}) (**Figure 6F**) was responsive even in the range of 50–100 kg MgO ha^{-1}. Notably, fruit crops responded to Mg application higher than 100 kg MgO ha^{-1} (**Figure 6E**). The difference was probably due to differential responses of crops to Mg, which conferred yield variations in relation to concentration changes of Mg in leaves (**Figure 5**). Importantly, there was a significant positive liner correlation between the crop yield and Mg concentration in leaves ($P < 0.01$, **Figure 5A**). With regard to different crop categories, the linear correlation was significant for vegetables ($P < 0.05$), fruits, and grasses ($P < 0.01$) (**Figures 5B, C**).

Soil Conditions and Fertilizer Types Affected Fertilization Effects

Crop roots explore heterogeneously available mineral nutrients in the soil for absorption to sustain plant growth and development (Hodge, 2004; Nibau et al., 2008). Soil conditions, e.g. concentrations of exchangeable Mg and soil pH levels, have a direct effect on Mg availability to crops thereby affecting crop yield in the long run (Foy and Barber, 1958; Fox and Piekielek, 1984; Clarka et al., 1997). Our meta-analysis suggested obvious stimulatory effects of Mg fertilization on crop yield in Mg-deficient acidic soils (**Figure 7**). Crop yield increased by 9.4%, 9.4%, and 4.9% due to Mg fertilization respectively under Mg deficient (exchangeable Mg <60 mg kg^{-1}), moderate (60–120 mg kg^{-1}), and relatively sufficient (> 120 mg kg^{-1}) conditions. Similarly, Mg improved crop production by 11.3%, 6.3%, and 3.9% respectively under acid (pH <6.5), neutral (pH 6.5–7.5),

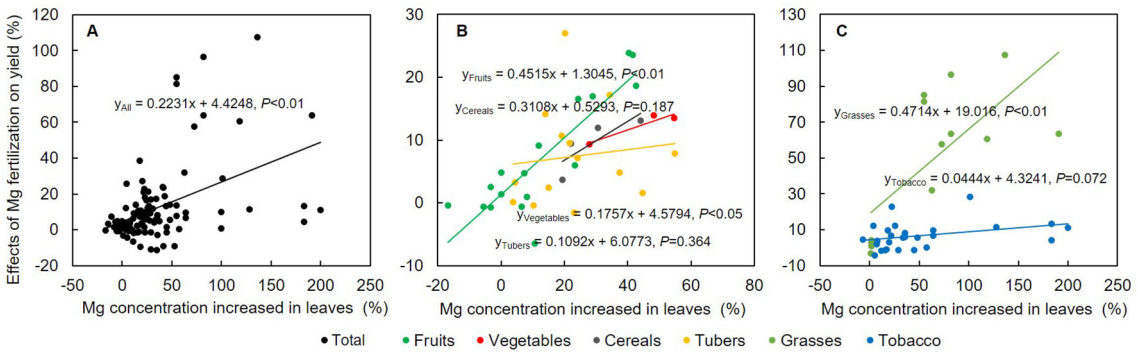

FIGURE 5 | The relationship between effects of Mg fertilization on yield and variations in Mg concentrations in all crops **(A)**, vegetables, tubers, fruits, cereals **(B)**, grasses and tobacco **(C)**. Individual crop was represented by colored circle, and the response relation is fitted by a straight line of the same color line. *P*-value, indicated the significance of the results.

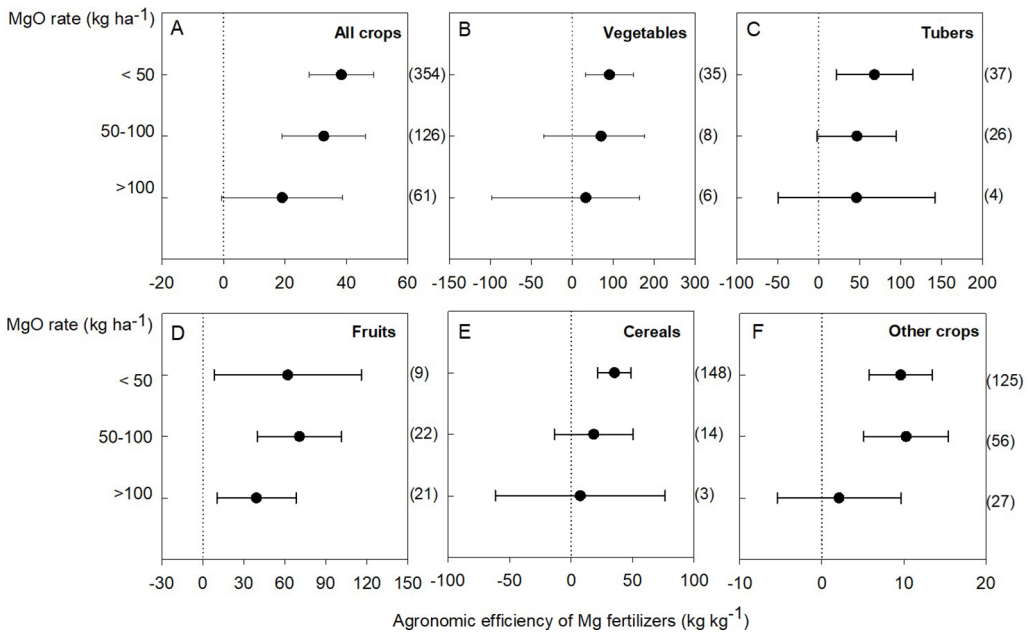

FIGURE 6 | Agronomic efficiency of Mg fertilizers (AE-Mg) in all crops **(A)**, vegetables **(B)**, tubers **(C)**, fruits **(D)**, cereals **(E)**, and other crops (tobacco, tea, grasses, oil, and other crops) **(F)**. The data points were means ± 95% CI (confidence interval), and the number of experimental observations were indicated in parentheses. MgO, magnesium oxide.

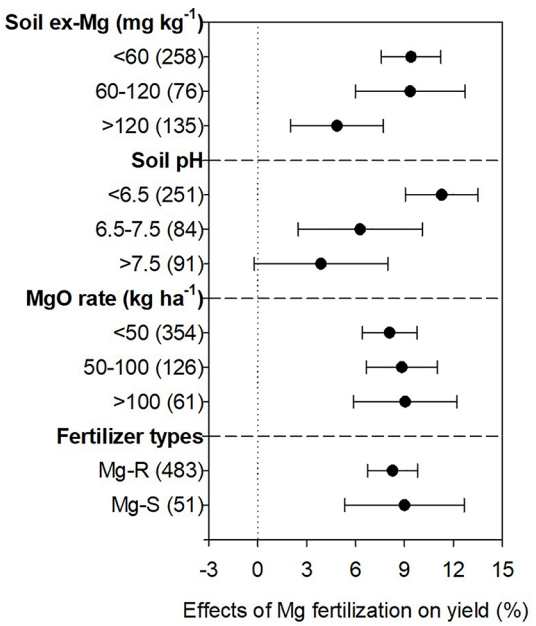

FIGURE 7 | Effects of Mg fertilizer on crop yield under different soil conditions (exchangeable-Mg concentrations, soil pH, rates of MgO application, and types of Mg fertilizers). The data points were means ± 95% CI (confidence interval), and the number of experimental observations were indicated in parentheses. Soil ex-Mg, soil exchangeable magnesium; MgO, magnesium oxide; Mg-R, rapidly released Mg fertilizers; Mg-S, slowly released Mg fertilizers.

and alkaline (pH >7.5) soil conditions (**Figure 7**). Yield increases were positively correlated with the amount of Mg fertilizers especially at application levels higher than 100 kg MgO ha^{-1} (9.0% yield-increment, **Figure 7**). Nevertheless, two different types of Mg fertilizers Mg-R (8.3%) and Mg-S (9.0%) showed no significant difference in yield improvement (**Figure 7**).

Interaction Effects of Ex-Mg and Fertilization Rates, Ex-Mg and pH, and pH and Fertilizer Types

Given large variations in fertilization regimes and soil conditions in field experiments, it's necessary to evaluate interaction effects of different influential factors on stimulatory effects of Mg fertilization on yield. The ex-Mg level was the significant factor compared with application rates of Mg fertilizers ($P < 0.05$, **Table S1**). With exchangeable-Mg concentrations in the soil increasing, crop yield responded moderately or slightly to Mg fertilization. Notably, Mg application higher than 100 kg MgO ha^{-1} in Mg deficient soils gave rise to the largest yield gain (12.5%) (**Figure 8A**). Adjustment of MgO rates caused no significant difference in soils with moderate or relatively sufficient ex-Mg (**Figure 8A**).

Indeed, the effect of Mg-fertilizers on crop production was combinatorically determined by pH levels and ex-Mg status of soils ($P = 0.803$, **Supplementary Table S2**), with the ex-Mg concentration as a main influential factor ($P = 0.05$, **Supplementary Table S2**). Average yield increases derived from Mg-fertilization under Mg deficiency were greater than those under moderate or relatively sufficient Mg conditions regardless of variations in soil pH (**Figure 8**). However, the

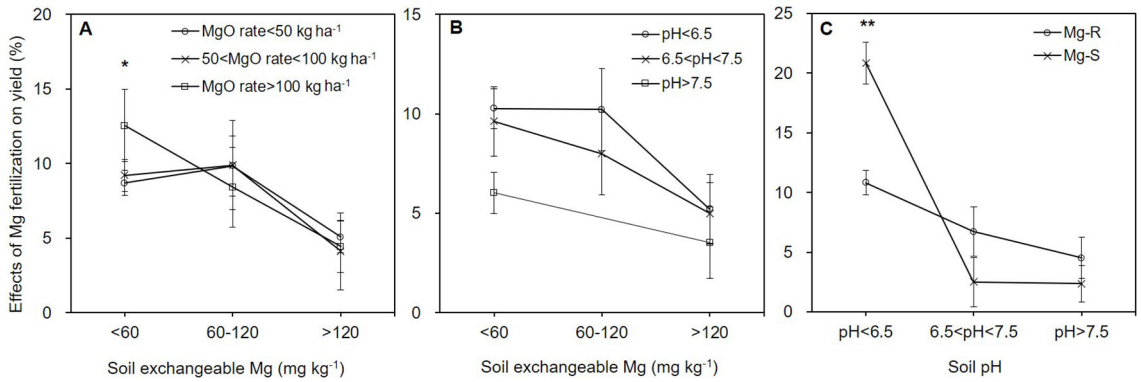

FIGURE 8 | Interaction effects of two factors on yield increases: soil exchangeable Mg and rates of Mg fertilizers **(A)**, soil exchangeable-Mg and pH **(B)**, soil pH and Mg fertilizer types **(C)**. * and **, indicated significant differences at $P < 0.05$ and $P < 0.01$, respectively. MgO, magnesium oxide; Mg-R, rapidly released Mg fertilizers; Mg-S, slowly released Mg fertilizers.

interaction effect of soil pH and Mg-fertilizer types was significant ($P < 0.05$, **Supplementary Table S3**). The Mg-S type significantly improved crop yield (20.9%) compared to the Mg-R type (10.8%) in acidic soils ($P < 0.01$, **Figure 8C**). Mg-S type also has a certain effect on improving soil acidity, which indirectly improves the utilization efficiency; and Mg-R performed better than Mg-S in neutral and alkaline soils (**Figure 8C**).

DISCUSSION

Magnesium Application Increases Crop Yield

Magnesium plays essential roles in ensuring crop productivity (Senbayram et al., 2015); unfortunately, Mg concentration in wheat, fruits, and vegetables has declined over the past 50 years (Andrea, 2013). Latent and acute Mg deficiencies are common phenomena in crop production (Römheld and Kirkby, 2007). Magnesium fertilization improves crop yield in the field (Mahdi et al., 2012; Kashinath et al., 2013; Nedim and Daml, 2015). Given large variations in crop species, fertilization regimes, and soil and climatic conditions in field experiments, it's necessary to systemically evaluate or quantify the overall effects of Mg fertilization on crop yield, corresponding agronomic efficiencies, and how pH and exchangeable Mg levels influence effects of Mg fertilization. Here, we selected 396 sets of observations from China and 174 outside of China to analyze how soil application of Mg fertilizers affect crop production in the field.

Our meta-analysis showed higher yield in fruit, grass, tobacco, tuber, vegetable, cereal, oil crop, tea, and other crops production with an overall 8.5% increase (**Figure 2**) when reasonable amount of Mg (i.e., 94.1, 46.9, 54.1, 58.3, 43.5, 27.8, 47.2, 34.1, and 76.8 kg MgO ha^{-1}, respectively) was applied. Under Mg deficiency, Mg fertilization leads to large yield increases; when not deficient, applied Mg meets high demand of crops during their rapid growth period. Alternatively, high concentrations of ions such as K^+, Ca^{2+}, and NH_4^+ likely antagonize Mg^{2+} uptake (Mulder, 1956; Seggewiss and Jungk, 1988; Wilkinson et al., 1990; Marschner, 2012); therefore, Mg fertilization upscales the Mg^{2+} proportion and weakens other cationic antagonism in the soil solution. Magnesium deficiency hampers nutrient uptake and reduces the leaf growth rate, affecting the assimilate supply to growing roots and their capacity to acquire nutrients and ultimately decreases the yield (Cakmak and Kirkby, 2008).

Magnesium is key component of several biological processes (CO_2 fixation in photosynthesis, photophosphorylation, protein and chlorophyll synthesis, phloem loading, and translocation of assimilates) in leaves (Cakmak and Yazici, 2010). The photosynthetic assimilates from leaves are transported to the sink organs (such as roots, shoot tips, and seeds), and stored as starch or converted to hexoses (Cakmak et al., 1994; Hermans et al., 2005; Lemoine et al., 2013) to increase crop yield under sufficient Mg status (Brohi et al., 2000; Laing et al., 2000). Sucrose transport from source to sink tissues occurs through phloem by invertase and sucrose synthase enzymes (Sturm and Tang, 1999; Winter and Huber, 2000; Welham et al., 2009). Hence, appropriate Mg concentration in leaves is essential to ensure activities of enzymes involved in source-to-sink transport of Mg and sugars, which can be achieved by planting proper species as well as managing Mg fertilizer rates (White and Broadley, 2009).

Mg^{2+} and closely related sugar production in leaves are of utmost importance for biomass accumulation and grain development (Koch, 1996; Orlovius and McHoul, 2015). Mg^{2+} also promotes assimilate partitioning and translocation to source tissues (Cakmak and Kirkby, 2008; Cakmak, 2013). Mg-deficiency reduces grain weight and lowers grain quality in wheat (Ceylan et al., 2016). We found that sugar concentrations in crops increased when Mg was applied compared to those without Mg application (**Figure 3B**). Enhanced sugar accumulation due to Mg fertilization is beneficial for crop production, regardless of plant species (Strebel and Duynisveld, 1989; Marschner, 2012; Orlovius and McHoul, 2015).

Agronomic Efficiencies of Mg Fertilizers Varies Depending on Crop Species

Mg^{2+} plays a critical role in regulating photosynthesis (Sun and Payn, 1999); Mg deficiency severely down-regulates photosynthesis rates, photo assimilates transport to sinks and crop yield (Nèjia et al., 2016). Magnesium application promoted Mg concentration in leaves (**Figure 3A**) and crop yield (**Figure 2**). The increased Mg concentration in leaves favored yield increases in all crops (**Figure 5A**) and significant responses were observed in fruits ($P < 0.01$), vegetables ($P < 0.05$) (**Figure 5B**), and grasses ($P < 0.01$, **Figure 5C**). However, the agronomic efficiencies of Mg fertilizers (AE-Mg) showed a different pattern due to variations in uptake or utilization of Mg across crop species (**Figure 4**). We analyzed 541 dataset and identified the AE-Mg as 34.4 kg kg^{-1} on average (**Figure 4**). Vegetables were always most responsive to Mg application, and cereals were least responsive (**Figure 4**). Even for cereals, the AE-Mg was 34.7 kg kg^{-1} (**Figure 4**), dramatically higher than that of nitrogen (8.0–10.4 kg kg^{-1}), phosphorus (7.3–9.0 kg kg^{-1}), and potassium (5.3–6.3 kg kg^{-1}) (Zhang et al., 2008). Plants generally have similar concentrations of Mg and P (Marschner, 2012); However, in contrast to long-term NPK fertilization, Mg removal from the soil by crop harvest has not been supplemented and Mg is more easily leached (Schachtschabel, 1954; Grzebise, 2011; Gransee and Führs, 2013), resulting in larger yield effects and higher AE-Mg upon Mg application.

Soil Conditions Primarily Determine Yield Effects of Mg Fertilization

Soil pH directly affects magnesium release from clay minerals and Mg uptake by plants (Schubert et al., 1990). Exchangeable Mg at pH <6.0 becomes non-exchangeable when soil pH becomes higher than 6.5 (Chan et al., 1979; Hailes et al., 1997). Mg is subjected to leaching in acidic soils, and H^+, Al^{3+}, and Mn^{2+} in rhizosphere may interfere with Mg uptake, thus hampering crop yield (Metson, 1974; Mayland and Wilkinson, 1989). Mg fertilization not only increases bioavailability of Mg^{2+}, but also mitigates Al^{3+} and Mn^{2+} toxicity (Bot et al., 1990; Goss and Carvalho, 1992; Bose et al., 2011; Marschner, 2012). Therefore, dramatic yield increases were observed when exchangeable Mg was lower than 60 mg kg^{-1} or pH was below 6.5, with less extent of yield effects under other conditions (**Figure 7**). Crops cultivated on Mg deficient soils show positive responses to the applied Mg fertilizers depending on the rate and timing of application (White and Broadley, 2009; Grzebisz, 2013). Thus, the application of Mg fertilizer in the acidic and Mg deficient soil is very important for crop nutrient management.

The yield effect was the largest in the magnesium deficient soil irrespective of MgO rates (**Figure 8A**) and soil pH (**Figure 8B**). Although exchangeable-Mg levels were the primary factors determining yield increases (**Supplementary Tables S1** and **S2**), there were clear interactions between soil pH and fertilizer types (**Supplementary Table S3**). Mg fertilizers are generally classified into rapidly released (Mg-R) and slowly released (Mg-S) types with distinct particle size and water solubility (Mayland and Wilkinson, 1989; Härdter et al., 2004; Loganathan et al., 2005). Mg-S releases slowly and improved yield more efficiently as compared to Mg-R (**Figure 8C**). Mg-S is also efficiently absorbed by crops and neutralizes soil acids. Both Mg-R and Mg-S improved crop yield with no significant difference between two types of Mg fertilizers (**Figure 8**).

CONCLUSIONS

Magnesium has similar concentrations to phosphorus in plant tissues. However, Mg is easily leached out in acidic soils and competition of excessive cations makes Mg less available to plant roots. Unfortunately, Mg deficiency is not well aware by farmers. Thus, Mg limitation is becoming an increasingly severe limitation factor in crop production. Our analysis suggested that Mg application improved crop yield by 8.5% under various field conditions across the world, along with elevation of Mg and sugar concentrations in plant tissues. The yield increase was 10.6% under severe Mg deficiency and 10.8% when soil pH was lower than 6.5.

The agronomic efficiency of magnesium fertilizers was 34.4 kg kg^{-1} and increased up to 38.3 kg kg^{-1} at lower MgO levels (0–50 kg ha^{-1}), which is dramatically higher than that of nitrogen, phosphorus, and potassium. Our findings indicate that it is more efficient in terms of yield improvement by applying Mg fertilizers compared to application of other macronutrients, opening up a novel path towards high nutrient efficiency, balanced fertilization for high crop yield and quality, as well as sustainable development of agriculture.

AUTHOR CONTRIBUTIONS

XL and FZ designed research. ZW, MH, FN, and LW collected data. ZW and XL wrote the paper. FZ revised the manuscript. All authors approved the final manuscript.

FUNDING

This work was funded by the International Magnesium Institute (IMI, Fujian Agriculture and Forestry University, China) and Chinese National Basic Research Program (2015CB150400).

SUPPLEMENTARY MATERIAL

The Supplementary Material for this article can be found online at: https://www.frontiersin.org/articles/10.3389/fpls.2019.01727/full#supplementary-material

SUPPLEMENTARY DATA SHEET S1 | Study list used for meta-analysis.

REFERENCES

Aggangan, N. S., Dell, B., and Malajczuk, N. (1996). Effects of soil pH on the ectomycorrhizal response of Eucalyptus urophylla seedlings. *New Phytol.* 134 (3), 539–546. doi: 10.1111/j.1469-8137.1996.tb04372.x

Andrea, R. (2013). Changing crop magnesium concentrations: impact on human health. *Plant Soil* 368, 139–153. doi: 10.1007/s11104-012-1471-5

Bergmann, W. (1992). *Nutritional disorders of plants-development, visual and analytical diagnosis* (Germany: Gustav Fischer Verlag).

Binh, T. N., Thanh, K. D., Thanh, V. T., Mui, K. D., Curtis, J. D., Phuc, V. L., et al. (2018). High soil Mn and Al, as well as low leaf P concentration, may explain for low natural rubber productivity on a tropical acid soil in Vietnam. *J. Plant Nutr.* 41 (7), 903–914. doi: 10.1080/01904167.2018.1431674

Bose, J., Babourina, O., and Rengel, Z. (2011). Role of Mg in alleviation of aluminium toxicity in plants. *J. Exp. Bot.* 62, 2251–2264. doi: 10.1093/jxb/erq456

Bot, J. L., Goss, M. J., Carvalho, M. J. G. P. R., Van Beusichem, M. L., and Kirkby, E. A. (1990). The significance of the magnesium to manganese ratio in plant tissues for growth and alleviation of manganese toxicity in tomato (*Lycopersicon esculentum*) and wheat (*Triticum aestivum*) plants. *Plant Soil* 124, 205–210. doi: 10.1007/BF00009261

Brohi, A. R., Karaman, M. R., Topbas, M. T., Aktas, A., and Savasli, E. (2000). Effect of potassium and magnesium fertilization on yield and nutrient content of rice crop grown on artificial siltation soil. *Turk. J. Agric. For.* 24, 429–435. doi: 5000029240

Cakmak, I., and Kirkby, E. A. (2008). Role of magnesium in carbon partitioning and alleviating photooxidative damage. *Physiol. Plantarum* 133, 692–704. doi: 10.1111/j.1399-3054.2007.01042.x

Cakmak, I., and Yazici, A. M. (2010). Magnesium: a forgotten element in crop production. *Better Crops* 94, 23–25. www.researchgate.net/publication/291869977.

Cakmak, I., Hengeler, C., and Marschner, H. (1994). Changes in phloem export of sucrose in leaves in response to phosphorus, potassium and Mg deficiency in bean plants. *J. Exp. Bot.* 45, 1251–1257. doi: 10.1093/jxb/45.9.1251

Cakmak, I. (2013). Magnesium in crop production, food quality and human health. *Plant Soil* 368, 1–4. doi: 10.1007/s11104-013-1781-2

Ceylan, Y., Kutman, U. B., Mengutay, M., and Cakmak, I. (2016). Magnesium applications to growth medium and foliage affect the starch distribution, increase the grain size and improve the seed germination in wheat. *Plant Soil* 406, 145–156. doi: 10.1007/s11104-016-2871-8

Chan, K. Y., Davey, B. G., and Geering, H. R. (1979). Adsorption of Mg and calcium by a soil with variable charge. *Soil Sci. Soc. Am. J.* 43, 301–304. doi: 10.2136/sssaj1979.03615995004300020012x

Clarka, R. B., Zetoa, S. K., Ritcheya, K. D., and BaligarMaize, V. C. (1997). Maize growth and mineral acquisition on acid soil amended with flue gas desulfurization by-products and magnesium. *Commun. Soil Sci. Plan.* 28 (15-16), 1441–1459. doi: 10.1080/00103629709369886

Fischer, E. S. (1997). Photosynthetic irradiance curves of Phaseolus vulgaris under moderate or severe magnesium deficiency. *Photosynthetica* 33 (3), 385–390.

Fox, R. H., and Piekielek, W. P. (1984). Soil magnesium level, corn (*Zeamays* L.) yield, and magnesium uptake. *Commun. Soil Sci. Plan.* 15, 109–123. doi: 10.1080/00103628409367459

Foy, C. D., and Barber, S. A. (1958). Magnesium deficiency and corn yield on two acid Indiana soils. *Soil Sci. Soc. Am. J.* 22 (2), 145–148. doi: 10.2136/sssaj1958.03615995002200020014x

Goss, M. J., and Carvalho, M. J. G. P. R. (1992). Manganese toxicity: the significance of magnesium for the sensitivity of wheat plants. *Plant Soil* 139, 91–98. doi: 10.1007/bf00012846

Graeff, S., Steffens, D., and Schubert, S. (2001). Use of reflectance measurements for the early detection of N, P, Mg and Fe deficiencies in *Zea mays* L. *J. Plant Nutr. Soil Sci.* 164, 445–450. doi: 10.1002/1522-2624(200108)164:4<445::AID-JPLN445>3.0.CO;2-1

Gransee, A., and Führs, H. (2013). Magnesium mobility in soils as a challenge for soil and plant analysis, magnesium fertilization and root uptake under adverse growth conditions. *Plant Soil* 368, 5–21. doi: 10.1007/s11104-012-1567-y

Grzebise, W. (2011). Magnesium - food and human health. *J. Elementol.* 16, 299–323. doi: 10.5601/jelem.2011.16.2.13

Grzebisz, W. (2013). Crop response to magnesium fertilization as affected by nitrogen supply. *Plant Soil* 368, 23–39.

Guo, J., Vogt, R. D., Zhang, X., Zhang, Y., Seip, H. M., and Tang, H. (2004). Ca–H–Al exchanges and aluminium mobility in two Chinese acidic forest soils: a bath experiment. *Environ. Geol.* 45, 1148–1153. doi: 10.1007/s00254-004-0979-2

Härdter, R., Rex, M., and Orlovius, K. (2004). Effects of different Mg fertilizer sources on the magnesium availability in soils. *Nutr. Cycl. Agroeco.* 70, 249–259. doi: 10.1007/s10705-005-0408-2

Hailes, K. J., Aitken, R. L., and Menzies, N. W. (1997). Magnesium in tropical and subtropical soils from north-eastern Australia. II. Response by glass house grown maize to applied magnesium. *Aust. J. Soil Res.* 35, 629–641. doi: 10.1071/s96082

Hariadi, Y., and Shabala, S. (2004). Screening broad beans (*Viciafaba*) for magnesium deficiency. I. Growth characteristics, visual deficiency symptomy and plant nutritional status. *Funct. Plant Biol.* 31, 529–537. doi: 10.1071/fp03201

Hedges, L. V., Gurevitch, J., and Curtis, P. S. (1999). The meta-analysis of response ratios in experimental ecology. *Ecology* 80, 1150–1156. doi: 10.2307/177062

Hermans, C., Johnson, G. N., Strasser, R. J., and Verbruggen, N. (2004). Physiological characterization of magnesium deficiency in sugar beet: acclimation to low magnesium differentially affects photosystems I and II. *Planta* 220, 344–355. doi: 10.1007/s00425-004-1340-4

Hermans, C., Bourgis, F., Faucher, M., Strasses, R. J., Delrot, S., and Verbruggen, N. (2005). Magnesium deficiency in sugar beets alters sugar partitioning and phloem lading in young mature leaves. *Planta* 220, 541–549. doi: 10.2307/23388758

Hodge, A. (2004). The plastic plant: root responses to heterogeneous supplies of nutrients. *New Phytol.* 162, 9–24. doi: 10.1111/j.1469-8137.2004.01015.x

Jeroen, H. F., de Baaij,, Joost, G. J., Hoenderop,, René, J. M., and Bindels, (2015). Magnesium in man: implications for health and disease. *Physiol. Rev.* 95, 1–46. doi: 10.1152/physrev.00012.2014

Kashinath, B. L., Ganesha, A. N., Murthy,, Senthivel, T., James, P. G., and Sadashiva, A. T. (2013). Effect of applied magnesium on yield and quality of tomato in Alfisols of Karnataka. *J. Hortic. Sci.* 8 (1), 55–59. doi: 10.4239/wjd.v4.i4.157

Koch, K. E. (1996). Carbohydrate modulated gene expression in plants. *Plant Mol. Biol.* 47, 509–540. doi: 10.1146/annurev.arplant.47.1.509

Laing, W., Greer, D., Sun, O., Beets, P., Lowe, A., and Payn, T. (2000). Physiological impacts of Mg deficiency in *Pinus radiata*: growth and photosynthesis. *New Phytol.* 146, 47–57. doi: 10.1046/j.1469-8137.2000.00616.x

Lemoine, R., Sylvain La, C., Rossitza, A., Fabienne, D., Thierry, A., and Nathalie, P. (2013). Source-to-sink transport of sugar and regulation by environmental factors. *Front. Plant Sci.*, 4, 272–292. doi: 10.3389/fpls.2013.00272

Loganathan, P., Hanly, J. A., and Currie, L. D. (2005). Effect of serpentine rock and its acidulated products as magnesium fertilisers for pasture, compared with magnesium oxide and Epsom salts, on a Pumice Soil. II. Dissolution and estimated leaching loss of fertiliser magnesium. *New Zeal. J. Agr. Res.* 48, 461–471. doi: 10.1080/00288233.2005.9513680

Mahdi, B., Yasser, E., Abolfazl, T., and Ahmad, A. (2012). Efficacy of different iron, zinc and magnesium fertilizers on yield and yield components of barley. *Afr. J. Microbiol. Res.* 6 (28), 5754–5756. doi: 10.5897/AJMR11.1638

Marschner, P. (2012). *Marschner"s mineral nutrition of higher plants. 3rd edn* (Netherlands: Amsterdam).

Mayland, H. F., and Wilkinson, S. R. (1989). Soil factors affecting magnesium availability in plant-animal systems: A review. *J. Anim. Sci.* 67, 3437–3444. doi: 10.2527/jas1989.67123437x

Metson, A. J. (1974). Magnesium in New Zealand soils. I. Some factors governing the availability of soil magnesium: A review. *New Z. J. Exp. Agric.* 2, 277–319. doi: 10.1080/03015521.1974.10427689

Mikkelsen, R. (2010). Soil and fertilizer magnesium. *Better Crops* 94, 26–28. www.researchgate.net/publication/308795926.

Mohebbi, S., and Mahler, R. L. (1989). The effect of soil pH on wheat and lentils grown on an agriculturally acidified northern Idaho soil under greenhouse conditions. *Commun. Soil Sci. Plan.* 20, 359–381. doi: 10.1080/00103628909368088

Mulder, E. G. (1956). Nitrogen-magnesium relationships in crop plants. *Plant Soil* 7, 341–376. doi: 10.1007/BF01394322

Nèjia, F., Amine, E., Walid, Z., Abderrazak, S., Chedly, A., and Mokded, R. (2016). Effects of magnesium deficiency on photosynthesis and carbohydrate partitioning. *Acta Physiol. Plant* 38, 145. doi: 10.1007/s11738-016-2165-z

Nedim, O., and Daml, B. O. (2015). Effect of Mg fertilization on some plant nutrient interactions and nut quality properties in Turkish hazelnut (*Corylus avellana* L.). *Sci. Res. Essays* 10 (14), 465–470. doi: 10.5897/SRE2014.5811

Nibau, C., Gibbs, D. J., and Coates, J. C. (2008). Branching out in new directions: the control of root architecture by lateral root formation. *New Phytol.* 179, 595–614. doi: 10.1111/j.1469-8137.2008.02472.x

Orlovius, K., and McHoul, J. (2015). Effect of two magnesium fertilizers on leaf magnesium concentration, yield, and quality of potato and sugar beet. *J. Plant Nutr.* 38 (13), 2044–2054. doi: 10.1080/01904167.2014.958167

Papenfuß, K. H., and Schlichting, E. (1979). Bestimmen de faktoren des Mg-haushaltes von böden in der bundesrepublik deutschland. *Magneiums-B.* 1, 12–14.

Pol, F., and Traore, B. (1993). Soil nutrient depletion by agricultural production in Southern Mali. *Fert. Res.* 36, 79–90. doi: 10.1007/BF00749951

Ridolfi, M., and Garrec, J. P. (2000). Consequences of an excess Al and a deficiency in Ca and Mg for stomatal functioning and net carbon assimilation of beech leaves. *Ann.For. Sci.* 57 (3), 209–218. doi: 10.1051/forest:2000112

Robert, K. R., and Helen, E. G. (2004). Magnesium deficiency and osteoporosis: animal and human observations. *J. Nutr. Biochem.* 15 (12), 710–716. doi: 10.1016/j.jnutbio.2004.08.001

Römheld, V., and Kirkby, E. A. (2007). Magnesium functions in crop nutrition and yield. *Proc. Conf. Cambridge*, 151–171.

Schachtschabel, P. (1954). Das pflanzenverfügbare magnesium des bodens und seine bestimmung. *J. Plant Nutr. Soil Sci.* 67, 9–23. doi: 10.1002/jpln.19540670103

Scheffer, F., and Schachtschabel, P. (2002). *Lehrbuch der Bodenkunde* (Heidelberg: Spektrum Akademischer Verlag).

Schubert, S., Schubert, E., and Mengel, K. (1990). Effect of low pH of the root medium on proton release, growth, and nutrient uptake of field beans (*Vicia faba*). *Plant Soil* 124, 239–244. doi: 10.1007/BF00009266

Seggewiss, B., and Jungk, A. (1988). Einfluss der kaliumdynamik im wurzelnahen boden auf die Mgaufnahme von pflanzen. *J. Plant Nutr. Soil Sci.* 151, 91–96. doi: 10.1002/jpln.19881510205

Senbayram, M., Bol, R., Dixon, L., Fisherd, A., Stevens, C., Quinton, J., et al. (2015). Potential use of rare earth oxides as tracers of organic matter in grassland. *J. Plant Nutr. Soil Sci.* 178, 288–296. doi: 10.1002/jpln.201400465

Strebel, O., and Duynisveld, W. H. M. (1989). Nitrogen supply to cereals and sugar beet by mass flow and diffusion on a silty loam soil. *J. Plant Nutr. Soil Sci.* 152 (2), 135–141. doi: 10.1002/jpln.19891520202

Sturm, A., and Tang, G. Q. (1999). The sucrose-cleaving enzymes of plants are crucial for development, growth and carbon partitioning. *Trends Plant Sci.* 4, 401–407. doi: 10.1016/s1360-1385(99)01470-3

Sun, O. J., and Payn, T. W. (1999). Magnesium nutrition and photosynthesis in *Pinus radiata*: clonal variation and influence of potassium. *Tree Physiol.* 19 (8), 535–540. doi: 10.1093/treephys/19.8.535

Verena, S., Navin, R., and Jonathan, A. F. (2012). Comparing the yields of organic and conventional agriculture. *Nature* 485, 229–232. doi: 10.1038/nature11069

Wang, J., Zhang, H., Xu, F., Xu, F., Zhang, K., and Zhang, Y. (2014). The antagonism of aluminum against fluoride-induced oxidative stress and c-Fos overexpression in rat testes. *Toxicol. Mech. Method.* 26 (2), 132–138. doi: 10.3109/15376516.2013.869779

Welham, T., Pike, J., Horst, I., Flemetakis, E., Katinakis, P., Kaneko, T., et al. (2009). A cytosolic invertase is required for normal growth and cell development in the model legume, *Lotus japonicus*. *J. Exp. Bot.* 60 (12), 3353–3365. doi: 10.1093/jxb/erp169

White, P. J., and Broadley, M. R. (2009). Biofortification of crops with seven mineral elements often lacking in human diets- iron, zinc, copper, calcium, magnesium, selenium and iodine. *New Phytol.* 182, 49–84. doi: 10.1111/j.1469-8137.2008.02738.x

Wilkinson, S. R., Welch, R. M., Mayland, H. F., and Grunes, D. L. (1990). Magnesium in plants: uptake, distribution, function, and utilization by man and animals. In: Siegel, Helmut, (ed.) *Metal Ions in Biological Systems*. (New York and Basel, Switzerland: Marcel Dekker, Inc.). 33–56. https://eprints.nwisrl.ars.usda.gov/id/eprint/776

Winter, H., and Huber, S. C. (2000). Regulation of sucrose metabolism in higher plants: localization and regulation of activity of key enzymes. *Crit. Rev. Biochem. Mol.* 35 (4), 253–289. doi: 10.1080/10409230008984165

Zhang, F. S., Wang, J. Q., Zhang, W. F., Cui, Z. L., Ma, W. Q., Chen, X. P., et al. (2008). Nutrient use efficiencies of major cereal crops in China and measures for improvement. *Acta Pedologica Scienca* 5 (45), 915–924. doi: 10.1163/156939308783122788

Zhu, M., Jiang, X., and Ji, G. (2004). Experimental investigation on aluminum release from haplic acrisols in southeastern China. *Appl. Geochem.* 19, 981–990. doi: 10.1016/j.apgeochem.2003.12.004

Conflict of Interest: The authors declare that the research was conducted in the absence of any commercial or financial relationships that could be construed as a potential conflict of interest.

frontiers in Plant Science

ORIGINAL RESEARCH
published: 30 January 2020
doi: 10.3389/fpls.2019.01797

High- and Low-Affinity Transport in Plants From a Thermodynamic Point of View

Ingo Dreyer[1]* *and Erwan Michard*[2]

[1] Centro de Bioinformática y Simulación Molecular, Facultad de Ingeniería, Universidad de Talca, Talca, Chile, [2] Cell Biology and Molecular Genetics, University of Maryland, College Park, College Park, MD, United States

Plants have to absorb essential nutrients from the soil and do this *via* specialized membrane proteins. Groundbreaking studies about half a century ago led to the identification of different nutrient uptake systems in plant roots. Historically, they have been characterized as "high-affinity" uptake systems acting at low nutrient concentrations or as "low-affinity" uptake systems acting at higher concentrations. Later this "high- and low-affinity" concept was extended by "dual-affinity" transporters. Here, in this study it is now demonstrated that the affinity concept based on enzyme kinetics does not have proper scientific grounds. Different computational cell biology scenarios show that affinity analyses, as they are often performed in wet-lab experiments, are not suited for reliably characterizing transporter proteins. The new insights provided here clearly indicate that the classification of transporters on the basis of enzyme kinetics is largely misleading, thermodynamically in no way justified and obsolete.

Keywords: computational cell biology, dual-affinity transport, high-affinity transport, low-affinity transport, modelling, nutrient transport, plant biophysics

OPEN ACCESS

Edited by:
Francisco Rubio, Spanish National Research Council, Spain

Reviewed by:
Stanley Joseph Miklavcic, University of South Australia, Australia
Igor Pottosin, University of Colima, Mexico

***Correspondence:**
Ingo Dreyer
idreyer@utalca.cl

Specialty section:
This article was submitted to Plant Nutrition, a section of the journal Frontiers in Plant Science

Received: *14 November 2019*
Accepted: *23 December 2019*
Published: *30 January 2020*

Citation:
Dreyer I and Michard E (2020) High- and Low-Affinity Transport in Plants From a Thermodynamic Point of View. Front. Plant Sci. 10:1797. doi: 10.3389/fpls.2019.01797

INTRODUCTION

For more than about half a century the scientific description of nutrient transport in plants has been dominated by the terminology of "high- and low-affinity" transport processes. Historically it goes back to the pioneering work of Emanuel Epstein and co-workers (Epstein et al., 1963). In their groundbreaking study, Epstein and colleagues could resolve two distinct mechanisms of potassium absorption by barley roots. In the absence of knowledge on channels and transporters, the nutrient fluxes were described in analogy to classical enzyme kinetics (Epstein and Hagen, 1952). This theoretical concept employing the Michaelis-Menten equation described the measurement data very satisfactorily and allowed to separate a low concentration uptake mechanism 1 (called "high-affinity") from a high concentration uptake mechanism 2 (called "low-affinity"). From then on, this concept began its triumphal march and was adopted by the scientific community largely without reflection. In the course of the molecular revolution with the cloning and molecular characterization of channels and transporters, it even developed a life of its own. Besides the categorization into either "high-affinity" or "low-affinity" uptake systems (Rodríguez-Navarro and Rubio, 2006; Sharma et al., 2013), some cloned transporters were assigned "dual affinities" (Fu and Luan, 1998; Kim et al., 1998; Liu et al., 1999). It was also suggested that post-translational modifications could switch between the affinity modes (Liu and Tsay, 2003). The "high-affinity/low-affinity" jargon suggests that the transported nutrient binds better

or less well to the respective transporter protein. As a consequence, "high-affinity" transporters are assumed to act better at low concentrations while at higher nutrient concentrations they are saturated in contrast to "low-affinity" transporters.

In this article it will be shown that all these far-reaching interpretations made on the basis of the historical enzyme kinetics concept are incorrect. Here, computationally assisted thought experiments are carried out exemplarily for K^+ channels and proton-coupled K^+ transporters with well-defined properties. H^+-coupled K^+ co-transporters are widely accepted as "high-affinity" transporters (Quintero and Blatt, 1997; Santa-María et al., 1997; Fu and Luan, 1998; Kim et al., 1998); K^+ channels are widely accepted as "low-affinity" transporters (Anderson et al., 1992; Schachtman et al., 1992; Sentenac et al., 1992). Different scenarios show that affinity analyses, as they are often performed in wet-lab experiments, are not suited for reliably characterizing transporter proteins.

METHOD

Mathematical Description of Transporter Activities

Irrespective of the exact transport mechanism, both K^+ channels and proton-coupled K^+ transporters can be considered as diffusion facilitators. A K^+ channel mediates the selective transport of K^+ along the transmembrane electrochemical gradient for potassium, while a 1:1 K^+/H^+ co-transporter allows the flux along the combined K^+/H^+ gradient (Rodriguez-Navarro et al., 1986). In its general form, the current through N open K^+ channels or N active K^+/H^+ transporters can be described by

$$I_X(V) = N \cdot z_X \cdot e_0 \cdot j_X(V) \cdot A \tag{1}$$

where $e_0 \approx 1.602\times10^{-19}C$ is the elementary charge, A the surface of a cross-section of the channel/transporter, z_X the valence of the transport, and $j_X(V)$ the flux density of ions per second per surface unit; X represents the respective transporter type (K, z_K = 1, or K/H, $z_{K/H}$ = 2). The current and the flux density are zero at V_{rev_X}, the voltage at which the electrochemical driving force is zero: $I_X(V_{rev\_X}) = j_X(V_{rev\_X}) = 0$. This fact can be used to simplify equation (1) by its first-order Taylor approximation:

$$\begin{aligned} I_X(V) &\approx I_X(V_{rev\_X}) + (V - V_{rev\_X}) \cdot \tfrac{dI_X(V)}{dV}\big|_{V=V_{rev\_X}} \\ &= g_X \cdot (V - V_{rev\_X}) \end{aligned} \tag{2}$$

with the membrane conductance of the respective transporter type:

$$g_X = N \cdot z_X \cdot e_0 \cdot A \cdot \frac{dj_X(V)}{dV}\big|_{V=V_{rev\_X}} \tag{3}$$

Higher order terms do not contribute significantly [$\sigma^2 \approx 0$], as *e.g.* the linear current-voltage properties of single open ion channels show. Equation (2) describes the current through open channels/transporters. Usually, these transporters are regulated by the environmental conditions, e.g. by the membrane voltage. This dependency can be included by a factor p_X that represents the probability of the channel/transporter being active/open resulting in the conductance G_X:

$$G_X = g_X \cdot p_X \tag{4}$$

At $V = V_{rev\_X}$ the driving energy gradient $\Delta\mu_X$ is zero. $\Delta\mu_X$ is the difference between the electrochemical potentials inside and outside the cell:

$$\Delta\mu_K = RT \cdot \ln\left(\frac{[K^+]_{int}}{[K^+]_{ext}}\right) + F \cdot (\psi_{int} - \psi_{ext}) \tag{5}$$

$$\Delta\mu_{K/H} = RT \cdot \ln\left(\frac{[K^+]_{int}\cdot[H^+]_{int}}{[K^+]_{ext}\cdot[H^+]_{ext}}\right) + 2 \cdot F \cdot (\psi_{int} - \psi_{ext}) \tag{6}$$

Here, $[K^+]_{int}$, $[K^+]_{ext}$, $[H^+]_{int}$, and $[H^+]_{ext}$ are the potassium and proton concentrations inside and outside the cell, respectively, ψ the electric potential ($V = \psi_{int} - \psi_{ext}$), F the Faraday constant, R the gas constant, and T the absolute temperature. At equilibrium ($\Delta\mu_X = 0$), the equilibrium voltages (V_{rev}) of the two transporter types are (Nernst-Equations):

$$V_{rev\_K} = E_K = \frac{RT}{F} \cdot \ln\left(\frac{[K^+]_{ext}}{[K^+]_{int}}\right) \tag{7}$$

$$V_{rev\_K/H} = E_{K/H} = \frac{RT}{2F} \cdot \ln\left(\frac{[K^+]_{ext}\cdot[H^+]_{ext}}{[K^+]_{int}\cdot[H^+]_{int}}\right) \tag{8}$$

Consequently, the transmembrane current *via* potassium channels is represented by:

$$I_K(V) = G_K \cdot \left(V - \frac{RT}{F} \cdot \ln\left(\frac{[K^+]_{ext}}{[K^+]_{\mathrm{int}}}\right)\right) \tag{9}$$

And the current *via* 1:1 proton-coupled potassium transporters is mathematically described by:

$$I_{H/K}(V) = G_{K/H} \cdot \left(V - \frac{RT}{2F} \cdot \ln\left(\frac{[K^+]_{ext}\cdot[H^+]_{ext}}{[K^+]_{\mathrm{int}}\cdot[H^+]_{\mathrm{int}}}\right)\right) \tag{10}$$

The conductances G_K and $G_{K/H}$ are in fact composite parameters [see equations (3–4)], which gather all dependencies on a variety of environmental parameters. Their values may change with the substrate concentration (via p_X) and may show saturation, or they may be regulated by the membrane voltage (via p_X), by gene expression (via N), and/or downstream signaling cascades (via N, p_X). Thus, the equations (9) and (10) cover all biological scenarios for these transporter types in a generalized way.

The action of the H^+-ATPase was mechanistically described by a six-state model (Dreyer, 2017), which is mathematically represented by a sigmoidal function (Gajdanowicz et al., 2011). Under normal physiological conditions (pH_{int} 7.0) an appropriate mathematical description for the dependency on the voltage and $[H^+]_{ext}$ is:

$$I_{pump}(V) = I_{\max} \cdot \frac{1}{1+\frac{[H^+]_{ext}}{100\mu M}} \cdot \frac{1 - \frac{[H^+]_{ext}}{0.1\mu M} \cdot e^{-\left(\frac{F}{RT}\cdot V+12.2\right)}}{1+e^{-\left(\frac{F}{RT}\cdot V+8\right)}+e^{-\left(0.32\cdot\frac{F}{RT}\cdot V+2.5\right)}} \tag{11}$$

Here, I_{max} denotes the maximal current at very positive voltages at low $[H^+]_{ext}$. The pump current amplitude decreases with increasing $[H^+]_{ext}$ and the voltage

$$V_{rev\_pump} = \frac{RT}{F} \cdot \left[\ln\left(\frac{[H^+]_{ext}}{0.1\mu M}\right) - 12.2 \right] \quad (12)$$

at which the energy from ATP-hydrolysis reaches its limit for pumping [$I_{pump}(V_{rev}) = 0$], shifts to less negative values. The numeric values in the equations (11) and (12) are empirical constants to describe the experimentally observed dependencies.

Computational Cell Biology

Following the mathematical description of all transporters, an *in silico* cellular system was programmed and computational cell biology (dry-laboratory) experiments were performed using the VCell Modeling and Analysis platform developed by the National Resource for Cell Analysis and Modeling, University of Connecticut Health Center (Loew and Schaff, 2001).

Michaelis-Menten Kinetics

To the present day, transport processes in plants are often described with the Michaelis-Menten kinetics developed for enzyme-catalyzed reactions. The reaction scheme

$$E + S \underset{k_2}{\overset{k_1}{\rightleftarrows}} ES \underset{k_4}{\overset{k_3}{\rightleftarrows}} E + P$$

is interpreted in the way that E is the free transporter, ES is the transporter with the bound nutrient, S is the transported nutrient at one side of the membrane (e.g. $S = [K^+]_{ext}$), and P the nutrient at the other side (e.g. $P = [K^+]_{int}$). In equilibrium ($\frac{dES}{dt} = \frac{dE}{dt} = 0$) the flux from the external to the internal medium is given by:

$$J = N \cdot \frac{k_1 \cdot k_3 \cdot [K^+]_{ext} - k_2 \cdot k_4 \cdot [K^+]_{int}}{k_2 + k_3 + k_1 \cdot [K^+]_{ext} + k_4 \cdot [K^+]_{int}} \quad (13)$$

Equation (13) is applied in plant biology almost exclusively with the approximation $k_4 \approx 0$-irrespective of the fact that this approximation is incompatible with the Nernst-Equation – yielding a Michaelis-Menten-type equation:

$$J \approx J_{max} \cdot \frac{[K^+]_{ext}}{K_m + [K^+]_{ext}} \quad (14)$$

with $J_{max} = N \times k_3$ and $K_m = (k_2 + k_3)/k_1$. In affinity analyses, equation (14) is employed alone or as a sum of two components, a "high-affinity" and a "low-affinity" component:

$$J = J_{max,high} \cdot \frac{[K^+]_{ext}}{K_{m,high} + [K^+]_{ext}} + J_{max,low} \cdot \frac{[K^+]_{ext}}{K_{m,low} + [K^+]_{ext}} \quad (15)$$

RESULTS

Apparent Affinities Can Be an Artifact of Data Display

Affinity analyses can be full of pitfalls. To illustrate this, a common voltage-clamp experiment as it can be found often in literature to characterize plant transporters has been computationally simulated: The currents flowing through a K^+ channel or a K^+/H^+ co-transporter were measured at a fixed membrane voltage with a constant internal K^+ concentration ($[K^+]_{int}$ = 100mM) under varying external K^+. In the simulations, K^+ channels and K^+/H^+ transporters were chosen that do *not* change their conductance with $[K^+]_{ext}$, *i.e.* G_K and $G_{K/H}$ are K^+-*in*dependent and have both the same constant value. Nevertheless, the "current vs. $[K^+]_{ext}$ display" suggests an apparent K^+-affinity of the K^+ channel of K_m = 1.7mM (**Figure 1A**) and of the K^+/H^+ co-transporter of K_m = 0.29mM (**Figure 1C**) when analyzed with the Michaelis-Menten formalism. Surprisingly, when displaying the same data in a different manner, both could be assigned even an apparent dual affinity. The K^+ channel was now characterized by a high-affinity component of K_m = 0.2mM and a low-affinity component of K_m = 7.3mM (**Figure 1B**), while the K^+/H^+ co-transporter had a high-affinity component of K_m = 0.01mM and a low-affinity component of K_m = 2.3mM (**Figure 1D**).

It should be emphasized again that in the simulation both, K^+ channel and K^+/H^+ co-transporter, are *in*dependent of $[K^+]_{ext}$. In fact, the apparent affinities originate from the $[K^+]_{ext}$-dependent change in V_{rev} [equations (7-10)]. If the data were displayed on a log-$[K^+]_{ext}$ scale they could be described by straight lines representing linear functions of the type $I = A + B \times \ln([K^+]_{ext})$ (**Figures 1E, F**). Were these curves presented in different linear intervals, as done in affinity analyses, several seemingly saturating affinity curves could be separated (**Figure 1G**). Thus, the K_m values obtained from the affinity analyses are artifacts of the data display and have no significant meaning.

Consequently, a similar K_m-analysis of real channels or transporters (with real experimental data) is meaningless and might be largely misguiding. Still, the simulations show that there are differences between the K^+ channel and the K^+/H^+ co-transporter. The apparent K_m-values, albeit misleading and without special meaning, are always smaller for the co-transporter than for the channel, despite the fact that $G_K = G_{K/H}$. The K_m-analysis is therefore a wrongly used tool that yet allows a distinction between the transporter types. Nevertheless, the widely used classification into "high-affinity" (= low K_m values) and "low-affinity" (= high K_m values) transporters becomes untenable (Dreyer, 2017) due to these new insights. They further raise the question, what is then the real difference between the K^+ transporter types from a biophysical and physiological point of view, if it is not the affinity of the proteins towards K^+?

The Features of the Proton Pump Lead to Believe in High- and Low-Affinity K^+ Transport

To assess the former question, another thought experiment has been carried out with the K^+-independent K^+ channel and K^+/H^+ co-transporter. This time the transporters were combined with a H^+-ATPase (**Figure 2A**), which energizes the K^+-uptake (**Figures 2B, C**), in order to approach further the physiological conditions and to simulate common K^+ uptake experiments. The concentrations ($[H^+]_{int}$, $[K^+]_{int}$, $[H^+]_{ext}$, $[K^+]_{ext}$) were kept constant and the membrane voltage was allowed to relax freely until a stabile equilibrium has been established. This occurred

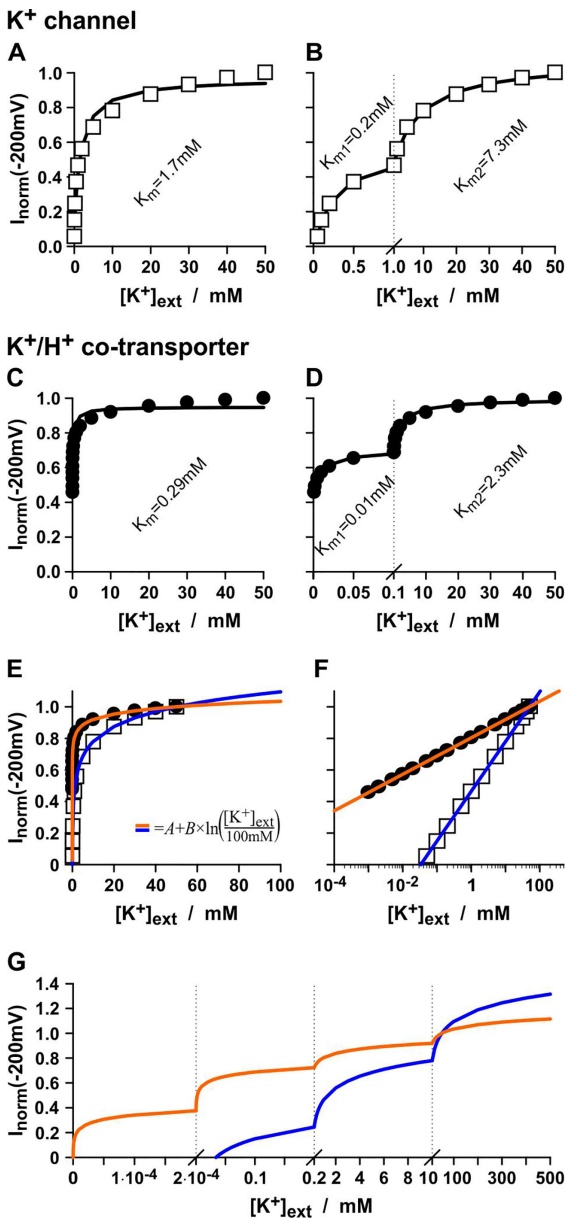

FIGURE 1 | The pitfalls of affinity analyses. Same data, different display = different affinities? Simulated experiments with a K^+-independent K^+ channel **(A, B)** and a K^+-independent K^+/H^+ 1:1 co-transporter **(C, D)**. Channel/transporter-mediated currents were determined at V = -200 mV with $[K^+]_{int}$ = 100 mM, pH_{int} = 7.0, pH_{ext} = 5.0 at varying $[K^+]_{ext}$. Currents were normalized to the values obtained with $[K^+]_{ext}$ = 50 mM. The same data were displayed linearly in the interval from 0 to 50 mM **(A, C)**, linearly split into the intervals from 0 to 1 mM and from 1 to 50 mM **(B)**, and linearly split into the intervals from 0 to 0.1 mM and from 0.1 to 50 mM **(D)**. The solid lines represent best fits with a Michaelis-Menten-equation [equation (14)] in the respective interval with the indicated K_m-values. **(E, F)** Fit of the data from A and C with logarithmic functions of the type $I = A+B\times\ln([K^+]_{ext}/100mM)$. For the K^+ channel (*white squares*) the fit parameters were A = 1.095 and B = 0.137 (*blue line*), while for the K^+/H^+ 1:1 co-transporter (black dots) the parameters were A = 1.035 and B = 0.05 (*orange line*). **(G)** Split-display of the fit curves from E and F in linear intervals (i) from 0 to 0.2 μM, (ii) from 0.2 μM to 0.2 mM, (iii) from 0.2 mM to 10 mM, and (iv) from 10 mM to 500 mM.

almost instantaneously within a few milliseconds. In this condition, the pumped protons compensate electrically the fluxes through the K^+-transporters. The magnitude of the steady-state fluxes depends on the ionic conditions on both sides of the membrane.

In a first experiment, the dependency of the steady state K^+ fluxes on the external potassium concentration was screened (**Figure 2D**). For both transporter modules, hyperbolic curves were obtained that saturated for the K^+/H^+ transporter at smaller $[K^+]_{ext}$ than for the K^+ channel. This result fueled again the interpretation that the K^+/H^+ transporter was a "high-affinity" transporter while the K^+ channel was a "low-affinity" transporter, despite the fact that both were K^+-*in*dependent in the thought experiment. However, also these data could be displayed as in **Figures 1B, D** in two different concentration intervals and would characterize both as "dual-affinity" K^+ transporters (not shown).

The concept of "high- and low-affinity K^+ transport" got more cracks in the analysis of the dependency of the K^+ fluxes on the external proton concentration. In contrast to the proton-coupled K^+ transport *via* the K^+/H^+ co-transporter, the flux through the K^+ channel should actually be independent of $[H^+]_{ext}$. However, this was not the case. Instead, the channel-mediated K^+ flux declined with increasing $[H^+]_{ext}$ (**Figure 2E**). The K^+ flux through the K^+/H^+ 1:1 co-transporter showed a bi-phasic behavior: as pH_{ext} dropped from 7.0 to 5.5, the K^+ flux increased slightly, while it decreased as the pH level dropped further. Thus, the K^+ fluxes are not determined by the activity of the K^+ transporters, alone.

Indeed, an in-depth analysis revealed that the apparent affinities are in fact not a feature of the K^+-transporters but were introduced into the system by the voltage- and pH-dependency of the H^+-ATPase. This became evident when replacing the physiological proton pump by a mechanical motor that is independent of the membrane voltage and the proton concentrations on both sides of the membrane (**Figures 2F–J**). The mechanical motor exported always the same number of protons per time irrespective of the voltage, pH_{ext} and pH_{int} (**Figure 2F**). The replacement of the pump eliminated the hyperbolic K^+-uptake kinetics for both transporter types (**Figures 2I, J**). The K^+ fluxes were independent of changes in $[K^+]_{ext}$ and $[H^+]_{ext}$, as it should be expected for transporters with $[K^+]$- and $[H^+]$-independent conductances, G_K and $G_{K/H}$.

Thus, K^+ flux measurements in our thought experiments as well as those in real wet-lab experiments are strongly influenced by the properties of the energizing proton-pump. The assigned affinities are therefore strongly misguiding and without any significant meaning for the K^+ transporter proteins.

The Real Difference Between K^+ Channels and K^+/H^+ Co-Transporters

The experiments presented in **Figure 2** were carried out with identical transporter conductances: $G_K = G_{K/H}$. That is why it is all the more amazing that the K^+/H^+ co-transporter transports just half the number of K^+ ions per time-interval than the K^+ channel (**Figures 2I, J**), despite the same energizing power source. Additionally, both modules, "pump & K^+ channel"

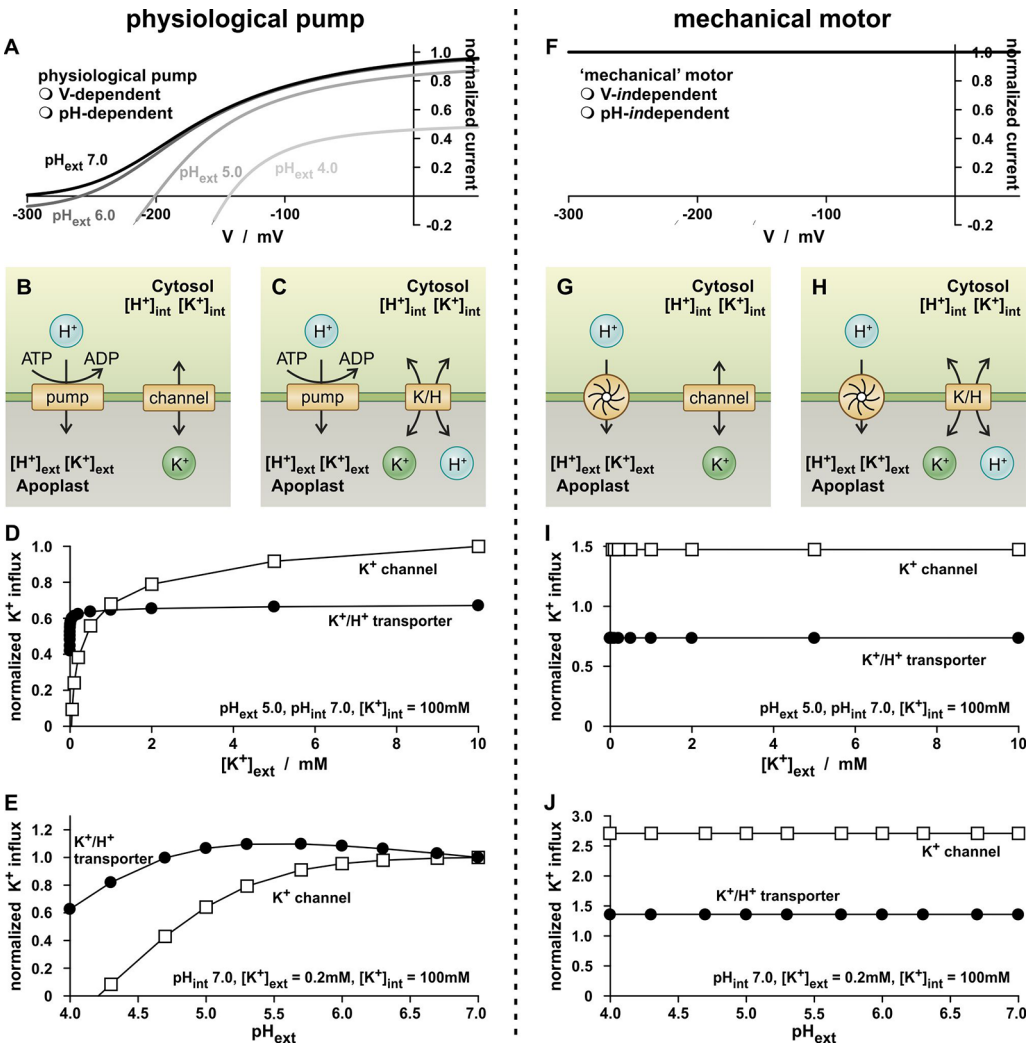

FIGURE 2 | Simple physiological K^+-uptake circuits. **(A–E)** K^+-uptake circuits fueled by a physiological proton ATPase. **(A)** As a consequence of the pump cycle driven by the energy from ATP hydrolysis, the activity of the proton pump inevitably depends on the membrane voltage (V) and the proton concentrations on both sides of the membrane. Shown is the current-voltage characteristic of the pump current [equation (11)] for pH_{int} 7.0 and four different pH_{ext} values. **(B, C)** Schematic representation of two simple K^+-uptake modules. A (pH- and voltage-dependent) proton pump energizes the uptake of potassium *via* a K^+ channel **(B)** and *via* a K^+/H^+ 1:1 co-transporter **(C)**. **(D, E)** Dependency of the K^+ flux mediated by the two modules on the external K^+ concentration **(D)** and on the external pH **(E)**. Please note that for both modules, the environmental conditions were the same and $G_K = G_{K/H}$. The observed differences thus result from the different transport mechanisms of the channel/transporter. Flux values were normalized to the K^+ flux mediated by the channel based module at $[K^+]_{ext}$ = 10 mM **(D)**, and pH_{ext} 7.0 **(E)**. **(F–J)** K^+-uptake circuits fueled by a voltage- and pH-*in*dependent proton motor. **(F)** The mechanical motor is independent of the voltage and the pH. **(G, H)** Schematic representation of two simple K^+-uptake modules. A mechanical proton motor energizes the uptake of potassium *via* a K^+ channel **(G)** and *via* a K^+/H^+ 1:1 co-transporter **(H)**. **(I, J)** Dependency of the K^+ flux mediated by the two modules on the external K^+ concentration **(I)** and on the external pH **(J)**. Please note that for both modules, the environmental conditions were the same and $G_K = G_{K/H}$. The observed differences thus result from the different transport mechanisms of the channel/transporter.

(**Figures 2B, G**) and "pump & K^+/H^+ co-transporter" (**Figures 2C, H**), do not differ in their net transfer ratios: both exchange 1 H^+ for 1 K^+. However, and this is the real crucial difference between the two modules, the K^+/H^+ co-transporter-based module pumped twice the number of protons per accumulated K^+ (Rodriguez-Navarro et al., 1986) than the K^+ channel-based module (**Figure 3**). Thus, the uptake of a K^+ ion *via* the "pump & K^+/H^+ co-transporter" module consumed the hydrolysis of 2 ATP molecules, while the uptake *via* the "pump & K^+ channel" module costed only 1 ATP molecule (**Figures 3C, D**).

The advantage of the channel-based module was the "cheap" accumulation of K^+; its disadvantage was its operating limit at low $[K^+]_{ext}$ and high $[H^+]_{ext}$. To enable K^+ uptake by a K^+ channel, the membrane voltage needed to be more negative than E_K, the equilibrium voltage for potassium [equation (7)], which depends on $[K^+]_{ext}$. For a 10-fold decrease in $[K^+]_{ext}$, E_K dropped

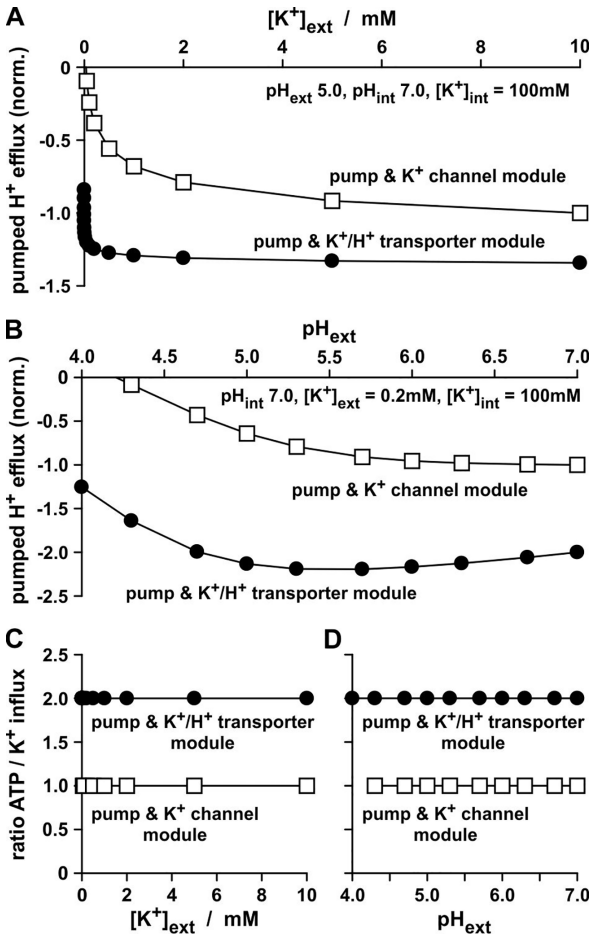

FIGURE 3 | Proton pump activity during K^+-uptake. **(A, B)** H^+ flux *via* the pump measured in the *in-silico* K^+-uptake experiments presented in Fig. 2D and E. The H^+ fluxes were normalized to the K^+ flux values measured for the channel-based module at $[K^+]_{ext}$ = 10 mM **(A)**, and pH_{ext} 7.0 **(B)**. The negative values indicate H^+ effluxes in contrast to the K^+ influxes presented in Fig. 2D and E. **(C, D)** For each pumped proton an ATP molecule has be to hydrolyzed. Ratios of the consumed ATP molecules per accumulated K^+ ion in the *in-silico* experiments presented in **Figures 2D, E** and **3 (A, B)**. To calculate the ratios, the absolute values of the data displayed in **(A)** were divided by the corresponding data from **Figure 2D** and the absolute values of the data displayed in **(B)** were divided by the corresponding data from **Figure 2E**.

by about 59 mV. Such a negative voltage could be established by the H^+-ATPase if the energy from ATP-hydrolysis was sufficient to pump protons against their electrochemical gradient out of the cell. The higher $[H^+]_{ext}$ was, however, the more difficulties the pump had to establish a sufficiently negative V (**Figure 2A**). As a consequence of both effects, the channel-based module reached the energy limit for K^+ uptake already at moderate conditions (**Figure 4A**). In contrast, the co-transporter-based module still operated as a K^+ uptake system under these conditions (**Figure 4B**). The reason was the coupling of the K^+- and the H^+-gradient. The equilibrium voltage of the K^+/H^+ 1:1 co-transporter [$E_{K/H}$, equation (8)] dropped only by about 29.5 mV for a 10-fold decrease in $[K^+]_{ext}$. Additionally, $E_{K/H}$ raised with increasing $[H^+]_{ext}$ which partially compensated the detrimental effect of $[H^+]_{ext}$ on the pump. Thus, the real difference between K^+ channels and K^+/H^+ co-transporters is not their affinity towards K^+ rather than the energization of the transport process.

DISCUSSION

Solidly based thought experiments have an inestimable value in gaining new insights. They allow, for instance, to test conditions that are hard to achieve in conventional wet-laboratory experiments. In the present study, different K^+ uptake systems were tested which were absolutely certain not to be dependent on $[K^+]$. With these transporters the half-century old concept of "high- and low-affinity uptake systems" has been challenged in computer-aided dry laboratory experiments. Interestingly, the results of the experiment-mimicking simulations mirrored those obtained in wet-lab experiments with hyperbolic curves that saturated for the K^+/H^+ co-transporter at smaller $[K^+]_{ext}$ than for the K^+ channel. The usual interpretation of such a result is that the co-transporter is a "high-affinity uptake system" while the K^+ channel is a "low-affinity uptake system". The fact that in the simulations channel and co-transporter had both the same affinity towards $[K^+]_{ext}$ clearly shows the absurdity of such an interpretation. Actually, the assigned affinities are not characteristics of the investigated transporters, but depend on several external parameters instead.

The equations (9) and (10) cover the mathematical description of the entire biological range of K^+ channels and K^+/H^+ 1:1 co-transporters. The parameters G_K and $G_{K/H}$, respectively, provide individual channels/transporters with their unique particular flair. The experimental characterization of channels and transporters in the wet-lab usually aims at getting knowledge about these parameters and their dependency on environmental conditions. Here, we carried out simulations with idealized transporters with conductances G_K and $G_{K/H}$ that did not depend on any environmental parameter. But even in this simplest case, the features of G_K and $G_{K/H}$ could only be resolved in artificial conditions (**Figures 2F–J**). In all other dry-lab experiments mimicking conventional wet-lab experiments artifactual affinities were assigned to the transporters. In real experiments the conductance of a transporter might depend on a variety of environmental parameters. The value may change with the substrate concentration and may show saturation, or it may be regulated by the membrane voltage, by gene expression and/or downstream signaling cascades. The presented simulations indicate that all these dependencies cannot be reliably resolved in affinity analyses.

The original "high- and low-affinity concept" proves to be largely misleading. Its further evolution to "dual-affinity", however, is an even more serious aberration. The examples presented in **Figure 1** illustrate clearly that an apparent "dual-affinity" can be "generated" just by a different display of the same data. Worse still, by further fragmentation of the x-axis it is

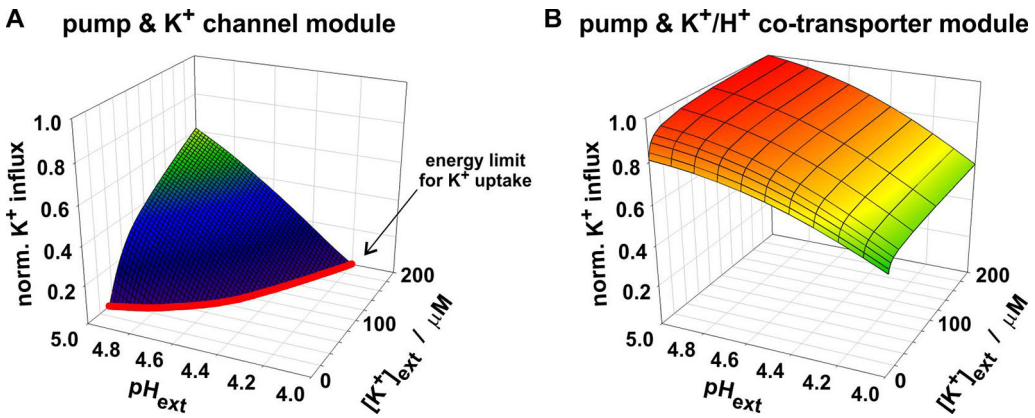

FIGURE 4 | Dependency of the two compared K^+ uptake modules on $[K^+]_{ext}$ and $[H^+]_{ext}$. Both modules mediate the net-antiport of K^+ and H^+ across the membrane. The module of proton pump and K^+ channel **(A)** reaches its energy limit (*red line*) at conditions in which the co-transporter-based module still allows K^+ uptake **(B)**. At very low $[K^+]_{ext}$ and/or high $[H^+]_{ext}$ the energy from ATP-hydrolysis is not sufficient anymore to energize the combined K^+-uptake/H^+-release *via* the pump & K^+ channel module.

possible to fake even a "triple or quadruple-affinity" (**Figure 1G**). Thus, the affinity analyses, as they are often performed in wet-lab experiments, are not suited for reliably characterizing transporter proteins. The classification of transporters on the basis of enzyme kinetics is largely misleading and obsolete.

DATA AVAILABILITY STATEMENT

All datasets generated for this study are included in the article/supplementary material.

AUTHOR CONTRIBUTIONS

ID conceived the project and prepared the original draft. EM and ID had intellectual input on the project and prepared the final manuscript.

FUNDING

This work was supported partially by the Fondo para Proyectos de Investigación Enlace Fondecyt of the Universidad Talca to ID.

REFERENCES

Anderson, J. A., Huprikar, S. S., Kochian, L. V., Lucas, W. J., and Gaber, R. F. (1992). Functional expression of a probable Arabidopsis thaliana potassium channel in Saccharomyces cerevisiae. *Proc. Natl. Acad. Sci. U. S. A.* 89, 3736–3740. doi: 10.1073/pnas.89.9.3736

Dreyer, I. (2017). Plant potassium channels are in general dual affinity uptake systems. *AIMS Biophys.* 4, 90–106. doi: 10.3934/biophy.2017.1.90

Epstein, E., and Hagen, C. E. (1952). A kinetic study of the absorption of alkali cations by barley roots. *Plant Physiol.* 27, 457–474. doi: 10.1104/pp.27.3.457

Epstein, E., Rains, D. W., and Elzam, O. E. (1963). Resolution of dual mechanisms of potassium absorption by barley roots. *Proc. Natl. Acad. Sci. U. S. A.* 49, 684–692. doi: 10.1073/pnas.49.5.684

Fu, H. H., and Luan, S. (1998). AtKuP1: a dual-affinity K+ transporter from Arabidopsis. *Plant Cell.* 10, 63–73. doi: 10.1105/tpc.10.1.63

Gajdanowicz, P., Michard, E., Sandmann, M., Rocha, M., Corrêa, L. G. G., Ramírez-Aguilar, S. J., et al. (2011). Potassium (K+) gradients serve as a mobile energy source in plant vascular tissues. *Proc. Natl. Acad. Sci. U. S. A.* 108, 864–869. doi: 10.1073/pnas.1009777108

Kim, E. J., Kwak, J. M., Uozumi, N., and Schroeder, J. I. (1998). AtKUP1: an Arabidopsis gene encoding high-affinity potassium transport activity. *Plant Cell.* 10, 51–62. doi: 10.1105/tpc.10.1.51

Liu, K.-H., and Tsay, Y.-F. (2003). Switching between the two action modes of the dual-affinity nitrate transporter CHL1 by phosphorylation. *EMBO J.* 22, 1005–1013. doi: 10.1093/emboj/cdg118

Liu, K. H., Huang, C. Y., and Tsay, Y. F. (1999). CHL1 is a dual-affinity nitrate transporter of Arabidopsis involved in multiple phases of nitrate uptake. *Plant Cell.* 11, 865–874. doi: 10.1105/tpc.11.5.865

Loew, L. M., and Schaff, J. C. (2001). The virtual cell: a software environment for computational cell biology. *Trends Biotechnol.* 19, 401–406. doi: 10.1016/S0167-7799(01)01740-1

Quintero, F. J., and Blatt, M. R. (1997). A new family of K + transporters from Arabidopsis that are conserved across phyla. *FEBS Lett.* 415, 206–211. doi: 10.1016/S0014-5793(97)01125-3

Rodríguez-Navarro, A., and Rubio, F. (2006). High-affinity potassium and sodium transport systems in plants. *J. Exp. Bot.* 57, 1149–1160. doi: 10.1093/jxb/erj068

Rodríguez-Navarro, A., Blatt, M. R., and Slayman, C. L. (1986). A potassium-proton symport in Neurospora crassa. *J. Gen. Physiol* 87, 649–674. doi: 10.1085/jgp.87.5.649

Santa-María, G. E., Rubio, F., Dubcovsky, J., and Rodríguez-Navarro, A. (1997). The HAK1 gene of barley is a member of a large gene family and encodes a high-affinity potassium transporter. *Plant Cell.* 9, 2281–2289. doi: 10.1105/tpc.9.12.2281

Schachtman, D. P., Schroeder, J. I., Lucas, W. J., Anderson, J. A., and Gaber, R. F. (1992). Expression of an inward-rectifying potassium channel by the Arabidopsis KAT1 cDNA. *Science* 258, 1654–1658. doi: 10.1126/science.8966547

Sentenac, H., Bonneaud, N., Minet, M., Lacroute, F., Salmon, J. M., Gaymard, F., et al. (1992). Cloning and expression in yeast of a plant potassium ion transport system. *Science* 256, 663–665. doi: 10.1126/science.1585180

Sharma, T., Dreyer, I., and Riedelsberger, J. (2013). The role of K+ channels in uptake and redistribution of potassium in the model plant Arabidopsis thaliana. *Front. Plant Sci.* 4, 224. doi: 10.3389/fpls.2013.00224

Conflict of Interest: The authors declare that the research was conducted in the absence of any commercial or financial relationships that could be construed as a potential conflict of interest.

frontiers in Plant Science

MINI REVIEW
published: 11 February 2020
doi: 10.3389/fpls.2020.00044

Calcium-Regulated Phosphorylation Systems Controlling Uptake and Balance of Plant Nutrients

Shunya Saito * *and Nobuyuki Uozumi* *

Department of Biomolecular Engineering, Graduate School of Engineering, Tohoku University, Sendai, Japan

Essential elements taken up from the soil and distributed throughout the whole plant play diverse roles in different tissues. Cations and anions contribute to maintenance of intracellular osmolarity and the formation of membrane potential, while nitrate, ammonium, and sulfate are incorporated into amino acids and other organic compounds. In contrast to these ion species, calcium concentrations are usually kept low in the cytosol and calcium displays unique behavior as a cytosolic signaling molecule. Various environmental stresses stimulate increases in the cytosolic calcium concentration, leading to activation of calcium-regulated protein kinases and downstream signaling pathways. In this review, we summarize the stress responsive regulation of nutrient uptake and balancing by two types of calcium-regulated phosphorylation systems: CPK and CBL-CIPK. CPK is a family of protein kinases activated by calcium. CBL is a group of calcium sensor proteins that interact with CIPK kinases, which phosphorylate their downstream targets. In *Arabidopsis*, quite a few ion transport systems are regulated by CPKs or CBL-CIPK complexes, including channels/transporters that mediate transport of potassium (KAT1, KAT2, GORK, AKT1, AKT2, HAK5, SPIK), sodium (SOS1), ammonium (AMT1;1, AMT1;2), nitrate and chloride (SLAC1, SLAH2, SLAH3, NRT1.1, NRT2.4, NRT2.5), and proton (AHA2, V-ATPase). CPKs and CBL-CIPKs also play a role in C/N nutrient response and in acquisition of magnesium and iron. This functional regulation by calcium-dependent phosphorylation systems ensures the growth of plants and enables them to acquire tolerance against various environmental stresses. Calcium serves as the key factor for the regulation of membrane transport systems.

Keywords: nutrition, calcium, membrane transport, *Arabidopsis thaliana*, ion homeostasis

OPEN ACCESS

Edited by:
Francisco Rubio,
Spanish National Research Council, Spain

Reviewed by:
Isabelle Chérel,
Institut National de la Recherche Agronomique (INRA), France
Ingo Dreyer,
University of Talca, Chile

***Correspondence:**
Shunya Saito
shunya.saito@tohoku.ac.jp
Nobuyuki Uozumi
uozumi@tohoku.ac.jp

Specialty section:
This article was submitted to Plant Nutrition, a section of the journal Frontiers in Plant Science

Received: *05 November 2019*
Accepted: *14 January 2020*
Published: *11 February 2020*

Citation:
Saito S and Uozumi N (2020) Calcium-Regulated Phosphorylation Systems Controlling Uptake and Balance of Plant Nutrients. Front. Plant Sci. 11:44. doi: 10.3389/fpls.2020.00044

INTRODUCTION

Plants require various ions as essential nutrients, which are taken up from the soil and distributed throughout the whole plant (Welch, 1995; Merchant, 2010; Grusak et al., 2016). Each of these nutrients, once they are transferred to their destination within plant tissues *via* corresponding transporters/ion channels, plays diverse and critical roles in maintaining plant growth. Potassium, nitrate, and chloride contribute to maintenance of intracellular osmolarity, enabling control of cell turgor pressure which is crucial for cell expansion, stomatal movement, and pollen tube growth (Kroeger et al., 2011; Saito and Uozumi, 2019). Nitrate, ammonium, sulfate, and phosphorus are

metabolized to produce various proteins and organic compounds (Leustek and Saito, 1999; López-Arredondo et al., 2013; López-Arredondo et al., 2014). Metal ions such as iron (Balk and Schaedler, 2014), manganese (Schmidt et al., 2016; Schmidt and Husted, 2019), magnesium (Gerendás and Führs, 2013), zinc (Broadley et al., 2007) and molybdenum (Mendel, 2013) work as essential cofactors for enzyme activity.

Among these essential nutrient ions, calcium exhibits some unique behaviors. In contrast to other macronutrient ions, such as potassium, for which the cellular concentration is normally in the range of 80 to 100 mM, calcium concentrations are usually relatively low and kept around 0.1 μM in the cytosol (Bush, 1995; Walker et al., 1996; Sanders et al., 1999; Hepler, 2005). However, when plants are exposed to environmental stresses such as drought, saline soil, pathogens, wounding, or nutrient deficiency, a rapid increase of the cytosolic calcium concentration occurs, either as a result of Ca^{2+} import *via* plasma membrane ion channels or Ca^{2+} release from intracellular calcium stores (Steinhorst and Kudla, 2013b; Zhu, 2016; Manishankar et al., 2018; Toyota et al., 2018). This leads to activation of calcium-regulated protein kinases, initiation of downstream phosphorylation signaling, and finally, achievement of stress resistance resulting from an activation of stress responsive genes or adjustment of ion channel activity. Ca^{2+}-regulated proteins which play a key role in this phosphorylation process can be divided into three major groups: Calcium dependent protein kinases (CPK), CPK-related protein kinases (CRK), and Calcineurin-B like proteins (CBL). CPK is a family of Ser/Thr kinases containing a calcium binding site (EF hand) in their C-terminal region. Binding of Ca^{2+} to the EF hand stimulates a conformational change, thus allowing autophosphorylation of the kinase (Hashimoto and Kudla, 2011; Schulz et al., 2013). There are 34 CPK members in the *Arabidopsis* genome, and over half of these have been functionally characterized (Kudla et al., 2010; Boudsocq and Sheen, 2013; Shi et al., 2018; Saito and Uozumi, 2019). CRKs, on the other hand, were recently shown to be able to phosphorylate Tyr residues (Nemoto et al., 2015). The function of only two of eight CRK members in *Arabidopsis* has been analyzed so far (Rigó et al., 2013; Baba et al., 2018). CBL differs from the other two groups with regard to CBL itself being a Ca^{2+} sensor protein but not a kinase. Ca^{2+}-bound and activated CBL interacts with another group of kinases called CBL-interacting protein kinases (CIPK), thereby enhancing CIPK autophosphorylation and recruitment to their target proteins (Batistic et al., 2008; Batistič and Kudla, 2009; Mao et al., 2016). Ten members of CBL and 26 members of CIPK exist in the *Arabidopsis* genome, each has a unique expression and subcellular localization profile. Together they form a specific interaction network, allowing regulation of genes and ion channels in various locations (Mahajan et al., 2006; Steinhorst and Kudla, 2013b; Manik et al., 2015; Manishankar et al., 2018; Saito and Uozumi, 2019). In this review, we focus on the stress responsive regulation of nutrient uptake and balancing by CPK and CBL-CIPK.

Calcium-Dependent Import of Potassium and Anions—Regulator of Intracellular Osmolarity

Potassium (K^+) is the most abundant ion in plant cells. As a soluble ion, it plays a critical role in adjusting cellular osmolarity, membrane electric potential, or intracellular pH (Almeida et al., 2017; Ragel et al., 2019). These processes are important for the regulation of cell expansion, which is a prerequisite for plant growth and stomatal movement. Other ion species that contribute to this regulation are nitrate (NO_3^-) and chloride (Cl^-). These anions work synergistically with K^+ in the regulation of guard cell turgor pressure, and ultimately the control of stomatal aperture. K^+, NO_3^-, and Cl^- fluxes across the plasma membrane of pollen tubes are also essential for its growth (Mouline et al., 2002; Wu et al., 2011; Gutermuth et al., 2013; Liu et al., 2016).

Early studies proposed a correlation between cytosolic calcium and the uptake of potassium in a variety of plant species (Hirata and Mitsui, 1965; Johansen et al., 1968; Rains and Floyd, 1970). Indeed, it has been reported that K^+ deficiency induces rapid Ca^{2+} increase in *Arabidopsis* roots (Behera et al., 2016). In *Arabidopsis* root cells, K^+ uptake from the soil and export to the xylem are orchestrated by several types of transporters. Main contributors to root K^+ uptake are the Shaker-type K^+ channel AKT1 and the KT/KUP/HAK type transporter HAK5 (Pyo et al., 2010; Rubio et al., 2010; Alemán et al., 2011). The activity of these two K^+ transport systems depends on CBL1 (or CBL9) and CIPK23 (Xu et al., 2006; Lee et al., 2007; Ragel et al., 2015). When cytosolic Ca^{2+} increases, activated CBL1/9 interacts with and recruits CIPK23 to the plasma membrane, enabling it to activate AKT1 and HAK5. Another CBL member, CBL10, is capable of CIPK-independent negative regulation of AKT1 activity, suggesting a role in maintaining balance of K^+ uptake (Ren et al., 2013). CIPK9, most likely paired with CBL2 or CBL3, also regulates K^+ homeostasis under low K^+ conditions *via* phosphorylation of a yet unknown target (Pandey et al., 2007a; Liu et al., 2012b; Singh et al., 2018). In addition, members of the cyclic-nucleotide gated channel family CNGC3, CNGC10, and CNGC13 (Kaplan et al., 2007; Caballero et al., 2012; Ragel et al., 2019), and the cation-proton antiporter CHX13 (Zhao et al., 2008) have also been reported to mediate K^+ flux into root cell. Activity of these CNGCs might be regulated by Ca^{2+}-activated calmodulin binding and resulting blocking of the cyclic-nucleotide binding domain (Kaplan et al., 2007; DeFalco et al., 2016; Pan et al., 2019). K^+ uptake by AKT1 and HAK5 is also conserved in rice, although systems corresponding to CNGCs and CHX remain to be identified in rice (Ragel et al., 2019). Increase of the K^+ concentration in root stellar cell enables drive of K^+ into the xylem mediated by the Shaker-type K^+ efflux channel SKOR, followed by translocation of K^+ to the shoot (Liu et al., 2006; Ragel et al., 2019).

In contrast to its role connected to potassium, the role of calcium as a second messenger for the nitrate response was only recently discovered (Riveras et al., 2015). Nitrate uptake and distribution throughout the plant is mainly mediated by members of the nitrate transporter (NRT) or nitrate transporter 1/peptide transporter (NPF) family (Léran et al., 2014). In *Arabidopsis* roots, NRT2.1/2.2/2.4/2.5 and NPF2.3/4.6/6.3 are responsible for NO_3^- uptake and translocation (Taochy et al., 2015; Noguero and Lacombe, 2016; Xuan et al., 2017; Zhao et al., 2018a). Among these transporters, NPF6.3, also known as NRT1.1 or CHL1, is well studied and considered a major contributor to NO_3^- transport (Léran et al., 2013; Leran et al., 2015; Undurraga et al., 2017). NPF6.3 is characterized as a dual affinity bidirectional NO_3^- transporter. This unique transporter switches its affinity from low-affinity to high-affinity mode by dimerization, which is controlled by phosphorylation of Thr101 by CBL1/9-CIPK23 (Liu and Tsay, 2003; Ho et al., 2009; Parker and Newstead, 2014; Sun et al., 2014). Two other members of CBL-CIPK are also involved in regulation of NRT/NPF. CIPK8 plays a role in the nitrate response by influencing the expression level of several nitrate-responsive genes including NPF6.3 and NRT2.1 (Hu et al., 2009). CBL7, on the other hand, was shown to regulate the expression levels of NRT2.4 and NRT2.5 (Ma et al., 2015). Other than NRT/NPF, two homologues of the guard cell S-type anion channel SLAC1, SLAH2 and SLAH3, are also suggested to mediate xylem loading of NO_3^- (Maierhofer et al., 2014a; Maierhofer et al., 2014b). Activation of these two SLAHs is also dependent on CBL1/9-CIPK23, and in addition, several members of the CPK family, such as CPK21 (Maierhofer et al., 2014a; Maierhofer et al., 2014b; Yao et al., 2017). Some members of the NRT/NPF or SLAH family are capable of transporting other ion species as well. NRT1.5/NPF7.3 can mediate K^+ and NO_3^- loading into the xylem, working synergistically with SKOR to maintain K^+/NO_3^- balance in root and shoot (Lin et al., 2008; Drechsler et al., 2015; Li et al., 2017b). Another NPF member, NPF2.4, is responsible for Cl^- loading into the xylem (Li et al., 2016). SLAH1, a silent channel subunit expressed together with SLAH3 in xylem-pole pericycle cells, mediates root to shoot Cl^- translocation by forming a heteromer with SLAH3 (Cubero-Font et al., 2016; Qiu et al., 2016).

Once imported into the xylem, K^+ travels long-distance from root to shoot to be exported into appropriate aerial tissues. In addition, K^+ can be transported from green cells into the phloem to be returned back to the roots. Detailed mechanism of this root-shoot translocation of K^+ still remains ambiguous, although transporters which affect the shoot/root ratio of K^+ might contribute, such as KUP7 (Han et al., 2016) and OsHAK16 from rice (Feng et al., 2019). Likewise, the identity of the transporters responsible for the retrieval of anions from the xylem remains unclear too, albeit several transporters such as NRT1.8/NPF7.2 (Li et al., 2010; Fan et al., 2017; Zhang et al., 2018) and Cation/Chloride Cotransporters (CCCs) (Li et al., 2017a) have been suggested.

Regulation of Cell Expansion and Movement

One of the key roles of K^+, NO_3^-, and Cl^- in aerial parts of plants is regulation of stomatal aperture. Stomatal movement occurs through change of osmolarity concomitantly with ion flow (mainly K^+) across the guard cell membrane. A number of guard cell-expressed transporters contribute to this regulation; KAT1, KAT2, AKT1, AKT2, NPF6.3, and H^+-ATPases such as AHA2 for stomatal opening (Szyroki et al., 2001; Guo et al., 2003; Saito and Uozumi, 2019), and SLAC1, SLAH3, GORK, and ALMT12 for stomatal closing (Hosy et al., 2003; Vahisalu et al., 2008; Meyer et al., 2010; Geiger et al., 2011; Saito and Uozumi, 2019). Stomata, being the site of water loss *via* transpiration and entrance of pathogens, are regulated by specific signal transduction pathways that ensure rapid closure in response to drought or pathogen attack. This signaling is mediated by an increase in guard cell cytosolic Ca^{2+} concentration and the resulting regulation of transporters by activated CPKs or CBL-CIPKs (Pandey et al., 2007b; Munemasa et al., 2015; Saito and Uozumi, 2019). Ca^{2+}-activated CPK3, CPK6, CPK21, CPK23 (Geiger et al., 2010; Geiger et al., 2011; Scherzer et al., 2012), and CBL1/9-CIPK23 (Maierhofer et al., 2014a) are capable of eliciting anion efflux through SLAC1 and SLAH3. In addition, CBL5-CIPK11 can also activate SLAC1 (Saito et al., 2018). Following this anion efflux, K^+ is driven out from guard cells *via* the Shaker K^+ efflux channel GORK, causing turgor pressure decrease and cell shrinkage, leading to stomatal closure. Moreover, GORK itself, either directly or indirectly, is activated by CPK21 (van Kleeff et al., 2018), CPK33 (Corratgé-Faillie et al., 2017), and CBL1-CIPK5 (Förster et al., 2019). In addition, Ca^{2+} also triggers attenuation of stomatal opening. CIPK11 (although its interacting CBL remains undetermined) has been reported to inhibit AHA2 activity (Fuglsang et al., 2007; Yang et al., 2010), and CPK13 reduces K^+ influx mediated by the Shaker K^+ channels KAT1 and KAT2 (Ronzier et al., 2014). Additionally, CBL2/3 and CIPK9/17 were reported to regulate stomatal movement *via* control of vacuolar morphology (Song et al., 2018), possibly achieved by phosphorylation of the vacuolar localized transporters like K^+/H^+ antiporter NHX (Barragán et al., 2012; Andres et al., 2014), two pore K^+ channel TPK1 (Gobert et al., 2007) and V-ATPase (Ratajczak, 2000; Eisenach and De Angeli, 2017). It is noteworthy that *cbl2 cbl3* double mutation in *Arabidopsis* results in reduced activity of V-ATPase (Tang et al., 2012).

Calcium is also well recognized as a predominant regulator of pollen germination and pollen tube elongation in a wide range of plant species (Steinhorst and Kudla, 2013a; Zheng et al., 2019). Control of cell volume through Ca^{2+}-dependent regulation of ion channels plays a crucial role in pollen tube growth. So far, CPKs and CBL-CIPKs reported to function in pollen tubes are CPK2/11/17/20/24/34, CBL1/2/3/9, and CIPK12/19 (Myers et al., 2009; Mähs et al., 2013; Zhou et al., 2015). CPK11, together with CPK24, modulates the activity of the pollen-expressed plasma membrane K^+ influx channel SPIK, which is required for pollen germination (Mouline et al., 2002; Zhao et al., 2013). Pollen tubes

also require an anion gradient at the tube tip, which was shown to be maintained by SLAH3 and its activator CPK2 and CPK20 (Gutermuth et al., 2013). CBL2/3-CIPK12 participate in pollen germination and tube growth by controlling vacuole morphology *via* regulation of a yet to be identified tonoplast protein (Steinhorst et al., 2015).

Sodium and Calcium—Resistance Against Salinity Stress

Sodium (Na^+) is widely considered the major cause of salt stress damage, osmotic stress, as well as K^+ deficiency due to their chemical and structural similarity (Benito et al., 2014). Uptake of Na^+ is likely mediated by non-selective cation channels and considered accidental (Demidchik and Tester, 2002; Keisham et al., 2018). In order to protect leaves and reproductive tissues, plants have developed a sophisticated system for sequestering Na^+ or sending it back to the soil. The salt overly sensitive (SOS) pathway, a major salt resistance mechanism, is initiated by rapid intracellular Ca^{2+} increase in response to salt treatment (Tester and Davenport, 2003; Köster et al., 2018), suggested to be achieved by opening of Ca^{2+} influx channels by Na^+-activated GIPC sphingolipids (Jiang et al., 2019). In this pathway, CIPK24 (SOS2), in combination with Ca^{2+}-activated CBL4 (SOS3), phosphorylates Na^+ efflux/H^+ influx antiporter SOS1 to remove Na^+ from cells (Qiu et al., 2002; Shi et al., 2002). Alternatively, CBL1-CIPK24 might also mediate this process (Kolukisaoglu, 2004; Manik et al., 2015). Tonoplast localized CBL10 is another CBL required for salt tolerance, presumably by activating a Na^+/H^+ antiporter together with CIPK24, allowing compartmentalization of Na^+ into the vacuole (Kim et al., 2007; Manik et al., 2015). Guard cell K^+ efflux channel GORK is also expressed in roots. Sudden salt stress induces membrane depolarization and cytosolic Ca^{2+} increase in root cell, which activates GORK *via* a mechanism mentioned earlier in this review. Activated GORK mediates K^+ efflux from root cells, which alongside with H^+ efflux by AHA2, repolarizes membrane potential and restores Ca^{2+} homeostasis (van Kleeff et al., 2018).

Calcium Controlling Ammonium Uptake Level

Plants absorb two kinds of nitrogen species from the soil, nitrate (NO_3^-) and ammonium (NH_4^+). NO_3^- import and translocation by multiple NRT/NPF and SLAH transporters and regulation of these by Ca^{2+} were described earlier in this review. NH_4^+ uptake, on the other hand, is mediated by ammonium transporters (AMT). While NH_4^+ is beneficial as an alternative nitrogen source, high levels of NH_4^+ can be toxic, and therefore its cellular level must be strictly controlled (Britto and Kronzucker, 2002; Zheng et al., 2015). Two members of the AMT family, AMT1;1 and AMT1;2, were shown to be inhibited by the CBL1-CIPK23 complex, also known as an activator of root-expressed AKT1, HAK5, and SLAH2/3

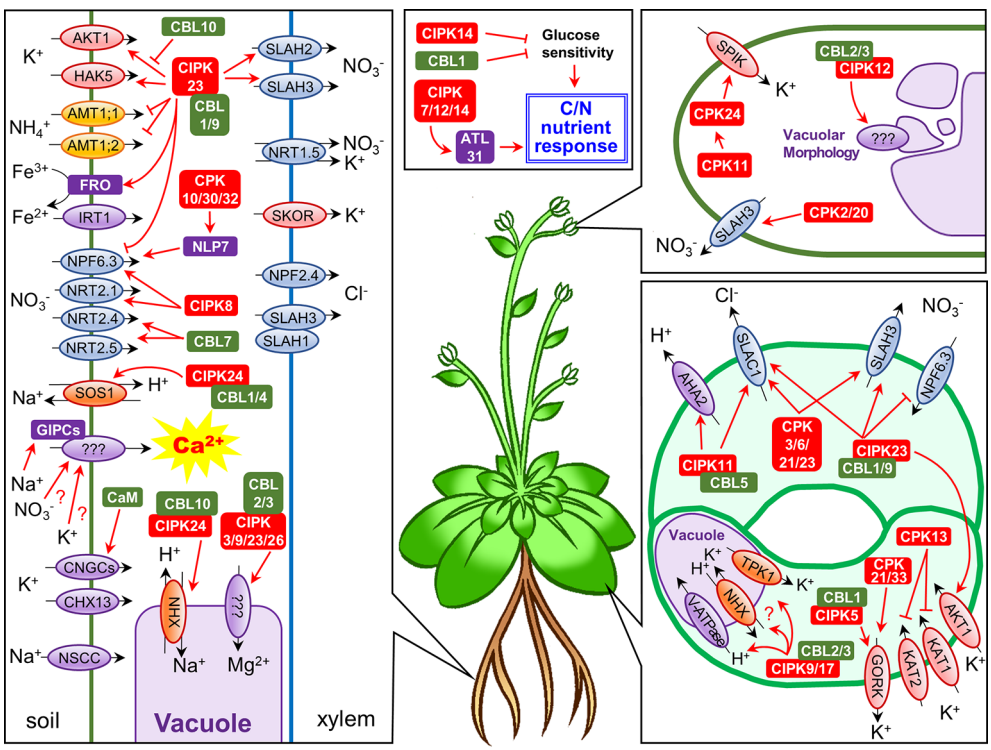

FIGURE 1 | Schematic representation of Ca^{2+}-regulated nutrient uptake and translocation in *Arabidopsis thaliana*. Each panel shows ion channel/transporter regulation by Ca^{2+}-dependent phosphorylation systems in roots, guard cells, and pollen tubes, or the roles of CBLs/CIPKs in C/N nutrient response, respectively. Abbreviations: NSCC, non-selective cation channel; IRT1, iron transporter 1; CaM, calmodulin.

TABLE 1 | Summary of ion channels/transporters and other Ca^{2+}-regulated proteins reviewed in this article.

Name	Activator	Deactivator	Type of transport	Expressed in	Role
AKT1	CBL1/9-CIPK23	CBL10	K^+ influx	Root, guard cell	K^+ uptake, stomatal opening
HAK5	CBL1/9-CIPK23		K^+ influx	Root	K^+ uptake
Unknown	CBL2/3-CIPK9				K^+ homeostasis
CNGC3	Calmodulin?		K^+ influx	Root	K^+ uptake
CNGC10	Calmodulin?		K^+ influx	Root	K^+ uptake
CNGC13	Calmodulin?		K^+ influx	Root	K^+ uptake
CHX13			K^+ influx	Root	K^+ uptake
SKOR			K^+ efflux	Root xylem pericycle	Xylem loading of K^+
NRT2.1	CIPK8		NO_3^- influx	Root	NO_3^- uptake
NRT2.2			NO_3^- influx	Root	NO_3^- uptake
NRT2.4	CBL7		NO_3^- influx	Root	NO_3^- uptake
NRT2.5	CBL7		NO_3^- influx	Root	NO_3^- uptake
NPF2.3			NO_3^- influx	Root	NO_3^- uptake
NPF4.6			NO_3^- influx	Root	NO_3^- uptake
NPF6.3	CIPK8, CPK10/30/32 (via NLP7 phosphorylation)	CBL1/9-CIPK23(via conversion of NO_3^- affinity mode)	NO_3^- influx	Root, guard cell	NO_3^- uptake, stomatal opening
NRT1.5			K^+/H^+ antiport, NO_3^- efflux	Root xylem pericycle	Xylem loading of K^+ and NO_3^-
NPF2.4			Cl^- efflux	Root xylem pericycle	Xylem loading of Cl^-
SLAH2	CBL1/9-CIPK23		NO_3^- efflux	Root stele	Xylem loading of NO_3^-
SLAH3	CBL1/9-CIPK23, CPK3/6/21/23, CPK2/20		NO_3^- efflux, Cl^- efflux (when forming heteromer with SLAH1)	Root xylem pericycle, guard cell, pollen tube	Xylem loading of NO_3^- and Cl^-, stomatal closure, pollen tube elongation
AKT2	CBL4-CIPK6		Weak/non-rectified K^+ transport (switched by phosphorylation)	Phloem, guard cell	Phloem membrane repolarization
KAT1		CPK13	K^+ influx	Guard cell	Stomatal opening
KAT2		CPK13	K^+ influx	Guard cell	Stomatal opening
AHA2		CIPK11	H^+ efflux	Guard cell	Stomatal opening
GORK	CPK21/33, CBL1-CIPK5 (via inhibition of ABI2)		K^+ efflux	Root, guard cell	Restoring root Ca^{2+} homeostasis, stomatal closure
SLAC1	CBL1/9-CIPK23, CPK3/6/21/23, CBL5-CIPK11		Cl^- efflux	Guard cell	Stomatal closure
ALMT12			Malate efflux	Guard cell	Stomatal closure
Unknown	CBL2/3-CIPK9/17			Guard cell tonoplast	Control of guard cell vacuolar morphology?
V-ATPase	CBL2/3-unidentified CIPK		H^+ influx	Guard cell tonoplast	Vacuolar pH homeostasis
SPIK	CPK11 and CPK24 together		K^+ influx	Pollen tube	Pollen tube growth
SOS1	CBL1/4-CIPK24		Na^+/H^+ antiport	Root	Removal of Na^+ from root cell

(Continued)

TABLE 1 | Continued

Name	Activator	Deactivator	Type of transport	Expressed in	Role
Unknown	CBL10-CIPK24		Na^+/H^+ antiport	Root vacuole	Na^+ compartment into vacuole
Unknown	Na^+ bound GIPC		Ca^{2+} influx	Root	Initiation of cytosolic Ca^{2+} increase
AMT1;1		CBL1/9-CIPK23	NH_4^+ influx	Root	NH_4^+ uptake
AMT1;2		CBL1/9-CIPK23	NH_4^+ influx	Root	NH_4^+ uptake
Unknown	CBL1, CIPK14		Glucose?		Glucose response
ATL31 (ubiquitin ligase)	CIPK7/12/14	–	–	Ubiquitous	Regulation of C/N-nutrient response
FROs (ferric chelate reductase)	CBL1/9-CIPK23	–	–	Varies	Iron acquisition
Unknown	CBL2/3-CIPK3/9/23			Tonoplast	Mg^{2+} storage
NIP1;1	CPK31		As^{3+} influx	Root	As^{3+} uptake

(Loqué and Von Wirén, 2004; Straub et al., 2017). Thus, it is likely that CBL1-CIPK23 plays a key role in maintaining ion homeostasis in root cells and in preventing the toxic effects of NH_4^+ (Britto and Kronzucker, 2002; Zheng et al., 2015). Another element that controls the NO_3^-/NH_4^+ balance is the transcription factor NLP7, which was recently shown to induce up-regulation of NPF6.3 transcripts in the presence of NH_4^+ (Zhao et al., 2018b). NLP7 is phosphoregulated by CPK10/30/32, which are activated by NO_3^--dependent elevation of intracellular Ca^{2+} (Liu et al., 2017).

Possible Role of Calcium in Balancing of Energy Source

Essential nutrients translocated through vascular tissues are not only limited to ions but also include organic compounds such as amino acids and sugars (Fischer et al., 1998; Liu et al., 2012a). Sugars are transported through phloem in the form of sucrose and distributed throughout the plant (Liu et al., 2012a). Loading of sucrose from the phloem to the apoplast requires activity of the shaker K^+ channel AKT2 (Shabala, 2003; Dreyer et al., 2017; Ragel et al., 2019). AKT2, usually weakly-rectified, can be converted into a non-rectifying K^+ channel *via* phosphorylation, thereby enabling K^+ efflux and phloem membrane repolarization and the consequent retrieval of sucrose (Deeken et al., 2002; Michard et al., 2005a; Michard et al., 2005b; Gajdanowicz et al., 2011; Sandmann et al., 2011; Saito et al., 2017). Though the kinase responsible for this phosphorylation remains to be identified, it must be noted that AKT2 activity can be enhanced by the CBL4-CIPK6 complex in a Ca^{2+}-dependent but phosphorylation-independent manner (Held et al., 2011).

The efficiency of cellular energy use is optimized by carbon/nitrogen (C/N) balance, and therefore its maintenance is of great significance for growth and development of plants (Coruzz and Bush, 2001; Zheng, 2009; Maekawa et al., 2014). In a recent study, three members of CIPK, CIPK7/12/14, were identified as key regulators of the C/N-nutrient response, achieved through their phosphorylation of ubiquitin ligase ATL31 (Yasuda et al., 2014; Yasuda et al., 2017).

Additionally, although most of the carbon compounds are derived from photosynthesis, plants respond to externally supplied sugars as well. These exogenous sugars, in addition to their use as energy source, show hormone-like behavior, working in parallel with some of the ABA-responsive genes (Rolland and Sheen, 2005; Yamada et al., 2011; Singh et al., 2014; Williams et al., 2014; Yuan et al., 2014). Among the calcium-regulated phosphorylation modules, CBL1 (Li et al., 2013) and CIPK14 (Yan et al., 2014) were found to positively regulate the response to glucose by an yet unidentified mechanism.

Uptake Regulation of Metal Ions and Toxins

Metal ions such as magnesium (Mg^{2+}), iron (Fe), zinc (Zn^{2+}), and manganese (Mn^{2+}) work as cofactors of numerous enzymes and are therefore indispensable for plant growth. Several Ca^{2+}-regulated phosphorylation components also participate in maintaining homeostasis of these ions. Iron deficiency was reported to elicit an increase of Ca^{2+} in *Arabidopsis* roots. This induces CBL1/9-CIPK23 to enhance Ferric chelate reductase (FRO) activity, which is required for converting Fe^{3+} in the soil into the transported form, Fe^{2+}, thereby substantially regulating iron acquisition (Tian et al., 2016). CIPK23 alongside with CBL2/3 and CIPK3/9, is also required for modulation of plant growth under high Mg^{2+} condition, likely mediated by Mg^{2+} compartmentalization to the vacuole (Mogami et al., 2015; Tang et al., 2015). Additionally, Zn^{2+} and Mn^{2+} levels were found to be reduced in *cipk23* mutant plants, suggesting some unidentified regulatory system of metal acquisition involving CIPK23 (Tian et al., 2016). On the other hand, some CPKs and

CBL-CIPKs are involved in uptake of toxic ions. For instance, CPK31 was reported to regulate uptake of non-essential and toxic arsenite (As^{3+}) (Ji et al., 2017), and in rice, several members of the CPK family exhibited increased phosphorylation in response to cadmium (Cd^{2+}) application (Zhong et al., 2017).

CONCLUSIONS

In this minireview we have summarized the Ca^{2+}-regulated uptake, storage, and translocation of nutrient ions, and possible role of Ca^{2+} in energy source balancing (**Figure 1**, **Table 1**). Most of these regulatory mechanisms are initiated by a rise of the cytosolic Ca^{2+} level in response to stress or nutrient depletion, and ultimately lead to resistance against unfavorable conditions. Thus, full understanding of the Ca^{2+}-dependent phosphorylation machinery would be a vital step for optimizing plant growth and reproduction.

AUTHOR CONTRIBUTIONS

Conceptualization, original draft preparation, review, and editing were done by SS, and NU contributed to the article by funding acquisition.

FUNDING

This work was supported by JSPS KAKENHI Grant Number (16H06558, 18H03762, 19H02880, 19K21140, and 19K22264).

ACKNOWLEDGMENTS

We thank Anke Reinders for critical reading of the manuscript.

REFERENCES

Alemán, F., Nieves-Cordones, M., Martínez, V., and Rubio, F. (2011). Root K^+ acquisition in plants: the Arabidopsis *thaliana* model. *Plant Cell Physiol.* 52, 1603–1612. doi: 10.1093/pcp/pcr096

Almeida, D. M., Margarida Oliveira, M., and Saibo, N. J. M. (2017). Regulation of Na^+ and K^+ homeostasis in plants: towards improved salt stress tolerance in crop plants. *Genet. Mol. Biol.* 40, 326–345. doi: 10.1590/1678-4685-gmb-2016-0106

Andres, Z., Perez-Hormaeche, J., Leidi, E. O., Schlucking, K., Steinhorst, L., McLachlan, D. H., et al. (2014). Control of vacuolar dynamics and regulation of stomatal aperture by tonoplast potassium uptake. *Proc. Natl. Acad. Sci.* 111, E1806–E1814. doi: 10.1073/pnas.1320421111

Baba, A. I., Rigó, G., Ayaydin, F., Rehman, A. U., Andrási, N., Zsigmond, L., et al. (2018). Functional analysis of the Arabidopsis *thaliana* CDPK-related kinase family: AtCRK1 regulates responses to continuous light. *Int. J. Mol. Sci.* 19, 1–21. doi: 10.3390/ijms19051282

Balk, J., and Schaedler, T. A. (2014). Iron cofactor assembly in plants. *Annu. Rev. Plant Biol.* 65, 125–153. doi: 10.1146/annurev-arplant-050213-035759

Barragán, V., Leidi, E. O., Andrés, Z., Rubio, L., de Luca, A., Fernández, J. A., et al. (2012). Ion exchangers NHX1 and NHX2 mediate active potassium uptake into vacuoles to regulate cell turgor and stomatal function in Arabidopsis. *Plant Cell* 24, 1127–1142. doi: 10.1105/tpc.111.095273

Batistič, O., and Kudla, J. (2009). Plant calcineurin B-like proteins and their interacting protein kinases. *Biochim. Biophys. Acta Mol. Cell Res.* 1793, 985–992. doi: 10.1016/j.bbamcr.2008.10.006

Batistic, O., Sorek, N., Schültke, S., Yalovsky, S., and Kudla, J. (2008). Dual fatty acyl modification determines the localization and plasma membrane targeting of CBL/CIPK Ca^{2+} signaling complexes in Arabidopsis. *Plant Cell* 20, 1346–1362. doi: 10.1105/tpc.108.058123

Behera, S., Long, Y., Schmitz-Thom, I., Wang, X.-P., Zhang, C., Li, H., et al. (2016). Two spatially and temporally distinct Ca^{2+} signals convey Arabidopsis *thaliana* responses to K^+ deficiency. *New Phytol.* 213, 739–750. doi: 10.1111/nph.14145

Benito, B., Haro, R., Amtmann, A., Cuin, T. A., and Dreyer, I. (2014). The twins K^+ and Na^+ in plants. *J. Plant Physiol.* 171, 723–731. doi: 10.1016/j.jplph.2013.10.014

Boudsocq, M., and Sheen, J. (2013). CDPKs in immune and stress signaling. *Trends Plant Sci.* 18, 30–40. doi: 10.1016/j.tplants.2012.08.008

Britto, D. T., and Kronzucker, H. J. (2002). NH4+ toxicity in higher plants: a critical review. *J. Plant Physiol.* 159, 567–584. doi: 10.1078/0176-1617-0774

Broadley, M. R., White, P. J., Hammond, J. P., Zelko, I., and Lux, A. (2007). Zinc in plants: Tansley review. *New Phytol.* 173, 677–702. doi: 10.1111/j.1469-8137.2007.01996.x

Bush, D. S. (1995). Calcium regulation in plant cells and its role in signaling. *Annu. Rev. Plant Physiol. Plant Mol. Biol.* 46, 95–122. doi: 10.1146/annurev.pp.46.060195.000523

Caballero, F., Botella, M. A., Rubio, L., Fernández, J. A., Martínez, V., and Rubio, F. (2012). A Ca^{2+}-sensitive system mediates low-affinity K^+ uptake in the absence of AKT1 in *Arabidopsis* plants. *Plant Cell Physiol.* 53, 2047–2059. doi: 10.1093/pcp/pcs140

Corratgé-Faillie, C., Ronzier, E., Sanchez, F., Prado, K., Kim, J.-H., Lanciano, S., et al. (2017). The *Arabidopsis* guard cell outward potassium channel GORK is regulated by CPK33. *FEBS Lett.*, 591, 1982–1992. doi: 10.1002/1873-3468.12687

Coruzz, G., and Bush, D. R. (2001). Nitrogen and carbon nutrient and metabolite signaling in plants. *Plant Physiol.* 125, 61–64. doi: 10.1104/pp.125.1.61

Cubero-Font, P., Maierhofer, T., Jaslan, J., Rosales, M. A., Espartero, J., Díaz-Rueda, P., et al. (2016). Silent S-type anion channel subunit SLAH1 gates SLAH3 open for chloride root-to-shoot translocation. *Curr. Biol.*, 26, 1–8. doi: 10.1016/j.cub.2016.06.045

Deeken, R., Geiger, D., Fromm, J., Koroleva, O., Ache, P., Langenfeld-Heyser, R., et al. (2002). Loss of the AKT2/3 potassium channel affects sugar loading into the phloem of *Arabidopsis*. *Planta* 216, 334–344. doi: 10.1007/s00425-002-0895-1

DeFalco, T. A., Marshall, C. B., Munro, K., Kang, H. G., Moeder, W., Ikura, M., et al. (2016). Multiple calmodulin-binding sites positively and negatively regulate *Arabidopsis* CYCLIC NUCLEOTIDE-GATED CHANNEL12. *Plant Cell* 28, 1738–1751. doi: 10.1105/tpc.15.00870

Demidchik, V., and Tester, M. (2002). Sodium fluxes through nonselective cation channels in the plasma membrane of protoplasts from *Arabidopsis* roots. *Plant Physiol.* 128, 379–387. doi: 10.1104/pp.010524

Drechsler, N., Zheng, Y., Bohner, A., Nobmann, B., von Wirén, N., Kunze, R., et al. (2015). Nitrate-dependent control of shoot K homeostasis by NPF7.3/NRT1.5 and SKOR in *Arabidopsis*. *Plant Physiol.* 169, 01152.2015. doi: 10.1104/pp.15.01152

Dreyer, I., Gomez-porras, J. L., and Riedelsberger, J. (2017). The potassium battery: a mobile energy source for transport processes in plant vascular tissues. *New Phytol.* 216, 1049–1053. doi: 10.1111/nph.14667

Eisenach, C., and De Angeli, A. (2017). Ion transport at the vacuole during stomatal movements. *Plant Physiol.* 174, 520–530. doi: 10.1104/pp.17.00130

Fan, X., Naz, M., Fan, X., Xuan, W., Miller, A. J., and Xu, G. (2017). Plant nitrate transporters: from gene function to application. *J. Exp. Bot.* 68, 2463–2475. doi: 10.1093/jxb/erx011

Feng, H., Tang, Q., Cai, J., Xu, B., Xu, G., and Yu, L. (2019). Rice OsHAK16 functions in potassium uptake and translocation in shoot, maintaining potassium homeostasis and salt tolerance. *Planta* 250, 549–561. doi: 10.1007/s00425-019-03194-3

Fischer, W. N., André, B., Rentsch, D., Krolkiewicz, S., Tegeder, M., Breitkreuz, K., et al. (1998). Amino acid transport in plants. *Trends Plant Sci.* 3, 188–195. doi: 10.1016/S1360-1385(98)01231-X

Förster, S., Schmidt, L. K., Kopic, E., Anschütz, U., Huang, S., Schlücking, K., et al. (2019). Wounding-induced stomatal closure requires jasmonate-mediated activation of GORK K^+ channels by a Ca^{2+} sensor-kinase CBL1-CIPK5 complex. *Dev. Cell* 48, 87–99.e6. doi: 10.1016/j.devcel.2018.11.014

Fuglsang, A. T., Guo, Y., Cuin, T. A., Qiu, Q., Song, C., Kristiansen, K. A., et al. (2007). *Arabidopsis* protein kinase PKS5 inhibits the plasma membrane H^+-ATPase by preventing interaction with 14-3-3 protein. *Plant Cell* 19, 1617–1634. doi: 10.1105/tpc.105.035626

Gajdanowicz, P., Michard, E., Sandmann, M., Rocha, M., Corrêa, L. G. G., Ramírez-Aguilar, S. J., et al. (2011). Potassium K^+ gradients serve as a mobile energy source in plant vascular tissues. *Proc. Natl. Acad. Sci. U. S. A.* 108, 864–869. doi: 10.1073/pnas.1009777108

Geiger, D., Scherzer, S., Mumm, P., Marten, I., Ache, P., Matschi, S., et al. (2010). Guard cell anion channel SLAC1 is regulated by CDPK protein kinases with distinct Ca^{2+} affinities. *Proc. Natl. Acad. Sci. U. S. A.* 107, 8023–8028. doi: 10.1073/pnas.0912030107

Geiger, D., Maierhofer, T., Al-Rasheid, K. A. S., Scherzer, S., Mumm, P., Liese, A., et al. (2011). Stomatal closure by fast abscisic acid signaling is mediated by the guard cell anion channel SLAH3 and the receptor RCAR1. *Sci. Signal.* 4, ra32. doi: 10.1126/scisignal.2001346

Gerendás, J., and Führs, H. (2013). The significance of magnesium for crop quality. *Plant Soil* 368, 101–128. doi: 10.1007/s11104-012-1555-2

Gobert, A., Isayenkov, S., Voelker, C., Czempinski, K., and Maathuis, F. J. M. (2007). The two-pore channel TPK1 gene encodes the vacuolar K^+ conductance and plays a role in K^+ homeostasis. *Proc. Natl. Acad. Sci.* 104, 10726–10731. doi: 10.1073/pnas.0702595104

Grusak, M. A., Broadley, M. R., and White, P. J. (2016). Plant macro- and micronutrient minerals. *eLS*, 1–6. doi: 10.1002/9780470015902.a0001306.pub2

Guo, F.-Q., Young, J., and Crawford, N. M. (2003). The nitrate transporter AtNRT1.1 (CHL1) functions in stomatal opening and contributes to drought susceptibility in *Arabidopsis*. *Plant Cell* 15, 107–117. doi: 10.1105/tpc.006312

Gutermuth, T., Lassig, R., Portes, M., Maierhofer, T., Romeis, T., Borst, J., et al. (2013). Pollen tube growth regulation by free anions depends on the interaction between the anion channel SLAH3 and calcium-dependent protein kinases CPK2 and CPK20. *Plant Cell* 25, 4525–4543. doi: 10.1105/tpc.113.118463

Han, M., Wu, W., Wu, W. H., and Wang, Y. (2016). Potassium transporter KUP7 is involved in K^+ acquisition and translocation in *Arabidopsis* root under K^+-limited conditions. *Mol. Plant* 9, 437–446. doi: 10.1016/j.molp.2016.01.012

Hashimoto, K., and Kudla, J. (2011). Calcium decoding mechanisms in plants. *Biochimie* 93, 2054–2059. doi: 10.1016/j.biochi.2011.05.019

Held, K., Pascaud, F., Eckert, C., Gajdanowicz, P., Hashimoto, K., Corratgé-Faillie, C., et al. (2011). Calcium-dependent modulation and plasma membrane targeting of the AKT2 potassium channel by the CBL4/CIPK6 calcium sensor/protein kinase complex. *Cell Res.* 21, 1116–1130. doi: 10.1038/cr.2011.50

Hepler, P. K. (2005). Calcium: a central regulator of plant growth and development. *Plant Cell* 17, 2142–2155. doi: 10.1105/tpc.105.032508

Hirata, H., and Mitsui, S. (1965). Role of calcium in potassium uptake by plant roots. *Plant Cell Physiol.* 6, 699–709. doi: 10.1093/oxfordjournals.pcp.a079142

Ho, C. H., Lin, S. H., Hu, H. C., and Tsay, Y. F. (2009). CHL1 functions as a nitrate sensor in plants. *Cell* 138, 1184–1194. doi: 10.1016/j.cell.2009.07.004

Hosy, E., Vavasseur, A., Mouline, K., Dreyer, I., Gaymard, F., Porée, F., et al. (2003). The *Arabidopsis* outward K^+ channel GORK is involved in regulation of stomatal movements and plant transpiration. *Proc. Natl. Acad. Sci. U. S. A.* 100, 5549–5554. doi: 10.1073/pnas.0733970100

Hu, H. C., Wang, Y. Y., and Tsay, Y. F. (2009). AtCIPK8, a CBL-interacting protein kinase, regulates the low-affinity phase of the primary nitrate response. *Plant J.* 57, 264–278. doi: 10.1111/j.1365-313X.2008.03685.x

Ji, R., Zhou, L., Liu, J., Wang, Y., Yang, L., Zheng, Q., et al. (2017). Calcium-dependent protein kinase CPK31 interacts with arsenic transporter AtNIP1;1 and regulates arsenite uptake in Arabidopsis *thaliana*. *PloS One* 12, 1–20. doi: 10.1371/journal.pone.0173681

Jiang, Z., Zhou, X., Tao, M., Yuan, F., Liu, L., Wu, F., et al. (2019). Plant cell-surface GIPC sphingolipids sense salt to trigger Ca^{2+} influx. *Nature* 572, 341–346. doi: 10.1038/s41586-019-1449-z

Johansen, C., Edwards, D. G., and Loneragan, J. F. (1968). Interaction between potassium and calcium in their absorption by intact barley plants. *Plant Physiol.* 43, 1722–1726. doi: 10.1104/pp.43.10.1722

Kaplan, B., Sherman, T., and Fromm, H. (2007). Cyclic nucleotide-gated channels in plants. *FEBS Lett.* 581, 2237–2246. doi: 10.1016/j.febslet.2007.02.017

Keisham, M., Mukherjee, S., and Bhatla, S. C. (2018). Mechanisms of sodium transport in plants—progresses and challenges. *Int. J. Mol. Sci.* 19, e647. doi: 10.3390/ijms19030647

Kim, B. G., Waadt, R., Cheong, Y. H., Pandey, G. K., Dominguez-Solis, J. R., Schültke, S., et al. (2007). The calcium sensor CBL10 mediates salt tolerance by regulating ion homeostasis in *Arabidopsis*. *Plant J.* 52, 473–484. doi: 10.1111/j.1365-313X.2007.03249.x

Kolukisaoglu, U. (2004). Calcium sensors and their interacting protein kinases: genomics of the *Arabidopsis* and rice CBL-CIPK signaling networks. *Plant Physiol.* 134, 43–58. doi: 10.1104/pp.103.033068

Köster, P., Wallrad, L., Edel, K. H., Faisal, M., Alatar, A. A., and Kudla, J. (2018). The battle of two ions: Ca^{2+} signalling against Na^+ stress. *Plant Biol.*, 1, 39–48. doi: 10.1111/plb.12704

Kroeger, J. H., Zerzour, R., and Geitmann, A. (2011). Regulator or driving force? The role of turgor pressure in oscillatory plant cell growth. *PloS One* 6, e18549. doi: 10.1371/journal.pone.0018549

Kudla, J., Batistic, O., and Hashimoto, K. (2010). Calcium signals: the lead currency of plant information processing. *Plant Cell* 22, 541–563. doi: 10.1105/tpc.109.072686

Lee, S. C., Lan, W.-Z., Kim, B.-G., Li, L., Cheong, Y. H., Pandey, G. K., et al. (2007). A protein phosphorylation/dephosphorylation network regulates a plant potassium channel. *Proc. Natl. Acad. Sci. U. S. A.* 104, 15959–15964. doi: 10.1073/pnas.0707912104

Leran, S., Edel, K. H., Pervent, M., Hashimoto, K., Corratge-Faillie, C., Offenborn, J. N., et al. (2015). Nitrate sensing and uptake in *Arabidopsis* are enhanced by ABI2, a phosphatase inactivated by the stress hormone abscisic acid. *Sci. Signal.* 8, ra43. doi: 10.1126/scisignal.aaa4829

Léran, S., Muños, S., Brachet, C., Tillard, P., Gojon, A., and Lacombe, B. (2013). *Arabidopsis* NRT1.1 is a bidirectional transporter involved in root-to-shoot nitrate translocation. *Mol. Plant* 6, 1984–1987. doi: 10.1093/mp/sst068

Léran, S., Varala, K., Boyer, J. C., Chiurazzi, M., Crawford, N., Daniel-Vedele, F., et al. (2014). A unified nomenclature of nitrate transporter 1/peptide transporter family members in plants. *Trends Plant Sci.* 19, 5–9. doi: 10.1016/j.tplants.2013.08.008

Leustek, T., and Saito, K. (1999). Sulfate transport and assimilation in plants. *Plant Physiol.* 120, 637–643. doi: 10.1104/pp.120.3.637

López-Arredondo, D. L., Leyva-González, M. A., Alatorre-Cobos, F., and Herrera-Estrella, L. (2013). Biotechnology of nutrient uptake and assimilation in plants. *Int. J. Dev. Biol.* 57, 595–610. doi: 10.1387/ijdb.130268lh

López-Arredondo, D. L., Leyva-González, M. A., González-Morales, S. I., López-Bucio, J., and Herrera-Estrella, L. (2014). Phosphate nutrition: improving low-phosphate tolerance in crops. *Annu. Rev. Plant Biol.* 65, 95–123. doi: 10.1146/annurev-arplant-050213-035949

Li, J. Y., Fu, Y. L., Pike, S. M., Bao, J., Tian, W., Zhang, Y., et al. (2010). The *Arabidopsis* nitrate transporter NRT1.8 functions in nitrate removal from the xylem sap and mediates cadmium tolerance. *Plant Cell* 22, 1633–1646. doi: 10.1105/tpc.110.075242

Li, Z. Y., Xu, Z. S., Chen, Y., He, G. Y., Yang, G. X., Chen, M., et al. (2013). A novel role for *Arabidopsis* CBL1 in affecting plant responses to glucose and gibberellin during germination and seedling development. *PloS One* 8. doi: 10.1371/journal.pone.0056412

Li, B., Byrt, C., Qiu, J., Baumann, U., Hrmova, M., Evrard, A., et al. (2016). Identification of a stelar-localized transport protein that facilitates root-to-shoot transfer of chloride in *Arabidopsis*. *Plant Physiol.* 170, 1014–1029. doi: 10.1104/pp.15.01163

Li, B., Tester, M., and Gilliham, M. (2017a). Chloride on the move. *Trends Plant Sci.* 22, 236–248. doi: 10.1016/j.tplants.2016.12.004

Li, H., Yu, M., Du, X.-Q., Wang, Z.-F., Wu, W.-H., Quintero, F. J., et al. (2017b). NRT1.5/NPF7.3 functions as a proton-coupled H^+/K^+ antiporter for K^+

loading into the xylem in *Arabidopsis*. *Plant Cell* 29, tpc.00972.2016. doi: 10.1105/tpc.16.00972

Lin, S.-H., Kuo, H.-F., Canivenc, G., Lin, C.-S., Lepetit, M., Hsu, P.-K., et al. (2008). Mutation of the *Arabidopsis* NRT1.5 nitrate transporter causes defective root-to-shoot nitrate transport. *Plant Cell Online* 20, 2514–2528. doi: 10.1105/tpc.108.060244

Liu, K. H., and Tsay, Y. F. (2003). Switching between the two action modes of the dual-affinity nitrate transporter CHL1 by phosphorylation. *EMBO J.* 22, 1005–1013. doi: 10.1093/emboj/cdg118

Liu, K., Li, L., and Luan, S. (2006). Intracellular K^+ sensing of SKOR, a Shaker-type K^+ channel from *Arabidopsis*. *Plant J.* 46, 260–268. doi: 10.1111/j.1365-313X.2006.02689.x

Liu, D. D., Chao, W. M., and Turgeon, R. (2012a). Transport of sucrose, not hexose, in the phloem. *J. Exp. Bot.* 63, 4315–4320. doi: 10.1093/jxb/ers127

Liu, L.-L., Ren, H.-M., Chen, L.-Q., Wang, Y., and Wu, W.-H. (2012b). A protein kinase CIPK9 interacts with calcium sensor CBL3 and regulates K^+ homeostasis under low-K^+ stress in *Arabidopsis*. *Plant Physiol.* 161, 266–277. doi: 10.1104/pp.112.206896

Liu, L., Zheng, C., Kuang, B., Wei, L., Yan, L., and Wang, T. (2016). Receptor-like kinase RUPO interacts with potassium transporters to regulate pollen tube growth and integrity in rice. *PloS Genet.* 12, 1–23. doi: 10.1371/journal.pgen.1006085

Liu, K. H., Niu, Y., Konishi, M., Wu, Y., Du, H., Sun Chung, H., et al. (2017). Discovery of nitrate-CPK-NLP signalling in central nutrient-growth networks. *Nature* 545, 311–316. doi: 10.1038/nature22077

Loqué, D., and Von Wirén, N. (2004). Regulatory levels for the transport of ammonium in plant roots. *J. Exp. Bot.* 55, 1293–1305. doi: 10.1093/jxb/erh147

Mähs, A., Steinhorst, L., Han, J. P., Shen, L. K., Wang, Y., and Kudla, J. (2013). The calcineurin B-like Ca^{2+} sensors CBL1 and CBL9 function in pollen germination and pollen tube growth in *Arabidopsis*. *Mol. Plant* 6, 1149–1162. doi: 10.1093/mp/sst095

Ma, Q., Tang, R. J., Zheng, X. J., Wang, S. M., and Luan, S. (2015). The calcium sensor CBL7 modulates plant responses to low nitrate in *Arabidopsis*. *Biochem. Biophys. Res. Commun.* 468, 59–65. doi: 10.1016/j.bbrc.2015.10.164

Maekawa, S., Inada, N., Yasuda, S., Fukao, Y., Fujiwara, M., Sato, T., et al. (2014). The carbon/nitrogen regulator ARABIDOPSIS TOXICOS EN LEVADURA31 controls papilla formation in response to powdery mildew fungi penetration by interacting with SYNTAXIN OF PLANTS121 in *Arabidopsis*. *Plant Physiol.* 164, 879–887. doi: 10.1104/pp.113.230995

Mahajan, S., Sopory, S. K., and Tuteja, N. (2006). CBL-CIPK paradigm: role in calcium and stress signaling in plants. *Proc. Indian Natl. Sci. Acad.* 78, 63–78. https://insa.nic.in/Default.aspx.

Maierhofer, T., Diekmann, M., Offenborn, J. N., Lind, C., Bauer, H., Hashimoto, K., et al. (2014a). Site- and kinase-specific phosphorylation-mediated activation of SLAC1, a guard cell anion channel stimulated by abscisic acid. *Sci. Signal.* 7, ra86. doi: 10.1126/scisignal.2005703

Maierhofer, T., Lind, C., Hüttl, S., Scherzer, S., Papenfuß, M., Simon, J., et al. (2014b). A single-pore residue renders the *Arabidopsis* root anion channel SLAH2 highly nitrate selective. *Plant Cell* 3, 1–15. doi: 10.1105/tpc.114.125849

Manik, S. M. N., Shi, S., Mao, J., Dong, L., Su, Y., Wang, Q., et al. (2015). The calcium sensor CBL-CIPK is involved in plant's response to abiotic stresses. *Int. J. Genomics* 2015, 1–10. doi: 10.1155/2015/493191

Manishankar, P., Wang, N., Köster, P., Alatar, A. A., and Kudla, J. (2018). Calcium signaling during salt stress and in the regulation of ion homeostasis. *J. Exp. Bot.* 69, 4215–4226. doi: 10.1093/jxb/ery201

Mao, J., Manik, S. M. N., Shi, S., Chao, J., Jin, Y., Wang, Q., et al. (2016). Mechanisms and physiological roles of the CBL-CIPK networking system in Arabidopsis *thaliana*. *Genes (Basel)* 7, 1–15. doi: 10.3390/genes7090062

Mendel, R. R. (2013). The molybdenum cofactor. *J. Biol. Chem.* 288, 13165–13172. doi: 10.1074/jbc.R113.455311

Merchant, S. S. (2010). The elements of plant micronutrients. *Plant Physiol.* 154, 512–515. doi: 10.1104/pp.110.161810

Meyer, S., Mumm, P., Imes, D., Endler, A., Weder, B., Al-Rasheid, K. A. S., et al. (2010). AtALMT12 represents an R-type anion channel required for stomatal movement in *Arabidopsis* guard cells. *Plant J.* 63, 1054–1062. doi: 10.1111/j.1365-313X.2010.04302.x

Michard, E., Dreyer, I., Lacombe, B., Sentenac, H., and Thibaud, J. B. (2005a). Inward rectification of the AKT2 channel abolished by voltage-dependent phosphorylation. *Plant J.* 44, 783–797. doi: 10.1111/j.1365-313X.2005.02566.x

Michard, E., Lacombe, B., Porée, F., Mueller-Roeber, B., Sentenac, H., Thibaud, J.-B., et al. (2005b). A unique voltage sensor sensitizes the potassium channel AKT2 to phosphoregulation. *J. Gen. Physiol.* 126, 605–617. doi: 10.1085/jgp.200509413

Mogami, J., Fujita, Y., Yoshida, T., Tsukiori, Y., Nakagami, H., Nomura, Y., et al. (2015). Two distinct families of protein kinases are required for plant growth under high external Mg^{2+} concentrations in *Arabidopsis*. *Plant Physiol.* 167, 1039–1057. doi: 10.1104/pp.114.249870

Mouline, K., Véry, A. A., Gaymard, F., Boucherez, J., Pilot, G., Devic, M., et al. (2002). Pollen tube development and competitive ability are impaired by disruption of a Shaker K^+ channel in *Arabidopsis*. *Genes Dev.* 16, 339–350. doi: 10.1101/gad.213902

Munemasa, S., Hauser, F., Park, J., Waadt, R., Brandt, B., and Schroeder, J. I. (2015). Mechanisms of abscisic acid-mediated control of stomatal aperture. *Curr. Opin. Plant Biol.* 28, 154–162. doi: 10.1016/j.pbi.2015.10.010

Myers, C., Romanowsky, S. M., Barron, Y. D., Garg, S., Azuse, C. L., Curran, A., et al. (2009). Calcium-dependent protein kinases regulate polarized tip growth in pollen tubes. *Plant J.* 59, 528–539. doi: 10.1111/j.1365-313X.2009.03894.x

Nemoto, K., Takemori, N., Seki, M., Shinozaki, K., and Sawasaki, T. (2015). Members of the plant CRK superfamily are capable of trans- and autophosphorylation of tyrosine residues. *J. Biol. Chem.* 290, 16665–16677. doi: 10.1074/jbc.M114.617274

Noguero, M., and Lacombe, B. (2016). Transporters involved in root nitrate uptake and sensing by *Arabidopsis*. *Front. Plant Sci.* 7, 1–7. doi: 10.3389/fpls.2016.01391

Pan, Y., Chai, X., Gao, Q., Zhou, L., Zhang, S., Li, L., et al. (2019). Dynamic interactions of plant CNGC subunits and calmodulins drive oscillatory Ca^{2+} channel activities. *Dev. Cell.* 48, 710–725. doi: 10.1016/j.devcel.2018.12.025

Pandey, G. K., Cheong, Y. H., Kim, B. G., Grant, J. J., Li, L., and Luan, S. (2007a). CIPK9: a calcium sensor-interacting protein kinase required for low-potassium tolerance in *Arabidopsis*. *Cell Res.* 17, 411–421. doi: 10.1038/cr.2007.39

Pandey, S., Zhang, W., and Assmann, S. M. (2007b). Roles of ion channels and transporters in guard cell signal transduction. *FEBS Lett.* 581, 2325–2336. doi: 10.1016/j.febslet.2007.04.008

Parker, J. L., and Newstead, S. (2014). Molecular basis of nitrate uptake by the plant nitrate transporter NRT1.1. *Nature* 507, 68–72. doi: 10.1038/nature13116

Pyo, Y. J., Gierth, M., Schroeder, J. I., and Cho, M. H. (2010). High-affinity K^+ transport in *Arabidopsis*: AtHAK5 and AKT1 are vital for seedling establishment and postgermination growth under low-potassium conditions. *Plant Physiol.* 153, 863–875. doi: 10.1104/pp.110.154369

Qiu, Q.-S., Guo, Y., Dietrich, M. A., Schumaker, K. S., and Zhu, J.-K. (2002). Regulation of SOS1, a plasma membrane Na^+/H^+ exchanger in Arabidopsis *thaliana*, by SOS2 and SOS3. *Proc. Natl. Acad. Sci. U. S. A.* 99, 8436–8441. doi: 10.1073/pnas.122224699

Qiu, J., Henderson, S. W., Tester, M., Roy, S. J., and Gilliham, M. (2016). SLAH1, a homologue of the slow type anion channel SLAC1, modulates shoot Cl– accumulation and salt tolerance in Arabidopsis *thaliana*. *J. Exp. Bot.* 67, 4495–4505. doi: 10.1093/jxb/erw237

Ragel, P., Ródenas, R., García-Martín, E., Andrés, Z., Villalta, I., Nieves-Cordones, M., et al. (2015). CIPK23 regulates HAK5-mediated high-affinity K^+ uptake in *Arabidopsis* roots. *Plant Physiol.* 169, 01401.2015. doi: 10.1104/pp.15.01401

Ragel, P., Raddatz, N., Leidi, E. O., Quintero, F. J., and Pardo, J. M. (2019). Regulation of K^+ nutrition in plants. *Front. Plant Sci.* 10, 281. doi: 10.3389/fpls.2019.00281

Rains, W. D., and Floyd, A. R. (1970). Influence of calcium on sodium and potassium absorption by fresh and aged bean stem slices. *Plant Physiol.* 46, 93–98. doi: 10.1104/pp.46.1.93

Ratajczak, R. (2000). Structure, function and regulation of the plant vacuolar H^+ translocating ATPase. *Biochim. Biophys. Acta Biomembr.* 1465, 17–36. doi: 10.1016/S0005-2736(00)00129-2

Ren, X. L., Qi, G. N., Feng, H. Q., Zhao, S., Zhao, S. S., Wang, Y., et al. (2013). Calcineurin B-like protein CBL10 directly interacts with AKT1 and modulates K^+ homeostasis in *Arabidopsis*. *Plant J.* 74, 258–266. doi: 10.1111/tpj.12123

Rigó, G., Ayaydin, F., Tietz, O., Zsigmond, L., Kovács, H., Páy, A., et al. (2013). Inactivation of plasma membrane-localized CDPK-RELATED KINASE5 decelerates PIN2 exocytosis and root gravitropic response in *Arabidopsis*. *Plant Cell* 25, 1592–1608. doi: 10.1105/tpc.113.110452

Riveras, E., Alvarez, J. M., Vidal, E. A., Oses, C., Vega, A., and Gutiérrez, R. A. (2015). The calcium ion is a second messenger in the nitrate signaling pathway of *Arabidopsis*. *Plant Physiol.* 169, 1397–1404. doi: 10.1104/pp.15.00961

Rolland, F., and Sheen, J. (2005). Sugar sensing and signalling networks in plants. *Biochem. Soc Trans.* 33, 269–271. doi: 10.1042/BST0330269

Ronzier, E., Corratgé-Faillie, C., Sanchez, F., Prado, K., Brière, C., Leonhardt, N., et al. (2014). CPK13, a noncanonical Ca^{2+}-dependent protein kinase, specifically inhibits KAT2 and KAT1 Shaker K^+ channels and reduces stomatal opening. *Plant Physiol.* 166, 314–326. doi: 10.1104/pp.114.240226

Rubio, F., Alemán, F., Nieves-Cordones, M., and Martínez, V. (2010). Studies on *Arabidopsis* athak5, atakt1 double mutants disclose the range of concentrations at which AtHAK5, AtAKT1 and unknown systems mediate K^+ uptake. *Physiol. Plant.* 139, 220–228. doi: 10.1111/j.1399-3054.2010.01354.x

Saito, S., and Uozumi, N. (2019). Guard cell membrane anion transport systems and their regulatory components: an elaborate mechanism controlling stress-induced stomatal closure. *Plants* 8, 9. doi: 10.3390/plants8010009

Saito, S., Hoshi, N., Zulkifli, L., Widyastuti, S., Goshima, S., Dreyer, I., et al. (2017). Identification of regions responsible for the function of the plant K^+ channels KAT1 and AKT2 in Saccharomyces cerevisiae and Xenopus laevis oocytes. *Channels* 11, 510–516. doi: 10.1080/19336950.2017.1372066

Saito, S., Hamamoto, S., Moriya, K., Matsuura, A., Sato, Y., Muto, J., et al. (2018). N -myristoylation and S-acylation are common modifications of Ca^{2+}-regulated *Arabidopsis* kinases and are required for activation of the SLAC1 anion channel. *New Phytol.* 218, 1504–1521. doi: 10.1111/nph.15053

Sanders, D., Brownlee, C., and Harper, J. F. (1999). Communicating with calcium. *Plant Cell* 11, 691–706. doi: 10.1105/tpc.11.4.691

Sandmann, M., Skłodowski, K., Gajdanowicz, P., Michard, E., Rocha, M., Gomez-Porras, J. L., et al. (2011). The K^+ battery-regulating *Arabidopsis* K^+ channel AKT2 is under the control of multiple post-translational steps. *Plant Signal. Behav.* 6, 558–562. doi: 10.4161/psb.6.4.14908

Scherzer, S., Maierhofer, T., Al-Rasheid, K. A. S., Geiger, D., and Hedrich, R. (2012). Multiple calcium-dependent kinases modulate ABA-activated guard cell anion channels. *Mol. Plant* 5, 1409–1412. doi: 10.1093/mp/sss084

Schmidt, S. B., and Husted, S. (2019). The biochemical properties of manganese in plants. *Plants* 8, 381. doi: 10.3390/plants8100381

Schmidt, S. B., Jensen, P. E., and Husted, S. (2016). Manganese deficiency in plants: the impact on photosystem II. *Trends Plant Sci.* 21, 622–632. doi: 10.1016/j.tplants.2016.03.001

Schulz, P., Herde, M., and Romeis, T. (2013). Calcium-dependent protein kinases: hubs in plant stress signaling and development. *Plant Physiol.* 163, 523–530. doi: 10.1104/pp.113.222539

Shabala, S. (2003). Regulation of potassium transport in leaves: from molecular to tissue level. *Ann. Bot.* 92, 627–634. doi: 10.1093/aob/mcg191

Shi, H., Quintero, F. J., Pardo, J. M., and Zhu, J. K. (2002). The putative plasma membrane Na^+/H^+ antiporter SOS1 controls long-distance Na^+transport in plants. *Plant Cell* 14, 465–477. doi: 10.1105/tpc.010371

Shi, S., Li, S., Asim, M., Mao, J., Xu, D., Ullah, Z., et al. (2018). The *Arabidopsis* calcium-dependent protein kinases (CDPKs) and their roles in plant growth regulation and abiotic stress responses. *Int. J. Mol. Sci.* 19, e1900. doi: 10.3390/ijms19071900

Singh, M., Gupta, A., and Laxmi, A. (2014). Glucose control of root growth direction in Arabidopsis *thaliana*. *J. Exp. Bot.* 65, 2981–2993. doi: 10.1093/jxb/eru146

Singh, A., Yadav, A. K., Kaur, K., Sanyal, S. K., Jha, S. K., Fernandes, J. L., et al. (2018). A protein phosphatase 2C, AP2C1, interacts with and negatively regulates the function of CIPK9 under potassium-deficient conditions in *Arabidopsis*. *J. Exp. Bot.* 69, 4003–4015. doi: 10.1093/jxb/ery182

Song, S.-J., Feng, Q.-N., Li, C., Li, E., Liu, Q., Kang, H., et al. (2018). A tonoplast-associated calcium-signaling module dampens ABA signaling during stomatal movement. *Plant Physiol.* 177, 00377.2018. doi: 10.1104/pp.18.00377

Steinhorst, L., and Kudla, J. (2013a). Calcium—a central regulator of pollen germination and tube growth. *Biochim. Biophys. Acta Mol. Cell Res.* 1833, 1573–1581. doi: 10.1016/j.bbamcr.2012.10.009

Steinhorst, L., and Kudla, J. (2013b). Calcium and reactive oxygen species rule the waves of signaling. *Plant Physiol.* 163, 471–485. doi: 10.1104/pp.113.222950

Steinhorst, L., Mähs, A., Ischebeck, T., Zhang, C., Zhang, X., Arendt, S., et al. (2015). Vacuolar CBL-CIPK12 Ca^{2+}-sensor-kinase complexes are required for polarized pollen tube growth. *Curr. Biol.* 25, 1475–1482. doi: 10.1016/j.cub.2015.03.053

Straub, T., Ludewig, U., and Neuhaeuser, B. (2017). The kinase CIPK23 inhibits ammonium transport in Arabidopsis *thaliana*. *Plant Cell*, 29, 409–422. doi: 10.1105/tpc.16.00806

Sun, J., Bankston, J. R., Payandeh, J., Hinds, T. R., Zagotta, W. N., and Zheng, N. (2014). Crystal structure of the plant dual-affinity nitrate transporter NRT1.1. *Nature* 507, 73–77. doi: 10.1038/nature13074

Szyroki, A., Ivashikina, N., Dietrich, P., Roelfsema, M. R. G., Ache, P., Reintanz, B., et al. (2001). KAT1 is not essential for stomatal opening. *Proc. Natl. Acad. Sci.* 98, 2917–2921. doi: 10.1073/pnas.051616698

Tang, R.-J., Liu, H., Yang, Y., Yang, L., Gao, X.-S., Garcia, V. J., et al. (2012). Tonoplast calcium sensors CBL2 and CBL3 control plant growth and ion homeostasis through regulating V-ATPase activity in *Arabidopsis*. *Cell Res.* 22, 1650–1665. doi: 10.1038/cr.2012.161

Tang, R.-J., Zhao, F.-G., Garcia, V. J., Kleist, T. J., Yang, L., Zhang, H.-X., et al. (2015). Tonoplast CBL–CIPK calcium signaling network regulates magnesium homeostasis in *Arabidopsis*. *Proc. Natl. Acad. Sci.* 112 (10), 3134–3139. doi: 10.1073/pnas.1420944112

Taochy, C., Gaillard, I., Ipotesi, E., Oomen, R., Leonhardt, N., Zimmermann, S., et al. (2015). The *Arabidopsis* root stele transporter NPF2.3 contributes to nitrate translocation to shoots under salt stress. *Plant J.* 83, 466–479. doi: 10.1111/tpj.12901

Tester, M., and Davenport, R. (2003). Na^+ tolerance and Na^+ transport in higher plants. *Ann. Bot.* 91, 503–527. doi: 10.1093/aob/mcg058

Tian, Q., Zhang, X., Yang, A., Wang, T., and Zhang, W. H. (2016). CIPK23 is involved in iron acquisition of *Arabidopsis* by affecting ferric chelate reductase activity. *Plant Sci.* 246, 70–79. doi: 10.1016/j.plantsci.2016.01.010

Toyota, M., Spencer, D., Sawai-toyota, S., Jiaqi, W., Zhang, T., Abraham, K. J., et al. (2018). Glutamate triggers long-distance, calcium-based plant defense signaling. *Science* (80-.), 1112–1115. doi: 10.1126/science.aat7744

Undurraga, S. F., Ibarra-Henríquez, C., Fredes, I., Álvarez, J. M., and Gutiérrez, R. A. (2017). Nitrate signaling and early responses in *Arabidopsis* roots. *J. Exp. Bot.* 68, 2541–2551. doi: 10.1093/jxb/erx041

Vahisalu, T., Kollist, H., Wang, Y.-F., Nishimura, N., Chan, W.-Y., Valerio, G., et al. (2008). SLAC1 is required for plant guard cell S-type anion channel function in stomatal signalling. *Nature* 452, 487–491. doi: 10.1038/nature06608

van Kleeff, P. J. M., Gao, J., Mol, S., Zwart, N., Zhang, H., Li, K. W., et al. (2018). The *Arabidopsis* GORK K^+-channel is phosphorylated by calcium-dependent protein kinase 21 (CPK21), which in turn is activated by 14-3-3 proteins. *Plant Physiol. Biochem.* 125, 219–231. doi: 10.1016/j.plaphy.2018.02.013

Walker, D. J., Leigh, R. A., and Miller, A. J. (1996). Potassium homeostasis in vacuolate plant cells. *Proc. Natl. Acad. Sci. U. S. A.* 93, 10510–10514. doi: 10.1073/pnas.93.19.10510

Welch, R. M. (1995). Micronutrient nutrition of plants. *CRC Crit. Rev. Plant Sci.* 14, 49–82. doi: 10.1080/07352689509701922

Williams, S. P., Rangarajan, P., Donahue, J. L., Hess, J. E., and Gillaspy, G. E. (2014). Regulation of sucrose non-fermenting related kinase 1 genes in Arabidopsis *thaliana*. *Front. Plant Sci.* 5, 1–13. doi: 10.3389/fpls.2014.00324

Wu, J. Y., Jin, C., and Zhang, S. L. (2011). Potassium flux in the pollen tubes was essential in plant sexual reproduction. *Plant Signal. Behav.* 6, 898–900. doi: 10.4161/psb.6.6.15322

Xu, J., Li, H. D., Chen, L. Q., Wang, Y., Liu, L. L., He, L., et al. (2006). A protein kinase, interacting with two calcineurin B-like proteins, regulates K^+ transporter AKT1 in *Arabidopsis*. *Cell* 125, 1347–1360. doi: 10.1016/j.cell.2006.06.011

Xuan, W., Beeckman, T., and Xu, G. (2017). Plant nitrogen nutrition: sensing and signaling. *Curr. Opin. Plant Biol.* 39, 57–65. doi: 10.1016/j.pbi.2017.05.010

Yamada, K., Kanai, M., Osakabe, Y., Ohiraki, H., Shinozaki, K., and Yamaguchi-Shinozaki, K. (2011). Monosaccharide absorption activity of *Arabidopsis* roots depends on expression profiles of transporter genes under high salinity conditions. *J. Biol. Chem.* 286, 43577–43586. doi: 10.1074/jbc.M111.269712

Yan, J., Niu, F., Liu, W. Z., Zhang, H., Wang, B., Yang, B., et al. (2014). *Arabidopsis* CIPK14 positively regulates glucose response. *Biochem. Biophys. Res. Commun.* 450, 1679–1683. doi: 10.1016/j.bbrc.2014.07.064

Yang, Y., Qin, Y., Xie, C., Zhao, F., Zhao, J., Liu, D., et al. (2010). The *Arabidopsis* chaperone J3 regulates the plasma membrane H^+-ATPase through interaction with the PKS5 kinase. *Plant Cell* 22, 1313–1332. doi: 10.1105/tpc.109.069609

Yao, F. Y., Qi, G. N., and Hussain, J. (2017). Investigation of the regulation mechanism of Arabidopsis *thaliana* anion channel SLAH2. *Turk. J. Bot.* 41, 543–551. doi: 10.3906/bot-1702-23

Yasuda, S., Sato, T., Maekawa, S., Aoyama, S., Fukao, Y., and Yamaguchi, J. (2014). Phosphorylation of arabidopsis ubiquitin ligase ATL31 is critical for plant carbon/nitrogen nutrient balance response and controls the stability of 14-3-3 proteins. *J. Biol. Chem.* 289, 15179–15193. doi: 10.1074/jbc.M113.533133

Yasuda, S., Aoyama, S., Hasegawa, Y., Sato, T., and Yamaguchi, J. (2017). *Arabidopsis* CBL-interacting protein kinases regulate carbon/nitrogen-nutrient response by phosphorylating ubiquitin ligase ATL31. *Mol. Plant* 10, 605–618. doi: 10.1016/j.molp.2017.01.005

Yuan, T.-T., Xu, H.-H., Zhang, K.-X., Guo, T.-T., and Lu, Y.-T. (2014). Glucose inhibits root meristem growth via ABA INSENSITIVE 5, which represses PIN1 accumulation and auxin activity in *Arabidopsis*. *Plant Cell Environ.* 37, 1338–1350. doi: 10.1111/pce.12233

Zhang, G. B., Meng, S., and Gong, J. M. (2018). The expected and unexpected roles of nitrate transporters in plant abiotic stress resistance and their regulation. *Int. J. Mol. Sci.* 19, 1–15. doi: 10.3390/ijms19113535

Zhao, J., Cheng, N. H., Motes, C. M., Blancaflor, E. B., Moore, M., Gonzales, N., et al. (2008). AtCHX13 is a plasma membrane K^+ transporter. *Plant Physiol.* 148, 796–807. doi: 10.1104/pp.108.124248

Zhao, L.-N., Shen, L.-K., Zhang, W.-Z., Zhang, W., Wang, Y., and Wu, W.-H. (2013). Ca^{2+}-dependent protein kinase11 and 24 modulate the activity of the inward rectifying K^+ channels in *Arabidopsis* pollen tubes. *Plant Cell* 25, 649–661. doi: 10.1105/tpc.112.103184

Zhao, L., Liu, F., Crawford, N. M., and Wang, Y. (2018a). Molecular regulation of nitrate responses in plants. *Int. J. Mol. Sci.* 19, e2039. doi: 10.3390/ijms19072039

Zhao, L., Zhang, W., Yang, Y., Li, Z., Li, N., Qi, S., et al. (2018b). The *Arabidopsis* NLP7 gene regulates nitrate signaling via NRT1.1-dependent pathway in the presence of ammonium. *Sci. Rep.* 8, 1–13. doi: 10.1038/s41598-018-20038-4

Zheng, X., He, K., Kleist, T., Chen, F., and Luan, S. (2015). Anion channel SLAH3 functions in nitrate-dependent alleviation of ammonium toxicity in *Arabidopsis*. *Plant Cell Environ.* 38, 474–486. doi: 10.1111/pce.12389

Zheng, R. H., de Su, S., Xiao, H., and Tian, H. Q. (2019). Calcium: a critical factor in pollen germination and tube elongation. *Int. J. Mol. Sci.* 20, e420. doi: 10.3390/ijms20020420

Zheng, Z.-L. (2009). Carbon and nitrogen nutrient balance signaling in plants. *Plant Signal. Behav.* 4, 584–591. doi: 10.4161/psb.4.7.8540

Zhong, M., Li, S., Huang, F., Qiu, J., Zhang, J., Sheng, Z., et al. (2017). The phosphoproteomic response of rice seedlings to cadmium stress. *Int. J. Mol. Sci.* 18, e2055. doi: 10.3390/ijms18102055

Zhou, L., Lan, W., Chen, B., Fang, W., and Luan, S. (2015). A calcium sensor-regulated protein kinase, CALCINEURIN B-LIKE PROTEIN-INTERACTING PROTEIN KINASE19, is required for pollen tube growth and polarity. *Plant Physiol.* 167, 1351–1360. doi: 10.1104/pp.114.256065

Zhu, J. K. (2016). Abiotic stress signaling and responses in plants. *Cell* 167, 313–324. doi: 10.1016/j.cell.2016.08.029

Conflict of Interest: The authors declare that the research was conducted in the absence of any commercial or financial relationships that could be construed as a potential conflict of interest.

frontiers in Plant Science

ORIGINAL RESEARCH
published: 26 February 2020
doi: 10.3389/fpls.2020.00168

Facile Coating of Urea With Low-Dose ZnO Nanoparticles Promotes Wheat Performance and Enhances Zn Uptake Under Drought Stress

Christian O. Dimkpa[1], Joshua Andrews[1], Job Fugice[1], Upendra Singh[1], Prem S. Bindraban[1], Wade H. Elmer[2], Jorge L. Gardea-Torresdey[3] and Jason C. White[2]*

[1] International Fertilizer Development Center (IFDC), Muscle Shoals, AL, United States, [2] The Connecticut Agricultural Experiment Station, New Haven, CT, United States, [3] Department of Chemistry and Biochemistry, The University of Texas at El Paso, El Paso, TX, United States

OPEN ACCESS

Edited by:
Michael A. Grusak, Edward T. Schafer Agricultural Research Center (USDA-ARS), United States

Reviewed by:
Muhammad Naveed, University of Agriculture Faisalabad, Pakistan
Anne J. Anderson, Utah State University, United States

***Correspondence:**
Christian O. Dimkpa
cdimkpa@ifdc.org

Specialty section:
This article was submitted to Plant Nutrition, a section of the journal Frontiers in Plant Science

Received: *10 November 2019*
Accepted: *04 February 2020*
Published: *26 February 2020*

Citation:
Dimkpa CO, Andrews J, Fugice J, Singh U, Bindraban PS, Elmer WH, Gardea-Torresdey JL and White JC (2020) Facile Coating of Urea With Low-Dose ZnO Nanoparticles Promotes Wheat Performance and Enhances Zn Uptake Under Drought Stress. Front. Plant Sci. 11:168. doi: 10.3389/fpls.2020.00168

Zinc oxide nanoparticles (ZnO-NPs) hold promise as novel fertilizer nutrients for crops. However, their ultra-small size could hinder large-scale field application due to potential for drift, untimely dissolution or aggregation. In this study, urea was coated with ZnO-NPs (1%) or bulk ZnO (2%) and evaluated in wheat (*Triticum aestivum* L.) in a greenhouse, under drought (40% field moisture capacity; FMC) and non-drought (80% FMC) conditions, in comparison with urea not coated with ZnO (control), and urea with separate ZnO-NP (1%) or bulk ZnO (2%) amendment. Plants were exposed to ≤ 2.17 mg/kg ZnO-NPs and ≤ 4.34 mg/kg bulk-ZnO, indicating exposure to a higher rate of Zn from the bulk ZnO. ZnO-NPs and bulk-ZnO showed similar urea coating efficiencies of 74–75%. Drought significantly ($p \leq 0.05$) increased time to panicle initiation, reduced grain yield, and inhibited uptake of Zn, nitrogen (N), and phosphorus (P). Under drought, ZnO-NPs significantly reduced average time to panicle initiation by 5 days, irrespective of coating, and relative to the control. In contrast, bulk ZnO did not affect time to panicle initiation. Compared to the control, grain yield increased significantly, 51 or 39%, with ZnO-NP-coated or uncoated urea. Yield increases from bulk-ZnO-coated or uncoated urea were insignificant, compared to both the control and the ZnO-NP treatments. Plant uptake of Zn increased by 24 or 8% with coated or uncoated ZnO-NPs; and by 78 or 10% with coated or uncoated bulk-ZnO. Under non-drought conditions, Zn treatment did not significantly reduce panicle initiation time, except with uncoated bulk-ZnO. Relative to the control, ZnO-NPs (irrespective of coating) significantly increased grain yield; and coated ZnO-NPs enhanced Zn uptake significantly. Zn fertilization did not significantly affect N and P uptake, regardless of particle size or coating. Collectively, these findings demonstrate that coating urea with ZnO-NPs enhances plant performance and Zn accumulation, thus potentiating field-scale deployment of nano-scale micronutrients. Notably, lower Zn inputs

from ZnO-NPs enhanced crop productivity, comparable to higher inputs from bulk-ZnO. This highlights a key benefit of nanofertilizers: a reduction of nutrient inputs into agriculture without yield penalities.

Keywords: drought, micronutrients, nutrient delivery, crop performance, ZnO nanoparticle-coated urea, Zn nutrition

INTRODUCTION

Zinc oxide nanoparticles (ZnO-NPs; ≤100 nm in at least one dimension) are incorporated into a variety of industrial, medical, and household products to enhance quality and functionality (Piccinno et al., 2012). However, ZnO is a bioreactant, causing beneficial, sublethal, or toxic effects. Compared to bulk ZnO particles, such effects could be accentuated if exposure is to ZnO-NPs. This is as a result of the enhanced reactivity of nanoparticles arising from their small size and greater surface area, compared to bulk particles. Such heightened or nanoscale-specific effects have been observed in microbes, plants, and other terrestrial species (Dimkpa et al., 2012b; Dimkpa, 2014; Anderson et al., 2018; Rajput et al., 2018). In addition to greater nanoscale reactivity, the degree of the effects of ZnO-NPs also depends on dose, plant species and age, exposure route and duration, and environmental conditions such as pH and surface interactions with other soil components (Jośko and Oleszczuk, 2013; Watson et al., 2015; Mukherjee et al., 2016; García-Gómez et al., 2017; Dimkpa et al., 2019a). The contrasting (toxic *vs*. beneficial) effects of ZnO-NPs suggest they can be used as plant fertilizer if supplied at judicious doses. Accordingly, in the context of agriculture and human and environmental health, ZnO-NPs are being systematically assessed in plants for their enhanced ability to modulate productivity and nutrient use efficiency; confer tolerance to biotic and abiotic stresses; and fortify edible plant parts with Zn (Elmer and White, 2016; Raliya et al., 2016; Dimkpa et al., 2017a; Dimkpa et al., 2017b; Elmer et al., 2018; Dimkpa et al., 2018b; Zhang et al., 2018; Adisa et al., 2019; Dimkpa et al., 2019a; Dimkpa et al., 2019b).

One of the potential benefits of nanoscale fertilizers is the possibility of reducing nutrient application rates without sacrificing yield (Kottegoda et al., 2017), thereby saving on input costs and reducing the environmental footprint of chemical fertilizers in a sustainable manner. As previously discussed (Dimkpa and Bindraban, 2018), despite these benefits, the use as nanofertilizers of Zn and other essential microelements in large-scale field crop production appears currently unfeasible due to several potential complications. In the case of broadcast application of dry nanoparticles, the suspensibility of nanopowders in air would lead to large drift losses and potential human inhalation and subsequent health hazards for the handler and unintended biological targets. Whereas deep placement of the powder into the soil may mitigate handling hazards, particle adhesion to equipment surfaces, especially under wet conditions, could hamper efficient delivery. Similarly, suspensions of nanoparticles in water, especially of non-stabilized products (i.e., bare nanomaterials not surface-functionalized), for use as soil drench, foliar spray, or fertigation have at least two potential problems. In aqueous environments, the particles can dissolve into ions; or they can aggregate into non-nanoscale particles. Particle dissolution at a high rate obfuscates the effect of the nanofertilizer treatment owing to prevalent ionic activity (García-Gómez et al., 2017; Qiu and Smolders, 2017). In contrast to dissolution, aggregation of nanoparticles negates the definition of "nano" and associated size-specific reactivity. Thus, in both cases, particle transformation counteracts the underlying functionality of the nanofertilizer. Furthermore, the large difference in weight between urea granules and ZnO bulk powder causes particle size-dependent segregation when they are blended together and packaged for transportation. This problem of particle segregation will worsen when using ZnO-NPs for blending with urea. There is, therefore, a need to develop efficient and safe methods of delivering nano-scale nutrients to plants that also simultaneously streamline fertilizer application events in multi-nutrient fertilization regimes. One strategy that has been discussed in this regard is coating of finished bulk fertilizers such as urea or NPK granules with a nanopowder, to generate nano-enabled urea or NPK fertilizers (Dimkpa and Bindraban, 2018). Previous studies have described the coating of urea with ZnO-NPs and investigated the Zn dissolution kinetics from urea (Milani et al., 2012; Milani et al., 2015); notably, the effect of ZnO-NP-coated urea on plant performance was not evaluated.

Upon developing nano-enabled fertilizers for soil application, product efficacy in field crop production may be affected by natural events such as drought, which reduces nutrient mobility in soil, and consequently, uptake by plants. Indeed, drought continues to ravage different regions of the globe, with devastating consequences on soil nutrient bioavailability and crop productivity (Lesk et al., 2016; Moreno-Jiménez et al., 2019). Mechanistically, Zn can mitigate drought effects in crops (Karim et al., 2012; Dimkpa et al., 2017a; Dimkpa et al., 2019b), due to the role of Zn in metabolic processes regulating water dynamics. For example, under water stress, plants produce elevated amounts of abscisic acid (ABA) to optimize stomatal closure so as to conserve water (Karim and Rahman, 2015; Yang et al., 2018). Zn is known to increase ABA production in plants (Zengin, 2006; Yang et al., 2018), thereby enhancing stomatal regulation by ABA under water limitation.

Little is known as to whether coating of ZnO-NPs onto urea leads to better outcomes, in terms of performance and nutrient acquisition, for plants growing in challenged and unchallenged environmental conditions, or how this novel material would compare to other fertilization regimes such as with urea and ZnO-NPs applied separately. The objectives of the present study

are to: i) understand differences in wheat performance using urea coated with ZnO-NPs *vs*. urea with separate ZnO-NP amendment; ii) determine whether ZnO-NPs coated on urea can mitigate the impact of drought stress on the performance of wheat; and iii) evaluate whether using a lower dose of ZnO-NPs can generate comparable effects as micro-scale (bulk) ZnO at a higher dose. Collectively, all effects were compared with those of bulk ZnO to determine the significance of nanoscale size.

MATERIALS AND METHODS

Chemicals

Commercial ZnO-NPs (18 nm) was purchased from US Research Nanomaterials, Inc., Houston, Texas, USA. Bulk (≥1,000 nm) ZnO powder was purchased from Sigma-Aldrich, St Louis, Missouri, USA. For *in vitro* characterization, a suspension of the ZnO-NPs in water was probe-sonicated, then allowed to precipitate. The supernatant was pipette-filtered (20 μm pore) and diluted 1:1 in methanol. A drop (3 μl) of the suspension was mounted on a 300-mesh carbon-coated Cu grid. The nanoparticles were imaged using a transmission electron microscope (TEM; Hitachi 7800) in high resolution mode at an accelerating voltage of 80 kV. Furthermore, the solubility of both types of oxide particles in the experimental soil was evaluated by separately loading 10 mg of each powder in 20 g soil and incubating at room temperature for 24 h. The spiked soils were extracted in diethylenetriaminepentaacetic acid (DTPA) extracting solution (Lindsay and Norvell, 1978), shaken, filtered and then centrifuged at 10,000 rpm for 10 min. The supernatants were collected and analyzed for soluble Zn using inductively coupled plasma-optical emission spectroscopy (ICP-OES; model Spectro Arcos, SPECTRO Analytical Instruments GmbH, Kleve, Germany). The ZnO-NPs were not further characterized in soil for size-related properties. This is because of the complexity of soil medium, such as the presence of natural nano-size colloids, that would obfuscate the outcome of NP size characterization in soil.

Facile Coating of Urea With ZnO Powder

Dry ZnO-NP (0.4 g) or bulk ZnO (0.8 g) powders were placed in transparent plastic bottles. To those were added 0.4 ml of commercial vegetable (canola) oil and 0.08 ml of black food color (McCormick, Hunt Valley, Maryland) for the nano-ZnO powder, or 0.8 ml vegetable oil and 0.16 ml of food color for the bulk ZnO powder. The urea granules and the ZnO powders are each white in color; thus, the food color provided a contrast that signaled the physical binding of the ZnO powders onto the urea surface that would otherwise be visually difficult to observe. The solutions were mixed to generate a grey-colored ZnO slurry. Urea granules were sieved in 2 mm cut-off sieves to obtain uniformly sized granules. Approximately 40 g of urea granules was added to the ZnO slurries. At these rates, the vegetable oil and food color amounted to 1.0 and 0.2% by weight, respectively, of the urea granule, for the control and nanopowder mixtures; and 2.0 and 0.4% of urea weight, respectively, for the bulk ZnO powder mixture. Similarly, the ZnO-NPs and the bulk ZnO corresponded to 1 and 2% by weight of the urea, respectively. The control urea was coated with vegetable oil and food coloring only and lacked addition of any ZnO powder. Each of the slurry-granular urea mixture was transferred to a low-speed mechanical shaker that generates roughly 32 rpm and all samples were allowed to mix overnight. The ZnO-coated urea was analyzed for the final Zn content by acid digestion (20 ml of 50% HCl), followed by boiling for 15 min, filtration, and dilution. ICP-OES was used to determine the Zn content. The original urea contained 46% N; after coating the N content was 45.7 and 45.3%, respectively, for the nano and bulk-coated products, indicating there was negligible change in the N content due to the coating process.

Soil Preparation

The experimental soil is a sandy loam with the following characteristics: pH 6.87; organic matter content of 0.92%; bioavailable N and P of 4 and 2 mg/kg, respectively; and a bioavailable (DTPA-extractable) Zn of 0.1 mg/kg, indicating a Zn status well below the critical soil level for most crops, 0.5–1.0 mg/kg. The soil was amended with P (75 mg/kg; from monocalcium phosphate) and added into pots at 8 kg/pot, in three replicates. No K was added, as the soil contained more than sufficient amounts, at 1,903 mg/kg.

Plant Growth

A greenhouse-based pot experiment involving winter wheat (*Triticum aestivum* var. Dyna-Gro 9522) was conducted in Muscle Shoals, Alabama (34.7448°N, 87.6675°W) during November-May of 2018–2019 (temperature, 1–33°C; relative humidity, 25–92%). Three wheat seeds were planted into the pots and were thinned to one seed upon germination. Two weeks after germination, the pots were fertilized with Zn-coated and uncoated urea; specifically, 217 mg of the urea was applied per kg of soil by sub-surface incorporation approximately 2 cm from the base of the plant and approximately 3 cm deep. Given 46% N, the amount of urea resulted in a nitrogen application rate of approximately 100 mg/kg (217 x 0.46). Coating of urea with 1 or 2% ZnO powder and applying 217 mg of the urea/kg soil resulted in the application of 2.17 mg ZnO/kg soil for nanoparticles, and 4.34 mg/kg soil for bulk particles. These levels of ZnO corresponded to ≈1.7 and ≈3.5 mg Zn/kg soil, respectively. Therefore, the respective Zn rates were directly used to amend in soil for the non-control uncoated urea treatments, corresponding to ≈17.4 mg ZnO-NPs, and ≈34.7 mg bulk ZnO powder per pot. Ultimately, five urea-Zn treatments were established, each in three replicates: i) control (urea coated with vegetable oil and food coloring); ii) control urea coated with ZnO-NPs (1%); iii) control urea + separate addition of ZnO-NPs (1%); iv) control urea coated with bulk ZnO (2%); and v) control urea + separate addition of bulk ZnO (2%). Each of these treatments was duplicated for the drought and non-drought conditions, resulting in a total of 10 treatments.

One week after Zn treatment, a portion of the plantlets were exposed to drought stress by maintaining the soil at 40% of field moisture capacity (FMC) until harvest. Forty % FMC was pre-

determined using non-experimental potted soil. To this end, each pot was flooded with water until complete leaching for 24 h into a holder underneath. Pots were then weighed, and water in the soil at 100% FMC was determined by subtracting the weight of leached soil from the weight at 100% FMC. With plants in the pot, individual pots were weighed periodically to determine the required water per pot, since plant biomass varied per pot. The required amount of water per pot was then added to reach 40% FMC. This regime was maintained throughout the remainder of the plant growth period so as to keep the droughted plants at 40% FMC. In contrast, the non-stressed plants were kept at 80% FMC. During growth, time to flowering (panicle initiation by the primary shoot) was monitored; and upon full maturity, plants were harvested, grain yield was analyzed, and above-ground plants parts were analyzed for nutrient content.

Plant Nutrient Analyses

Harvested plant tissues were oven-dried at 60°C until constant weight was achieved. Dried tissues were ground into powder using a Model 4 Thomas Wiley Laboratory Mill (Pennsylvania, USA). The ground tissues were acid-digested in a solution of 75% sulfuric acid (3 ml acid + 1 ml of 50% H_2O_2), heated for 1 h at 350°C, cooled to ambient temperature, and equilibrated with distilled H_2O. Sub-samples of the prepared tissues were then subjected to Skalar segmented flow analysis for N and P, or to ICP-OES for Zn as noted above. Soil samples were also collected from the harvested pots for each treatment, to determine pH and bioavailable levels of N (as ammonium and nitrate fractions), P, and Zn. To this end, soil devoid of any root particles was collected for each treatment. The detailed procedures for the soil extraction and analyses of these elements have been described previously (Dimkpa et al., 2018a).

Data Analysis

A two-way analysis of variance (ANOVA; OriginPro 2018) was used to determine significant differences in plant responses to the Zn treatments as a function of water status, for each variable, including vegetative and reproductive development, and nutrient content of plant and soil samples. A Fisher least significant difference (LSD) mean comparison was performed to further explore the differences with significant ($p = 0.05$) ANOVA. Considering that the actual Zn exposure rates among the ZnO treatments are different, the obtained values for the different plant measurement variables with significant ANOVA for Zn treatment (namely, time to panicle initiation, grain yield, and Zn uptake) were normalized by dividing the values by the respective exposure Zn rate.

RESULTS

Characterization of ZnO Nanoparticles

Images of the ZnO-NPs obtained by TEM are presented in **Figure 1**. The ZnO-NPs were present in multiple shapes, including rectangular, tubular, angular, and somewhat circular shapes. However, particles with amorphous shapes could also be seen. Particles with dimensions of less than 100 nm and others with dimensions greater than 100 nm were present, confirming the presence of both discrete nanoscale and aggregated structures. Solubility in the soil of the particles after 24 h was similar between the ZnO-NPs and bulk ZnO, with recoveries around 100% when 10 mg of ZnO was applied in 20 g of soil without plants.

Facile Coating of Urea With ZnO Nano and Bulk Particles

Coating of urea with the nano-ZnO and bulk ZnO powders in a vegetable oil and food color slurry resulted in urea granules that were dark grey in color, in contrast to uncoated urea which is white. Visual observation showed that the entire surface of each urea granule became coated with the slurry, indicating uniform coverage (**Figure 2**). However, post-coating evaluation of the

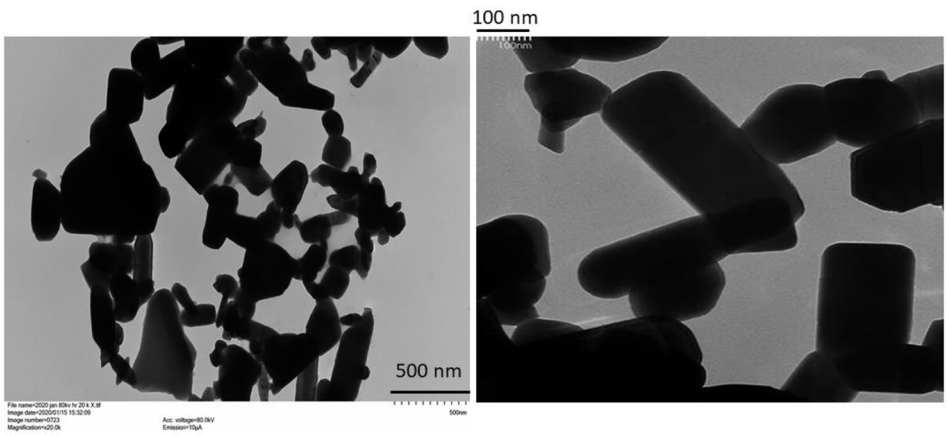

FIGURE 1 | Transmission electron microscopy images of the ZnO-nanoparticles (NPs) used in the study (left: 500 nm resolution; right: 100 nm resolution). For the 500 nm image, each little vertical scale mark on lower right-hand side represents a 50-nm increment. For the 100 nm image, each little scale mark on upper left-hand side represents a 10-nm increment.

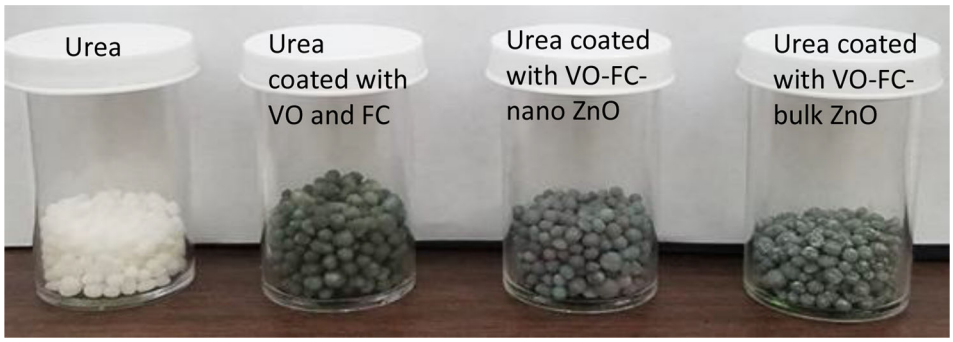

FIGURE 2 | Urea granules, and urea granules coated with vegetable oil (VO) and food coloring (FC), without and with, ZnO nano or bulk powders.

procedure indicated that not all of the slurry coated onto the urea; some dry particles with grey color stuck to the walls of the plastic container used for mixing the slurry and urea. Accordingly, the Zn content of the Zn-coated urea granules was determined, which showed that Zn in the nano-coated urea was only 0.74 ± 0.002% by weight of urea, contrary to the initial 1% target. Similarly, Zn in the bulk-coated urea was 1.51 ± 0.003% by weight of urea, as opposed to the 2% target. Given initial ZnO amounts of 0.4 and 0.8 g, this finding implies that only ≈0.3 g of the nano and ≈0.6 g of the bulk ZnO powder were eventually coated onto the 40 g urea. This suggested similar, 74 and 75%, urea coating efficiencies for the nano and bulk ZnO powders. From the point of view of plant exposure, this suggests that plants treated with the coated urea were exposed to slightly lower Zn rates of 1.6 and 3.3 mg/kg respectively, for the nanoscale and bulk oxide treatment, instead of the pre-targeted Zn rates of 1.7 and 3.5 mg/kg soil that plants treated with uncoated urea were exposed to (**Table 1**).

Effect of Zn-Coated Urea on the Development of Panicle in Wheat Under Drought Stress

Compared to the adequate (80% FMC) water condition, drought (40% FMC) significantly delayed the time to panicle initiation in the wheat plants by 4–11 days, depending on the treatment (**Figure 3**; left panel). Under drought, ZnO-NPs strongly alleviated the delay in panicle initiation time, irrespective of whether the metal was coated onto urea or not. In contrast, bulk ZnO irrespective of coating did not affect the time to panicle formation under drought conditions. Overall, Zn fertilization had less significant effect on time to panicle initiation under the non-drought scenario, although there was a clear trend for reducing the time to panicle formation in all Zn treatments. Only in the case of uncoated bulk ZnO was time to panicle formation significantly different from the control (**Figure 3**; left panel). However, when the effects of the actual exposure Zn rates were considered by expressing the values per mg Zn in terms of change in panicle time initiation and normalizing per unit Zn exposure, it can be seen that ZnO-NPs, regardless of coating or not onto urea, specifically facilitated plant development under drought, relative to the bulk ZnO treatments (**Figure 3**; right panel). However, as suggested by data in the left panel, this nano-specific effect was not apparent under the non-drought condition.

TABLE 1 | Targeted and actual rates of added Zn exposure to wheat in soil. The term uncoated is with respect to Zn.

Trt/rate (mg/kg)	Control	Nano coated	Nano uncoated	Bulk coated	Bulk uncoated
Targeted Zn rate	0	1.7	1.7	3.5	3.5
Actual Zn rate	0	1.6	1.7	3.3	3.5

Effect of Zn-Coated Urea on Wheat Grain Yield Under Drought Stress

Drought strongly reduced grain yield, relative to the non-drought condition, 59–73%, depending on the treatment. Under drought, ZnO-NPs significantly increased grain yield compared to the control and irrespective of whether coated onto urea or not. In contrast, bulk ZnO resulted in intermediate, non-significant effects on grain yield, relative to both the control and ZnO-NPs treatments. As with the nanoscale treatment, coating of urea with bulk ZnO did not produce a significantly different effect, compared to separate application of bulk ZnO (**Figure 4**; left panel). The effect of Zn on grain yield in the non-drought treatments mimicked that with the drought treatments. Unfortunately, the larger variation in the replicates (as indicated by the large error bars) of the bulk oxide treatments under both growth conditions, more so under non-drought, resulted in non-significant effects of that treatment, relative to the control (**Figure 4**; left panel). When the Zn effect was evaluated by normalizing in terms of per unit Zn, coating with Zn generated similar effect as not coating on grain yield, for both ZnO-NPs and bulk ZnO in the drought condition. However, the effect of nanoscale was apparent. Similar to the drought condition, the effect of nanoscale on yield was also clearly demonstrated, independent of Zn coating (**Figure 4**; right panel).

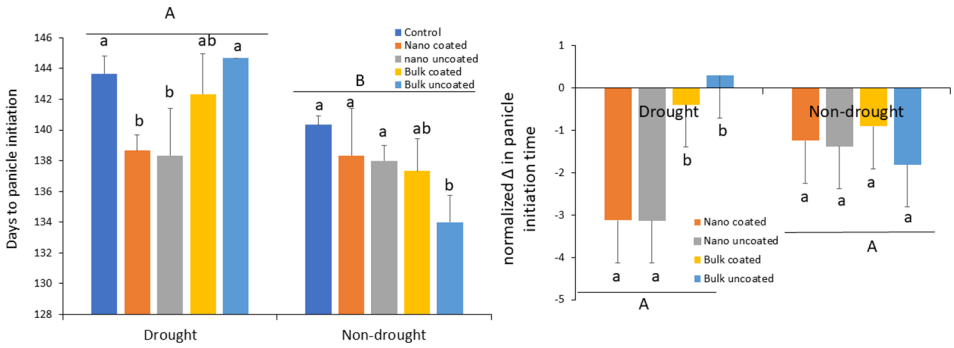

FIGURE 3 | Left panel: effect of urea coated with ZnO-nanoparticles (NPs) or bulk ZnO and of separate ZnO-NP or bulk ZnO amendment with urea on the time to panicle development in wheat under drought and non-drought growth conditions. Right panel: change in panicle initiation time due to ZnO-NPs and bulk ZnO treatments normalized per unit (mg) of Zn. Values are means and standard deviations. Different uppercase letters above horizontal lines represent significant difference between the drought and non-drought condition. Different lowercase letters on bars indicate significant differences among the Zn treatments for each growth condition (n = 3). The term uncoated is with respect to Zn.

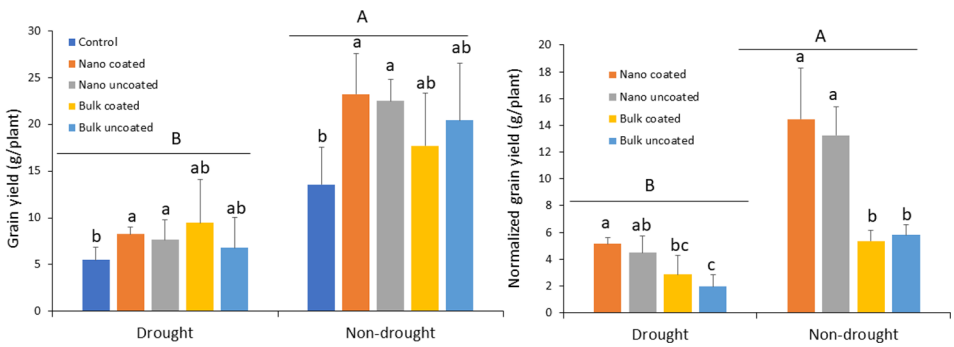

FIGURE 4 | Left panel: effect of urea coated with ZnO-nanoparticles (NPs) or bulk ZnO and of separate ZnO-NP or bulk ZnO amendment with urea on the grain yield of wheat under drought and non-drought growth conditions. Right panel: normalized [per unit (mg) of Zn] values for the effect of ZnO-NPs and bulk ZnO on grain yield. Values are means and standard deviations. Different uppercase letters above horizontal lines represent significant difference between the drought and non-drought condition. Different lowercase letters on bars indicate significant differences among the Zn treatments for each growth condition (n = 3). The term uncoated in the legend is with respect to Zn.

Effect of Zn-Coated Urea on Zinc Uptake in Wheat Under Drought Stress

Drought strongly reduced Zn uptake into above-ground wheat tissues relative to the non-drought condition, 29–116%, depending on the treatment. Under drought condition, coating of nanoscale or bulk ZnO particles onto urea significantly increased Zn uptake, relative to the control urea treatment. The effect of coating with nanoscale oxide particles was not significantly different from that of separate amendment of the nanoparticles. In contrast, urea coated with bulk oxide yielded significantly greater Zn uptake, compared to urea with the separately added bulk oxide (**Figure 5**; left panel). Under non-drought condition, only the ZnO-NP-coated urea significantly increased Zn uptake relative to the control; other treatments resulted in median values on Zn uptake when compared to the control and the ZnO-NP-coated urea (**Figure 5**; left panel). The normalized data confirmed coating of urea with ZnO-NPs to be more effective for Zn accumulation, relative to separate amendments. Similarly, ZnO-NPs were more effective for above-ground tissue Zn delivery than was bulk ZnO Zn type. These effects were consistent in both the drought and non-drought growth conditions (**Figure 5**; right panel).

Effect of Zn-Coated Urea on Nitrogen and Phosphorus Uptake in Wheat Under Drought Stress

Drought strongly reduced N uptake into above-ground (shoot and grain) wheat tissues relative to the non-drought condition by 12–23%, depending on the treatment. However, Zn amendment did not mitigate the effect of drought stress on N uptake, regardless of Zn type, coating or not on urea, and water status of the plants (**Figure 6**; left panel). As with N, drought significantly reduced P uptake into above-ground wheat tissues by 18–37%, relative to the non-drought condition. Notably, Zn

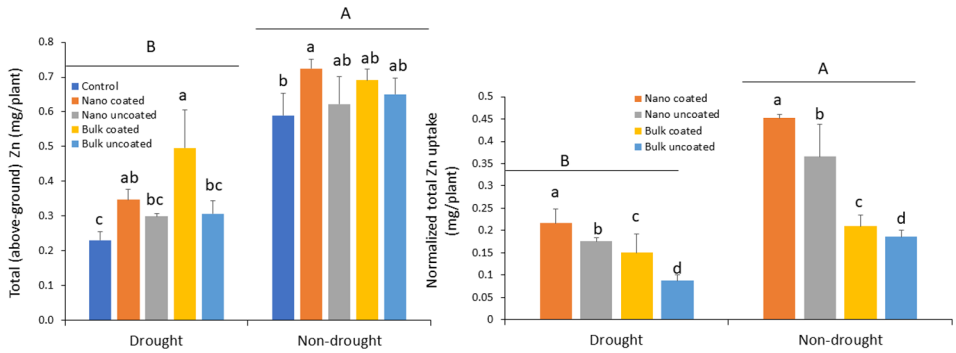

FIGURE 5 | Left panel: effect of urea coated with ZnO-nanoparticles (NPs) or bulk ZnO and of separate ZnO-NP or bulk ZnO amendment with urea on above-ground accumulation of Zn in wheat under drought and non-drought growth conditions. Right panel: normalized [per unit (mg) of Zn] values for the effect of ZnO-NPs and bulk ZnO on Zn accumulation. Values are means and standard deviations. Different uppercase letters above horizontal lines represent significant difference between the drought and non-drought condition. Different lowercase letters on bars indicate significant differences among the Zn treatments for each growth condition (n = 3). The term uncoated in the legend is with respect to Zn.

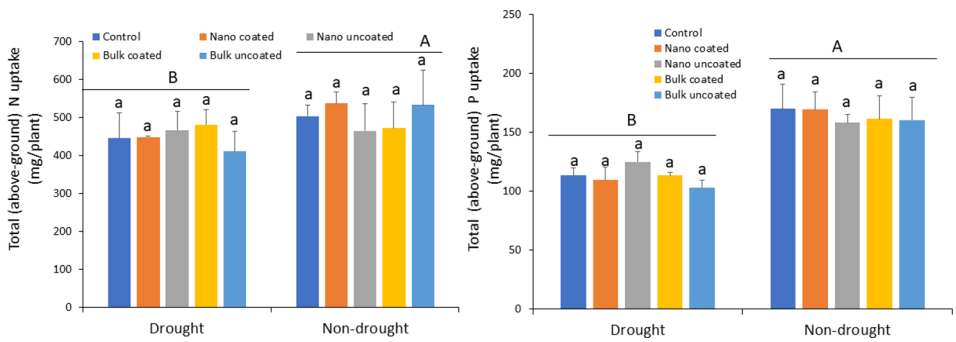

FIGURE 6 | Effect of urea coated with ZnO-nanoparticles (NPs) or bulk ZnO and of separate ZnO-NP or bulk ZnO amendment with urea on above-ground accumulation of nitrogen (left panel) and phosphorus (right panel) in wheat under drought and non-drought growth conditions. Values are means and standard deviations. Different uppercase letters above horizontal lines represent significant difference between the drought and non-drought condition. Different lowercase letters on bars indicate significant differences among the Zn treatments for each growth condition (n = 3). The term uncoated in the legend is with respect to Zn.

amendment also did not mitigate the negative effects of drought on P uptake, regardless of Zn type, whether coated onto urea or not, and the water status of the plants (**Figure 6**; right panel).

Effects of Zn-Coated Urea on Post-Harvest Soil pH and Residual N, P, and Zn

Plant growth in the soil under drought with and without Zn amendment did not significantly alter soil pH from the pre-planting value of 6.87. Conversely, soil pH was significantly altered by adequate watering as compared to the drought condition; the pH increase under normal watering condition was, however, not significantly influenced by Zn treatment (**Table 2**). Drought caused significantly higher residual N in the soil both as ammonium and nitrate fractions. In both fractions, amendment with Zn did not significantly influence residual N, regardless of water status. However, N existed in the soil more as nitrate than as ammonium in all cases, except for the treatment with separately amended bulk ZnO under both growth conditions (**Table 2**). The residual P level was affected by water status, but not by Zn treatment (**Table 2**). Residual Zn was unaffected by water status of soil but was significantly affected by Zn treatment. Under drought, all Zn treatments increased residual Zn, more so with the bulk ZnO particles. Under non-drought condition, only the bulk oxide treatments significantly increased residual soil Zn (**Table 2**). These effects were similar in each case, regardless of whether urea was coated or not with Zn.

DISCUSSION

ZnO-NPs of similar shapes as obtained in this study have previously been observed, and aggregation of ZnO-NPs when suspended in water is also documented (see for e.g., Dimkpa et al., 2012a; Zhang et al., 2018). However, aggregation could also have resulted from drying of the suspension on the TEM grid. Nevertheless, we demonstrate in this study that coating of urea

TABLE 2 | Post-harvest soil pH and residual bioavailable N, P, and Zn (mg/kg) as affected by drought and Zn treatment.

Trt.	Drought					Non-Drought				
	Control	Nano coated	Nano uncoated	Bulk coated	Bulk uncoated	Control	Nano coated	Nano uncoated	Bulk coated	Bulk uncoated
pH	6.93aB	6.88aB	6.99aB	7.08aB	6.85aB	7.04aA	7.20aA	7.04aA	7.08aA	7.09aA
NH_4-N	4.86aA	5.99aA	4.45aA	5.16aA	5.13aA	1.99aB	2.04aB	2.08aB	1.89aB	3.86aB
NO_3-N	6.74aA	8.00aA	5.03aA	6.13aA	4.01aA	2.64aB	3.23aB	3.33aB	2.68aB	3.50aB
P	25.3aA	23.5aA	25.1aA	22.5aA	25.6aA	19.5aB	19.7aB	20.4aB	19.6aB	21.5aB
Zn	0.28cA	0.81bA	0.81bA	1.43aA	1.43aA	0.39cA	0.66bA	0.59cA	1.03abA	1.28aA

Values are means. Different uppercase letters after values represent significant difference between the drought and non-drought condition. Different lowercase letters after values indicate significant differences among the Zn treatments for each growth condition (n = 3). The term uncoated is with respect to Zn.

with a low dose of the dry ZnO-NP powder can enhance wheat performance by accelerating phenological development (panicle initiation) and enhancing grain yield and Zn nutrition from a Zn-deficient soil stressed with drought. To the best of our knowledge, this is the first report on the effect of urea coated with ZnO-NPs on crop performance under a challenged growth condition, in this case drought. Coating of bulk fertilizers such as urea can facilitate fertilizer regimes requiring the co-application of macro- and micro- nutrients. However, large-scale field application of micronutrients such as Zn that are required in small amounts by themselves can result in non-uniform distribution of the analytes in the field, resulting in sporadic and unpredictable effects on crop productivity (Santos et al., 2018). Accordingly, physical coating of micronutrient nanoparticles onto bulk fertilizers has been recommended as a viable option to address this problem (Dimkpa and Bindraban, 2018).

Milani et al. (2015) coated urea with ZnO-NPs and bulk ZnO (each at 1.5%) by spraying with a small amount of water that served as a binding agent for the particles, followed by drying. They reported similarly low, < 1%, Zn dissolution from the products in an alkaline calcareous soil, wherein high pH induced by urea affected Zn dissolution due to pH-dependent particle aggregation. However, unlike the alkaline soil, the soil used in the present study was slightly acidic (pH 6.87), and the urea-Zn treatments did not significantly alter pH after plant growth (**Table 2**), likely due to exudation of organic acids that counteracted any urea-induced alkalinity. This suggests that dissolution was the major fate of ZnO for both Zn types, in the coated and uncoated urea systems. This is indicated by the similarly high residual bioavailable Zn levels in the post-harvest soils (**Table 2**), which agrees with a previous study (García-Gómez et al., 2017). Irfan et al. (2018) also coated urea with bulk ZnO particles (2%) using a slurry composed of honey wax, gum arabica (5% each), paraffin wax, or molasses, without and with heating (60°C) under stirring. They reported that Zn solubility after 24 h was greater in the heated system. Compared to the methods of Milani et al. (2012) and Irfan et al. (2018), the procedure described in the present study, though equally facile, was different because vegetable oil and food coloring were used. This could provide different binding properties and Zn solubility, compared to water or the other described binding agents, in addition to adding carbon into a low organic matter containing soil.

Notably, the rate of plant exposure to Zn from urea coated with ZnO-NPs was slightly (6%) lower than with urea with separate ZnO-NP amendment (1.6 *vs*. 1.7 mg/kg). Compared to the bulk ZnO, it was lower by 52–54%, depending on whether coated or not onto urea (see **Table 1**). Importantly, the ZnO-NP-coated urea not only affected panicle initiation time, grain yield and Zn accumulation to the same degree as the uncoated urea with separate ZnO-NP amendment at a slightly higher Zn exposure rate, it also performed well against the bulk ZnO even with significantly lower (52%) Zn rate. Notably, the effect of Zn on panicle initiation at the actual exposure rates was nanoscale-specific under drought stress. We previously reported acceleration of sorghum development by ZnO-NPs, wherein emergence of the flag leaf and grain head was prolonged by drought, but that delay was alleviated by ZnO-NPs (Dimkpa et al., 2019b); bulk ZnO or Zn salt was not co-evaluated in that study. In wheat, Zn salt (1–3 kg/ha; ≈ 0.5–1.5 mg/kg) alone did not affect the number of days to anthesis in plants grown in soil originally containing 0.17 mg/kg Zn. However, the interaction of N and Zn application significantly reduced time to anthesis (Sher et al., 2018). Therefore, the present study in which ZnO-NPs but not bulk ZnO reduced panicle initiation time in the drought-stressed but not in the unstressed plants lends credence to both the nano-specificity and the water status-dependence of these effects. The mechanism surrounding ZnO-NP effects on plant development under drought stress may be related to Zn effecting hormonal induction to regulate root growth for improved adaptation to limited water supply. Indeed, expression of genes related to hormones such as ABA and cytokinins was enhanced by ZnO-NPs in droughted wheat plants, concomitant with modulation of root architecture that helped tolerate the stress (Yang et al., 2018). In addition, soil microbes can facilitate hormonal activity in plants, as microbially-produced hormones can be accessed by plants, contributing to tolerance to drought stress (Defez et al., 2017; Yang et al., 2018). Whereas hormones such as indole acetic acid (IAA) can prolong plant vegetative growth, heavy metals can lower plant IAA levels, as reported in cowpea with impaired vegetative growth in a heavy metal-polluted soil (Dimkpa et al., 2009). Thus, as with some other metals, ZnO-NPs may alter IAA effects in plants by lowering its level, as reported for bacteria (Dimkpa et al., 2012c; Haris and Ahmad, 2017). Hence, the time to initiation of reproductive development in wheat was accelerated in the presence of ZnO-NPs under drought conditions.

The important finding that a lower rate of Zn from ZnO-NPs increased grain yield similarly to higher rates from bulk ZnO highlights the value of nano-scale fertilizers as a tool for reducing the rate of fertilizer input in agriculture, while still maintaining equivalent or even increased yields, compared to bulk-scale fertilizers. Along these lines, Subbaiah et al. (2016) demonstrated that maize yield could be increased to greater extents by ZnO-NPs at doses 60–98% lower than the bulk Zn-sulfate dose. However, unlike our study, the Zn rates evaluated by Subbaiah et al. (2016) were already high, 50–2,000 mg/L, and the application route was foliar, rather than through the soil. In studies involving urea coated with bulk ZnO or Zn-sulfate (0.5–2.0%), wheat grain yield was increased between 5 and 18 or 8 and 22%, compared to the control (Shivay et al., 2008a). The present report of grain yield increase by ZnO-NPs aligns with previous studies with other crops (Dimkpa et al., 2017a; Dimkpa et al., 2017b; Dimkpa et al., 2018b; Dimkpa et al., 2019a; Dimkpa et al., 2019b), while also confirming that coating of Zn onto urea does not lower its fertilizer efficacy due to potential effects on solubility, as indicated by Milani et al. (2012).

Accordingly, the above-ground tissue accumulation of Zn from the nanoscale and bulk ZnO particles was not decreased by coating of the particles onto urea. In fact, Zn accumulation was facilitated by coating at the higher Zn rate in the bulk oxide treatments under drought; and coating was slightly more effective than separate amendment for Zn delivery under non-drought condition in the ZnO-NP system. Moreover, tissue Zn levels were similar between the nanoscale and bulk ZnO treatments, despite lower Zn exposure levels from the nanoscale form. Zn fortification of crops through fertilization has been amply reported (Joy et al., 2015; Dimkpa and Bindraban, 2016). However, limited studies are available on the use of Zn-coated urea for enhancing Zn nutrition of crops; notably, these studies involved bulk ZnO or Zn salt (Shivay et al., 2008a; Shivay et al., 2008b). Therefore, as demonstrated for the first time in the present study for ZnO-NPs, coating of urea with Zn represents a clear strategy for facilitating the delivery of Zn into plants, even at relatively low Zn rates, and irrespective of soil water status. Plausibly, the speciation of Zn in the NP-exposed plants, though not assessed in this study, is likely to be Zn-phosphate, given other reports involving ZnO-NPs and wheat (Dimkpa et al., 2013; Zhang et al., 2018). We observed no effect of Zn treatment on N and P accumulation in the wheat plants. This was somewhat surprising, given previous observations to the contrary (Dimkpa et al., 2018b). For N, such prior observation as it relates to wheat shows that uptake into above-ground plant parts can be increased by as much as 21% with 6 mg Zn/kg soil from ZnO-NPs (same batch used in the current study). However, in the study in question, the N source was ammonium nitrate, rather than urea. Apparently, the effect of Zn as an element in stimulating N uptake can be both N-fertilizer-type and Zn-dose dependent. For example, 4 mg/kg Zn (from Zn-sulfate) had no effect on N uptake, but higher doses of 6 and 8 mg/kg resulted in greater N uptake than in the controls (Abbas et al., 2009). Also, the Zn dose-dependency of N uptake by plants seems species-specific; N uptake was strongly enhanced in soybean when exposure to Zn from ZnO-NPs was at a low rate of 2–3 mg/kg, under drought and non-drought conditions (Dimkpa et al., 2017a; Dimkpa et al., 2019a). With regard to P, Zn amendment is known to inhibit P uptake (Zhao et al., 2000; Abbas et al., 2009; Watts-Williams et al., 2014; Bindraban et al., 2020), due to the formation of insoluble Zn-phosphate complexes. We hypothesize that the temporal and spatial separation of Zn and P applications in the current work could have contributed to the lack of antagonistic effect between these nutrients. Plants are known to utilize significant amounts of P in early root development, which could have lowered the plant-available P concentration prior to Zn-N application.

Collectively, when data on plant development, grain yield and Zn uptake are normalized, there are some interesting hypothetical scenarios based on plant exposure to the same amount (one gram) of Zn. Overall (i.e., under drought and non-drought conditions), these data indicated that there are indeed differences based on particle size. When expressed on the basis of per gram of Zn, panicle initiation time was accelerated with ZnO-NPs than with the bulk ZnO, and coating had no effect in each case. However, this effect was only found in the drought condition; whereas in the non-drought condition only uncoated bulk ZnO facilitated panicle initiation. For grain yield, a nano-specific effect was found in both growth conditions, and there was no effect of coating. For Zn uptake, size effect of ZnO-NPs was strongly demonstrated, as was the effect of coating of ZnO, irrespective of growth condition. Drought enhances plant root exudation for stress adaptation (Karlowsky et al., 2018), which likely would affect the rate of particle dissolution, depending on specific metabolites in the exudate (Martineau et al., 2014; Yang et al., 2018). Hence, Zn was sufficiently bioavailable from ZnO-NPs under drought, even at a lower exposure rate than bulk ZnO. Nevertheless, additional studies to optimize coating efficiency to deliver same Zn rate in urea as the separate Zn addition for both ZnO-NPs and bulk ZnO could provide important insight on the significance of these assumptions.

The significantly higher residual soil N in the drought-exposed plants relative to the normal watering regime may reflect the fact that biomass growth, and thus, N assimilation, was lower in the droughted plants (data not shown). It was observed that N generally existed in the soil more as nitrate than as ammonium, except in the case of uncoated bulk ZnO in both growth conditions. The significance of bulk ZnO altering the dynamics of N types in the soil is currently unclear. However, the presence in soil of more nitrate than ammonium may reflect the transformation dynamics of different N-fertilizer types. Moreover, soil pH and specific plant uptake requirements for either ammonium or nitrate would also play a role in the ratios of the residual nutrients. In this case, the soil being more acidic than alkaline could have induced a preference for ammonium uptake (Maathuis, 2009), resulting in more nitrate being left as residual N in the soil. In our prior study with wheat (Dimkpa et al., 2018b), ZnO-NPs did not reduce residual soil N levels, similar to the current finding. As with N, Zn treatment with either nanoscale or bulk ZnO did not affect residual soil P levels,

similar to the previous finding with ZnO-NPs (Dimkpa et al., 2018b). However, these are contrary to ZnO-NPs increasing residual soil P in sorghum (Dimkpa et al., 2017b). In terms of residual Zn, the difference in the levels of Zn exposure between the ZnO-NP and the bulk ZnO soils directly reflects the exposure rates, although merely doubling the obtained mean values for the nanoscale form would suggest higher soluble Zn from the NPs than from the bulk product.

As noted, the soil used in the study has a low organic matter content. The role of the carbon that would be added to the soil by the trace amounts of oil and food coloring used for coating in enhancing soil organic matter is unknown at this time. However, it should be noted that all the urea, with and without ZnO, also was coated with the oil, which makes any effect of coating uniform among the treatments.

The findings reported herein indicate that Zn in nanoparticle form can accelerate wheat phenological development, reproductive yield and Zn nutrition under drought stress, as previously reported for sorghum. A broader implication of this study is that a lower Zn rate from ZnO-NPs may suffice for enhancing crop productivity under drought stress, compared to higher input from bulk ZnO. This clearly demonstrates one of the goals of nano-enabled agriculture, which is to reduce the rate of nutrient inputs into the biosphere without a yield penalty. Coating urea or other N-fertilizers with nano-scale micronutrients such as Zn may increase crop yield; facilitate the use of nanoscale micronutrients in field applications; eliminate the problem of segregation of the smaller and larger nutrient particles in bulk fertilizer blends; and facilitate one-time Zn-urea application. However, coating may not necessarily influence yield to a greater extent than separate Zn and urea applications, as observed in this study. This is especially true as the Zn particles will eventually dissolve from the urea surface and undergo independent transformation to ions or larger aggregates, similar to separately-applied ZnO particles. That being said, it is very likely that making improvements to the urea coating process to increase the coating efficiency of ZnO-NPs will further improve outcomes on crop performance and Zn acquisition.

DATA AVAILABILITY STATEMENT

The raw data supporting the conclusions of this article will be made available by the authors, without undue reservation, to any qualified researcher.

AUTHOR CONTRIBUTIONS

CD: acquired research funding, conceived research, designed experiments, conducted experiments and wrote manuscript. JA: conducted experiments and revised manuscript. JF: conducted experiments, evaluated data and revised manuscript. US: designed experiments evaluated data, and revised manuscript; PB: conceived research and revised manuscript. WE: acquired research funding, conceived research and revised manuscript. JG-T: acquired research funding, conceived research and revised manuscript. JW: acquired research funding, conceived research and revised manuscript.

FUNDING

This study was funded by United States Agency for International Development (USAID)'s Feed the Future Soil Fertility Technology Adoption, Policy Reform and Knowledge Management Project (Cooperative Agreement Number AIDBFS-IO-15-00001), and by a U.S. Department of Agriculture (USDA) Agriculture and Food Research Initiative (AFRI) Nanotechnology for Agriculture and Food Systems Grant (2016-67021-24985).

ACKNOWLEDGMENTS

Thanks to Vaughn Henry, Wendie Bible, Celia Sylvester and Katherine Glass, for greenhouse activities and nutrient analyses; and to Dr. Nubia Zuverza-Mena for TEM.

REFERENCES

Abbas, G., Khan, M. Q., Jamil, M., Tahir, M., and Hussain, F. (2009). Nutrient uptake, growth and yield of wheat (*Triticum aestivum*) as affected by zinc application rates. *Int. J. Agric. Biol.* 11, 389–396.

Adisa, I. O., Pullagurala, V. L. R., Peralta-Videa, J. R., Dimkpa, C. O., Elmer, W. H., Gardea-Torresdey, J. L., et al. (2019). Recent advances in nano-enabled fertilizers and pesticides: a critical review of mechanisms of action. *Environ. Sci. Nano.* 6, 2002–2030. doi: 10.1039/C9EN00265K

Anderson, A. J., McLean, J. E., Jacobson, A. R., and Britt, D. W. (2018). CuO and ZnO Nanoparticles modify interkingdom cell signaling processes relevant to crop production. *J. Agric. Food Chem.* 66, 6513–6524. doi: 10.1021/acs.jafc.7b01302

Bindraban, P. S., Dimkpa, C. O., and Pandey, R. (2020). Exploring phosphorus fertilizers and fertilization strategies for improved human and environmental health. *Biol. Fert. Soils*. doi: 10.1007/s00374-019-01430-2

Defez, R., Andreozzi, A., Dickinson, M., Charlton, A., Tadini, L., Pesaresi, P., et al. (2017). Improved drought stress response in alfalfa plants nodulated by an IAA over-producing *Rhizobium* strain. *Front. Microbiol.* 8, 2466. doi: 10.3389/fmicb.2017.02466

Dimkpa, C. O., and Bindraban, P. S. (2016). Micronutrients fortification for efficient agronomic production. *Agron. Sustain. Dev.* 36, 1–26. doi: 10.1007/s13593-015-0346-6

Dimkpa, C., and Bindraban, P. (2018). Nanofertilizers: new products for the industry? *Agric. Food Chem.* 66, 6462–6473. doi: 10.1021/acs.jafc.7b02150

Dimkpa, C. O., Merten, D., Svatoš, A., Büchel, G., and Kothe, E. (2009). Metal-induced oxidative stress impacting plant growth in contaminated soil is alleviated by microbial siderophores. *Soil Biol. Biochem.* 41, 154–162. doi: 10.1016/j.soilbio.2008.10.010

Dimkpa, C. O., McLean, J. E., Latta, D. E., Manangón, E., Britt, D. W., Johnson, W. P., et al. (2012a). CuO and ZnO nanoparticles: phytotoxicity, metal speciation and induction of oxidative stress in sand-grown wheat. *J. Nanopart. Res.* 14, 9. doi: 10.1007/s11051-012-1125-9

Dimkpa, C. O., McLean, J. E., Britt, D. W., and Anderson, A. J. (2012b). Bioactivity and biomodification of Ag, ZnO and CuO nanoparticles with relevance to plant performance in agriculture. *Industr. Biotechnol.* 8, 344–357. doi: 10.1089/ind.2012.0028

Dimkpa, C. O., Zeng, J., McLean, J. E., Britt, D. W., Zhan, J., and Anderson, A. J. (2012c). Production of indole-3-acetic acid *via the* indole-3-acetamide pathway in the plant-beneficial bacterium, *Pseudomonas chlororaphis* O6 is inhibited by

ZnO nanoparticles but enhanced by CuO nanoparticles. *Appl. Environ. Microbiol.* 78, 1404–1410. doi: 10.1128/AEM.07424-11

Dimkpa, C. O., Latta, D. E., McLean, J. E., Britt, D. W., Boyanov, M. I., and Anderson, A. J. (2013). Fate of CuO and ZnO nano- and microparticles in the plant. *Environ. Sci. Technol.* 47, 4734–4742. doi: 10.1021/es304736y

Dimkpa, C., Bindraban, P., Fugice, J., Agyin-Birikorang, S., Singh, U., and Hellums, D. (2017a). Composite micronutrient nanoparticles and salts decrease drought stress in soybean. *Agron. Sustain. Dev.* 37, 5. doi: 10.1007/s13593-016-0412-8

Dimkpa, C. O., White, J. C., Elmer, W. H., and Gardea-Torresdey, J. (2017b). Nanoparticle and ionic Zn promote nutrient loading of sorghum grain under low NPK fertilization. *J. Agric. Food Chem.* 65, 8552–8559. doi: 10.1021/acs.jafc.7b02961

Dimkpa, C. O., Singh, U., Adisa, I. O., Bindraban, P. S., Elmer, W. H., Gardea-Torresdey, J. L., et al. (2018a). Effects of manganese nanoparticle exposure on nutrient acquisition in wheat (*Triticum aestivum* L.). *Agronomy* 8, 158. doi: 10.3390/agronomy8090158

Dimkpa, C. O., Singh, U., Bindraban, P. S., Elmer, W. H., Gardea-Torresdey, J. L., and White, J. C. (2018b). Exposure to weathered and fresh nanoparticle and ionic Zn in soil promotes grain yield and modulates nutrient acquisition in wheat (*Triticum aestivum* L.). *J. Agric. Food Chem.* 66, 9645–9656. doi: 10.1021/acs.jafc.8b03840

Dimkpa, C. O., Singh, U., Bindraban, P. S., Adisa, I. O., Elmer, W. H., Gardea-Torresdey, J. L., et al. (2019a). Addition-omission of zinc, copper, and boron nano and bulk particles demonstrate element and size -specific response of soybean to micronutrients exposure. *Sci. Total Environ.* 665, 606–616. doi: 10.1016/j.scitotenv.2019.02.142

Dimkpa, C. O., Singh, U., Bindraban, P. S., Elmer, W. H., Gardea-Torresdey, J. L., and White, J. C. (2019b). Zinc oxide nanoparticles alleviate drought-induced alterations in sorghum performance, nutrient acquisition, and grain fortification. *Sci. Total Environ.* 688, 926–934. doi: 10.1016/j.scitotenv.2019.06.392

Dimkpa, C. O. (2014). Can nanotechnology deliver the promised benefits without negatively impacting soil microbial life? *J. Basic Microbiol.* 54, 889–904. doi: 10.1002/jobm.201400298

Elmer, W., and White, J. C. (2016). The use of metallic oxide nanoparticles to enhance growth of tomatoes and eggplants in disease infested soil or soilless medium. *Environ. Sci.: Nano.* 3, 1072–1079. doi: 10.1039/C6EN00146G

Elmer, W., De La Torre-Roche, R., Pagano, L., Majumdar, S., Zuverza-Mena, N., Dimkpa, C., et al. (2018). Effect of metalloid and metallic oxide nanoparticles on *Fusarium* wilt of watermelon. *Plant Dis.* 102, 1394–1401. doi: 10.1094/PDIS-10-17-1621-RE

García-Gómez, C., Obrador, A., González, D., Babin, M., and Fernández, M. D. (2017). Comparative effect of ZnO NPs, ZnO bulk and $ZnSO_4$ in the antioxidant defences of two plant species growing in two agricultural soils under greenhouse conditions. *Sci. Total Environ.* 589, 11–24. doi: 10.1016/j.scitotenv.2017.02.153

Haris, Z., and Ahmad, I. (2017). Impact of metal oxide nanoparticles on beneficial soil microorganisms and their secondary metabolites. *Int. J. Life. Sci. Scienti. Res.* 3, 1020–1030. doi: 10.21276/ijlssr.2017.3.3.10

Irfan, M., Niazi, M. B. K., Hussain, A., Farooq, W., and Zia, M. H. (2018). Synthesis and characterization of zinc-coated urea fertilizer. *J. Plant Nutr.* 41, 1625–1635. doi: 10.1080/01904167.2018.1454957

Jośko, I., and Oleszczuk, P. (2013). Influence of soil type and environmental conditions on ZnO, TiO_2 and Ni nanoparticles phytotoxicity. *Chemosphere* 92, 91–99. doi: 10.1016/j.chemosphere.2013.02.048

Joy, E. J. M., Stein, A. J., Young, S. D., Ander, E. L., Watts, M. J., and Broadley, M. R. (2015). Zinc-enriched fertilisers as a potential public health intervention in Africa. *Plant Soil* 389, 1–24. doi: 10.1007/s11104-015-2430-8

Karim, M. R., and Rahman, M. A. (2015). Drought risk management for increased cereal production in asian least developed countries. *Weath. Clim. Extr.* 7, 24–35. doi: 10.1016/j.wace.2014.10.004

Karim, M. R., Zhang, Y.-Q., Zhao, R.-R., Chen, X.-P., Zhang, F.-S., and Zou, C.-Q. (2012). Alleviation of drought stress in winter wheat by late foliar application of zinc, boron, and manganese. *J. Plant Nutri. Soil Sci.* 175, 142–151. doi: 10.1002/jpln.201100141

Karlowsky, S., Augusti, A., Ingrisch, J., Akanda, M. K. U., Bahn, M., and Gleixner, G. (2018). Drought-induced accumulation of root exudates supports post-drought recovery of microbes in mountain grassland. *Front. Plant Sci.* 9, 1593. doi: 10.3389/fpls.2018.01593

Kottegoda, N., Sandaruwan, C., Priyadarshana, G., Siriwardhana, A., Rathnayake, U. A., Arachchige, D. M. B., et al. (2017). Urea-hydroxyapatite nanohybrids for slow release of nitrogen. *ACS Nano.* 11, 1214–1221. doi: 10.1021/acsnano.6b07781

Lesk, C., Rowhani, P., and Ramankutty, N. (2016). Influence of extreme weather disasters on global crop production. *Nature* 529, 84–87. doi: 10.1038/nature16467

Lindsay, W. L., and Norvell, W. A. (1978). Development of a DTPA soil test for zinc, iron, manganese, and copper 1. *Soil Sci. Soc Ame. J.* 42, 421–428. doi: 10.2136/sssaj1978.03615995004200030009x

Maathuis, F. (2009). Physiological functions of mineral nutrients. *Curr. Opin. Plant Biol.* 12, 250–258. doi: 10.1016/j.pbi.2009.04.003

Martineau, N., McLean, J. E., Dimkpa, C. O., Britt, D. W., and Anderson, A. J. (2014). Components from wheat roots modify the bioactivity of ZnO and CuO NPs in a soil bacterium. *Environ. Pollut.* 187, 65–72. doi: 10.1016/j.envpol.2013.12.022

Milani, N., McLaughlin, M. J., Stacey, S. P., Kirby, J. K., Hettiarachchi, G. M., Beak, D. G., et al. (2012). Dissolution kinetics of macronutrient fertilizers coated with manufactured zinc oxide nanoparticles. *J. Agric. Food Chem.* 60, 3991–3998. doi: 10.1021/jf205191y

Milani, N., Hettiarachchi, G. M., Kirby, J. K., Beak, D. G., Stacey, S. P., and McLaughlin, M. J. (2015). Fate of zinc oxide nanoparticles coated onto macronutrient fertilizers in an alkaline calcareous soil. *PloS One* 10, e0126275. doi: 10.1371/journal.pone.0126275

Moreno-Jiménez, E., Plaza, C., Saiz, H., Manzano, R., Flagmeier, M., and Maestre, F. T. (2019). Aridity and reduced soil micronutrient availability in global drylands. *Nat. Sust.* 2, 371–377. doi: 10.1038/s41893-019-0262-x

Mukherjee, A., Sun, Y., Morelius, E., Tamez, C., Bandyopadhyay, S., Niu, G., et al. (2016). Differential toxicity of bare and hybrid ZnO nanoparticles in green pea (*Pisum sativum* L.): a life cycle study. *Front. Plant Sci.* 6, 1242. doi: 10.3389/fpls.2015.01242

Piccinno, F., Gottschalk, F., Seeger, S., and Nowack, B. (2012). Industrial production quantities and uses of ten engineered nanomaterials in Europe and the world. *J. Nanopart. Res.* 14, 1109. doi: 10.1007/s11051-012-1109-9

Qiu, H., and Smolders, E. (2017). Nanospecific phytotoxicity of CuO nanoparticles in soils disappeared when bioavailability factors were considered. *Environ. Sci. Technol.* 51, 11976–11985. doi: 10.1021/acs.est.7b01892

Rajput, V. D., Minkina, T. M., Behal, A., Sushkova, S. N., Mandzhieva, S., Singh, R., et al. (2018). Effects of zinc-oxide nanoparticles on soil, plants, animals and soil organisms: a review. *Environ. Nanotechnol. Monit. Manage.* 9, 76–84. doi: 10.1016/j.enmm.2017.12.006

Raliya, R., Tarafdar, J. C., and Biswas, P. (2016). Enhancing the mobilization of native phosphorus in mung bean rhizosphere using ZnO nanoparticles synthesized by fungi. *J. Agric. Food Chem.* 64, 3111–3118. doi: 10.1021/acs.jafc.5b05224

Santos, G. A., Korndorfer, G. H., Pereira, H. S., and Paye, W. (2018). Addition of micronutrients to NPK formulation and initial development of maize plants. *Biosci. J.* 34, 927–936. doi: 10.14393/BJ-v34n1a2018-36690

Sher, A. K., Naveed, G., Ahmad, K. A., Saeed, M., and Masaud, S. (2018). Phenology and biomass production of wheat in response to micronutrients and nitrogen application. *Sarhad. J. Agric.* 34, 712–723. doi: 10.17582/journal.sja/2018/34.4.712.723

Shivay, Y. S., Prasad, R., and Rahal, A. (2008a). Relative efficiency of zinc oxide and zinc sulphate-enriched urea for spring wheat. *Nutr. Cycl. Agroecosyst.* 82, 259–264. doi: 10.1007/s10705-008-9186-y

Shivay, Y. S., Kumar, D., Prasad, R., and Ahlawat, I. P. S. (2008b). Relative yield and zinc uptake by rice from zinc sulphate and zinc oxide coatings onto urea. *Nutr. Cycl. Agroecosyst.* 80, 181–188. doi: 10.1007/s10705-007-9131-5

Subbaiah, L. V., Prasad, T. N. V. K. V., Krishna, T. G., Sudhakar, P., Reddy, B. R., and Pradeep, T. (2016). Novel effects of nanoparticulate delivery of zinc on growth, productivity, and zinc biofortification in maize (*Zea mays* L.). *J. Agric. Food Chem.* 64, 3778–3788. doi: 10.1021/acs.jafc.6b00838

Watson, J.-L., Fang, T., Dimkpa, C. O., Britt, D. W., McLean, J. E., Jacobson, A., et al. (2015). The phytotoxicity of ZnO nanoparticles on wheat varies with soil properties. *Biometals* 28, 101–112. doi: 10.1007/s10534-014-9806-8

Watts-Williams, S. J., Turney, T. W., Patti, A. F., and Cavagnaro, T. R. (2014). Uptake of zinc and phosphorus by plants is affected by zinc fertilizer material and arbuscular mycorrhizas. *Plant Soil* 376, 165–175. doi: 10.1007/s11104-013-1967-7

Yang, K.-Y., Doxey, S., McLean, J. E., Britt, D., Watson, A., Al Qassy, D., et al. (2018). Remodeling of root morphology by CuO and ZnO nanoparticles: effects on drought tolerance for plants colonized by a beneficial pseudomonad. *Botany* 96, 175–186. doi: 10.1139/cjb-2017-0124

Zengin, F. K. (2006). The effects of Co^{2+} and Zn^{2+} on the contents of protein, abscisic acid, proline and chlorophyll in bean (*Phaseolus vulgaris* cv. Strike) seedlings. *J. Environ. Biol.* 27, 441–448.

Zhang, T., Sun, H., Lv, Z., Cui, L., Mao, H., and Kopittke, P. M. (2018). Using synchrotron-based approaches to examine the foliar application of $ZnSO_4$ and ZnO nanoparticles for field-grown winter wheat. *J. Agric. Food Chem.* 66, 2572–2579. doi: 10.1021/acs.jafc.7b04153

Zhao, F. J., Lombi, E., Breedon, T., and McGrath, S. P. (2000). Zinc hyperaccumulation and cellular distribution in *Arabidopsis halleri*. *Plant Cell Environ.* 23, 507–514. doi: 10.1046/j.1365-3040.2000.00569.x

Conflict of Interest: The authors declare that the research was conducted in the absence of any commercial or financial relationships that could be construed as a potential conflict of interest.

frontiers in Plant Science

MINI REVIEW
published: 26 February 2020
doi: 10.3389/fpls.2020.00123

Grapevine Potassium Nutrition and Fruit Quality in the Context of Climate Change

Jérémy Villette[1], *Teresa Cuéllar*[2], *Jean-Luc Verdeil*[2], *Serge Delrot*[3] *and Isabelle Gaillard*[1]*

[1] BPMP, Univ Montpellier, CNRS, INRAE, SupAgro, Montpellier, France, [2] CIRAD, UMR AGAP, Univ Montpellier, INRA, Montpellier SupAgro, Montpellier, France, [3] EGFV, Bordeaux Sciences Agro, INRAE, Université de Bordeaux, ISVV, Villenave d'Ornon, France

Potassium (K^+) nutrition is of relevant interest for winegrowers because it influences grapevine growth, berry composition, as well as must and wine quality. Indeed, wine quality strongly depends on berry composition at harvest. However, K^+ content of grape berries increased steadily over the last decades, in part due to climate change. Currently, the properties and qualities of many fruits are also impacted by environment. In grapevine, this disturbs berry properties resulting in unbalanced wines with poor organoleptic quality and low acidity. This requires a better understanding of the molecular basis of K^+ accumulation and its control along grape berry development. This mini-review summarizes our current knowledge on K^+ nutrition in relation with fruit quality in the context of a changing environment.

Keywords: potassium nutrition, potassium transport, fruit quality, grape berries, climate change

OPEN ACCESS

Edited by:
Guillermo Esteban Santa María, National University of General San Martín, Argentina

Reviewed by:
Begona Benito, Polytechnic University of Madrid, Spain
Ingo Dreyer, University of Talca, Chile

***Correspondence:**
Isabelle Gaillard
isabelle.gaillard@inrae.fr

Specialty section:
This article was submitted to Plant Nutrition, a section of the journal Frontiers in Plant Science

Received: *09 December 2019*
Accepted: *28 January 2020*
Published: *26 February 2020*

Citation:
Villette J, Cuéllar T, Verdeil J-L, Delrot S and Gaillard I (2020) Grapevine Potassium Nutrition and Fruit Quality in the Context of Climate Change. Front. Plant Sci. 11:123. doi: 10.3389/fpls.2020.00123

INTRODUCTION

Plant growth and development rely on a balanced distribution of different mineral elements that are needed for various physiological processes. The beneficial effects of adding mineral elements to soils to improve plant growth has been known and used in agriculture for more than several thousand years. However, in the context of climate change, plants are facing increasing challenges to maintain balanced growth. High temperatures and soil water deficits associated with climate change affect agriculture and largely constrain plant productivity. Moreover, final product quality is also altered by excessive solar radiation, atmospheric CO_2 levels, and rainfalls (Schultz, 2000; Korres et al., 2016). Grapevine (*Vitis vinifera*) is the most economically important fruit crop in the world. Wine grapes are particularly threatened by this phenomenon because its oenological potential is directly linked to its composition, in turn depending on pedoclimatic conditions (vintage effect). In this context, it is therefore important for the vine growers and wine makers to adapt many field practices including mineral nutrition.

Great wines are famous for their high standard and characteristic flavors that are distinguishable and reflect their environment (climate, soils, and grown varieties). In France, the southern regions have a typical Mediterranean climate with warm and long summers whereas central and northern regions undergo more humid climates. These climatic aspects have been properly taken into account in the past, to adapt various grapevine varieties and best suit their environmental conditions. But today the berry properties such as color, flavor, and aroma components are

modified by the current climate environment, which results in unbalanced wines, with high alcoholic content and excessively low acidity (Jones et al., 2005). This is due to the regular increase of grape berry K^+ and sugar contents that have been observed during the last decades.

Obviously, deficiencies in major minerals like potassium (K^+), nitrogen (N), and phosphorus (P) strongly affect metabolism with subsequent impacts on plant growth, crop yield, nutritional value, and composition of grape berries (Amtmann and Armengaud, 2009; Fernandes et al., 2016). But with the effects of climate change, impact of mineral nutrition might change. This has been extensively studied for K^+ nutrition because several reports mentioned that when K^+ accumulation in grape berries at harvest is too high, berry acidity is too low (Conde et al., 2007; Walker and Blackmore, 2012).

Potassium is the major cation in plants. It can be present up to 10% of dry mass. It is a highly mobile osmolyte and a major component in the cation/anion balance. K^+ is involved in neutralization of negative charges and organic acids and contributes to cellular turgor and elongation and mechanical movements such as stomata aperture or leaf movements (Maathuis, 2009; Sharma et al., 2013; Dreyer, 2014). Cytoplasmic concentration of K^+ is maintained around 80 to 100 mM. Preserving this concentration range is important for many physiological processes as the control of electrical membrane potential, the maintenance of pH homeostasis in the cells, enzyme activations, and stabilization of protein synthesis. These different functions explain why K^+ is so important for plants and is present in all tissues and subcellular compartments of cells. Indeed, it has been shown that plants accumulate large amounts of K^+ in their vacuoles, surpassing purely nutritional requirements. K^+ deficiency has negative impact on plant growth. K^+ starvation reduces also the ability to use N and provokes chlorosis at the tip of older leaves in cereal crops, increasing crop's susceptibility to diseases and affecting plant metabolism (Armengaud et al., 2009; Zörb et al., 2014; Coskun et al., 2017). Plant performance depends on K^+ availability in soil and K^+ uptake efficiency. To perform an optimal preservation of K^+ homeostasis, a large group of K^+ transporters and channels has been identified in plants. They are involved in K^+ uptake by roots, ion translocation between organs and tissues, and storage in cellular vacuoles.

In grapevine, K^+ plays an essential role in the initiation and control of massive fluxes that are necessary for berry growth during maturation (Cuéllar et al., 2013; Nieves-Cordones et al., 2019). In addition, grape acidity at harvest is a key factor to obtain wines of great quality. Grape acidity results from the ratio between free organic acids (i.e. malic and tartaric acids) and organic acids neutralized by K^+. In the context of warmer climates, K^+ ion accumulation increases during grape ripening, leading to an excessive neutralization of organic acids (Cuéllar et al., 2010; Cuéllar et al., 2013; Rogiers et al., 2017; Nieves-Cordones et al., 2019). Moreover, high temperature also affects the organic acid content of berries inducing the consumption of malic acid as a respiratory substrate (Famiani et al., 2016). This results in a low-acidic must context leading to the formation of insoluble K^+ bitartrate during winemaking. Not only this amplifies the loss of acidity but this also gives rise to unstable wines with poor organoleptic properties. This is a major concern for grape production, although the molecular determinants that control berry acidity and K^+ accumulation during ripening are still poorly known. Adaptation to climate changes is becoming a major challenge for grapevine. This mini-review focuses on K^+ nutrition in grapevine in the context of our current environment and summarizes the knowledge available nowadays.

PLANTS K^+ TRANSPORT SYSTEMS AND PHYSIOLOGICAL FUNCTIONS

In the model plant *Arabidopsis thaliana*, a total of about 70 K^+ channels and transporters, differing in transport affinity, energetic coupling, voltage sensitivity, or ionic selectivity, have been identified (Mäser et al., 2001; Lebaudy et al., 2008; Sharma et al., 2013; Véry et al., 2014). In grapevine, because excess of K^+ levels in berries may have a negative impact on wine quality, molecular determinants of K^+ transport are under investigation. Plant major multi-gene families encoding K^+ permeable transport systems belong to one of the following five families (i) HAK-KUP-KT transporters, (ii) HKT transporters, (iii) cation-proton antiporters (CPA), (iv) Shaker-like K^+ channels, and (v) two pore K (TPKs) channels. This review only focuses on the three transporters families and the K^+ Shaker channels which are briefly presented below (**Figure 1**, Mäser et al., 2001; Sharma et al., 2013; Véry et al., 2014).

K^+-Selective Transporters HAK-KUP-KT

The HAK-KUP-KT family is usually selective for K^+. Plant HAK-KUP-KT proteins possess 10 to 14 transmembrane domains with both N- and C-termini at the membrane intracellular side. These transporters are present in plants, fungi, bacteria, and even viruses but not in animals. They are crucial for organisms facing external solutions containing very low K^+ concentrations (μM range) (Nieves-Cordones et al., 2010). In flowering plants, the HAK-KUP-KT family displays variable number of members: 13 genes have been identified in *A. thaliana* and 18 in grapevine which are classified among clades I-V (Nieves-Cordones et al., 2016). High-affinity K^+ transport has been demonstrated for all members of the clade I sub-family to which belongs, e.g. HAK5 (high affinity K^+ 5). HAK5, located at the plasma membrane, contributes to high affinity K^+ uptake from soil and to root elongation (Ragel et al., 2019). HAK5 transporters are transcriptionally up-regulated under K^+ starvation conditions in *A. thaliana*, but also in agronomic crop species like rice, barley, pepper, and tomato (Santa-María et al., 1997; Bañuelos et al., 2002; Martínez-Cordero et al., 2004; Nieves-Cordones et al., 2008). Moreover, HAK5 is also up-regulated in -K, -N, and -P starvation in tomato, whereas in *A. thaliana*, HAK5 is up-regulated only in -K^+ and -N deficiencies (Rubio et al., 2014). This suggests different responses and regulation between plant species.

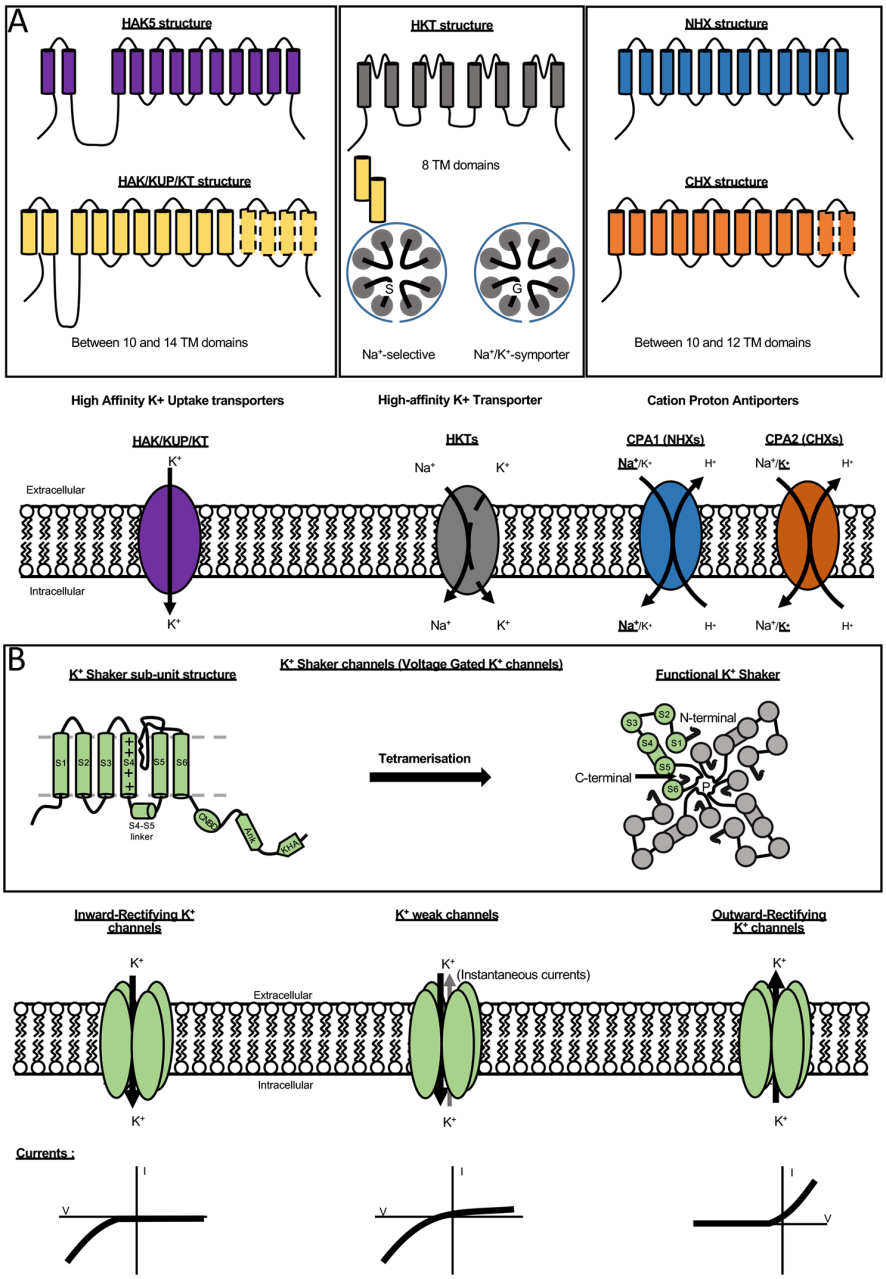

FIGURE 1 | K^+ transporter and channel families. **(A)** Structure and function of different transporter families. The family HAK/KUP/KT (left panel) is present in all plant genomes and contains 13 members in *A. thaliana* and 18 in vine distributed into five clades. Arabidopsis has just one member belonging to cluster I, AtHAK5, which has been extensively studied and its structure is shown in the top. The general structure of the HAK/KUP/KT transporters is conserved. The number of transmembrane segments (TMS) is ranged from 10 to14, with the most common being 11–12 TMS. The HKT (High-affinity K^+ Transporter) transporters (middle panel) are distributed into two families depending of the presence of a glycine into the first pore loop proposed as a K^+ selectivity determinant. All members of HKT family are composed of eight transmembrane domains. The last family of K^+ transporters is the CPA family (right panel) for Cation Proton Antiporters. CPAs are composed of 10 to 12 transmembrane domains. This family is divided in two sub-families (CPA1 and CPA2). CPA1 mainly consists in NHX antiporters ($Na^+(K^+)/H^+$ exchangers). CPA2 is mainly constituted by CHXs (cation/H^+ exchangers). Information on the CPA family is still fragmentary. **(B)** Description of K^+ Shaker channels. The structure of different members is strictly conserved with six transmembrane domains. The fourth transmembrane segment (S4) harbors positively charged amino acids and acts together with S1, S2, and S3 as voltage sensor. The pore domain is located between the TMS5 and TMS6 domains. The C-terminal extremity of Shaker sub-unit is composed of three distinct domains: a cyclic nucleotide-binding domain (CNBD), an ankyrin domain allowing protein-protein interactions and a KHA domain rich in hydrophobic and acidic amino acids. Functional Shaker channels are multimeric proteins formed by the assembly of four Shaker gene products (Dreyer et al., 2019). In plants, three types of K^+ Shaker channel localized at the plasma membrane have been exhaustively characterized: the inwardly, weak inwardly or outwardly rectifying K^+ channels which drive inward or outward K^+ fluxes across the plasma membrane according to the membrane potential.

In *A. thaliana*, the 12 other members of this family are present in different tissues and are probably involved in many diverse physiological functions in plants (Ahn et al., 2004). Among them, AtKUP2, 4, 6, and 7 are involved in cell enlargement, K^+ translocation, and long-distance K^+ transport (Han et al., 2016; Santa-María et al., 2018). Some studies showed a large reduction of HAK-KUP-KT transcripts under high salt conditions and K^+ deficiencies (Nieves-Cordones et al., 2010; Li et al., 2018). An interplay between sodium (Na^+) and K^+, at elevated concentrations of Na^+, is described to have a negative effect on the expression of members of this family. In maize, it has recently been shown that some HAK transporters can transport Na^+ instead of K^+ (Zhang et al., 2019). These transporters belong to clade IV of the HAK-KUP-KT family. In grapevine, only one member was identified in this sub-group (Benito et al, 2012).

In grape, only two HAK-KUP-KT-type K^+ transporters have been studied so far. They are expressed most highly in the berry skin during the first phase of berry development (Davies et al., 2006) and therefore do not participate to the berry loading after veraison (the onset of ripening).

Non-Selective Cation-Transporters HKT and CPA

Transporters of the HKT (high-affinity K^+ transporter) and CPA families display varying permeabilities for K^+ and Na^+.

The HKT transporters can be divided into two sub-families; "Na^+-selective transporters" or "Na/K^+"-symporters. The Na^+ selective transporter sub-family (sub-family I) is found in all higher plant species whereas the sub-family II which contains Na^+/K^+ symporters and K^+-selective transporters, has been so far only identified in the monocotyledonous plants. The division into the two sub-families is associated with a molecular determinant of permeability to K^+ that has been identified in the selectivity filter. The key amino acid of this determinant, located in the first pore loop, is a serine for all members of sub-family I which is replaced by glycine for the Na^+/K^+ symporters (sub-family II) (Mäser et al., 2002; Platten et al., 2006). In *A. thaliana*, a single HKT gene has been identified in the sub-family I, and is a strong actor of the tolerance to salinity in this species (Berthomieu et al., 2003). In grapevine, six HKTs have been identified, all belonging to the sub-family I. One of them, named VisHKT1:1, has been shown to be involved in the control of leaf Na^+ exclusion and so in Na^+ tolerance (Henderson et al., 2018). Water shortage induced by climate change leads to the use of water containing high levels of sodium chloride in some countries. The HKT1 K^+ transporter may be a good candidate to avoid Na^+ toxicity (Henderson et al., 2018). In the monocotyledonous crop species, several genes distributed into the two sub-families have been identified, e.g. rice (eight or nine genes depending on the cultivar) or wheat (nine genes) (Véry et al., 2014). The members belonging to the sub-family II are thought to play an important role in the regulation of K^+ homeostasis at saline conditions in different species (Platten et al., 2006; Hamamoto et al., 2015; Cao et al., 2019).

The CPA family is divided in two sub-families. In *A. thaliana*, there are the NHX (Na^+/H^+ exchanger) antiporter sub-family, composed of eight members, and the CHX antiporter (cation/H^+ exchanger) sub-family, including 33 members (Pardo et al., 2006). These two sub-families are composed of cation transporters present in the endomembranes as AtNHX5 and AtNHX6 (Dragwidge et al., 2019), at the vacuolar membrane as AtNHX1 or AtNHX2 (Bassil et al., 2011a), or at the plasma membrane like AtCHX17 (Chanroj et al., 2013). Some of these antiporters are involved in the regulation of K^+ homeostasis, intravacuolar and cellular pH homeostasis, cell expansion, and salt stress tolerance (Chanroj et al., 2012). This family of antiporters is not well characterized, but some studies with double knock-out mutants showed disturbed phenotypes in *A. thaliana* (Apse et al., 1999; Bassil et al., 2011a; Bassil et al., 2011b). In grapevine genome, six genes belonging to NHX sub-family, distributed in two distinct groups: vacuolar (VvNHX1-5) and endosomal members (VvNHX6) (Ayadi et al., 2020) and eight genes belonging to CHX sub-family have been identified (Ma et al., 2015). One member of the NHX family (VvNHX1) which is expressed in the tonoplast of mesocarp cells, is involved in the accumulation of K^+ in the vacuole and in the control of homeostasis of cytosolic K^+ during grape ripening (Hanana et al., 2007).

Voltage-Gated K^+ Shaker Channels

Shaker channels are the best-characterized family related to K^+ transport in plants. These channels dominate K^+ fluxes in plants and are crucial to drive sustained fluxes across the plasma membranes. In *A. thaliana*, nine sub-units have been identified and characterized. Functional channels are tetrameric proteins arranged around a central pore (Dreyer et al., 2004; Sharma et al., 2013; Véry et al., 2014) and are composed by assembling of four Shaker subunits encoded either by the same gene (homomeric channel) or by different genes (heteromeric channel). Heterotetramerization is known to increase channel functional diversity (Jeanguenin et al., 2008; Sharma et al., 2013; Véry et al., 2014). Depending on their functional features, these channels drive inwardly or outwardly rectifying K^+ fluxes according to the plasma membrane potential. Thereby, they mediate K^+ translocation out of or into the cell (Sharma et al., 2013; Véry et al., 2014).

In addition to their functional properties, it is worth to note that the role of these channels *in planta* strongly depends on the tissue in which they are expressed. Indeed the same channel, expressed in both the phloem and stomata, is involved in the two different physiological processes taking place in these tissues. For example, one recent study focusing on the phloem highlights the importance of the outward Shaker channel GORK, which drives K^+ efflux, in the membrane repolarization (Cuin et al., 2018) whereas this same channel, expressed in guard cells, is involved in stomatal closure (Hosy et al., 2003). In *A. thaliana*, the underlying mechanisms controlling stomatal movements have been extensively studied in relation with the K^+ transport. Whereas GORK is the only outward K^+ Shaker channel controlling stomatal closure, the inward-rectifying K^+ currents involved in stomatal opening are driven by multiple inward Shaker channels named KAT1, KAT2, and AKT1 (Lebaudy et al.,

2008). Otherwise, AKT1 is also expressed in the root where it is involved in K^+ uptake from the soil and its activity is regulated by interacting with different CIPK/CBL complexes (Xu et al., 2006). In tomato and grapevine, orthologous K^+ channels of AKT1, named LKT1 and VvK1.1, respectively, have been shown to be involved in the K^+ uptake from the soil but also in pips K^+ accumulation in grapevine (Hartje et al., 2000; Cuéllar et al., 2010).

Similarly to *A. thaliana*, the grapevine genome also contains nine Shaker genes coding for nine channel subunits with a number of members within each Shaker sub-family that is not strictly conserved between the two species. The VvK1.2 channel (an AKT1-like channel), is only expressed in the plasma membrane of the grape berry flesh cells and its unique function is to load K^+ ions into these cells (Cuéllar et al., 2013). The VvK3.1 channel which, as its most related *A. thaliana* AKT2 channel, forms a weakly rectifying channel, giving rise to two current components with different gating modes. This unique property allows the AKT2-like channels to mediate inward as well as outward K^+ currents. These channels are known to dominate phloem K^+ conductance where they have a major role in phloem K^+ loading and unloading (Marten et al., 1999; Lacombe et al., 2000; Ache et al., 2001; Hafke et al., 2007). In grapevine, VvK3.1 channel mediates K^+ unloading in the berries and is also involved in the maintenance of transmembrane K^+ gradients of phloem cells, which refers to the concept of K^+ battery (Gajdanowicz et al., 2011; Dreyer et al., 2017; Nieves-Cordones et al., 2019). The K^+ battery explains how an open AKT2-like channel can compensate for the reduced pH gradient present under energy limitation and can provide additional energy stored in the K^+ gradient between the phloem cytosol and the berry apoplast for transmembrane transport processes (Dreyer et al., 2017). This plays a major role in driving sugar, amino acid, and water transport across plant cell membranes during phloem unloading and allows the phloem stream flux toward the berry may persist over a long period of time. Finally, four K^+ outward Shaker subunits have been identified in grapevine whereas only two outward subunits exist in *A. thaliana.* Among them, the VvK5.1 Shaker exhibits an expression territory strongly enlarged in comparison with SKOR, its most related *A. thaliana* gene (Villette et al., 2019). As SKOR, this grapevine Shaker is also involved in K^+ root to shoot translocation but its larger expression profile reveals new roles not described so far, e.g. the involvement of a K^+ Shaker in the process of lateral root primordium development (Villette et al., 2019). In response to climate change, K^+ transporters and particularly K^+ Shaker channels identified in grapevine appear to be key molecular actors to sustain a suitable K^+ uptake and distribution.

GRAPEVINE K^+ NUTRITION IN THE CONTEXT OF CLIMATE CHANGE

The current climatic context with increasing temperatures and carbon dioxide levels, ozone depletion, and decrease in precipitation patterns is becoming a major challenge for agriculture (Korres et al., 2016). These adverse conditions influence productivity by affecting overall plant performance and disturbing plant phenology. Obviously, grapevine is affected by this climatic conditions, and doubly so, since wine production depends on both maintaining a good yield and grape composition at harvest.

Among the climate parameters that affect the most the berry content at harvest, temperature and water availability play a prominent role. High temperature affects the phenology of grape berry development and ripening, resulting in a shift of picking dates toward earlier periods depending on the region, the variety, and the wine type. Heat waves directly increase sugar import (Mori et al., 2007; Parker et al., 2011) and K^+ accumulation (Mpelasoka et al., 2003; Cuéllar et al., 2010; Kodur, 2011; Cuéllar et al., 2013; Rogiers et al., 2017; Nieves-Cordones et al., 2019). Phloem transport and berry metabolism also increase at high temperature. From the onset of the ripening (veraison), berry loading is ensured from the phloem by a directional flow of water, sugar, and nutrients driven by massive K^+ fluxes (Nieves-Cordones et al., 2019). In addition, it is also known that vineyards grown in warmer areas give wines with low acidity. This is due to an excessive accumulation of K^+ leading to an increase of the electrical neutralization of organic acids, which disturbs the control of the pH and of the acid-base balance of the flesh cells (Kodur, 2011). High temperatures also decrease the atmospheric water potential and favor plant transpiration and soil dehydration, which in turn favor water stress. Upon drought stress, it is worth to note that the shaker channels VvK1.1, VvK1.2, and VvK3.1, whose expression located in berry phloem vasculature or in berry flesh cells, are strongly up-regulated (Cuéllar et al., 2010; Cuéllar et al., 2013; Nieves-Cordones et al., 2019).These Shaker channels could thus play a role in K^+ loading into berries during drought stress. We (and others) have invested in the identification of K^+ transport systems and molecular regulators involved in grape berry K^+ loading. Current understanding of these processes is summarized in **Figure 2**.

Plant responses to environmental stresses under a K^+-limiting scenario are poorly understood. Field studies have observed that K^+ as an osmolyte, can enhance osmotic adjustment or osmoprotection by maintenance of leaf turgor. This is directly linked to the improved capacity to retain water (Babita et al., 2010; Levi et al., 2011). Moreover, Rivas-Ubach et al. (2012) showed that in leaves of *Erica multiflora* (Heather) K^+ concentrations increase under warm and drought conditions, in agreement with the role of K^+ in osmotic protection. However, in *Olea europea* (olive) the stomatal conductance is disturbed when plants grow under moderate K^+ deficiency in water stress conditions (Arquero et al., 2006). This behavior suggests that plants are impaired in their ability to grow during drought conditions when it is not possible to take up K^+. This could explain why in grapevine, the berry K^+ concentration during ripening enhances when high temperatures are combined with water stress. This higher K^+ accumulation should contribute to a better osmotic adjustment

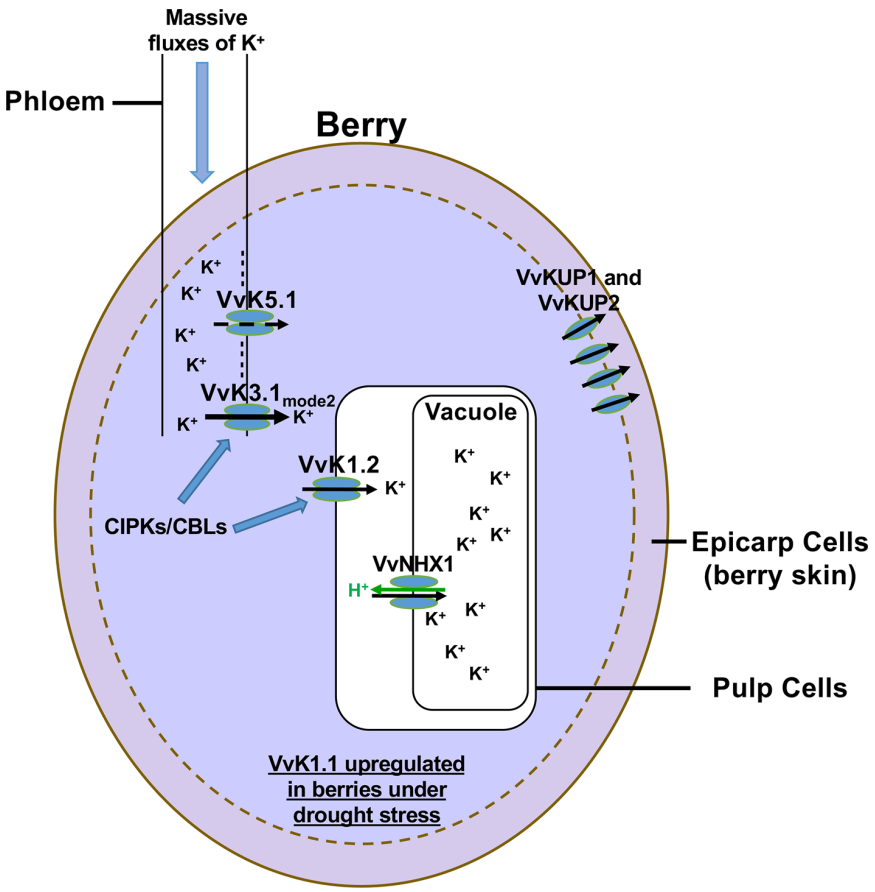

FIGURE 2 | Map of K^+ transport in grape berry. Seven K^+ transport systems have been identified and characterized to be involved in K^+ fluxes into or out of the berry cells. The first identified K^+ transport systems belonging to the HAK/KUP-KT family are VvKUP1 and VvKUP2. These transporters are involved in K^+ transport into the berry skin only during the first phase of berry development. In contrast, three K^+ Shaker channels and one antiporter belonging to the CPA family have been characterized to be involved in K^+ berry loading during its ripening. Recently, two other Shaker channels have been characterized in phloem cells. VvK5.1, which is a typical outwardly rectifying K^+ channel, is involved in the repolarization of the plasma membrane of phloem cells (Villette et al., 2019). The second one, VvK3.1, is a weakly rectifying K^+ Shaker channel that can switch between two gating modes driving either inwardly rectifying or instantaneous currents. The latter mode allows to drive K^+ influx or efflux through phloem cell membranes according to membrane potentials and K^+ gradients. At the unloading site, the K^+ gradient is in favor of K^+ efflux (100 mM in the cytosol of phloem cells and 1 mM in the apoplast). The VvK3.1 channel is the main molecular actor involved in K^+ unloading into berries, thanks to massive K^+ efflux into the apoplast (Nieves-Cordones et al., 2019). Then, apoplastic K^+ is directly recovered by the inwardly rectifying K^+ channel VvK1.2 expressed in pulp cell plasma membranes. The CPA transporter, VvNHX1, expressed in the tonoplast of pulp cells, is involved in K^+ storage in the vacuole during berry ripening (Hanana et al., 2007). It is important to note that some members of the CIPK/CBL families increase the functional activity of VvK3.1 and VvK1.2. Finally, another inwardly rectifying K^+ channel, named VvK1.1, involved in K^+ uptake from the soil in roots, is up-regulated in berries in drought stress conditions (Cuéllar et al, 2010).

in grape berry cells. In the context of climate change, many fruits present similar symptoms and suffer of detrimental effects that greatly affect their features and qualities. Under high temperature exposure, during maturing, apples become less acid with a decrease of fruit firmness and watercore (Sugiura et al., 2013). In sweet orange (*Citrus sinensis*) and clementine (*Citrus clementina*) sugar content increases and fruit acidity decreases (Albrigo and Galán Saúco, 2004; Cercós et al., 2006). During flowering, high temperatures can have a deleterious impact on olive production (Gabaldón-Leal et al., 2017). Altogether, understanding the underlying mechanisms to face to the climate change is now an important challenge for fruit production.

AUTHOR CONTRIBUTIONS

All authors listed have made a substantial and intellectual contribution to the work, and approved it for publication.

FUNDING

This work was supported by SweetKaliGrape ANR (ANR-33 14-CE20-0002-02). JV was the recipient of a PhD fellowship from the Institut National Recherche Agronomique and from Agropolis fondation in the context of APLIM (Advanced Plant Life Imaging) project (contract 1504-005).

REFERENCES

Ache, P., Becker, D., Deeken, R., Dreyer, I., Weber, H., Fromm, J., et al. (2001). VFK1, a Vicia faba K^+ channel involved in phloem unloading. *ThePlant J.* 27, 571–580. doi: 10.1046/j.1365-313X.2001.t01-1-01116.x

Ahn, S. J., Shin, R., and Schachtman, D. P. (2004). Expression of KT/KUP genes in arabidopsis and the role of root hairs in K^+ uptake. *Plant Physiol.* 134 (3), 1135. doi: 10.1104/pp.103.034660

Albrigo, G., and Galán Saúco, V. (2004). Flower bud induction, flowering and fruit-set of some tropical and subtropical fruit tree crops with special reference to citrus. *Acta Hortic.* 632, 81–90. doi: 10.17660/ActaHortic.2004.632.10

Amtmann, A., and Armengaud, P. (2009). Effects of N, P, K and S on metabolism: new knowledge gained from multi-level analysis. *Curr. Opin. In Plant Biol.* 12 (3), 275–283. doi: 10.1016/j.pbi.2009.04.014

Apse, M. P., Aharon, G. S., Snedden, W. A., and Blumwald, E. (1999). Salt tolerance conferred by overexpression of a vacuolar Na^+/H^+ antiport in arabidopsis. *Science* 285 (5431), 1256. doi: 10.1126/science.285.5431.1256

Armengaud, P., Sulpice, R., Miller, A. J., Stitt, M., Amtmann, A., and Gibon, Y. (2009). Multilevel analysis of primary metabolism provides new insights into the role of potassium nutrition for glycolysis and nitrogen assimilation in arabidopsis roots. *Plant Physiol.* 150 (2), 772. doi: 10.1104/pp.108.133629

Arquero, O., Diego, B., and Benlloch, M. (2006). Potassium starvation increases stomatal conductance in olive trees. *HortScience: A Publ. Am. Soc. Hortic. Sci.* 41 (2), 433–436. doi: 10.21273/HORTSCI.41.2.433

Ayadi, M., Martins, V., Ben Ayed, R., Jbir, R., Feki, M., Mzid, R., et al. (2020). Genome wide identification, molecular characterization, and gene expression analyses of grapevine NHX antiporters suggest their involvement in growth, ripening, seed dormancy, and stress response. *Biochem. Genet.* 58 (1), 102–128 doi: 10.1007/s10528-019-09930-4

Bañuelos, M., Garciadeblas, B., Cubero, B., and Rodríguez-Navarro, A. (2002). Inventory and functional characterization of the HAK potassium transporters of rice. *Plant Physiol.* 130 (2), 784. doi: 10.1104/pp.007781

Babita, M., Maheswari, M., Rao, L. M., Shanker, A. K., and Rao, D. G. (2010). Osmotic adjustment, drought tolerance and yield in castor (Ricinus communis L.) hybrids. *Environ. Exp. Bot.* 69 (3), 243–249. doi: 10.1016/j.envexpbot.2010.05.006

Bassil, E., Tajima, H., Liang, Y.-C., Ohto, M.-A., Ushijima, K., Nakano, R., et al. (2011a). The arabidopsis Na+/H+ antiporters nhx1 and nhx2 control vacuolar ph and k^+ homeostasis to regulate growth, flower development, and reproduction. *Plant Cell* 23 (9), 3482. doi: 10.1105/tpc.111.089581

Bassil, E., Ohto, M.-A., Esumi, T., Tajima, H., Zhu, Z., Cagnac, O., et al. (2011b). The arabidopsis intracellular Na+/H+ antiporters NHX5 and NHX6 are endosome associated and necessary for plant growth and development. *Plant Cell* 23 (1), 224. doi: 10.1105/tpc.110.079426

Benito, B., Garciadeblas, B., and Rodriguez-Navarro, A. (2012). HAK transporters from Physcomitrella patens and Yarrowia lipolytica mediate sodium uptake. *Plant Cell Physiol.* 53 (6), 1117–1123. doi: 10.1093/pcp/pcs056

Berthomieu, P., Conéjéro, G., Nublat, A., Brackenbury, W. J., Lambert, C., Savio, C., et al. (2003). Functional analysis of AtHKT1 in Arabidopsis shows that Na(+) recirculation by the phloem is crucial for salt tolerance. *EMBO J.* 22 (9), 2004–2014. doi: 10.1093/emboj/cdg207

Cao, Y., Liang, X., Yin, P., Zhang, M., and Jiang, C. (2019). A domestication-associated reduction in K^+-preferring HKT transporter activity underlies maize shoot K^+ accumulation and salt tolerance. *New Phytol.* 222 (1), 301–317. doi: 10.1111/nph.15605

Cercós, M., Soler, G., Iglesias, D. J., Gadea, J., Forment, J., and Talón, M. (2006). Global analysis of gene expression during development and ripening of citrus fruit flesh. a proposed mechanism for citric acid utilization. *Plant Mol. Biol.* 62 (4), 513–527. doi: 10.1007/s11103-006-9037-7

Chanroj, S., Wang, G., Venema, K., Zhang, M., Delwiche, C., and Sze, H. (2012). Conserved and diversified gene families of monovalent cation/h+ antiporters from algae to flowering plants. *Front. In Plant Sci.* 3, 25. doi: 10.3389/fpls.2012.00025

Chanroj, S., Padmanaban, S., Czerny, D. D., Jauh, G.-Y., and Sze, H. (2013). K+ Transporter AtCHX17 with Its hydrophilic c tail localizes to membranes of the secretory/endocytic system: role in reproduction and seed set. *Mol. Plant* 6 (4), 1226–1246. doi: 10.1093/mp/sst032

Conde, C., Silva, P., Fontes, N., Dias, A., Tavares, R., Sousa, M., et al. (2007). Biochemical changes throughout Grape Berry development and fruit and wine quality. *Food* 1, 1–22. http://hdl.handle.net/1822/6820.

Coskun, D., Britto, D. T., Shi, W., and Kronzucker, H. J. (2017). Nitrogen transformations in modern agriculture and the role of biological nitrification inhibition. *Nat. Plants* 3 (6), 17074. doi: 10.1038/nplants.2017.74

Cuéllar, T., Pascaud, F., Verdeil, J.-L., Torregrosa, L., Adam-Blondon, A.-F., Thibaud, J.-B., et al. (2010). A grapevine Shaker inward K+ channel activated by the calcineurin B-like calcium sensor 1–protein kinase CIPK23 network is expressed in grape berries under drought stress conditions. *Plant J.* 61 (1), 58–69. doi: 10.1111/j.1365-313X.2009.04029.x

Cuéllar, T., Azeem, F., Andrianteranagna, M., Pascaud, F., Verdeil, J.-L., Sentenac, H., et al. (2013). Potassium transport in developing fleshy fruits: the grapevine inward K + channel VvK1.2 is activated by CIPK–CBL complexes and induced in ripening berry flesh cells. *Plant J.* 73 (6), 1006–1018. doi: 10.1111/tpj.12092

Cuin, A. T., Dreyer, I., and Michard, E. (2018). The role of potassium channels in arabidopsis thaliana long distance electrical signalling: AKT2 modulates tissue excitability while GORK shapes action potentials. *Int. J. Mol. Sci.* 19 (4), 926. doi: 10.3390/ijms19040926

Davies, C., Shin, R., Liu, W., Thomas, M. R., and Schachtman, D. P. (2006). Transporters expressed during grape berry (Vitis vinifera L.) development are associated with an increase in berry size and berry potassium accumulation. *J. Exp. Bot.* 57 (12), 3209–3216. doi: 10.1093/jxb/erl091

Dragwidge, J. M., Scholl, S., Schumacher, K., and Gendall, A. R. (2019). NHX-type $Na^+(K^+)/H^+$ antiporters are required for TGN/EE trafficking and endosomal ion homeostasis in Arabidopsis thaliana. *J. Cell Sci.* 132 (7), jcs226472. doi: 10.1242/jcs.226472

Dreyer, I., Porée, F., Schneider, A., Mittelstädt, J., Bertl, A., Sentenac, H., et al. (2004). Assembly of plant shaker-like kout channels requires two distinct sites of the channel α-Subunit. *Biophys. J.* 87 (2), 858–872. doi: 10.1529/biophysj.103.037671

Dreyer, I., Gomez-Porras, J. L., and Riedelsberger, J. (2017). The potassium battery: a mobile energy source for transport processes in plant vascular tissues. *New Phytol.* 216 (4), 1049–1053. doi: 10.1111/nph.14667

Dreyer, I., Vergara-Jaque, A., Riedelsberger, J., and González, W. (2019). Exploring the fundamental role of potassium channels in novel model plants. *J. Exp. Bot.* -70 (21), 5985–5989. doi: 10.1093/jxb/erz413

Dreyer, I. (2014). Potassium K^+ in plants. *J. Plant Physiol.* 171, 655. doi: 10.1016/j.jplph.2014.03.001

Famiani, F., Farinelli, D., Frioni, T., Palliotti, A., Battistelli, A., Moscatello, S., et al. (2016). Malate as substrate for catabolism and gluconeogenesis during ripening in the pericarp of different grape cultivars. *Biol. Plant.* 60 (1), 155–162. doi: 10.1007/s10535-015-0574-2

Fernandes, J. C., Goulao, L. F., and Amâncio, S. (2016). Immunolocalization of cell wall polymers in grapevine (Vitis vinifera) internodes under nitrogen, phosphorus or sulfur deficiency. *J. Plant Res.* 129 (6), 1151–1163. doi: 10.1007/s10265-016-0851-y

Gabaldón-Leal, C., Ruiz-Ramos, M., de la Rosa, R., León, L., Belaj, A., Rodríguez, A., et al. (2017). Impact of changes in mean and extreme temperatures caused by climate change on olive flowering in southern Spain. *Int. J. Climatol.* 37 (S1), 940–957. doi: 10.1002/joc.5048

Gajdanowicz, P., Michard, E., Sandmann, M., Rocha, M., Corrêa, L. G. G., Ramírez-Aguilar, S. J., et al. (2011). Potassium (K^+) gradients serve as a mobile energy source in plant vascular tissues. *Proc. Natl. Acad. Sci.* 108 (2), 864. doi: 10.1073/pnas.1009777108

Hafke, J. B., Furch, A. C., Reitz, M. U., and van Bel, A. J. (2007). Functional sieve element protoplasts. *Plant Physiol.* 145, 703–711. doi: 10.1104/pp.107.105940

Hamamoto, S., Horie, T., Hauser, F., Deinlein, U., Schroeder, J. I., and Uozumi, N. (2015). HKT transporters mediate salt stress resistance in plants: from structure and function to the field. *Curr. Opin. In Biotechnol.* 32, 113–120. doi: 10.1016/j.copbio.2014.11.025

Han, M., Wu, W., Wu, W.-H., and Wang, Y. (2016). Potassium transporter KUP7 Is involved in K+ acquisition and translocation in arabidopsis root under K +-limited conditions. *Mol. Plant* 9 (3), 437–446. doi: 10.1016/j.molp.2016.01.012

Hanana, M., Cagnac, O., Yamaguchi, T., Hamdi, S., Ghorbel, A., and Blumwald, E. (2007). A grape berry (Vitis vinifera L.) cation/proton antiporter is associated with berry ripening. *Plant Cell Physiol.* 48 (6), 804–811. doi: 10.1093/pcp/pcm048

Hartje, S., Zimmermann, S., Klonus, D., and Mueller-Roeber, B. (2000). Functional characterisation of LKT1, a K+ uptake channel from tomato root hairs, and comparison with the closely related potato inwardly rectifying K+ channel SKT1 after expression in Xenopus oocytes. *Planta* 210 (5), 723–731. doi: 10.1007/s004250050673

Henderson, S. W., Dunlevy, J. D., Wu, Y., Blackmore, D. H., Walker, R. R., Edwards, E. J., et al. (2018). Functional differences in transport properties of natural HKT1;1 variants influence shoot Na^+ exclusion in grapevine rootstocks. *New Phytol.* 217 (3), 1113–1127. doi: 10.1111/nph.14888

Hosy, E., Vavasseur, A., Mouline, K., Dreyer, I., Gaymard, F., Porée, F., et al. (2003). The Arabidopsis outward K+ channel GORK is involved in regulation of stomatal movements and plant transpiration. *Proc. Natl. Acad. Sci.* 100 (9), 5549. doi: 10.1073/pnas.0733970100

Jeanguenin, L., Lebaudy, A., Xicluna, J., Alcon, C., Hosy, E., Duby, G., et al. (2008). Heteromerization of Arabidopsis Kv channel α-subunits. *Plant Signaling Behav.* 3 (9), 622–625. doi: 10.4161/psb.3.9.6209

Jones, G., White, M., Cooper, O., and Storchmann, K. (2005). Climate Change and Global Wine Quality. *Clim Change* 73, 319–343. doi: 10.1007/s10584-005-4704-2

Kodur, S. (2011). Effects of juice pH and potassium on juice and wine quality, and regulation of potassium in grapevines through rootstocks (Vitis): A short review. *Vitis - J. Grapevine Res.* 50 (1), 1–6.

Korres, N. E., Norsworthy, J. K., Tehranchian, P., Gitsopoulos, T. K., Loka, D. A., Oosterhuis, D. M., et al. (2016). Cultivars to face climate change effects on crops and weeds: a review. *Agron. Sustain. Dev.* 36 (1), 12. doi: 10.1007/s13593-016-0350-5

Lacombe, B., Pilot, G., Michard, E., Gaymard, F., Sentenac, H., and Thibaud, J.-B. (2000). A Shaker-like K^+ Channel with Weak Rectification Is Expressed in Both Source and Sink Phloem Tissues of Arabidopsis. *Plant Cell* 12 (6), 837. doi: 10.1105/tpc.12.6.837

Lebaudy, A., Vavasseur, A., Hosy, E., Dreyer, I., Leonhardt, N., Thibaud, J.-B., et al. (2008). Plant adaptation to fluctuating environment and biomass production are strongly dependent on guard cell potassium channels. *Proc. Natl. Acad. Sci.* 105 (13), 5271. doi: 10.1073/pnas.0709732105

Levi, A., Paterson, A. H., Cakmak, I., and Saranga, Y. (2011). Metabolite and mineral analyses of cotton near-isogenic lines introgressed with QTLs for productivity and drought-related traits. *Physiologia Plant.* 141 (3), 265–275. doi: 10.1111/j.1399-3054.2010.01438.x

Li, W., Xu, G., Alli, A., and Yu, L. (2018). Plant HAK/KUP/KT K+ transporters: Function and regulation. *Semin. In Cell Dev. Biol.* 74, 133–141. doi: 10.1016/j.semcdb.2017.07.009

Mäser, P., Thomine, S., Schroeder, J. I., Ward, J. M., Hirschi, K., Sze, H., et al. (2001). Phylogenetic Relationships within Cation Transporter Families of Arabidopsis. *Plant Physiol.* 126 (4), 1646. doi: 10.1104/pp.126.4.1646

Mäser, P., Hosoo, Y., Goshima, S., Horie, T., Eckelman, B., Yamada, K., et al. (2002). Glycine residues in potassium channel-like selectivity filters determine potassium selectivity in four-loop-per-subunit HKT transporters from plants. *Proc. Natl. Acad. Sci.* 99 (9), 6428. doi: 10.1073/pnas.082123799

Ma, Y., Wang, J., Zhong, Y., Cramer, G. R., and Cheng, Z.-M. (2015). Genome-wide analysis of the cation/proton antiporter (CPA) super family genes in grapevine (Vitis vinifera L.). *Plant Omics J.* 8 (4), 300–311.

Maathuis, F. J. M. (2009). Physiological functions of mineral macronutrients. *Curr. Opin. In Plant Biol.* 12 (3), 250–258. doi: 10.1016/j.pbi.2009.04.003

Martínez-Cordero, M. A., Martínez, V., and Rubio, F. (2004). Cloning and functional characterization of the high-affinity K^+ transporter HAK1 of pepper. *Plant Mol. Biol.* 56 (3), 413–421. doi: 10.1007/s11103-004-3845-4

Marten, I., Hoth, S., Deeken, R., Ache, P., Ketchum, K. A., Hoshi, T., et al. (1999). AKT3, a phloem-localized K+ channel, is blocked by protons. *Proc. Natl. Acad. Sci.* 96 (13), 7581. doi: 10.1073/pnas.96.13.7581

Mori, K., Goto-Yamamoto, N., Kitayama, M., and Hashizume, K. (2007). Loss of anthocyanins in red-wine grape under high temperature. *J. Exp. Bot.* 58 (8), 1935–1945. doi: 10.1093/jxb/erm055

Mpelasoka, B. S., Schachtman, D. P., Treeby, M. T., and Thomas, M. R. (2003). A review of potassium nutrition in grapevines with special emphasis on berry accumulation. *Aust. J. Grape Wine Res.* 9 (3), 154–168. doi: 10.1111/j.1755-0238.2003.tb00265.x

Nieves-Cordones, M., Miller, A. J., Alemán, F., Martínez, V., and Rubio, F. (2008). A putative role for the plasma membrane potential in the control of the expression of the gene encoding the tomato high-affinity potassium transporter HAK5. *Plant Mol. Biol.* 68 (6), 521. doi: 10.1007/s11103-008-9388-3

Nieves-Cordones, M., Alemán, F., Martínez, V., and Rubio, F. (2010). The Arabidopsis thaliana HAK5 K+ Transporter Is Required for Plant Growth and K+ Acquisition from Low K+ Solutions under Saline Conditions. *Mol. Plant* 3 (2), 326–333. doi: 10.1093/mp/ssp102

Nieves-Cordones, M., Ródenas, R., Chavanieu, A., Rivero, R. M., Martinez, V., Gaillard, I., et al. (2016). Uneven HAK/KUP/KT Protein Diversity Among Angiosperms: Species Distribution and Perspectives. *Front. In Plant Sci.* 7, 127. doi: 10.3389/fpls.2016.00127

Nieves-Cordones, M., Andrianteranagna, M., Cuéllar, T., Chérel, I., Gibrat, R., Boeglin, M., et al. (2019). Characterization of the grapevine Shaker K+ channel VvK3.1 supports its function in massive potassium fluxes necessary for berry potassium loading and pulvinus-actuated leaf movements. *New Phytol.* 222 (1), 286–300. doi: 10.1111/nph.15604

Pardo, J. M., Cubero, B., Leidi, E. O., and Quintero, F. J. (2006). Alkali cation exchangers: roles in cellular homeostasis and stress tolerance. *J. Exp. Bot.* 57 (5), 1181–1199. doi: 10.1093/jxb/erj114

Parker, A. K., Garcia de Cortazar-Atauri, I., van Leeuwen, C., and Chuine, I. (2011). General phenological model to characterise the timing of flowering and veraison of Vitis vinifera L. *Aust. J. Grape Wine Res.* 17, 206–216. doi: 10.1111/j.1755-0238.2011.00140.x

Platten, J. D., Cotsaftis, O., Berthomieu, P., Bohnert, H., Davenport, R. J., Fairbairn, D. J., et al. (2006). Nomenclature for HKT transporters, key determinants of plant salinity tolerance. *Trends In Plant Sci.* 11 (8), 372–374. doi: 10.1016/j.tplants.2006.06.001

Ragel, P., Raddatz, N., Leidi, E. O., Quintero, F. J., and Pardo, J. M. (2019). Regulation of K^+ Nutrition in Plants. *Front. Plant Sci.* 10, 281. doi: 10.3389/fpls.2019.002

Rivas-Ubach, A., Sardans, J., Pérez-Trujillo, M., Estiarte, M., and Peñuelas, J. (2012). Strong relationship between elemental stoichiometry and metabolome in plants. *Proc. Natl. Acad. Sci.* 109 (11), 4181. doi: 10.1073/pnas.1116092109

Rogiers, S. Y., Coetzee, Z. A., Walker, R. R., Deloire, A., and Tyerman, S. D. (2017). Potassium in the grape (Vitis vinifera L.) berry: transport and function. *Front. In Plant Sci.* 8, 1629. doi: 10.3389/fpls.2017.01629

Rubio, F., Fon, M., Ródenas, R., Nieves-Cordones, M., Alemán, F., Rivero, R. M., et al. (2014). A low K+ signal is required for functional high-affinity K+ uptake through HAK5 transporters. *Physiologia Plant.* 152 (3), 558–570. doi: 10.1111/ppl.12205

Santa-María, G. E., Rubio, F., Dubcovsky, J., and Rodríguez-Navarro, A. (1997). The HAK1 gene of barley is a member of a large gene family and encodes a high-affinity potassium transporter. *Plant Cell* 9 (12), 2281. doi: 10.1105/tpc.9.12.2281

Santa-María, G. E., Oliferuk, S., and Moriconi, J. I. (2018). KT-HAK-KUP transporters in major terrestrial photosynthetic organisms: A twenty years tale. *J. Plant Physiol.* 226, 77–90. doi: 10.1016/j.jplph.2018.04.008

Schultz, H. R. (2000). Climate change and viticulture: a European perspective on climatology, carbon dioxide and UV-B effects. *Aust. J. Grape Wine Res.* 6, 2–12. doi: 10.1111/j.1755-0238.2000.tb00156.x

Sharma, T., Dreyer, I., and Riedelsberger, J. (2013). The role of K+ channels in uptake and redistribution of potassium in the model plant Arabidopsis thaliana. *Front. In Plant Sci.* 4, 224. doi: 10.3389/fpls.2013.00224

Sugiura, T., Ogawa, H., Fukuda, N., and Moriguchi, T. (2013). Changes in the taste and textural attributes of apples in response to climate change. *Sci. Rep.* 3, 2418. doi: 10.1038/srep02418

Véry, A.-A., Nieves-Cordones, M., Daly, M., Khan, I., Fizames, C., and Sentenac, H. (2014). Molecular biology of K+ transport across the plant cell membrane: What do we learn from comparison between plant species? *J. Plant Physiol.* 171 (9), 748–769. doi: 10.1016/j.jplph.2014.01.011

Villette, J., Cuéllar, T., Zimmermann, S. D., Verdeil, J.-L., and Gaillard, I. (2019). Unique features of the grapevine VvK5.1 channel support novel functions for outward K+ channels in plants. *J. Exp. Bot*. 70 (21), 6181–6193. doi: 10.1093/jxb/erz341

Walker, R. R., and Blackmore, D. H. (2012). Potassium concentration and pH inter-relationships in grape juice and wine of Chardonnay and Shiraz from a range of rootstocks in different environments. *Aust. J. Grape Wine Res.* 18 (2), 183–193. doi: 10.1111/j.1755-0238.2012.00189.x

Xu, J., Li, H.-D., Chen, L.-Q., Wang, Y., Liu, L.-L., He, L., et al. (2006). A Protein Kinase, Interacting with Two Calcineurin B-like Proteins, Regulates K+ Transporter AKT1 in Arabidopsis. *Cell* 125 (7), 1347–1360. doi: 10.1016/j.cell.2006.06.011

Zörb, C., Senbayram, M., and Peiter, E. (2014). Potassium in agriculture – Status and perspectives. *J. Plant Physiol*. 171 (9), 656–669. doi: 10.1016/j.jplph.2013.08.008

Zhang, M., Liang, X., Wang, L., Cao, Y., Song, W., Shi, J., et al. (2019). A HAK family Na^+ transporter confers natural variation of salt tolerance in maize. *Nat. Plants.* 12, 1297–1308. doi: 10.1038/s41477-019-0565-y

Conflict of Interest: The authors declare that the research was conducted in the absence of any commercial or financial relationships that could be construed as a potential conflict of interest.

frontiers in Plant Science

REVIEW
published: 06 March 2020
doi: 10.3389/fpls.2020.00247

Coordinated Transport of Nitrate, Potassium, and Sodium

*Natalia Raddatz†, Laura Morales de los Ríos†, Marika Lindahl, Francisco J. Quintero and José M. Pardo**

Institute of Plant Biochemistry and Photosynthesis, Consejo Superior de Investigaciones Científicas and Universidad de Sevilla, Seville, Spain

Potassium (K^+) and nitrogen (N) are essential nutrients, and their absorption and distribution within the plant must be coordinated for optimal growth and development. Potassium is involved in charge balance of inorganic and organic anions and macromolecules, control of membrane electrical potential, pH homeostasis and the regulation of cell osmotic pressure, whereas nitrogen is an essential component of amino acids, proteins, and nucleic acids. Nitrate (NO_3^-) is often the primary nitrogen source, but it also serves as a signaling molecule to the plant. Nitrate regulates root architecture, stimulates shoot growth, delays flowering, regulates abscisic acid-independent stomata opening, and relieves seed dormancy. Plants can sense K^+/NO_3^- levels in soils and adjust accordingly the uptake and root-to-shoot transport to balance the distribution of these ions between organs. On the other hand, in small amounts sodium (Na^+) is categorized as a "beneficial element" for plants, mainly as a "cheap" osmolyte. However, at high concentrations in the soil, Na^+ can inhibit various physiological processes impairing plant growth. Hence, plants have developed specific mechanisms to transport, sense, and respond to a variety of Na^+ conditions. Sodium is taken up by many K^+ transporters, and a large proportion of Na^+ ions accumulated in shoots appear to be loaded into the xylem by systems that show nitrate dependence. Thus, an adequate supply of mineral nutrients is paramount to reduce the noxious effects of salts and to sustain crop productivity under salt stress. In this review, we will focus on recent research unraveling the mechanisms that coordinate the K^+-NO_3^-; Na^+-NO_3^-, and K^+-Na^+ transports, and the regulators controlling their uptake and allocation.

Keywords: plant nutrition, salinity, potassium, nitrate, sodium, long-distance transport

OPEN ACCESS

Edited by:
Guillermo Esteban Santa María, National University of General San Martín, Argentina

Reviewed by:
Sergey Shabala, University of Tasmania, Australia
Rosario Haro, Polytechnic University of Madrid, Spain

***Correspondence:**
José M. Pardo
jose.pardo@csic.es

†These authors have contributed equally to this work

Specialty section:
This article was submitted to Plant Nutrition, a section of the journal Frontiers in Plant Science

Received: *23 December 2019*
Accepted: *18 February 2020*
Published: *06 March 2020*

Citation:
Raddatz N, Morales de los Ríos L, Lindahl M, Quintero FJ and Pardo JM (2020) Coordinated Transport of Nitrate, Potassium, and Sodium. Front. Plant Sci. 11:247. doi: 10.3389/fpls.2020.00247

INTRODUCTION

Plants take up essential nutrients and other minerals from the soil in various chemical forms. Some of them (K^+ or NO_3^-) are essential for growth and taken in large quantities if available, while others (Na^+ or NH_4^+) are potentially toxic at high concentrations. Contrary to nitrate and phosphate, K^+ is not incorporated into organic matter, and hence it is the most abundant cation in tissues of well-fed plants, constituting between 2 to 10% of the dry weight of the plant (Leigh, 2001).

The physiological function of K^+ ions include enzyme activation, osmotic regulation, turgor generation, cell expansion, pH homeostasis, regulation of electrical membrane potentials and electrical neutralization of the abundant negative charges within cells (Clarkson and Hanson, 1980;

Pettigrew, 2008; Hawkesford et al., 2012; Zorb et al., 2014). Thus, large quantities of K^+ are taken up from the soil solution by root epidermal and cortical cells, and then distributed throughout the plant. The concentration of K^+ in the cytoplasm is kept rather constant, typically in the range of 75−100 mM when measured as K^+ activity by ion-selective microelectrodes in several species (Maathuis and Sanders, 1993; Walker et al., 1996; Leidi et al., 2010; Planes et al., 2015). The vacuolar K^+ pool is highly dynamic and serves as a repository that is replenished in times of abundance or wasted to preserve the homeostatic cytosolic concentration upon starvation (Martinoia et al., 2012; Ahmad and Maathuis, 2014). In barley roots, cytosolic K^+ content began to decline only after the total tissue concentration dropped below 25 mM, while vacuolar concentrations ranged widely from 10 to 125 mM depending on the K^+ status of the plant (Walker et al., 1996). Despite the homeostatic design to preserve optimal cytosolic K^+ levels, both abiotic and biotic stresses result in the disturbance of intracellular K^+ levels (Shabala and Pottosin, 2014). Relatively small changes in K^+ concentration have profound effects on the electrical charge of the plasma membrane, which in turn initiates signaling events that trigger pertinent responses in K^+ acquisition (Rubio et al., 2014), salinity (Leidi et al., 2010; Shabala, 2017), plant immunity (Brauer et al., 2016), and programmed cell death (Demidchik et al., 2010). Consequently, a signaling role has been proposed for the shifting levels of cytosolic K^+ (Shabala, 2017).

Nitrogen is another macronutrient required by plants in the greatest amounts for optimal growth, and incorporated into numerous organic compounds (Mengel et al., 2001). For most plants, NO_3^- and NH_4^+ are the prevalent nitrogen sources (Crawford, 1995; Gazzarrini et al., 1999). To be assimilated, NO_3^- has to be taken up from the soil and converted into ammonium by nitrate and nitrite reductases, and then incorporated into amino acids via the glutamine-synthetase and glutamate synthase (GS-GOGAT) pathway. On the other hand, ammonium, as nitrogen source, is preferred over nitrate by most plants, but ammonium uptake through roots is tightly controlled because an elevated ammonium concentration in the cytosol becomes toxic to the plant (Gazzarrini et al., 1999; Straub et al., 2017). Potassium plays an essential role as counter-ion of NO_3^-, facilitating the uptake, translocation, and distribution of these ions between roots and shoots (Engels and Marschner, 1993; Zhang et al., 2010; Rodenas et al., 2017). Hence, the acquisition rates of K^+ and NO_3^- are often positively correlated (reviewed by Coskun et al., 2017). Under nutrient-sufficient conditions, K^+:NO_3^- co-translocation from the root-to-shoot is enhanced, while on the contrary, under nutrient-limited conditions the transport of both nutrients is restricted (Pettersson, 1984; Lin et al., 2008; Drechsler et al., 2015; Meng et al., 2016). The amount of supplied N and K must also be balanced to achieve maximum growth (Coskun et al., 2017). However, the mechanistic basis for the mutual influences exerted by these nutrients is poorly understood. By contrast, NH_4^+ is a strong inhibitor of the high-affinity K^+ uptake by roots and translocation to shoots (Scherer et al., 1984; Wang et al., 1996; Spalding et al., 1999; Santa-Maria et al., 2000; ten Hoopen et al., 2010).

Sodium is the 7th most abundant element in the earth's crust (2.4 vs. 2.1% of K^+), present in all soils and surface and subterranean water bodies. However, unlike K^+ and NO_3^-, it is not essential for either development or for the reproduction of plants with the exception of a subgroup of C4 plants that require traces of Na^+ to drive the Na^+-pyruvate co-transporter chloroplasts (Furumoto et al., 2011). In all other plants, this function is mediated by a H^+-coupled pyruvate carrier. Under typical physiological conditions, plants maintain a high cytosolic K^+:Na^+ ratio with relatively low Na^+ concentrations (20–30 mM) (Carden et al., 2003; Rodriguez-Navarro and Rubio, 2006; Kronzucker et al., 2013). However, as the ionic radii of Na^+ and K^+ in their hydrated forms are similar, under sodic conditions a failure in the discrimination among them often occurs, thus facilitating the Na^+ influx through pathways that generally function for K^+ uptake (Benito et al., 2014). The accumulation of toxic concentrations of Na^+ in cells may have harmful effects, such as induction of cytosolic K^+ efflux from both root and leaf cells and, subsequently an imbalance in cellular homeostasis, oxidative stress, interference with Ca^{2+} and K^+ functions, disruption of protein synthesis, retarded growth and even plant death (Tester and Davenport, 2003; Munns and Tester, 2008; Craig Plett and Moller, 2010; Cabot et al., 2014).

Considering the extent and physiological importance of these interactions between NO_3^-, K^+, and Na^+, in this review we describe the operation and diversity of the main mechanisms that coordinate the K^+-NO_3^-, Na^+-NO_3^-, and K^+-Na^+ transports, and their regulators that control their uptake and movements. Most of the proteins and processes described herein belong to *Arabidopsis thaliana* and rice because of the wealth of information available in these model species.

POTASSIUM–NITRATE INTERACTIONS

In most plant species, the uptake rates of K^+ and NO_3^- from the soil are positively correlated and to enhance one another. This effect can be explained by the improved charge balance during nutrient uptake and long-distance transport and by the K^+-induced activation of the enzymes involved in nitrate assimilation. Consequently, plants grown in the presence of NO_3^- take up and accumulate more K^+ than when grown with NH_4^+. However, little is known about the direct influences produced by one ion on the transport of the other (Coskun et al., 2017).

To cope with variable nitrate concentrations in soil, tissues and within cells, plants have developed both a High-Affinity Transport System (HATS; K_m in the μM range) and a Low-Affinity Transport System (LATS; K_m of mM) for the acquisition and distribution of nitrate. When the external nitrate concentration is high (e.g., >1 mM), LATS is preferentially used; otherwise, the inducible HATS are activated and take over nitrate transport (Glass et al., 1992; Crawford and Glass, 1998). Two protein families, NRT1/NPF and NRT2, have been identified as responsible for LATS and HATS, respectively. Exceptions are NRT1.1, which has a dual high- and low-affinity for nitrate, depending on the phosphorylation state, and NRT2.7 which

despite belonging to NRT2 family, shows low nitrate affinity (Glass et al., 1992; Orsel et al., 2002; Chopin et al., 2007; Tsay et al., 2007). Some endosomal channel-like exchangers of the CLC family, and the slow anion channels SLAC1/SLAH also transport nitrate. Collectively, these four families of anion transporters amount to 70 genes in *A. thaliana*, albeit just a few of them have been confirmed to transport nitrate (Fan et al., 2017).

The NRT1/NPF family shares significant sequence identity to mammalian and bacterial PTR peptide transporters. The NRT1/NPF family belongs to the Major Facilitator Superfamily (MFS) of secondary active transporters that use the proton electrochemical gradient to drive substrate uptake into cells. Although several members of the NRT1/NPF have been shown to mediate nitrate transport, other members of this large family may not be competent for this process but instead mobilize diverse substrates ranging from dipeptides to hormones, including ABA and auxin (Leran et al., 2015a; Fan et al., 2017). NRT1.1/CHL1 is the most studied nitrate transporter and represents a major pathway for nitrate uptake (Tsay et al., 1993, 2007; **Figure 1**). Notably, the Arabidopsis NRT1.1 is a dual-affinity nitrate transporter that also serves as a sensor for its substrate (Wang et al., 1998). In conditions of high nitrate availability (>1mM) NRT1.1 behaves as a low-affinity transporter (K_m ~4 mM). However, when nitrate levels fall below 1 mM, NRT1.1 is phosphorylated by the CIPK23 protein kinase, switching into a high-affinity mode (K_m ~40 μM) (Wang et al., 1998; Liu et al., 1999; Ho et al., 2009). NRT1.2, expressed in root epidermis and cortex also contributes in low-affinity nitrate uptake, together with other LATS yet to be identified (**Figure 1**; Huang et al., 1999; Nacry et al., 2013). On top of the nitrate transport activity of NRT1.1, this sensor protein governs essential physiological, developmental and molecular features of the plant response to nitrate availability by means of its capacity for auxin transport. Under low nitrate conditions, NRT1.1 functions to take up and remove auxin from the lateral root primordia, thus repressing the development of lateral roots. Nitrate inhibits NRT1.1-dependent auxin uptake, which in turn stimulates lateral root development (Krouk et al., 2010). Mutations in residues P492 and T101, the later being phosphorylated by CIPK23, decrease auxin transport of NRT1.1 and impair the regulation of lateral root development (Bouguyon et al., 2015, 2016).

The *NRT2* family consists of seven members in the *Arabidopsis* genome. NRT2.1, NRT2.2, NRT2.4 and NRT2.5 are involved in inducible high-affinity nitrate uptake (**Figure 1**; Cerezo et al., 2001; Li et al., 2007; Kiba et al., 2012; Kiba and Krapp, 2016). These four NRT2 transporters are responsible of approximately 95% of high-affinity nitrate influx activity under nitrate-limited conditions, as evidenced by the phenotype of the quadruple mutant *nrt2.1/nrt2.2/nrt2.4/nrt2.5* (Lezhneva et al., 2014). Although NRT1 and NRT2 proteins are functionally and phylogenetically distinct, both are believed to couple nitrate and proton translocation to sustain nitrate transport regardless of the thermodynamical constraints imposed by the nitrate gradient across biological membranes (Paulsen and Skurray, 1994; Orsel et al., 2002). Passive efflux, i.e., downward the electrochemical gradient of nitrate, is facilitated by channels, including SLAH3 in guard cells (Geiger et al., 2011; Zheng et al., 2015). Efflux in the cortex of mature roots is achieved by the electroneutral NO_3^-/H^+ symporter NAXT1/NPF2.7 (**Figure 1**; Segonzac et al., 2007). The biological role of this nitrate leak leading to a decrease in root NO_3^- content is unclear because interference with *NAXT1* gene expression did not reveal a role in plant N nutrition in standard culture conditions (Segonzac et al., 2007). A NAXT-like protein, NPF2.3, contributes to nitrate efflux in the root pericycle and loading into the xylem sap (Taochy et al., 2015).

Long-distance transport of nitrate involves xylem loading and unloading, two successive steps that determine net distribution and assimilation efficiency (**Figure 2**; Krapp, 2015). After entering the root cytoplasm, nitrate can be loaded into xylem vessels by NRT1.5, expressed in root pericycle cells, and subsequently retrieved from the xylem sap in plant roots and aerial tissues by NRT1.8, expressed predominantly in xylem parenchyma cells (Lin et al., 2008; Li et al., 2010). Under stress conditions (salinity, drought, and cadmium treatment), *NRT1.5* expression in roots decreases and nitrate loading into xylem vessels is reduced. By contrast, *NRT1.8* expression in roots increases, enhancing nitrate unloading back into roots. This coordinated regulation is mediated by ethylene and jasmonic pathways (Li et al., 2010; Zhang et al., 2014). Once nitrate has reached the aerial tissues, the low-affinity nitrate transporter NRT1.4, preferentially expressed in leaf petioles, gates nitrate distribution within leaves (**Figure 2**). The activity of NRT1.4 contributes to cell expansion. Under high nitrate conditions, NRT1.9 mediates nitrate transport back to roots via phloem (**Figure 2**). This mechanism prevents excess amounts of nitrate being accumulated in shoots (Wang and Tsay, 2011). Moreover, nitrate can be remobilized from older leaves to feed young leaves via NRT1.7, expressed in the phloem of minor veins (Fan et al., 2009). At destination, nitrate is either stored inside vacuoles using K^+ as counterion, where both ions contribute to osmotic adjustment (Barragan et al., 2012; Martinoia et al., 2012), or reduced to nitrite and then partitioned into plastids to be assimilated to organic nitrogen (Wang et al., 2012, 2018). The low-affinity nitrate transporter NRT2.7 and the channel-like NO_3^-/H^+ exchanger CLCa were identified as responsible for nitrate translocation into vacuoles (De Angeli et al., 2006; Chopin et al., 2007; **Figure 2**). The transporters responsible for exporting nitrate out of vacuoles remain to be identified.

Potassium uptake by roots often exhibits complex biphasic kinetics in response to increasing external concentrations. At least two transport systems are involved in potassium uptake, corresponding to high- and low- affinity transports systems, which work at low (<1 mM) and high (>1 mM) external K^+ concentrations, respectively (Nieves-Cordones et al., 2014; Ragel et al., 2019). At high concentrations outside, K^+ crosses the plasma membrane mostly through selective channels, e.g., the *Shaker*-like channel AKT1 (Lagarde et al., 1996; Nieves-Cordones et al., 2016; **Figure 1**). At low K^+ concentrations, proton-coupled transport systems, such as HAK5 of Arabidopsis and HAK1 of rice, are needed in order to pull potassium inside cells against its electrochemical gradient (Gierth et al., 2005; Nieves-Cordones et al., 2016; Santa-Maria et al., 2018). The cryo-EM structure of KimA, a KUP-like protein from *Bacillus subtilis*, has been resolved recently (Tascon et al., 2020). The structure

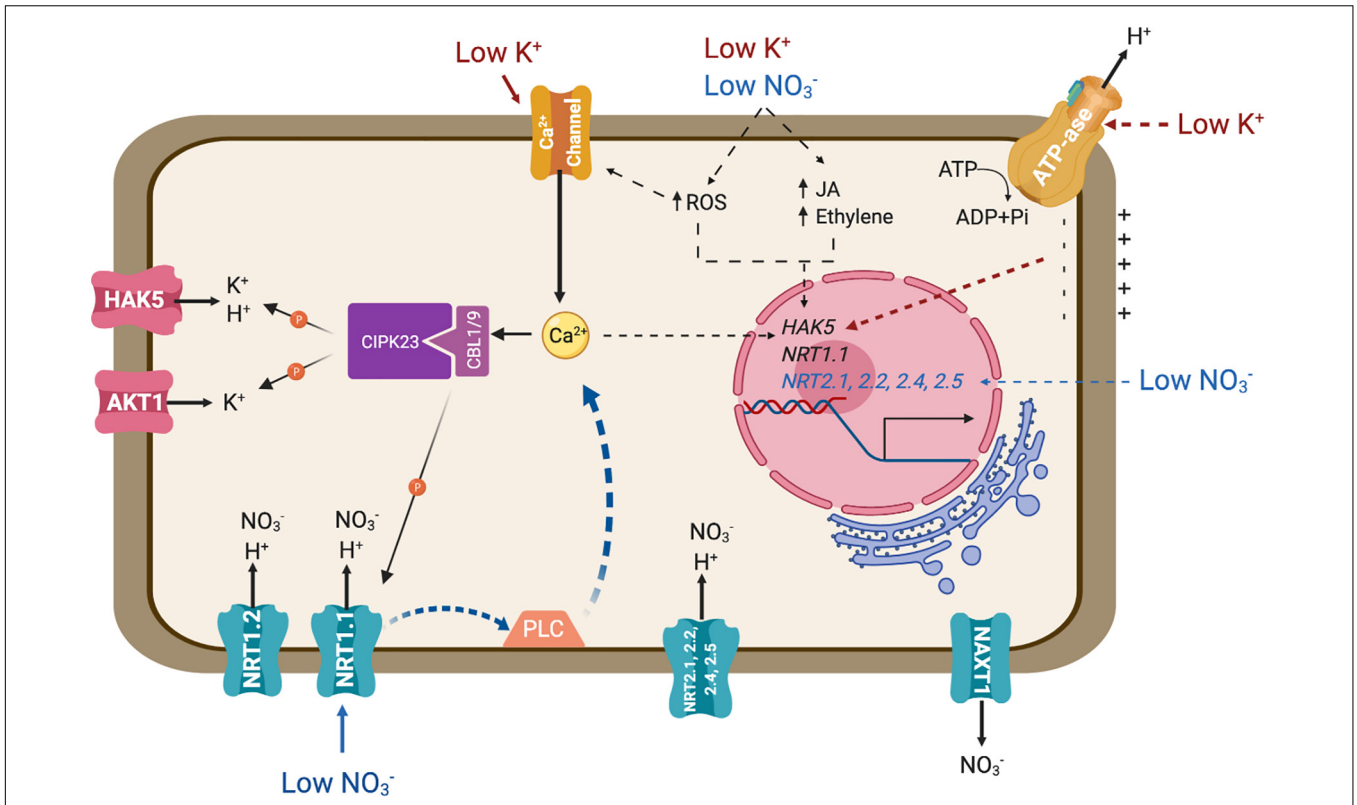

FIGURE 1 | Transporters involved in the main pathways for the uptake of nitrate and potassium. The diagram represents an idealized root cell disregarding developmental differentiation. Major signaling pathways regulating the expression and biochemical activity of these transporters are also represented. Solid lines represent signaling events and connections that have been confirmed experimentally. Dotted lines signify known or suspected connections for which the molecular events involved remain to be defined. PLC represents an unidentified phospholipase C. Further details are given in the main text.

shows a homodimer alternating between occluded and opened arrangements formed by tilted protomers that likely rock with a "breading" motion during K^+/H^+ symport.

Plants respond to K^+ availability by different means. Hyperpolarization of the root cell membrane is considered to be the earliest signaling event elicited by K^+ deficiency (Nieves-Cordones et al., 2008; **Figure 1**). Also associated to K^+ starvation are increases in cytosolic calcium (Ca^{2+}), the alteration of different hormone levels (such as ethylene and jasmonate), and production of reactive oxygen species (ROS) (Armengaud et al., 2004; Shin and Schachtman, 2004; Jung et al., 2009; Behera et al., 2017; **Figure 1**). Together, these stimuli lead to transcriptional and post-translational regulation of K^+ uptake systems. At the transcriptional level, the *HAK5* transporter is activated by K^+ starvation, specifically responding to hyperpolarization of the plasma membrane (Nieves-Cordones et al., 2008), and quickly repressed after K^+ supply (Ahn et al., 2004; Gierth et al., 2005; Aleman et al., 2009). At the post-transcriptional level, Ca^{2+} signaling under K^+ deprivation is registered by the CBL1/CBL9 Ca^{2+} sensors, that activate and recruit the kinase CIPK23 to the plasma membrane to achieve the phosphorylation and activation of both AKT1 and HAK5 transporters (Li et al., 2006; Xu et al., 2006; Ragel et al., 2015; **Figure 1**). HAK5 activation produced an increase in the affinity and the V_{max} of K^+ transport, ensuring the entry of K^+ inside the cell at concentrations lower than 0.1 mM (Nieves-Cordones et al., 2014; Ragel et al., 2015), whereas phosphorylation of AKT1 results in channel activation that maximizes K^+ influx (Geiger et al., 2009).

The CIPK23/CBL1-9 module not only phosphorylates and activates K^+ uptake systems AKT1 and HAK5, but also mediates high- and low-affinity transition of the nitrate transporter and sensor (transceptor) NRT1.1 (Ho et al., 2009; Leran et al., 2015b; **Figure 1**). The crystal structure of NRT1.1 reveals a biologically relevant dimer, whose dynamic coupling and decoupling of monomers is controlled by the phosphorylation of a single residue, Thr101, by CIPK23 (Ho et al., 2009; Parker and Newstead, 2014; Sun et al., 2014). This residue is strictly conserved among plant NRT1.1 orthologs. Non-phosphorylated NRT1.1 is a low-affinity nitrate transporter working as a dimer. According to the common view, at low external nitrate concentration, a Ca^{2+} signaling cascade leads to the phosphorylation of NRT1.1 by CIPK23/CBL1-9 and dimer dissociation. Phosphorylated NRT1.1 monomers show a higher nitrate affinity than the dimers (Tsay et al., 2011; Li et al., 2017). These findings bring about two questions. One is how the CIPK23/CBL1-9 complex is capable of resolving different nutrient-related stimuli and then targets the pertinent K^+ or nitrate transporter. One reason could be the sequence

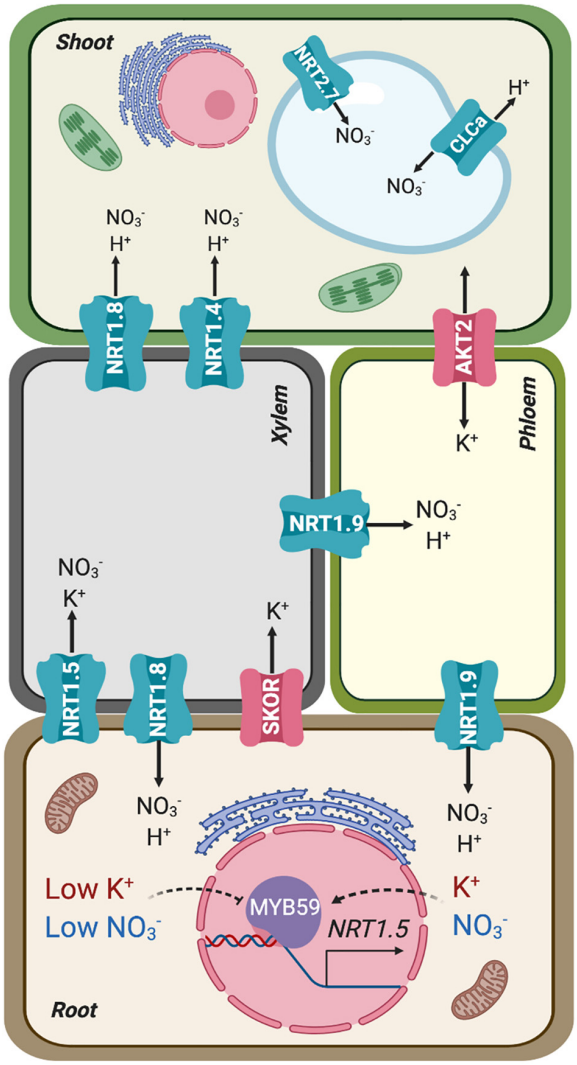

FIGURE 2 | Simplified representation of the source (root) and sink (shoot) organs in terms of mineral uptake and distribution, connected by xylem and phloem. Transporters involved in the root-shoot partition of nitrate and potassium are represented in their preferential placement based on gene expression and protein activity. AKT2 is represented as bidirectional owing to its facultative inward-rectification.

of events leading to transporter phosphorylation/activation. Rashid et al. (2019) proposed that nitrate binding by only one NRT1.1 monomer triggers dimer dissociation and exposes the Thr101 residue to enable phosphorylation by CIPK23. This phosphorylation stabilizes the monomeric state of NRT1.1. However, at higher nitrate concentrations, substrate binding by both monomers promotes NRT1.1 dimerization, which attenuates CIPK23 activity and thereby maintains the low-affinity mode of nitrate signaling and transport (Rashid et al., 2019). Moreover, a functional NRT1.1 is necessary to trigger nitrate-induced Ca^{2+} waves through the action of an unknown phospholipase C (Riveras et al., 2015; **Figure 1**). Whether this kinetic model also applies to HAK5 and AKT1, which likely are dimers and tetramers themselves (Daram et al., 1997; Daras et al., 2015; Tascon et al., 2020), is unknown. In K^+ transport, it is assumed that K^+ starvation elicits a Ca^{2+} signal perceived by CBL1 and CBL9 (Behera et al., 2017), which then recruit CIPK23 to the plasma membrane to phosphorylate and activate AKT1 and HAK5 transporters. In other words, Ca^{2+}-induced phosphorylation of K^+ transport protein leads to conformational and kinetics changes, whereas for NRT1.1 the low availability of the substrate is what induces the phase transition from dimers to monomers. This, in turn, facilitates phosphorylation to stabilize the new conformation, which also elicits a Ca^{2+} signal that reinforces the output by stimulating CBL1/9-dependent CIPK23 activity (Rashid et al., 2019). How those alternative models apply to ammonium, magnesium and iron transporters, and channels SLAC1 and SLAH3, all of which are also regulated by CIPK23, is unclear (Maierhofer et al., 2014; Tang et al., 2015; Straub et al., 2017; Dubeaux et al., 2018).

The second, broader question is why nitrate and potassium transporters need to be regulated by the same kinase in the first place. The answer to this question likely relates to the tight linkage between K^+ and nitrate uptake and distribution. The expression of *NRT1.1* in roots is enhanced by low K^+-treatment, and the transporter is required for plants to resist K^+ deficiency under sufficient NO_3^- in concert with K^+ uptake channels (Fang et al., 2019). In these conditions, the *nrt1.1* knockout mutant exhibited severe leaf senescence, shorter roots and less biomass than Col-0 plants, while the quadruple mutant *nrt2.1*, *nrt2.2*, *nrt2.4*, and *nrt2.5* lacking several high-affinity nitrate transporters showed a phenotype similar to wild-type plants. In addition, the rates of root Rb^+ uptake (the closest analog of K^+) in *nrt1.1* mutant were considerably less than those in Col-0 plants in low-Rb^+ medium. How low-K^+ stress up-regulates NRT1.1 activity is not yet known, but it likely involves activation of the CIPK23/CBL1-CBL9 module.

Potassium and nitrate are also linked with each other in their translocation to shoots (**Figure 2**). In general, under nutrient sufficient conditions, the root-to-shoot transport of K^+ and NO_3^- is enhanced (Coskun et al., 2017). Conversely, co-translocation is restricted in plants under limited availability of either nutrient. However, under low-NO_3^- and K^+-sufficient conditions, NO_3^- can be partially substituted by other anions such a chloride, indicating that charge balance is a key factor behind the observed linkage. The cooperative translocation of K^+ and NO_3^- via the vasculature has been interpreted as an internal ion cycling by which NO_3^- is transported from root to shoot using K^+ as counterion in the xylem sap. In the shoot NO_3^- is assimilated into amino acids and organic acids. Malate is then transported to roots via the phloem, again accompanied by K^+ as counterion (Zioni et al., 1971; Kirkby and Knight, 1977; Touraine et al., 1988; Engels and Kirkby, 2001). Potassium circulating in the phloem is also involved in supporting sucrose transport from source to sink tissues. The K^+ channel AKT2, a facultative inward-rectifier controlled by phosphorylation (**Figure 2**), energizes sucrose loading into the phloem of Arabidopsis (Michard et al., 2005; Gajdanowicz et al., 2011).

Molecular mechanisms that directly coordinate the long-distance transport of NO_3^- and K^+ are beginning to emerge. To transport ions to the shoot, they must be loaded into the xylem vessels of the root vascular stele (Ahmad and Maathuis, 2014). Until recently, only the K^+ channel SKOR had been implicated in root-to-shoot K^+ translocation in *Arabidopsis* (Gaymard et al., 1998; **Figure 2**). SKOR belongs to the voltage-dependent *Shaker*-like superfamily of K^+ channels. SKOR is expressed in the root pericycle and xylem parenchyma of *Arabidopsis*, and mediates K^+ secretion into xylem vessels. At high external K^+ concentration in the vasculature, the channel stabilizes in a closed state. However, with a low external K^+ concentration and when the plasma membrane of xylem parenchyma cells becomes depolarized, SKOR opens and mediates the release of cellular K^+ to the stele apoplast and xylem vessels. Since the cell interior is electrically negative relative to the exterior, the uptake of the nitrate anion driven by the co-transport of two protons would initially depolarize the plasma membrane. Likewise, the efflux of anions, such as NO_3^- or Cl^-, out of parenchyma cells in the stele could lead to membrane depolarization that in turn would elicit K^+ release via SKOR, thereby explaining the observed linkage between anionic (NO_3^-, SO_4^-, Cl^-) and cationic (K^+, Ca^{2+}, Mg^{2+}) nutrients (Leigh, 2001; Drechsler et al., 2015). The *skor* mutation strongly reduced the K^+ content in the shoot and xylem sap with little effect on the root K^+ content (Gaymard et al., 1998), but surprisingly *skor* null mutants do not exhibit a particular K^+-deficient phenotype, which suggests that other proteins may also participate in this process. Notably, one nitrate transporter, NRT1.5, has been shown to affect root-to-shoot K^+ translocation under low NO_3^- availability (Drechsler et al., 2015) and to be involved in K^+ and NO_3^- transport by xylem under K^+ limited conditions (Li et al., 2017; **Figure 2**).

As said before, nitrate can be assimilated into ammonium and then to amino acids. A significant proportion of nitrate assimilation takes place in shoot because the reducing power required for the assimilation processes comes from photosynthesis (Searles and Bloom, 2003; Krapp, 2015). NRT1.5 of Arabidopsis was first identified as a *bona fide* nitrate transporter in *Xenopus* oocytes and shown to facilitate nitrate loading into xylem vessels (Lin et al., 2008). However, NRT1.5 has later been shown to operate as a proton-coupled H^+/K^+ antiporter (Li et al., 2017). Thus, at external acidic pH (as in the xylem sap) NRT1.5 promotes K^+ release out of cells into the xylem. In *nrt1.5* mutants, the amount of K^+ transported to the shoot is reduced in K^+-sufficient and K^+- deficient conditions, while the mutant *nrt1.5* accumulates higher K^+ and NO_3^- in the root under K^+-deficient conditions (Lin et al., 2008; Li et al., 2017). According to the crystal structure of NRT1.1, which is an electrogenic NO_3^-/H^+ symporter, the "ExxER" motif (containing three conserved residues) on transmembrane TM1 together with the conserved residue Lys-164 on TM4 is responsible for proton coupling (Parker and Newstead, 2014). These four charged residues are highly conserved in most Arabidopsis NRT1 members. By contrast, NRT1.5 only has non-charged residues in these four sites, suggesting that this transporter must have an alternative proton-coupling mechanism compared with other NRT1 members. One possibility that deserves further exploration is whether differences in amino acids related to proton-binding in NRT1.1 allow NRT1.5 to couple the co-transport K^+ and nitrate as substrates. Despite the controversial mechanism of transport by NRT1.5, the consensus is that NRT1.5 affects the homeostatic balance between K^+ and nitrate in the xylem stream (Lin et al., 2008; Li et al., 2017). Inactivation of *NRT1.5* also promoted the expression of genes responsive to phosphate deficiency and increased the concentration of phosphate in tissues compared to wild-type plants under phosphate starvation. However, this appeared to be an indirect effect of ethylene production in the mutant since inhibition of ethylene synthesis canceled differences between *nrt1.5* and wild-type plants with regard to the phosphate response (Cui et al., 2019).

Coordinated regulation between K^+ and NO_3^- in translocation to xylem also exists at the transcriptional level. The expression of genes *SKOR* and *NRT1.5* was up-regulated by nitrate supply. During low-K^+ stress, the *NRT1.5* transcript is down-regulated, presumably to adjust root-to-shoot K^+/NO_3^- transport to K^+ levels (Wang et al., 2004; Lin et al., 2008; Li et al., 2017). Similar results have been reported in rice regarding the nitrate transporter OsNPF2 expressed in the root epidermis, xylem parenchyma, and phloem companion cells (Xia et al., 2015). Knockout of *OsNPF2.4* decreased K^+ concentration in xylem sap. Conversely, K^+ deprivation resulted in the up-regulation of the nitrate transporters *NRT1.2* and *NRT2.1* in tomato roots (Wang et al., 2001) and of NRT1.1 in Arabidopsis (Armengaud et al., 2004).

Recently, the Arabidopsis transcription factor *MYB59* has been shown to positively regulate *NRT1.5* expression and to balance K^+/NO_3^- transport (Du et al., 2019). Under K^+/NO_3^- sufficient conditions, MYB59 binds to the *NRT1.5* promoter and facilitates NRT1.5-mediated root to shoot K^+/NO_3^- transport (**Figure 2**). When plants are subjected to K^+/NO_3^- deficient conditions, *MYB59* is down-regulated, which subsequently impairs the accumulation of the *NRT1.5* transcript. These data further support a co-regulation at the level of xylem transport that maintains the balance between NO_3^- and K^+.

Guard cells represent a paradigmatic example of how NO_3^- and K^+ transport are functionally linked at the cellular level (**Figure 3**). Stomata consist of pairs of guard cells that dynamically and reversibly change their turgor and volume to adjust the size of the stomatal pore. This is accomplished by the massive uptake and release of K^+ and nitrate ions among other solutes, and by the biosynthesis of organic compounds (Eisenach and De Angeli, 2017; Hedrich and Shabala, 2018). To open the stomata, firstly the activation of H^+-ATPase AHA1 hyperpolarizes the plasma membrane, negative inside, which then triggers the influx of K^+ into the cytoplasm following the electrochemical gradient (**Figure 3**). The influx of K^+ partly depolarizes the membrane, which in turn favors that charge-balancing anions accumulate in the guard cell (Yamauchi et al., 2016; Jezek and Blatt, 2017). The inward-directed H^+ gradient allows the symport of sugars, and of organic (malate) and inorganic anions (Cl^-, NO_3^-) in co-transport with H^+ (Eisenach and De Angeli, 2017; Jezek and Blatt, 2017). This increased uptake of osmolytes triggers water influx, inflates the guard cells and

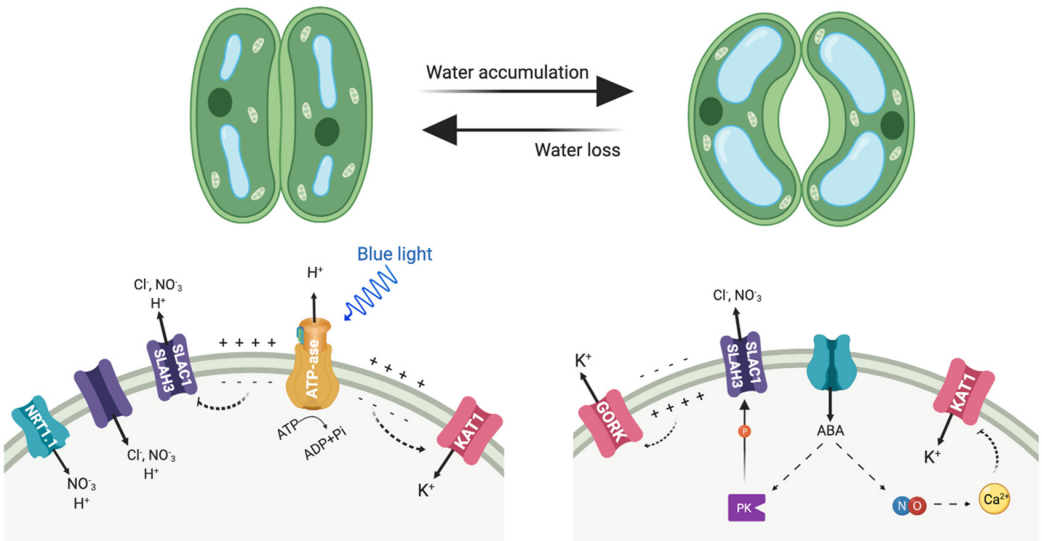

FIGURE 3 | Depicted are the main transporters mediating anion and cation fluxes at the plasma membrane of guard cells and involved in stomatal movements. Left side, stomata opening; right side, stomata closure. PK represents protein kinases, including OST1 and CPK3.

the stomatal pore opens. NRT1.1, which is expressed not only in roots but also in the guard cells, contributes to promoting stomatal opening (Guo et al., 2003). Conversely, stomatal closure activates the anion channels SLAC1 and SLAH3, which differ in their Cl^-/NO_3^- permeability and are activated by a distinct set of protein kinases that are stimulated by ABA (Vahisalu et al., 2008; Geiger et al., 2009, 2010, 2011; Lee et al., 2009; **Figure 3**). As result of anion exit through these channels, the plasma membrane depolarizes. This voltage drop at the plasma membrane activates the potassium outward-rectifying channel GORK, what finally leads to K^+ efflux for decreasing turgor and stomatal closure.

Abscisic acid (ABA) promotes stomatal closure at least in part by driving the increase in nitric oxide, which in turn leads cytosolic calcium elevation (Chen et al., 2016). The effects in elevating cytosolic calcium results in the suppression of currents at the plasma membrane through the K^+ inward channel to prevent K^+ influx and activation of K^+ outward and anion channels for ion efflux and stomatal closure. The main source of nitric oxide is the reduction of nitrite to nitric oxide, catalyzed by two nitrate reductases encoded by *NIA1* and *NIA2* genes (Wilson et al., 2008). Accordingly, stomatal opening is significantly affected in the double mutant *nia1 nia2* in normal growth conditions throughout the day. Beside this, *nia1 nia2* was unable to fully open its stomata even under high external K^+, suggesting the mutations may affect guard cell K^+ transport, as K^+ is the main solute for stomatal opening (Chen et al., 2016).

NITRATE–SODIUM INTERACTIONS

Substantial interactions between nitrate and sodium transport could be expected in marine plants and algae thriving in a medium with high salinity and moderately alkaline pH (pH 7.5–8.4). Nitrate is present at low (1–10 μM) concentrations in seawater and must be captured against a steep electrochemical gradient across the plasma membrane, which theoretically could be coupled to the co-transport of H^+ or the abundant Na^+ ions (Rubio et al., 2005). However, only few reports have described Na^+-linked nutrient uptake in marine plants. One example is the seagrass *Zostera marina*, which evolved from a terrestrial angiosperm that returned to the sea. Like extant land species, the ancestor of *Z. marina* presumably transported NO_3^- from the soil using H^+-coupled transport systems. Therefore, an interesting question is how Na^+-coupled NO_3^- transport evolved in *Z. marina* (Garcia-Sanchez et al., 2000). Identifying the transporter(s) involved in Na^+/NO_3^- co-transport could potentially yield important structural information regarding the ion selectivity of nitrate transporters.

Not surprisingly, there are very few reports about Na^+-coupled transport systems in terrestrial plants. Na^+-dependent nitrate transport has been described in the halophytes *Suaeda physophora* and *Salicornia europea* (Junfeng et al., 2010; Nie et al., 2015). In *Beta vulgaris*, Na^+ enhances both nitrate uptake and translocation to shoots (Kaburagi et al., 2014, 2015). On the other hand, a large proportion of Na^+ ions accumulated in Arabidopsis shoots were loaded into the xylem by transport systems that appeared to couple the movement of Na^+ to that of nitrate (Alvarez-Aragon and Rodriguez-Navarro, 2017). The nitrate-dependent loading of Na^+ into the xylem was additive to that of SOS1, a Na/H exchanger mediating Na^+ efflux at the xylem parenchyma cells (Shi et al., 2002; El Mahi et al., 2019). Nitrate-dependent Na^+ transport was partially interrupted in the *nrt1.1* mutant but not in *nrt1.2*, implying that unidentified nitrate transporters under the regulation of the NRT1.1 transceptor were involved in this process (Alvarez-Aragon and Rodriguez-Navarro, 2017). Notably, this linked Na^+/NO_3^- transport served the purpose of osmotic adjustment since it prevented the wilting of plants challenged with a hyperosmotic medium. The combined

use of nitrate and chloride as permeable anions showed a predominant role of nitrate to stimulate Na^+ accumulation, suggesting that nitrate fulfilled a specific function that chloride did not achieve. Thus, it appears that under high salinity Na^+ may partly substitute for K^+ in the extensive K^+-NO_3^- interactions described above, particularly in those connected to charge balance and the re-distribution of K^+ as a cellular osmoticum.

Under stress conditions, a significant amount of nitrate assimilation into organic matter is shifted from shoots to roots (Krapp, 2015). As explained above, the coordinate action of NRT1.5/NPF7.3 and NRT1.8/NPF7.2 determines the root/shoot partition of nitrate in Arabidopsis. Upon salinity or heavy metal stress, expression of *NRT1.5* in roots decreases to limit the nitrate load of xylem vessels, while that of *NRT1.8* is induced to favor nitrate unloading back into the root symplasm (Li et al., 2010; Chen et al., 2012; Zhang et al., 2014). Cadmium and sodium stresses initiated ethylene (ET) and jasmonic acid (JA) signaling pathways, which promoted the binding of the ET-responsive transcription factors ERF59, *ERF1B*, and *ERF104* to the *NRT1.8* promoter, and of EIN3 to the *NRT1.5* promoter (Zhang et al., 2014). Moreover, EIN3 further induced the expression of ERF59, *ERF1B*, and *ERF104*, thereby acting as an integrator of ET and JA signaling.

The nitrate efflux protein NPF2.3 is preferentially expressed in the root pericycle, where it contributes to nitrate loading in the xylem together with NRT1.5/NPF7.3 (Taochy et al., 2015). *NPF2.3* gene disruption resulted in salt sensitivity and reduced nitrate translocation to shoots, but only under salt stress even though *NPF2.3* was expressed at similar levels to control conditions. The prevalence of NPF2.3 under salt stress may result from transcriptional repression of *NRT1.5*/NPF7.3. Presumably, the salinity-induced repression of *NRT1.5/NPF7.3* likely prevents detrimental Na^+ accumulation in shoots since disruption of this gene led to decreased Na^+ content in shoots and enhanced tolerance to salinity (Chen et al., 2012). Hence, it is unlikely that NRT1.5/NPF7.3 is involved in the nitrate-dependent Na^+ transport reported by Alvarez-Aragon and Rodriguez-Navarro (2017) because these authors evidenced the beneficial effect of Na^+ distribution along the plant axis to improve osmotic adjustment. On the other hand, translocation of nitrate to shoots by NPF2.3 proceeded without inducing any significant increase in shoot Na^+ content, and growth impairment probably resulted from defective nitrate assimilation (Taochy et al., 2015). It remains to be resolved whether the patterns of Na^+ distribution in *nrt1.5* and *npf2.3* mutants result from altered xylematic transport K^+, an antagonist of Na^+, as we discuss in the next Section, and whose transport is intimately connected to that of nitrate.

SODIUM–POTASSIUM INTERACTIONS

Sodium and potassium interact at two main levels: the interference of Na^+ with K^+ nutrition, and the substitution of Na^+ for K^+ as highly dynamic and mobile cellular osmolyte in conditions of K^+ shortage (Haro et al., 2010; Kronzucker and Britto, 2011; Kronzucker et al., 2013; Alvarez-Aragon et al., 2016). Soil salinity is often associated with elevated levels of Na^+ (Munns and Tester, 2008). Although it is not clear what cytosolic levels of Na^+ are harmful to the plant cell (Kronzucker and Britto, 2011; Alvarez-Aragon et al., 2016), this cation is usually excluded from the cytosol. Due to their physicochemical similarity, Na^+ and K^+ can compete for binding to amino acids of protein surfaces, pockets of allosteric regulation or selectivity filters of ion channels (Benito et al., 2014). As a result, high Na^+ concentrations in plants trigger K^+-deficiency symptoms and disrupt many physiological processes mediated by K^+ such as protein synthesis and enzymatic reactions. Moreover, membrane depolarization caused by the entry of Na^+ into the cell results in compromised K^+ uptake through inward-rectifying K^+ channels, making it thermodynamically unfavorable, together with the increased K^+ efflux through outward-rectifying channels (Shabala et al., 2006; Coskun et al., 2013). Contrary to the debate regarding whether NRT proteins transport NO_3^-, K^+ or both, it is clear that Na^+ competes with K^+ in plant uptake specifically through High-Affinity K^+/K^+ UPtake/K^+ Transporter (HAK/KUP/KT), High-Affinity Potassium Transporters (HKTs) and Non-Selective Cation Channels (NSCCs) (Kronzucker and Britto, 2011).

HAK transporters are essential for K^+ absorption related to mineral nutrition, root hair formation and adaptation to abiotic stresses (Osakabe et al., 2013; Nieves-Cordones et al., 2014; Very et al., 2014). However, they could also have an important role in enabling Na^+ uptake. Indeed, different members of this family have been shown to mediate high-affinity Na^+ uptake. PpHAK13 from the moss *Physcomitrella patens* transports Na^+ but not K^+. This transporter appears to be a major pathway for Na^+ entry at low external concentration in *P. patens* because high-affinity Na^+ uptake was abolished in the *hak13* knockout (Benito et al., 2012). PhaHAK2 from reed plants (*Phragmites australis*) is permeable to Na^+, and its gene induced by low-K^+ conditions but repressed under salt stress, thereby limiting toxic Na^+ uptake through this transporter (Takahashi et al., 2007a). Another *P. australis* protein, PhaHAK5, could also be involved in Na^+ transport, as suggested from heterologous expression in yeast (Takahashi et al., 2007b). Recently, a *bona fide* high-affinity Na^+-selective transporter of higher plants, ZmHAK4, has been identified in maize (Zhang et al., 2019). *ZmHAK4* is predominantly expressed in the root vascular tissue. Knock-out mutants and natural hypomorphic alleles with reduced expression of this gene had increased Na^+ contents in shoot and xylem sap, and reduced root Na^+ content under high-Na^+ conditions. Thus, ZmHAK4 appears to promote shoot Na^+ exclusion and salt tolerance by retrieving Na^+ from xylem sap and preventing root-to-shoot Na^+ translocation (**Figure 4**). *HAK4* orthologs in rice and wheat are also preferentially expressed in the root stele and encode Na^+-selective transporters. Thus, *HAK4* orthologs in cereals probably constitute a conserved salt-tolerance mechanism governing Na^+ delivery to shoots. Last, HvHAK1 of barley (*Hordeum vulgare*) and the rice OsHAK2 could also be involved in Na^+ influx (Santa-Maria et al., 1997; Horie et al., 2011).

In parallel with HAK transporters, several HKTs also contribute to Na^+ uptake from the soil, functioning as Na^+:K^+ symporters or as Na^+ uniporters at high Na^+ concentrations

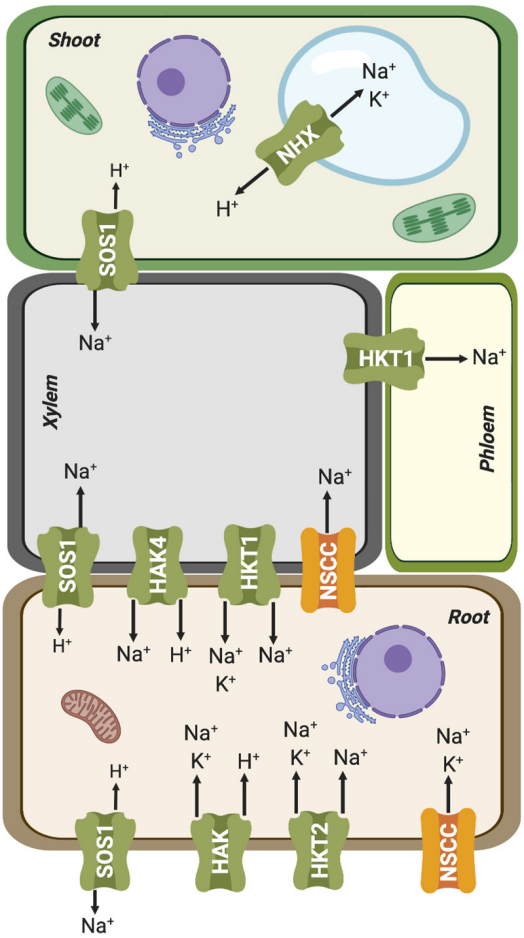

FIGURE 4 | Simplified representation of plant organs and vascular tissues, and the Na^+ and K^+ fluxes mediated by ion transporters involved in root uptake and root-shoot partition. Further details are given in the main text.

(reviewed by Benito et al., 2014; Hamamoto et al., 2015; **Figure 4**). Plant HKT proteins display a core structure similar to that of the K^+ transporter TrkH from *Vibrio parahaemolyticus* (Cao et al., 2011), comprising eight transmembrane (TM) and four pore-forming (P) domains successively arranged in four TM1-P-TM2 motifs in a single polypeptide chain. The assembly of these four TM1-P-TM2 motifs results in the formation of a central permeation pathway similar to that of tetrameric *Shaker*-like K^+ channels. The plant HKT family has been divided into at least two classes based on a distinguishing feature that lies in the selectivity filter. Class-I (HKT1) members are ubiquitous in plants, mostly Na^+-selective, and often involved in Na^+ recirculation through vascular tissues (Maathuis, 2014; Very et al., 2014; **Figure 4**). Most members of this clade have a highly conserved serine (SGGG motif) in the first pore-loop domain of the protein, while class-II (HKT2) members, found exclusively in monocots, have a glycine instead of the serine (GGGG motif) in this domain and are generally permeable to both Na^+ and K^+ (Hauser and Horie, 2010). This classification is not strict as HKT proteins may display different permeation modes depending on the external concentrations of Na^+ and K^+. At concentrations of Na^+ and K^+ below 1–10 mM, these transporters function essentially as Na^+:K^+ symporters (Rubio et al., 1995; Haro et al., 2005), whereas at high external Na^+ concentrations, above 1–10 mM, HKTs lose their permeability to K^+ and become Na^+ uniporters (Gassman et al., 1996; Horie et al., 2001; Jabnoune et al., 2009). On the other hand, an increase in K^+ concentration reduces the transport rate of both the Na^+:K^+ symport and Na^+ uniport modes (Gassman et al., 1996; Garciadeblas et al., 2003; Jabnoune et al., 2009). These different permeation mechanisms have been explained through two mechanistic models: (i) carrier-mediated transport by an alternating-access model (Gassman et al., 1996; Rubio et al., 1999; Haro and Rodriguez-Navarro, 2002) and (ii) a pore-mediated model very similar to that of K^+ channels (Durell and Guy, 1999; Tholema et al., 2005; Corratge et al., 2007). The first mechanism posits the existence of two high-affinity binding sites, named K^+- and Na^+-coupling sites. In this model, both binding sites need to be occupied for uptake to occur (Rubio et al., 1995; Jabnoune et al., 2009). Thus, the competitive binding of K^+ and Na^+ at the K^+-coupling site would explain both permeation modes, Na^+:K^+ symport or Na^+ uniport. On the other hand, high external K^+ could inhibit the symport activity assuming that the binding of K^+ at the Na^+ coupling site results in a non- or weakly conductive state (Jabnoune et al., 2009). While this mechanism can readily explain the different uniport and symport modes, it does not explain the large currents measured for different HKTs in oocytes for Na^+ and/or K^+ (5–10 μA) (Oomen et al., 2012). Considering that the turnover rate reaches values around 10^6 ions per second, it is likely that HKTs have a pore and they function as ion channels. According to the channel-like model of transport, Na^+ ions would be bound by two coordination sites in a partially dehydrated form, i.e., retaining only its first hydration shell (Benito et al., 2014). One or two water molecules of the shell might be substituted with polar oxygens of the side chain of the serine residue in the SGGG signature in the first P-loop region. The flexible hydration shell of K^+ would also allow the coordination of this ion in the two coordination sites. Thus, the molecular permeation model proposed for HKTs, based on Na^+ permeation in a channel-like structure, could account for the different transport modes observed in the HKT, namely Na^+ uniport, Na^+:K^+ symport and K^+ uniport (Benito et al., 2014).

An interesting example of the fuzzy classification of HKT proteins is that of two class-II HKT proteins of rice, OsHKT2;1, isolated from Nipponbare, and OsHKT2;2 present in the salt-tolerant Pokkali cultivar. Both proteins share high homology (91%), and yet they exhibit differential Na^+:K^+ transport selectivity when expressed in heterologous expression systems. OsHKT2;1 mediates mainly Na^+ uptake (Jabnoune et al., 2009; Yao et al., 2010), whereas OsHKT2;2 transports both K^+ and Na^+ (Horie et al., 2001, 2007). Protein OsHKT2;2 has the typical four Gly residues (GGGG motif) of class-II HKT transporters, permeates both K^+ and Na^+ in a large range of concentrations, and functions preferentially as a Na^+:K^+ symport, and with low concentration of K^+ ions exerting an stimulating effect on Na^+ transport (Horie et al., 2001; Yao et al., 2010; Oomen et al., 2012; Riedelsberger et al., 2018). However, OsHKT2;1 is an atypical

HKT class-II member because it contains the SGGG signature in the first pore-loop and mediates selective Na^+ uptake, which are typical features of class-I HKT transporters (Horie et al., 2001; Garciadeblas et al., 2003). OsHKT2;1 enables Na^+ uptake into K^+-starved roots, thereby compensating for the lack of K^+ as cellular osmolyte (Horie et al., 2007). In wheat, *TaHKT2;1* is preferentially expressed in the root cortex and induced by K^+ deficiency (Schachtman and Schroeder, 1994) and seems to have a function similar to that of OsHKT2;1 (Horie et al., 2009). *HvHKT2;1* from barley (*Hordeum vulgare*) is also induced by K^+ deficiency, and the protein demonstrated the co-transports Na^+ and K^+ over a large range of concentrations (Mian et al., 2011; Hmidi et al., 2019). Together, these result suggest that HKT2;1 proteins may contribute both to the K^+ uptake in the presence of Na^+, and to Na^+ uptake for osmotic adjustment.

Of note is that substrate selectivity of HKT1 transporters could be modified by single amino acid changes outside the SGGG/GGGD motif dichotomy. Using 3D comparative modeling, Cotsaftis et al. (2012) suggested that K^+ can be transported unfavorably in class-I members due to a steric hindrance imposed through the G to S substitution, while the G in class-II HKTs would facilitate the transport of K^+, although under certain conditions these proteins also could transport Na^+ (Maser et al., 2002a). Some exceptions to this general rule are EcHKT1;2 from *Eucalyptus camaldulensis*, EsHKT1;2 from *Eutrema salsugineum (*formerly *Thellungiella salsuginea or T. halophila)*, SpHKT1;2 from *Schrenkiella parvula (*formerly *T. parvula)*, and McHKT1;1 from *Mesembryantemum crystallinum*, all of which have a Ser in the first pore-loop domain and are permeable to K^+ (Fairbairn et al., 2000; Su et al., 2003; Jabnoune et al., 2009; Ali et al., 2012). This indicates that K^+ permeability in HKTs does not depend only on the Gly residue at the pore. Indeed, the alignment of HKTs homologs from *Arabidopsis*, *Eutrema* and *Schrenkiella* species with ScTRK1, a high-affinity potassium transporter of *Saccharomyces cerevisiae*, showed that both EsHKT1;2 (*E. salsugineum*) and SpHKT1;2 (*S. parvula*) contained, alike ScTRK1, conserved Asp residues in their second pore-loop domains (Asp207 and Asp205, respectively) (Ali et al., 2012). However, in most HKT1-like proteins an Asn is present at the corresponding position. The change of Asp207 to Asn207 in EsHKT1;2 and Asp205 to Asn205 in SpHKT1;2 abolished K^+ uptake and generated the typical Na^+-selective transport of class-I HKTs (Ali et al., 2012, 2018). Moreover, changing the Asn residue in the 2nd pore-loop domain of AtHKT1 to Asp, converted a highly selective Na^+ transporter into a transporter more similar to EsHKT1;2, with high affinity for K^+. Transgenic *Arabidopsis* plants that expressed the AtHKT1-Asn211Asp variant were more tolerant to salt stress than controls with wild type AtHKT1, and showed the same tolerance phenotype than having EsHKT1;2 or SpHKT1;2 overexpressed in *Arabidopsis* plants (Ali et al., 2016, 2018). Consequently, Ser in the SGGG motif of the first pore-loop domain appears not to be the only essential amino acid favoring Na^+ uptake (at least in *Arabidopsis*, *Eutrema*, and *Schrenkiella* species), but it possibly functions as a supporting residue. All these examples show that the cation selectivity of HKT transporters could be convertible by exchanging single amino acids, and that structural elements localized in regions outside the selectivity filter can determine the ionic selectivity for Na^+ and/or K^+ of HKT proteins.

Notably, mutations inactivating Na^+-selective HKT1-like transporters reduce the K^+ contents of shoots during salt exposure. For instance, mutations of *hkt1* in Arabidopsis cause opposite effects on the K^+ content with respect to that of Na^+ both in roots and shoots, maintaining lower K^+ levels in shoots but higher K^+ in roots (Maser et al., 2002b; Sunarpi et al., 2005). In rice, the *SKC1* locus identified as a QTL for shoot K^+ content encodes the Na^+-selective protein HKT1;5 whose activity, however, determines the accumulation of K^+ in aerial parts (Ren et al., 2005). A similar situation has been described for the salt-tolerance *NAX2* locus of wheat, also encoding an HKT1;5 protein (Munns et al., 2012). These results suggest a connection between Na^+ unloading via HKT1-like proteins and K^+ loading from xylem parenchyma cells under salt stress. This phenomenon could be explained if the uptake of Na^+ through HKT1 proteins caused membrane depolarization in xylem parenchyma cells, thereby promoting the opening of outward-rectifying K^+ channels, such as SKOR, and the K^+ accumulation in the xylem and leaves (Horie et al., 2009). SKOR allows of K^+ release into the xylem vessels from xylem parenchyma cells (Gaymard et al., 1998). Together, these results suggest that HKT1-like proteins provide two essential mechanisms toward mediating salt tolerance: (i) prevention of Na^+ over-accumulation in leaves; and (ii) allowing the K^+ accumulation in leaves through outward-rectifying K^+ channels.

Additional pathways for Na^+ entry in plant cells may be provided by Non-Selective Cation Channels (NSCC) (**Figure 4**). Negative electrical membrane potential and high extracellular Na^+ concentrations promote passive entry of Na^+ into roots through ion channels. Electrophysiological experiments in *A. thaliana* protoplasts have shown that NSCCs could be Na^+ influx pathways (Demidchik and Tester, 2002; Tyerman, 2002). These proteins form a heterogeneous group of plasma membrane channels with a high selectivity for cations over anions, while differing in their ability to conduct mono- and divalent cations (Tyerman, 2002; Zhang et al., 2002; Demidchik et al., 2002a,b; Demidchik and Maathuis, 2007). NSCC channels are classified into three major families according to their response to changes in membrane electrical potential: depolarization-activated NSCCs (DA-NSCCs), hyperpolarization-activated NSCCS (HA-NSCCs) and voltage-insensitive NSCCs (VI-NSCCs) (Demidchik and Maathuis, 2007). This last group is commonly found in plasma membrane of roots and leaves of different plant species (Tyerman et al., 1997; Demidchik and Tester, 2002; Demidchik et al., 2002b; Shabala et al., 2006, 2007; Zhao et al., 2007, 2011; Velarde-Buendia et al., 2012). VI-NSCCs weakly differentiate among different cations, with the preference $K^+ > NH^{+4} > Rb^+ \sim Cs^+ \sim Na^+ > Li^+ >$ tetraethylammonium (TEA^+). In general, they have significant Na^+ conductance, but still lower than that of K^+ (Kronzucker and Britto, 2011). Cyclic nucleotide-gated channel (CNGC), have been suggested to be VI-NSCCs channels (Maathuis and Sanders, 2001; Demidchik et al., 2002b; Demidchik and Maathuis, 2007), or weakly voltage-sensitive (Leng et al., 2002; Lemtiri-Chlieh and Berkowitz, 2004;

Wang et al., 2013; Mori et al., 2018). CNGCs permit the diffusion of monovalent and divalent cations such as Na^+, K^+, and Ca^{2+} (Leng et al., 1999, 2002; Demidchik and Maathuis, 2007; Mian et al., 2011; Hanin et al., 2016). They are ligand-gated channels regulated by reversible binding of adenosine 3′,5′-cyclic monophosphate (cAMP), guanosine 3,5-cyclic monophosphate (cGMP) (Balague et al., 2003; Chin et al., 2009; Ramanjaneyulu et al., 2010), or calmodulin (CaM) to the cyclic nucleotide binding domain (Kohler and Neuhaus, 2000; Hua et al., 2003). In fact, the first *CNGC* gene in plants was identified during a screen for CaM binding partners in *Hordeum vulgare* (Schuurink et al., 1998). Subsequently, 20 CNGC family members have been identified in *A. thaliana* (Kohler et al., 1999), 16 in rice, *Oryza sativa* (Nawaz et al., 2014), 18 in tomato, *Solanum lycopersicum* (Saand et al., 2015), 21 in pear, *Pyrus bretschneideri* (Chen et al., 2015) and 26 in the Chinese cabbage *Brassica oleracea* (Kakar et al., 2017). The largest family was recently described in wheat, *Triticum aestivum*, with 47 *TaCNGC* genes (Guo et al., 2018). These proteins share structural homology with *Shaker*-like channels, with six transmembrane segments and a long cytosolic C-terminal domain harboring a cyclic nucleotide-binding domain. However, they lack the canonical motif TxGYG, a hallmark of K^+-selective channels (Talke et al., 2003; Szczerba et al., 2009). All CNGCs of *P. bretschneideri* and *A. thaliana* contain positively charged residues in the S4 motif, similar to voltage-dependent K^+ channels (Chen et al., 2015). Likewise, in HvCNGC2-3, four arginine residues and a lysine are present through S2 to S4 (Mori et al., 2018). Thus, it is possible that the voltage sensitivity observed in some CNGCs could discredit a significant involvement in mediating Na^+ fluxes for extended periods of time (Kronzucker and Britto, 2011). More electrophysiological experiments are required to determine the real importance of the charged residues in the voltage sensitivity of these channels. Moreover, salt stress increases cGMP level in *Arabidopsis* roots, thereby inhibiting the permeability of CNGC channels to Na^+ and reducing its entry to root cells (Maathuis and Sanders, 2001; Donaldson et al., 2004). Together, these findings question that CNGC could represent a significant pathway for Na^+ entry.

Some members of *A. thaliana*, like AtCNGC2, appears to be selective for K^+ over other alkali metal cations (Cs^+, Li^+, and Rb^+) and to exclude Na^+ (Leng et al., 2002), while others are able to transport both K^+ as well as Na^+, thereby impacting on cytosolic K^+:Na^+ ratios under saline conditions. AtCNGC3 is mostly expressed in epidermal and cortical root tissues. The loss of function of CNGC3 alters the ionic composition of seedlings of *Arabidopsis*, reducing the net Na^+ uptake and promoting K^+ accumulation (Gobert et al., 2006). AtCNGC10 is also permeable to Na^+ and K^+, and antisense lines exhibited alterations in the content of both cations within roots and shoots (Guo et al., 2008) while overexpression could partially compensate the knockout mutation *akt1-1* inactivating a *Shaker*-type channel implicated in uptake of K^+ by roots (Li et al., 2005). Recently, electrophysiological analysis of the barley HvCNGC2-3 (*Hordeum vulgare)* has shown that this channel is activated only by the co-presence of K^+ and Na^+ (Mori et al., 2018). This property has not been reported for any other CNGC, and although its meaning is still unclear, the root-expressed HvCNGC2-3 could be involved in the response to salinity stress, improving the osmotic adjustment of roots. In the case of barley, the permeability of Na^+ and K^+ by CNGC2-3 could have a role in balancing the ratio of these cations in the cells sustaining osmotic potential in the roots.

As mentioned before, Na^+ can partially substitute for K^+ as a cellular osmolyte, particularly in conditions in which K^+ is limiting. The Na^+ acquired for osmotic purposes must be sequestered within the vacuoles to avert its cytotoxic effect in the cytosol and other intracellular components (Mittler and Blumwald, 2010). Cation/H^+ antiporters are thought to mediate the transport of Na^+ into the vacuole, driven by the electrochemical gradient of protons generated by the vacuolar ATPase (V-ATPase) and pyrophosphatase (V-PPase) enzymes (Sze and Chanroj, 2018; Shabala et al., 2019; **Figure 4**). Na^+/H^+ exchange is mediated by members of a family of transporters referred to as Na^+-H^+ exchangers, named NHXs in plants and NHEs in animals (Jiang et al., 2010; Chanroj et al., 2012). However, detailed biochemical and molecular genetic analyses have shown that members of the plant NHX family have different ion selectivities that correlate with the cellular membrane in which they are placed (Jiang et al., 2010; Chanroj et al., 2012; Ragel et al., 2019). Thus, the plasma membrane localized proteins SOS1/NHX7 and NHX8 show great selectivity for Na^+ and Li^+, respectively, and they are involved in the plant tolerance to high levels of these cations (Shi et al., 2002; An et al., 2007; Quintero et al., 2011), whereas family members sorted to endosomal membranes show various degrees of non-selective transport of the monovalent alkali cations Na^+, K^+ and Li^+ (Jiang et al., 2010; Huertas et al., 2013; Bassil et al., 2019; **Figure 4**).

Shortly after the identification of plant NHXs, Apse et al. (1999) showed that overexpression of the vacuolar isoform *AtNHX1* of *Arabidopsis* increased salinity tolerance and greater Na^+/H^+ exchange activity in isolated leaf vacuoles. Although this first report concluded that AtNHX1 was specific to Na^+ transport, later studies have shown that AtNHX1 and other tonoplast localized NHXs mediate vacuolar K^+ uptake under normal growth conditions and in the presence of moderate Na^+ concentrations (Venema et al., 2002; Leidi et al., 2010; Bassil et al., 2011; Barragan et al., 2012; Andres et al., 2014). Overexpression of *AtNHX1* in tomato plants promoted higher vacuolar K^+ content under different growth conditions, and increased the salinity tolerance of transgenic plants via retention of intracellular K^+ and without influencing vacuolar Na^+ accumulation (Leidi et al., 2010). Similarly, transgenic alfalfa overexpressing the wheat TaNHX2 exchanger, a vacuolar isoform, decreased K^+ efflux by reducing plasma membrane depolarization and activation of K^+ outwardly rectifying channels, thereby retaining more intracellular K^+ under salt stress conditions (Zhang et al., 2015). LeNHX2 protein, which is preferentially localized in non- endomembranes from tomato, catalyzes specifically K^+/H^+ antiport in proteoliposomes, showing very low activities with other monovalent cations, including Na^+ (Venema et al., 2003; Huertas et al., 2013). Endosomes have been identified as a target for Na^+ toxicity (Hernandez et al., 2009) and it has been suggested that intracellular non-vacuolar isoforms, such as

LeNHX2 or Arabidopsis NHX5 and NHX6 could have greater selectivity for K^+ over Na^+ as to prevent excessive Na^+ uptake into endosomes (Hernandez et al., 2009; Jiang et al., 2010), whereas those NHXs localized to the tonoplast would not discriminate since their main function is to accumulate ions in the vacuolar lumen for osmotic adjustment, cell turgor and control of the vacuolar pH (Venema et al., 2002; Bassil et al., 2011; Barragan et al., 2012; Andres et al., 2014).

Recently, multiple knockout mutants of Arabidopsis lacking all but one of the four vacuolar isoforms (NHX1, NHX2, NHX3, NHX4) and quadruple knockout plants lacking all vacuolar NHX activity, have been analyzed (Bassil et al., 2019). Kinetic analysis of K^+ and Na^+ transport indicated that NHX1, NHX2, and NHX4, are the main transporters of K^+ in the vacuoles, while AtNHX3 could mediate Na^+ transport. The lack of NHX activity at the tonoplast (*nhx1–nhx4*) resulted in no K^+ uptake and in highly acidic vacuolar lumen. This mutant displayed Na^+ transport with an apparent Km of 9.9 mM, suggesting the existence of an alternative, cation/H^+-independent mechanism that permitted the transport of Na^+ into vacuoles, as previously suggested (Barragan et al., 2012). These results confirm a large amount of evidence demonstrating the polyvalent role of NHX as Na^+/H^+ and/or K^+/H^+ exchangers in vacuolar membranes. Refined structural modeling combined with the identification of amino acid residues involved in ion coordination and transport (Wang et al., 2015) could allow the rational design of Na^+-selective tonoplast-localized NHXs that would be instrumental in achieving salt tolerance based on efficacious Na^+ sequestration into vacuoles. This strategy should most likely be combined with the reduction of Na^+ leaks back to the cytosol through vacuolar channels (Shabala et al., 2019).

AUTHOR CONTRIBUTIONS

All authors have contributed to literature search, discussion, and writing of the manuscript. LM prepared the figures. JP assembled all the sections. All authors checked and approved the manuscript.

FUNDING

This work was supported by grants RTI2018-094027-B-I00 and BIO2016-81957-REDT from the Spanish AEI-MCIU (co-financed by the European Regional Development Fund), and the SSAC grant PJ01318205 from the Rural Development Administration, South Korea, to JP. We acknowledge support of the publication fee by the CSIC Open Access Publication Support Initiative through its Unit of Information Resources for Research (URICI).

ACKNOWLEDGMENTS

We apologize to all authors whose work relevant to this topic could not be cited because of space limitations.

REFERENCES

Ahmad, I., and Maathuis, F. J. (2014). Cellular and tissue distribution of potassium: physiological relevance, mechanisms and regulation. *J. Plant Physiol.* 171, 708–714. doi: 10.1016/j.jplph.2013.10.016

Ahn, S. J., Shin, R., and Schachtman, D. P. (2004). Expression of KT/KUP genes in *Arabidopsis* and the role of root hairs in K(+) uptake. *Plant Physiol.* 134, 1135–1145. doi: 10.1104/pp.103.034660

Aleman, F., Nieves-Cordones, M., Martinez, V., and Rubio, F. (2009). Differential regulation of the HAK5 genes encoding the high-affinity K(+) transporters of *Thellungiella halophila* and *Arabidopsis thaliana*. *Environ. Exp. Bot.* 65, 263–269. doi: 10.1016/j.envexpbot.2008.09.011

Ali, A., Khan, I. U., Jan, M., Khan, H. A., Hussain, S., Nisar, M., et al. (2018). The high-affinity potassium transporter EpHKT1;2 from the extremophile Eutrema parvula mediates salt tolerance. *Front. Plant Sci.* 9:1108. doi: 10.3389/fpls.2018.01108

Ali, A., Raddatz, N., Aman, R., Kim, S., Park, H. C., Jan, M., et al. (2016). A single amino-acid substitution in the sodium transporter HKT1 associated with plant salt tolerance. *Plant Physiol.* 171, 2112–2126. doi: 10.1104/pp.16.00569

Ali, Z., Park, H. C., Ali, A., Oh, D. H., Aman, R., Kropornicka, A., et al. (2012). TsHKT1;2, a HKT1 homolog from the extremophile *Arabidopsis* relative *Thellungiella salsuginea*, shows K(+) specificity in the presence of NaCl. *Plant Physiol.* 158, 1463–1474. doi: 10.1104/pp.111.193110

Alvarez-Aragon, R., Haro, R., Benito, B., and Rodriguez-Navarro, A. (2016). Salt intolerance in *Arabidopsis*: shoot and root sodium toxicity, and inhibition by sodium-plus-potassium overaccumulation. *Planta* 243, 97–114. doi: 10.1007/s00425-015-2400-7

Alvarez-Aragon, R., and Rodriguez-Navarro, A. (2017). Nitrate-dependent shoot sodium accumulation and osmotic functions of sodium in *Arabidopsis* under saline conditions. *Plant J.* 91, 208–219. doi: 10.1111/tpj.13556

An, R., Chen, Q. J., Chai, M. F., Lu, P. L., Su, Z., Qin, Z. X., et al. (2007). AtNHX8, a member of the monovalent cation: proton antiporter-1 family in *Arabidopsis thaliana*, encodes a putative Li/H antiporter. *Plant J.* 49, 718–728. doi: 10.1111/j.1365-313X.2006.02990.x

Andres, Z., Perez-Hormaeche, J., Leidi, E. O., Schlucking, K., Steinhorst, L., McLachlan, D. H., et al. (2014). Control of vacuolar dynamics and regulation of stomatal aperture by tonoplast potassium uptake. *Proc. Natl. Acad. Sci. U.S.A.* 111, E1806–E1814. doi: 10.1073/pnas.1320421111

Apse, M. P., Aharon, G. S., Snedden, W. A., and Blumwald, E. (1999). Salt tolerance conferred by overexpression of a vacuolar Na(+)/H(+) antiport in *Arabidopsis*. *Science* 285, 1256–1258. doi: 10.1126/science.285.5431.1256

Armengaud, P., Breitling, R., and Amtmann, A. (2004). The potassium-dependent transcriptome of *Arabidopsis* reveals a prominent role of jasmonic acid in nutrient signaling. *Plant Physiol,* 136, 2556–2576. doi: 10.1104/pp.104.046482

Balague, C., Lin, B., Alcon, C., Flottes, G., Malmstrom, S., Kohler, C., et al. (2003). HLM1, an essential signaling component in the hypersensitive response, is a member of the cyclic nucleotide-gated channel ion channel family. *Plant Cell* 15, 365–379. doi: 10.1105/tpc.006999

Barragan, V., Leidi, E. O., Andres, Z., Rubio, L., De Luca, A., Fernandez, J. A., et al. (2012). Ion exchangers NHX1 and NHX2 mediate active potassium uptake into vacuoles to regulate cell turgor and stomatal function in *Arabidopsis*. *Plant Cell* 24, 1127–1142. doi: 10.1105/tpc.111.095273

Bassil, E., Tajima, H., Liang, Y. C., Ohto, M. A., Ushijima, K., Nakano, R., et al. (2011). The *Arabidopsis* Na(+)/H(+) antiporters NHX1 and NHX2 control vacuolar pH and K(+) homeostasis to regulate growth, flower development, and reproduction. *Plant Cell* 23, 3482–3497. doi: 10.1105/tpc.111.089581

Bassil, E., Zhang, S., Gong, H., Tajima, H., and Blumwald, E. (2019). Cation specificity of vacuolar NHX-type cation/H(+) antiporters. *Plant Physiol.* 179, 616–629. doi: 10.1104/pp.18.01103

Behera, S., Long, Y., Schmitz-Thom, I., Wang, X. P., Zhang, C., Li, H., et al. (2017). Two spatially and temporally distinct Ca(2+) signals convey *Arabidopsis*

thaliana responses to K(+) deficiency. *New Phytol.* 213, 739–750. doi: 10.1111/nph.14145

Benito, B., Garciadeblas, B., and Rodriguez-Navarro, A. (2012). HAK transporters from *Physcomitrella patens* and Yarrowia lipolytica mediate sodium uptake. *Plant Cell Physiol.* 53, 1117–1123. doi: 10.1093/pcp/pcs056

Benito, B., Haro, R., Amtmann, A., Cuin, T. A., and Dreyer, I. (2014). The twins K(+) and Na(+) in plants. *J. Plant Physiol.* 171, 723–731. doi: 10.1016/j.jplph.2013.10.014

Bouguyon, E., Brun, F., Meynard, D., Kubes, M., Pervent, M., Leran, S., et al. (2015). Multiple mechanisms of nitrate sensing by *Arabidopsis* nitrate transceptor NRT1.1. *Nat. Plants* 1:15015. doi: 10.1038/nplants.2015.15

Bouguyon, E., Perrine-Walker, F., Pervent, M., Rochette, J., Cuesta, C., Benkova, E., et al. (2016). Nitrate controls root development through posttranscriptional regulation of the NRT1.1/*NPF*6.3 transporter/sensor. *Plant Physiol.* 172, 1237–1248. doi: 10.1104/pp.16.01047

Brauer, E. K., Ahsan, N., Dale, R., Kato, N., Coluccio, A. E., Pineros, M. A., et al. (2016). The Raf-like kinase ILK1 and the high affinity K(+) transporter HAK5 are required for innate immunity and abiotic stress response. *Plant Physiol.* 171, 1470–1484. doi: 10.1104/pp.16.00035

Cabot, C., Sibole, J. V., Barcelo, J., and Poschenrieder, C. (2014). Lessons from crop plants struggling with salinity. *Plant Sci.* 226, 2–13. doi: 10.1016/j.plantsci.2014.04.013

Cao, Y., Jin, X., Huang, H., Derebe, M. G., Levin, E. J., Kabaleeswaran, V., et al. (2011). Crystal structure of a potassium ion transporter. *TRKH Nature* 471, 336–340. doi: 10.1038/nature09731

Carden, D. E., Walker, D. J., Flowers, T. J., and Miller, A. J. (2003). Single-cell measurements of the contributions of cytosolic Na(+) and K(+) to salt tolerance. *Plant Physiol.* 131, 676–683. doi: 10.1104/pp.011445

Cerezo, M., Tillard, P., Filleur, S., Munos, S., Daniel-Vedele, F., and Gojon, A. (2001). Major alterations of the regulation of root NO3(-) uptake are associated with the mutation of Nrt2.1 *and Nrt*2.2 genes in *Arabidopsis*. *Plant Physiol.* 127, 262–271. doi: 10.1104/pp.127.1.262

Chanroj, S., Wang, G., Venema, K., Zhang, M. W., Delwiche, C. F., and Sze, H. (2012). Conserved and diversified gene families of monovalent cation/H(+) antiporters from algae to flowering plants. *Front. Plant Sci.* 3:25. doi: 10.3389/fpls.2012.00025

Chen, C. Z., Lv, X. F., Li, J. Y., Yi, H. Y., and Gong, J. M. (2012). *Arabidopsis* NRT1.5 is another essential component in the regulation of nitrate reallocation and stress tolerance. *Plant Physiol.* 159, 1582–1590. doi: 10.1104/pp.112.199257

Chen, J., Yin, H., Gu, J., Li, L., Liu, Z., Jiang, X., et al. (2015). Genomic characterization, phylogenetic comparison and differential expression of the cyclic nucleotide-gated channels gene family in pear (Pyrus bretchneideri Rehd.). *Genomics* 105, 39–52. doi: 10.1016/j.ygeno.2014.11.006

Chen, Z. H., Wang, Y., Wang, J. W., Babla, M., Zhao, C., Garcia-Mata, C., et al. (2016). Nitrate reductase mutation alters potassium nutrition as well as nitric oxide-mediated control of guard cell ion channels in *Arabidopsis*. *New Phytol.* 209, 1456–1469. doi: 10.1111/nph.13714

Chin, K., Moeder, W., and Yoshioka, K. (2009). Biological roles of cyclic-nucleotide-gated ion channels in plants: what we know and don't know about this 20 member ion channel family. *Botany* 87, 668–677. doi: 10.1139/B08-147

Chopin, F., Orsel, M., Dorbe, M. F., Chardon, F., Truong, H. N., Miller, A. J., et al. (2007). The *Arabidopsis* ATNRT2.7 nitrate transporter controls nitrate content in seeds. *Plant Cell* 19, 1590–1602. doi: 10.1105/tpc.107.050542

Clarkson, D. T., and Hanson, J. B. (1980). The mineral nutrition of higher plants. *Annu. Rev. Plant Physiol.* 31, 239–298. doi: 10.1146/annurev.pp.31.060180.001323

Corratge, C., Zimmermann, S., Lambilliotte, R., Plassard, C., Marmeisse, R., Thibaud, J. B., et al. (2007). Molecular and functional characterization of a Na(+)-K(+) transporter from the Trk family in the ectomycorrhizal fungus Hebeloma cylindrosporum. *J. Biol. Chem.* 282, 26057–26066. doi: 10.1074/jbc.M611613200

Coskun, D., Britto, D. T., Jean, Y. K., Kabir, I., Tolay, I., Torun, A. A., et al. (2013). K(+) efflux and retention in response to NaCl stress do not predict salt tolerance in contrasting genotypes of rice (Oryza sativa L.). *PLoS One* 8:e57767. doi: 10.1371/journal.pone.0057767

Coskun, D., Britto, D. T., and Kronzucker, H. J. (2017). The nitrogen-potassium intersection: membranes, metabolism, and mechanism. *Plant Cell Environ.* 40, 2029–2041. doi: 10.1111/pce.12671

Cotsaftis, O., Plett, D., Shirley, N., Tester, M., and Hrmova, M. (2012). A two-staged model of Na(+) exclusion in rice explained by 3D modeling of HKT transporters and alternative splicing. *PLoS One* 7:e39865. doi: 10.1371/journal.pone.0039865

Craig Plett, D., and Moller, I. S. (2010). Na(+) transport in glycophytic plants: what we know and would like to know. *Plant Cell Environ.* 33, 612–626. doi: 10.1111/j.1365-3040.2009.02086.x

Crawford, N. M. (1995). Nitrate: nutrient and signal for plant growth. *Plant Cell* 7, 859–868. doi: 10.1105/tpc.7.7.859

Crawford, N. M., and Glass, A. D. (1998). Molecular and physiological aspects of nitrate uptake in plants. *Trends Plant Sci.* 3, 389–395. doi: 10.1016/S1360-1385(98)01311-9

Cui, Y. N., Li, X. T., Yuan, J. Z., Wang, F. Z., Wang, S. M., and Ma, Q. (2019). Nitrate transporter NPF7.3/*NRT*1.5 plays an essential role in regulating phosphate deficiency responses in *Arabidopsis*. *Biochem. Biophys. Res. Commun.* 508, 314–319. doi: 10.1016/j.bbrc.2018.11.118

Daram, P., Urbach, S., Gaymard, F., Sentenac, H., and Cherel, I. (1997). Tetramerization of the AKT1 plant potassium channel involves its C-terminal cytoplasmic domain. *EMBO J.* 16, 3455–3463. doi: 10.1093/emboj/16.12.3455

Daras, G., Rigas, S., Tsitsekian, D., Iacovides, T. A., and Hatzopoulos, P. (2015). Potassium transporter TRH1 subunits assemble regulating root-hair elongation autonomously from the cell fate determination pathway. *Plant Sci.* 231, 131–137. doi: 10.1016/j.plantsci.2014.11.017

De Angeli, A., Monachello, D., Ephritikhine, G., Frachisse, J. M., Thomine, S., Gambale, F., et al. (2006). The nitrate/proton antiporter AtCLCa mediates nitrate accumulation in plant vacuoles. *Nature* 442, 939–942. doi: 10.1038/nature05013

Demidchik, V., Bowen, H. C., Maathuis, F. J., Shabala, S. N., Tester, M. A., White, P. J., et al. (2002a). *Arabidopsis thaliana* root non-selective cation channels mediate calcium uptake and are involved in growth. *Plant J.* 32, 799–808. doi: 10.1046/j.1365-313x.2002.01467.x

Demidchik, V., Cuin, T. A., Svistunenko, D., Smith, S. J., Miller, A. J., Shabala, S., et al. (2010). *Arabidopsis* root K(+)-efflux conductance activated by hydroxyl radicals: single-channel properties, genetic basis and involvement in stress-induced cell death. *J. Cell Sci.* 123(Pt 9), 1468–1479. doi: 10.1242/jcs.064352

Demidchik, V., Davenport, R. J., and Tester, M. (2002b). Nonselective cation channels in plants. *Annu Rev. Plant Biol.* 53, 67–107. doi: 10.1146/annurev.arplant.53.091901.161540

Demidchik, V., and Maathuis, F. J. (2007). Physiological roles of nonselective cation channels in plants: from salt stress to signalling and development. *New Phytol.* 175, 387–404. doi: 10.1111/j.1469-8137.2007.02128.x

Demidchik, V., and Tester, M. (2002). Sodium fluxes through nonselective cation channels in the plasma membrane of protoplasts from *Arabidopsis* roots. *Plant Physiol.* 128, 379–387. doi: 10.1104/pp.010524

Donaldson, L., Ludidi, N., Knight, M. R., Gehring, C., and Denby, K. (2004). Salt and osmotic stress cause rapid increases in *Arabidopsis thaliana* cGMP levels. *FEBS Lett.* 569, 317–320. doi: 10.1016/j.febslet.2004.06.016

Drechsler, N., Zheng, Y., Bohner, A., Nobmann, B., von Wiren, N., Kunze, R., et al. (2015). Nitrate-dependent control of shoot K homeostasis by the nitrate transporter1/peptide transporter family member NPF7.3/*NRT*1.5 and the stelar K(+) outward rectifier SKOR in *Arabidopsis*. *Plant Physiol.* 169, 2832–2847. doi: 10.1104/pp.15.01152

Du, X. Q., Wang, F. L., Li, H., Jing, S., Yu, M., Li, J., et al. (2019). The transcription factor MYB59 regulates K(+)/NO3 (-) translocation in the *Arabidopsis* response to low K(+) stress. *Plant Cell* 31, 699–714. doi: 10.1105/tpc.18.00674

Dubeaux, G., Neveu, J., Zelazny, E., and Vert, G. (2018). Metal sensing by the IRT1 transporter-receptor orchestrates its own degradation and plant metal nutrition. *Mol Cell* 69, 953.e4–955.e5. doi: 10.1016/j.molcel.2018.02.009

Durell, S. R., and Guy, H. R. (1999). Structural models of the KtrB, TrkH, and Trk1,2 symporters based on the structure of the KcsA K(+) channel. *Biophys. J.* 77, 789–807. doi: 10.1016/S0006-3495(99)76932-8

Eisenach, C., and De Angeli, A. (2017). Ion transport at the vacuole during stomatal movements. *Plant Physiol.* 174, 520–530. doi: 10.1104/pp.17.00130

El Mahi, H., Perez-Hormaeche, J., De Luca, A., Villalta, I., Espartero, J., Gamez-Arjona, F., et al. (2019). A critical role of sodium flux via the plasma membrane Na(+)/H(+) exchanger SOS1 in the salt tolerance of rice. *Plant Physiol.* 180, 1046–1065. doi: 10.1104/pp.19.00324

Engels, C., and Kirkby, E. A. (2001). Cycling of nitrogen and potassium between shoot and roots in maize as affected by shoot and root growth. *J. Plant Nutr. Soil Sci.* 164, 183–191.

Engels, C., and Marschner, H. (1993). Influence of the form of nitrogen supply on root uptake and translocation of cations in the xylem exudate of maize (Zea mays L). *J. Exp. Bot.* 44, 1695–1701. doi: 10.1093/jxb/44.11.1695

Fairbairn, D. J., Liu, W., Schachtman, D. P., Gomez-Gallego, S., Day, S. R., and Teasdale, R. D. (2000). Characterisation of two distinct HKT1-like potassium transporters from Eucalyptus camaldulensis. *Plant Mol. Biol.* 43, 515–525. doi: 10.1023/a:1006496402463

Fan, S. C., Lin, C. S., Hsu, P. K., Lin, S. H., and Tsay, Y. F. (2009). The *Arabidopsis nitrate* transporter NRT1.7, expressed in phloem, is responsible for source-to-sink remobilization of nitrate. *Plant Cell* 21, 2750–2761. doi: 10.1105/tpc.109.067603

Fan, X., Naz, M., Fan, X., Xuan, W., Miller, A. J., and Xu, G. (2017). Plant nitrate transporters: from gene function to application. *J. Exp. Bot.* 68, 2463–2475. doi: 10.1093/jxb/erx011

Fang, X. Z., Liu, X. X., Zhu, Y. X., Ye, J. Y., and Jin, C. W. (2019). K(+) uptake and root-to-shoot allocation in *Arabidopsis* require coordination of nitrate transporter1/peptide transporter family member NPF6. 3/NRT1.1. *bioRxiv*. [Preprint]. Available at https://www.biorxiv.org/content/10.1101/674903v1.abstract (accessed June 20, 2019).

Furumoto, T., Yamaguchi, T., Ohshima-Ichie, Y., Nakamura, M., Tsuchida-Iwata, Y., Shimamura, M., et al. (2011). A plastidial sodium-dependent pyruvate transporter. *Nature* 476, 472–475. doi: 10.1038/nature10250

Gajdanowicz, P., Michard, E., Sandmann, M., Rocha, M., Corrêa, L. G. G., Ramiìrez-Aguilar, S. J., et al. (2011). Potassium K^+ gradients serve as a mobile energy source in plant vascular tissues. *Proc. Natl. Acad. Sci. U.S.A.* 108, 864–869. doi: 10.1073/pnas.1009777108

Garciadeblas, B., Senn, M. E., Banuelos, M. A., and Rodriguez-Navarro, A. (2003). Sodium transport and HKT transporters: the rice model. *Plant J.* 34, 788–801. doi: 10.1046/j.1365-313x.2003.01764.x

Garcia-Sanchez, M. J., Jaime, M. P., Ramos, A., Sanders, D., and Fernandez, J. A. (2000). Sodium-dependent nitrate transport at the plasma membrane of leaf cells of the marine higher plant Zostera marina L. *Plant Physiol.* 122, 879–885. doi: 10.1104/pp.122.3.879

Gassman, W., Rubio, F., and Schroeder, J. I. (1996). Alkali cation selectivity of the wheat root high-affinity potassium transporter HKT1. *Plant J.* 10, 869–852. doi: 10.1046/j.1365-313x.1996.10050869.x

Gaymard, F., Pilot, G., Lacombe, B., Bouchez, D., Bruneau, D., Boucherez, J., et al. (1998). Identification and disruption of a plant shaker-like outward channel involved in K(+) release into the xylem sap. *Cell* 94, 647–655. doi: 10.1016/s0092-8674(00)81606-2

Gazzarrini, S., Lejay, L., Gojon, A., Ninnemann, O., Frommer, W. B., and von Wiren, N. (1999). Three functional transporters for constitutive, diurnally regulated, and starvation-induced uptake of ammonium into *Arabidopsis* roots. *Plant Cell* 11, 937–948. doi: 10.1105/tpc.11.5.937

Geiger, D., Becker, D., Vosloh, D., Gambale, F., Palme, K., Rehers, M., et al. (2009). Heteromeric AtKC1-AKT1 channels in *Arabidopsis* roots facilitate growth under K(+)-limiting conditions. *J. Biol. Chem.* 284, 21288–21295. doi: 10.1074/jbc.M109.017574

Geiger, D., Maierhofer, T., Al-Rasheid, K. A., Scherzer, S., Mumm, P., Liese, A., et al. (2011). Stomatal closure by fast abscisic acid signaling is mediated by the guard cell anion channel SLAH3 and the receptor RCAR1. *Sci. Signal.* 4:ra32. doi: 10.1126/scisignal.2001346

Geiger, D., Scherzer, S., Mumm, P., Marten, I., Ache, P., Matschi, S., et al. (2010). Guard cell anion channel SLAC1 is regulated by CDPK protein kinases with distinct Ca2(+) affinities. *Proc. Natl. Acad. Sci. U.S.A.* 107, 8023–8028. doi: 10.1073/pnas.0912030107

Gierth, M., Maser, P., and Schroeder, J. I. (2005). The potassium transporter AtHAK5 functions in K(+) deprivation-induced high-affinity K(+) uptake and AKT1 K(+) channel contribution to K(+) uptake kinetics in *Arabidopsis* roots. *Plant Physiol.* 137, 1105–1114. doi: 10.1104/pp.104.057216

Glass, A. D., Shaff, J. E., and Kochian, L. V. (1992). Studies of the uptake of nitrate in barley : IV. Electrophysiology. *Plant Physiol.* 99, 456–463. doi: 10.1104/pp.99.2.456

Gobert, A., Park, G., Amtmann, A., Sanders, D., and Maathuis, F. J. (2006). *Arabidopsis thaliana* cyclic nucleotide gated channel 3 forms a non-selective ion transporter involved in germination and cation transport. *J. Exp. Bot.* 57, 791–800. doi: 10.1093/jxb/erj064

Guo, F. Q., Young, J., and Crawford, N. M. (2003). The nitrate transporter AtNRT1.1 *(CHL*1) functions in stomatal opening and contributes to drought susceptibility in *Arabidopsis*. *Plant Cell* 15, 107–117. doi: 10.1105/tpc.006312

Guo, J., Islam, M. A., Lin, H., Ji, C., Duan, Y., Liu, P., et al. (2018). Genome-wide identification of cyclic nucleotide-gated ion channel gene family in wheat and functional analyses of TaCNGC14 and TaCNGC16. *Front. Plant Sci.* 9:18. doi: 10.3389/fpls.2018.00018

Guo, K. M., Babourina, O., Christopher, D. A., Borsics, T., and Rengel, Z. (2008). The cyclic nucleotide-gated channel, AtCNGC10, influences salt tolerance in *Arabidopsis*. *Physiol. Plant* 134, 499–507. doi: 10.1111/j.1399-3054.2008.01157.x

Hamamoto, S., Horie, T., Hauser, F., Deinlein, U., Schroeder, J. I., and Uozumi, N. (2015). HKT transporters mediate salt stress resistance in plants: from structure and function to the field. *Curr. Opin. Biotechnol.* 32, 113–120. doi: 10.1016/j.copbio.2014.11.025

Hanin, M., Ebel, C., Ngom, M., Laplaze, L., and Masmoudi, K. (2016). New insights on plant salt tolerance mechanisms and their potential use for breeding. *Front. Plant Sci.* 7:1787. doi: 10.3389/fpls.2016.01787

Haro, R., Banuelos, M. A., and Rodriguez-Navarro, A. (2010). High-affinity sodium uptake in land plants. *Plant Cell Physiol.* 51, 68–79. doi: 10.1093/pcp/pcp168

Haro, R., Banuelos, M. A., Senn, M. E., Barrero-Gil, J., and Rodriguez-Navarro, A. (2005). HKT1 mediates sodium uniport in roots. *Pitfalls in the expression of HKT*1 in yeast. *Plant Physiol.* 139, 1495–1506. doi: 10.1104/pp.105.067553

Haro, R., and Rodriguez-Navarro, A. (2002). Molecular analysis of the mechanism of potassium uptake through the TRK1 transporter of Saccharomyces cerevisiae. *Biochim. Biophys. Acta* 1564, 114–122. doi: 10.1016/s0005-2736(02)00408-x

Hauser, F., and Horie, T. (2010). A conserved primary salt tolerance mechanism mediated by HKT transporters: a mechanism for sodium exclusion and maintenance of high K(+)/Na(+) ratio in leaves during salinity stress. *Plant Cell Environ.* 33, 552–565. doi: 10.1111/j.1365-3040.2009.02056.x

Hawkesford, M., Horst, W., Kichey, T., Lambers, H., Schjoerring, J., Møller, I. S., et al. (2012). "Functions of macronutrients," in *Marschner's Mineral Nutrition of Higher Plants* (3rd Edn), ed. P. Marschner (San Diego: Academic Press), 135–189.

Hedrich, R., and Shabala, S. (2018). Stomata in a saline world. *Curr. Opin. Plant Biol.* 46, 87–95. doi: 10.1016/j.pbi.2018.07.015

Hernandez, A., Jiang, X., Cubero, B., Nieto, P. M., Bressan, R. A., Hasegawa, P. M., et al. (2009). Mutants of the *Arabidopsis thaliana* cation/H(+) antiporter AtNHX1 conferring increased salt tolerance in yeast: the endosome/prevacuolar compartment is a target for salt toxicity. *J. Biol. Chem.* 284, 14276–14285. doi: 10.1074/jbc.M806203200

Hmidi, D., Messedi, D., Corratgi-Faillie, C., Marhuenda, T. O., Fizames, C. C., Zorrig, W., et al. (2019). Investigation of Na(+) and K(+) transport in halophytes: functional analysis of the HmHKT2;1 transporter from Hordeum maritimum and expression under saline conditions. *Plant Cell Physiol.* 60, 2423–2435. doi: 10.1093/pcp/pcz136

Ho, C. H., Lin, S. H., Hu, H. C., and Tsay, Y. F. (2009). CHL1 functions as a nitrate sensor in plants. *Cell* 138, 1184–1194. doi: 10.1016/j.cell.2009.07.004

Horie, T., Costa, A., Kim, T. H., Han, M. J., Horie, R., Leung, H. Y., et al. (2007). Rice OsHKT2;1 transporter mediates large Na(+) influx component into K(+)-starved roots for growth. *EMBO J.* 26, 3003–3014. doi: 10.1038/sj.emboj.7601732

Horie, T., Hauser, F., and Schroeder, J. I. (2009). HKT transporter-mediated salinity resistance mechanisms in *Arabidopsis* and monocot crop plants. *Trends Plant Sci.* 14, 660–668. doi: 10.1016/j.tplants.2009.08.009

Horie, T., Sugawara, M., Okada, T., Taira, K., Kaothien-Nakayama, P., Katsuhara, M., et al. (2011). Rice sodium-insensitive potassium transporter, OsHAK5, confers increased salt tolerance in tobacco BY2 cells. *J. Biosci. Bioeng.* 111, 346–356. doi: 10.1016/j.jbiosc.2010.10.014

Horie, T., Yoshida, K., Nakayama, H., Yamada, K., Oiki, S., and Shinmyo, A. (2001). Two types of HKT transporters with different properties of Na(+) and K(+)

transport in Oryza sativa. *Plant J.* 27, 129–138. doi: 10.1046/j.1365-313x.2001.01077.x

Hua, B. G., Mercier, R. W., Zielinski, R. E., and Berkowitz, G. A. (2003). Functional interaction of calmodulin with a plant cyclic nucleotide gated cation channel. *Plant Physiol. Biochem.* 41, 945–954. doi: 10.1016/j.plaphy.2003.07.006

Huang, N. C., Liu, K. H., Lo, H. J., and Tsay, Y. F. (1999). Cloning and functional characterization of an *Arabidopsis* nitrate transporter gene that encodes a constitutive component of low-affinity uptake. *Plant Cell* 11, 1381–1392. doi: 10.1105/tpc.11.8.1381

Huertas, R., Rubio, L., Cagnac, O., Garcia-Sanchez, M. J., Alche Jde, D., Venema, K., et al. (2013). The K(+)/H(+) antiporter LeNHX2 increases salt tolerance by improving K(+) homeostasis in transgenic tomato. *Plant Cell Environ.* 36, 2135–2149. doi: 10.1111/pce.12109

Jabnoune, M., Espeout, S., Mieulet, D., Fizames, C., Verdeil, J. L., Conejero, G., et al. (2009). Diversity in expression patterns and functional properties in the rice HKT transporter family. *Plant Physiol.* 150, 1955–1971. doi: 10.1104/pp.109.138008

Jezek, M., and Blatt, M. R. (2017). The membrane transport system of the guard cell and its integration for stomatal dynamics. *Plant Physiol.* 174, 487–519. doi: 10.1104/pp.16.01949

Jiang, X., Leidi, E. O., and Pardo, J. M. (2010). How do vacuolar NHX exchangers function in plant salt tolerance? *Plant Signal. Behav.* 5, 792–795. doi: 10.4161/psb.5.7.11767

Junfeng, Y., Changyan, T., and Gu, F. (2010). Effects of sodium on nitrate uptake and osmotic adjustment of Suaeda physophora. *J. Arid Land* 2, 190–196. doi: 10.3724/SP.J.1227.2010.00190

Jung, J. Y., Shin, R., and Schachtman, D. P. (2009). Ethylene mediates response and tolerance to potassium deprivation in *Arabidopsis*. *Plant Cell* 21, 607–621. doi: 10.1105/tpc.108.063099

Kaburagi, E., Morikawa, Y., Yamada, M., and Fujiyama, H. (2014). Sodium enhances nitrate uptake in Swiss chard (*Beta vulgaris var. cicla* L.). *Soil Sci. Plant Nutr.* 60, 651–658. doi: 10.1080/00380768.2014.938595

Kaburagi, E., Yamada, M., and Fujiyama, H. (2015). Sodium, but not potassium, enhances root to leaf nitrate translocation in Swiss chard (*Beta vulgaris var*. cicla L.). *Environ. Exp.Bot,* 112, 27–32. doi: 10.1016/j.envexpbot.2014.11.007

Kakar, K. U., Nawaz, Z., Kakar, K., Ali, E., Almoneafy, A. A., Ullah, R., et al. (2017). Comprehensive genomic analysis of the CNGC gene family in *Brassica oleracea*: novel insights into synteny, structures, and transcript profiles. *BMC Genomics* 18:869. doi: 10.1186/s12864-017-4244-y

Kiba, T., Feria-Bourrellier, A. B., Lafouge, F., Lezhneva, L., Boutet-Mercey, S., Orsel, M., et al. (2012). The *Arabidopsis* nitrate transporter NRT2.4 plays a double role in roots and shoots of nitrogen-starved plants. *Plant Cell* 24, 245–258. doi: 10.1105/tpc.111.092221

Kiba, T., and Krapp, A. (2016). Plant nitrogen acquisition under low availability: regulation of uptake and root architecture. *Plant Cell Physiol.* 57, 707–714. doi: 10.1093/pcp/pcw052

Kirkby, E. A., and Knight, A. H. (1977). Influence of the level of nitrate nutrition on ion uptake and assimilation, organic acid accumulation, and cation-anion balance in whole tomato plants. *Plant Physiol.* 60, 349–353. doi: 10.1104/pp.60.3.349

Kohler, C., Merkle, T., and Neuhaus, G. (1999). Characterisation of a novel gene family of putative cyclic nucleotide- and calmodulin-regulated ion channels in *Arabidopsis thaliana*. *Plant J.* 18, 97–104. doi: 10.1046/j.1365-313x.1999.00422.x

Kohler, C., and Neuhaus, G. (2000). Characterisation of calmodulin binding to cyclic nucleotide-gated ion channels from *Arabidopsis thaliana*. *FEBS Lett.* 471, 133–136. doi: 10.1016/s0014-5793(00)01383-1

Krapp, A. (2015). Plant nitrogen assimilation and its regulation: a complex puzzle with missing pieces. *Curr. Opin. Plant Biol.* 25, 115–122. doi: 10.1016/j.pbi.2015.05.010

Kronzucker, H. J., and Britto, D. T. (2011). Sodium transport in plants: a critical review. *New Phytol.* 189, 54–81. doi: 10.1111/j.1469-8137.2010.03540.x

Kronzucker, H. J., Coskun, D., Schulze, L. M., Wong, J. R., and Britto, D. T. (2013). Sodium as nutrient and toxicant. *Plant Soil* 369, 1–23. doi: 10.1007/s11104-013-1801-2

Krouk, G., Lacombe, B., Bielach, A., Perrine-Walker, F., Malinska, K., Mounier, E., et al. (2010). Nitrate-regulated auxin transport by NRT1.1 defines a mechanism for nutrient sensing in plants. *Dev. Cell* 18, 927–937. doi: 10.1016/j.devcel.2010.05.008

Lagarde, D., Basset, M., Lepetit, M., Conejero, G., Gaymard, F., Astruc, S., et al. (1996). Tissue-specific expression of *Arabidopsis* AKT1 gene is consistent with a role in K(+) nutrition. *Plant J.* 9, 195–203. doi: 10.1046/j.1365-313x.1996.09020195.x

Lee, S. C., Lan, W., Buchanan, B. B., and Luan, S. (2009). A protein kinase-phosphatase pair interacts with an ion channel to regulate ABA signaling in plant guard cells. *Proc. Natl.Acad. Sci. U.S.A.* 106, 21419–21424. doi: 10.1073/pnas.0910601106

Leidi, E. O., Barragan, V., Rubio, L., El-Hamdaoui, A., Ruiz, M. T., Cubero, B., et al. (2010). The AtNHX1 exchanger mediates potassium compartmentation in vacuoles of transgenic tomato. *Plant J.* 61, 495–506. doi: 10.1111/j.1365-313X.2009.04073.x

Leigh, R. A. (2001). Potassium homeostasis and membrane transport. *J. Plant Nutr. Soil Sci.* 164, 193–198.

Lemtiri-Chlieh, F., and Berkowitz, G. A. (2004). Cyclic adenosine monophosphate regulates calcium channels in the plasma membrane of *Arabidopsis* leaf guard and mesophyll cells. *J. Biol. Chem.* 279, 35306–35312. doi: 10.1074/jbc.M400311200

Leng, Q., Mercier, R. W., Hua, B. G., Fromm, H., and Berkowitz, G. A. (2002). Electrophysiological analysis of cloned cyclic nucleotide-gated ion channels. *Plant Physiol.* 128, 400–410. doi: 10.1104/pp.010832

Leng, Q., Mercier, R. W., Yao, W., and Berkowitz, G. A. (1999). Cloning and first functional characterization of a plant cyclic nucleotide-gated cation channel. *Plant Physiol.* 121, 753–761. doi: 10.1104/pp.121.3.753

Leran, S., Edel, K. H., Pervent, M., Hashimoto, K., Corratge-Faillie, C., Offenborn, J. N., et al. (2015a). Nitrate sensing and uptake in *Arabidopsis* are enhanced by ABI2, a phosphatase inactivated by the stress hormone abscisic acid. *Sci. Signal.* 8:ra43. doi: 10.1126/scisignal.aaa4829

Leran, S., Garg, B., Boursiac, Y., Corratge-Faillie, C., Brachet, C., Tillard, P., et al. (2015b). AtNPF5.5, a nitrate transporter affecting nitrogen accumulation in *Arabidopsis* embryo. *Sci. Rep.* 5:7962. doi: 10.1038/srep07962

Lezhneva, L., Kiba, T., Feria-Bourrellier, A. B., Lafouge, F., Boutet-Mercey, S., Zoufan, P., et al. (2014). The *Arabidopsis* nitrate transporter NRT2.5 plays a role in nitrate acquisition and remobilization in nitrogen-starved plants. *Plant J.* 80, 230–241. doi: 10.1111/tpj.12626

Li, H., Yu, M., Du, X. Q., Wang, Z. F., Wu, W. H., Quintero, F. J., et al. (2017). NRT1.5/*NPF*7.3 functions as a proton-coupled H(+)/K(+) antiporter for K(+) loading into the xylem in *Arabidopsis*. *Plant Cell* 29, 2016–2026. doi: 10.1105/tpc.16.00972

Li, J. Y., Fu, Y. L., Pike, S. M., Bao, J., Tian, W., Zhang, Y., et al. (2010). The *Arabidopsis* nitrate transporter NRT1.8 functions in nitrate removal from the xylem sap and mediates cadmium tolerance. *Plant Cell* 22, 1633–1646. doi: 10.1105/tpc.110.075242

Li, L., Kim, B. G., Cheong, Y. H., Pandey, G. K., and Luan, S. (2006). A Ca(2)+ signaling pathway regulates a K(+) channel for low-K response in *Arabidopsis*. *Proc. Natl. Acad. Sci. U.S.A.* 103, 12625–12630. doi: 10.1073/pnas.0605129103

Li, W., Wang, Y., Okamoto, M., Crawford, N. M., Siddiqi, M. Y., and Glass, A. D. (2007). Dissection of the AtNRT2.1:*AtNRT*2.2 inducible high-affinity nitrate transporter gene cluster. *Plant Physiol.* 143, 425–433. doi: 10.1104/pp.106.091223

Li, X. T., Borsics, T., Harrington, H. M., and Christopher, D. A. (2005). *Arabidopsis* AtCNGC10 rescues potassium channel mutants of *E. coli*, yeast and *Arabidopsis* and is regulated by calcium/calmodulin and cyclic GMP in *E. coli*. *Funct. Plant Biol.* 32, 643–653. doi: 10.1071/FP04233

Lin, S. H., Kuo, H. F., Canivenc, G., Lin, C. S., Lepetit, M., Hsu, P. K., et al. (2008). Mutation of the *Arabidopsis* NRT1.5 nitrate transporter causes defective root-to-shoot nitrate transport. *Plant Cell* 20, 2514–2528. doi: 10.1105/tpc.108.060244

Liu, K. H., Huang, C. Y., and Tsay, Y. F. (1999). CHL1 is a dual-affinity nitrate transporter of *Arabidopsis* involved in multiple phases of nitrate uptake. *Plant Cell* 11, 865–874. doi: 10.1105/tpc.11.5.865

Maathuis, F. J. (2014). Sodium in plants: perception, signalling, and regulation of sodium fluxes. *J. Exp. Bot.* 65, 849–858. doi: 10.1093/jxb/ert326

Maathuis, F. J., and Sanders, D. (2001). Sodium uptake in *Arabidopsis* roots is regulated by cyclic nucleotides. *Plant Physiol.* 127, 1617–1625. doi: 10.1104/pp.010502

Maathuis, F. J. M., and Sanders, D. (1993). Energization of potassium uptake in *Arabidopsis thaliana*. *Planta* 191, 302–307. doi: 10.1007/bf00195686

Maierhofer, T., Diekmann, M., Offenborn, J. N., Lind, C., Bauer, H., Hashimoto, K., et al. (2014). Site- and kinase-specific phosphorylation-mediated activation of SLAC1, a guard cell anion channel stimulated by abscisic acid. *Sci. Signal.* 7:ra86. doi: 10.1126/scisignal.2005703

Martinoia, E., Meyer, S., De Angeli, A., and Nagy, R. (2012). Vacuolar transporters in their physiological context. *Annu. Rev. Plant Biol.* 63, 183–213. doi: 10.1146/annurev-arplant-042811-105608

Maser, P., Eckelman, B., Vaidyanathan, R., Horie, T., Fairbairn, D. J., Kubo, M., et al. (2002a). Altered shoot/root Na(+) distribution and bifurcating salt sensitivity in *Arabidopsis* by genetic disruption of the Na(+) transporter AtHKT1. *FEBS Lett.* 531, 157–161. doi: 10.1016/s0014-5793(02)03488-9

Maser, P., Hosoo, Y., Goshima, S., Horie, T., Eckelman, B., Yamada, K., et al. (2002b). Glycine residues in potassium channel-like selectivity filters determine potassium selectivity in four-loop-per-subunit HKT transporters from plants. *Proc. Natl. Acad. Sci. U.S.A.* 99, 6428–6433. doi: 10.1073/pnas.082123799

Meng, S., Peng, J. S., He, Y. N., Zhang, G. B., Yi, H. Y., Fu, Y. L., et al. (2016). *Arabidopsis* NRT1.5 mediates the suppression of nitrate starvation-induced leaf senescence by modulating foliar potassium level. *Mol. Plant.* 9, 461–470. doi: 10.1016/j.molp.2015.12.015

Mengel, K., Kirkby, E. A., Kosegarten, H., and Appel, T. (2001). "Nitrogen," in *Principles of Plant Nutrition*, (Dordrecht: Springer Netherlands), 397–434.

Mian, A., Oomen, R. J., Isayenkov, S., Sentenac, H., Maathuis, F. J., and Very, A. A. (2011). Over-expression of an Na(+)-and K(+)-permeable HKT transporter in barley improves salt tolerance. *Plant J.* 68, 468–479. doi: 10.1111/j.1365-313X.2011.04701.x

Michard, E., Dreyer, I., Lacombe, B., Sentenac, H., and Thibaud, J. B. (2005). Inward rectification of the AKT2 channel abolished by voltage-dependent phosphorylation. *Plant J.* 44, 783–797. doi: 10.1111/j.1365-313X.2005.02566.x

Mittler, R., and Blumwald, E. (2010). Genetic engineering for modern agriculture: challenges and perspectives. *Annu. Rev. Plant Biol,.* 61, 443–462. doi: 10.1146/annurev-arplant-042809-112116

Mori, I. C., Nobukiyo, Y., Nakahara, Y., Shibasaka, M., Furuichi, T., and Katsuhara, M. (2018). A cyclic nucleotide-gated channel, HvCNGC2-3, is activated by the co-presence of Na(+) and K(+) and permeable to Na(+) and K(+) non-selectively. *Plants* 7:61. doi: 10.3390/plants7030061

Munns, R., James, R. A., Xu, B., Athman, A., Conn, S. J., Jordans, C., et al. (2012). Wheat grain yield on saline soils is improved by an ancestral Na(+) transporter gene. *Nat. Biotechnol.* 30, 360–364. doi: 10.1038/nbt.2120

Munns, R., and Tester, M. (2008). Mechanisms of salinity tolerance. *Annu. Rev. Plant Biol.* 59, 651–681. doi: 10.1146/annurev.arplant.59.032607.092911

Nacry, P., Bouguyon, E., and Gojon, A. (2013). Nitrogen acquisition by roots: physiological and developmental mechanisms ensuring plant adaptation to a fluctuating resource. *Plant Soil* 370, 1–29. doi: 10.1007/s11104-013-1645-9

Nawaz, Z., Kakar, K. U., Saand, M. A., and Shu, Q. Y. (2014). Cyclic nucleotide-gated ion channel gene family in rice, identification, characterization and experimental analysis of expression response to plant hormones, biotic and abiotic stresses. *BMC Genomics* 15:853. doi: 10.1186/1471-2164-15-853

Nie, L., Feng, J., Fan, P., Chen, X., Guo, J., Lv, S., et al. (2015). Comparative proteomics of root plasma membrane proteins reveals the involvement of calcium signalling in NaCl-facilitated nitrate uptake in Salicornia europaea. *J. Exp. Bot.* 66, 4497–4510. doi: 10.1093/jxb/erv216

Nieves-Cordones, M., Aleman, F., Martinez, V., and Rubio, F. (2014). K(+) uptake in plant roots. The systems involved, their regulation and parallels in other organisms. *J. Plant Physiol.* 171, 688–695. doi: 10.1016/j.jplph.2013.09.021

Nieves-Cordones, M., Martinez, V., Benito, B., and Rubio, F. (2016). Comparison between *Arabidopsis* and rice for main pathways of K(+) and Na(+) uptake by roots. *Front. Plant Sci.* 7:992. doi: 10.3389/fpls.2016.00992

Nieves-Cordones, M., Miller, A. J., Aleman, F., Martinez, V., and Rubio, F. (2008). A putative role for the plasma membrane potential in the control of the expression of the gene encoding the tomato high-affinity potassium transporter HAK5. *Plant Mol. Biol.* 68, 521–532. doi: 10.1007/s11103-008-9388-3

Oomen, R. J., Benito, B., Sentenac, H., Rodriguez-Navarro, A., Talon, M., Very, A. A., et al. (2012). HKT2;2/1, a K(+)-permeable transporter identified in a salt-tolerant rice cultivar through surveys of natural genetic polymorphism. *Plant J.* 71, 750–762. doi: 10.1111/j.1365-313X.2012.05031.x

Orsel, M., Krapp, A., and Daniel-Vedele, F. (2002). Analysis of the NRT2 nitrate transporter family in *Arabidopsis*. Structure and gene expression. *Plant Physiol.* 129, 886–896. doi: 10.1104/pp.005280

Osakabe, Y., Arinaga, N., Umezawa, T., Katsura, S., Nagamachi, K., Tanaka, H., et al. (2013). Osmotic stress responses and plant growth controlled by potassium transporters in *Arabidopsis*. *Plant Cell* 25, 609–624. doi: 10.1105/tpc.112.105700

Parker, J. L., and Newstead, S. (2014). Molecular basis of nitrate uptake by the plant nitrate transporter NRT1.1. *Nature* 507, 68–72. doi: 10.1038/nature13116

Paulsen, I. T., and Skurray, R. A. (1994). The POT family of transport proteins. *Trends Biochem. Sci.* 19:404. doi: 10.1016/0968-0004(94)90087-6

Pettersson, S. (1984). Effects of nitrate on influx, efflux and translocation of potassium in young sunflower plants. *Physiol. Plant.* 61, 663–669. doi: 10.1111/j.1399-3054.1984.tb05188.x

Pettigrew, W. T. (2008). Potassium influences on yield and quality production for maize, wheat, soybean and cotton. *Physiol. Plant* 133, 670–681. doi: 10.1111/j.1399-3054.2008.01073.x

Planes, M. D., Ninoles, R., Rubio, L., Bissoli, G., Bueso, E., Garcia-Sanchez, M. J., et al. (2015). A mechanism of growth inhibition by abscisic acid in germinating seeds of *Arabidopsis thaliana* based on inhibition of plasma membrane H(+)-ATPase and decreased cytosolic pH, K(+), and anions. *J. Exp. Bot.* 66, 813–825. doi: 10.1093/jxb/eru442

Quintero, F. J., Martinez-Atienza, J., Villalta, I., Jiang, X., Kim, W. Y., Ali, Z., et al. (2011). Activation of the plasma membrane Na/H antiporter Salt-Overly-Sensitive 1 (SOS1) by phosphorylation of an auto-inhibitory C-terminal domain. *Proc. Natl. Acad. Sci. U.S.A.* 108, 2611–2616. doi: 10.1073/pnas.1018921108

Ragel, P., Raddatz, N., Leidi, E. O., Quintero, F. J., and Pardo, J. M. (2019). Regulation of K(+) nutrition in plants. *Front. Plant Sci.* 10:281. doi: 10.3389/fpls.2019.00281

Ragel, P., Rodenas, R., Garcia-Martin, E., Andres, Z., Villalta, I., Nieves-Cordones, M., et al. (2015). The CBL-interacting protein kinase CIPK23 regulates HAK5-mediated high-affinity K(+) uptake in *Arabidopsis* roots. *Plant Physiol.* 169, 2863–2873. doi: 10.1104/pp.15.01401

Ramanjaneyulu, G., Seshapani, P., Naidu, B. R., Rayalu, D. J., Raju, P. C., and Kumari, J. P. (2010). Genome wide analysis and identification of genes related to cyclic nucleotide gated channels (CNGC) in Oryza sativa. *Bull. Pure Appl. Sci.* 29b, 83–91.

Rashid, M., Bera, S., Banerjee, M., Medvinsky, A. B., Sun, G. Q., Li, B. L., et al. (2019). Feedforward control of plant nitrate transporter NRT1.1 biphasic adaptive activity. *Biophys. J.* 118, 1–11. doi: 10.1016/j.bpj.2019.10.018

Ren, Z. H., Gao, J. P., Li, L. G., Cai, X. L., Huang, W., Chao, D. Y., et al. (2005). A rice quantitative trait locus for salt tolerance encodes a sodium transporter. *Nat. Genet.* 37, 1141–1146. doi: 10.1038/ng1643

Riedelsberger, J., Vergara-Jaque, A., Piñeros, M., Dreyer, I., and González, W. (2018). Extracellular cation binding pocket is essential for ion conduction of OsHKT2; 2. *bioRxiv*. [Preprint]. Available at https://www.biorxiv.org/content/10.1101/471003v1.abstract (accessed November 16, 2018).

Riveras, E., Alvarez, J. M., Vidal, E. A., Oses, C., Vega, A., and Gutierrez, R. A. (2015). The calcium ion is a second messenger in the nitrate signaling pathway of *Arabidopsis*. *Plant Physiol.* 169, 1397–1404. doi: 10.1104/pp.15.00961

Rodenas, R., Garcia-Legaz, M. F., Lopez-Gomez, E., Martinez, V., Rubio, F., and Angeles Botella, M. (2017). NO3(-), PO4(3)(-) and SO4(2)(-) deprivation reduced LKT1-mediated low-affinity K(+) uptake and SKOR-mediated K(+) translocation in tomato and *Arabidopsis* plants. *Physiol. Plant* 160, 410–424. doi: 10.1111/ppl.12558

Rodriguez-Navarro, A., and Rubio, F. (2006). High-affinity potassium and sodium transport systems in plants. *J. Exp. Bot.* 57, 1149–1160. doi: 10.1093/jxb/erj068

Rubio, F., Fon, M., Rodenas, R., Nieves-Cordones, M., Aleman, F., Rivero, R. M., et al. (2014). A low K(+) signal is required for functional high-affinity K(+) uptake through HAK5 transporters. *Physiol. Plant* 152, 558–570. doi: 10.1111/ppl.12205

Rubio, F., Gassmann, W., and Schroeder, J. I. (1995). Sodium-driven potassium uptake by the plant potassium transporter HKT1 and mutations conferring salt tolerance. *Science* 270, 1660–1663. doi: 10.1126/science.270.5242.1660

Rubio, F., Schwarz, M., Gassmann, W., and Schroeder, J. I. (1999). Genetic selection of mutations in the high affinity K(+) transporter HKT1 that define functions

of a loop site for reduced Na(+) permeability and increased Na(+) tolerance. *J. Biol. Chem.* 274, 6839–6847. doi: 10.1074/jbc.274.11.6839

Rubio, L., Linares-Rueda, A., Garcia-Sanchez, M. J., and Fernandez, J. A. (2005). Physiological evidence for a sodium-dependent high-affinity phosphate and nitrate transport at the plasma membrane of leaf and root cells of *Zostera marina* L. *J. Exp. Bot.* 56, 613–622. doi: 10.1093/jxb/eri053

Saand, M. A., Xu, Y. P., Munyampundu, J. P., Li, W., Zhang, X. R., and Cai, X. Z. (2015). Phylogeny and evolution of plant cyclic nucleotide-gated ion channel (CNGC) gene family and functional analyses of tomato CNGCs. *DNA Res.* 22, 471–483. doi: 10.1093/dnares/dsv029

Santa-Maria, G. E., Danna, C. H., and Czibener, C. (2000). High-affinity potassium transport in barley roots. Ammonium-sensitive and -insensitive pathways. *Plant Physiol.* 123, 297–306. doi: 10.1104/pp.123.1.297

Santa-Maria, G. E., Oliferuk, S., and Moriconi, J. I. (2018). KT-HAK-KUP transporters in major terrestrial photosynthetic organisms: a twenty years tale. *J. Plant Physiol.* 226, 77–90. doi: 10.1016/j.jplph.2018.04.008

Santa-Maria, G. E., Rubio, F., Dubcovsky, J., and Rodriguez-Navarro, A. (1997). The HAK1 gene of barley is a member of a large gene family and encodes a high-affinity potassium transporter. *Plant Cell* 9, 2281–2289. doi: 10.1105/tpc.9.12.2281

Schachtman, D. P., and Schroeder, J. I. (1994). Structure and transport mechanism of a high-affinity potassium uptake transporter from higher plants. *Nature* 370, 655–658. doi: 10.1038/370655a0

Scherer, H. W., Mackown, C. T., and Leggett, J. E. (1984). Potassium-ammonium uptake interactions in tobacco seedlings. *J. Exp. Bot.* 35, 1060–1070. doi: 10.1093/jxb/35.7.1060

Schuurink, R. C., Shartzer, S. F., Fath, A., and Jones, R. L. (1998). Characterization of a calmodulin-binding transporter from the plasma membrane of barley aleurone. *Proc. Natl. Acad. Sci. U.S.A.* 95, 1944–1949. doi: 10.1073/pnas.95.4.1944

Searles, P. S., and Bloom, A. J. (2003). Nitrate photo-assimilation in tomato leaves under short-term exposure to elevated carbon dioxide and low oxygen. *Plant Cell Environ.* 26, 1247–1255. doi: 10.1046/j.1365-3040.2003.01047.x

Segonzac, C., Boyer, J. C., Ipotesi, E., Szponarski, W., Tillard, P., Touraine, B., et al. (2007). Nitrate efflux at the root plasma membrane: identification of an *Arabidopsis* excretion transporter. *Plant Cell* 19, 3760–3777. doi: 10.1105/tpc.106.048173

Shabala, S. (2017). Signalling by potassium: another second messenger to add to the list? *J. Exp. Bot.* 68, 4003–4007. doi: 10.1093/jxb/erx238

Shabala, S., Chen, G., Chen, Z. H., and Pottosin, I. (2019). The energy cost of the tonoplast futile sodium leak. *New Phytol.* 225, 1105–1110. doi: 10.1111/nph.15758

Shabala, S., Cuin, T. A., and Pottosin, I. (2007). Polyamines prevent NaCl-induced K(+) efflux from pea mesophyll by blocking non-selective cation channels. *FEBS Lett.* 581, 1993–1999. doi: 10.1016/j.febslet.2007.04.032

Shabala, S., Demidchik, V., Shabala, L., Cuin, T. A., Smith, S. J., Miller, A. J., et al. (2006). Extracellular Ca(2+) ameliorates NaCl-induced K(+) loss from *Arabidopsis* root and leaf cells by controlling plasma membrane K(+) -permeable channels. *Plant Physiol.* 141, 1653–1665. doi: 10.1104/pp.106.082388

Shabala, S., and Pottosin, I. (2014). Regulation of potassium transport in plants under hostile conditions: implications for abiotic and biotic stress tolerance. *Physiol. Plant* 151, 257–279. doi: 10.1111/ppl.12165

Shi, H., Quintero, F. J., Pardo, J. M., and Zhu, J. K. (2002). The putative plasma membrane Na(+)/H(+) antiporter SOS1 controls long-distance Na(+) transport in plants. *Plant Cell* 14, 465–477. doi: 10.1105/tpc.010371

Shin, R., and Schachtman, D. P. (2004). Hydrogen peroxide mediates plant root cell response to nutrient deprivation. *Proc. Natl. Acad. Sci. U.S.A.* 101, 8827–8832. doi: 10.1073/pnas.0401707101

Spalding, E. P., Hirsch, R. E., Lewis, D. R., Qi, Z., Sussman, M. R., and Lewis, B. D. (1999). Potassium uptake supporting plant growth in the absence of AKT1 channel activity: inhibition by ammonium and stimulation by sodium. *J. Gen. Physiol.* 113, 909–918. doi: 10.1085/jgp.113.6.909

Straub, T., Ludewig, U., and Neuhauser, B. (2017). The kinase CIPK23 inhibits ammonium transport in *Arabidopsis thaliana*. *Plant Cell* 29, 409–422. doi: 10.1105/tpc.16.00806

Su, H., Balderas, E., Vera-Estrella, R., Golldack, D., Quigley, F., Zhao, C., et al. (2003). Expression of the cation transporter McHKT1 in a halophyte. *Plant Mol. Biol.* 52, 967–980. doi: 10.1023/a:1025445612244

Sun, J., Bankston, J. R., Payandeh, J., Hinds, T. R., Zagotta, W. N., and Zheng, N. (2014). Crystal structure of the plant dual-affinity nitrate transporter NRT1.1. *Nature* 507, 73–77. doi: 10.1038/nature13074

Sunarpi, H. T., Motoda, J., Kubo, M., Yang, H., Yoda, K., Horie, R., et al. (2005). Enhanced salt tolerance mediated by AtHKT1 transporter-induced Na(+) unloading from xylem vessels to xylem parenchyma cells. *Plant J* 44, 928–938. doi: 10.1111/j.1365-313X.2005.02595.x

Szczerba, M. W., Britto, D. T., and Kronzucker, H. J. (2009). K(+) transport in plants: physiology and molecular biology. *J. Plant Physiol.* 166, 447–466. doi: 10.1016/j.jplph.2008.12.009

Sze, H., and Chanroj, S. (2018). Plant endomembrane dynamics: studies of K(+)/H(+) antiporters provide insights on the effects of pH and ion homeostasis. *Plant Physiol.* 177, 875–895. doi: 10.1104/pp.18.00142

Takahashi, R., Nishio, T., Ichizen, N., and Takano, T. (2007a). Cloning and functional analysis of the K(+) transporter, PhaHAK2, from salt-sensitive and salt-tolerant reed plants. *Biotechnol. Lett.* 29, 501–506. doi: 10.1007/s10529-006-9246-9

Takahashi, R., Nishio, T., Ichizen, N., and Takano, T. (2007b). High-affinity K(+) transporter PhaHAK5 is expressed only in salt-sensitive reed plants and shows Na(+) permeability under NaCl stress. *Plant Cell Rep.* 26, 1673–1679. doi: 10.1007/s00299-007-0364-1

Talke, I. N., Blaudez, D., Maathuis, F. J., and Sanders, D. (2003). CNGCs: prime targets of plant cyclic nucleotide signalling? *Trends Plant Sci.* 8, 286–293. doi: 10.1016/S1360-1385(03)00099-2

Tang, R. J., Zhao, F. G., Garcia, V. J., Kleist, T. J., Yang, L., Zhang, H. X., et al. (2015). Tonoplast CBL-CIPK calcium signaling network regulates magnesium homeostasis in *Arabidopsis*. *Proc. Natl. Acad. Sci. U.S.A.* 112, 3134–3139. doi: 10.1073/pnas.1420944112

Taochy, C., Gaillard, I., Ipotesi, E., Oomen, R., Leonhardt, N., Zimmermann, S., et al. (2015). The *Arabidopsis* root stele transporter NPF2.3 contributes to nitrate translocation to shoots under salt stress. *Plant J.* 83, 466–479. doi: 10.1111/tpj.12901

Tascon, I., Sousa, J. S., Corey, R. A., Mills, D. J., Griwatz, D., Aumuller, N., et al. (2020). Structural basis of proton-coupled potassium transport in the KUP family. *Nat. Commun.* 11:626. doi: 10.1038/s41467-020-14441-7

ten Hoopen, F., Cuin, T. A., Pedas, P., Hegelund, J. N., Shabala, S., Schjoerring, J. K., et al. (2010). Competition between uptake of ammonium and potassium in barley and *Arabidopsis* roots: molecular mechanisms and physiological consequences. *J. Exp. Bot.* 61, 2303–2315. doi: 10.1093/jxb/erq057

Tester, M., and Davenport, R. (2003). Na(+) tolerance and Na(+) transport in higher plants. *Ann. Bot.* 91, 503–527. doi: 10.1093/aob/mcg058

Tholema, N., Vor der Bruggen, M., Maser, P., Nakamura, T., Schroeder, J. I., Kobayashi, H., et al. (2005). All four putative selectivity filter glycine residues in KtrB are essential for high affinity and selective K(+) uptake by the KtrAB system from *Vibrio alginolyticus*. *J. Biol. Chem.* 280, 41146–41154. doi: 10.1074/jbc.M507647200

Touraine, B., Grignon, N., and Grignon, C. (1988). Charge balance in NO3(-) fed soybean: estimation of K and carboxylate recirculation. *Plant Physiol.* 88, 605–612. doi: 10.1104/pp.88.3.605

Tsay, Y. F., Chiu, C. C., Tsai, C. B., Ho, C. H., and Hsu, P. K. (2007). Nitrate transporters and peptide transporters. *FEBS Lett.* 581, 2290–2300. doi: 10.1016/j.febslet.2007.04.047

Tsay, Y. F., Ho, C. H., Chen, H. Y., and Lin, S. H. (2011). Integration of nitrogen and potassium signaling. *Annu. Rev. Plant Biol.* 62, 207–226. doi: 10.1146/annurev-arplant-042110-103837

Tsay, Y. F., Schroeder, J. I., Feldmann, K. A., and Crawford, N. M. (1993). The herbicide sensitivity gene CHL1 of *Arabidopsis* encodes a nitrate-inducible nitrate transporter. *Cell* 72, 705–713. doi: 10.1016/0092-8674(93)90399-b

Tyerman, S. D. (2002). Nonselective cation channels. Multiple functions and commonalities. *Plant Physiol.* 128, 327–328. doi: 10.1104/pp.900021

Tyerman, S. D., Skerrett, M., Garrill, A., Findlay, G. P., and Leigh, R. A. (1997). Pathways for the permeation of Na(+) and Cl(-) into protoplasts derived from the cortex of wheat roots. *J. Exp. Bot.* 48, 459–480. doi: 10.1093/jxb/48.Special_Issue.459

Vahisalu, T., Kollist, H., Wang, Y. F., Nishimura, N., Chan, W. Y., Valerio, G., et al. (2008). SLAC1 is required for plant guard cell S-type anion channel function in stomatal signalling. *Nature* 452, 487–491. doi: 10.1038/nature06608

Velarde-Buendia, A. M., Shabala, S., Cvikrova, M., Dobrovinskaya, O., and Pottosin, I. (2012). Salt-sensitive and salt-tolerant barley varieties differ in the extent of potentiation of the ROS-induced K(+) efflux by polyamines. *Plant Physiol. Biochem.* 61, 18–23. doi: 10.1016/j.plaphy.2012.09.002

Venema, K., Belver, A., Marin-Manzano, M. C., Rodriguez-Rosales, M. P., and Donaire, J. P. (2003). A novel intracellular K(+)/H(+) antiporter related to Na(+)/H(+) antiporters is important for K(+) ion homeostasis in plants. *J. Biol. Chem.* 278, 22453–22459. doi: 10.1074/jbc.M210794200

Venema, K., Quintero, F. J., Pardo, J. M., and Donaire, J. P. (2002). The *Arabidopsis* Na(+)/H(+) exchanger AtNHX1 catalyzes low affinity Na(+) and K(+) transport in reconstituted liposomes. *J. Biol. Chem.* 277, 2413–2418. doi: 10.1074/jbc.M105043200

Very, A. A., Nieves-Cordones, M., Daly, M., Khan, I., Fizames, C., and Sentenac, H. (2014). Molecular biology of K(+) transport across the plant cell membrane: what do we learn from comparison between plant species? *J. Plant Physiol.* 171, 748–769. doi: 10.1016/j.jplph.2014.01.011

Walker, D. J., Leigh, R. A., and Miller, A. J. (1996). Potassium homeostasis in vacuolate plant cells. *Proc. Natl. Acad. Sci. U.S.A.* 93, 10510–10514. doi: 10.1073/pnas.93.19.10510

Wang, L., Wu, X., Liu, Y., and Qiu, Q. S. (2015). AtNHX5 and AtNHX6 control cellular K(+) and pH homeostasis in *Arabidopsis*: three conserved acidic residues are essential for K(+) transport. *PLoS One* 10:e0144716. doi: 10.1371/journal.pone.0144716

Wang, M. Y., Siddiqi, M. Y., and Glass, A. D. M. (1996). Interactions between K(+) and NH4(+): effects on ion uptake by rice roots. *Plant Cell Environ.* 19, 1037–1046. doi: 10.1111/j.1365-3040.1996.tb00210.x

Wang, R., Liu, D., and Crawford, N. M. (1998). The *Arabidopsis* CHL1 protein plays a major role in high-affinity nitrate uptake. *Proc. Natl. Acad. Sci. U.S.A.* 95, 15134–15139. doi: 10.1073/pnas.95.25.15134

Wang, R., Tischner, R., Gutierrez, R. A., Hoffman, M., Xing, X., Chen, M., et al. (2004). Genomic analysis of the nitrate response using a nitrate reductase-null mutant of *Arabidopsis*. *Plant Physiol.* 136, 2512–2522. doi: 10.1104/pp.104.044610

Wang, Y. F., Munemasa, S., Nishimura, N., Ren, H. M., Robert, N., Han, M., et al. (2013). Identification of cyclic GMP-activated nonselective Ca(2+)-permeable cation channels and associated CNGC5 and CNGC6 genes in *Arabidopsis* guard cells. *Plant Physiol.* 163, 578–590. doi: 10.1104/pp.113.225045

Wang, Y. H., Garvin, D. F., and Kochian, L. V. (2001). Nitrate-induced genes in tomato roots. Array analysis reveals novel genes that may play a role in nitrogen nutrition. *Plant Physiol.* 127, 345–359. doi: 10.1104/pp.127.1.345

Wang, Y. Y., Cheng, Y. H., Chen, K. E., and Tsay, Y. F. (2018). Nitrate transport, signaling, and use efficiency. *Annu. Rev. Plant Biol.* 69, 85–122. doi: 10.1146/annurev-arplant-042817-040056

Wang, Y. Y., Hsu, P. K., and Tsay, Y. F. (2012). Uptake, allocation and signaling of nitrate. *Trends Plant Sci.* 17, 458–467. doi: 10.1016/j.tplants.2012.04.006

Wang, Y. Y., and Tsay, Y. F. (2011). *Arabidopsis* nitrate transporter NRT1.9 is important in phloem nitrate transport. *Plant Cell* 23, 1945–1957. doi: 10.1105/tpc.111.083618

Wilson, I. D., Neill, S. J., and Hancock, J. T. (2008). Nitric oxide synthesis and signalling in plants. *Plant Cell Environ.* 31, 622–631. doi: 10.1111/j.1365-3040.2007.01761.x

Xia, X., Fan, X., Wei, J., Feng, H., Qu, H., Xie, D., et al. (2015). Rice nitrate transporter OsNPF2.4 functions in low-affinity acquisition and long-distance transport. *J. Exp. Bot.* 66, 317–331. doi: 10.1093/jxb/eru425

Xu, J., Li, H. D., Chen, L. Q., Wang, Y., Liu, L. L., He, L., et al. (2006). A protein kinase, interacting with two calcineurin B-like proteins, regulates K(+) transporter AKT1 in *Arabidopsis*. *Cell* 125, 1347–1360. doi: 10.1016/j.cell.2006.06.011

Yamauchi, S., Takemiya, A., Sakamoto, T., Kurata, T., Tsutsumi, T., Kinoshita, T., et al. (2016). The plasma membrane H(+)-ATPase AHA1 plays a major role in stomatal opening in response to blue light. *Plant Physiol.* 171, 2731–2743. doi: 10.1104/pp.16.01581

Yao, X., Horie, T., Xue, S., Leung, H. Y., Katsuhara, M., Brodsky, D. E., et al. (2010). Differential sodium and potassium transport selectivities of the rice OsHKT2;1 and OsHKT2;2 transporters in plant cells. *Plant Physiol.* 152, 341–355. doi: 10.1104/pp.109.145722

Zhang, F., Niu, J., Zhang, W., Chen, X., Li, C., Yuan, L., et al. (2010). Potassium nutrition of crops under varied regimes of nitrogen supply. *Plant Soil* 335, 21–34. doi: 10.1007/s11104-010-0323-4

Zhang, G. B., Yi, H. Y., and Gong, J. M. (2014). The *Arabidopsis* ethylene/jasmonic acid-NRT signaling module coordinates nitrate reallocation and the trade-off between growth and environmental adaptation. *Plant Cell* 26, 3984–3998. doi: 10.1105/tpc.114.129296

Zhang, M., Liang, X., Wang, L., Cao, Y., Song, W., Shi, J., et al. (2019). A HAK family Na(+) transporter confers natural variation of salt tolerance in maize. *Nat. Plants* 5, 1297–1308. doi: 10.1038/s41477-019-0565-y

Zhang, W. H., Skerrett, M., Walker, N. A., Patrick, J. W., and Tyerman, S. D. (2002). Nonselective currents and channels in plasma membranes of protoplasts from coats of developing seeds of bean. *Plant Physiol.* 128, 388–399. doi: 10.1104/pp.010566

Zhang, Y. M., Zhang, H. M., Liu, Z. H., Li, H. C., Guo, X. L., and Li, G. L. (2015). The wheat NHX antiporter gene TaNHX2 confers salt tolerance in transgenic alfalfa by increasing the retention capacity of intracellular potassium. *Plant Mol. Biol.* 87, 317–327. doi: 10.1007/s11103-014-0278-6

Zhao, F., Song, C. P., He, J., and Zhu, H. (2007). Polyamines improve K(+)/Na(+) homeostasis in barley seedlings by regulating root ion channel activities. *Plant Physiol.* 145, 1061–1072. doi: 10.1104/pp.107.105882

Zhao, X., Wang, Y. J., Wang, Y. L., Wang, X. L., and Zhang, X. (2011). Extracellular Ca(2+) alleviates NaCl-induced stomatal opening through a pathway involving H2O2-blocked Na(+) influx in Vicia guard cells. *J. Plant Physiol.* 168, 903–910. doi: 10.1016/j.jplph.2010.11.024

Zheng, X., He, K., Kleist, T., Chen, F., and Luan, S. (2015). Anion channel SLAH3 functions in nitrate-dependent alleviation of ammonium toxicity in *Arabidopsis*. *Plant Cell Environ.* 38, 474–486. doi: 10.1111/pce.12389

Zioni, A. B., Vaadia, Y., and Lips, S. H. (1971). Nitrate uptake by roots as regulated by nitrate reduction products of the shoot. *Physiol.Plant.* 24, 288–290. doi: 10.1111/j.1399-3054.1971.tb03493.x

Zorb, C., Senbayram, M., and Peiter, E. (2014). Potassium in agriculture–status and perspectives. *J Plant Physiol.* 171, 656–669. doi: 10.1016/j.jplph.2013.08.008

Conflict of Interest: The authors declare that the research was conducted in the absence of any commercial or financial relationships that could be construed as a potential conflict of interest.

frontiers in Plant Science

REVIEW
published: 26 March 2020
doi: 10.3389/fpls.2020.00300

Manganese in Plants: From Acquisition to Subcellular Allocation

Santiago Alejandro, Stefanie Höller, Bastian Meier and Edgar Peiter**

Plant Nutrition Laboratory, Institute of Agricultural and Nutritional Sciences, Martin Luther University Halle-Wittenberg, Halle (Salle), Germany

Manganese (Mn) is an important micronutrient for plant growth and development and sustains metabolic roles within different plant cell compartments. The metal is an essential cofactor for the oxygen-evolving complex (OEC) of the photosynthetic machinery, catalyzing the water-splitting reaction in photosystem II (PSII). Despite the importance of Mn for photosynthesis and other processes, the physiological relevance of Mn uptake and compartmentation in plants has been underrated. The subcellular Mn homeostasis to maintain compartmented Mn-dependent metabolic processes like glycosylation, ROS scavenging, and photosynthesis is mediated by a multitude of transport proteins from diverse gene families. However, Mn homeostasis may be disturbed under suboptimal or excessive Mn availability. Mn deficiency is a serious, widespread plant nutritional disorder in dry, well-aerated and calcareous soils, as well as in soils containing high amounts of organic matter, where bio-availability of Mn can decrease far below the level that is required for normal plant growth. By contrast, Mn toxicity occurs on poorly drained and acidic soils in which high amounts of Mn are rendered available. Consequently, plants have evolved mechanisms to tightly regulate Mn uptake, trafficking, and storage. This review provides a comprehensive overview, with a focus on recent advances, on the multiple functions of transporters involved in Mn homeostasis, as well as their regulatory mechanisms in the plant's response to different conditions of Mn availability.

Keywords: manganese transport, manganese uptake, manganese deficiency, manganese toxicity, intracellular distribution, Arabidopsis, rice, barley

OPEN ACCESS

Edited by:
Manuel Nieves-Cordones, Center for Edaphology and Applied Biology of Segura, Spanish National Research Council, Spain

Reviewed by:
Sebastien Thomine, UMR 9198 Institut de Biologie Intégrative de la Cellule (I2BC), France
Mathieu Pottier, University of Liège, Belgium

****Correspondence:***
Santiago Alejandro
santiago.alejandro-martinez@landw.uni-halle.de
Edgar Peiter
edgar.peiter@landw.uni-halle.de

Specialty section:
This article was submitted to Plant Nutrition, a section of the journal Frontiers in Plant Science

Received: *05 December 2019*
Accepted: *02 March 2020*
Published: *26 March 2020*

Citation:
Alejandro S, Höller S, Meier B and Peiter E (2020) Manganese in Plants: From Acquisition to Subcellular Allocation. Front. Plant Sci. 11:300. doi: 10.3389/fpls.2020.00300

INTRODUCTION

Manganese (Mn) is an essential element in virtually all living organisms where it can fulfill two different functions: acting as an enzyme cofactor or as a metal with catalytic activity in biological clusters (Andresen et al., 2018). In humans, Mn functions as a cofactor for a variety of enzymes, including arginase, glutamine synthetase, pyruvate carboxylase, and Mn superoxide dismutase (MnSOD). But in comparison to other essential micronutrients, such as iron (Fe) and zinc (Zn), whose deficiencies in humans are responsible for major health problems, Mn deficiency in humans is rare. However, Mn poisoning may be encountered more frequently upon overexposure to this metal causing hepatic cirrhosis, polycythemia, dystonia, and Parkinson-like symptoms (Li and Yang, 2018). In plants, Mn is one of the 17 essential elements for growth and reproduction. It is needed in only small quantities by plants, but is ultimately as critical to growth as are the other nutrients. In photosynthetic organisms, Mn is an essential element of the metalloenzyme cluster

of the oxygen-evolving complex (OEC) in photosystem II (PSII). In spite of its importance for photosynthetic activity, Mn homeostasis in plants has been poorly investigated. Nevertheless, Mn deficiency can be a serious plant nutritional disorder in soils with high pH and high partial pressure of O_2 (pO_2), where the bio-availability of Mn can decrease far below the level that is required for normal plant growth (Broadley et al., 2012). Fertilization with Mn salts at soil level is often not effective, since soluble Mn (Mn^{2+}) is rapidly converted to plant-unavailable Mn oxides, particularly in sandy alkaline soils. (In this review, we use the general term "Mn," unless we refer to a specific oxidation state). However, it has been argued that the application of Mn fertilizers to the soil can be an effective way to alleviate Mn deficiencies, but only if soil pH is also corrected (White and Greenwood, 2013). Foliar Mn application can supply sufficient Mn to overcome Mn deficiency, but this strategy is expensive and often impractical for farmers on marginal lands. Moreover, foliar Mn sprays are only effective for a limited time period since Mn is very little mobile in the plant and does not remobilize from older leaves to Mn-deficient young leaves (Li et al., 2017). On the other extreme, Mn toxicity can occur in poorly drained and in strongly acidic soils, where it is usually associated with other acidity-related soil fertility problems, such as aluminum toxicity and deficiencies of calcium (Ca), magnesium (Mg), and molybdenum (Mo) (Goulding, 2016).

Depending on Mn availability, plants either need to efficiently acquire and utililize Mn under limiting conditions, or to detoxify the metal under superfluous supply. Transport processes are at the core of those adaptations. In the past, Mn transporters have been identified at the molecular level in many eukaryotic organisms (Pittman, 2005). Furthermore, recent progress in Mn homeostasis has mainly focused on Arabidopsis and rice, which represent dicot and graminaceous monocot plants, respectively (Socha and Guerinot, 2014; Shao et al., 2017). Only recently, transporters involved in uptake and subcellular distribution of Mn have been characterized in a wider range of plant species. This article reviews the current knowledge of Mn uptake, translocation and subcellular distribution, as well as the functions of Mn in different plant species. **Table 1** lists the Mn transporters discussed in the text.

FUNCTIONS OF MANGANESE IN PLANTS

Mn plays a role in diverse processes of a plant's life cycle such as photosynthesis, respiration, scavenging of reactive oxygen species (ROS), pathogen defense, and hormone signaling. In Arabidopsis, 398 enzymes are predicted to contain Mn in the metal-binding site (The UniProt Knowledgebase[1]). Among them, 20% showed an experimental evidence to require Mn as a cofactor. In many enzymes, Mn is interchangeable with other divalent cations such as Ca, cobalt (Co), copper (Cu), Mg, or Zn. In plants, only the OEC in PSII, MnSOD, and oxalate oxidase have been shown to require exclusively Mn.

The most-well-studied function in plant metabolism that depends on Mn is the water-splitting reaction in PSII, which is the first step of photosynthesis. This process requires the tetra-Mn cluster Mn_4O_5Ca to split two water molecules into four electrons, four protons, and molecular O_2 (Bricker et al., 2012). However, the delivery of Mn^{2+} and Ca^{2+} to the OEC reaction center in land plants is still under investigation. In the unicellular photosynthetic organism *Synechocystis*, PratA functions as an assembly factor and chaperone protein for efficient delivery of Mn to the PSII reaction core (Stengel et al., 2012). In green plants, it is speculated that the extrinsic protein PsbP, the closest homolog to PratA, acts as a Mn carrier protein to introduce Mn into the OEC reaction center, where it subsequently stabilizes the Mn cluster in association with PsbO and PsbQ (Bondarava et al., 2007).

Another process in plants dependent on Mn is the detoxification of ROS. In plant cells, ROS are formed mainly in chloroplasts, mitochondria, peroxisomes, and in the cytosol. Mn is a cofactor of MnSODs located in mitochondria as also in peroxisomes (Bowler et al., 1994; Corpas et al., 2017). In addition, oxalate oxidase is a Mn-dependent enzyme which catalyzes the oxidation of oxalate to CO_2 coupled with a reduction of O_2 to H_2O_2 (Requena and Bornemann, 1999). Oxalate oxidase is located in the apoplast, where it is involved in pathogen defense likely by the generation of microcidal concentrations of H_2O_2 and by the formation of effective barriers against pathogen penetration by H_2O_2-mediated lignification (Lane, 2002). Oxalate oxidase activity has been identified mainly in monocot plant species including wheat, barley, and rice (Svedruzic et al., 2005). Interestingly, germin-like proteins (GLPs) in Arabidopsis, which are homologous to oxalate oxidase, showed neither oxalate oxidase activity nor a Mn-dependent activation (Membré et al., 2000; Li et al., 2016). Intriguingly, the Mn^{2+} cation itself may act as an antioxidant molecule. In fact, it has been shown in yeast that elevated intracellular Mn was associated with a reduction of oxidative damage in yeast cells (Reddi et al., 2009). It is likely that Mn-phosphate (Mn-P) complexes act as antioxidants whereby the Mn speciation is altered by changes in phosphate concentrations (McNaughton et al., 2010).

Furthermore, Mn is an important cofactor of enzymes involved in isoprenoid biosynthesis (Wilkinson and Ohki, 1988; Köllner et al., 2008). Mn and Mg are two major cofactors of terpene synthases (Rohdich et al., 2006; Köllner et al., 2008). Therefore, it has been proposed that different patterns of plant terpene profiles are often closely correlated with Mg/Mn ratios rather than with concentrations of each cofactor element alone in the growth media (Farzadfar et al., 2017). Beside this, Mn is involved in lignin biosynthesis at two different levels: (i) Mn, besides Mg, can serve as cofactor of the phenylalanine ammonia-lyase (PAL) (Engelsma, 1972), a key enzyme in the phenylpropanoid pathway to produce monolignols; (ii) Lignin can be synthesized from monolignols that are oxidized by Mn^{3+} into monolignol radicals, which can then be added to existing phenolic groups to form lignin polymers (Önnerud et al., 2002).

[1]http://www.uniprot.org, accessed 20 October 2019

Intriguingly, it has been shown that Mn can replace Mg in the active site of some enzymes of the photosynthetic pathway, including Ribulose-1,5-bisphosphate carboxylase/oxygenase (Rubisco), changing the functional role of these enzymes (Bloom and Lancaster, 2018; Bloom, 2019). Furthermore, *in vitro* experiments demonstrated that Mn is an important cofactor in abscisic acid (ABA) and auxin signaling by activating PP2C phosphatases and IAA-amino acid conjugate hydrolases, respectively (LeClere et al., 2002; Meinhard et al., 2002; Schweighofer et al., 2004). Since diverse Golgi-localized glycosyl transferases require Mn for their activity, Mn is also essential for protein glycosylation and the biosynthesis of pectin and hemicellulose polymers (Egelund et al., 2006; Strasser et al., 2007; Basu et al., 2015). Other enzymes that require Mn as a cofactor are purple acid phosphatases (PAPs) (Schenk et al., 1999; Venkidasamy et al., 2019). Also, different decarboxylases (e.g., NAD malic enzyme) and dehydrogenases (e.g., phosphoenolpyruvate carboxylase) of the tricarboxylic acid cycle can be activated by Mn, but in many cases Mn can be replaced by Mg (Burnell, 1988; Gregory et al., 2009).

Another Mn-dependent process lies in the deposition of cuticular waxes in leaves. In barley, it has been demonstrated that Mn deficiency may decrease the cuticular wax layer, which leads to a higher transpiration rate (Hebbern et al., 2009). Moreover, Mn deficiency caused a decrease of cuticular waxes in Arabidopsis leaves (Alejandro et al., 2017).

In addition, Mn plays a role in such diverse processes as chloroplast development (Rohdich et al., 2000; Hsieh et al., 2008), purine and urea catabolism (Werner et al., 2008; Cao et al., 2010), phospholipid biosynthesis (Collin et al., 1999; Nowicki et al., 2005), Ca^{2+} signaling (Kim et al., 2003; Hashimoto et al., 2012), DNA repair (Takahashi et al., 2007; Szurmak et al., 2008), or histidine biosynthesis (Glynn et al., 2005).

MANGANESE DEFICIENCY AND TOXICITY

In plants, Mn deficiency often occurs as a latent disorder, without clear visual symptoms. Thus, the magnitude to which Mn deficiency affects crop yield is difficult to quantify. The critical concentration for Mn deficiency is generally below 10–20 $mg.kg^{-1}$ dry weight (Broadley et al., 2012). One of the consequences of Mn deficiency in plants is an impaired growth, leading to a decrease in biomass (Longnecker et al., 1991; Hebbern et al., 2005; Pedas et al., 2005). This can be caused by lower numbers of chloroplasts, lower net photosynthetic efficiency, and a decrease in chlorophyll content

TABLE 1 | Manganese transport proteins reviewed in this article.

Family/name	Organ(s)/tissue(s) expression	Subcellular localization	Gene expression response	Other substrates	References
CaCA					
AtCAX2	Root (stele and root tip), stem, leaf, flower, pollen, fruit	Tonoplast	Unaffected by +Cu, +Mn, +Zn	Ca, Cd	Hirschi et al., 2000; Shigaki et al., 2003; Pittman et al., 2004; Edmond et al., 2009
AtCAX4	Root, stem, leaf, flower, fruit	Tonoplast	Up-regulated by +Mn, +Ni, -Ca	Cd, Ca, Zn	Cheng et al., 2002; Koren'kov et al., 2007; Mei et al., 2009
AtCAX5	Root, stem, leaf, flower, fruit	Tonoplast	Up-regulated by +Mn down-regulated by +Zn	Ca	Edmond et al., 2009
HvCAX2	Root, leaf, seed	–	Up-regulated by +Ca, +Na unaffected by +Mn	Ca	Edmond et al., 2009
LeCAX2	Root, leaf, fruit	–	–	Ca	Edmond et al., 2009
OsCAX1a	Root, shoot, flower, seed	Tonoplast	–	Ca	Kamiya et al., 2005
OsCAX3	Root, shoot, flower, seed	–	–	Ca	Kamiya et al., 2005
OsCAX4	Root	–	Up-regulated by +Ca	Ca,Cu	Yamada et al., 2014
VvCAX3	Root, stem, leaf, fruit	Tonoplast	Up-regulated by +Ca, +Na unaffected by +Mn	Ca, Cu, Li, Na	Martins et al., 2017
AtCCX3	Root, stem, leaf, flower	Tonoplast, endomembranes	Up-regulated by +K, +Na unaffected by +Mn	K, Na	Morris et al., 2008
BICAT					
AtBICAT1/PAM71/CCHA1	Leaf	Chloroplast (thylakoid membrane)	Unaffected by +Mn	Ca	Schneider et al., 2016; Wang et al., 2016; Eisenhut et al., 2018; Frank et al., 2019
AtBICAT2/CMT1	Root, stem, leaf, flower, fruit	Chloroplast (inner envelope)	Down-regulated by +Mn	Ca, Mg	Eisenhut et al., 2018; Frank et al., 2019; Zhang et al., 2018

(Continued)

TABLE 1 | Continued

Family/name	Organ(s)/tissue(s) expression	Subcellular localization	Gene expression response	Other substrates	References
CDF/MTP					
AtMTP8	Root (epidermis, cortex), seed	Tonoplast	Up-regulated by +Mn -Fe	Fe	Eroglu et al., 2016, 2017
AtMTP9	–	–	Unaffected by +Mn	–	Delhaize et al., 2007; Chu et al., 2017
AtMTP10	–	–	Unaffected by +Mn	–	Delhaize et al., 2007; Chu et al., 2017
AtMTP11	Root (root tip), leaf (guard cells)	Golgi/PVC	Unaffected by +Mn	–	Delhaize et al., 2007; Peiter et al., 2007
ShMTP8	–	Tonoplast	–	–	Delhaize et al., 2003, 2007
BmMTP10	Root, leaf	Endomembranes*	Up-regulated by +Mn	–	Erbasol et al., 2013
BmMTP11	Root, leaf	Endomembranes*	Unaffected by +Mn	Ni	Erbasol et al., 2013
OsMTP8.1	Root, shoot	Tonoplast	–	–	Chen et al., 2013; Takemoto et al., 2017
OsMTP8.2	Root, shoot	Tonoplast	–	–	Takemoto et al., 2017
OsMTP9	Root (endodermis, exodermis)	Plasma membrane	Unaffected by +Mn -Mn		Ueno et al., 2015
OsMTP11	Root, shoot	Golgi/TGN	Up-regulated by +Mn +Zn +Cd +Ni	Co, Ni	Zhang and Liu, 2017; Ma et al., 2018; Tsunemitsu et al., 2018
HvMTP8.1	Root, leaf	Golgi	Down-regulated by -Mn (root) down-regulated by +Mn (shoot)	–	Pedas et al., 2014
HvMTP8.2	Root, leaf	Golgi	Down-regulated by +Mn	–	Pedas et al., 2014
PtMTP11.1	–	TGN	–	–	Peiter et al., 2007
PtMTP11.2	–	TGN	–	–	Peiter et al., 2007
PbMTP8.1	–	–	–	Fe	Hou et al., 2019
PbMTP8.2	–	–	–	Fe	Hou et al., 2019
PbMTP9	–	–	–	Fe	Hou et al., 2019
PbMTP10	–	–	–	Fe	Hou et al., 2019
PbMTP11.1	–	–	–	–	Hou et al., 2019
PbMTP11.2	–	–	–	–	Hou et al., 2019
NtMTP8.1	Root, stem, leaf, flower	–	Up-regulated by +Co +Zn unaffected by +Mn	–	Liu et al., 2019
NtMTP8.4	Stem, leaf, flower	–	Up-regulated by +Cd +Co +Mn (root) up-regulated by +Cd +Co +Mg +Zn (shoot)	–	Liu et al., 2019
NtMTP11.1	Root, stem, leaf, flower	–	Up-regulated by +Co +Cd +Mn +Zn	–	Liu et al., 2019
CsMTP9	Root (endodermis)	Plasma membrane	Up-regulated by +Cd +Mn +Ni down-regulated by –Mn -Zn	Cd	Migocka et al., 2015
NRAMP					
AtNRAMP1	Root (Cortex, endodermis) > > shoot	Plasma membrane	Up-regulated by -Fe -Mn	Cd, Fe	Curie et al., 2000; Thomine et al., 2000; Cailliatte et al., 2010; Castaings et al., 2016
AtNRAMP2	Root (pericycle, root tip), leaf vasculature, flower, trichome	TGN	Up-regulated by -Mn down-regulated by -Fe	–	Curie et al., 2000; Alejandro et al., 2017; Gao et al., 2018

(Continued)

TABLE 1 | Continued

Family/name	Organ(s)/tissue(s) expression	Subcellular localization	Gene expression response	Other substrates	References
AtNRAMP3	Root (stele), leaf vasculature, developing seed	Tonoplast	Up-regulated by -Fe unaffected by -Mn	Cd, Fe	Thomine et al., 2000, 2003; Lanquar et al., 2005, 2010
AtNRAMP4	Root (stele), leaf vasculature, developing seed	Tonoplast	Up-regulated by -Fe unaffected by -Mn	Cd, Fe	Thomine et al., 2000; Lanquar et al., 2005, 2010
OsNRAMP3	Node, leaf vasculature	Plasma membrane	Unaffected by +Mn -Mn	–	Yamaji et al., 2013; Yang et al., 2013
OsNRAMP5	Root (exodermis, endodermis, stele), panicle	Plasma membrane	Up-regulated by -Fe (shoot) up-regulated by -Fe, -Zn (root) unaffected by -Mn	Cd, Fe	Ishimaru et al., 2012; Sasaki et al., 2012; Yang et al., 2014
OsNRAMP6	Leaves	Plasma membrane	–	Fe	Peris-Peris et al., 2017
HvNRAMP5	Root (epidermis, stele)	Plasma membrane	Up-regulated by -Fe unaffected by +Mn	Cd	Wu et al., 2016
BnNRAMP1b	Root, shoot	–	Up-regulated by +Cd	Cd, Zn	Meng et al., 2017
TcNRAMP3	–	Tonoplast	–	Cd, Fe	Oomen et al., 2009
TcNRAMP4	–	Tonoplast	–	Cd, Fe, Zn	Oomen et al., 2009
TcNRAMP3 (*T. cacao*)	Root, shoot	–	Up-regulated by -Fe unaffected by -Mn	Fe	Ullah et al., 2018
TcNRAMP5 (*T. cacao)*	Root	–	Up-regulated by -Fe unaffected by -Mn	Cd, Fe, Zn	Ullah et al., 2018
TcNRAMP6 (*T. cacao)*	Root, shoot	–	–	–	Ullah et al., 2018
LeNRAMP1	Root	Endomembranes*	up-regulated by -Fe	–	Bereczky et al., 2003
LeNRAMP3	Root, shoot	Endomembranes*	Up-regulated by -Fe	–	Bereczky et al., 2003
AhNRAMP1	Root, stem	–	Up-regulated by -Mn, -Zn	Zn	Wang et al., 2019
MbNRAMP1	Root	Endomembranes*	Up-regulated by -Fe	Fe	Xiao et al., 2008
P-TYPE ATPASE					
AtECA1	Root, stem, leaf, guard cells, trichome	ER	–	Ca, Zn	Liang et al., 1997; Wu et al., 2002; Li et al., 2008
AtECA3	Root (stele), stem, leaf vasculature, guard cells, flower, fruit	Golgi	Unaffected by -Mn	Ca, Zn	Mills et al., 2007; Li et al., 2008
LeLCA1	–	ER?	–	Ca	Johnson et al., 2009
VIT					
AtVIT1	Root, cotyledon, developing seed	Tonoplast	–	Fe	Kim et al., 2006
OsVIT1	Leaf > > root, stem, panicle, embryo	Tonoplast	Down-regulated by -Fe	Fe, Zn	Zhang et al., 2012; Wang et al., 2017
OsVIT2	Leaf, stem, panicle, embryo	Tonoplast	Up-regulated by +Fe down-regulated by -Fe	Fe, Zn	Zhang et al., 2012
TaVIT2	Root, shoot, seed	Tonoplast	–	Fe	Connorton et al., 2017
AtMEB1	–	ER bodies	–	Fe	Yamada et al., 2013
AtMEB2	–	ER bodies	–	Fe	Yamada et al., 2013
YSL					
OsYSL2	Root (phloem), leaf, vascular bundle, developing seed	Plasma membrane	Up-regulated by -Fe down-regulated by -Mn	Fe	Koike et al., 2004; Yang et al., 2014
OsYSL6	Root, shoot	Plasma membrane	Unaffected by +Mn -Mn	–	Sasaki et al., 2011
HvYSL2	Root (endodermis), shoot	–	Up-regulated by -Fe	Fe, Zn, Co, Ni, Cu	Araki et al., 2011

(Continued)

TABLE 1 | Continued

Family/name	Organ(s)/tissue(s) expression	Subcellular localization	Gene expression response	Other substrates	References
ZIP					
AtIRT1	Root (epidermis, cortex) > > shoot	Plasma membrane	Up-regulated by -Fe	Fe, Zn, Co, Ni	Korshunova et al., 1999; Curie et al., 2000; Thomine et al., 2000; Vert et al., 2002
AtZIP1	Root (stele), leaf vasculature	Tonoplast	Up-regulated by -Fe -Zn (root) up-regulated by -Mn (shoot) down-regulated by -Zn (shoot)	Zn	Milner et al., 2013
AtZIP2	Root (stele)	Plasma membrane	Down-regulated by -Fe -Mn	Zn	Milner et al., 2013
AtZIP5	Root, shoot	–	–	–	Milner et al., 2013
AtZIP6	Root, shoot	–	–	–	Milner et al., 2013
AtZIP7	Shoot > > root	–	–	Fe, Zn	Milner et al., 2013; Fu et al., 2017
AtZIP9	Root, shoot	–	–	–	Milner et al., 2013
HvIRT1	Root (epidermis, cortex**, endodermis**, pericycle), seed	Plasma membrane	Up-regulated by -Fe, -Mn	Fe, Zn	Pedas et al., 2008; Long et al., 2018
LeIRT1	Root, flower	–	–	Cd, Fe, Zn	Eckhardt et al., 2001
LeIRT2	Root	–	–	Cd, Fe, Zn	Eckhardt et al., 2001
MtZIP4	Root***, leaf	–	Down-regulated by -Fe -Mn up-regulated by +Zn	–	López-Millán et al., 2004
MtZIP7	Leaf	–	Unaffected by -Mn	–	López-Millán et al., 2004
PtIRT1	Root, leaf	–	Down-regulated by -Mn	Fe, Zn	Fu et al., 2017

*+ excess, − deficiency, * in yeast cells, ** only under +Fe, *** only under +Zn.*

(Henriques, 2004; Hebbern et al., 2009; Alejandro et al., 2017), as well as higher susceptibility to pathogen infections (Heckman et al., 2003; Heine et al., 2011), imbalance in plant water relations (Ohki, 1985; Hebbern et al., 2009), and decreased tolerance to low temperatures (Ihnatowicz et al., 2014; Stoltz and Wallenhammar, 2014). Mn deficiency leads to a reduced number of Mn-complexes in the PSII core, which causes the destabilization and disintegration of PSII complexes that lowers the net photosynthesis rate (Schmidt et al., 2016). Besides, the disintegration of PSII complexes directly affects the thylakoid structure and promotes chlorophyll degradation leading to the development of characteristic interveinal leaf chlorosis (Papadakis et al., 2007). Due to the low phloem mobility of Mn (Ferrandon and Chamel, 1988; Li et al., 2017), typical symptoms of Mn deficiency first develop in younger leaves. Pale mottled leaves and interveinal chlorosis are the most visible symptoms of the disorder (Schmidt et al., 2016). Under severe Mn deficiency, leaves may also develop gray speck symptoms, which are characterized by brownish or necrotic spots (Broadley et al., 2012). It has been proposed that necrotic spots are a consequence of an increase in free oxygen radicals in damaged chloroplasts and a decrease in MnSOD activity (Broadley et al., 2012; Hajiboland, 2012). Similar responses have been described in Chlamydomonas, where a decrease in photosynthesis and mitochondrial MnSOD function was observed under Mn-deficient conditions (Allen et al., 2007). However, Mn-starved Arabidopsis seedlings showed a decrease in net photosynthesis while there was no loss of MnSOD activity (Lanquar et al., 2010). This suggests that the use of the cellular Mn pool for Mn-requiring metabolic reactions under low Mn conditions is variable among photosynthetic organisms.

In roots, an increase in the frequency of root hairs can be observed under Mn deficiency (Yang et al., 2008). If the deficiency becomes more severe, root tips may develop serious necrosis (Yamaji et al., 2013).

Toxic Mn concentrations are highly dependent on plant species and genotypes (Husted et al., 2009; Broadley et al., 2012; Fernando and Lynch, 2015). Excess Mn may be stored in vacuoles (Dučić and Polle, 2007; Dou et al., 2009), cell walls (Führs et al., 2010), and distributed to different leaf tissues (Fernando et al., 2006a,b). Also, Mn can be chelated in Mn-P complexes in trichomes (McNear and Küpper, 2014; Blamey et al., 2015) and complexed by organic acids in leaves (Lambers et al., 2015). Therefore, it is likely that differences between plant species lie in the cellular distribution and speciation of Mn, dominated by complexes with malate or citrate (Fernando et al., 2010). At the molecular level, excessive Mn can prevent the uptake and translocation of other essential elements such as Ca, Mg, Fe, and P (Alam et al., 2005; St.Clair and Lynch, 2005; Blamey et al., 2015; Lešková et al., 2017), inhibit chlorophyll biosynthesis (Clairmont et al., 1986; Subrahmanyam and Rathore, 2001), cause a decline in the photosynthetic rate (Nable et al., 1988; Amao and Ohashi, 2008), reduce the meristematic cell division in roots by inhibiting auxin biosynthesis (Morgan et al., 1966;

Zhao et al., 2017), and lead to an increase in the accumulation of oxidized Mn and oxidized phenolic compounds in the apoplast (Fecht-Christoffers et al., 2006).

The symptoms of Mn toxicity vary widely among plant species, with chlorotic leaves and necrotic spots as the most common symptoms (Millaleo et al., 2010). Accordingly, Mn stress in plants has been explained by two main hypotheses based on either symplastic or apoplastic processes (Fernando and Lynch, 2015). The symplastic hypothesis proposes that Mn toxicity acts via photo-oxidative stress in the chloroplast that causes chlorosis. Conversely, in the apoplastic hypothesis, Mn stress damage is mainly due to the accumulation of Mn oxides, oxidized phenolic compounds, and ROS, in the cell wall, leading to necrosis. Necrotic spots have thus been associated with the accumulation and oxidation of Mn and of oxidized phenolic compounds, while chlorosis has been often attributed to Fe deficiency induced by high Mn. Surprisingly, necrotic spots are high in Mn and appear first on older leaves, whereas in chlorotic areas no Mn accumulation can be observed. It is hence conceivable that the mechanism resulting in necrotic spots differs from that which causes chlorosis.

Several lines of evidence suggest that the early target of Mn toxicity is the photosynthetic process (Millaleo et al., 2010). In fact, plants exposed to Mn excess showed a decline in net photosynthesis rate and chlorophyll content (Li et al., 2010). Although in chloroplasts the occurrence of thylakoid swelling has been associated with the administration of excess Mn (Lidon et al., 2004; Doncheva et al., 2009), the target of Mn in these photosynthetic membranes is still unclear. It has been proposed that the oxidation of Mn in chloroplasts by light-activated chlorophyll generates ROS, and thereby damages chlorophyll (Panda et al., 1987; Baldisserotto et al., 2007). At the same time, Mn may substitute Mg in chlorophyll molecules or bind to ferredoxin in the thylakoid matrix, eventually destroying the ultrastructure of chloroplasts (Panda et al., 1987; Hauck et al., 2003). Moreover, the lack of physiologically active Fe would be a secondary effect of Mn toxicity (Nian, 1989; Huang et al., 2016), which might block chlorophyll synthesis and the correct assembly of photosystem I (PSI) (Chereskin and Castelfranco, 1982; Cornah et al., 2002; Millaleo et al., 2013). Consequently, photoinhibition of PSII would likely be a late side effect of Mn exposure.

MANGANESE DYNAMICS IN SOIL

Mn is one of the most abundant and widely distributed metals in nature and comprises about 0.1% of the Earth's crust (Emsley, 2003). The element is found in minerals, combined with other elements such as oxygen, sulfur, carbon, silicon, and chlorine (Turekian and Wedepohl, 1961). Mn can exist in 11 oxidation states, ranging from −3 to +7, but in soils, Mn is mainly present as +2 (e.g., Mn^{2+}), +3 (e.g., Mn_2O_3) and +4 (e.g., MnO_2). Availability of Mn to plants depends on its oxidation state: Mn^{2+} is the only plant-available form and can be readily transported into root cells and translocated to the shoot, whereas the oxidized species Mn(III) and Mn(IV) form insoluble oxides that rapidly sediment (Stumm and Morgan, 1996). Thus, Mn dynamics in soils are mostly represented by the concept of a balance between soluble Mn^{2+} and insoluble Mn oxides (MnO_x).

Mn deficiency in plants is particularly prevalent in alkaline soils, in which the oxidization of Mn^{2+} to unavailable MnO_x is favored. Such soils are common in the northern part of Europe, the UK, USA, China, and in southern Australia (Husted et al., 2009; George et al., 2014). In addition to pH, the oxygen level (pO_2) in soil and soil microorganisms are also relevant factors of Mn dynamics in soils. Beside this, root exudates can modify the Mn availability in the rhizosphere. The Mn redox status in soils involves primarily the competition of soluble highly mobile oxidants, such as molecular O_2, and soluble reducing organic molecules, derived from soil organic matter and biological sources. In aerobic soils, due to the high mobility and redox potential of O_2, Mn oxidation is favored rather than reduction of MnO_x by microorganisms (Lovely, 1995). By contrast, waterlogging causes a reduction of MnO_x most likely by decreasing the O_2 concentration, leading to an increase of plant-available Mn^{2+} in soil solution up to toxic levels (Khabaz-Saberi et al., 2006).

However, it has been proposed that the oxidation of Mn^{2+} in environments with abundant O_2 is sluggish, particularly in the absence of biological catalysts, and that the oxidation of Mn^{2+} in soil is carried out predominantly by microorganisms (Sparrow and Uren, 2014). Indeed, microorganisms can catalyze Mn^{2+} oxidation in order of 10^3 times faster than abiotic oxidation (Morgan, 2005). Some microorganisms produce enzymes which directly oxidize Mn^{2+}, or produce extracellular superoxide leading to the production of insoluble MnO_x (Hansel et al., 2012; Zhang et al., 2014). Conversely, other microorganisms can reduce MnO_x and thereby increase Mn availability for plant uptake (Rengel, 2015). Also, environmental conditions (temperature, humidity) affect soil Mn availability by modulating the activity of Mn-oxidizing microorganisms (Sparrow and Uren, 2014). Therefore, the population of Mn-oxidizing and Mn-reducing microorganisms is a key factor in the availability of soil Mn for plant uptake.

Another important factor of Mn dynamics in soils is the exudation of protons (H^+), carboxylates, and enzymes by plant roots. Proton exudation increases the Mn availability in the rhizosphere by exchanging Mn that is immobilized by negatively charged organic matter and clay minerals, and also by lowering the pH of alkaline soils (Rengel, 2015). Mn uptake by some Mn-hyperaccumulators, such as *Phytolacca* species, is based on a strong rhizosphere acidification (Lambers et al., 2015). Noteworthy, Mn availability is also increased by root exudation of carboxylates which chelate Mn and reduce Mn(IV) to Mn^{2+} in either acidic or alkaline soils (Jauregui and Reisenauer, 1982; Gherardi and Rengel, 2004).

Phytate (inositol hexaphosphate) is generally the dominant form of organic P in soils and has the potential to complex Mn^{2+} and other divalent cations. Exudation of phytases, which catalyze the degradation of phytate thus increases the Mn availability by releasing Mn^{2+} (George et al., 2014).

The release of carboxylates into the rhizosphere is a mechanism for the acquisition of not only Mn, but in particular

of P. Carboxylates mobilize P absorbed to Fe/Al hydroxides by ligand exchange, especially under low P availability (Nuruzzaman et al., 2006). By contrast, elevated levels of soil-P lead to a reduction of carboxylate and phytase exudation, in turn decreasing Mn^{2+} acquisition (Lambers et al., 2015; Giles et al., 2017). However, hydroponic experiments in barley, where most likely no Mn–P complexes were formed, have also shown a decrease in Mn uptake under elevated P supply (Pedas et al., 2011). Hence, it has been proposed that there is a competition between Mn^{2+} and P during Mn uptake.

MANGANESE TRANSPORT PROTEINS IN PLANTS

As mentioned above, reduced Mn (Mn^{2+}) is the only available form for plants. To maintain an optimal supply, acquisition from the rhizosphere and distribution of Mn have to be regulated. One of the most important mechanisms to regulate the acquisition from the soil is the uptake by specific transporters into root cells (**Figure 1**). Once Mn reaches the symplast, the main pathways for the translocation and distribution of Mn in the whole plant involve transport toward and into the xylem, transfer to the phloem, and translocation to and between the different tissues. However, most of the Mn transporters and mechanisms required for Mn loading into the xylem of the root stele, for loading Mn into the phloem, and for Mn transport into the plant cell in shoots have not been identified yet. Interestingly, the mobility of Mn in the phloem is supposed to be low (Li et al., 2017), but there is evidence that a small amount of Mn may be recycled via the phloem. In fact, it has been reported that after application of ^{52}Mn to a cut barley leaf, radioactivity was detectable in the discrimination center of the shoot, in other leaves, as also in root tips (Tsukamoto et al., 2006). These results suggested that ^{52}Mn was transported by unknown transporters with low affinity.

An intriguing property of Mn transport across membranes is that most of the proteins that transport Mn are not specific for the metal. Plant Mn^{2+} transporters can transport, to varying extent, other divalent cations, such as Fe^{2+}, Zn^{2+}, Cu^{2+}, Cd^{2+}, Ca^{2+}, Co^{2+}, and Ni^{2+}. The physiological relevance of this low specificity needs further investigations, including the modification of specificity. For instance, in the Mn/Fe transporter AtMTP8, Fe transport activity was inhibited by introducing point mutations in different Fe-binding domains without affecting its Mn^{2+} transport capability (Chu et al., 2017).

Diverse families of transport proteins are known to be components of the Mn homeostatic network in plants and can be classified into importers and exporters. Importers translocate Mn from the extracellular space or from internal compartments into the cytosol, whereas exporters are responsible for the exclusion of Mn out of the cytosol into intracellular compartments or into the apoplast. The Natural Resistance Associated Macrophage Protein (NRAMP) family, the Zinc-Regulated Transporter/Iron-Regulated Transporter (ZRT/IRT)-related Protein (ZIP) family, and the Yellow Stripe-Like (YSL) family have members involved in the transport of Mn^{2+} into the cytosol. In contrast, the Cation Diffusion Facilitator/Metal Transport Protein (CDF/MTP) family, the Vacuolar Iron Transporter (VIT) family, the Ca^{2+}/Cation Antiporter (CaCA) superfamily, the Bivalent Cation Transporter (BICAT) family, and the P_{2A}-type ATPase family have members involved in the transport of Mn^{2+} out of the cytosol. **Figure 1** shows the tissue specificity and subcellular localization of Mn transport proteins in roots of Arabidopsis, rice, and other plant species. Genes encoding encoding Mn transport proteins in aerial parts of the plant species are depicted in **Figure 2**, and the subcellular localization of these proteins is displayed in **Figure 3**. The NRAMP family has been characterized in a number of species including bacteria, fungi, plants, and animals. These proteins act as metal/H^+ symporters and are capable of transporting divalent metal cations (Fe^{2+}, Mn^{2+}, Zn^{2+}, Cd^{2+}, Co^{2+}, Ni^{2+}, Cu^{2+}) into the cytosol (Nevo and Nelson, 2006), with the exceptions of OsNRAMP4 (syn. OsNrat1), that transports the trivalent cation Al^{3+} (Xia et al., 2010; Li et al., 2014), and OsNRAMP1, that appears to mediate also As(III) transport (Tiwari et al., 2014).

The ZIP transporters have been found widely in bacteria, fungi, plants, and animals and are predicted to be involved in Fe^{2+}, Zn^{2+}, Cd^{2+}, Co^{2+}, Cu^{2+}, and Mn^{2+} transport. They have 8 transmembrane domains (TMD) with extracellular N- and C-termini and a cytosolic histidine-rich loop (Guerinot, 2000). YSL transporters are related to the OligoPeptide Transporter (OPT) family and are exclusively found in plants, bacteria, fungi, and archaea. Members of the YSL family are predicted to transport metals (Mn^{2+}, Zn^{2+}, Cu^{2+}, Ni^{2+}, Cd^{2+}, Fe^{2+}) complexed to non-proteinogenic amino acids, such as nicotianamine (NA) or phytosiderophores (PS) (Schaaf et al., 2004).

The CDF family has members in all organisms. Most CDFs are Metal^{2+}/H^+(K^+) antiporters and mediate the efflux of Zn^{2+}, Co^{2+}, Fe^{2+}, Cd^{2+}, Ni^{2+}, and/or Mn^{2+}. Most of them have six TMDs with histidine-rich regions at their cytosolic N- and/or C-terminus and additionally between the 4th and 5th TMD. Based on phylogenetic relationships, the CDF family can be classified, corresponding to the main transported metal, into three major subgroups: Zn-CDFs, Fe/Zn-CDFs, and Mn-CDFs (Montanini et al., 2007).

BICAT proteins, also denominated Photosynthesis-Affected Mutant71 (PAM71) or Chloroplast Manganese Transporter (CMT) proteins, belong to the Uncharacterized Protein Family 0016 (UPF0016), which represents a new family of cation transporters present in all eukaryotes and prokaryotes, except in *Lactobacillales* and *Bacillales* (Demaegd et al., 2013, 2014; Hoecker et al., 2017). The protein structure of the plant homologs is characterized by two clusters of three transmembrane domains separated by a central loop. BICAT proteins act as Mn^{2+} and Ca^{2+} transporters (Hoecker et al., 2017; Frank et al., 2019).

CaCA transporters are present in all kingdoms of life and have a conserved core structure of ten transmembrane domains and two conserved α-repeat regions containing acidic amino acids (Pittman and Hirschi, 2016). In particular, the Cation/Ca^{2+} exchanger (CCX) and the H^+/Cation exchanger (CAX) families, which are both members of the CaCA superfamily, are present within all plants.

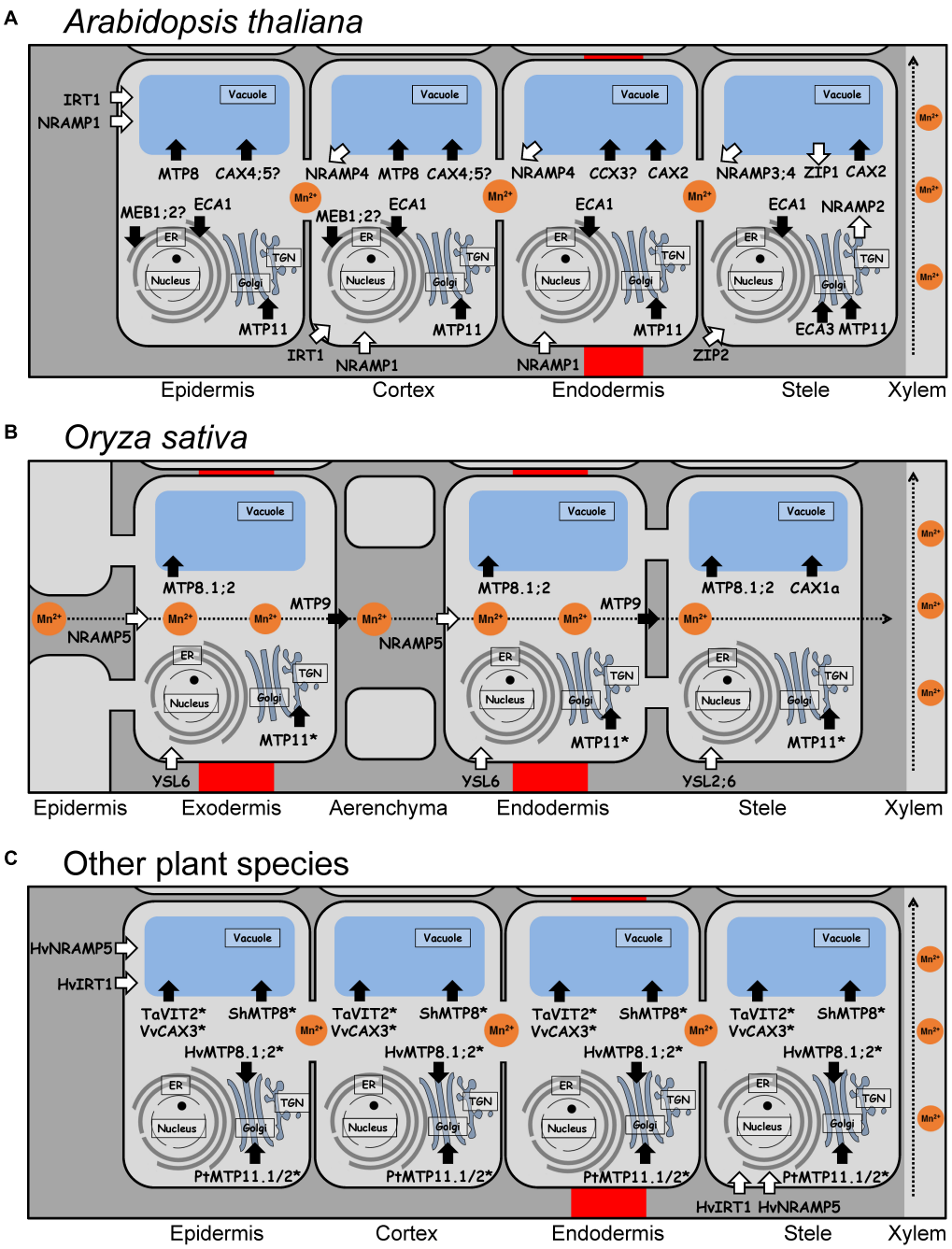

FIGURE 1 | Tissue specificity and subcellular localization of Mn transport proteins in roots of different plant species. **(A)** Mn transport proteins in epidermis, endodermis, cortex, and stele (including pericycle) of Arabidopsis roots. **(B)** Mn transport proteins in exodermis, endodermis, and stele of rice roots. Radial transport of Mn^{2+} is carried out by OsNRAMP5 and OsMTP9, which are polarly localized transporters at both the exodermis and the endodermis, providing a unidirectional flux of Mn from the soil to the stele (indicated as dashed arrow). **(C)** Mn transport proteins in epidermis, endodermis, cortex, and stele of roots of other plant species. **(A–C)** White arrows indicate import into the cytosol, black arrows indicate export out of the cytosol. Transport proteins with yet unknown root tissue specificity are marked by asterisks. Proteins which subcellular localization only shown in yeast but not in plants are indicated by a question mark. Hv, *Hordeum vulgare*; Pt, *Populus trichocarpa*; Sh, *Stylosanthes hamata*; Ta, *Triticum aestivum*; Vv, *Vitis vinifera*.

VIT transporters are found in plants, fungi, and bacteria, but are absent in animals. Members of the VIT family in plants share a high degree of sequence similarity and most of them are capable to transport Fe^{2+} in addition to Mn^{2+}, but their biological functions have been poorly investigated (Cao, 2019).

Plant P-type Ca^{2+}-ATPases are divided into two groups, 2A and 2B, whereby the first one does not contain an N-terminal

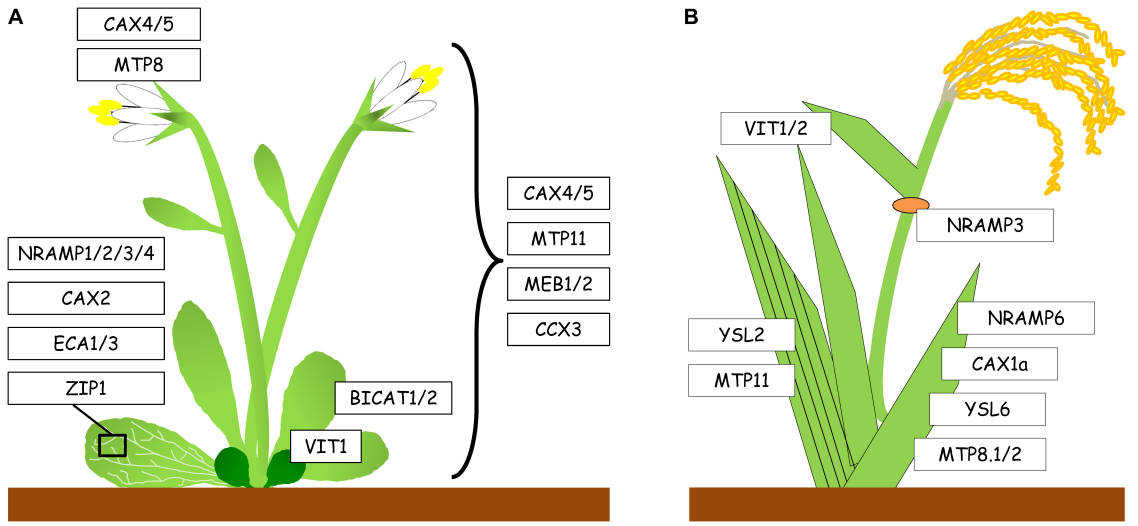

FIGURE 2 | Expression of genes encoding Mn transport proteins in aerial parts of Arabidopsis and rice. **(A)** Mn transport proteins in shoots of Arabidopsis. Transporters listed on the left are expressed in the vasculature of leaves, transporters listed on the right are expressed throughout the above-ground tissues of the plant. In vegetative tissues, *AtVIT1* is only expressed in cotyledons. **(B)** Mn transport proteins in shoots of rice. *OsMTP11* and *OsYSL2* are expressed in the vasculature. *OsNRAMP3* is expressed in the first node (orange). *OsYSL6* and *OsMTP8.1/2* are expressed in older leaves, whereas expression of *OsVIT1/2* is more pronounced in younger leaves.

autoinhibitory domain (Johnson et al., 2009). Those P_{2A}-type Ca^{2+}-ATPases have also a role in Mn^{2+} transport.

MANGANESE UPTAKE FROM THE SOIL AND TRANSLOCATION TO THE SHOOT

Despite the importance of Mn in plant physiology, our knowledge of systems mediating Mn uptake followed by translocation from the roots to the shoot is limited. This is mainly due to the lack of information about the expression and subcellular localization of Mn transporters in most plants. In fact, only few Mn transporters involved in uptake and root radial transport have been identified so far. Uptake of Mn^{2+} has been assumed to be mediated by plasma membrane Ca^{2+} channels, which are generally permeable to Mn^{2+} (Wymer et al., 1997; White et al., 2002). However, this is likely to be a minor Mn^{2+} uptake pathway due to its competition with Ca^{2+}, only relevant when Mn^{2+} is present in high concentrations. However, in soil, Mn^{2+} is usually far less abundant than Ca^{2+} (Broadley et al., 2012). Since this assumption, few Mn transporters have been identified mainly in *A. thaliana* and rice. Their tissue-specific localizations in roots are shown in **Figure 1A** for Arabidopsis, in **Figure 1B** for rice, and in **Figure 1C** for other plant species including barley, wheat, tomato, poplar, and grapevine.

In Arabidopsis, there is plenty of evidence that Mn^{2+} uptake is mainly mediated by AtNRAMP1 (**Figure 1A**), which is localized in the plasma membrane of epidermis and cortex cells in roots, and less in vascular tissues of young leaves (Cailliatte et al., 2010; Castaings et al., 2016). Under Mn-deficient conditions, the expression of *AtNRAMP1* is moderately up-regulated, and *nramp1* knockout mutants accumulate less Mn in shoots under Mn deficiency, which points to a function of this protein as a high-affinity Mn^{2+} uptake transporter (Cailliatte et al., 2010). *NRAMP1* orthologs in cacao, rapeseed, and peanut are also expressed in roots and complement a Mn uptake-deficient yeast strain, *smf1*, lacking a Mn transporter located in the plasma membrane (Meng et al., 2017; Ullah et al., 2018; Wang et al., 2019). In addition, active Mn^{2+} uptake may be accomplished by the ZIP transporter AtIRT1 (Castaings et al., 2016), that is considered as the major Fe uptake transporter of dicots. However, AtIRT1 is not strongly selective for Fe^{2+}, but also transports Zn^{2+}, Cu^{2+}, Co^{2+}, Ni^{2+}, and Mn^{2+} (Korshunova et al., 1999). *IRT1* orthologs expressed in roots have also been identified in tomato and trifoliate orange, but their function in Mn^{2+} uptake remains to be confirmed (Eckhardt et al., 2001; Fu et al., 2017). Furthermore, two ZIP transporters expressed in the root stele are described to be involved in root-to-shoot translocation of Mn in Arabidopsis (Milner et al., 2013). AtZIP1 is a transporter localized to the tonoplast and probably involved in remobilizing Mn^{2+} from vacuoles to the cytosol in root stele cells, whereas AtZIP2 is localized to the plasma membrane and may mediate Mn^{2+} uptake into cells of the root stele. Other Mn^{2+} transporters of the AtZIP family are also expressed in roots, but their function in Mn^{2+} uptake and remobilization is still unknown (Milner et al., 2013).

In comparison with other plant species, in rice, transporters involved in uptake, xylem loading, and root-to-shoot translocation of Mn have been functionally characterized more extensively (Shao et al., 2017). The first Mn^{2+} transporter identified in rice roots was OsNRAMP5, which contributes to Mn^{2+} uptake and translocation (Sasaki et al., 2012). Further investigations showed that Mn^{2+} uptake and translocation works in conjunction with another transporter next to OsNRAMP5,

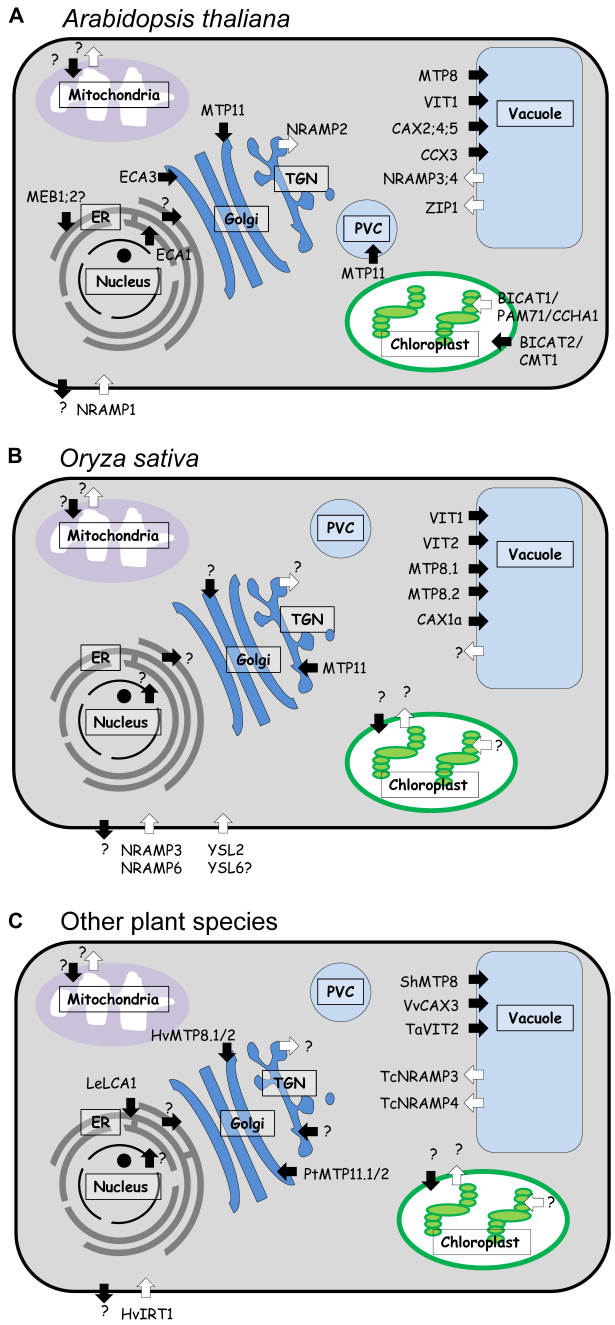

FIGURE 3 | Subcellular localization of Mn transport proteins in aerial parts of different plant species. **(A)** Arabidopsis, **(B)** rice, and **(C)** other species. White arrows represent import into the cytosol, black arrows represent export from the cytosol. Transport pathways with uncharacterized Mn transporters are indicated by a question mark. Hv, *Hordeum vulgare*; Le, *Lycopersicum esculentum* (syn. *Solanum lycopersicum*); Pt, *Populus trichocarpa*; Sh, *Stylosanthes hamata*; Ta, *Triticum aestivum*; Vv, *Vitis vinifera*.

namely OsMTP9 (Ueno et al., 2015). OsNRAMP5, localized to the plasma membrane of the distal side of the exo- and endodermis was shown to be responsible for the import of Mn^{2+} from the soil solution (**Figure 1B**). Subsequently, OsMTP9, localized to the plasma membrane of the proximal side of these cell layers, mediates the export of Mn^{2+} into the stele (Sasaki et al., 2012; Ueno et al., 2015). Knockout of either *OsMTP9* or *OsNRAMP5* significantly decreased Mn^{2+} uptake and root-to-shoot translocation, indicating that both transporters are responsible for transporting Mn^{2+} from the soil to the xylem.

Interestingly, in barley, the plasma membrane transporter HvIRT1 is implicated in the uptake and translocation of Mn^{2+}, but not Fe^{2+} (Long et al., 2018). *HvIRT1* is constitutively expressed in cells of the epidermis and in pericycle funder cells (**Figure 1C**), but under Mn deficiency, its expression is extended to the entire pericycle and the cortex. In *hvirt1* RNAi lines, a reduced shoot Mn concentration was observed without changes in Fe or Zn concentrations. Barley is characterized as a strategy II plant species that requires HvYSL transporters for the uptake of Fe^{3+} complexed with phytosiderophores (PS) (Araki et al., 2011). Therefore, the Fe transport function of HvIRT1 has become redundant because Fe is acquired via strategy II processes. Although HvIRT1 may transport Fe in yeast (Pedas et al., 2008), HvIRT1 plays actually a key role in uptake and root-to-shoot translocation of Mn rather than Fe. HvNRAMP5 is another Mn transporter localized to the plasma membranes of cells in root tips of barley (Wu et al., 2016). In contrast to *HvIRT1*, its expression is slightly upregulated by Fe deficiency, but not by Mn deficiency. Since *HvIRT1* is up-regulated by Mn deficiency and *HvNRAMP5* is constitutively expressed in roots (Wu et al., 2016), both transporters may play different roles. Therefore, it has been suggested that HvNRAMP5 may confer constitutive Mn^{2+} uptake, while HvIRT1 plays a role in Mn^{2+} uptake only under Mn-deficient conditions (Wu et al., 2016). The barley transporter HvYSL2 appears to mediate the transport of PS complexes with metals, including Mn, in the endodermis, and it may thus be involved in the transport of minerals from the cortex to the pericycle (Araki et al., 2011). However, further analyses of HvYSL2 are required to fully understand its biological role in barley.

Once Mn has been absorbed by the root, it needs to be translocated to the shoot. To date, the molecular basis of xylem loading of Mn is still unclear, and there is no clear evidence of which Mn complex is required to translocate Mn to the shoot via the xylem. Nevertheless, transporters of the YSL family may be involved in Mn translocation. In fact, during senescence, Mn concentration decreased in Arabidopsis wild type leaves, whereas no change was observed in the *ysl1ysl3* double mutant (Waters et al., 2006). Hence, it has been proposed that both AtYSL1 and AtYSL3 are putative Mn-nicotianamine (Mn^{2+}-NA) transporters, but so far, there is no direct evidence supporting this hypothesis. In rice, Mn^{2+} is transferred by OsNRAMP3 from the xylem to the phloem at the basal node, followed by its distribution to young leaves, panicles and root tips (Yamaji et al., 2013). However, at high Mn availability, Mn is distributed to mature tissues. Therefore, in rice nodes OsNRAMP3 functions as a switch for Mn distribution, whereby the protein is activated or deactivated in response to fluctuating Mn concentrations (**Figure 2B**). Moreover, a rice YSL transporter, OsYSL2, was proposed to be implicated in long-distance transport and distribution of Mn, since it may transport Mn^{2+}-NA, as well

as Fe^{2+}-NA complexes (Koike et al., 2004). Because OsYSL2 is localized in phloem companion cells, it is probably involved in phloem loading of Mn^{2+}-NA (Ishimaru et al., 2010), although its exact role in rice needs to be further investigated.

MANGANESE UPTAKE BY LEAF CELLS

As described above, a number of plasma membrane transporters involved in Mn^{2+} import into the cytosol of root cells has been characterized. In contrast, the identity of Mn^{2+} transporters in the plasma membrane of leaf cells remains largely elusive. Recently, it has been reported that OsNRAMP6, which is expressed in shoots, is localized to the plasma membrane (**Figure 3B**) and functions as Fe and Mn^{2+} transporter when expressed in yeast (Peris-Peris et al., 2017). Interestingly, OsNRAMP6 rescued, to some extent, the growth of yeast strains mutated in *SMF1* (plasma membrane Mn^{2+} transporter) or *SMF2* (Mn^{2+} transporter in intracellular vesicles) under Mn-limited conditions. In plants, OsNRAMP6 accumulated in vesicles in the vicinity of the plasma membrane. Whether these vesicles represent an anterograde or retrograde trafficking stage of OsNRAMP6, depending on the Mn^{2+} status, remains to be elucidated. Moreover, an *OsNRAMP6* knock-out plant showed enhanced resistance to infection by the rice fungus *M. oryzae* and a reduced biomass compared to wild type plants (Peris-Peris et al., 2017). Therefore, it is likely that OsNRAMP6 plays a role in regulating the Mn and/or Fe contents in infected tissues which would boost the expression of defense genes. Based on the decreased root and shoot biomass of the *nramp6* mutant under non-stress conditions, it was hypothesized that OsNRAMP6 functions as a Mn uptake transporter. Future studies are needed to establish the importance of OsNRAMP6 in cellular Mn^{2+} uptake and plant growth.

A second mechanism for Mn uptake into leaf cells of rice may be conferred by the OsYSL6 transporter, which was described to transport Mn^{2+}-NA complexes from the leaf apoplast to the symplast (Sasaki et al., 2011). *OsYSL6* is expressed in roots and shoots, particularly in older leaves. Due to the ability of OsYSL6 to increase Mn^{2+} influx when expressed in the *smf1* yeast mutant, it is likely localized in the plasma membrane (Sasaki et al., 2011). *ysl6* mutant plants accumulate high Mn concentrations in the apoplast of shoots and exhibit symptoms of Mn toxicity. Therefore, it is likely that OsYSL6 translocates Mn^{2+} from the apoplast to the symplast where it is sequestered under Mn excess. However, since its expression level remains unchanged under either Mn deficiency or excess, OsYSL6 may also act as a constitutive Mn importer in leaf cells.

INTRACELLULAR TRANSPORT OF MANGANESE

Once Mn has entered a plant cell, it must be moved to the appropriate location for the adequate supply of Mn-dependent targets or for storage. Mn is present in all cellular compartments, including ER, Golgi apparatus, mitochondria, plastids, and peroxisomes, where it performs specific cellular functions (see section Functions of Manganese in Plants), whereas vacuoles can serve as a reservoir to regulate cellular Mn homeostasis. Consequently, cells contain a plethora of transporters that are responsible for the distribution of Mn to the different compartments. **Figure 3** shows an overview of Mn transporters previously described in different plant species and their subcellular localization. To structure the description of these Mn transporters in the following sections, they are organized based on their demonstrated or putative subcellular localization.

Vacuoles as Manganese Stores

Vacuoles generally function as a primary compartment for metal internalization to avoid metal toxicity. In the case of Mn, vacuoles also serve as a temporal Mn storage pool for a proper distribution to other organelles, e.g., chloroplasts (Lanquar et al., 2010). Many transporters have been described to contribute to vacuolar Mn sequestration and unloading processes.

In the tropical legume *Stylosanthes hamata*, a plant tolerant to acidic soils in which high concentrations of plant-available Mn^{2+} can occur, the tonoplast-localized Mn transporter ShMTP8 was identified (Delhaize et al., 2003). This protein was the first characterized member of the Mn-CDF subgroup and is involved in Mn detoxification by sequestering Mn into vacuoles. Sequence analysis of *ShMTP8* showed that this protein lacks the complete N-terminal sequence and the histidine-rich loop common for members of the CDF family. When expressed in Arabidopsis, *ShMTP8* conferred tolerance to Mn toxicity (Delhaize et al., 2003). In pear and tobacco, members of the Mn-CDF subclade have also been described as Mn transporters, but their subcellular localization and relevance in Mn homeostasis is unknown (Hou et al., 2019; Liu et al., 2019). In Arabidopsis, the Mn-CDF subclade of the CDF/MTP family has four members, AtMTP8 through AtMTP11 (Montanini et al., 2007). All of them were shown to transport Mn^{2+} in yeast (Chu et al., 2017), but so far, only *AtMTP8* and *AtMTP11* have been described in more detail (**Figure 3A**). AtMTP8 was characterized as Mn^{2+} and Fe^{2+} transporter localized in the tonoplast (Eroglu et al., 2016; Chu et al., 2017; Eroglu et al., 2017). *AtMTP8* expression was specific to cells of the epidermis and the cortex in roots and strongly induced by Fe deficiency (Eroglu et al., 2016). Moreover, *mtp8* mutants showed chlorosis and critically low Fe levels in shoots on media with limited Fe availability, if Mn was present in the medium. This further demonstrated a Mn-specific role of AtMTP8 during Fe limitation, which lies in the detoxification of Mn taken up by the non-specific Fe transporter AtIRT1. In accord with a function of AtMTP8 in Mn detoxification, growth of *mtp8* mutants was impaired by high Mn, and *AtMTP8* expression was increased under excess Mn^{2+} supply (Eroglu et al., 2016). Besides its role in the Fe deficiency response, AtMTP8 plays a second role during seed development. An analysis of metal localization in the embryo by μXRF tomography showed that AtMTP8 is responsible for the specific accumulation of Mn in subepidermal cells on the abaxial side of the cotyledons and in cortical cells of the hypocotyl (Chu et al., 2017; Eroglu et al., 2017). In mutant embryos lacking the vacuolar Fe/Mn transporter AtVIT1, AtMTP8 built up Fe hotspots in those *AtMTP8*-expressing

cell types, suggesting that AtMTP8 transports Fe in addition to Mn. This was supported by complementation of the Fe-sensitive yeast strain *ccc1*. An *mtp8vit1* double mutant showed a homogeneous distribution of both metals in all cell types of the embryo, demonstrating that both are the primary transporters determining Mn and Fe allocation (Chu et al., 2017; Eroglu et al., 2017). Mn^{2+} transport and vacuolar localization were also demonstrated for MTP8 orthologs in rice (**Figure 3B**). *OsMTP8.1* was highly expressed in older leaves, and it was induced and repressed by high and low Mn^{2+} levels, respectively (Chen et al., 2013). *OsMTP8.2* was expressed in roots and shoots, and it showed lower expression levels than *OsMTP8.1* (Takemoto et al., 2017). The *mtp8.1mtp8.2* double mutant suffered from necrotic leaf blades. Since Mn concentrations were comparable to those in healthy wild type plants, it has been suggested that this phenotype was the result of an insufficient Mn sequestration in the double mutant. Unlike AtMTP8 in Arabidopsis, there is no evidence that OsMTP8.1 and OsMTP8.2 are able to transport Fe or that their transcript levels are increased upon Fe deficiency (Chen et al., 2013; Takemoto et al., 2017).

VIT proteins in plants are mainly Fe transporters (Cao, 2019). AtVIT1, the most-studied VIT transporter in Arabidopsis, was identified as a vacuolar Fe transporter that is responsible for the localization of Fe primarily to the provascular strands of the embryo in seeds (Kim et al., 2006). The ability of AtVIT1 to transport Mn^{2+} was shown by metal analysis of vacuoles from the Fe-sensitive yeast strain *ccc1* expressing *AtVIT1* (Kim et al., 2006). Interestingly, seeds of a *vit1* mutant showed a localization of Fe that coincided with the localization of Mn in the subepidermal cells on the abaxial side of the cotyledons and that was dependent on AtMTP8, as discussed above (Chu et al., 2017; Eroglu et al., 2017). VIT transporters of rice, OsVIT1 and OsVIT2, not only partially rescued the Fe^{2+}-sensitive phenotype, but also the Zn^{2+}-sensitive phenotypes of yeast mutant strains. Similar to AtVIT1, an analysis of vacuolar metal composition of these cells showed an increased accumulation of Mn (Zhang et al., 2012). Moreover, *OsVIT1* and *OsVIT2* were shown to be highly expressed in flag leaf blades and leaf sheath. Consistent with these results, decreased accumulation of Fe and Zn was observed in flag leaves of *osvit1* and *osvit2* mutants. However, both mutants showed no significant change of Mn in these tissues or in grains (Zhang et al., 2012). These results suggest that OsVIT1 and OsVIT2 may function primarily in flag leaves to mediate vacuolar sequestration of Fe and Zn. Moreover, the Fe and Zn accumulation in seeds and the decrease of those metals in flag leaves (the source organ) of *osvit1* and *osvit2* mutants indicates an indirect involvement of both gene products in translocation of both metals to sink organs, since they are only weakly expressed in embryos, which is in contrast to *AtVIT1* (Zhang et al., 2012). Finally, there are two VIT homologs in wheat, which are located to the tonoplast (**Figure 3C**), but only one of them, namely TaVIT2, was shown to complement a Mn-sensitive yeast strain, *pmr1*. TaVIT2 was also able to transport Fe^{2+} and has been employed for biofortification of wheat grains with Fe (Connorton et al., 2017).

Members of the CAX family are metal transporters that mediate efflux of cations into the vacuole (Martinoia et al., 2012). All plant CAX transporters characterized to date appear to be able to transport Ca^{2+}. Nevertheless, a broad metal substrate range, including Mn^{2+}, is a common characteristic of these proteins. Based on amino acid sequences, the plant CAX family is divided into two clusters, type 1-A and 1-B. Their capability to transport Mn^{2+} is not related to their phylogenetic association, with *AtCAX4*, *OsCAX1a*, and *VvCAX3* being members of the type 1-A subfamily and *AtCAX2*, *AtCAX5*, *OsCAX3*, and *OsCAX4* being members of the type 1-B subfamily (Martins et al., 2017). AtCAX2 transports a range of cations into the vacuole, including Mn^{2+}, Zn^{2+}, and Cd^{2+} (Koren'kov et al., 2007). Knockout analysis suggested that AtCAX2 does not play a major physiological role in Ca homeostasis, but is more important for vacuolar Mn accumulation (Pittman et al., 2004). However, vacuolar Mn^{2+} transport was not completely abolished in *cax2*. AtCAX5 is a likely candidate for this residual activity. AtCAX5 showed a lower Ca^{2+} and Mn^{2+} transport activity than AtCAX2 as also a reduced Ca^{2+} transport capacity (Edmond et al., 2009). Despite the significant sequence similarity and substrate specificity of AtCAX2 and AtCAX5, a clear distinction appeared in their expression pattern and transcriptional regulation. *AtCAX5* was expressed in all tissues of Arabidopsis seedlings, particularly in the stem and the root, and at a lower level in the leaf. In addition, there was an increase in *AtCAX5* transcripts under conditions of excess Mn, and a reduction in response to excess Zn. In contrast, *AtCAX2* was detected at fairly low levels in all tissues, but was not greatly induced by any metal (Edmond et al., 2009). The relevance of these CAX transporters in intracellular Mn homeostasis is unclear. Since only the Arabidopsis *cax2* mutant showed a growth defect under Mn deficiency (Connorton et al., 2012), future genetic analysis by using *cax2cax5* double mutant plants may uncover the physiological function of these transporters in plants.

CAX2-like transporters of other species, as tomato LeCAX2 and barley HvCAX2, transport Ca^{2+} and Mn^{2+} into yeast vacuoles upon heterologous expression, but with different transport kinetics (Edmond et al., 2009). *HvCAX2* is expressed ubiquitously in roots, shoot, immature spikes, and in seeds, preferentially in the embryo rather than the endosperm. Transcripts of *HvCAX2* increased under excess Ca^{2+} and Na^{+}. Likewise, *LeCAX2* was also expressed in roots and to a higher extend in leaves and fruits (Edmond et al., 2009).

AtCAX4 was expressed at low level in all tissues, and expression increased after Mn^{2+}, Na^{+}, and Ni^{2+} treatment (Cheng et al., 2002). Specifically, *AtCAX4* transcript levels increased in the root apex and lateral root primordia upon Mn^{2+} and Ni^{2+} treatment and decreased if Ca^{2+} was depleted. Mutation of *AtCAX4* led to an arrested growth in seedlings under excess Cd^{2+}, Mn^{2+}, and auxin (Mei et al., 2009). Previously, a link between auxin-regulated plant development, cytosolic Ca^{2+}, and kinases was described (Robert and Offringa, 2008). Therefore, these findings suggest that the *cax4* mutant may have increased cytosolic Ca^{2+} levels (because of reduced Ca^{2+} transport into the vacuole), that cause an impaired auxin gradient and altered root development (Mei et al., 2009). Alternatively, the auxin sensitivity phenotype may be a result of altered Mn homeostasis in *cax4* mutants, since Mn has an influence

on auxin responses and auxin metabolism (Mei et al., 2009). VvCAX3 is a ubiquitously expressed vacuolar transporter for both, monovalent and divalent cations in grapevine. Expression of *VvCAX3* in yeast restored the growth on media with high Na^+, Li^+, Cu^{2+}, and Mn^{2+} concentrations (Martins et al., 2017). Interestingly, expression of *VvCAX3* decreased during the development in parallel with Ca^{2+} accumulation in the fruit. It is likely that VvCAX3 is not only involved in Ca^{2+} sequestration, but also in the detoxification of trace elements and the mitigation of salt stress, since its transcript level increased under NaCl treatment (Martins et al., 2017).

Other members of the type 1-B subfamily of CAX transporters are *OsCAX3* and *OsCAX4* in rice. *OsCAX3* is expressed in all plant tissues, and the protein has a capacity to transport Mn^{2+}. Interestingly, when expressed in yeast, next to Mn tolerance *OsCAX3* also conferred Ca^{2+} tolerance, but to a lower extent compared to other OsCAX transporters. Therefore, OsCAX3, as AtCAX2, might preferentially transport Mn^{2+}, rather than Ca^{2+}, into the vacuole (Kamiya et al., 2005). Nevertheless, future work is needed to confirm its vacuolar localization. By contrast, expression of *OsCAX4* provides Mn and Cu tolerance to yeast, and *OsCAX4* transcripts were increased upon prolonged salt stress *in planta* (Yamada et al., 2014). A type 1-A transporter of rice, OsCAX1a, transports Ca^{2+} and Mn^{2+} into yeast vacuoles, but is involved mainly in Ca^{2+} homeostasis in plant cells under high concentrations of Ca^{2+} (Kamiya et al., 2006). Further analysis of the function of OsCAX1a *in planta* showed that the transcript level in roots was increased by Ca^{2+} and decreased by Mn^{2+}, Ni^{2+}, Mg^{2+}, and Cu^{2+}, while shoots showed only an increase of *OsCAX1a* transcript levels after treatment with Ca^{2+}. The decreased expression of *OsCAX1a* in response to other divalent cations might be a mechanism to keep high concentrations of cytosolic Ca^{2+} in order to protect the cell from toxic levels of ions like Mn^{2+} (Kamiya et al., 2006). Therefore, OsCAX1a may transport Ca^{2+} into the vacuole under Ca^{2+} toxicity or regulate Ca^{2+} homeostasis in the cytosol. In rice, further studies using combined mutants of *OsCAX1a*, *OsCAX3*, and *OsCAX4* are needed to confirm their relevance in plant Mn^{2+} and Ca^{2+} homeostasis.

Members of the CCX family were previously described as transporters of the CAX family. However, because they are phylogenetically closer to the mammalian plasma membrane K^+-dependent Na^+/Ca^{2+} exchangers (NCXs), this gene family, which has five members in Arabidopsis (CCX1-5), was re-classified (Pittman and Hirschi, 2016). Expression of *AtCCX3* was induced in roots and flowers upon treatment with Mn^{2+}, and in yeast the expression of *AtCCX3* complemented strains defective in Mn^{2+} export (Morris et al., 2008). Tobacco cells expressing *AtCCX3* showed enhanced Mn levels, further suggesting an ability of AtCCX3 to transport Mn^{2+}. The transcript level of *AtCCX3* increased in plants upon a treatment with Na^+, K^+, and Mn^{2+}, albeit a mutation in *AtCCX3* provoked no discernible growth abnormalities under those conditions (Morris et al., 2008).

The genome of Arabidopsis contains six genes encoding NRAMP transporters, whereby AtNRAMP3 and AtNRAMP4 have been localized to the tonoplast (Thomine et al., 2003; Lanquar et al., 2005). The NRAMP homologs TcNRAMP3 and TcNRAMP4 from *Thlaspi caerulescens* were also localized to the tonoplast (Oomen et al., 2009). These NRAMP transporters from both species are involved in the transport of Cd^{2+}, Fe^{2+}, and Mn^{2+} (Thomine et al., 2000; Oomen et al., 2009; Pottier et al., 2015). In addition, AtNRAMP4 and TcNRAMP4 also transport Zn^{2+} when expressed in yeast (Lanquar et al., 2004; Oomen et al., 2009; Pottier et al., 2015). AtNRAMP3 and AtNRAMP4 protein levels in leaves were unaffected by Mn deficiency, but expression of *AtNRAMP4* was induced under Fe-limited conditions (Lanquar et al., 2010). Both proteins were shown to be responsible for the retrieval of Fe from vacuoles during seed germination and to mediate the export of vacuolar Mn in photosynthetic tissues of adult plants (Lanquar et al., 2005, 2010). The *nramp3nramp4* double mutant had comparable Mn concentrations in leaf mesophyll cells as wild type plants, but it showed a strong accumulation of Mn in the vacuoles (Lanquar et al., 2010). Under Mn deficiency, the double mutant showed a decreased growth which was correlated with reduced photosynthetic activity as a consequence of a shortage of Mn for the formation of OEC complexes in PSII. In contrast, *nramp3nramp4* did not show altered mitochondrial MnSOD activity under Mn deficiency (Lanquar et al., 2010). These results suggest an important role for AtNRAMP3/AtNRAMP4-dependent Mn transit through the vacuole prior to the import into chloroplasts of mesophyll cells.

Manganese Accumulation in Chloroplasts

Mn plays an extremely important role in chloroplast function, as it is essential for photosynthetic activity. There is a high demand for Mn in the photosynthetic apparatus, mainly for the formation of the Mn_4Ca -cluster in the OEC of PSII, which is essential for water splitting. In spite of the importance of Mn for chloroplast function, only recent studies have reported the identification and characterization of Mn transporters in chloroplast membranes. Two members of the BICAT family, which are related to the GDT1 protein in yeast (Demaegd et al., 2013) and the Mnx protein in the cyanobacterium *Synechocystis* (Brandenburg et al., 2017), are involved in Mn loading of the chloroplast and the distribution within this organelle (**Figure 3A**).

The Arabidopsis AtBICAT1 (syn. PAM71, CCHA1) protein is localized in the thylakoid membrane and transports Ca^{2+} and Mn^{2+} into the thylakoid lumen (Schneider et al., 2016; Wang et al., 2016; Frank et al., 2019). AtBICAT1 complemented the Mn-sensitive phenotype of the *pmr1* yeast mutant and mediated Ca^{2+} influx upon expression in *E. coli*. *bicat1* knockout mutants showed slightly pale green leaves along with compromised growth. Interestingly, growth retardation and photosynthetic activity of *bicat1* could be partially restored by exogenous treatment with Mn^{2+} (Schneider et al., 2016). In addition, transient elevations of the stromal free Ca^{2+} concentration, induced by a light-to-dark shift, were increased in *bicat1* mutants (Frank et al., 2019). Based on these findings, AtBICAT1

presumably functions in Mn^{2+} and Ca^{2+} flux into thylakoids for assembly of the Mn_4Ca-cluster, and also in the homeostasis of stromal Ca^{2+}, which regulates numerous processes in chloroplasts (Sello et al., 2018).

AtBICAT2 (syn. PAM71HL, CMT1), the second member of this family, was also described to fulfill functions in chloroplast Mn and Ca^{2+} homeostasis (Eisenhut et al., 2018; Frank et al., 2019). In contrast to AtBICAT1, it resides in the chloroplast envelope. Like *AtBICAT1*, the expression of *AtBICAT2* can also alleviate the Mn^{2+} and Ca^{2+} sensitivity phenotypes of the *pmr1* and *pmr1gdt1* yeast mutants, respectively. Disruption of *AtBICAT2* resulted in strong chlorosis, severely impaired plant growth, defective thylakoid stacking, and severe reduction of PS II complexes, resulting in diminished photosynthetic activity (Eisenhut et al., 2018; Frank et al., 2019). Consistent with a reduced oxygen evolution capacity, *bicat2* mutant chloroplasts contained less Mn than those of the wild type (Zhang et al., 2018). Also, mutants were defective in Ca^{2+} uptake across the chloroplast envelope and showed a strongly dampened dark-induced Ca^{2+} signal in the stroma (Frank et al., 2019). As consequence, the disruption of *AtBICAT2* should also lead to a decreased Ca^{2+} import into the thylakoid lumen. Taken together, these results indicate that AtBICAT2 functions as an inner envelope transporter responsible for chloroplast Mn^{2+} and Ca^{2+} uptake. Ca^{2+} dynamics and Mn concentrations in both, stroma and lumen, were likely diminished in *bicat2* mutants, which may explain the stronger phenotype compared to that of *bicat1* mutants. The phenotype of *bicat1bicat2* double mutants suggest that *AtBICAT2* is the limiting step in Mn^{2+} and Ca^{2+} delivery to the chloroplast. Further work is needed to unravel the bi-functionality and regulation of BICATs in Ca^{2+} and Mn^{2+} homeostasis in chloroplasts.

Manganese Transport Proteins in Endomembranes

The Arabidopsis CDF protein AtMTP11 was shown to exhibit an important role in Mn detoxification. The promoter of *AtMTP11* had a high activity in root tips, shoot margins, and hydathodes, but not in epidermal cells and trichomes. Expression of *AtMTP11* in yeast complemented the Mn^{2+} hypersensitivity of the *pmr1* mutant (Peiter et al., 2007). In Arabidopsis, *mtp11* mutants were hypersensitive to elevated Mn^{2+} levels, whereas *AtMTP11*-overexpressing lines were hypertolerant (Delhaize et al., 2007; Peiter et al., 2007). As AtMTP11 appeared to be localized to the prevacuolar compartment (PVC) or to the Golgi apparatus (**Figure 3A**), it was suggested that it functions in the accumulation of excess Mn either into vacuoles via the PVC or in the secretion to the apoplastic space via vesicle-mediated exocytosis (Delhaize et al., 2007; Peiter et al., 2007). The latter pathway was supported by increased Mn concentrations in *mtp11* mutants (Peiter et al., 2007). Two poplar homologs of this protein, PtMTP11.1 and PtMTP11.2, were also able to complement the Mn-sensitive yeast mutant *pmr1* and targeted to the same Golgi compartments as AtMTP11 (**Figure 3C**; Peiter et al., 2007). Those genes are therefore likely to function in a similar way. Another MTP11 ortholog in rice, OsMTP11, was also described to be involved in Mn detoxification. *OsMTP11* is induced by high Mn and expressed specifically in conducting tissues (Zhang and Liu, 2017). Interestingly, epigenetic mechanisms (e.g., DNA methylation) were a major factor regulating the expression level of *OsMTP11* (Zhang and Liu, 2017). Knockdown of *OsMTP11* resulted in growth inhibition in the presence of high concentrations of Mn^{2+} and also led to increased accumulation of Mn in shoots and roots. By contrast, the overexpression of *OsMTP11* enhanced Mn tolerance of rice and decreased the accumulation of Mn in shoots and roots (Ma et al., 2018). Stable expression of *OsMTP11-GFP* in Arabidopsis and transient expression of this construct in rice and tobacco protoplasts showed that OsMTP11 was also located to the Golgi (**Figure 3B**; Farthing et al., 2017). However, recent studies suggested that OsMTP11 localized to the trans-Golgi network (TGN) when it was expressed in rice protoplasts and tobacco epidermal cells (Ma et al., 2018). Surprisingly, in tobacco epidermal cells, OsMTP11 relocalized to the plasma membrane upon treatment with high extracellular Mn^{2+} concentrations. These findings suggest that OsMTP11 is required for Mn homeostasis and contributes to Mn^{2+} tolerance in rice (Ma et al., 2018).

In the sugar beet relative *B. vulgaris* spp. *maritima*, the MTP11 homologs BmMTP10 and BmMTP11 were also characterized as Mn^{2+} transporters by complementation of the *pmr1* yeast strain (Erbasol et al., 2013). In barley, transient expression in onion epidermal cells showed that the HvMTP8.1 and HvMTP8.2 proteins, which are most closely related to the vacuolar AtMTP8 (see section Vacuoles as Manganese Stores), were localized to the Golgi apparatus and also complemented the *pmr1* strain (Pedas et al., 2014). However, the function of those CDF proteins *in planta* is still unclear.

The Arabidopsis genome encodes 15 P-type Ca^{2+}-ATPases, of which the P_{2A} -type or ECA (ER-type Calcium ATPase) subfamily has two members involved in endomembrane Mn^{2+} transport (Kamrul Huda et al., 2013). AtECA1 and AtECA3 both function as a pump for Ca^{2+} and Mn^{2+}, and localize to the ER and Golgi apparatus, respectively (**Figure 3A**). Furthermore, AtECA3 was shown to be localized also in subpopulations of endosomes or PVC (Li et al., 2008). *AtECA1* and *AtECA3* expression in the K616 yeast mutant, defective in the Golgi Ca^{2+} and Mn^{2+} pump PMR1 and in the vacuolar Ca^{2+} pump PMC1, increased its tolerance to toxic levels of Mn^{2+} and to Ca^{2+} deficiency (Liang et al., 1997; Wu et al., 2002; Mills et al., 2007). Another ER-localized ECA transporter in tomato, LCA1, also complemented the growth of K616 yeast under conditions of high Mn^{2+} and low Ca^{2+} (Johnson et al., 2009). *eca1* mutants of Arabidopsis showed impaired growth under Ca^{2+} deprivation and Mn^{2+} excess. On high-Mn^{2+} media, root hair elongation was inhibited in the mutants, suggesting an impairment in tip growth (Wu et al., 2002). Taken together, AtECA1 and LeLCA1 are likely involved in the transport of Ca^{2+} and Mn^{2+} from the cytosol into the ER. On the other hand, *eca3* was shown to be sensitive to Mn deficiency and also to Mn toxicity, but not to Ca^{2+} deficiency (Mills et al., 2007; Li et al., 2008). Thus, the phenotype of *eca3*, observed under Mn-deficient conditions, may be due

to a reduction of the Mn content in the Golgi. Based on these studies, CDF and ECA proteins may be responsible for Mn^{2+} loading of Golgi-related vesicular compartments, for delivering Mn to Mn-dependent enzymes and/or for detoxification of Mn via a secretory pathway.

In Arabidopsis, AtNRAMP2 is located in the TGN (**Figure 3A**) and was shown to be involved in the intracellular allocation of Mn (Alejandro et al., 2017; Gao et al., 2018). *AtNRAMP2* is mainly expressed in the vasculature of roots and shoots and was barely induced upon Mn deficiency. Nevertheless, *nramp2* mutants showed a hypersensitivity to Mn deficiency and a reduction in Mn contents in vacuoles and chloroplasts with an accompanying reduction in PSII activity under those conditions (Alejandro et al., 2017). Surprisingly, the *nramp2nramp3nramp4* triple mutant did not exhibit higher sensitivity to Mn deficiency than the single *nramp2* and double *nramp3nramp4* mutants (Alejandro et al., 2017). This suggests that the three transporters act in the same pathway to deliver Mn to the chloroplasts.

NRAMP transporters from tomato (LeNRAMP1 and LeNRAMP3) and apple (MbNRAMP1) were also able to transport Mn^{2+} and located to intracellular vesicles when expressed in yeast cells, but their function in Mn homeostasis is still unclear (Bereczky et al., 2003; Xiao et al., 2008).

ER bodies are fusiform compartments connected to the ER that were found specifically in Brassicales (Matsushima et al., 2003). It has been proposed that ER bodies might play a role in the defense against pathogens and herbivores (Yamada et al., 2011). In Arabidopsis, two VIT transporters, AtMEB1 (Membrane protein of Endoplasmic reticulum Body) and AtMEB2, that localize to the ER body membrane but not to the ER network, have been identified (Yamada et al., 2013). Heterologous expression of *AtMEB1* and *AtMEB2* in yeast suppressed Fe and Mn toxicity, suggesting that they possibly act as metal transporters. ER bodies are present in hypocotyls of seedlings where they disappear during plant development. In contrast, in roots, ER bodies are constitutively present. Therefore, it has been suggested that MEB transporters may be involved in the sequestration of metals into root ER bodies under metal stress conditions (Yamada et al., 2013).

Manganese Homeostasis in Other Organelles

In mitochondria, Mn is crucial for the activity of MnSOD which scavenges ROS generated within the citric acid cycle and the electron transport chain. However, the transport mechanisms for Mn^{2+} in plant mitochondria still remain to be elucidated. To date, no transporter involved in Mn^{2+} transport to and from plant mitochondria has been characterized. Nevertheless, in humans, a mitochondrial Ca^{2+} uniporter (MCU) that is responsible for Ca^{2+} and Mn^{2+} loading into the mitochondria has been described (Kirichok et al., 2004). Arabidopsis has six MCU isoforms which are predicted to be localized in mitochondria, except one, cMCU, that is targeted to the chloroplast (Stael et al., 2012). The cMCU protein mediates Ca^{2+} fluxes across the chloroplast envelope (Teardo et al., 2019). In humans, MCU is part of a complex named MCUC (MCU complex) which includes other subunits, including the EF hand-containing proteins MICU1 and MICU2 (Ca^{2+}-sensing inhibitory subunit). MICU1 plays a decisive role in ion specificity of MCU, allowing it to distinguish between Ca^{2+} vs. Mn^{2+} (Kamer et al., 2018). In Arabidopsis, a MICU homolog, AtMICU, that binds Ca^{2+} and localizes to the mitochondria, was described (Wagner et al., 2015). These findings provoke the idea that a conserved uniporter system, similar to MCUC in humans, may mediate Ca^{2+} and Mn^{2+} uptake by plant mitochondria.

In peroxisomes, Mn is important as a cofactor of the peroxisomal MnSOD. This enzyme is present in some plant species, including pea, cucumber, and pepper (Corpas et al., 2017). However, so far, transporters to load Mn into the peroxisomes are still missing.

CONCLUSION AND PERSPECTIVES

The relevance of manganese as a micronutrient of plants is still largely underestimated. For a long time, the accepted dogma among animal and plant biologists has been that the physiological requirement for Mn by living cells is low and that Mn uptake exceeds the requirement. However, in natural and in agricultural settings, Mn availability can be a seriously limiting factor for plant growth, which necessitates the operation of high-affinity Mn transporters in roots and efficient mechanisms of Mn distribution in the plant to cope with Mn shortage. Crops with improved Mn uptake capacity and Mn use efficiency will achieve higher growth and yield under suboptimal Mn availability, primarily by providing sufficient Mn to PSII and thus increasing their photosynthetic efficiency.

There are many unresolved issues in our understanding of Mn transport and homeostasis, such as the transport of Mn into the xylem – Is it mediated by a vesicle-based secretory mechanism or by plasma membrane-bound exporters? How Mn is imported by different cell types in the shoot is another open question. Most Mn^{2+} transporters are not specific, but also able to move other divalent cations, like Ca^{2+}, Fe^{2+}, Zn^{2+}, or Cu^{2+}, but so far it is still unclear if and how they discriminate between the cations. In humans, the substrate selectivity of a mitochondrial Mn transporter is altered by interacting EF hand proteins (Kamer et al., 2018). In this respect, the ability of diverse Ca^{2+} transport proteins to also permeate Mn^{2+} (or vice versa) is particular interesting. The possibility that Ca^{2+} and Mn^{2+} share transport pathways mediated by ECAs, BICATs, CAXs, and Ca^{2+} channels, implies an interference of Mn^{2+} in Ca^{2+} signaling. In fact, Mn^{2+} has been demonstrated to act as a signaling agent *per se* in humans (Wang et al., 2018).

The sensing and signaling of the plant's Mn status is another area yet to be explored: On which level is Mn transport activity regulated by the nutritional status of the plant? This review pointed out some transcriptional changes of Mn transporter-encoding genes under Mn-toxic and Mn-deficient conditions, but the signaling networks that underlie these changes are still missing. Furthermore, a

recent systems-wide analysis indicated that Mn deficiency responses are primarily regulated at the posttranscriptional level (Rodríguez-Celma et al., 2016). Moreover, our understanding of how Mn transport proteins are regulated is very rudimentary. In this respect, a couple of proteins that regulate the subcellular localization of AtNRAMP1 have been identified, revealing links to inositol phosphate and choline homeostasis (Agorio et al., 2017; Gao et al., 2017). As another fascinating case, it has been demonstrated that phosphorylation, ubiquitination, and metal binding modify the stability and localization of AtIRT1, an Fe^{2+} transporter that contributes to the uptake of Mn^{2+} (Dubeaux et al., 2018). However, for the vast majority of Mn transporters, posttranslational modifications and protein-protein interactions are unknown.

Future research has to be focused on all these fundamental aspects. The function, regulation, and co-operation of Mn^{2+} transport proteins in different plant tissues upon Mn deficiency and excess ought to be understood at transcriptional and at protein level. Such studies will eventually elucidate the mechanisms controlling Mn acquisition, subcellular compartmentation, and homeostasis in plants, a knowledge that can be harnessed to develop Mn-efficient germplasm of staple crops.

AUTHOR CONTRIBUTIONS

SA, SH, and BM drafted the manuscript. SA, SH, BM, and EP finalized the manuscript, approved the final version of the manuscript, and agreed to be accountable for all aspects of the work.

FUNDING

This work was supported by the European Regional Development Fund (ERDF) within the State Research Focus Program "Molecular Biosciences as a Motor for a Knowledge-Based Economy" (Grant No. ZS/2016/06/79740 to EP). We acknowledge the financial support within the funding program Open Access Publishing by the German Research Foundation (DFG).

REFERENCES

Agorio, A., Giraudat, J., Bianchi, M. W., Marion, J., Espagne, C., Castaings, L., et al. (2017). Phosphatidylinositol 3-phosphate–binding protein AtPH1 controls the localization of the metal transporter NRAMP1 in *Arabidopsis*. *Proc. Natl. Acad. Sci. U.S.A.* 114, E3354–E3363. doi: 10.1073/pnas.1702975114

Alam, S., Akiha, F., Kamei, S., Huq, S. M. I., and Kawai, S. (2005). Mechanism of potassium alleviation of manganese phytotoxicity in barley. *J. Plant Nutr.* 28, 889–901. doi: 10.1081/pln-200055572

Alejandro, S., Cailliatte, R., Alcon, C., Dirick, L., Domergue, F., Correia, D., et al. (2017). Intracellular distribution of manganese by the trans-Golgi network transporter NRAMP2 is critical for photosynthesis and cellular redox homeostasis. *Plant Cell* 29, 3068–3084. doi: 10.1105/tpc.17.00578

Allen, M. D., Kropat, J., Tottey, S., Del Campo, J. A., and Merchant, S. S. (2007). Manganese deficiency in *Chlamydomonas* results in loss of photosystem II and MnSOD function, sensitivity to peroxides, and secondary phosphorus and iron deficiency. *Plant Physiol.* 143, 263–277. doi: 10.1104/pp.106.088609

Amao, Y., and Ohashi, A. (2008). Effect of Mn ion on the visible light induced water oxidation activity of photosynthetic organ grana from spinach. *Catal. Commun.* 10, 217–220. doi: 10.1016/j.catcom.2008.08.022

Andresen, E., Peiter, E., and Küpper, H. (2018). Trace metal metabolism in plants. *J. Exp. Bot.* 69, 909–954. doi: 10.1093/jxb/erx465

Araki, R., Murata, J., and Murata, Y. (2011). A novel barley yellow stripe 1-like transporter (HvYSL2) localized to the root endodermis transports metal-phytosiderophore complexes. *Plant Cell Physiol.* 52, 1931–1940. doi: 10.1093/pcp/pcr126

Baldisserotto, C., Ferroni, L., Anfuso, E., Pagnoni, A., Fasulo, M. P., and Pancaldi, S. (2007). Responses of *Trapa natans* L. floating laminae to high concentrations of manganese. *Protoplasma* 231, 65–82. doi: 10.1007/s00709-007-0242-2

Basu, D., Tian, L., Wang, W., Bobbs, S., Herock, H., Travers, A., et al. (2015). A small multigene hydroxyproline-*O*-galactosyltransferase family functions in arabinogalactan-protein glycosylation, growth and development in Arabidopsis. *BMC Plant Biol.* 15:295. doi: 10.1186/s12870-015-0670-7

Bereczky, Z., Wang, H. Y., Schubert, V., Ganal, M., and Bauer, P. (2003). Differential regulation of *nramp* and *irt* metal transporter genes in wild type and iron uptake mutants of tomato. *J. Biol. Chem.* 278, 24697–24704. doi: 10.1074/jbc.m301365200

Blamey, F. P. C., Hernandez-Soriano, M., Cheng, M., Tang, C., Paterson, D., Lombi, E., et al. (2015). Synchrotron-based techniques shed light on mechanisms of plant sensitivity and tolerance to high manganese in the root environment. *Plant Physiol.* 169, 2006–2020. doi: 10.1104/pp.15.00726

Bloom, A. J. (2019). Metal regulation of metabolism. *Curr. Opin. Chem. Biol.* 49, 33–38. doi: 10.1016/j.cbpa.2018.09.017

Bloom, A. J., and Lancaster, K. M. (2018). Manganese binding to Rubisco could drive a photorespiratory pathway that increases the energy efficiency of photosynthesis. *Nat. Plants* 4, 414–422. doi: 10.1038/s41477-018-0191-0

Bondarava, N., Un, S., and Krieger-Liszkay, A. (2007). Manganese binding to the 23 kDa extrinsic protein of photosystem II. *Biochim. Biophys. Acta Bioenerg.* 1767, 583–588. doi: 10.1016/j.bbabio.2007.01.001

Bowler, C., Van Camp, W., Van Montagu, M., Inzé, D., and Asada, K. (1994). Superoxide dismutase in plants. *Crit. Rev. Plant Sci.* 13, 199–218.

Brandenburg, F., Schoffman, H., Kurz, S., Krämer, U., Keren, N., Weber, A. P. M., et al. (2017). The *Synechocystis* manganese exporter Mnx is essential for manganese homeostasis in cyanobacteria. *Plant Physiol.* 173, 1798–1810. doi: 10.1104/pp.16.01895

Bricker, T. M., Roose, J. L., Fagerlund, R. D., Frankel, L. K., and Eaton-Rye, J. J. (2012). The extrinsic proteins of Photosystem II. *Biochim. Biophys. Acta Bioenerg.* 1817, 121–142.

Broadley, M., Brown, P., Cakmak, I., Rengel, Z., and Zhao, F. (2012). "Function of nutrients: micronutrients," in *Marschner's Mineral Nutrition of Higher Plants*, 3rd Edn, ed. P. Marschner (Oxford: Elsevier), 191–249.

Burnell, J. N. (1988). "The biochemistry of manganese in plants," in *Manganese in Soils and Plants*, eds R. D. Graham, R. J. Hannam, and N. C. Uren (Dordrecht: Springer), 125–137.

Cailliatte, R., Schikora, A., Briat, J.-F., Mari, S., and Curie, C. (2010). High-affinity manganese uptake by the metal transporter NRAMP1 is essential for Arabidopsis growth in low manganese conditions. *Plant Cell* 22, 904–917. doi: 10.1105/tpc.109.073023

Cao, F. Q., Werner, A. K., Dahncke, K., Romeis, T., Liu, L. H., and Witte, C. P. (2010). Identification and characterization of proteins involved in rice urea and arginine catabolism. *Plant Physiol.* 154, 98–108. doi: 10.1104/pp.110.160929

Cao, J. (2019). Molecular evolution of the vacuolar iron transporter (VIT) family genes in 14 plant species. *Genes* 10:144. doi: 10.3390/genes10020144

Castaings, L., Caquot, A., Loubet, S., and Curie, C. (2016). The high-affinity metal transporters NRAMP1 and IRT1 team up to take up iron under sufficient metal provision. *Sci. Rep.* 6, 37222–37222. doi: 10.1038/srep37222

Chen, Z., Fujii, Y., Yamaji, N., Masuda, S., Takemoto, Y., Kamiya, T., et al. (2013). Mn tolerance in rice is mediated by MTP8.1, a member of the cation diffusion facilitator family. *J. Exp. Bot.* 64, 4375–4387. doi: 10.1093/jxb/ert243

Cheng, N.-H., Pittman, J. K., Shigaki, T., and Hirschi, K. D. (2002). Characterization of CAX4, an Arabidopsis H^+ /cation antiporter. *Plant Physiol.* 128, 1245–1254. doi: 10.1104/pp.010857

Chereskin, B. M., and Castelfranco, P. A. (1982). Effects of iron and oxygen on chlorophyll biosynthesis. *Plant Physiol.* 69, 112–116. doi: 10.1104/pp.69.1.112

Chu, H.-H., Car, S., Socha, A. L., Hindt, M. N., Punshon, T., and Guerinot, M. L. (2017). The *Arabidopsis* MTP8 transporter determines the localization of manganese and iron in seeds. *Sci. Rep.* 7, 11024–11024. doi: 10.1038/s41598-017-11250-9

Clairmont, K. B., Hagar, W. G., and Davis, E. A. (1986). Manganese toxicity to chlorophyll synthesis in tobacco callus. *Plant Physiol.* 80, 291–293. doi: 10.1104/pp.80.1.291

Collin, S., Justin, A. M., Cantrel, C., Arondel, V., and Kader, J. C. (1999). Identification of AtPIS, a phosphatidylinositol synthase from *Arabidopsis*. *Eur. J. Biochem.* 262, 652–658. doi: 10.1046/j.1432-1327.1999.00378.x

Connorton, J. M., Jones, E. R., Rodríguez-Ramiro, I., Fairweather-Tait, S., Uauy, C., and Balk, J. (2017). Wheat vacuolar iron transporter TaVIT2 transports Fe and Mn and is effective for biofortification. *Plant Physiol.* 174, 2434–2444. doi: 10.1104/pp.17.00672

Connorton, J. M., Webster, R. E., Cheng, N., and Pittman, J. K. (2012). Knockout of multiple *Arabidopsis* cation/H^+ exchangers suggests isoform-specific roles in metal stress response, germination and seed mineral nutrition. *PLoS One* 7:e47455. doi: 10.1371/journal.pone.0047455

Cornah, J. E., Roper, J. M., Singh, D. P., and Smith, A. G. (2002). Measurement of ferrochelatase activity using a novel assay suggests that plastids are the major site of haem biosynthesis in both photosynthetic and non-photosynthetic cells of pea (*Pisum sativum* L.). *Biochem. J.* 362, 423–432. doi: 10.1042/bj3620423

Corpas, F. J., Barroso, J. B., Palma, J. M., and Rodriguez-Ruiz, M. (2017). Plant peroxisomes: a nitro-oxidative cocktail. *Redox Biol.* 11, 535–542. doi: 10.1016/j.redox.2016.12.033

Curie, C., Alonso, J. M., Le Jean, M., Ecker, J. R., and Briat, J.-F. (2000). Involvement of NRAMP1 from *Arabidopsis thaliana* in iron transport. *Biochem. J.* 347:749. doi: 10.1042/0264-6021:3470749

Delhaize, E., Gruber, B. D., Pittman, J. K., White, R. G., Leung, H., Miao, Y., et al. (2007). A role for the *AtMTP11* gene of Arabidopsis in manganese transport and tolerance. *Plant J.* 51, 198–210. doi: 10.1111/j.1365-313x.2007.03138.x

Delhaize, E., Kataoka, T., Hebb, D. M., White, R. G., and Ryan, P. R. (2003). Genes encoding proteins of the cation diffusion facilitator family that confer manganese tolerance. *Plant Cell* 15, 1131–1142. doi: 10.1105/tpc.009134

Demaegd, D., Colinet, A. S., Deschamps, A., and Morsomme, P. (2014). Molecular evolution of a novel family of putative calcium transporters. *PLoS One* 9:e100851. doi: 10.1371/journal.pone.0100851

Demaegd, D., Foulquier, F., Colinet, A. S., Gremillon, L., Legrand, D., Mariot, P., et al. (2013). Newly characterized Golgi-localized family of proteins is involved in calcium and pH homeostasis in yeast and human cells. *Proc. Natl. Acad. Sci. U.S.A.* 110, 6859–6864. doi: 10.1073/pnas.1219871110

Doncheva, S., Poschenrieder, C., Stoyanova, Z., Georgieva, K., Velichkova, M., and Barceló, J. (2009). Silicon amelioration of manganese toxicity in Mn-sensitive and Mn-tolerant maize varieties. *Environ. Exp. Bot.* 65, 189–197. doi: 10.1016/j.envexpbot.2008.11.006

Dou, C. M., Fu, X. P., Chen, X. C., Shi, J. Y., and Chen, Y. X. (2009). Accumulation and detoxification of manganese in hyperaccumulator *Phytolacca americana*. *Plant Biol.* 11, 664–670. doi: 10.1111/j.1438-8677.2008.00163.x

Dubeaux, G., Neveu, J., Zelazny, E., and Vert, G. (2018). Metal sensing by the IRT1 transporter-receptor orchestrates its own degradation and plant metal nutrition. *Mol. Cell* 69, 953–964. doi: 10.1016/j.molcel.2018.02.009

Dučić, T., and Polle, A. (2007). Manganese toxicity in two varieties of Douglas fir (*Pseudotsuga menziesii* var. *viridis* and *glauca*) seedlings as affected by phosphorus supply. *Funct. Plant Biol.* 34, 31–40.

Eckhardt, U., Mas Marques, A., and Buckhout, T. J. (2001). Two iron-regulated cation transporters from tomato complement metal uptake-deficient yeast mutants. *Plant Mol. Biol.* 45, 437–448.

Edmond, C., Shigaki, T., Ewert, S., Nelson, M. D., Connorton, J. M., Chalova, V., et al. (2009). Comparative analysis of CAX2-like cation transporters indicates functional and regulatory diversity. *Biochem. J.* 418, 145–154. doi: 10.1042/BJ20081814

Egelund, J., Petersen, B. L., Motawia, M. S., Damager, I., Faik, A., Olsen, C. E., et al. (2006). *Arabidopsis thaliana* RGXT1 and RGXT2 encode Golgi-localized (1,3)-alpha-D-xylosyltransferases involved in the synthesis of pectic rhamnogalacturonan-II. *Plant Cell* 18, 2593–2607. doi: 10.1105/tpc.105.036566

Eisenhut, M., Hoecker, N., Schmidt, S. B., Basgaran, R. M., Flachbart, S., Jahns, P., et al. (2018). The plastid envelope CHLOROPLAST MANGANESE TRANSPORTER1 is essential for manganese homeostasis in *Arabidopsis*. *Mol. Plant* 11, 955–969. doi: 10.1016/j.molp.2018.04.008

Emsley, J. (2003). *Nature's Building Blocks: An A-Z Guide to the Elements*. Oxford: Oxford University Press.

Engelsma, G. (1972). A possible role of divalent manganese ions in the photoinduction of phenylalanine ammonia-lyase. *Plant Physiol.* 50, 599–602. doi: 10.1104/pp.50.5.599

Erbasol, I., Bozdag, G. O., Koc, A., Pedas, P., and Karakaya, H. C. (2013). Characterization of two genes encoding metal tolerance proteins from *Beta vulgaris* subspecies *maritima* that confers manganese tolerance in yeast. *Biometals* 26, 795–804. doi: 10.1007/s10534-013-9658-7

Eroglu, S., Giehl, R. F. H., Meier, B., Takahashi, M., Terada, Y., Ignatyev, K., et al. (2017). Metal tolerance protein 8 mediates manganese homeostasis and iron reallocation during seed development and germination. *Plant Physiol.* 174, 1633–1647. doi: 10.1104/pp.16.01646

Eroglu, S., Meier, B., von Wirén, N., and Peiter, E. (2016). The vacuolar manganese transporter MTP8 determines tolerance to iron deficiency-induced chlorosis in Arabidopsis. *Plant Physiol.* 170, 1030–1045. doi: 10.1104/pp.15.01194

Farthing, E. C., Menguer, P. K., Fett, J. P., and Williams, L. E. (2017). OsMTP11 is localised at the Golgi and contributes to Mn tolerance. *Sci. Rep.* 7:15258. doi: 10.1038/s41598-017-15324-6

Farzadfar, S., Zarinkamar, F., and Hojati, M. (2017). Magnesium and manganese affect photosynthesis, essential oil composition and phenolic compounds of *Tanacetum parthenium*. *Plant Physiol. Biochem.* 112, 207–217. doi: 10.1016/j.plaphy.2017.01.002

Fecht-Christoffers, M. M., Führs, H., Braun, H. P., and Horst, W. J. (2006). The role of hydrogen peroxide-producing and hydrogen peroxide-consuming peroxidases in the leaf apoplast of cowpea in manganese tolerance. *Plant Physiol.* 140, 1451–1463. doi: 10.1104/pp.105.070474

Fernando, D. R., Bakkaus, E. J., Perrier, N., Baker, A. J., Woodrow, I. E., Batianoff, G. N., et al. (2006a). Manganese accumulation in the leaf mesophyll of four tree species: a PIXE/EDAX localization study. *New Phytol.* 171, 751–758. doi: 10.1111/j.1469-8137.2006.01783.x

Fernando, D. R., Batianoff, G. N., Baker, A. J., and Woodrow, I. E. (2006b). In vivo localization of manganese in the hyperaccumulator *Gossia bidwillii* (Benth.) N. Snow & Guymer (Myrtaceae) by cryo-SEM/EDAX. *Plant Cell Environ.* 29, 1012–1020. doi: 10.1111/j.1365-3040.2006.01498.x

Fernando, D. R., and Lynch, J. P. (2015). Manganese phytotoxicity: new light on an old problem. *Annals Bot.* 116, 313–319. doi: 10.1093/aob/mcv111

Fernando, D. R., Mizuno, T., and Woodrow, I. E. (2010). Characterization of foliar manganese (Mn) in Mn (hyper) accumulators using X−ray absorption spectroscopy. *New Phytol.* 188, 1014–1027. doi: 10.1111/j.1469-8137.2010.03431.x

Ferrandon, M., and Chamel, A. R. (1988). Cuticular retention, foliar absorption and translocation of Fe, Mn and Zn supplied in organic and inorganic form. *J. Plant Nutr.* 11, 247–263. doi: 10.1080/01904168809363800

Frank, J., Happeck, R., Meier, B., Hoang, M. T. T., Stribny, J., Hause, G., et al. (2019). Chloroplast-localized BICAT proteins shape stromal calcium signals and are required for efficient photosynthesis. *New Phytol.* 221, 866–880. doi: 10.1111/nph.15407

Fu, X.-Z., Zhou, X., Xing, F., Ling, L.-L., Chun, C.-P., Cao, L., et al. (2017). Genome-wide identification, cloning and functional analysis of the Zinc/Iron-Regulated Transporter-Like Protein (ZIP) gene family in trifoliate orange (*Poncirus trifoliata* L. *Raf.*). *Front. Plant Sci.* 8:588. doi: 10.3389/fpls.2017.00588

Führs, H., Behrens, C., Gallien, S., Heintz, D., Van Dorsselaer, A., Braun, H. P., et al. (2010). Physiological and proteomic characterization of manganese sensitivity and tolerance in rice (*Oryza sativa*) in comparison with barley (*Hordeum vulgare*). *Ann. Bot.* 105, 1129–1140. doi: 10.1093/aob/mcq046

Gao, H., Xie, W., Yang, C., Xu, J., Li, J., Wang, H., et al. (2018). NRAMP2, a trans-Golgi network-localized manganese transporter, is required for *Arabidopsis* root growth under manganese deficiency. *New Phytol.* 217, 179–193. doi: 10.1111/nph.14783

Gao, Y. Q., Chen, J. G., Chen, Z. R., An, D., Lv, Q. Y., Han, M. L., et al. (2017). A new vesicle trafficking regulator CTL1 plays a crucial role in ion homeostasis. *PLoS Biol.* 15:e2002978. doi: 10.1371/journal.pbio.2002978

George, T. S., French, A. S., Brown, L. K., Karley, A. J., White, P. J., Ramsay, L., et al. (2014). Genotypic variation in the ability of landraces and commercial cereal varieties to avoid manganese deficiency in soils with limited manganese availability: is there a role for root-exuded phytases? *Physiol. Plant.* 151, 243–256. doi: 10.1111/ppl.12151

Gherardi, M. J., and Rengel, Z. (2004). The effect of manganese supply on exudation of carboxylates by roots of lucerne (Medicago sativa). *Plant Soil* 260, 271–282. doi: 10.1023/b:plso.0000030182.11473.3b

Giles, C. D., Brown, L. K., Adu, M. O., Mezeli, M. M., Sandral, G. A., Simpson, R. J., et al. (2017). Response-based selection of barley cultivars and legume species for complementarity: root morphology and exudation in relation to nutrient source. *Plant Sci.* 255, 12–28. doi: 10.1016/j.plantsci.2016.11.002

Glynn, S. E., Baker, P. J., Sedelnikova, S. E., Davies, C. L., Eadsforth, T. C., Levy, C. W., et al. (2005). Structure and mechanism of imidazoleglycerol-phosphate dehydratase. *Structure* 13, 1809–1817. doi: 10.1016/j.str.2005.08.012

Goulding, K. W. T. (2016). Soil acidification and the importance of liming agricultural soils with particular reference to the United Kingdom. *Soil Use Manag.* 32, 390–399. doi: 10.1111/sum.12270

Gregory, A. L., Hurley, B. A., Tran, H. T., Valentine, A. J., She, Y. M., Knowles, V. L., et al. (2009). In vivo regulatory phosphorylation of the phosphoenolpyruvate carboxylase AtPPC1 in phosphate-starved *Arabidopsis thaliana*. *Biochem. J.* 420, 57–65. doi: 10.1042/BJ20082397

Guerinot, M. L. (2000). The ZIP family of metal transporters. *Biochim. Biophys. Acta Biomembr.* 1465, 190–198. doi: 10.1016/s0005-2736(00)00138-3

Hajiboland, R. (2012). "Effect of micronutrient deficiencies on plants stress responses," in *Abiotic Stress Responses in Plants*, eds P. Ahmad and M. Prasad (New York, NY: Springer), 283–329. doi: 10.1007/978-1-4614-0634-1_16

Hansel, C. M., Zeiner, C. A., Santelli, C. M., and Webb, S. M. (2012). Mn(II) oxidation by an ascomycete fungus is linked to superoxide production during asexual reproduction. *Proc. Natl. Acad. Sci. U.S.A.* 109, 12621–12625. doi: 10.1073/pnas.1203885109

Hashimoto, K., Eckert, C., Anschütz, U., Scholz, M., Held, K., Waadt, R., et al. (2012). Phosphorylation of calcineurin B-like (CBL) calcium sensor proteins by their CBL-interacting protein kinases (CIPKs) is required for full activity of CBL-CIPK complexes toward their target proteins. *J. Biol. Chem.* 287, 7956–7968. doi: 10.1074/jbc.M111.279331

Hauck, M., Paul, A., Gross, S., and Raubuch, M. (2003). Manganese toxicity in epiphytic lichens: chlorophyll degradation and interaction with iron and phosphorus. *Environ. Exp. Bot.* 49, 181–191. doi: 10.1016/s0098-8472(02)00069-2

Hebbern, C. A., Laursen, K. H., Ladegaard, A. H., Schmidt, S. B., Pedas, P., Bruhn, D., et al. (2009). Latent manganese deficiency increases transpiration in barley (*Hordeum vulgare*). *Physiol. Plant.* 135, 307–316. doi: 10.1111/j.1399-3054.2008.01188.x

Hebbern, C. A., Pedas, P., Schjoerring, J. K., Knudsen, L., and Husted, S. (2005). Genotypic differences in manganese efficiency: field experiments with winter barley (*Hordeum vulgare* L.). *Plant Soil* 272, 233–244. doi: 10.1007/s11104-004-5048-9

Heckman, J. R., Clarke, B. B., and Murphy, J. A. (2003). Optimizing manganese fertilization for the suppression of take-all patch disease on creeping bentgrass. *Crop Sci.* 43, 1395–1398. doi: 10.2135/cropsci2003.1395

Heine, G., Max, J. F. J., Führs, H., Moran-Puente, D. W., Heintz, D., and Horst, W. J. (2011). Effect of manganese on the resistance of tomato to *Pseudocercospora fuligena*. *J. Plant Nutr. Soil Sci.* 174, 827–836. doi: 10.1002/jpln.201000440

Henriques, F. S. (2004). Reduction in chloroplast number accounts for the decrease in the photosynthetic capacity of Mn-deficient pecan leaves. *Plant Sci.* 166, 1051–1055. doi: 10.1016/j.plantsci.2003.12.022

Hirschi, K. D., Korenkov, V. D., Wilganowski, N. L., and Wagner, G. J. (2000). Expression of *Arabidopsis CAX2* in tobacco. Altered metal accumulation and increased manganese tolerance. *Plant Physiol.* 124, 125–134. doi: 10.1104/pp.124.1.125

Hoecker, N., Leister, D., and Schneider, A. (2017). Plants contain small families of UPF0016 proteins including the PHOTOSYNTHESIS AFFECTED MUTANT71 transporter. *Plant Signal. Behav* 12:e1278101. doi: 10.1080/15592324.2016.1278101

Hou, L., Gu, D., Li, Y., Li, J., Li, J., Chen, X., et al. (2019). Phylogenetic and expression analysis of Mn-CDF transporters in pear (*Pyrus bretschneideri* Rehd.). *Plant Mol. Biol. Report.* 37, 98–110. doi: 10.1007/s11105-019-01142-9

Hsieh, M. H., Chang, C. Y., Hsu, S. J., and Chen, J. J. (2008). Chloroplast localization of methylerythritol 4-phosphate pathway enzymes and regulation of mitochondrial genes in *ispD* and *ispE* albino mutants in Arabidopsis. *Plant Mol. Biol.* 66, 663–673. doi: 10.1007/s11103-008-9297-5

Huang, Y. L., Yang, S., Long, G. X., Zhao, Z. K., Li, X. F., and Gu, M. H. (2016). Manganese toxicity in sugarcane plantlets grown on acidic soils of southern China. *PLoS One* 11:e0148956. doi: 10.1371/journal.pone.0148956

Husted, S., Laursen, K. H., Hebbern, C. A., Schmidt, S. B., Pedas, P., Haldrup, A., et al. (2009). Manganese deficiency leads to genotype-specific changes in fluorescence induction kinetics and state transitions. *Plant Physiol.* 150, 825–833. doi: 10.1104/pp.108.134601

Ihnatowicz, A., Siwinska, J., Meharg, A. A., Carey, M., Koornneef, M., and Reymond, M. (2014). Conserved histidine of metal transporter AtNRAMP1 is crucial for optimal plant growth under manganese deficiency at chilling temperatures. *New Phytol.* 202, 1173–1183. doi: 10.1111/nph.12737

Ishimaru, Y., Masuda, H., Bashir, K., Inoue, H., Tsukamoto, T., Takahashi, M., et al. (2010). Rice metal-nicotianamine transporter, OsYSL2, is required for the long-distance transport of iron and manganese. *Plant J.* 62, 379–390. doi: 10.1111/j.1365-313X.2010.04158.x

Ishimaru, Y., Takahashi, R., Bashir, K., Shimo, H., Senoura, T., Sugimoto, K., et al. (2012). Characterizing the role of rice NRAMP5 in manganese, iron and cadmium transport. *Sci. Rep.* 2:286. doi: 10.1038/srep00286

Jauregui, M. A., and Reisenauer, H. M. (1982). Dissolution of oxides of manganese and iron by root exudate components. *Soil Sci. Soc. Am. J.* 46, 314–317. doi: 10.2136/sssaj1982.03615995004600020020x

Johnson, N. A., Liu, F., Weeks, P. D., Hentzen, A. E., Kruse, H. P., Parker, J. J., et al. (2009). A tomato ER-type Ca^{2+}-ATPase, LCA1, has a low thapsigargin-sensitivity and can transport manganese. *Arch. Biochem. Biophys.* 481, 157–168. doi: 10.1016/j.abb.2008.11.010

Kamer, K. J., Sancak, Y., Fomina, Y., Meisel, J. D., Chaudhuri, D., Grabarek, Z., et al. (2018). MICU1 imparts the mitochondrial uniporter with the ability to discriminate between Ca^{2+} and Mn^{2+}. *Proc. Natl. Acad. Sci. U.S.A.* 115, E7960–E7969. doi: 10.1073/pnas.1807811115

Kamiya, T., Akahori, T., Ashikari, M., and Maeshima, M. (2006). Expression of the vacuolar Ca^{2+}/H^{+} exchanger, OsCAX1a, in rice: cell and age specificity of expression, and enhancement by Ca^{2+}. *Plant Cell Physiol.* 47, 96–106. doi: 10.1093/pcp/pci227

Kamiya, T., Akahori, T., and Maeshima, M. (2005). Expression profile of the genes for rice cation/H^{+} exchanger family and functional analysis in yeast. *Plant Cell Physiol.* 46, 1735–1740. doi: 10.1093/pcp/pci173

Kamrul Huda, K. M., Yadav, S., Akhter Banu, M. S., Trivedi, D. K., and Tuteja, N. (2013). Genome-wide analysis of plant-type II Ca^{2+} ATPases gene family from rice and Arabidopsis: potential role in abiotic stresses. *Plant Physiol. Biochem.* 65, 32–47. doi: 10.1016/j.plaphy.2013.01.002

Khabaz-Saberi, H., Setter, T. L., and Waters, I. (2006). Waterlogging induces high to toxic concentrations of iron, aluminum, and manganese in wheat varieties on acidic soil. *J. Plant Nutr.* 29, 899–911. doi: 10.1080/01904160600649161

Kim, K. N., Lee, J. S., Han, H., Choi, S. A., Go, S. J., and Yoon, I. S. (2003). Isolation and characterization of a novel rice Ca^{2+}-regulated protein kinase gene involved in responses to diverse signals including cold, light, cytokinins, sugars and salts. *Plant Mol. Biol.* 52, 1191–1202. doi: 10.1023/b:plan.0000004330.62660.a2

Kim, S. A., Punshon, T., Lanzirotti, A., Li, L., Alonso, J. M., Ecker, J. R., et al. (2006). Localization of iron in *Arabidopsis* seed requires the vacuolar membrane transporter VIT1. *Science* 314, 1295–1298. doi: 10.1126/science.1132563

Kirichok, Y., Krapivinsky, G., and Clapham, D. E. (2004). The mitochondrial calcium uniporter is a highly selective ion channel. *Nature* 427, 360–364. doi: 10.1038/nature02246

Koike, S., Inoue, H., Mizuno, D., Takahashi, M., Nakanishi, H., Mori, S., et al. (2004). OsYSL2 is a rice metal-nicotianamine transporter that is regulated by iron and expressed in the phloem. *Plant J.* 39, 415–424. doi: 10.1111/j.1365-313x.2004.02146.x

Köllner, T. G., Held, M., Lenk, C., Hiltpold, I., Turlings, T. C. J., Gershenzon, J., et al. (2008). A maize (E)-β-caryophyllene synthase implicated in indirect

defense responses against herbivores is not expressed in most American maize varieties. *Plant Cell* 20, 482–494. doi: 10.1105/tpc.107.051672

Koren'kov, V., Park, S., Cheng, N. H., Sreevidya, C., Lachmansingh, J., Morris, J., et al. (2007). Enhanced Cd^{2+}-selective root-tonoplast-transport in tobaccos expressing Arabidopsis cation exchangers. *Planta* 225, 403–411. doi: 10.1007/s00425-006-0352-7

Korshunova, Y. O., Eide, D., Clark, W. G., Guerinot, M. L., and Pakrasi, H. B. (1999). The IRT1 protein from *Arabidopsis thaliana* is a metal transporter with a broad substrate range. *Plant Mol. Biol.* 40, 37–44.

Lambers, H., Hayes, P. E., Laliberté, E., Oliveira, R. S., and Turner, B. L. (2015). Leaf manganese accumulation and phosphorus-acquisition efficiency. *Trends Plant Sci.* 20, 83–90. doi: 10.1016/j.tplants.2014.10.007

Lane, B. G. (2002). Oxalate, germins, and higher-plant pathogens. *IUBMB Life* 53, 67–75. doi: 10.1080/15216540211474

Lanquar, V., Lelièvre, F., Barbier-Brygoo, H., and Thomine, S. (2004). Regulation and function of AtNRAMP4 metal transporter protein. *Soil Sci. Plant Nutr.* 50, 1141–1150. doi: 10.1080/00380768.2004.10408587

Lanquar, V., Lelièvre, F., Bolte, S., Hamès, C., Alcon, C., Neumann, D., et al. (2005). Mobilization of vacuolar iron by AtNRAMP3 and AtNRAMP4 is essential for seed germination on low iron. *EMBO J.* 24, 4041–4051. doi: 10.1038/sj.emboj.7600864

Lanquar, V., Schnell Ramos, M., Lelièvre, F., Barbier-Brygoo, H., Krieger-Liszkay, A., Krämer, U., et al. (2010). Export of vacuolar manganese by AtNRAMP3 and AtNRAMP4 is required for optimal photosynthesis and growth under manganese deficiency. *Plant Physiol.* 152, 1986–1999. doi: 10.1104/pp.109.150946

LeClere, S., Tellez, R., Rampey, R. A., Matsuda, S. P. T., and Bartel, B. (2002). Characterization of a family of IAA-amino acid conjugate hydrolases from *Arabidopsis*. *J. Biol. Chem.* 277, 20446–20452. doi: 10.1074/jbc.m111955200

Lešková, A., Giehl, R. F. H., Hartmann, A., Fargašová, A., and von Wirén, N. (2017). Heavy metals induce iron deficiency responses at different hierarchic and regulatory levels. *Plant Physiol.* 174, 1648–1668. doi: 10.1104/pp.16.01916

Li, C., Wang, P., Menzies, N. W., Lombi, E., and Kopittke, P. M. (2017). Effects of changes in leaf properties mediated by methyl jasmonate (MeJA) on foliar absorption of Zn, Mn and Fe. *Ann. Bot.* 120, 405–415. doi: 10.1093/aob/mcx063

Li, J. Y., Liu, J., Dong, D., Jia, X., Mccouch, S. R., and Kochian, L. V. (2014). Natural variation underlies alterations in Nramp aluminum transporter (NRAT1) expression and function that play a key role in rice aluminum tolerance. *Proc. Natl. Acad. Sci. U.S.A.* 111, 6503–6508. doi: 10.1073/pnas.1318975111

Li, L., Xu, X., Chen, C., and Shen, Z. (2016). Genome-wide characterization and expression analysis of the Germin-like protein family in rice and Arabidopsis. *Int. J. Mol. Sci.* 17:1622. doi: 10.3390/ijms17101622

Li, L., and Yang, X. (2018). The essential element manganese, oxidative stress, and metabolic diseases: links and interactions. *Oxid. Med. Cell. Longev.* 2018:7580707. doi: 10.1155/2018/7580707

Li, Q., Chen, L. S., Jiang, H. X., Tang, N., Yang, L. T., Lin, Z. H., et al. (2010). Effects of manganese-excess on CO_2 assimilation, ribulose-1,5-bisphosphate carboxylase/oxygenase, carbohydrates and photosynthetic electron transport of leaves, and antioxidant systems of leaves and roots in *Citrus grandis* seedlings. *BMC Plant Biol.* 10:42. doi: 10.1186/1471-2229-10-42

Li, X., Chanroj, S., Wu, Z., Romanowsky, S. M., Harper, J. F., and Sze, H. (2008). A distinct endosomal Ca^{2+}/Mn^{2+} pump affects root growth through the secretory process. *Plant Physiol.* 147, 1675–1689. doi: 10.1104/pp.108.119909

Liang, F., Cunningham, K. W., Harper, J. F., and Sze, H. (1997). ECA1 complements yeast mutants defective in Ca^{2+} pumps and encodes an endoplasmic reticulum-type Ca^{2+}-ATPase in *Arabidopsis thaliana*. *Proc. Natl. Acad. Sci. U.S.A.* 94, 8579–8584. doi: 10.1073/pnas.94.16.8579

Lidon, F. C., Barreiro, M. G., and Ramalho, J. C. (2004). Manganese accumulation in rice: implications for photosynthetic functioning. *J. Plant Physiol.* 161, 1235–1244. doi: 10.1016/j.jplph.2004.02.003

Liu, J., Gao, Y., Tang, Y., Wang, D., Chen, X., Yao, Y., et al. (2019). Genome-wide identification, comprehensive gene feature, evolution, and expression analysis of plant metal tolerance proteins in tobacco under heavy metal toxicity. *Front. Genet.* 10:345. doi: 10.3389/fgene.2019.00345

Long, L., Persson, D. P., Duan, F., Jørgensen, K., Yuan, L., Schjoerring, J. K., et al. (2018). The iron-regulated transporter 1 plays an essential role in uptake, translocation and grain-loading of manganese, but not iron, in barley. *New Phytol.* 217, 1640–1653. doi: 10.1111/nph.14930

Longnecker, N. E., Graham, R. D., and Card, G. (1991). Effects of manganese deficiency on the pattern of tillering and development of barley (*Hordeum vulgare* c.v. galleon). *Field Crops Res.* 28, 85–102. doi: 10.1016/0378-4290(91)90076-8

López-Millán, A. F., Ellis, D. R., and Grusak, M. A. (2004). Identification and characterization of several new members of the ZIP family of metal ion transporters in *Medicago truncatula*. *Plant Mol. Biol.* 54, 583–596. doi: 10.1023/b:plan.0000038271.96019.aa

Lovely, D. R. (1995). Microbial reduction of iron, manganese, and other metals. *Adv. Agron.* 54, 175–231. doi: 10.1016/s0065-2113(08)60900-1

Ma, G., Li, J., Li, J., Li, Y., Gu, D., Chen, C., et al. (2018). OsMTP11, a trans-Golgi network localized transporter, is involved in manganese tolerance in rice. *Plant Sci.* 274, 59–69. doi: 10.1016/j.plantsci.2018.05.011

Martinoia, E., Meyer, S., De Angeli, A., and Nagy, R. (2012). Vacuolar transporters in their physiological context. *Annu. Rev. Plant Biol.* 63, 183–213. doi: 10.1146/annurev-arplant-042811-105608

Martins, V., Carneiro, F., Conde, C., Sottomayor, M., and Gerós, H. (2017). The grapevine VvCAX3 is a cation/H^+ exchanger involved in vacuolar Ca^{2+} homeostasis. *Planta* 246, 1083–1096. doi: 10.1007/s00425-017-2754-0

Matsushima, R., Hayashi, Y., Yamada, K., Shimada, T., Nishimura, M., and Hara-Nishimura, I. (2003). The ER body, a novel endoplasmic reticulum-derived structure in *Arabidopsis*. *Plant Cell Physiol.* 44, 661–666. doi: 10.1093/pcp/pcg089

McNaughton, R. L., Reddi, A. R., Clement, M. H. S., Sharma, A., Barnese, K., Rosenfeld, L., et al. (2010). Probing *in vivo* Mn^{2+} speciation and oxidative stress resistance in yeast cells with electron-nuclear double resonance spectroscopy. *Proc. Natl. Acad. Sci U.S.A.* 107, 15335–15339. doi: 10.1073/pnas.1009648107

McNear, D. H., and Küpper, J. V. (2014). Mechanisms of trichome-specific Mn accumulation and toxicity in the Ni hyperaccumulator *Alyssum murale*. *Plant Soil* 377, 407–422. doi: 10.1007/s11104-013-2003-7

Mei, H., Cheng, N. H., Zhao, J., Park, S., Escareno, R. A., Pittman, J. K., et al. (2009). Root development under metal stress in *Arabidopsis thaliana* requires the H^+/cation antiporter CAX4. *New Phytol.* 183, 95–105. doi: 10.1111/j.1469-8137.2009.02831.x

Meinhard, M., Rodriguez, P. L., and Grill, E. (2002). The sensitivity of ABI2 to hydrogen peroxide links the abscisic acid-response regulator to redox signalling. *Planta* 214, 775–782. doi: 10.1007/s00425-001-0675-3

Membré, N., Bernier, F., Staiger, D., and Berna, A. (2000). *Arabidopsis thaliana* germin-like proteins: common and specific features point to a variety of functions. *Planta* 211, 345–354. doi: 10.1007/s004250000277

Meng, J. G., Zhang, X. D., Tan, S. K., Zhao, K. X., and Yang, Z. M. (2017). Genome-wide identification of Cd-responsive NRAMP transporter genes and analyzing expression of NRAMP1 mediated by miR167 in *Brassica napus*. *Biometals* 30, 917–931. doi: 10.1007/s10534-017-0057-3

Migocka, M., Papierniak, A., Kosieradzka, A., Posyniak, E., Maciaszczyk-Dziubinska, E., Biskup, R., et al. (2015). Cucumber metal tolerance protein CsMTP9 is a plasma membrane H^+-coupled antiporter involved in the Mn^{2+} and Cd^{2+} efflux from root cells. *Plant J.* 84, 1045–1058. doi: 10.1111/tpj.13056

Millaleo, R., Reyes-Díaz, M., Alberdi, M., Ivanov, A. G., Krol, M., and Hüner, N. P. A. (2013). Excess manganese differentially inhibits photosystem I versus II in *Arabidopsis thaliana*. *J. Exp. Bot.* 64, 343–354. doi: 10.1093/jxb/ers339

Millaleo, R., Reyes-Diaz, M., Ivanov, A. G., Mora, M. L., and Alberdi, M. (2010). Manganese as essential and toxic element for plants: transport, accumulation and resistance mechanisms. *J. Soil Sci. Plant Nutr.* 10, 470–481. doi: 10.4067/s0718-95162010000200008

Mills, R. F., Doherty, M. L., Lopez-Marques, R. L., Weimar, T., Dupree, P., Palmgren, M. G., et al. (2007). ECA3, a Golgi-localized P_{2A}-type ATPase, plays a crucial role in manganese nutrition in Arabidopsis. *Plant Physiol.* 146, 116–128. doi: 10.1104/pp.107.110817

Milner, M. J., Seamon, J., Craft, E., and Kochian, L. V. (2013). Transport properties of members of the ZIP family in plants and their role in Zn and Mn homeostasis. *J. Exp. Bot.* 64, 369–381. doi: 10.1093/jxb/ers315

Montanini, B., Blaudez, D., Jeandroz, S., Sanders, D., and Chalot, M. (2007). Phylogenetic and functional analysis of the Cation Diffusion Facilitator (CDF) family: improved signature and prediction of substrate specificity. *BMC Genomics* 8:107. doi: 10.1186/1471-2164-8-107

Morgan, J. J. (2005). Kinetics of reaction between O_2 and Mn(II) species in aqueous solutions. *Geochim. Cosmochim. Acta* 69, 35–48. doi: 10.1016/j.gca.2004.06.013

Morgan, P. W., Joham, H. E., and Amin, J. V. (1966). Effect of manganese toxicity on the indoleacetic acid oxidase system of cotton. *Plant Physiol.* 41, 718–724. doi: 10.1104/pp.41.4.718

Morris, J., Tian, H., Park, S., Sreevidya, C. S., Ward, J. M., and Hirschi, K. D. (2008). AtCCX3 is an Arabidopsis endomembrane H^+-dependent K^+ transporter. *Plant Physiol.* 148, 1474–1486. doi: 10.1104/pp.108.118810

Nable, R. O., Houtz, R. L., and Cheniae, G. M. (1988). Early inhibition of photosynthesis during development of Mn toxicity in tobacco. *Plant Physiol.* 86, 1136–1142. doi: 10.1104/pp.86.4.1136

Nevo, Y., and Nelson, N. (2006). The NRAMP family of metal-ion transporters. *Biochim. Biophys. Acta Mol. Cell Res.* 1763, 609–620. doi: 10.1016/j.bbamcr.2006.05.007

Nian, L. S. (1989). Manganese induced iron chlorosis in pineapple and its control by foliar application of iron-citrate. *J. Plant Nutr. Soil Sci.* 152, 125–126. doi: 10.1002/jpln.19891520122

Nowicki, M., Müller, F., and Frentzen, M. (2005). Cardiolipin synthase of *Arabidopsis thaliana*. *FEBS Lett.* 579, 2161–2165. doi: 10.1016/j.febslet.2005.03.007

Nuruzzaman, M., Lambers, H., Bolland, M. D. A., and Veneklaas, E. J. (2006). Distribution of carboxylates and acid phosphatase and depletion of different phosphorus fractions in the rhizosphere of a cereal and three grain legumes. *Plant Soil* 281, 109–120. doi: 10.1007/s11104-005-3936-2

Ohki, K. (1985). Manganese deficiency and toxicity effects on photosynthesis, chlorophyll, and transpiration in Wheat. *Crop Sci.* 25, 187–191. doi: 10.2135/cropsci1985.0011183x002500010045x

Önnerud, H., Zhang, L., Gellerstedt, G., and Henriksson, G. (2002). Polymerization of monolignols by redox shuttle–mediated enzymatic oxidation. *Plant Cell* 14, 1953–1962. doi: 10.1105/tpc.001487

Oomen, R. J. F. J., Wu, J., Lelièvre, F., Blanchet, S., Richaud, P., Barbier-Brygoo, H., et al. (2009). Functional characterization of NRAMP3 and NRAMP4 from the metal hyperaccumulator *Thlaspi caerulescens*. *New Phytol.* 181, 637–650. doi: 10.1111/j.1469-8137.2008.02694.x

Panda, S., Mishra, A. K., and Biswal, U. C. (1987). Manganese induced peroxidation of thylakoid lipids and changes in chlorophyll-α fluorescence during aging of cell free chloroplasts in light. *Phytochemistry* 26, 3217–3219. doi: 10.1016/s0031-9422(00)82472-3

Papadakis, I. E., Giannakoula, A., Therios, I. N., Bosabalidis, A. M., Moustakas, M., and Nastou, A. (2007). Mn-induced changes in leaf structure and chloroplast ultrastructure of *Citrus volkameriana* (L.) plants. *J. Plant Physiol.* 164, 100–103. doi: 10.1016/j.jplph.2006.04.011

Pedas, P., Hebbern, C. A., Schjoerring, J. K., Holm, P. E., and Husted, S. (2005). Differential capacity for high-affinity manganese uptake contributes to differences between barley genotypes in tolerance to low manganese availability. *Plant Physiol.* 139, 1411–1420. doi: 10.1104/pp.105.067561

Pedas, P., Husted, S., Skytte, K., and Schjoerring, J. K. (2011). Elevated phosphorus impedes manganese acquisition by barley plants. *Front. Plant Sci.* 2:37. doi: 10.3389/fpls.2011.00037

Pedas, P., Stokholm, M. S., Hegelund, J. N., Ladegård, A. H., Schjoerring, J. K., and Husted, S. (2014). Golgi localized barley MTP8 proteins facilitate Mn transport. *PLoS One* 9:e113759. doi: 10.1371/journal.pone.0113759

Pedas, P., Ytting, C. K., Fuglsang, A. T., Jahn, T. P., Schjoerring, J. K., and Husted, S. (2008). Manganese efficiency in barley: identification and characterization of the metal ion transporter HvIRT1. *Plant Physiol.* 148, 455–466. doi: 10.1104/pp.108.118851

Peiter, E., Montanini, B., Gobert, A., Pedas, P., Husted, S., Maathuis, F. J. M., et al. (2007). A secretory pathway-localized cation diffusion facilitator confers plant manganese tolerance. *Proc. Natl. Acad. Sci. U.S.A.* 104, 8532–8537. doi: 10.1073/pnas.0609507104

Peris-Peris, C., Serra-Cardona, A., Sánchez-Sanuy, F., Campo, S., Ariño, J., and San Segundo, B. (2017). Two NRAMP6 isoforms function as iron and manganese transporters and contribute to disease resistance in rice. *Mol. Plant Microbe Interact.* 30, 385–398. doi: 10.1094/MPMI-01-17-0005-R

Pittman, J. K. (2005). Managing the manganese: molecular mechanisms of manganese transport and homeostasis. *New Phytol.* 167, 733–742. doi: 10.1111/j.1469-8137.2005.01453.x

Pittman, J. K., and Hirschi, K. D. (2016). Phylogenetic analysis and protein structure modelling identifies distinct Ca^{2+}/cation antiporters and conservation of gene family structure within Arabidopsis and rice species. *Rice* 9:3. doi: 10.1186/s12284-016-0075-8

Pittman, J. K., Shigaki, T., Marshall, J. L., Morris, J. L., Cheng, N., and Hirschi, K. D. (2004). Functional and regulatory analysis of the *Arabidopsis thaliana* CAX2 cation transporter. *Plant Mol. Biol.* 56, 959–971. doi: 10.1007/s11103-004-6446-3

Pottier, M., Oomen, R., Picco, C., Giraudat, J., Scholz-Starke, J., Richaud, P., et al. (2015). Identification of mutations allowing natural resistance associated macrophage proteins (NRAMP) to discriminate against cadmium. *Plant J.* 83, 625–637. doi: 10.1111/tpj.12914

Reddi, A. R., Jensen, L. T., Naranuntarat, A., Rosenfeld, L., Leung, E., Shah, R., et al. (2009). The overlapping roles of manganese and Cu/Zn SOD in oxidative stress protection. *Free Radic. Biol. Med.* 46, 154–162. doi: 10.1016/j.freeradbiomed.2008.09.032

Rengel, Z. (2015). Availability of Mn, Zn and Fe in the rhizosphere. *J. Soil Sci. Plant Nutr.* 15, 397–409.

Requena, L., and Bornemann, S. (1999). Barley (*Hordeum vulgare*) oxalate oxidase is a manganese-containing enzyme. *Biochem. J.* 343, 185–190. doi: 10.1042/bj3430185

Robert, H. S., and Offringa, R. (2008). Regulation of auxin transport polarity by AGC kinases. *Curr. Opin. Plant Biol.* 11, 495–502. doi: 10.1016/j.pbi.2008.06.004

Rodríguez-Celma, J., Tsai, Y.-H., Wen, T.-N., Wu, Y.-C., Curie, C., and Schmidt, W. (2016). Systems-wide analysis of manganese deficiency-induced changes in gene activity of *Arabidopsis* roots. *Sci. Rep.* 6, 35846–35846. doi: 10.1038/srep35846

Rohdich, F., Lauw, S., Kaiser, J., Feicht, R., Köhler, P., Bacher, A., et al. (2006). Isoprenoid biosynthesis in plants - 2C-methyl-D-erythritol-4-phosphate synthase (IspC protein) of *Arabidopsis thaliana*. *FEBS J.* 273, 4446–4458. doi: 10.1111/j.1742-4658.2006.05446.x

Rohdich, F., Wungsintaweekul, J., Eisenreich, W., Richter, G., Schuhr, C. A., Hecht, S., et al. (2000). Biosynthesis of terpenoids: 4-diphosphocytidyl-2C-methyl-D-erythritol synthase of *Arabidopsis thaliana*. *Proc. Natl. Acad. Sci. U.S.A.* 97, 6451–6456. doi: 10.1073/pnas.97.12.6451

Sasaki, A., Yamaji, N., Xia, J., and Ma, J. F. (2011). OsYSL6 is involved in the detoxification of excess manganese in rice. *Plant Physiol.* 157, 1832–1840. doi: 10.1104/pp.111.186031

Sasaki, A., Yamaji, N., Yokosho, K., and Ma, J. F. (2012). Nramp5 is a major transporter responsible for manganese and cadmium uptake in rice. *Plant Cell* 24, 2155–2167. doi: 10.1105/tpc.112.096925

Schaaf, G., Ludewig, U., Erenoglu, B. E., Mori, S., Kitahara, T., and von Wirén, N. (2004). ZmYS1 functions as a proton-coupled symporter for phytosiderophore- and nicotianamine-chelated metals. *J. Biol. Chem.* 279, 9091–9096. doi: 10.1074/jbc.m311799200

Schenk, G., Ge, Y., Carrington, L. E., Wynne, C. J., Searle, I. R., Carroll, B. J., et al. (1999). Binuclear metal centers in plant purple acid phosphatases: Fe-Zn in sweet potato and Fe-Zn in soybean. *Arch. Biochem. Biophys.* 370, 183–189. doi: 10.1006/abbi.1999.1407

Schmidt, S. B., Jensen, P. E., and Husted, S. (2016). Manganese deficiency in plants: The impact on photosystem II. *Trends Plant Sci.* 21, 622–632. doi: 10.1016/j.tplants.2016.03.001

Schneider, A., Steinberger, I., Herdean, A., Gandini, C., Eisenhut, M., Kurz, S., et al. (2016). The evolutionarily conserved protein PHOTOSYNTHESIS AFFECTED MUTANT71 is required for efficient manganese uptake at the thylakoid membrane in Arabidopsis. *Plant Cell* 28, 892–910. doi: 10.1105/tpc.15.00812

Schweighofer, A., Hirt, H., and Meskiene, I. (2004). Plant PP2C phosphatases: Emerging functions in stress signaling. *Trends Plant Sci.* 9, 236–243. doi: 10.1016/j.tplants.2004.03.007

Sello, S., Moscatiello, R., Mehlmer, N., Leonardelli, M., Carraretto, L., Cortese, E., et al. (2018). Chloroplast Ca^{2+} fluxes into and across thylakoids revealed by thylakoid-targeted aequorin probes. *Plant Physiol.* 177, 38–51. doi: 10.1104/pp.18.00027

Shao, J. F., Yamaji, N., Shen, R. F., and Ma, J. F. (2017). The key to Mn homeostasis in plants: regulation of Mn transporters. *Trends Plant Sci.* 22, 215–224. doi: 10.1016/j.tplants.2016.12.005

Shigaki, T., Pittman, J. K., and Hirschi, K. D. (2003). Manganese specificity determinants in the *Arabidopsis* metal/H^+ antiporter CAX2. *J. Biol. Chem.* 278, 6610–6617. doi: 10.1074/jbc.M209952200

Socha, A. L., and Guerinot, M. L. (2014). Mn-euvering manganese: the role of transporter gene family members in manganese uptake and mobilization in plants. *Front. Plant Sci.* 5:106. doi: 10.3389/fpls.2014.00106

Sparrow, L. A., and Uren, N. C. (2014). Manganese oxidation and reduction in soils: effects of temperature, water potential, pH and their interactions. *Soil Res.* 52, 483–494. doi: 10.1071/SR13159

St.Clair, S. B., and Lynch, J. P. (2005). Element accumulation patterns of deciduous and evergreen tree seedlings on acid soils: implications for sensitivity to manganese toxicity. *Tree Physiol.* 25, 85–92. doi: 10.1093/treephys/25.1.85

Stael, S., Wurzinger, B., Mair, A., Mehlmer, N., Vothknecht, U. C., and Teige, M. (2012). Plant organellar calcium signalling: an emerging field. *J. Exp. Bot.* 63, 1525–1542. doi: 10.1093/jxb/err394

Stengel, A., Gügel, I. L., Hilger, D., Rengstl, B., Jung, H., and Nickelsen, J. (2012). Initial steps of photosystem II de novo assembly and preloading with manganese take place in biogenesis centers in Synechocystis. *Plant Cell* 24, 660–675. doi: 10.1105/tpc.111.093914

Stoltz, E., and Wallenhammar, A. C. (2014). Manganese application increases winter hardiness in barley. *Field Crops Res.* 164, 148–153. doi: 10.1016/j.fcr.2014.05.008

Strasser, R., Bondili, J. S., Vavra, U., Schoberer, J., Svoboda, B., Glossl, J., et al. (2007). A unique β1,3-galactosyltransferase is indispensable for the biosynthesis of N-glycans containing Lewis a structures in *Arabidopsis thaliana*. *Plant Cell* 19, 2278–2292. doi: 10.1105/tpc.107.052985

Stumm, W., and Morgan, J. J. (1996). *Aquatic Chemistry: Chemical Equilibria and Rates in Natural Waters*. New York, NY: Wiley.

Subrahmanyam, D., and Rathore, V. S. (2001). Influence of manganese toxicity on photosynthesis in ricebean (*Vigna umbellata*) seedlings. *Photosynthetica* 38, 449–453.

Svedruzic, D., Jonsson, S., Toyota, C. G., Reinhardt, L. A., Ricagno, S., Lindqvist, Y., et al. (2005). The enzymes of oxalate metabolism: unexpected structures and mechanisms. *Arch. Biochem. Biophys.* 433, 176–192. doi: 10.1016/j.abb.2004.08.032

Szurmak, B., Wysłouch-Cieszyńska, A., Wszelaka-Rylik, M., Bal, W., and Dobrzańska, M. (2008). A diadenosine 5′,5″-P1P4 tetraphosphate (Ap_4A) hydrolase from *Arabidopsis thaliana* that is activated preferentially by Mn^{2+} ions. *Acta Biochim. Polon.* 55, 151–160. doi: 10.18388/abp.2008_3173

Takahashi, S., Sakamoto, A. N., Tanaka, A., and Shimizu, K. (2007). AtREV1, a Y-family DNA polymerase in Arabidopsis, has deoxynucleotidyl transferase activity *in vitro*. *Plant Physiol.* 145, 1052–1060. doi: 10.1104/pp.107.101980

Takemoto, Y., Tsunemitsu, Y., Fujii-Kashino, M., Mitani-Ueno, N., Yamaji, N., Ma, J. F., et al. (2017). The tonoplast-localized transporter MTP8.2 contributes to manganese detoxification in the shoots and roots of *Oryza sativa* L. *Plant Cell Physiol.* 58, 1573–1582. doi: 10.1093/pcp/pcx082

Teardo, E., Carraretto, L., Moscatiello, R., Cortese, E., Vicario, M., Festa, M., et al. (2019). A chloroplast-localized mitochondrial calcium uniporter transduces osmotic stress in *Arabidopsis*. *Nat. Plants* 5, 581–588. doi: 10.1038/s41477-019-0434-8

Thomine, S., Lelièvre, F., Debarbieux, E., Schroeder, J. I., and Barbier-Brygoo, H. (2003). AtNRAMP3, a multispecific vacuolar metal transporter involved in plant responses to iron deficiency. *Plant J.* 34, 685–695. doi: 10.1046/j.1365-313X.2003.01760.x

Thomine, S., Wang, R., Ward, J. M., Crawford, N. M., and Schroeder, J. I. (2000). Cadmium and iron transport by members of a plant metal transporter family in *Arabidopsis* with homology to *Nramp* genes. *Proc. Natl. Acad. Sci. U.S.A.* 97, 4991–4996. doi: 10.1073/pnas.97.9.4991

Tiwari, M., Sharma, D., Dwivedi, S., Singh, M., Tripathi, R. D., and Trivedi, P. K. (2014). Expression in *Arabidopsis* and cellular localization reveal involvement of rice NRAMP, OsNRAMP1, in arsenic transport and tolerance. *Plant Cell Environ.* 37, 140–152. doi: 10.1111/pce.12138

Tsukamoto, T., Nakanishi, H., Kiyomiya, S., Watanabe, S., Matsuhashi, S., Nishizawa, N. K., et al. (2006). ^{52}Mn translocation in barley monitored using a positron-emitting tracer imaging system. *Soil Sci. Plant Nutr.* 52, 717–725. doi: 10.1111/j.1747-0765.2006.00096.x

Tsunemitsu, Y., Genga, M., Okada, T., Yamaji, N., Ma, J. F., Miyazaki, A., et al. (2018). A member of cation diffusion facilitator family, MTP11, is required for manganese tolerance and high fertility in rice. *Planta* 248, 231–241. doi: 10.1007/s00425-018-2890-1

Turekian, K. K., and Wedepohl, K. H. (1961). Distribution of the elements in some major units of the earth's crust. *GSA Bull.* 72, 175–192.

Ueno, D., Sasaki, A., Yamaji, N., Miyaji, T., Fujii, Y., Takemoto, Y., et al. (2015). A polarly localized transporter for efficient manganese uptake in rice. *Nat. Plants* 1:15170. doi: 10.1038/nplants.2015.170

Ullah, I., Wang, Y., Eide, D. J., and Dunwell, J. M. (2018). Evolution, and functional analysis of natural resistance-associated macrophage proteins (NRAMPs) from *Theobroma cacao* and their role in cadmium accumulation. *Sci. Rep.* 8:14412. doi: 10.1038/s41598-018-32819-y

Venkidasamy, B., Selvaraj, D., and Ramalingam, S. (2019). Genome-wide analysis of purple acid phosphatase (PAP) family proteins in *Jatropha curcas* L. *Int. J. Biol. Macromol.* 123, 648–656. doi: 10.1016/j.ijbiomac.2018.11.027

Vert, G., Grotz, N., Dédaldéchamp, F., Gaymard, F., Guerinot, M., Lou, B. J., et al. (2002). IRT1, an Arabidopsis transporter essential for iron uptake from the soil and for plant growth. *Plant Cell* 14, 1223–1233. doi: 10.1105/tpc.001388

Wagner, S., Behera, S., De Bortoli, S., Logan, D. C., Fuchs, P., Carraretto, L., et al. (2015). The EF-hand Ca^{2+} binding protein MICU choreographs mitochondrial Ca^{2+} dynamics in Arabidopsis. *Plant Cell* 27, 3190–3212. doi: 10.1105/tpc.15.00509

Wang, C., Guan, Y., Lv, M., Zhang, R., Guo, Z., Wei, X., et al. (2018). Manganese increases the sensitivity of the cGAS-STING pathway for double-stranded DNA and is required for the host defense against DNA viruses. *Immunity* 48, 675.e7–687.e7. doi: 10.1016/j.immuni.2018.03.017

Wang, C., Xu, W., Jin, H., Zhang, T., Lai, J., Zhou, X., et al. (2016). A putative chloroplast-localized Ca^{2+}/H^+ antiporter CCHA1 is involved in calcium and pH homeostasis and required for PSII function in *Arabidopsis*. *Mol. Plant* 9, 1183–1196. doi: 10.1016/j.molp.2016.05.015

Wang, N., Qiu, W., Dai, J., Guo, X., Lu, Q., Wang, T., et al. (2019). AhNRAMP1 enhances manganese and zinc uptake in plants. *Front. Plant Sci.* 10:415. doi: 10.3389/fpls.2019.00415

Wang, X., Zhong, F., Woo, C. H., Miao, Y., Grusak, M. A., Zhang, X., et al. (2017). A rapid and efficient method to study the function of crop plant transporters in *Arabidopsis*. *Protoplasma* 254, 737–747. doi: 10.1007/s00709-016-0987-6

Waters, B. M., Chu, H. H., Didonato, R. J., Roberts, L. A., Eisley, R. B., Lahner, B., et al. (2006). Mutations in Arabidopsis *Yellow Stripe-Like1* and *Yellow Stripe-Like3* reveal their roles in metal ion homeostasis and loading of metal ions in seeds. *Plant Physiol.* 141, 1446–1458. doi: 10.1104/pp.106.082586

Werner, A. K., Sparkes, I. A., Romeis, T., and Witte, C. P. (2008). Identification, biochemical characterization, and subcellular localization of allantoate amidohydrolases from Arabidopsis and soybean. *Plant Physiol.* 146, 418–430. doi: 10.1104/pp.107.110809

White, P. J., Bowen, H. C., Demidchik, V., Nichols, C., and Davies, J. M. (2002). Genes for calcium-permeable channels in the plasma membrane of plant root cells. *Biochim. Biophys. Acta Biomembr.* 1564, 299–309. doi: 10.1016/S0005-2736(02)00509-6

White, P. J., and Greenwood, D. J. (2013). "Properties and management of cationic elements for crop growth," in *Soil Conditions and Plant Growth*, eds P. J. Gregory and S. Nortcliff (Oxford: Blackwell Publishing), 160–194 doi: 10.1002/9781118337295.ch6

Wilkinson, R. E., and Ohki, K. (1988). Influence of manganese deficiency and toxicity on isoprenoid syntheses. *Plant Physiol.* 87, 841–846. doi: 10.1104/pp.87.4.841

Wu, D., Yamaji, N., Yamane, M., Kashino-Fujii, M., Sato, K., and Ma, J. F. (2016). The HvNramp5 transporter mediates uptake of cadmium and manganese, but not iron. *Plant Physiol.* 172, 1899–1910. doi: 10.1104/pp.16.01189

Wu, Z., Liang, F., Hong, B., Young, J. C., Sussman, M. R., Harper, J. F., et al. (2002). An endoplasmic reticulum-bound Ca^{2+}/Mn^{2+} pump, ECA1, supports plant growth and confers tolerance to Mn^{2+} stress. *Plant Physiol.* 130, 128–137. doi: 10.1104/pp.004440

Wymer, C. L., Bibikova, T. N., and Gilroy, S. (1997). Cytoplasmic free calcium distributions during the development of root hairs of *Arabidopsis thaliana*. *Plant J.* 12, 427–439. doi: 10.1046/j.1365-313X.1997.12020427.x

Xia, J., Yamaji, N., Kasai, T., and Ma, J. F. (2010). Plasma membrane-localized transporter for aluminum in rice. *Proc. Natl. Acad. Sci. U.S.A.* 107, 18381–18385. doi: 10.1073/pnas.1004949107

Xiao, H., Yin, L., Xu, X., Li, T., and Han, Z. (2008). The iron-regulated transporter, MbNRAMP1, isolated from *Malus baccata* is involved in Fe, Mn and Cd trafficking. *Ann. Bot.* 102, 881–889. doi: 10.1093/aob/mcn178

Yamada, K., Hara-Nishimura, I., and Nishimura, M. (2011). Unique defense strategy by the endoplasmic reticulum body in plants. *Plant Cell Physiol.* 52, 2039–2049. doi: 10.1093/pcp/pcr156

Yamada, K., Nagano, A. J., Nishina, M., Hara-Nishimura, I., and Nishimura, M. (2013). Identification of two novel endoplasmic reticulum body-specific integral membrane proteins. *Plant Physiol.* 161, 108–120. doi: 10.1104/pp.112.207654

Yamada, N., Theerawitaya, C., Cha-Um, S., Kirdmanee, C., and Takabe, T. (2014). Expression and functional analysis of putative vacuolar Ca^{2+}-transporters (CAXs and ACAs) in roots of salt tolerant and sensitive rice cultivars. *Protoplasma* 251, 1067–1075. doi: 10.1007/s00709-014-0615-2

Yamaji, N., Sasaki, A., Xia, J. X., Yokosho, K., and Ma, J. F. (2013). A node-based switch for preferential distribution of manganese in rice. *Nat. Commun.* 4:2442. doi: 10.1038/ncomms3442

Yang, M., Zhang, W., Dong, H., Zhang, Y., Lv, K., Wang, D., et al. (2013). OsNRAMP3 is a vascular bundles-specific manganese transporter that is responsible for manganese distribution in rice. *PLoS One* 8:e83990. doi: 10.1371/journal.pone.0083990

Yang, M., Zhang, Y., Zhang, L., Hu, J., Zhang, X., Lu, K., et al. (2014). OsNRAMP5 contributes to manganese translocation and distribution in rice shoots. *J. Exp. Bot.* 65, 4849–4861. doi: 10.1093/jxb/eru259

Yang, T. J. W., Perry, P. J., Ciani, S., Pandian, S., and Schmidt, W. (2008). Manganese deficiency alters the patterning and development of root hairs in *Arabidopsis*. *J. Exp. Bot.* 59, 3453–3464. doi: 10.1093/jxb/ern195

Zhang, B., Zhang, C., Liu, C., Jing, Y., Wang, Y., Jin, L., et al. (2018). Inner envelope CHLOROPLAST MANGANESE TRANSPORTER 1 supports manganese homeostasis and phototrophic growth in *Arabidopsis*. *Mol. Plant* 11, 943–954. doi: 10.1016/j.molp.2018.04.007

Zhang, M., and Liu, B. (2017). Identification of a rice metal tolerance protein OsMTP11 as a manganese transporter. *PLoS One* 12:e0174987. doi: 10.1371/journal.pone.0174987

Zhang, Y., Xu, Y. H., Yi, H. Y., and Gong, J. M. (2012). Vacuolar membrane transporters OsVIT1 and OsVIT2 modulate iron translocation between flag leaves and seeds in rice. *Plant J.* 72, 400–410. doi: 10.1111/j.1365-313X.2012.05088.x

Zhang, Z., Yin, H., Tan, W., Koopal, L. K., Zheng, L., Feng, X., et al. (2014). Zn sorption to biogenic bixbyite-like Mn_2O_3 produced by *Bacillus* CUA isolated from soil: XAFS study with constraints on sorption mechanism. *Chem. Geol.* 389, 82–90. doi: 10.1016/j.chemgeo.2014.09.017

Zhao, J., Wang, W., Zhou, H., Wang, R., Zhang, P., Wang, H., et al. (2017). Manganese toxicity inhibited root growth by disrupting auxin biosynthesis and transport in *Arabidopsis*. *Front. Plant Sci.* 8:272. doi: 10.3389/fpls.2017.00272

Conflict of Interest: The authors declare that the research was conducted in the absence of any commercial or financial relationships that could be construed as a potential conflict of interest.

frontiers in Plant Science

REVIEW
published: 15 April 2020
doi: 10.3389/fpls.2020.00413

An Update on Nitric Oxide Production and Role Under Phosphorus Scarcity in Plants

*Andrea Galatro[1], Facundo Ramos-Artuso[1,2], Melisa Luquet[1], Agustina Buet[1,2] and Marcela Simontacchi[1,2]**

[1] Instituto de Fisiología Vegetal (INFIVE), CONICET-UNLP, La Plata, Argentina, [2] Facultad de Ciencias Agrarias y Forestales, Universidad Nacional de La Plata, La Plata, Argentina

Phosphate (P) is characterized by its low availability and restricted mobility in soils, and also by a high redistribution capacity inside plants. In order to maintain P homeostasis in nutrient restricted conditions, plants have developed mechanisms which enable P acquisition from the soil solution, and an efficient reutilization of P already present in plant cells. Nitric oxide (NO) is a bioactive molecule with a plethora of functions in plants. Its endogenous synthesis depends on internal and environmental factors, and is closely tied with nitrogen (N) metabolism. Furthermore, there is evidence demonstrating that N supply affects P homeostasis and that P deficiency impacts on N assimilation. This review will provide an overview on how NO levels *in planta* are affected by P deficiency, the interrelationship with N metabolism, and a summary of the current understanding about the influence of this reactive N species over the processes triggered by P starvation, which could modify P use efficiency.

Keywords: abiotic stress, acid phosphatases, plant mineral nutrition, phosphate, reactive nitrogen species

OPEN ACCESS

Edited by:
Manuel Nieves-Cordones, Spanish National Research Council, Spain

Reviewed by:
John Hancock, University of the West of England, United Kingdom
Sylvia Morais De Sousa, Embrapa Maize and Sorghum, Brazil

***Correspondence:**
Marcela Simontacchi
marcelasimontacchi@agro.unlp.edu.ar

Specialty section:
This article was submitted to Plant Nutrition, a section of the journal Frontiers in Plant Science

Received: *03 December 2019*
Accepted: *23 March 2020*
Published: *15 April 2020*

Citation:
Galatro A, Ramos-Artuso F, Luquet M, Buet A and Simontacchi M (2020) An Update on Nitric Oxide Production and Role Under Phosphorus Scarcity in Plants. Front. Plant Sci. 11:413. doi: 10.3389/fpls.2020.00413

INTRODUCTION

It is not uncommon for plant roots to be exposed to temporary changes in local P availability. Considering the pivotal roles of this macronutrient in energy dynamics and metabolic regulation, P fluxes coordinately adjust to balance growth and development at the level of the whole plant. In the same way as it occurs with other mineral nutrients, both local signals acting on the cellular level, and long-distance or systemic signaling pathways, communicating internal nutrient status across different tissues and plant organs, must act coordinately to improve nutrient acquisition and internal utilization (Giehl et al., 2009; Lin et al., 2014; Ham et al., 2018; Wang et al., 2018; Ueda and Yanagisawa, 2019). The signaling compounds, such as NO and hormones, are involved in regulatory pathways when availability of nutrients is scarce (Giehl et al., 2009; Lei et al., 2011).

Abbreviations: AM, arbuscular mycorrhizal; APases, acid phosphatases; ARC, amidoxime reducing component; cPTIO, 2-(4-carboxyphenyl)-4,4,5,5-tetramethylimidazoline-1-oxyl-3-oxide; DAF-FM DA, 4-amino-5-methylamino-2′,7′-difluorofluorescein diacetate; GA, gibberellic acid; GSNO, S-nitrosoglutathione; IAA, indolacetic acid; N, nitrogen; NiNOR, nitrite:nitric oxide reductase; NO, nitric oxide; NOFNiR, NO-forming nitrite reductase; NOS, nitric oxide synthase; NR, nitrate reductase; P, phosphate; PAPs, purple acid phosphatases; Pi, inorganic phosphate; PTIO, 2-phenyl-4,4,5,5-tetramethylimidazoline-1-oxyl-3-oxide; ROS, reactive oxygen species; SNAP, S-nitroso-N-acetyl-penicillamine; SNP, sodium nitroprusside; WT, wild type; XOR, xanthine oxidoreductase.

In the case of P starvation, other signaling compounds come into play, including P itself, inositol polyphosphate, miRNAs, photosynthates, and calcium (Ruffel, 2018). Recently, a red-light signaling in the regulation of nutrient uptake and use was suggested, as it was found that expression levels of P starvation-responsive genes in Arabidopsis were modulated by PIF4/PIF5 and HY5 transcription factors, which activity is under the control of phytochromes (Sakuraba et al., 2018).

Reactive oxygen species (ROS) and NO have been recognized as early components in several mineral nutrient signaling events (Baxter et al., 2014; Kolbert, 2016). Even though there is a specific localization, timing and intensity of response depending on the depleted nutrient, it has been proposed that ROS and NO may be frequent elements in plant signal transduction cascades in response to nutrient imbalance (Xu et al., 2010; Zhu et al., 2019).

Sensing, signaling and the elaboration of acclimation responses will determine plant survival and performance in conditions of spatial and temporal variability of soil nutrient concentrations. To that end, in this review, we will discuss the current state of knowledge regarding NO functions in plants specifically under P restriction. We will focus on NO levels (and sources) in plants suffering from P deficiency, and its influence over the processes triggered by P starvation, which could modify P acquisition and use efficiency.

PHOSPHATE IN SOIL AND PLANTS

Plants are often exposed to growth-limiting levels of P during their life cycle. As this is also true in crops, in order to maintain yields in low P soils, chemical P fertilizers obtained from mineral deposits are applied in each crop cycle (Baker et al., 2015). Each year around 148 million tonnes of phosphoric rock are mined, and 90% of that is used for food production (Cordell et al., 2009). A fraction of the applied fertilizer is lost to run-off, consequently reaching seas and lakes and resulting in eutrophication processes (Childers et al., 2011). Thus, current agriculture generates massive P mobilization from mineral deposits to water bodies: a one-way flux of a resource considered "non-renewable" (Cordell et al., 2009; Elser and Bennett, 2011). Throughout the whole process of P extraction and use, two main critical points can be identified: depletion of P reserves from mines, affecting future global food production's sustainability, and eutrophication of water reserves, recently reviewed by Schoumans et al. (2014). It is clear that the understanding of diverse processes involved in soil-plant P dynamics constitutes a key point, to face not only an agronomic problem, but also worldwide environmental and economic ones, with a direct impact on water-food-energy security (Jarvie et al., 2015).

The fact that P in soil can be found in a variety of chemical forms – as organic compounds, in the mineral pool as poorly soluble salts, and adsorbed to particle surfaces – turns this nutrient into one of the least available for plant nutrition in the rhizosphere (Raghothama and Karthikeyan, 2005; McLaughlin et al., 2011; Shen et al., 2011). P from organic sources needs to be released through mineralization processes carried out by soil microorganisms and enzymes present in root exudates. Roots are able to uptake P from the soil solution in the form of $H_2PO_4^-$ and HPO_4^{2-}, and whereas the dynamic balance of available and non-available P is determined by diverse soil and climate conditions (Marschner, 2011), it is also modified by plant roots (Wang et al., 2015), microorganisms (Khan et al., 2016), and other physiological traits (Pang et al., 2018). Therefore in this complex matrix only a small portion of total P in soil is available for plants (Pierre and Parker, 1927). As a consequence only 10–20% of P-containing fertilizers applied are available in the short term (reviewed by Chien et al., 2012). Plants with limited P supply induce changes in pH, organic acids (carboxylates) concentration, and activity of enzymes in the rhizosphere (Hallama et al., 2019), improving P solubility and availability (**Figure 1**).

Phosphorus is easily remobilized internally, and this is of great agronomic importance. According to some authors, P use-efficiency in crops is determined not only by uptake efficiency but also other factors including utilization inside the plant, once the P is taken up, and the production of economically relevant plant tissues per unit of incorporated P (Schröder et al., 2011). P remobilization increases under external P restriction or during senescence. Remobilization occurs, in general, from leaves but also from proteoid roots as is the case of the harsh hakea where ∼85% of P can be reallocated (Shane et al., 2014). Vacuoles are the

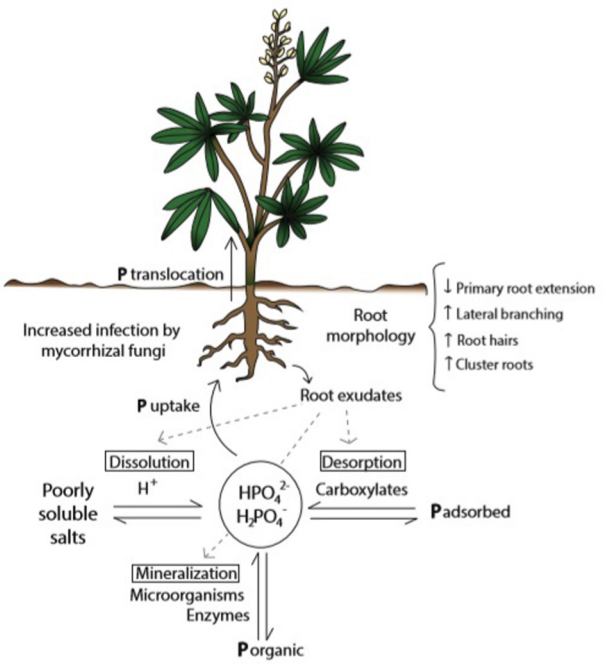

FIGURE 1 | Plant's strategies to improve P availability and uptake from soil solution in conditions of P scarcity. Acclimation responses tend to increase soil exploration (through morphological changes in roots), P desorption, dissolution, and interaction with microorganisms, as well as P internal remobilization (reallocation and interaction between P pools). P from the soil solution is taken up by the roots in the form of HPO_4^{2-} and $H_2PO_4^-$. Figure shows the dynamic equilibrium between available and not available P forms in soil, influenced by root exudations.

primary intracellular compartments for inorganic P (Pi) storage, with active participation in remobilization (Yang et al., 2017). In vacuoles at pH 5.0, monoanion $H_2PO_4^-$ predominates as the Pi species occurring in the efflux with a concentration in the millimolar range (Pratt et al., 2009). Using *in vivo* ^{31}P-NMR, which allows for the discrimination between cytosolic-Pi and organelles-Pi pools, it has been found that, following the onset of P starvation, the Pi efflux from vacuoles is insufficient to compensate for a rapid decrease in the cytosolic Pi concentration. The sudden drop of cytosolic-Pi could be the first endogenous consequence to P starvation, triggering a signal transduction pathway which activates the P starvation rescue metabolism (Pratt et al., 2009). In addition to vacuole stock, when plants are exposed to P restriction, cell walls, membranes, RNA, and available organic compounds containing P, become important sources for the delivery of P to the actively growing tissues.

To better understand P fluxes in order to improve P use-efficiency by plants, a holistic interpretation of agroecosystems needs to be developed. This would identify the impacts of anthropic intervention through fertilization and diverse agricultural practices, soil P dynamics in connection with climate and microbiota, and plant physiological traits which modulate P acquisition and resulting internal reutilization (Macintosh et al., 2019).

Investigation of plant traits associated with agricultural P management is on the rise. New approaches are emerging such as the global-scale ecosystem services connected to soil fertility management (Macintosh et al., 2019) which is intended to overcome traditional agricultural perspectives, mainly focused on crop yield and short-term economic profits. In close connection with a global focus, P dynamic should also be studied at plant cellular and physiological levels. In this context, NO has influence on mechanisms which could increase soil exploration (Wu et al., 2014) and P availability (Ramos-Artuso et al., 2018), as well as mechanisms which could improve internal reutilization (Zhu et al., 2017). Thus, NO could be a key component in agro-ecosystem P flux interpretation, through modulation of P dynamics on plant physiological and plant-soil relationship levels.

NITRIC OXIDE IN SOIL AND PLANTS

Nitric Oxide Synthesis in Plant Cells

Nitric Oxide can be endogenously produced by plant cells, but it can also be incorporated from the environment where it is generated as a result of activity of soil microorganisms. NO is a direct intermediate of nitrification (biological oxidation of ammonium, NH_4^+, to nitrate, NO_3^-) and denitrification processes (reduction of NO_3^-, to nitrogen gas, N_2) carried out by microorganisms (Payne, 1976; Skiba et al., 1993; Feelisch and Martin, 1995). Soils are an important source of NO, and environmental conditions such as the presence of inorganic fertilizers can affect NO emissions. In this context, questions arise as to whether increased NO fluxes derived from N fertilization may affect growth and development, influence plant nutrition, and also affect a range of other plant responses (Lamattina et al., 2003). On the other hand, associative or symbiotic relationships between roots and microorganisms may contribute to NO production, and could also influence NO synthesis on each other (Molina-Favero et al., 2007).

Regarding NO synthesis, in mammals, nitric oxide synthase (NOS) enzymes use L-arginine, O_2, and NADPH, to produce NO (Stuehr, 1999). In plants, different enzymatic and non-enzymatic sources can contribute to the generation of NO (Moreau et al., 2010; Fröhlich and Durner, 2011; Gupta et al., 2011; Mur et al., 2013; Astier et al., 2017), which have been classified as either oxidative or reductive pathways depending on the substrate involved (Gupta et al., 2011). NO production associated with NR, plasma membrane-associated nitrite:NO reductase (NiNOR) and other molibdo-enzymes (such as xanthine oxidoreductase, XOR), in addition to mitochondrial and chloroplastic electron transport chains, are all reductive pathways and depend on NO_2^- as a primary substrate. Meanwhile, NO production from arginine, polyamines or hydroxylamine, belongs to the oxidative pathways.

Progress has recently been made concerning the two main sources of NO, arginine-dependent (known as NOS-like activity) and NR in plant tissues. Jeandroz et al. (2016) searched for the presence of transcripts encoding NOS proteins in over 1000 species of land plants and did not find typical NOS sequences. In photosynthetic organisms, only a few algae species contained NOS orthologs (Jeandroz et al., 2016; Santolini et al., 2017), such as the green alga *Ostreococcus tauri* (Foresi et al., 2010). However, the presence of proteins structurally unrelated to known NOS, or the cooperation between proteins or peptides, which combined can form a complex with similar NOS activity, cannot be discarded in higher plants (Fröhlich and Durner, 2011; Corpas and Barroso, 2017). In this scenario, NO production from NR seems to gain more relevance, considering the importance of NO_3^- reduction and assimilation in plants. According to Chamizo-Ampudia et al. (2016), in *Chlamydomonas reinhardtii*, NR can supply electrons from NAD(P)H, through its diaphorase/dehydrogenase activity, to the molybdoenzyme NOFNiR (NO-forming nitrite reductase, also known as Amidoxime Reducing Component, ARC), which is in fact responsible for NO synthesis from NO_2^-, even in the presence of NO_3^-, condition under which NR is unable to do that. In addition, NR participates in the control of NO levels in cell by supplying electrons to the truncated hemoglobin THB1, which has dioxygenase activity (it can dioxygenate NO to produce NO_3^-). THB1 would then act by removing the very reactive NO and simultaneously inhibiting NR by uncoupling the electron transfer from NAD(P)H to NO_3^- (redirecting the electrons from FAD to THB1). THB1 then plays a dual role in NO detoxification and in the modulation of NR activity (Sanz-Luque et al., 2015). Further research on the conditions that regulate NO or NO_2^- production (such as the factors which favor the activity of NOFNiR and hemoglobins over NR) is required (Chamizo-Ampudia et al., 2017).

Over the last few years, research in the field of NO generation in plants has advanced. However, knowledge of the regulation of the multiple proposed pathways, especially under stress conditions, and in particular under mineral nutrient

deprivation, is still limited. Different sources may come together, depending on stress conditions, substrate availability, species, and plant's organs. Knowledge of the sources (and fates) of NO which operate under nutrient deficiency, in addition to the understanding of the specific roles of this molecule, are key tools to unraveling the mechanisms which trigger acclimation responses, where the modulation of endogenous levels of this molecule could be involved.

Nitric Oxide Targets in Plants

Nitric oxide may exert its biological functions through protein modifications, such as tyrosine nitration or S-nitrosation (also termed as S-nitrosylation), or through interaction with metalloproteins (metal-nitrosylation) (**Figure 2**), besides performing a broad spectrum of biochemical events through the interaction with hormones, and ROS among others (Gupta et al., 2020).

Although in animals the NO/cGMP-signaling (cyclic guanosine monophosphate) pathway has a main role in transmitting NO signal, plants have developed specific NO signaling different from other eukariotic lineages. According to recent studies, typical NO/cGMP signaling module is absent from representative plant species, while S-nitrosation has emerged as major NO-dependent signaling mechanisms in plants (Astier et al., 2019). Proteins and low-molecular-weight thiols can undergo S-nitrosation, where NO binds the thiol group of cysteinyl residues. S-nitrosation is a reversible post-translational modification by which NO can modulate protein activity.

S-nitrosoglutathione (GSNO) is the most abundant low-molecular-weight nitrosothiol and, in turn, it is considered to be a form of NO storage and long-distance transport (reviewed in Begara-Morales et al., 2019). NADPH-dependent thioredoxin reductase (NTR)/thioredoxin (Trx) system and GSNO reductase (GSNOR) control the extent of S-nitrosation through the regulation of GSNO levels and catalyzing denitrosation reactions (Begara-Morales and Loake, 2016).

Tyrosine nitration is mediated by reactive nitrogen species, such as $ONOO^-$ and nitrogen dioxide (NO_2), formed as secondary products of NO metabolism in the presence of oxidants, such as superoxide radicals (O_2^-), hydrogen peroxide (H_2O_2), and transition metal centers (Radi, 2004). In a relevant position, Tyr nitration can alter protein function and conformation, impose steric restrictions, and also inhibit Tyr phosphorylation. The result may be a loss-of-function (if a large fraction of protein is nitrated in specific critical tyrosines) or a gain-of-function (a small fraction of nitrated protein can elicit a substantive biological signal) (Radi, 2004). Evidence shows that protein Tyr nitration is an important NO-dependent signaling mechanism in plants, as well as nitration of fatty acids and ribonucleic acids (Arasimowicz-Jelonek and Floryszak-Wieczorek, 2019).

It is necessary to understand NO effects in the context of a complex network of molecules (Kolbert et al., 2019). The interaction of NO with other small signaling molecules, such as ROS and hydrogen sulfide (H_2S), contributes to the regulation of growth, development, and of biotic and abiotic stresses responses (Singh et al., 2019; **Figure 2**). So far, there is insufficient knowledge of the specific crosstalk involving RNS, ROS and H_2S under P-scarcity.

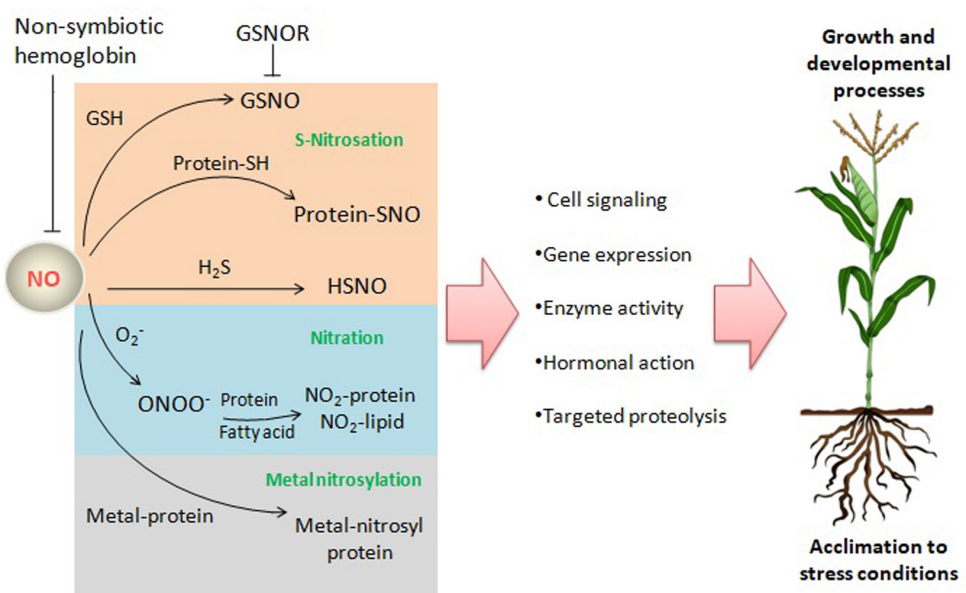

FIGURE 2 | NO reactions and targets in plants. NO may exert its biological functions through interaction with ROS, the gasotransmitter H_2S, proteins, and lipids leading to a broad range of biochemical events affecting signaling pathways and processes related to growth, development and acclimation to stress conditions. GSNO, S-nitrosoglutathione; GSNOR, GSNO reductase; O_2^-, superoxide anion; $ONOO^-$, peroxynitrite; H_2S, hydrogen sulfide; HSNO, thionitrous acid (the smallest S-nitrosothiol); Protein-SNO, nitrosated protein.

These mechanisms may account, in part, for the broad spectrum of NO actions in plants exposed to P imbalances, including posttranslational modification of proteins, enzymes, transporters and transcription factors, which may participate, in addition to hormones, in some of the physiological responses summarized here.

The Levels of Nitric Oxide Are Influenced by P Deficiency

Wang et al. (2010) described a relationship between NO generation and P restriction in white lupin (*Lupinus albus*), where P deficiency enhanced NO production in primary and lateral root tips, with a bigger increase in juvenile and mature cluster roots (bottlebrush like structures). In searching for NO sources, root treatment with the mammalian NOS inhibitor (NG-nitro-L-arginine) and the XOR inhibitor (allopurinol) was found to reduce NO concentration in cluster roots, whereas with the NR inhibitor (tungstate), no effect of treatment was observed. Thus NOS-like activity and XOR may be two of the sources involved in NO production under P deficiency in white lupin.

In *Arabidopsis thaliana*, however, the NR double mutant (*nia1,2*) resulted in more sensitivity to P scarcity than WT plants, which indicated an impairment of the mechanisms involved in the acclimation to low P in these mutants. Moreover, P deprivation led to an increased NO production in roots from WT plants but not from *nia1,2*, which suggested a role for the NR pathway in NO production under P restriction conditions in Arabidopsis (Royo et al., 2015). In regards to soybean plants, P deprivation led to higher levels of NO in the leaves and an increase in NR activity as early as 24 h of P deprivation (Ramos-Artuso et al., 2019). Interestingly, the levels of total N, NO_3^-, NO_2^-, and the activities of other enzymes from N metabolism, were not affected. NR activity and NO generation may play a part in sensing P levels in cells triggering early metabolic responses to deal with P scarcity, as was suggested by the changes observed in the proteome in soybean leaves (Ramos-Artuso et al., 2019). Moreover, P deficiency induced an increase in NO level in rice roots (Zhu et al., 2016) where it was involved in cell-wall P reutilization, upstream of ethylene (Zhu et al., 2017).

Overall, NO seems to have a role in conditions of P scarcity in plants, not only in root response but also in shoot, where early changes are triggered as a consequence of P decrease. The two main ways of NO production in plants, NR and arginine-dependent, seem to be involved in the regulation of NO levels in the cell, but other potential sources (such as polyamines and other ways of NO_2^- reduction) cannot be ruled out, and may also contribute to NO synthesis in conditions of P restriction. Future research will clarify this variable scenario dependent on multiple factors, including plant species, organ, source of N, and the level of P in the cell.

Phosphorus Deficiency Affects N Metabolism and Impacts on NO Levels: Potential Regulatory Implications

It is known that P deprivation leads to alterations in N assimilation (Rabe and Lovatt, 1986; Rufty et al., 1993), but how these changes in N metabolism modify NO levels in cell and affect signaling events, is still unknown. Recent studies of P deficiency in plants have shown an increase in NO levels and suggest this molecule takes part in some responses related to acclimation conditions. Taking into account this scenario, changes in NO levels may either result in or be the result of alteration in N metabolism under conditions of P scarcity since N assimilation and NO generation are strongly connected. As mentioned before NO_2^- and arginine, both derived from N assimilation and metabolism, are substrates for NO synthesis, and both the amount and the form of N supply (NO_3^- or NH_4^+) could affect NO generation (Buet et al., 2019). Zhu et al. (2016) observed an increased NO content in roots from two rice cultivars under P-deficient conditions, where the feeding with NH_4^+ significantly increased the NO level as compared with NO_3^- treatment. The effect of NH_4^+ over the NO levels was also observed in Arabidopsis plants with Fe deficiency (Zhu et al., 2019). In the case of soybean plants fed with NH_4^+, N assimilation occurs mainly in the roots, where the incorporation into amino acids is faster and stronger than with NO_3^- as N source. This suggests a protective role, to avoid accumulation of high levels of NH_4^+, which can produce deleterious effects on cellular functions (Oliveira et al., 2013). In P-deficient leaves, it has been proposed that arginine biosynthesis may act as a protective mechanism for NH_4^+ detoxification (Rabe and Lovatt, 1986; Rufty et al., 1993). This highlights the need for an evaluation of arginine and polyamines levels in roots, as potential sources of NO in conditions of P deficiency.

In soybean (*Glycine max*), long-term P deprivation (20 days) led to several changes in N assimilation: rates of $^{15}NO_3^-$ uptake and net translocation of ^{15}N from roots to shoots decreased, resulting in the alteration of NO_3^- assimilation. Asparagine accumulated to high levels in stems and roots, and arginine accumulated to high levels in leaves was also observed (Rufty et al., 1993). Arginine levels increased in leaves of rough lemon (*Citrus limon*) and summer squash (*Cucurbita pepo*), when grown under P deficient conditions (Rabe and Lovatt, 1986). Nitrite levels increased in WT Arabidopsis roots after exposure of P restriction for 14-days (Royo et al., 2015) but not in soybean leaves after 24 h of P scarcity (Ramos-Artuso et al., 2019). However, in both plant species, NO increased and NR activity seemed to be involved in NO generation. If the amount of substrates for NO synthesis is affected under P deficiency, its availability may affect NO levels, but this factor is not the only one point of control for NO generation.

During P deficiency, the alteration of nutrient transport may be a non-specific result of changes in energy (low ATP), rates of water flow (hydraulic conductance), and membrane permeability; but other feedback control factors could affect NO_3^- uptake (Rufty et al., 1993). It is worth mentioning that in *C. reinhardtii*, NO inhibited the high-affinity uptake of NH_4^+ and NO_3^-/NO_2^-, as well as NR activity in a reversible form which may include post-translational regulation (Sanz-Luque et al., 2013). It has been extensively noted that NO affects NR activity, but the effect depends on several factors, such as the N source (e.g., NO_3^- concentration in the growth medium) and the level of NO or GSNO reached in each system (Buet

TABLE 1 | Summary of NO effects on some physiological responses observed under P starvation and the potential components involved.

Plant species	Treatment	Physiological effect observed	Major components involved	References
Lupinus albus	P-deficiency (0 P) + SNP (50 μM)	Increased number of cluster roots and first-order lateral roots	Interaction with auxins (?)	Wang et al., 2010
		Increased concentration of citrate in exudation from cluster roots	Activation of plasma membrane H^+-ATPase (?) Citrate metabolism (?)	
	P-deficiency (0 P) + cPTIO (500 μM)	Decreased number of cluster roots	Expression of genes that regulate cell division and radial root patterning	Meng et al., 2012
Arabidopsis thaliana	P-deficiency (5 μM P) + SNP (10–100 μM)	Primary root growth inhibition	DELLA proteins stabilization in root tip nuclei	Wu et al., 2014
Arabidopsis thaliana (nia1,2)	P-deficiency (0 P) + GSNO (200 μM)	Improved plant growth and alternative respiration rate	Alternative oxidase pathway (AOX)	Royo et al., 2015
Zea mays	P-deficiency (0 P) + GSNO (100 μM)	Increased Pi uptake from diluted solutions	P transporters (?)	Ramos-Artuso et al., 2018
		Increased P release from organic compounds	Activity of root APases	
		Increased external medium acidification	H^+-ATPase (?) Citrate metabolism (?)	
Oryza sativa	P-deficiency (0 P) + SNP (2.5 μM)	Increased P translocation from roots to shoots	Expression of a phosphate transporter gene (OsPT2)	Zhu et al., 2016, 2017
		Increased soluble P	Cell wall pectin content	

SNP and GSNO are NO donors, cPTIO is an NO scavenger, nia1,2 is the nitrate reductase double mutant, (?) stands for proposed or potential components involved. Physiological effect refers to that observed as compared to P-deficient treatment.

et al., 2019, and references therein). Frungillo et al. (2014) has proposed that NO regulates NO_3^- assimilation pathways and also controls its bioavailability by modulating its own consumption in *A. thaliana*. The authors observed that high levels of NO and S-nitrosothiols induced a switch from high- to low-affinity NO_3^- transport reducing NO_3^- uptake. The authors also observed that genetically elevated levels of GSNO inhibited the activity of NR while reduced levels promoted its activity. Also the enzyme GSNO reductase (GSNOR1) was inhibited by S-nitrosation. As this enzyme catalyses the NADH-dependent reduction of GSNO (stable pool of NO) to oxidized glutathione and NH_4^+, its inhibition could prevent this GSNO degradation and amplify S-nitrosothiols signals (Frungillo et al., 2014). Further research would highlight whether this regulation of N assimilation could also operate in conditions of P scarcity, modulate NO levels and, in turn, P deficiency responses.

In P scarcity conditions, diverse factors such as changes in the availability of substrates (as NO_2^- or/and arginine) and modulation in the activity of some enzymes, including NR, XOR or NOS-like, can contribute to modify NO levels *in planta*. Despite NO origin, it may regulate N assimilation and, as a result, its own levels to participate in signaling events to afford P deficiency.

PLANT'S ACCLIMATION TO P RESTRICTION

Plants sense low P availability, leading to the activation of a complex signaling network, which runs morphological, metabolic and physiological modifications often with great variations among species or even cultivars. In general, main modifications allow plants to enhance soil exploration, and P availability in the soil solution, as well as to maintain P homeostasis at the whole-plant level.

In this section we will discuss the extent to which the presence of NO could affect key plant acclimation responses to P scarcity (**Table 1**).

Root Morphology

Cluster Roots

As a response to P starvation, root architecture sustains modifications which shows a higher presence of roots in the topsoil horizon- usually the P-enriched fraction- (Peret et al., 2014; Del-Saz et al., 2018). These morphological responses probably contribute to an efficient acquisition of this nutrient (Aibara and Miwa, 2014).

One of the most remarkable adaptations for some species consists in the development of proteoid or cluster roots when they are growing in conditions of P scarcity. These roots expose an enhanced surface area and strongly acidify the rhizosphere. White lupin (*Lupinus albus*) is frequently used as a model plant to study the formation and function of cluster roots under P-deficient conditions (Cheng et al., 2011). Shoot P concentration, sucrose and hormones (cytokinins, ethylene, and auxins) have been identified as participants in cluster root development (Cheng et al., 2011; Meng et al., 2013; Müller et al., 2015). In addition, after 32 days of P restriction, cluster roots showed a massive change in gene

transcription (Venuti et al., 2019). A relationship between NO and morphological changes in roots has been described in lupin plants under P restriction. Using the fluorescent probe DAF-FM DA, NO was found to increase in the pericycle, endodermis cells and rootlet primordia from plants exposed to P restriction during 20 days. These results, and the timing of NO accumulation, led the authors to suggest NO was involved in the initiation, development and emergence of rootlets in the P deficiency-induced cluster-root formation (Wang et al., 2010; Meng et al., 2012). In addition, treatments with NO donors SNP and GSNO induced changes in roots morphology (Wang et al., 2010; Meng et al., 2012).

Primary and Lateral Roots

In species with non-proteoid roots, the reshaping of the root system architecture under P-deficiency usually includes the development of lateral roots and the inhibition of primary root extension (Peret et al., 2014). A crosstalk between auxins (known as root growth regulators) and NO has been described for cucumber explants. In this system, NO accumulation was detected after exposure to indolacetic acid (IAA, an auxin), and treatment with NO donors SNP (10 μM) and S-nitroso-N-acetyl-penicillamine (SNAP 10 μM) induced the production of adventitious roots to the same extent as IAA (Pagnussat et al., 2002). In tomato and maize plants, treatment with auxins (1-naphthylacetic acid and IAA) or SNP (200 μM) induced similar lateral root formation (Correa-Aragunde et al., 2004; Zandonadi et al., 2010). Further research has led to suggest that NO is required for cell cycle progression and establishment of lateral root primordia in the pericycle as NO modulates cell cycle regulatory genes (Correa-Aragunde et al., 2006). However, the relationship between NO and auxins in the context of root development under P deprivation still needs addressing.

The effect of NO on primary roots was described for tomato growing under sufficient nutrient conditions, where treatment with SNP (200 μM) strongly reduced primary root length, whose effect was reversed in the presence of NO scavenger cPTIO (Correa-Aragunde et al., 2004). In Arabidopsis, the inhibitory effect of exogenous NO treatment (SNP 10–100 μM) was observed for both P-sufficient and P-deprived plants (Wu et al., 2014). Even though the use of cPTIO confirmed a direct action of NO, there remained doubt as only the Fe-containing NO donor (SNP) was used as exogenous NO source (Wu et al., 2014). In Arabidopsis, it was described that localized Fe accumulation in the root tip – rather than the reduction in P concentration- was responsible for the growth inhibition under P restriction (Ward et al., 2008). Growth arrest requires accumulation of transcription factor STOP1 in the nucleus. Under P-restriction, it has been proposed that Fe stimulates the accumulation of STOP1 in root nuclei which, in turn, activates the transcription of malate transporter gene ALMT1 (Godon et al., 2019). The use of other NO donors, and the measurement of NO levels in each system, will confirm the effect of NO on primary root morphology under P scarcity.

Other mechanisms involving GA and NO may play a part in primary root inhibition under P restriction. Knowing that P starvation decreases GA biosynthesis in Arabidopsis, and that the addition of exogenous GA acts as a positive regulator for primary root growth (Jiang et al., 2007; Wu et al., 2014), the interaction between NO and GA on primary root growth has been analyzed and showed that the treatments, both with NO donor SNP and with NO scavenger cPTIO, modulated the effect of P restriction on primary root growth. In assays using Arabidopsis mutants in DELLA proteins (negative regulators of GA signaling), it was found that exogenous NO (SNP 10 μM) stabilized these proteins in root tip nuclei. Thus NO inhibition of primary root growth involves, at least in part, the DELLA-degradation pathway (Wu et al., 2014).

Root Hairs

Enhanced root hair development is a typical adaptive plant response to P starvation, where increasing root surface area for nutrient uptake is mediated by ethylene (Zhang et al., 2003; Song et al., 2016). The description of NO participation as a regulator of root hair development has long been documented. Lettuce plants treated with SNP (10 μM) showed increased root hair number and elongation, and Arabidopsis root hair development was inhibited by cPTIO (0.5–1 mM). Moreover, NO has been proposed as a mediator of auxin action in root hair growth (Lombardo et al., 2006).

Other nutrient's availability usually affects root hair development, as is the case of Mg deficiency (Liu et al., 2017). Arabidopsis plants exposed to Mg deficiency exhibited increased levels of NO as well as ethylene, and, interestingly, both species were reciprocally influenced and interactively regulated root hair morphogenesis (Liu et al., 2017). Recently, a scheme including auxins has been proposed for plants exposed to Mg deficiency. In Arabidopsis plants subjected to Mg deficiency, both ethylene and NO were required to regulate the rise of auxins in roots (Liu et al., 2018). A positive feedback loop involving auxins, ethylene and NO production under Mg deficiency was found. However, there remains a lack of information regarding the role of ethylene, NO and auxins interaction in root hair development during P scarcity. A similar interaction between NO and phytohormones occurring under P-restriction regulating root hair growth could be anticipated.

P Transport

The upregulation of high-affinity P transporters is a common phenomenon in response to P restriction in order to coordinate nutrient acquisition and distribution (Nussaume et al., 2011). As expected when compared with P-sufficient plants, there was a significant increase in the uptake of Pi from a diluted solution in maize plants exposed for 6 days to P-restriction, and the presence of an NO donor (GSNO 100 μM) further increased the potential capability of roots to incorporate P (Ramos-Artuso et al., 2018). Regulatory pathways integrated by microRNA and ubiquitin/26S proteasome degradation have been proposed for the selective modulation of P transport activity in response to P levels (Lin et al., 2014; Ye et al., 2018). The degradation of P transporters in P-sufficient conditions occurs through ubiquitin-mediated pathways which are reduced under P deficiency, activating Pi uptake as well as root-to-shoot translocation (Wang et al., 2017;

Yue et al., 2017). In this regard, NO has been reported to be involved in ubiquitin-targeted protein degradation events in plants and animals (Arnaud et al., 2006; Kapadia et al., 2009). There is no knowledge directly related to how NO may affect P transport in plants; however, the activity of P transporters is regulated at both transcriptional and post-transcriptional levels (Nussaume et al., 2011), remarkably these processes are affected by NO under abiotic stress (Umbreen et al., 2018; Kolbert et al., 2019).

As mentioned before, P is easily redistributed, especially in plants under P-restriction. This includes the internal redistribution of P pools, the release of P from vacuoles, cell walls, and phospholipids in membranes, while at the whole plant level, P is reallocated to the young actively growing tissues (Veneklaas et al., 2012; Baker et al., 2015; Yang et al., 2017). P-translocation and the interconversion of different pools are related to the up-regulation of P transporters and enzymes (RNAses and phosphatases, among others), which release Pi from a broad range of P monoesters.

P starvation induced a specific group of cell-wall localized and intracellular APases, the PAPs (Shane et al., 2014; Ramos-Artuso et al., 2019), and in soybean the expression of a particular PAP (PAP21) increased in roots and old leaves, playing an important role in the utilization and recycling of P from intracellular reserves under P-starving conditions (Li et al., 2016). The same authors found that the overexpression of *GmPAP21* enabled plants to achieve around 96% higher fresh weight under P restriction as compared with WT plants, pointing out the role of this enzyme in internal P use efficiency in plants. Results of assays on maize plants (*Zea mays*) exposed to an NO donor during P restriction suggested NO played a part in the enhanced activity of root APases (Ramos-Artuso et al., 2018). Short term P-deprivation experiments (48 h) showed that the increase in gene expression and in activity of PAP1 in roots from *Medicago falcata* were dependent on the presence of the ethylene hormone (Li et al., 2011). Also in Arabidopsis, ethylene positively regulates P starvation-induced gene expression and activity of APase (Lei et al., 2011). In addition, during senescence of petunia corolla, ethylene regulated P remobilization and the expression of a P transporter gene (*PhPT1*) (Chapin and Jones, 2009). An interplay between NO and ethylene occurs not only during plant growth and development, but also when the plant is exposed to abiotic stress (Kolbert et al., 2019), as it has been proposed for rice, where P-restriction led to a quick enhanced NO production followed by an ethylene peak (Zhu et al., 2017). As a result, pectin content increased allowing reutilization of P from the cell wall, and at the same time, the expression of a P transporter (*OsPT2*) was up-regulated to facilitate the translocation of P from root to shoot, improving growth under P restriction (Zhu et al., 2016, 2017). To our knowledge this is the only study over the effect of NO (applied as SNP), showing that NO increases the expression of a P transporter gene under P deficiency (Zhu et al., 2017).

Since P-restriction produces an increase in NO (Wang et al., 2010; Ramos-Artuso et al., 2019) and in ethylene levels (Borch et al., 1999; Zhu et al., 2016), both species could interact, and contribute to optimizing P availability and translocation inside plant, affecting P use efficiency.

Changes in the Rhizosphere

As a large proportion of P in soil is precipitated, chelated with metals, or becomes a constituent of organic compounds, the exudation of organic acids, protons and enzymes by roots contributes to improving plant's P availability (Gaume et al., 2001; Shen et al., 2006; Pang et al., 2015). The "strategy" used varies greatly depending on plant species, genotypes and soil conditions (Hallama et al., 2019).

The induced secretion of ribonucleases, nucleases, phosphodiesterases, and APases is involved in P release from soil-localized organic substrates, such as nucleic acids and their degradation products, making P available for root uptake (Plaxton and Tran, 2011). Organic acids released from roots in the form of anions also contribute to increase P availability since they dissolve precipitates and chelate metal cations, and also block binding sites on soil particles. Citrate, malate and succinate from leaves can be transported via the phloem and directed to roots for exudation (Alexova et al., 2017). Citrate is the major organic acid released, and is one of the most effective species for solubilization of sparingly soluble P forms in soils (Igamberdiev and Eprintsev, 2016). NO was found to affect organic acid metabolism in citrus plants (*Citrus grandis*), where citrate content in roots increased after treatment with SNP (10 and 500 μM), due to an alteration in transport from leaves, whereas malate content increased (after treatment with 500 μM SNP), probably due to changes in the activity of the enzymes responsible for its synthesis and degradation (Yang et al., 2012). However, the dose of SNP used was toxic since plant growth was inhibited. As it has been previously discussed, lupin plants develop cluster roots under P-deficient conditions, characterized by their capacity to exude huge amounts of organic acids with citrate as the main component. Incubation of cluster roots from P-deficient lupin plants in the presence of an NO donor (SNP 50 μM, during 24 h) stimulated even more citrate exudation from the root, while the presence of cPTIO (an NO scavenger) had an inhibitory effect (Wang et al., 2010). Considering the side effects of SNP (León and Costa-Broseta, 2019), it would be interesting to test the effect of NO on organic acids production and exudation when using other NO donors in addition to carefully designed experimental approaches (such as the use of appropriate controls and scavengers).

Plant plasma membrane H^+-ATPases transport protons out of the cell, controlling cell's membrane potential and enabling the major transport processes in the plant, such as root nutrient uptake (Duby and Boutry, 2009). Enhanced H^+ release to the rhizosphere occurs as a response to P-shortage and plays an important role in the acclimation to P-deficiency (Shen et al., 2006). Decrease in rhizosphere pH helps to dissolve P from Ca, Al or Fe phosphates and to increase P availability in calcareous soils (Hallama et al., 2019). It has been shown that the activity of plasma membrane H^+-ATPase increases in P-restricted proteoid roots from lupin plants (Yan et al., 2002), and the enzyme has been described as an important component in responses to P restriction in soybean roots, where pharmacological and genetic approaches showed a parallel between enzyme activity and P uptake (Shen et al., 2006). Humic substances are naturally present in soils and, in addition to affecting root morphology,

they stimulate the activity of H^+-ATPase (Canellas et al., 2002). Interestingly, a link was found between NO and the humic-acid stimulation of H^+-ATPase. In maize roots, plasma membrane H^+-ATPase activity increased in the presence of NO donor SNP (200 μM), and the stimulatory effects of humic acids were inhibited by the addition of NO scavenger PTIO (Zandonadi et al., 2010). Moreover, data supporting a role for NO in the expression and activity of H^+-ATPase were described in other systems under study. Calluses from reed (*Phragmites communis* Trin.) exhibited enhanced H^+-ATPase activity 48 h after incubation with SNP (200 μM), and a reduced activity after treatment with PTIO (Zhao et al., 2004). None of the previous studies regarding the influence of NO or humic acids on the activity of H^+-ATPase were performed under P restriction. Recently, maize plants exposed 6 days to P deprivation, being simultaneously in the presence of an NO donor (GSNO 100 μM), were found to exhibit higher capacity of external medium acidification as compared with P-deprived plants (Ramos-Artuso et al., 2018). It is worth considering that NO can be generated non-enzymatically in the apoplast, and its synthesis is favored when pH is low (Stöhr and Ullrich, 2002; Bethke et al., 2004). Thus, a mechanism in which NO induces external medium acidification, which, in turn, enhances NO synthesis under P-restricted conditions, may be suggested. Further experiments are necessary to unravel the role of NO over H^+-ATPase activity in plants under P-restriction.

Apoplast acidification, through the activity of plasma membrane H^+-ATPase, is also influenced by auxins, and it is involved not only in nutrient uptake, but also in cell growth (Rayle and Cleland, 1992). Auxins also induce accumulation of NO in roots, as has been evaluated in Arabidopsis, soybean, tomato, and cucumber (Pagnussat et al., 2002; Correa-Aragunde et al., 2004; Hu et al., 2005; Terrile et al., 2012). It is therefore possible to speculate an interplay between NO and auxins in the modulation of H^+-ATPase activity under P scarcity.

Symbiotic Associations

The broad range of adaptive P stress responses includes the establishment of symbiotic association with AM fungi (Mensah et al., 2015), through which plants can enhance their capacity to acquire P from soils by increasing root uptake volume, dissolving insoluble P, mineralizing organic P, and avoiding P slow diffusion from the soil solution to root surface (Zhang et al., 2014). AM symbiosis has been associated with changes in the amount of plant hormones in roots (cytokinins, auxins, ethylene, jasmonic acid, abscisic acid and strigolactones), and NO has recently been described as playing a role at the early stages of that interaction (reviewed in Martínez-Medina et al., 2019b). Five days after inoculation of *Medicago truncatula* with *Glomus mosseae*, the expression of the NR gene was significantly upregulated in roots. It was suggested that a diffusible fungal factor was perceived by the host tissues, since the same result was obtained when roots had been physically separated from *G. mosseae* hyphae by a semipermeable barrier (Weidmann et al., 2004). In search for a link between NR transcript accumulation and NO levels, roots of *M. truncatula* were exposed to fungal exudates obtained from germinating *Gigaspora margarita*, simulating the presymbiotic phase of the interaction (Calcagno et al., 2012). During the first minutes after exposure, increases in NO levels were found in the epidermal and cortical tissues of roots evaluated using DAF-2DA and confocal microscopy. Moreover, NR transcript level increased after 10 min of treatment, and AM-dependent NO accumulation was suppressed when NR activity was inhibited with tungstate (Calcagno et al., 2012).

Increased levels of NO, associated with AM-plant interaction, were also confirmed in: roots of *Trifolium repens* L. inoculated with *G. mosseae* (Zhang et al., 2013); olive roots in association with *Rhizophagus irregularis* (Espinosa et al., 2014); *P. trifoliata* seedlings colonized by *D. versiformis* (Zou et al., 2017); and tomato plants at the onset of the AM symbiosis with *R. irregularis* (Martínez-Medina et al., 2019a). Based on these results, Martínez-Medina et al. (2019b) has proposed a model for the establishment of mycorrhizal symbiosis which, during the pre-symbiotic stages, diffusible fungal signals are perceived by the plant, triggering a burst of NO linked with the activation of the symbiotic regulatory pathway. This partially suppresses the host immune responses and prepares the plant for fungal colonization. In later stages, the level of NO in root cells is controlled by the action of phytoglobins (Martínez-Medina et al., 2019b). However, experimental data regarding NO participation during mutualistic interaction in P-restricted conditions are not available. NO's role in some key P-deficiency responses, on the one hand, and in the interaction with AMF, on the other, opens up interesting queries regarding whether integrated responses involving NO and soil microorganisms may occur under P scarcity.

CONCLUDING REMARKS

To date there is little research on NO levels that have been conducted in plants exposed to P scarcity. NO increased after imposition of P-restriction treatments in lupin, Arabidopsis and rice roots, as well as in soybean leaves. NO seems to be implicated in acclimation responses to low P-availability, as it was described for citrate exudation, transcription and activity of a P transporter, P uptake from diluted solutions, external medium acidification and phosphatase activity, as well as modulation of some metabolic pathways. However, other functions of NO (for example, increasing H^+-ATPase activity, role in symbiotic interaction, root hairs development, and lateral roots growth) remain to be studied in plants exposed to low P conditions.

Considering that a large amount of research has been developed using NO donors, caution should be taken regarding some observed side effects. In this regard, the use of other NO donors or scavengers in assays should be encouraged to strongly support some of the results. In addition, measurement of NO levels inside the plant as well as in different organs should be promoted to obtain a more integrated view.

Different mechanisms could be involved in NO synthesis during P scarcity but NR seems to have a critical role because of the close relationship between N metabolism and NO generation. Once NO concentration rises to a critical value, it may regulate its own specific level to exert a particular function. An interesting

interaction of NO with hormones, such as ethylene, GA, and auxins during P deficiency may be proposed in some key acclimation responses. Moreover, future research in this field may confirm and show additional actors to this scenario. Overall, we encourage research in NO participation during P deficiency in order to find new tools to improve agricultural practices, avoiding fertilizers misuse and consequently, environmental damage.

AUTHOR CONTRIBUTIONS

AG, FR-A, AB, and MS contributed equally to conceive and write the manuscript. ML prepared the figures and contributed to the writing. All the authors approved it for publication.

FUNDING

This work was supported by funds from the Agencia Nacional de Promoción Científica y Tecnológica (ANPCyT) (PICT 2017-2492), and Universidad Nacional de La Plata (A322).

ACKNOWLEDGMENTS

AB, AG, and MS are researchers from Consejo Nacional de Investigaciones Científicas y Técnicas (CONICET). FR-A and ML thank CONICET and ANPCyT for a fellowship. We are grateful to M. J. Doiny and C. Warwick-Foster for language proofreading.

REFERENCES

Aibara, I., and Miwa, K. (2014). Strategies for optimization of mineral nutrient transport in plants: multilevel regulation of nutrient-dependent dynamics of root architecture and transporter activity. *Plant Cell Physiol.* 55, 2027–2036. doi: 10.1093/pcp/pcu156

Alexova, R., Nelson, C. J., and Millar, A. H. (2017). Temporal development of the barley leaf metabolic response to P i limitation. *Plant Cell Environ.* 40, 645–657. doi: 10.1111/pce.12882

Arasimowicz-Jelonek, M., and Floryszak-Wieczorek, J. (2019). A physiological perspective on targets of nitration in NO-based signaling networks in plants. *J. Exp. Bot.* 70, 4379–4389. doi: 10.1093/jxb/erz300

Arnaud, N., Murgia, I., Boucherez, J., Briat, J. F., Cellier, F., and Gaymard, F. (2006). An iron-induced nitric oxide burst precedes ubiquitin-dependent protein degradation for *Arabidopsis AtFer1* ferritin gene expression. *J. Biol. Chem.* 281, 23579–23588. doi: 10.1074/jbc.M602135200

Astier, J., Gross, I., and Durner, J. (2017). Nitric oxide production in plants: an update. *J. Exp. Bot.* 69, 3401–3411. doi: 10.1093/jxb/erx420

Astier, J., Mounier, A., Santolini, J., Jeandroz, S., and Wendehenne, D. (2019). The evolution of nitric oxide signalling diverges between the animal and the green lineages. *J. Exp. Bot.* 70, 4355–4364. doi: 10.1093/jas/sky123/4962501

Baker, A., Ceasar, S. A., Palmer, A. J., Paterson, J. B., Qi, W., Muench, S. P., et al. (2015). Replace, reuse, recycle: improving the sustainable use of phosphorus by plants. *J. Exp. Bot.* 66, 3523–3540. doi: 10.1093/jxb/erv210

Baxter, A., Mittler, R., and Suzuki, N. (2014). ROS as key players in plant stress signalling. *J. Exp. Bot.* 65, 1229–1240. doi: 10.1093/jxb/ert375

Begara-Morales, J. C., Chaki, M., Valderrama, R., Mata-Pérez, C., Padilla, M. N., and Barroso, J. B. (2019). The function of S-nitrosothiols during abiotic stress in plants. *J. Exp. Bot.* 70, 4429–4439. doi: 10.1093/jxb/erz197

Begara-Morales, J. C., and Loake, G. J. (2016). "Protein denitrosylation in plant biology, Protein," in *Gasotransmitters in Plants. Signaling and Communication in Plants*, eds L. Lamattina and C. García-Mata (Cham: Springer).

Bethke, P. C., Badger, M. R., and Jones, R. L. (2004). Apoplastic synthesis of nitric oxide by plant tissues. *Plant Cell* 16, 332–341. doi: 10.1105/tpc.017822

Borch, K., Bouma, T. J., Lynch, J. P., and Brown, K. M. (1999). Ethylene: a regulator of root architectural responses to soil phosphorus availability. *Plant Cell Environ.* 22, 425–431. doi: 10.1046/j.1365-3040.1999.00405.x

Buet, A., Galatro, A., Ramos-Artuso, F., and Simontacchi, M. (2019). Nitric oxide and plant mineral nutrition: current knowledge. *J. Exp. Bot.* 70, 4461–4476. doi: 10.1093/jxb/erz129

Calcagno, C., Novero, M., Genre, A., Bonfante, P., and Lanfranco, L. (2012). The exudate from an arbuscular mycorrhizal fungus induces nitric oxide accumulation in *Medicago truncatula* roots. *Mycorrhiza* 22, 259–269. doi: 10.1007/s00572-011-0400-4

Canellas, L. P., Olivares, F. L., Okorokova-Façanha, A. L., and Façanha, A. R. (2002). Humic acids isolated from earthworm compost enhance root elongation, lateral root emergence, and plasma membrane H+-ATPase activity in maize roots. *Plant Physiol.* 130, 1951–1957. doi: 10.1104/pp.007088

Chamizo-Ampudia, A., Sanz-Luque, E., Llamas, A., Galván, A., and Fernández, E. (2017). Nitrate reductase regulates plant nitric oxide homeostasis. *Trends Plant Sci.* 22, 163–174. doi: 10.1016/j.tplants.2016.12.001

Chamizo-Ampudia, A., Sanz-Luque, E., Llamas, Á., Ocaña-Calahorro, F., Mariscal, V., Carreras, A., et al. (2016). A dual system formed by the ARC and NR molybdoenzymes mediates nitrite-dependent NO production in Chlamydomonas. *Plant Cell Environ.* 39, 2097–2107. doi: 10.1111/pce.12739

Chapin, L.-J., and Jones, M. L. (2009). Ethylene regulates phosphorus remobilization and expression of a phosphate transporter (PhPT1) during petunia corolla senescence. *J. Exp. Bot.* 60, 2179–2190. doi: 10.1093/jxb/erp092

Cheng, L., Bucciarelli, B., Shen, J., Allan, D., and Vance, C. P. (2011). Update on white lupin cluster root acclimation to phosphorus deficiency update on lupin cluster roots. *Plant Physiol.* 156, 1025–1032. doi: 10.1104/pp.111.175174

Chien, S. H., Sikora, F. J., Gilkes, R. J., and McLaughlin, M. J. (2012). Comparing of the difference and balance methods to calculate percent recovery of fertilizer phosphorus applied to soils: a critical discussion. *Nutr. Cycl. Agroecosyst.* 92, 1–8. doi: 10.1007/s10705-011-9467-8

Childers, D. L., Corman, J., Edwards, M., and Elser, J. J. (2011). Sustainability challenges of phosphorus and food: solutions from closing the human phosphorus cycle. *Bioscience* 61, 117–124. doi: 10.1525/bio.2011.61.2.6

Cordell, D., Drangert, J. O., and White, S. (2009). The story of phosphorus: global food security and food for thought. *Glob. Environ. Change* 19, 292–305. doi: 10.1016/j.gloenvcha.2008.10.009

Corpas, F. J., and Barroso, J. B. (2017). Nitric oxide synthase-like activity in higher plants. *Nitric Oxide* 68, 5–6. doi: 10.1016/j.niox.2016.10.009

Correa-Aragunde, N., Graziano, M., Chevalier, C., and Lamattina, L. (2006). Nitric oxide modulates the expression of cell cycle regulatory genes during lateral root formation in tomato. *J. Exp. Bot.* 57, 581–588. doi: 10.1093/jxb/erj045

Correa-Aragunde, N., Graziano, M., and Lamattina, L. (2004). Nitric oxide plays a central role in determining lateral root development in tomato. *Planta* 218, 900–905. doi: 10.1007/s00425-003-1172-7

Del-Saz, N. F., Romero-Munar, A., Cawthray, G. R., Palma, F., Aroca, R., Baraza, E., et al. (2018). Phosphorus concentration coordinates a respiratory bypass, synthesis and exudation of citrate, and the expression of high-affinity phosphorus transporters in Solanum lycopersicum. *Plant Cell Environ.* 41, 865–875. doi: 10.1111/pce.13155

Duby, G., and Boutry, M. (2009). The plant plasma membrane proton pump ATPase: a highly regulated P-type ATPase with multiple physiological roles. *Pflügers Arch. Eur. J. Physiol.* 457, 645–655. doi: 10.1007/s00424-008-0457-x

Elser, J., and Bennett, E. (2011). Phosphorus cycle: a broken biogeochemical cycle. *Nature* 478, 29–31. doi: 10.1038/478029a

Espinosa, F., Garrido, I., Ortega, A., Casimiro, I., and Álvarez-Tinaut, M. C. (2014). Redox activities and ROS, NO and phenylpropanoids production by axenically cultured intact olive seedling roots after interaction with a mycorrhizal or a pathogenic fungus. *PLoS One* 9:e100132. doi: 10.1371/journal.pone.0100132

Feelisch, M., and Martin, J. F. (1995). The early role of nitric oxide in evolution. *Trends Ecol. Evol.* 10, 496–499. doi: 10.1016/s0169-5347(00)89206-x

Foresi, N., Correa-Aragunde, N., Parisi, G., Caló, G., Salerno, G., and Lamattina, L. (2010). Characterization of a nitric oxide synthase from the plant kingdom:

NO generation from the green alga Ostreococcus tauri is light irradiance and growth phase dependent. *Plant Cell* 22, 3816–3830. doi: 10.1105/tpc.109.07351

Fröhlich, A., and Durner, J. (2011). The hunt for plant nitric oxide synthase (NOS): Is one really needed? *Plant Sci.* 181, 401–404. doi: 10.1016/j.plantsci.2011.07.014

Frungillo, L., Skelly, M. J., Loake, G. J., Spoel, S. H., and Salgado, I. (2014). S-nitrosothiols regulate nitric oxide production and storage in plants through the nitrogen assimilation pathway. *Nat. Commun.* 5:5401. doi: 10.1038/ncomms6401

Gaume, A., Machler, F., De Leon, C., Narro, L., and Frossard, E. (2001). Low-P tolerance by maize (*Zea mays* L.) genotypes: significance of root growth, and organic acids and acid phosphatase root exudation. *Plant Soil* 228, 253–264.

Giehl, R. F. H., Meda, A. R., and von Wirén, N. (2009). Moving up, down, and everywhere: signaling of micronutrients in plants. *Curr. Opin. Plant Biol.* 12, 320–327. doi: 10.1016/j.pbi.2009.04.006

Godon, C., Mercier, C., Wang, X., David, P., Richaud, P., Nussaume, L., et al. (2019). Under phosphate starvation conditions, Fe and Al trigger accumulation of the transcription factor STOP1 in the nucleus of Arabidopsis root cells. *Plant J.* 937–949. doi: 10.1111/tpj.14374

Gupta, K. J., Fernie, A. R., Kaiser, W. M., and van Dongen, J. T. (2011). On the origins of nitric oxide. *Trends Plant Sci.* 6, 160–168.

Gupta, K. J., Hancock, J. T., Petrivalsky, M., Kolbert, Z., Lindermayr, C., Durner, J., et al. (2020). Recommendations on terminology and experimental best practice associated with plant nitric oxide research. *New Phytol.* 225, 1828–1834. doi: 10.1111/nph.16157

Hallama, M., Pekrun, C., Lambers, H., and Kandeler, E. (2019). Hidden miners – the roles of cover crops and soil microorganisms in phosphorus cycling through agroecosystems. *Plant Soil* 434, 7–45. doi: 10.1007/s11104-018-3810-7

Ham, B. K., Chen, J., Yan, Y., and Lucas, W. J. (2018). Insights into plant phosphate sensing and signaling. *Curr. Opin. Biotechnol.* 49, 1–9. doi: 10.1016/j.copbio.2017.07.005

Hu, X., Neill, S. J., Tang, Z., and Cai, W. (2005). Nitric oxide mediates gravitropic bending in soybean roots. *Plant Physiol.* 137, 663–670. doi: 10.1104/pp.104.054494

Igamberdiev, A. U., and Eprintsev, A. T. (2016). Organic acids: the pools of fixed carbon involved in redox regulation and energy balance in higher plants. *Front. Plant Sci.* 7:1042. doi: 10.3389/fpls.2016.01042

Jarvie, H. P., Sharpley, A. N., Flaten, D., Kleinman, P. J., Jenkins, A., and Simmons, T. (2015). The pivotal role of phosphorus in a resilient water–energy–food security nexus. *J. Environ. Qual.* 44, 1049–1062. doi: 10.2134/jeq2015.01.0030

Jeandroz, S., Wipf, D., Stuehr, D. J., Lamattina, L., Melkonian, M., Tian, Z., et al. (2016). Occurrence, structure, and evolution of nitric oxide synthase–like proteins in the plant kingdom. *Sci. Signal.* 9:re2. doi: 10.1126/scisignal.aad4403

Jiang, C., Gao, X., Liao, L., Harberd, N. P., and Fu, X. (2007). Phosphate starvation root architecture and anthocyanin accumulation responses are modulated by the gibberellin-DELLA signaling pathway in Arabidopsis. *Plant Physiol.* 145, 1460–1470. doi: 10.1104/pp.107.103788

Kapadia, M. R., Eng, J. W., Jiang, Q., Stoyanovsky, D. A., and Kibbe, M. R. (2009). Nitric oxide regulates the 26S proteasome in vascular smooth muscle cells. *Nitric Oxide* 20, 279–288. doi: 10.1016/j.niox.2009.02.005

Khan, M. S., Zaidi, A., and Ahmad, E. (2016). "Mechanism of phosphate solubilization and physiological functions of phosphate-solubilizing microorganisms," in *Phosphate Solubilizing Microorganisms*, eds M. S. Khan, A. Zaidi, and J. Musarrat (Cham: Springer), 31–62. doi: 10.1007/978-3-319-08216-5_2

Kolbert, Z. (2016). Implication of nitric oxide (NO) in excess element-induced morphogenic responses of the root system. *Plant Physiol. Biochem.* 101, 149–161. doi: 10.1016/j.plaphy.2016.02.003

Kolbert, Z., Feigl, G., Freschi, L., and Poór, P. (2019). Gasotransmitters in action: nitric oxide-ethylene crosstalk during plant growth and abiotic stress responses. *Antioxidants* 8:167. doi: 10.3390/antiox8060167

Lamattina, L., García-Mata, C., Graziano, M., and Pagnussat, G. (2003). Nitric oxide: the versatility of an extensive signal molecule. *Ann. Rev. Plant Biol.* 54, 109–136. doi: 10.1146/annurev.arplant.54.031902.134752

Lei, M., Zhu, C., Liu, Y., Karthikeyan, A. S., Bressan, R. A., Raghothama, K. G., et al. (2011). Ethylene signalling is involved in regulation of phosphate starvation-induced gene expression and production of acid phosphatases and anthocyanin in Arabidopsis. *New Phytol.* 189, 1084–1095. doi: 10.1111/j.1469-8137.2010.03555.x

León, J., and Costa-Broseta, Á. (2019). Present knowledge and controversies, deficiencies and misconceptions on nitric oxide synthesis, sensing and signaling in plants. *Plant Cell Environ.* 43, 1–15. doi: 10.1111/pce.13617

Li, C., Li, C., Zhang, H., Liao, H., and Wang, X. (2016). The purple acid phosphatase GmPAP21 enhances internal phosphorus utilization and possibly plays a role in symbiosis with rhizobia in soybean. *Physiol. Plant.* 159, 215–227. doi: 10.1111/ppl.12524

Li, Y. S., Gao, Y., Tian, Q. Y., Shi, F. L., Li, L. H., and Zhang, W. H. (2011). Stimulation of root acid phosphatase by phosphorus deficiency is regulated by ethylene in *Medicago falcata*. *Environ. Exp. Bot.* 71, 114–120. doi: 10.1016/j.envexpbot.2010.11.007

Lin, W. Y., Huang, T. K., Leong, S. J., and Chiou, T. J. (2014). Long-distance call from phosphate: systemic regulation of phosphate starvation responses. *J. Exp. Bot.* 65, 1817–1827. doi: 10.1093/jxb/ert431

Liu, M., Liu, X. X., He, X. L., Liu, L. J., Wu, H., Tang, C. X., et al. (2017). Ethylene and nitric oxide interact to regulate the magnesium deficiency-induced root hair development in Arabidopsis. *New Phytol.* 213, 1242–1256. doi: 10.1111/nph.14259

Liu, M., Zhang, H., Fang, X., Zhang, Y., and Jin, C. (2018). Auxin acts downstream of ethylene and nitric oxide to regulate magnesium deficiency-induced root hair development in *Arabidopsis thaliana*. *Plant Cell Physiol.* 59, 1452–1465. doi: 10.1093/pcp/pcy078

Lombardo, M. C., Graziano, M., Polacco, J. C., and Lamattina, L. (2006). Nitric oxide functions as a positive regulator of root hair development. *Plant Signal. Behav.* 1, 28–33. doi: 10.4161/psb.1.1.2398

Macintosh, K. A., Doody, D. G., Withers, P. J., McDowell, R. W., Smith, D. R., Johnson, L. T., et al. (2019). Transforming soil phosphorus fertility management strategies to support the delivery of multiple ecosystem services from agricultural systems. *Sci. Total Environ.* 649, 90–98. doi: 10.1016/j.scitotenv.2018.08.272

Marschner, H. (2011). "Plant-soil relationship," in *Marschner's Mineral Nutrition of Higher Plants*, ed. P. Marschner (Cambridge, MA: Academic Press), 315–371.

Martínez-Medina, A., Pescador, L., Fernández, I., Rodríguez-Serrano, M., García, J. M., Romero-Puertas, M. C., et al. (2019a). Nitric oxide and phytoglobin PHYTOGB1 are regulatory elements in the *Solanum lycopersicum–Rhizophagus irregularis* mycorrhizal symbiosis. *New Phytol.* 223, 1560–1574. doi: 10.1111/nph.15898

Martínez-Medina, A., Pescador, L., Terrón-Camero, L. C., Pozo, M. J., and Romero-Puertas, M. C. (2019b). Nitric oxide in plant–fungal interactions. *J. Exp. Bot.* 70, 4489–4503. doi: 10.1093/jxb/erz289

McLaughlin, M. J., McBeath, T. M., Smernik, R., Stacey, S. P., Ajiboye, B., and Guppy, C. (2011). The chemical nature of P accumulation in agricultural soils—implications for fertiliser management and design: an Australian perspective. *Plant Soil* 349, 69–87. doi: 10.1007/s11104-011-0907-7

Meng, Z. B., Chen, L. Q., Suo, D., Li, G. X., Tang, C. X., and Zheng, S. J. (2012). Nitric oxide is the shared signalling molecule in phosphorus- and iron-deficiency-induced formation of cluster roots in white lupin (*Lupinus albus*). *Ann. Bot.* 109, 1055–1064. doi: 10.1093/aob/mcs024

Meng, Z. B., Di You, X., Suo, D., Chen, Y. L., Tang, C., Yang, J. L., et al. (2013). Root-derived auxin contributes to the phosphorus-deficiency-induced cluster-root formation in white lupin (*Lupinus albus*). *Physiol. Plant.* 148, 481–489. doi: 10.1111/j.1399-3054.2012.01715.x

Mensah, J. A., Koch, A. M., Antunes, P. M., Kiers, E. T., Hart, M., and Bücking, H. (2015). High functional diversity within species of arbuscular mycorrhizal fungi is associated with differences in phosphate and nitrogen uptake and fungal phosphate metabolism. *Mycorrhiza* 25, 533–546. doi: 10.1007/s00572-015-0631-x

Molina-Favero, C., Creus, C. M., Lanteri, M. L., Correa-Aragunde, N., Lombardo, M. C., Barassi, C. A., et al. (2007). Nitric oxide and plant growth promoting rhizobacteria: common features influencing root growth and development. *Adv. Bot. Res.* 46, 1–33. doi: 10.1016/s0065-2296(07)46001-3

Moreau, M., Lindermayr, C., Durner, J., and Klessig, D. F. (2010). NO synthesis and signaling in plants – where do we stand? *Physiol. Plant.* 138, 372–383. doi: 10.1111/j.1399-3054.2009.01308.x

Müller, J., Gödde, V., Niehaus, K., and Zörb, C. (2015). Metabolic adaptations of white lupin roots and shoots under phosphorus deficiency. *Front. Plant Sci.* 6:1014. doi: 10.3389/fpls.2015.01014

Mur, L. A. J., Mandon, J., Persijn, S., Cristescu, S. M., Moshkov, I. E., Novikova, G. V., et al. (2013). Nitric oxide in plants: an assessment of the current state of knowledge. *AoB Plants* 5:ls052. doi: 10.1093/aobpla/pls052

Nussaume, L., Kanno, S., Javot, H., Marin, E., Pochon, N., Ayadi, A., et al. (2011). Phosphate import in plants: focus on the PHT1 transporters. *Front. Plant Sci.* 2:83. doi: 10.3389/fpls.2011.00083

Oliveira, H. C., Freschi, L., and Sodek, L. (2013). Nitrogen metabolism and translocation in soybean plants subjected to root oxygen deficiency. *Plant Physiol. Biochem.* 66, 141–149. doi: 10.1016/j.plaphy.2013.02.015

Pagnussat, G. C., Simontacchi, M., Puntarulo, S., and Lamattina, L. (2002). Nitric oxide is required for root organogenesis. *Plant Physiol.* 129, 954–956. doi: 10.1104/pp.004036

Pang, J., Yang, J., and Lambers, H. (2015). Physiological and morphological adaptations of herbaceous perennial legumes allow differential access to sources of varyingly soluble phosphate. *Physiol. Plant.* 154, 511–525. doi: 10.1111/ppl.12297

Pang, J., Zhao, H., Bansal, R., Bohuon, E., Lambers, H., Ryan, M. H., et al. (2018). Leaf transpiration plays a role in phosphorus acquisition among a large set of chickpea genotypes. *Plant Cell Environ.* 41, 2069–2079. doi: 10.1111/pce.13139

Payne, W. J. (1976). Denitrification. *Trends Biochem. Sci.* 1, 220–222.

Peret, B., Desnos, T., Jost, R., Kanno, S., Berkowitz, O., and Nussaume, L. (2014). Root architecture responses: in search of phosphate. *Plant Physiol.* 166, 1713–1723. doi: 10.1104/pp.114.244541

Pierre, W. H., and Parker, F. W. (1927). Soil phosphorus studies: II. The concentration of organic and inorganic phosphorus in the soil solution and soil extracts and the availability of the organic phosphorus to plants. *Soil Sci.* 24, 119–128. doi: 10.1097/00010694-192708000-00005

Plaxton, W. C., and Tran, H. T. (2011). Metabolic adaptations of phosphate-starved plants. *Plant Physiol.* 156, 1006–1015. doi: 10.1104/pp.111.175281

Pratt, J., Boisson, A. M., Gout, E., Bligny, R., Douce, R., and Aubert, S. (2009). Phosphate (Pi) starvation effect on the cytosolic Pi concentration and Pi exchanges across the tonoplast in plant cells: an *in vivo* 31P-nuclear magnetic resonance study using methylphosphonate as a Pi analog. *Plant Physiol.* 151, 1646–1657. doi: 10.1104/pp.109.144626

Rabe, E., and Lovatt, C. J. (1986). Increased arginine biosynthesis during phosphorus deficiency. *Plant Physiol.* 81, 774–779. doi: 10.1104/pp.81.3.774

Radi, R. (2004). Nitric oxide, oxidants, and protein tyrosine nitration. *Proc. Natl. Acad. Sci. U.S.A.* 101, 4003–4008. doi: 10.1073/pnas.0307446101

Raghothama, K. G., and Karthikeyan, A. S. (2005). Phosphate acquisition. *Plant Soil* 274:37. doi: 10.1007/1-4020-4099-7_2

Ramos-Artuso, F., Galatro, A., Buet, A., Santa-María, G. E., and Simontacchi, M. (2018). Key acclimation responses to phosphorus deficiency in maize plants are influenced by exogenous nitric oxide. *J. Plant Physiol.* 222, 51–58. doi: 10.1016/j.jplph.2018.01.001

Ramos-Artuso, F., Galatro, A., Lima, A., Batthyány, C., and Simontacchi, M. (2019). Early events following phosphorus restriction involve changes in proteome and affects nitric oxide metabolism in soybean leaves. *Environ. Exp. Bot.* 161, 203–217. doi: 10.1016/j.envexpbot.2019.01.002

Rayle, D. L., and Cleland, R. E. (1992). The acid growth theory of auxin-induced cell elongation is alive and well. *Plant Physiol.* 99, 1271–1274. doi: 10.1104/pp.99.4.1271

Royo, B., Moran, J. F., Ratcliffe, R. G., and Gupta, K. J. (2015). Nitric oxide induces the alternative oxidase pathway in *Arabidopsis* seedlings deprived of inorganic phosphate. *J. Exp. Bot.* 66, 6273–6280. doi: 10.1093/jxb/erv338

Ruffel, S. (2018). Nutrient-related long-distance signals: common players and possible cross-talk. *Plant Cell Physiol.* 59, 1723–1732. doi: 10.1093/pcp/pcy152

Rufty, T. W. Jr., Israel, D. W., Volk, R. J., Qiu, J., and Sa, T. (1993). Phosphate regulation of nitrate assimilation in soybean. *J. Exp. Bot.* 44, 879–891. doi: 10.1007/s00425-014-2165-4

Sakuraba, Y., Kanno, S., Mabuchi, A., Monda, K., Iba, K., and Yanagisawa, S. (2018). A phytochrome-B-mediated regulatory mechanism of phosphorus acquisition. *Nat. Plants* 4, 1089–1101. doi: 10.1038/s41477-018-0294-7

Santolini, J., André, F., Jeandroz, S., and Wendehenne, D. (2017). Nitric oxide synthase in plants: Where do we stand? *Nitric Oxide* 63, 30–38. doi: 10.1016/j.niox.2016.09.005

Sanz-Luque, E., Ocaña-Calahorro, F., de Montaigu, A., Chamizo-Ampudia, A., Llamas, Á., Galván, A., et al. (2015). THB 1, a truncated hemoglobin, modulates nitric oxide levels and nitrate reductase activity. *Plant J.* 81, 467–479. doi: 10.1111/tpj.12744

Sanz-Luque, E., Ocaña-Calahorro, F., Llamas, A., Galván, A., and Fernández, E. (2013). Nitric oxide controls nitrate and ammonium assimilation in *Chlamydomonas reinhardtii*. *J. Exp. Bot.* 64, 3373–3383. doi: 10.1093/jxb/ert175

Schoumans, O. F., Chardon, W. J., Bechmann, M. E., Gascuel-Odoux, C., Hofman, G., Kronvang, B., et al. (2014). Mitigation options to reduce phosphorus losses from the agricultural sector and improve surface water quality: a review. *Sci. Total Environ.* 468, 1255–1266. doi: 10.1016/j.scitotenv.2013.08.061

Schröder, J. J., Smit, A. L., Cordell, D., and Rosemarin, A. (2011). Improved phosphorus use efficiency in agriculture: a key requirement for its sustainable use. *Chemosphere* 84, 822–831. doi: 10.1016/j.chemosphere.2011.01.065

Shane, M. W., Stigter, K., Fedosejevs, E. T., and Plaxton, W. C. (2014). Senescence-inducible cell wall and intracellular purple acid phosphatases: implications for phosphorus remobilization in *Hakea prostrata* (Proteaceae) and *Arabidopsis thaliana* (Brassicaceae). *J. Exp. Bot.* 65, 6097–6106. doi: 10.1093/jxb/eru348

Shen, H., Chen, J., Wang, Z., Yang, C., Sasaki, T., Yamamoto, Y., et al. (2006). Root plasma membrane H+-ATPase is involved in the adaptation of soybean to phosphorus starvation. *J. Exp. Bot.* 57, 1353–1362. doi: 10.1093/jxb/erj111

Shen, J., Yuan, L., Zhang, J., Li, H., Bai, Z., Chen, X., et al. (2011). Phosphorus dynamics: from soil to plant. *Plant Physiol.* 156, 997–1005. doi: 10.1104/pp.111.175232

Singh, S., Kumar, V., Kapoor, D., Kumar, S., and Singh, S. (2019). Revealing on hydrogen sulfide and nitric oxide signals co-ordination for plant growth under stress conditions. *Physiol. Plant.* 168, 301–317. doi: 10.1111/ppl.13002

Skiba, U., Smith, K. A., and Fowler, D. (1993). Nitrification and denitrification as sources of nitric oxide and nitrous oxide in a sandy loam soil. *Soil Biol. Biochem.* 25, 1527–1536. doi: 10.1073/pnas.1219993110

Song, L., Yu, H., Dong, J., Che, X., Jiao, Y., and Liu, D. (2016). The molecular mechanism of ethylene-mediated root hair development induced by phosphate starvation. *PLoS Genet.* 12:e1006194. doi: 10.1371/journal.pgen.1006194

Stöhr, C., and Ullrich, W. R. (2002). Generation and possible roles of NO in plant roots and their apoplastic space. *J. Exp. Bot.* 53, 2293–2303. doi: 10.1093/jxb/erf110

Stuehr, D. J. (1999). Mammalian nitric oxide synthases. *Biochim. Biophys. Acta* 1411, 217–230. doi: 10.1016/S0005-2728(99)00016-X

Terrile, M. C., París, R., Calderón-Villalobos, L. I. A., Iglesias, M. J., Lamattina, L., Estelle, M., et al. (2012). Nitric oxide influences auxin signaling through S-nitrosylation of the *Arabidopsis* TRANSPORT INHIBITOR RESPONSE 1 auxin receptor. *Plant J.* 70, 492–500. doi: 10.1111/j.1365-313X.2011.04885.x

Ueda, Y., and Yanagisawa, S. (2019). Perception, transduction and integration of nitrogen and phosphorus nutritional signals in the transcriptional regulatory network in plants. *J. Exp. Bot.* 70, 3709–3717. doi: 10.1093/jxb/erz148

Umbreen, S., Lubega, J., Cui, B., Pan, Q., Jiang, J., and Loake, G. J. (2018). Specificity in nitric oxide signalling. *J. Exp. Bot.* 69, 3439–3448. doi: 10.1093/jxb/ery184

Veneklaas, E. J., Lambers, H., Bragg, J., Finnegan, P. M., Lovelock, C. E., Plaxton, W. C., et al. (2012). Opportunities for improving phosphorus-use efficiency in crop plants. *New Phytol.* 195, 306–320. doi: 10.1111/j.1469-8137.2012.04190.x

Venuti, S., Zanin, L., Marroni, F., Franco, A., Morgante, M., Pinton, R., et al. (2019). Physiological and transcriptomic data highlight common features between iron and phosphorus acquisition mechanisms in white lupin roots. *Plant Sci.* 285, 110–121. doi: 10.1016/j.plantsci.2019.04.026

Wang, B. L., Tang, X. Y., Cheng, L. Y., Zhang, A. Z., Zhang, W. H., Zhang, F. S., et al. (2010). Nitric oxide is involved in phosphorus deficiency-induced cluster-root development and citrate exudation in white lupin. *New Phytol.* 187, 1112–1123. doi: 10.1111/j.1469-8137.2010.03323.x

Wang, D., Lv, S., Jiang, P., and Li, Y. (2017). Roles, regulation, and agricultural application of plant phosphate transporters. *Front. Plant Sci.* 8:817. doi: 10.3389/fpls.2017.00817

Wang, F., Deng, M., Xu, J., Zhu, X., and Mao, C. (2018). Molecular mechanisms of phosphate transport and signaling in higher plants. *Semin. Cell Dev. Biol.* 74, 114–122. doi: 10.1016/j.semcdb.2017.06.013

Wang, Y. L., Almvik, M., Clarke, N., Eich-Greatorex, S., Øgaard, A. F., Krogstad, T., et al. (2015). Contrasting responses of root morphology and root-exuded organic acids to low phosphorus availability in three important food crops with divergent root traits. *AoB Plants* 7:lv097. doi: 10.1093/aobpla/plv097

Ward, J. T., Lahner, B., Yakubova, E., Salt, D. E., and Raghothama, K. G. (2008). The effect of iron on the primary root elongation of Arabidopsis during phosphate deficiency. *Plant Physiol.* 147, 1181–1191. doi: 10.1104/pp.108.118562

Weidmann, S., Sanchez, L., Descombin, J., Chatagnier, O., Gianinazzi, S., and Gianinazzi-Pearson, V. (2004). Fungal elicitation of signal transduction-related plant genes precedes mycorrhiza establishment and requires the dmi3 gene in *Medicago truncatula*. *Mol. Plant Microbe Interact.* 17, 1385–1393. doi: 10.1094/MPMI.2004.17.12.1385

Wu, A. P., Gong, L., Chen, X., and Wang, J. X. (2014). Interactions between nitric oxide, gibberellic acid, and phosphorus regulate primary root growth in *Arabidopsis*. *Biol. Plant.* 58, 335–340. doi: 10.1007/s10535-014-0408-7

Xu, J., Yin, H., Li, Y., and Liu, X. (2010). Nitric oxide is associated with long-term zinc tolerance in *Solanum nigrum*. *Plant Physiol.* 154, 1319–1334. doi: 10.1104/pp.110.162982

Yan, F., Zhu, Y., Mü, C., Zo, C., and Schubert, S. (2002). Adaptation of H+ -pumping and plasma membrane H+ ATPase activity in proteoid roots of white lupin under phosphate deficiency. *Plant Physiol.* 1, 50–63. doi: 10.1104/pp.010869.50

Yang, L. T., Chen, L. S., Peng, H. Y., Guo, P., Wang, P., and Ma, C. L. (2012). Organic acid metabolism in *Citrus grandis* leaves and roots is differently affected by nitric oxide and aluminum interactions. *Sci. Hortic.* 133, 40–46. doi: 10.1016/j.scienta.2011.10.011

Yang, S. Y., Huang, T. K., Kuo, H. F., and Chiou, T. J. (2017). Role of vacuoles in phosphorus storage and remobilization. *J. Exp. Bot* 68, 3045–3055. doi: 10.1093/jxb/erw481

Ye, Q., Wang, H., Su, T., Wu, W.-H., and Chen, Y.-F. (2018). The Ubiquitin E3 Ligase PRU1 regulates WRKY6 degradation to modulate phosphate homeostasis in response to low-Pi stress in Arabidopsis. *Plant Cell* 30, 1062–1076. doi: 10.1105/tpc.17.00845

Yue, W., Ying, Y., Wang, C., Zhao, Y., Dong, C., Whelan, J., et al. (2017). OsNLA1, a RING-type ubiquitin ligase, maintains phosphate homeostasis in Oryza sativa via degradation of phosphate transporters. *Plant J.* 90, 1040–1051. doi: 10.1111/tpj.13516

Zandonadi, D. B., Santos, M. P., Dobbss, L. B., Olivares, F. L., Canellas, L. P., Binzel, M. L., et al. (2010). Nitric oxide mediates humic acids-induced root development and plasma membrane H+-ATPase activation. *Planta* 231, 1025–1036. doi: 10.1007/s00425-010-1106-0

Zhang, R. Q., Zhu, H. H., Zhao, H. Q., and Yao, Q. (2013). Arbuscular mycorrhizal fungal inoculation increases phenolic synthesis in clover roots via hydrogen peroxide, salicylic acid and nitric oxide signaling pathways. *J. Plant Physiol.* 170, 74–79. doi: 10.1016/j.jplph.2012.08.022

Zhang, Y., Lynch, J. P., and Brown, K. M. (2003). Ethylene and phosphorus availability have interacting yet distinct effects on root hair development. *J. Exp. Bot.* 54, 2351–2361. doi: 10.1093/jxb/erg250

Zhang, Z., Liao, H., and Lucas, W. J. (2014). Molecular mechanisms underlying phosphate sensing, signaling, and adaptation in plants. *J. Integr. Plant Biol.* 56, 192–220. doi: 10.1111/jipb.12163

Zhao, L., Zhang, F., Guo, J., Yang, Y., Li, B., and Zhang, L. (2004). Nitric oxide functions as a signal in salt resistance in the calluses from two ecotypes of reed. *Plant Physiol.* 134, 849–857. doi: 10.1104/pp.103.030023

Zhu, C. Q., Zhu, X. F., Hu, A. Y., Wang, C., Wang, B., Dong, X. Y., et al. (2016). Differential effects of nitrogen forms on cell wall phosphorus remobilization in rice (Oryza sativa) are mediated by nitric oxide, pectin content and the expression of the phosphate transporter OsPT2. *Plant Physiol.* 171, 1407–1417. doi: 10.1104/pp.16.00176

Zhu, X. F., Dong, X. Y., Wu, Q., and Shen, R. F. (2019). Ammonium regulates Fe deficiency responses by enhancing nitric oxide signaling in *Arabidopsis thaliana*. *Planta* 250, 1089–1102. doi: 10.1007/s00425-019-03202-6

Zhu, X. F., Zhu, C. Q., Wang, C., Dong, X. Y., and Shen, R. F. (2017). Nitric oxide acts upstream of ethylene in cell wall phosphorus reutilization in phosphorus-deficient rice. *J. Exp. Bot.* 68, 753–760. doi: 10.1093/jxb/erw480

Zou, Y. N., Wang, P., Liu, C. Y., Ni, Q. D., Zhang, D. J., and Wu, Q. S. (2017). Mycorrhizal trifoliate orange has greater root adaptation of morphology and phytohormones in response to drought stress. *Sci. Rep.* 7:41134. doi: 10.1038/srep41134

Conflict of Interest: The authors declare that the research was conducted in the absence of any commercial or financial relationships that could be construed as a potential conflict of interest.

frontiers in Plant Science

ORIGINAL RESEARCH
published: 15 May 2020
doi: 10.3389/fpls.2020.00586

Differential Regulation of Kernel Set and Potential Kernel Weight by Nitrogen Supply and Carbohydrate Availability in Maize Genotypes Contrasting in Nitrogen Use Efficiency

Ivan A. Paponov[1]†‡, Martina Paponov[1‡], Paolo Sambo[2] and Christof Engels[3]*

[1] Division of Food Production and Society, Norwegian Institute of Bioeconomy Research, Ås, Norway, [2] Department of Agronomy, Food, Natural Resources, Animals and Environment, University of Padova, Legnaro, Italy, [3] Albrecht Daniel Thaer-Institute of Agricultural and Horticultural Sciences, Plant Nutrition and Fertilisation, Humboldt-Universitat zu Berlin, Berlin, Germany

Sub-optimal nitrogen (N) conditions reduce maize yield due to a decrease in two sink components: kernel set and potential kernel weight. Both components are established during the lag phase, suggesting that they could compete for resources during this critical period. However, whether this competition occurs or whether different genotypic strategies exist to optimize photoassimilate use during the lag phase is not clear and requires further investigation. We have addressed this knowledge gap by conducting a nutrient solution culture experiment that allows abrupt changes in N level and light intensity during the lag phase. We investigated plant growth, dry matter partitioning, non-structural carbohydrate concentration, N concentration, and ^{15}N distribution (applied 4 days before silking) in plant organs at the beginning and the end of the lag phase in two maize hybrids that differ in grain yield under N-limited conditions: one is a nitrogen-use-efficient (EFFI) genotype and the other is a control (GREEN) genotype that does not display high N use efficiency. We found that the two genotypes used different mechanisms to regulate kernel set. The GREEN genotype showed a reduction in kernel set associated with reduced dry matter allocation to the ear during the lag phase, indicating that the reduced kernel set under N-limited conditions was related to sink restrictions. This idea was supported by a negative correlation between kernel set and sucrose/total sugar ratios in the kernels, indicating that the capacity for sucrose cleavage might be a key factor defining kernel set in the GREEN genotype. By contrast, the kernel set of the EFFI genotype was not correlated with dry matter allocation to the ear or to a higher capacity for sucrose cleavage; rather, it showed a relationship with the different EFFI ear morphology with bigger kernels at the apex of the ear than in the GREEN genotype. The potential kernel

OPEN ACCESS

Edited by:
Guillermo Esteban Santa María, National University of General San Martín, Argentina

Reviewed by:
Juan Guiamet, National University of La Plata, Argentina
Peng Ning, Northwest A&F University, China

***Correspondence:**
Ivan A. Paponov
ivpa@food.au.dk

†Present address:
Ivan A. Paponov, Department of Food Science, Aarhus University, Aarhus, Denmark

‡These authors have contributed equally to this work

Specialty section:
This article was submitted to Plant Nutrition, a section of the journal Frontiers in Plant Science

Received: *22 November 2019*
Accepted: *17 April 2020*
Published: *15 May 2020*

Citation:
Paponov IA, Paponov M, Sambo P and Engels C (2020) Differential Regulation of Kernel Set and Potential Kernel Weight by Nitrogen Supply and Carbohydrate Availability in Maize Genotypes Contrasting in Nitrogen Use Efficiency. Front. Plant Sci. 11:586. doi: 10.3389/fpls.2020.00586

weight was independent of carbohydrate availability but was related to the N flux per kernel in both genotypes. In conclusion, kernel set and potential kernel weight are regulated independently, suggesting the possibility of simultaneously increasing both sink components in maize.

Keywords: kernel set, potential kernel weight, nitrogen, nitrogen use efficiency, maize, sink strength, non-structural carbohydrate

INTRODUCTION

Nitrogen (N) is a key nutrient for plant growth and is therefore one of the main factors that can be manipulated to increase crop yields (Erisman et al., 2008). However, extensive application of N has adverse environmental impacts due to N losses in the form of volatilized ammonia, nitrous oxide, and nitrate, a water pollutant (Cameron et al., 2013). Therefore, strategies promoting more efficient N use are important to decrease these N losses. One strategy that can increase N use efficiency (NUE) is to grow plants under a suboptimal N supply, but this requires plant breeding programs that can generate new crop genotypes that produce satisfactory yields under N restriction (Moll et al., 1982; Sattelmacher et al., 1994). In this context, the NUE was defined as the ability of a genotype to realize superior grain yields at low soil N conditions when compared with other genotypes (Sattelmacher et al., 1994). New genotypes can be identified by marker-assisted selection, which can pinpoint genes or QTLs responsible for agriculturally important physiological traits. The identification and characterization of the physiological traits with the highest impact on NUE are important for the successful implementation of marker-assisted selection for breeding of genotypes with high NUE.

In maize, a sub-optimal N supply can decrease yield due to reductions in several key yield components, including the number of ears per plant (Monneveux et al., 2005), kernel number (KN) per ear (Uhart and Andrade, 1995; Andrade et al., 2002; Paponov et al., 2005b), and/or weight of individual kernels (Hisse et al., 2019). Numerous experiments have shown that KN per plant is the main determinant of yield. The KN is established in the period that extends from 2 weeks before to 2 weeks after silking and is controlled by three factors: plant growth (plant dry mass increment) during this critical period, dry mass (DM) partitioning to the ears, and kernel set efficiency (i.e., the number of kernels set per unit DM flux to the ears) (Borras and Vitantonio-Mazzini, 2018). Restrictions in N supply during this critical phase bracketing silking can decrease both plant growth (Andrade et al., 2002) and DM partitioning to the ears (D'Andrea et al., 2008), but these responses can vary depending on the maize genotype. The questions of how different genotypes respond to N limitation and why some genotypes show higher kernel set under sub-optimal N supply remain unanswered and require further investigation.

The potential KN is determined by the number of mature florets on the ear inflorescence and is established well in advance of silking (Gonzalez et al., 2019). KN can be reduced during the lag phase due to failure of kernels to develop from ovaries, termed kernel abortion (Hanft et al., 1986). Under suboptimal levels of N supply, kernel abortion is considered the most sensitive component regulating kernel set (Monneveux et al., 2005). However, the reduction in KN might be also related to delayed emergence of apical silking under stress conditions (Lemcoff and Loomis, 1986, 1994). By contrast, the floret number is insensitive or only weakly affected by N and carbohydrate limitation (Lemcoff and Loomis, 1986; DeBruin et al., 2018), whereas extreme drought stress reduces the floret set (Gonzalez et al., 2019).

Variations in kernel weight (KW) can also strongly affect the crop yield (Borras and Gambin, 2010). The potential KW is established during the 2 weeks period after silking, called the "lag phase," and is characterized by the number of cells per endosperm and the number of starch granules per cell at the end of the lag phase (Jones et al., 1996). The final KW is determined during the grain filling stage, when the potential KW is realized. Notably, the "lag phase" period is therefore critical for two sink components: the kernel set and the potential KW. The simultaneous establishment of these two sink components assumes that these components would compete for resources (i.e., assimilates), meaning that a higher investment in one component would be offset by a lower investment in the other (Ordonez et al., 2018).

The potential KW, like the KN, is also closely associated with the amount of assimilates available per kernel during the lag phase (Gambin et al., 2006). However, which type of assimilate (i.e., carbohydrates or amino acids) contributes to a higher potential KW is difficult to determine based on field experiments, because carbohydrate and N metabolism share close relationships. Experiments with *in vitro* culture have shown a direct role of N in enhancing potential KW (Cazetta et al., 1999); however, this effect of N has not been tested in intact maize plants. Moreover, the role of genotypic differences in the regulation of potential KW under sub-optimal N supply remains unexplored.

In the present study, we sought to gain insights into the regulation of kernel set and potential KW during the lag phase using hydroponic culture, as this allows rapid decreases or increases in the N level during the lag phase. We used abrupt changes in N level and plant shading to decouple N and carbohydrate fluxes and to provide insights into the use of different resources by sinks under stress conditions. This hydroponic system can serve as a prototype for the development of a phenotyping platform for robust characterization of NUE and can aid in the accurate dissection of different physiological traits that contribute to NUE.

The aim of the present work was to determine whether common or different mechanisms are responsible for the regulation of the two main components of sink capacity (KN

and potential KW) in maize when growth is restricted by N and C limitations during the lag phase. A further aim was to elucidate the strategies by which NUE genotypes adapt to sub-optimal N and C conditions to maintain high sink capacity. Specifically, we addressed the question of the importance of carbohydrates, N, or some other unknown factors in establishing the KN and KW sink capacity components. We decoupled the effects of N and carbohydrate availability with an abrupt change in the N (NO_3^-) level in the nutrient solution or by an abrupt change in carbohydrate availability by shading the plants, and we estimated the carbohydrate and N status at the critical lag phase stages when the two sink components of KN and potential KW are established.

MATERIALS AND METHODS

Plant Material and Growing Conditions

The experiment was conducted at the University of Hohenheim (48°43′N, 9°13′E, 407 m altitude) from 26 May (sowing) to 19 September (final harvest) 1997. The average temperature in the summer was 19.8°C, which was 2.9°C warmer than the average values between 1961 and 1990. The sunshine duration reached 822.5 h, which represented 125% of the average values. The plants were cultivated in an area protected from birds by a wire cage but were otherwise exposed to the natural temperature and light conditions (**Figure 1A**). The experiment compared two maize (*Zea mays* L.) hybrids that had shown similar yields at optimal N supply but different yields at suboptimal N supply in field experiments carried out in 1992 and 1997 (Presterl et al., 2002; Paponov et al., 2005a,b). At suboptimal N supply, the grain yields had been significantly lower for the commercial variety GREEN than for the experimental hybrid EFFI. This latter hybrid had been selected in a breeding program for its high N use efficiency at low levels of N availability (Presterl et al., 2002).

Seeds were germinated for 24 h in 1 mM $CaSO_4$ at 25°C under continuous aeration. The kernels were then placed between filter papers fixed with foam and incubated in the darkness. On the 5th day, the emerging seedlings were exposed to light. At day 7, the seedlings were transferred to a dilute nutrient solution containing 10% concentrations of the macronutrients and 100% concentrations of the micronutrients of the standard nutrient solution, along with 0.5 mM of $Ca(NO_3)_2$. At 14 days of age, the seedlings were transferred to 20 L pots containing the standard nutrient solution of 0.1 mM KH_2PO_5, 0.5 mM K_2SO_4, 0.6 mM $MgSO_4$, 150 μM Fe-EDTA, 1 μM H_3BO_3, 0.5 μM $MnSO_4$, 0.5 μM $ZnSO_4$, 0.2 μM $CuSO_4$, and 0.01 μM $(NH_4)_6Mo_7O_{24}$. The nutrient solution was changed every 5–7 days. The N supply, in the form of $Ca(NO_3)_2$, varied depending on the treatment. To prevent Ca deficiency, the low-N plants received sufficient $CaCl_2$ to provide equivalent Ca to that provided by $Ca(NO_3)_2$ in the high-N treatment. The nutrient solution was maintained between pH 5.5 and 6.5.

The design of the experiment included six treatments (**Figure 1B**). Plants received the high N supply (N) before silking in three treatments, and the low N supply (n) before silking in three treatments. For both groups of treatments, N supply and light intensity were varied from silking to 16 days after silking. During these 16 days, the plants received either the high N supply (NN, nN) or the low N supply (Nn, nn) to modify the N-nutritional status. The role of plant carbohydrate status on kernel yield was assessed in plants growing in high N status [N(N + S)] or low N status [n(n + S)] by shading the plants to reduce the light intensity by 80%. A lack of a sufficient number of plants prevented sampling for the n(n + S) treatment at the second harvest.

Initially (i.e., after a change of nutrient solution), the nitrate concentration was 0.5 mM in the treatments with high N supply. For this treatment, the nitrate concentration in the nutrient solution was measured daily using the Reflektoquant method (Rqflex, Merck), and nitrate was added regularly to satisfy plant N demand (excluding the complete depletion of nitrate in nutrient solution). With this N supply, plants accumulated about 4948 mg N per plant in the aboveground parts at maturity. This was a significantly higher N uptake than that observed (about 2700 mg per plant) in the aboveground parts in the same genotypes growing in the field under high N supply (Paponov et al., 2005b). These data indicate that N supply in hydroponics was more luxurious than in the field under high N supply. The size of the shoot under these growth conditions was similar to that of the field-grown plants.

In hydroponics, the external concentration is inadequate as a driving variable for N supply because it offers two options for concentration-controlled culture: excess supply and uncontrolled deficiency (Macduff et al., 1993). For this reason, we used a simplified method of N limitation based on relative addition rates, which involved frequent additions of small quantities of nutrient to each pot of nutrient solution (Ingestad and Lund, 1986). This approach was previously applied successfully for comparison of wheat genotypes grown to maturity (Oscarson, 2000). In our study, plants at low N supply until the silking were supplied regularly with 50% of the N amount given to the plants grown under high N supply. During the lag phase, the low N level plants received 200 mg N, whereas N availability was unrestricted for the high N supply plants. Beyond the 16 days after silking and until maturity, all plants received the high N supply to ensure that no limitation of N existed so that the final KW would reflect the potential KW and would not be limited by the growth conditions during the effective grain filling stage.

We used a randomized complete block design with two environmental treatments before silking. During the 16 days of the lag phase, the plants were distributed according to a split-plot design with the main plot being light intensity (shading). We used six environmental treatments during the lag phase. The plant density before the effective grain filling was 4 plants m^{-2}. After the end of the lag phase, the plant density was reduced to 3 plants m^{-2} to ensure luxury carbohydrate supply. Rows of border plants were not sampled in this experiment.

Harvest

Plants were harvested at the beginning of silking, at the end of the lag phase (i.e., 16 days after silking), and at maturity (**Figure 1B**). One individual plant was used for one replication, with four replications for every time point and every treatment.

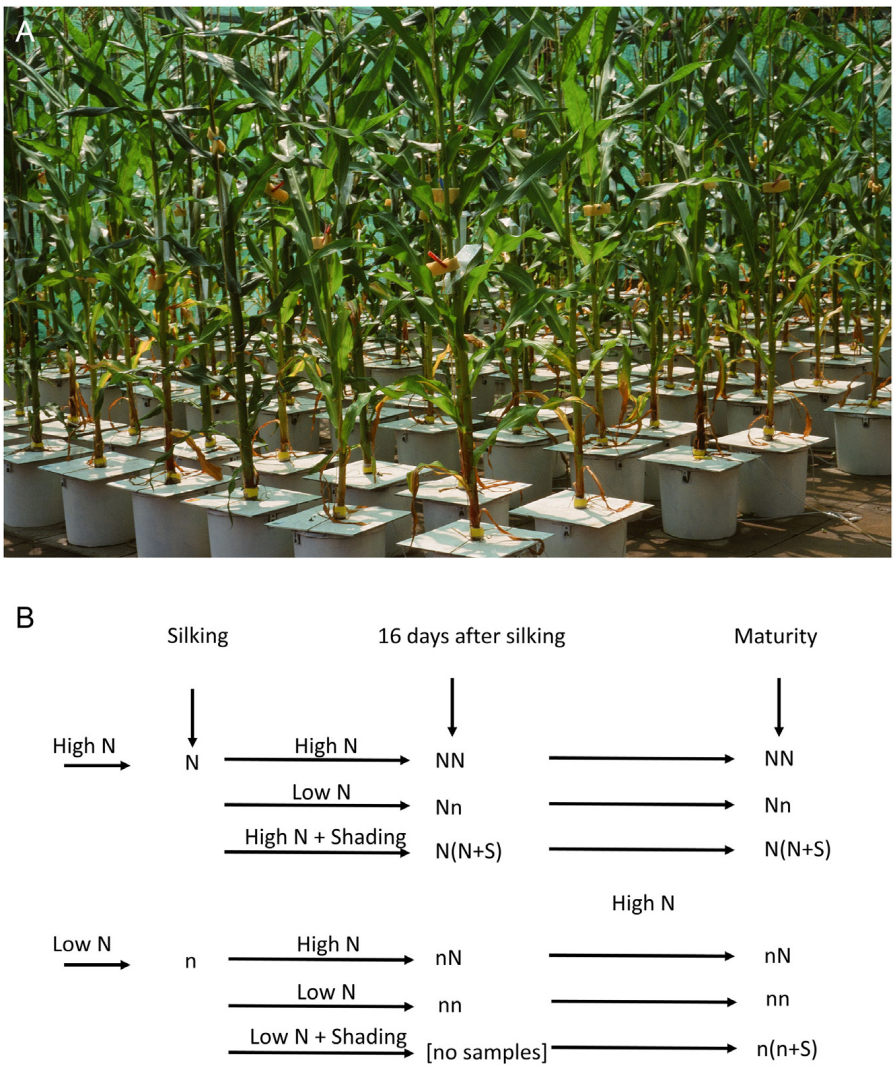

FIGURE 1 | Design of the hydroponics experiment. **(A)** Maize cultivation in 20 L pots in hydroponics with continuous aeration. **(B)** The scheme of the experimental design: high and low N supply before silking, high and low N for 16 days after silking, and shading of the plants under constant N supply; all plants were given excess N and full light during the grain filling stage. Plants were harvested at the beginning of silking, at the end of the lag phase (i.e., 16 days after silking), and at maturity.

At the first harvest, the plants were divided into roots, stalk, leaves, ear, and husks. At the second and third harvests, plants were divided into the same organs, but the ear was divided into the cob and kernels. At the end of the lag phase, kernels in a whole row along the rachis of the ear were removed, frozen with liquid nitrogen, and freeze-dried for the analysis of soluble sugars and starch. The other plant organs were dried at 65°C to a constant weight and weighed for dry matter (DM) determination. Leaf weight ratio (LWR), stalk weight ratio (SWR), root weight ratio (RWR), and ear and husk weight ratio (Ear + huskWR) were calculated as DM of leaves, stalk, roots, and ear and husks, respectively, divided by the total DW biomass of the plants. Leaf sheath weights were added to the stalk weights. The plants were harvested according to a randomized complete block design from 10:00 to 12:00, 10:00 to 14:00, and 10:00 to 16:00 for the first, second, and third harvest, respectively. Kernel number was determined for the third harvest by counting all kernels per ear. Individual KW was determined as the ratio between the total kernel weight per ear and the kernel number per ear.

Soluble Sugars and Starch

A 50 mg sample of ground tissue was mixed with 3.3 mL 70% (v/v) ethanol for sample extraction. Each sample was extracted two more times and sample tubes were centrifuged (3000 × *g*) for 10 min after each extraction. The three supernatants were combined in a test tube and brought to a 10 ml final volume with 70% (v/v) ethanol. Reducing sugars and sucrose were estimated colorimetrically at 415 nm using *p*-hydroxybenzoic acid hydrazide (Blakeney and Mutton, 1980) before and after the digestion of sucrose with invertase for 2 h at 37°C. For starch determination, the ethanol-extracted plant residue was

suspended in dimethyl sulfoxide (DMSO) for 10 min (Perez et al., 1971). After centrifugation the supernatant was incubated with amyloglucosidase (2 mL 0.M sodium acetate containing 1.2 U mL^{-1}) overnight at 37°C to hydrolyze the starch. The released glucose was then measured colorimetrically at 510 nm (Blakeney and Mutton, 1980) and starch equivalents were calculated.

Total N and ^{15}N Analysis and Calculations

Leaf N content was measured with an automatic N analyzer (Carlo Erba, Milan, Italy, Model 1400). Total plant N uptake was measured as the sum of nitrogen content in different plant parts. The amount of N in different plant parts was calculated by multiplying the dry weight by the N concentration in those parts. Labeled N [^{15}N in form of $Ca(NO_3)_2$] was applied at four days before silking. Every plant with low N supply received 53.7 mg (^{15}N, 12.1904% excess) and those with high N supply received 55.9 mg (^{15}N, 16.8635% excess).

Heavy-isotope concentrations were determined by mass spectrometry (Tracermass, stable isotope analyzer, Europa Scientific) after combustion of the samples in quartz-sealed tubes in the presence of CuO (Roboprep-CN, Europa Scientific). The A% excess was defined as the atom% ^{15}N in the plant material minus the atom% in the control sample that did not receive labeled N. The partitioning of recently assimilated N ($\%P_N$) to different organs was determined as previously described (Paponov and Engels, 2005):

$\%P_N$ = (A% excess(^{15}N) in organ)/(A% excess (^{15}N) in plant) *(N organ)/(N plant)*100

N flux per ear during the lag phase was measured as the difference between ear N content at the end of the lag phase and ear N content at the beginning of the lag phase.

Analysis of Ear Morphology in the Field Experiment

The field experiment was conducted in 1998 at the experimental station of the University of Hohenheim Muttergarten in the southern part of Germany (48°43′N, 9°13′E, 407 m altitude). The average temperature in the summer was 20.5°C, which was 3.6°C warmer than the average values between 1961 and 1990. The sunshine duration reached 851.4 h, which represented 129% of the average values. The experiments were randomized block designs with four replications. The soil characteristics, techniques of phosphorus and potassium application, and size of experimental plots were as described previously (Paponov et al., 2005b). Plants were sown on 11 May at a uniform density of 10 plants m^{-2}. N fertilizer (calcium ammonium nitrate) was applied at rates of 0 or 150 kg N ha^{-1}. Before silk appearance, the ears were covered with paper bags to prevent pollination. The ears were then hand pollinated for two consecutive days, and the paper bags were removed to ensure complete pollination of each ear. Synchronize pollination was used to diminish any differences in pollination time between kernels that might affect on kernel size. Four ears were selected for analysis of the kernel size at different positions along the ear.

Statistics

The treatments were replicated four times. Data were statistically analyzed by analysis of variance (two-way analysis or three-way analysis, using the ANOVA variables Nv, nitrogen supply before silking, Nf, nitrogen supply during lag phase, Sh, shading during lag phase, G, genotypes). When significant treatment effects were indicated by ANOVA, Fisher's protected LSD test was used to compare the individual means (Statistica for Windows, version 13).

RESULTS

Genotype-Specific Responses to N Supply During the Vegetative Growing Phase: Growth and Dry Matter Partitioning

On average, for both genotypes, a low N supply reduced the plant biomass by 28% when compared with the high N supply (**Table 1**). Dry mass partitioning among the vegetative plant organs (leaves, stalks, and roots) was not significantly influenced by genotype or rate of N supply, with the exception of a slightly higher leaf weight ratio (LWR) observed at low N than at high N supply. The fact that RWR was not increased at a low N supply was surprising, as the DM partitioning in the roots usually increases under N limitation (Poorter et al., 2012). However, for maize, also other investigations have shown that DM partitioning to the roots is not modulated by the availability of N (Guo and York, 2019). DM partitioning to generative organs, by contrast, was affected differently by N supply in the two genotypes. At the high N supply, DM partitioning to ear 1 and husks (Ear + husk1WR) was greater in the GREEN than in the EFFI genotype, whereas at the low level of N supply, no difference was observed between the two genotypes for DM partitioning to ear 1 and husks. For the GREEN genotype, the DM partitioning to ear 2 and husk (Ear + husk2WR) was reduced to zero at the low level of N supply. By contrast, for the EFFI genotype, the development of ear 2 was not stopped by the low level of N supply.

Genotype-Specific Responses to N Supply During the Vegetative Growing Phase: Plant Carbohydrate Status

The concentration of non-structural carbohydrates in the stalks, which was measured as an indicator of plant carbohydrate status, did not differ significantly between the two genotypes (**Table 2**). Low N decreased the carbohydrate status due to lower sucrose concentrations, but it did not affect the concentrations of reducing sugars and starch. Taken together, the data on N and genotype effects on plant biomass, the ratio of stalk biomass in total plant biomass (SWR), and the non-structural carbohydrate concentrations in the stalks indicated that the amount of reserve carbohydrates in plants at silking was substantially lower in plants given a low N than a high N supply. The genotypes did not differ in their carbohydrate status.

TABLE 1 | The influence of N supply up to silking on plant biomass and dry matter distribution at the start of silking for two genotypes with different N-use efficiency.

Nitrogen (N)	Genotype (G)	Biomass, g	LWR	SWR	RWR	Ear + husk1 WR	Ear + husk2 WR
High							
	GREEN	129 ± 2^{a}	20.1 ± 0.2^{a}	45.4 ± 0.9^{a}	25.9 ± 1.3^{a}	6.99 ± 0.31^{b}	1.64 ± 0.45^{b}
	EFFI	130 ± 5^{a}	20.4 ± 1.0^{a}	45.6 ± 2.2^{a}	27.9 ± 3.0^{a}	3.31 ± 0.32^{a}	2.73 ± 0.14^{c}
Low							
	GREEN	89 ± 1^{b}	22.1 ± 0.3^{a}	52.0 ± 0.5^{a}	22.9 ± 1.0^{a}	2.97 ± 0.47^{a}	0.00 ± 0.00^{a}
	EFFI	98 ± 7^{b}	22.0 ± 0.4^{a}	45.6 ± 1.7^{a}	27.9 ± 2.1^{a}	3.35 ± 0.53^{a}	1.10 ± 0.08^{b}
ANOVA, source of variation							
N		***	*	NS	NS	**	***
G		NS	NS	NS	NS	**	***
N × G		NS	NS	NS	NS	**	NS

*Dry matter distribution: LWR, leaf weight ratio; SWR, stalk weight ratio; RWR, root weight ratio; Ear + husk1WR, ear 1 and husk weight ratio; Ear + husk2WR, ear 2 and husk weight ratio. Values are means ± SE of four independent biological replicates; different lower case letters behind means indicate significant differences ($p \leq 0.05$, Fisher's protected LSD). *, **, *** Significant at the 0.05, 0.01, and 0.001 probability level, NS, not significant. Factors N level (N), Genotype (G).*

Genotype-Specific Responses to N Supply During the Vegetative Growing Phase: N Status

Plants under low N supply absorbed about 50% less N than plants under high N supply (**Table 3**). The N concentrations in the vegetative plant organs were significantly lower in plants supplied with low N than with high N (**Table 3**). With the high N supply, the N concentrations in leaves and stalks were lower in the EFFI than in GREEN genotype; by contrast, when grown at the low N supply, neither the leaf nor the stalk N concentrations differed between the genotypes. The N concentrations in the generative plant organs were only slightly affected by the N supply rate. The N concentrations in ears 1 and 2 in the EFFI genotype were not significantly reduced by low N compared to high N supply. For the GREEN genotype, the N concentration in ear 1 was even higher at low than at high N supply, which might reflect a dilution effect of N in the ear during development (Ciampitti and Vyn, 2013).

TABLE 2 | The influence of N supply up to silking on carbohydrate concentration (mg g^{-1}) in the stalks at the start of silking for two genotypes with different N-use efficiency.

Nitrogen (N)	Genotype (G)	Red. sugars	Sucrose	Starch
High				
	GREEN	66 ± 5^{a}	137 ± 9^{b}	3.33 ± 0.25^{a}
	EFFI	76 ± 8^{a}	164 ± 21^{b}	2.92 ± 0.33^{a}
Low				
	GREEN	82 ± 2^{a}	40 ± 8^{a}	3.86 ± 0.56^{a}
	EFFI	72 ± 8^{a}	51 ± 11^{a}	3.97 ± 0.22^{a}
ANOVA, source of variation				
N		NS	***	NS
G		NS	NS	NS
N × G		NS	NS	NS

*Values are means ± SE of four independent biological replicates; different lower case letters behind means indicate significant differences ($p \leq 0.05$, Fisher's protected LSD). *** Significant at the 0.001 probability level, NS, not significant. Factors N level (N), Genotype (G).*

We assessed the partitioning of recently acquired N among plant organs by supplying the plants with ^{15}N-labeled nitrate 4 days before silking, and we then quantified the percentages of total plant ^{15}N in the vegetative and generative plant organs at silking. Partitioning of recently acquired ^{15}N among the plant organs was affected by the previous N supply and by the genotype (**Table 4**). The partitioning of recently acquired N to leaves and stalks, at the expense of N partitioning to roots, was higher for plants supplied with low N than with high N (**Table 4**). N partitioning to leaves and stalks tended to be higher, and N partitioning to roots lower, for the GREEN than for the EFFI genotype at both levels of N supply. At the high N supply, ^{15}N partitioning to ear 1 and husks was greater in GREEN than in EFFI; however, at the low N supply, no differences were found in ^{15}N partitioning to ear 1 and husks between the genotypes (**Table 4**), in agreement with the genotypic differences observed in biomass partitioning (**Table 1**). For GREEN, ^{15}N partitioning to ear 2 and husks was reduced to zero at low N supply. By contrast, for EFFI, ^{15}N partitioning to the ear 2 and husks at low and high levels of N supply were similar.

Genotype-Specific Responses to Modification of N Supply and/or to Shading During the Lag Phase: Growth and DM Partitioning

In the 16 days between silking and the end of the lag phase, the DM per plant increased by about 100 g in plants that were previously (i.e., during the vegetative growing phase) supplied optimally with N, and by 60 g in plants previously supplied with sub-optimal N levels (compare **Table 1** and **Figure 2A**). For both groups of plants, the short-term modification of growing conditions during the lag phase [i.e., the reduction in N supply (Nn) for high N plants and the increase in the N supply for low N plants (nN)] did not significantly change the total plant DM (**Figure 2A** and **Supplementary Table S1**).

The level of N supply and the shading during the lag phase had different effects on DM allocation between the vegetative organs: a low N supply during the lag phase increased DM partitioning into the stalks (the main storage

TABLE 3 | The influence of N supply up to silking on N uptake by plants and N concentrations in plant organs at the start of silking for two maize genotypes with different N-use efficiency.

Nitrogen (N)	Genotype (G)	Plants, mg	Leaf (%)	Stem (%)	Roots (%)	Ear 1 (%)	Ear 2 (%)
High							
	GREEN	1906 ± 55^{b}	2.71 ± 0.11^{c}	0.92 ± 0.03^{c}	1.36 ± 0.07^{ab}	2.69 ± 0.03^{a}	3.93 ± 0.04^{b}
	EFFI	1752 ± 66^{b}	2.39 ± 0.12^{b}	0.76 ± 0.04^{b}	1.47 ± 0.11^{b}	3.50 ± 0.15^{b}	3.09 ± 0.13^{a}
Low							
	GREEN	893 ± 5^{a}	1.63 ± 0.05^{a}	0.63 ± 0.02^{a}	1.16 ± 0.04^{ab}	3.20 ± 0.11^{b}	
	EFFI	988 ± 18^{a}	1.68 ± 0.03^{a}	0.60 ± 0.03^{a}	1.04 ± 0.14^{a}	3.12 ± 0.13^{ab}	3.13 ± 0.18^{a}
ANOVA, source of variation							
N		***	***	***	*	NS	
G		NS	NS	**	NS	*	
N × G		*	NS	*	NS	**	

*Values are means ± SE of four independent biological replicates; different lower case letters behind means indicate significant differences ($p \leq 0.05$, Fisher's protected LSD). *, **, *** Significant at the 0.05, 0.01, and 0.001 probability level, NS, not significant. Factors N level (N), Genotype (G).*

TABLE 4 | The percentages of total plant ^{15}N in the vegetative and generative plant organs at silking after supplying the plants with ^{15}N-labeled nitrate four days before silking, as affected by level of N supply for two maize genotypes with different N-use efficiency.

Nitrogen (N)	Genotype (G)	Leaf	Stem	Roots	Ear + husk 1	Ear + husk 2
High						
	GREEN	15.0 ± 1.3^{a}	28.3 ± 0.4^{a}	38.5 ± 0.01^{ab}	16.31 ± 0.75^{b}	1.84 ± 0.11^{b}
	EFFI	13.9 ± 0.9^{a}	24.4 ± 2.4^{a}	46.8 ± 2.8^{b}	9.61 ± 0.68^{a}	5.31 ± 0.51^{c}
Low						
	GREEN	20.8 ± 0.8^{b}	39.0 ± 3.0^{b}	33.2 ± 2.1^{a}	7.07 ± 2.05^{a}	0.00 ± 0.00^{a}
	EFFI	15.2 ± 0.9^{a}	27.9 ± 2.1^{a}	40.1 ± 2.5^{a}b	11.07 ± 1.11^{a}	5.74 ± 0.16^{c}
ANOVA, source of variation						
N		**	*	*	*	NS
G		**	*	*	NS	***
N × G		NS	NS	NS	**	**

*Values are means ± SE of four independent biological replicates; different lower case letters behind means indicate significant differences ($p \leq 0.05$, Fisher's protected LSD). *, **, *** Significant at the 0.05, 0.01, and 0.001 probability level, NS, not significant. Factors N level (N), Genotype (G).*

organ for carbohydrates) in plants grown at low levels of N before silking but had no effect on DM partitioning in plants grown at high N before silking. These responses indicated a sink limitation in N-deficient plants. By contrast, shading increased DM partitioning into the leaves, in agreement with the common trend of plant adaptation to low light intensity (Poorter et al., 2012) (**Figures 2B,C** and **Supplementary Table S1**). This indicates that plants have different mechanisms for adapting to N and carbohydrate limitations. A reduction in the N supply (Nn) or an increase in the N supply for low-N supplied (nN) plants did not change the DM partitioning to the roots, whereas shading [N(N + S)] increased the DM allocation to roots. Analysis of variance showed a significant genotypic effect in the DM partitioning into roots (**Supplementary Table S1**), as root DM allocation was higher for the EFFI than for the GREEN genotype; however, the genotypic significant difference was not identified under specific treatments (**Figure 2D**).

In plants grown at high N supply before silking, a low N supply during the lag phase did not significantly change DM partitioning to ear 1 and husks, whereas for the GREEN genotype DM partitioning to ear 1 and husks was reduced by shading. Plants exposed to a continuously low level of N supply before silking and during the lag phase showed decreased DM partitioning to the ear 1 and husks when compared to plants grown at a continuously high N supply. Genotypic differences were also apparent in DM partitioning into the first ear and husks, as the EFFI genotype partitioned less DM to ear 1 and husks in all but one treatment [the same amount was partitioned in the (nn) treatment] (**Figure 2E**). However, a high N supply during the lag phase caused a stronger increase in DM partitioning into ear 2 and husks in the EFFI than in the GREEN genotype when grown at low N before silking. A similar tendency for higher DM partitioning was also evident in the EFFI versus the GREEN genotype when the plants were grown at high N supply before silking (**Figure 2F** and **Supplementary Table S1**).

Genotype-Specific Response to Modification of N Supply and Shading During the Lag Phase: Carbohydrate Status of Plants and Kernels

The whole-plant carbohydrate status at the end of the lag phase, as indicated by the concentrations of non-structural carbohydrates in the stalk, was significantly affected by the rate

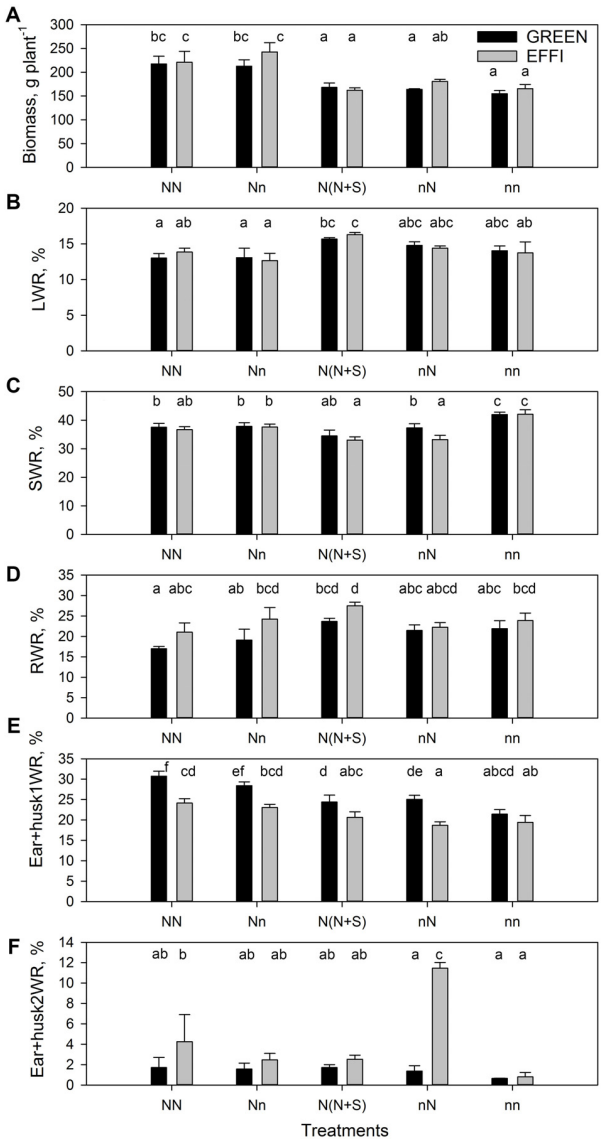

FIGURE 2 | Plant biomass and dry matter distribution in two genotypes with different N-use efficiency at the end of the lag phase. **(A)** Plant biomass, **(B)** leaf weight ratio (LWR), **(C)** stalk weight ratio (SWR), **(D)** root weight ratio (RWR), **(E)** ear 1 and husk weight ratio (Ear + husk1WR), **(F)** ear 2 and husk weight ratio (Ear + husk2WR). Treatments: High N before silking and during the lag phase (NN), high N before silking and low N during the lag phase (Nn), high N before silking and during the lag phase and shading during the lag phase [N(N + S)], low N before silking and high N during the lag phase (nN), low N before silking and during the lag phase (nn). Means ± SE are presented. Different lower case letters indicate significant differences ($p \leq 0.05$, Fisher's protected LSD). The data was analyzed by 2-factor-ANOVA. The first factor was treatments (T) [NN, Nn, N(N + S), nN, nn] and the second factor was genotype (G). Excluding shading from the analysis, the experiment was also analyzed by 3-factor ANOVA, using factors Nv, Nf, and G. The results of ANOVAs are presented in **Supplementary Table S1**.

of N supply before silking (Nv) and by the modifications in the growing conditions during the lag phase (Nf, shading). The response of GREEN plants that were well supplied with N during the vegetative stage to a reduction in the N supply during the lag phase was a significantly increased concentration of reducing sugars, but the EFFI genotype did not show this response (**Figure 3A** and **Supplementary Table S2**). The concentrations of sucrose (**Figure 3B**) and starch (**Figure 3C**) were not changed in either genotype (compare NN with Nn in **Figures 3B,C**). Shading drastically diminished the concentrations of reducing sugars, sucrose, and starch in both genotypes [compare NN with N(N + S) in **Figures 3A–C**].

The response of GREEN plants supplied with sub-optimal N during the vegetative phase to an increase in N supply during the lag phase was a decrease in the concentration of reducing sugars in the stalk, but again the EFFI genotype did not show this response. The concentrations of sucrose and starch in both genotypes were unchanged by the short-term increase in N supply (compare nn with nN in **Figures 3A–C**). The lower concentration of reducing sugars and starch in the stalks of the EFFI than in the GREEN genotypes under sub-optimal conditions [nn, Nn, N(N + S)] indicates a more efficient carbohydrate utilization at the plant level.

In the kernels, the reduction of N supply during the lag phase (compare NN with Nn) did not change the soluble carbohydrate (sucrose and reducing sugars) concentrations in the GREEN genotype but did increase the sucrose concentration in the EFFI genotype (**Figures 3D,E**). By contrast, low N supply during lag phase tended to decrease the starch concentration in the kernels in both genotypes, although the difference did not reach statistical significance (**Figure 3F**). Shading tended to increase the concentration of sucrose but decreased the concentration of reducing sugars in the kernels for both genotypes [compare NN with N(N + S)]. An increased N supply during the lag phase in plants grown at low N supply during the vegetative stage tended to decrease the concentration of sucrose but did not change the concentration of reducing sugars and starch (compare nn with nN). Genotypic comparisons showed that EFFI tended to accumulate higher concentrations of sucrose at both optimal and sub-optimal N conditions (**Table 3E** and **Supplementary Table S2**); however, a greater accumulation of reducing sugars in EFFI only occurred in the plants supplied with low levels of N during the vegetative and the lag phases.

Genotype-Specific Response to Modification of N Supply and Shading During the Lag Phase: N Concentration and Allocation

The change in N supply during the lag phase quickly modulated the N content in plants (**Figure 4A** and **Supplementary Table S3**). Low N supply during the lag phase decreased the N concentration in all vegetative organs for plants grown at high N supply before silking (compare NN and Nn); however, low N supply had a weaker effect on N concentration in the generative organs (kernels and cob) (**Figures 4B–F** and **Supplementary Table S3**). The N concentration was still higher in these plants than in plants grown at continuously low levels of N (nn).

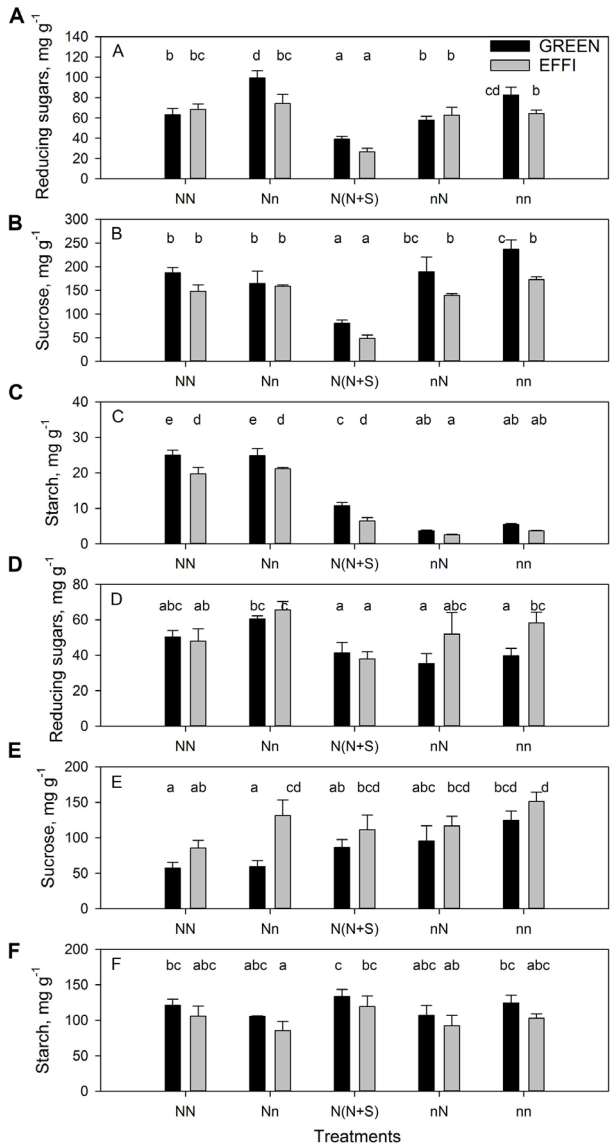

FIGURE 3 | The concentration of carbohydrates in stalk and kernels of two genotypes with different N-use efficiency at the end of the lag phase. Reducing sugars, sucrose, and starch in the stalk **(A–C)** and kernels **(D–F)**. Treatments: High N before silking and during the lag phase (NN), high N before silking and low N during the lag phase (Nn), high N before silking and during the lag phase and shading during the lag phase [N(N + S)], low N before silking and high N during the lag phase (nN), low N before silking and during the lag phase (nn). Means ± SE are presented. Different lower case letters indicate significant differences ($p \leq 0.05$, Fisher's protected LSD). The experiment was analyzed by 2-factor-ANOVA. The first factor was treatments (T) [NN, Nn, N(N + S), nN, nn] and the second factor was genotype (G). Excluding shading from the analysis, the experiment was also analyzed by 3-factor ANOVA, using factors Nv, Nf, and G. The results of ANOVAs are presented in **Supplementary Table S2**.

Interestingly, the supply of high N to plants cultivated at a low N level before silking (nN) increased the N concentration to the same level as that seen in plants continuously cultivated at high N. This quick increase in N concentration in these plants indicates a large capacity of the plants to absorb limiting nutrients, as regulated by the demand-driven regulator mechanisms of nitrate uptake (Imsande and Touraine, 1994). Genotypic differences in N concentration were found in the roots (**Figure 4D**) of plants grown at various N supply conditions (NN, Nn, and nN). The root N concentrations were lower in EFFI than in GREEN, indicating a higher internal N utilization efficiency for root growth. Moreover, under optimal conditions during lag phase, the stalk N concentrations tended to be lower in the EFFI than the GREEN genotype.

Data for the ^{15}N distribution showed that low lag phase N supply for plants grown at high N supply during the vegetative stage tended to decrease N partitioning into the leaves. Shading increased N partitioning into the stalk (**Figures 5A,B** and **Supplementary Table S4**). The GREEN genotype plants grown at low N supply during the vegetative stage responded to an increased N supply by increasing the N partitioning into the leaves and into the stalk, whereas the EFFI genotype tended to allocate more ^{15}N into the roots when grown with a high N supply before silking, regardless of the N supply during the lag phase (**Figure 5C**). Depletion of N during the lag phase increased ^{15}N partitioning into ear 1 and husks, whereas the presence of N during the lag phase increased ^{15}N partitioning into ear 2 and husks in the EFFI genotype (**Figures 5D,E** and **Supplementary Table S4**). Shading did not significantly affect ^{15}N allocation to the ears. The ^{15}N distribution to the first ear and husks was lower in the EFFI than in the GREEN genotype under both optimal and sub-optimal conditions and showed significant differences for the Nn, N(N + S), and nN treatments.

Genotypes Responded Differently in KN to Changes of N and Light Supply During the Lag Phase

The KN per plant was higher in EFFI than in GREEN (**Figure 6A**) because of the formation of the second ear in EFFI under conditions of high N and light during the lag phase. However, a low level of N supply in the lag phase for plants grown under luxury conditions during the vegetative stage did not significantly change KN in the first ear in either genotype (comparing NN vs. Nn) (**Figure 6A** and **Supplementary Table S5**). Shading of the plants grown at high N level decreased the KN only in the GREEN and not in the EFFI genotype. Because the floret set is established before silking (Gonzalez et al., 2019), we assume that this kernel number reduction was due to the kernel abortion that occurs during the lag phase. Transfer of plants supplied with low N during the vegetative stage to high N did not increase KN in either genotype; however, shading during the lag phase resulted in a more pronounced decrease in KN in the GREEN than in the EFFI genotype, further indicating that a higher kernel abortion was induced in GREEN than in EFFI under unfavorable conditions during the lag phase. Taken together, the results showed that the EFFI genotype was able to maintain a similar KN under either stress or control conditions, whereas the KN of the GREEN genotype was sensitive to both low N and low light conditions.

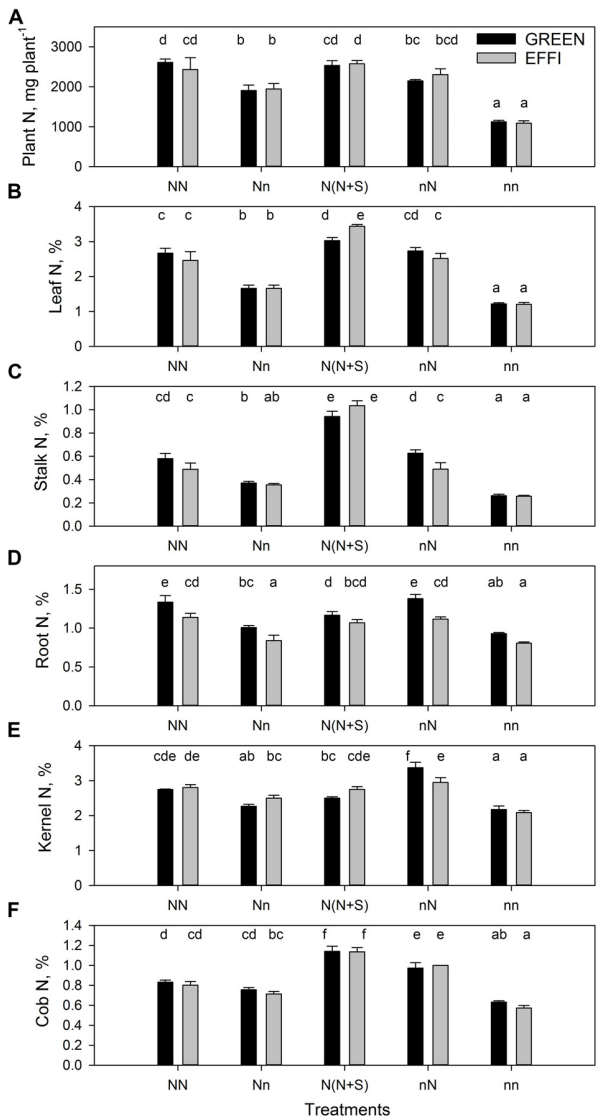

FIGURE 4 | Plant N uptake and N concentration in two genotypes with different N-use efficiency at the end of the lag phase. **(A)** Plant N uptake, N concentration in **(B)** leaves, **(C)** stalk, **(D)** roots, **(E)** kernels, and **(F)** cob. Treatments: High N before silking and during the lag phase (NN), high N before silking and low N during the lag phase (Nn), high N before silking and during the lag phase and shading during the lag phase [N(N + S)], low N before silking and high N during the lag phase (nN), low N before silking and during the lag phase (nn). Means ± SE are presented. Different lower case letters indicate significant differences ($p \leq 0.05$, Fisher's protected LSD). The experiment was analyzed by 2-factor-ANOVA. The first factor was treatments (T) [NN, Nn, N(N + S), nN, nn] and the second factor was genotype (G). Excluding shading from the analysis, the experiment was also analyzed by 3-factor ANOVA, using factors Nv, Nf, and G. The results of ANOVAs are presented in **Supplementary Table S3**.

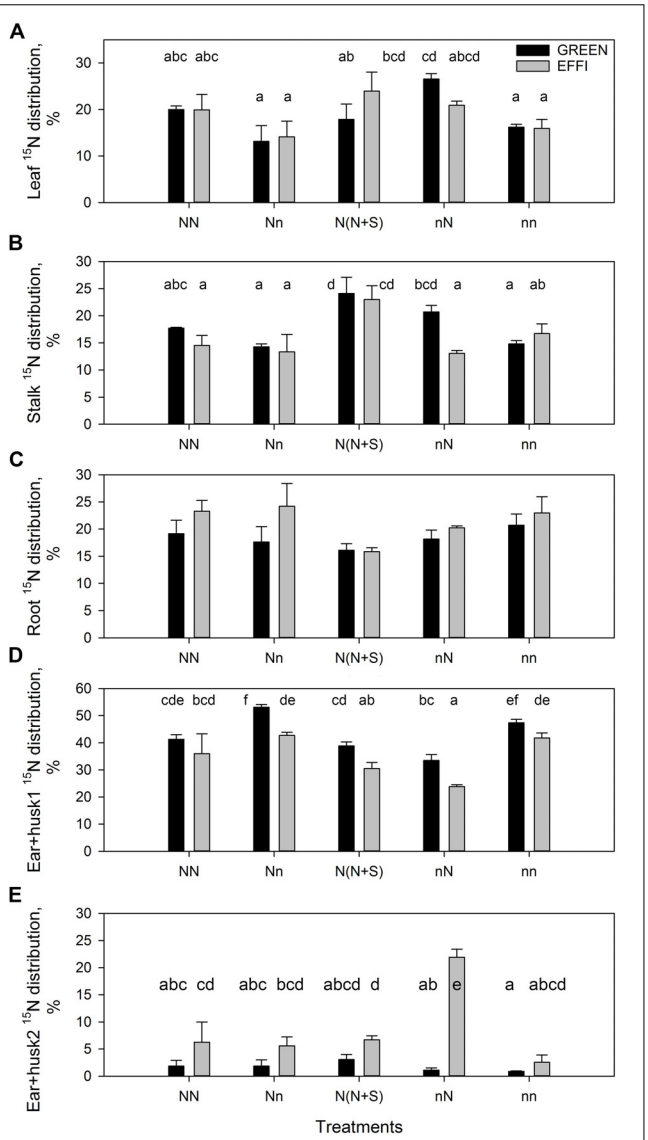

FIGURE 5 | Percentage of ^{15}N distribution at the end of the lag phase in two genotypes with different N-use efficiency at the end of the lag phase. ^{15}N distribution to **(A)** leaves, **(B)** stalk, **(C)** roots, **(D)** first ear and husks, **(E)** second ear and husks. Treatments: High N before silking and during the lag phase (NN), high N before silking and low N during the lag phase (Nn), high N before silking and during the lag phase and shading during the lag phase [N(N + S)], low N before silking and high N during the lag phase (nN), low N before silking and during the lag phase (nn). Means ± SE are presented. Different lower case letters indicate significant differences ($p \leq 0.05$, Fisher's protected LSD). The experiment was analyzed by 2-factor-ANOVA. The first factor was treatments (T) [NN, Nn, N(N + S), nN, nn] and the second factor was genotype (G). Excluding shading from the analysis, the experiment was also analyzed by 3-factor ANOVA, using factors Nv, Nf, and G. The results of ANOVAs are presented in **Supplementary Table S4**.

Regulation of KW by N Supply and Shading During the Lag Phase

The mean KW for both genotypes was higher at high than at low N supply during the vegetative stage (**Figure 6B** and **Supplementary Table S5**). A reduction in N supply or shading of plants grown under luxury N conditions during the vegetative stage did not decrease the mean KW in either genotype. However, increasing the N supply during the lag phase for plants grown at a low N supply

before silking (compare nn vs. nN) increased KW, with a significant effect observed for the GREEN but not for the EFFI genotype. Shading had weak reducing effect on KW in both genotypes.

Association of KN With N and Carbohydrate Status at the End of the Lag Phase

The reduction in DM partitioning into the ear and the reduced kernel set under stress conditions resulted in a close correlation between these two traits in the GREEN genotype (**Figure 7A**), whereas for the EFFI genotype, KN was not related to the stress-induced variation in ear growth (**Figure 7A**). A closer correlation was also observed between ear growth per kernel during the lag phase and KN in the GREEN than in the EFFI genotype (**Figure 7B**). The GREEN genotype showed a negative correlation between KN and total soluble sugars (**Figure 7C**) and between KN and the sucrose/sugar ratio (**Figure 7D**) indicating that, for this genotype, a higher utilization of soluble sugars in the kernels and a higher cleavage of sucrose were related to the higher KN set. Interestingly, the KN for the EFFI genotype was not associated with soluble sugar concentrations in the kernels. The N concentration and fluxes were less associated with KN than was the DM distribution to the ear and KN (**Figures 7E–H**), indicating that the N supply to the ear was not associated with KN set. The relatively high value of the paired correlation coefficient between KN and N supply to the ear for GREEN (r = 0.83) was strongly affected by the high correlation between the DM distribution and N supply to the ear (r = 0.89). Indeed, the calculation of the partial correlation coefficient between KN and N supply to the ear show no positive effect of N supply on KN ($r = -0.69$).

Association of KW With N and Carbohydrate Status at the End of the Lag Phase

No close correlation was detected between KW and ear growth or ear growth per kernel (**Figures 8A,B**) in either genotype. A weak negative correlation was found between KW and total sugars, indicating that utilization of sugars might be important for both kernel set and KW (**Figure 8C**). In the GREEN genotype, the correlation between KW and sucrose/total sugar ratio (**Figure 8D**) was weaker than the correlation between KN and sucrose/total sugar (**Figure 7D**), indicating that the sucrose cleavage capacity was more important for KN than for potential KW. No strong correlations were found between KW and N% in the kernels and ^{15}N distribution (**Figures 8E,F**); however, closer correlations were found between KW and N flux into the ear and KW and N flux into ear per kernel (**Figures 8G,H**) for both genotypes, indicating that KW might be associated with N flux to the ear.

Genotypic Differences in Ear Morphology

Analysis of the kernel size at 4 days after pollination (**Figure 9**) showed that the genotypes differed in the gradient of kernel size: the GREEN genotype showed a strong gradient in kernel size along the ear, with smaller sized kernels at the top and larger sized kernels at the base of ear. By contrast, the EFFI genotype had bigger apical kernels that reduced the gradient of kernel size along the entire ear.

DISCUSSION

In grain crops, the sink capacity (i.e., the ability of kernels to accumulate assimilates) is determined by the KN and potential KW (Tollenaar, 1977). In maize, both components of sink capacity are fixed during the lag phase of grain growth (Ordonez et al., 2018). Therefore, the processes involved in the determination of KN and potential KW can be assumed to compete for a given pool of resources during this phase, resulting in a restriction of either KN or potential KW. However, if these two components of sink capacity are regulated by different processes and resource pools, then an increase in one component should be possible without a decrease in the other. In the present study, we found indication that these two sink components are regulated independently, implying the possibility of simultaneously increasing both sink components in maize breeding programs.

Independent regulation of KN and potential KW is indicated by the finding that KN and potential KW responded differently to modifications in the supply of either N or carbohydrates during the lag phase in the two genotypes with contrasting N efficiency. The KN per ear (i) was related to the level of available assimilates and their utilization in the kernels during the lag phase in the GREEN genotype, (ii) showed a genotypic difference that was related to morphological traits of the ear determined before silking, and (iii) was regulated by an unknown signal that strongly modulated ear formation and kernel abortion. The potential KW, by contrast, was related to the N flux to the kernels during the lag phase.

In the Control GREEN Genotype, Kernel Number Was Associated With the Level of Available Assimilates and Their Utilization During the Lag Phase

In the first ear of the GREEN genotype, KN strongly responded to the level of pre-silking N supply and to the light intensity during the lag phase (**Figure 6A** and **Supplementary Table S5**). A low pre-silking N supply tend to reduce KN when compared with a high pre-silking N supply. Shading reduced KN for plants with either high N [N(N + S)] or low N supply [n(n + S)]. The tendency toward a reduction in KN under low N supply compared to high N supply before silking indicates a possible inhibitory effect of low N supply on spikelet number; however, limiting conditions during the lag phase have a greater impact on kernel set. Indeed, numerous investigations in maize have shown that KN is closely correlated with crop growth during

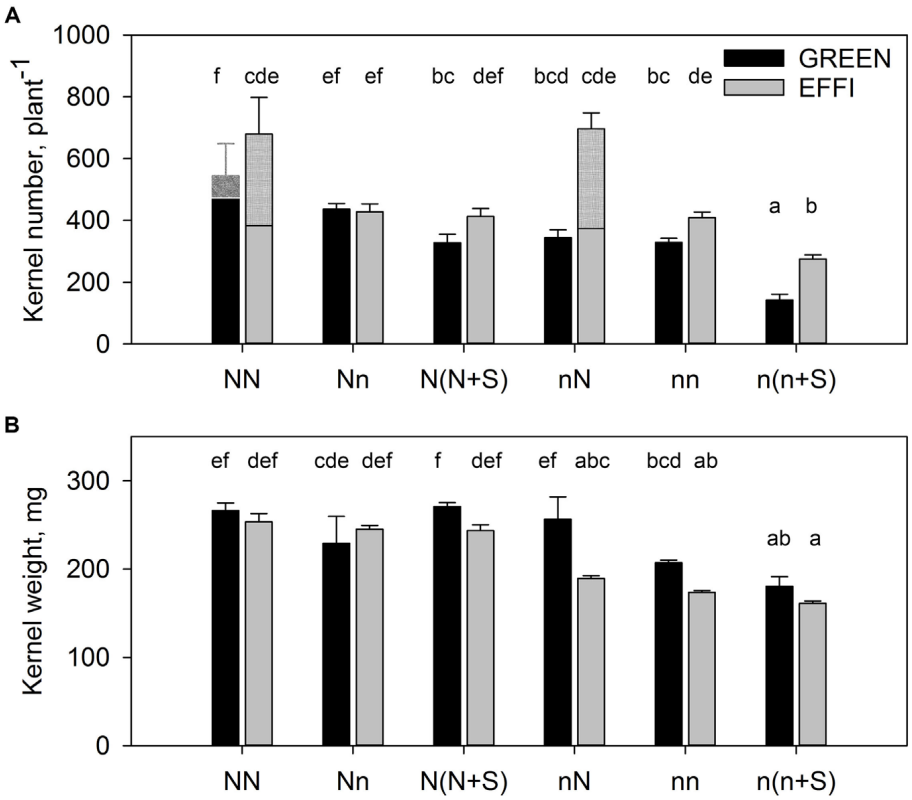

FIGURE 6 | Kernel number **(A)** and kernel weight **(B)** for two genotypes with different N-use efficiency grown under high or low N supply during vegetative growth or during the lag phase and under full light or shading during the lag phase. Treatments: High N before silking and during the lag phase (NN), high N before silking and low N during the lag phase (Nn), high N before silking and during the lag phase and shading during the lag phase [N(N + S)], low N before silking and high N during the lag phase (nN), low N before silking and during the lag phase (nn), and low N before silking and during the lag phase and shading [n(n + S)]. All plants were grown under luxury conditions during the effective grain filling stage to ensure that the final kernel weight corresponded to the potential kernel weight established at the end of the lag phase. Means ± SE are presented. Different lower case letters indicate significant differences ($p \leq 0.05$, Fisher's protected LSD). The treatments NN for both genotypes and nN for the EFFI genotype induced formation of a second ear. The kernel number of the second ear is shown in the hatched part of the columns **(A)**, so that the contribution of every ear is presented. The statistical analysis is presented for the first ear. Two separate 3-factor-ANOVAs were carried out. In the first analysis, the factors N level during vegetative stage up to silking (Nv), N level after flowering from silking to 16 days after silking (Nf), and genotype (G) were tested (NN, Nn, nN, nn). In the second analysis, the factors N level (both during vegetative and the lag phase), shading (S), and genotype (G) were tested [NN, N(N + S), nn, n(n + S)]. The results of ANOVAs are presented in **Supplementary Table S5**.

the lag phase (Andrade et al., 2002; D'Andrea et al., 2009). Crop growth is considered an indicator of a crop's ability to produce assimilates, i.e., its source strength. In agreement with the well-documented positive relationship between KN and crop growth, all the treatments in the present study that reduced KN also decreased plant growth during the lag phase. The level of N supply during pre-silking and during the lag phase, and the light intensity during the lag phase, also affected N concentrations in various plant organs (**Figure 4**) and the supply of recently acquired ^{15}N to those organs during the lag phase (**Figure 5**). However, the treatment-induced modification of plant N status and resulting changes of the N delivery to generative organs was not associated with corresponding changes in KN. For example, the abrupt change in N supply from high N during the vegetative growth phase to low N at silking significantly reduced N concentrations in the generative organs, but did not reduce KN. Shading was associated with an increase in plant N concentration, whereas the KN of the GREEN genotype decreased with shading. This suggests that the KN of the GREEN genotype was not directly regulated by the N status of the plants.

Interestingly, experimental conditions that decreased plant growth during the lag phase [nn and N(N + S)] also decreased DM partitioning to the ear (**Figure 2**). The decrease in DM partitioning to the ear indicates that the sink capacity of the generative plant organs was diminished relative to the sink capacity of other plant organs, resulting in a further reduction of assimilate flux to kernels. This indicates that reduced source strength of the plants was not the only mechanism decreasing kernel set under stress conditions. Under low N and, to a lesser extent, under shading conditions, the concentrations of sucrose in kernels were increased rather than decreased (**Figure 3E**). Obviously, under these conditions, the sink activity of kernels (i.e., their ability to utilize assimilates for growth and storage) was more depressed than the assimilate supply. This suggestion of lower kernel sink activity under stress conditions is further supported by the

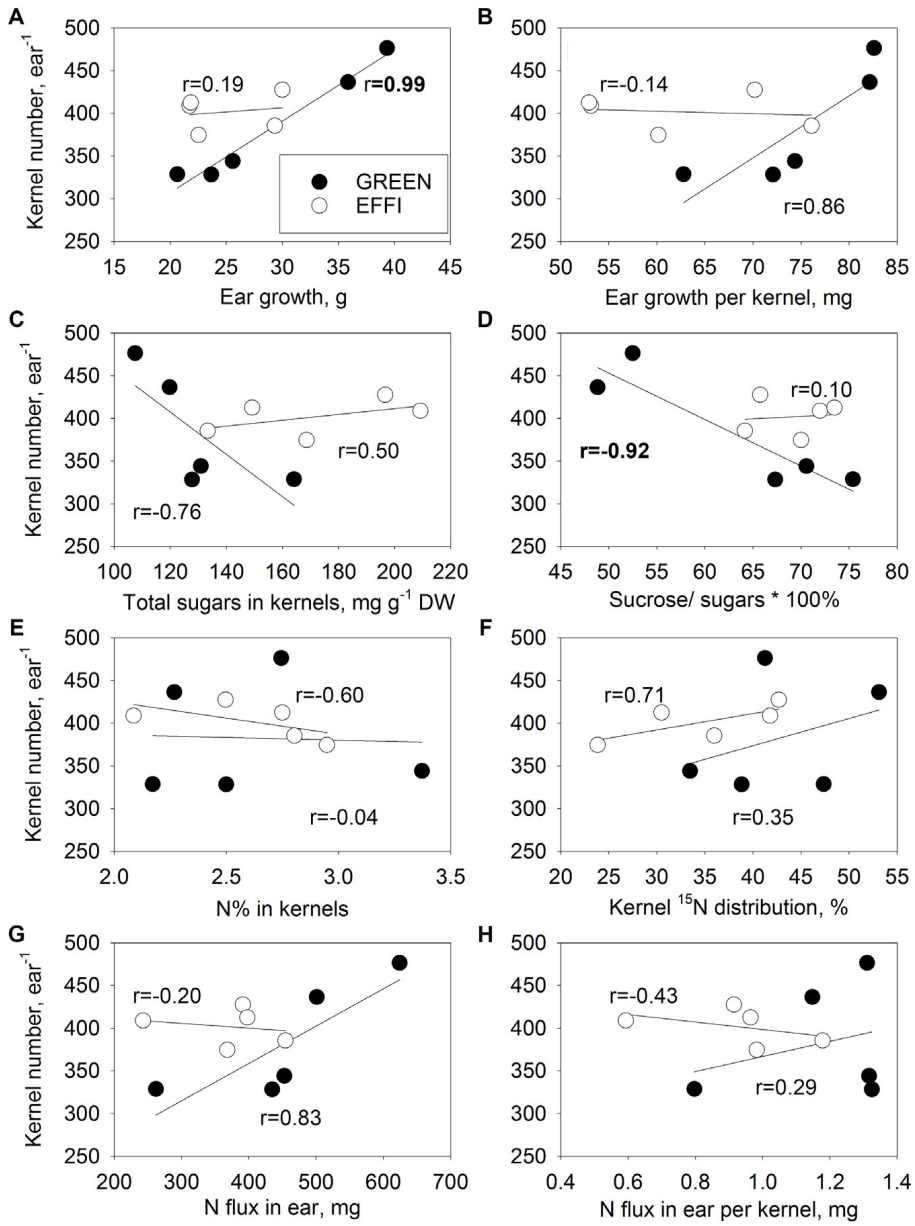

FIGURE 7 | Relationships between kernel number (KN) of the first ear and parameters describing the supply of the first ear with N and carbohydrates during the lag phase for two genotypes with different N-use efficiency. Relationships between KN and ear growth **(A)**, ear growth per kernel **(B)**, total soluble sugar concentrations in kernels **(C)**, ratio of sucrose to total soluble sugar concentrations in kernels **(D)**, kernel N concentrations **(E)**, ^{15}N distribution to kernels **(F)**, N flux into ear **(G)**, and N flux into ear per kernel **(H)**. The correlation coefficients (r) in bold are statistically significant at $p < 0.05$.

increase in the sucrose/total soluble carbohydrate ratio in kernels (**Figure 3**). This ratio increase indicates that the kernels have a lower sucrose cleavage capacity, which is a crucial factor that determines the high sink activity of kernels. The cleavage of sucrose to hexoses occurs mostly in the pedicel and basal endosperm layer (Shannon, 1972), where apoplastic invertases play a crucial role in establishment of sink strength by maintaining a favorable sucrose concentration gradient between the phloem sieve tubes and the apoplast (Zinselmeier et al., 1999; McLaughlin and Boyer, 2004). A lower ability to metabolize sucrose results in kernel abortion (Bihmidine et al., 2013). The suggestion that plant growth and KN under low N conditions were limited by assimilate utilization (i.e., the sink strength) is also supported by the increased accumulation of hexoses and sucrose in the stalks of GREEN when cultivated at low N (nn) versus high N (NN) conditions (**Figures 3A,B**).

The suggestion that KN and yield at low N supply are controlled by sink activity rather than source activity is also supported by other investigations. Field experiments on plants

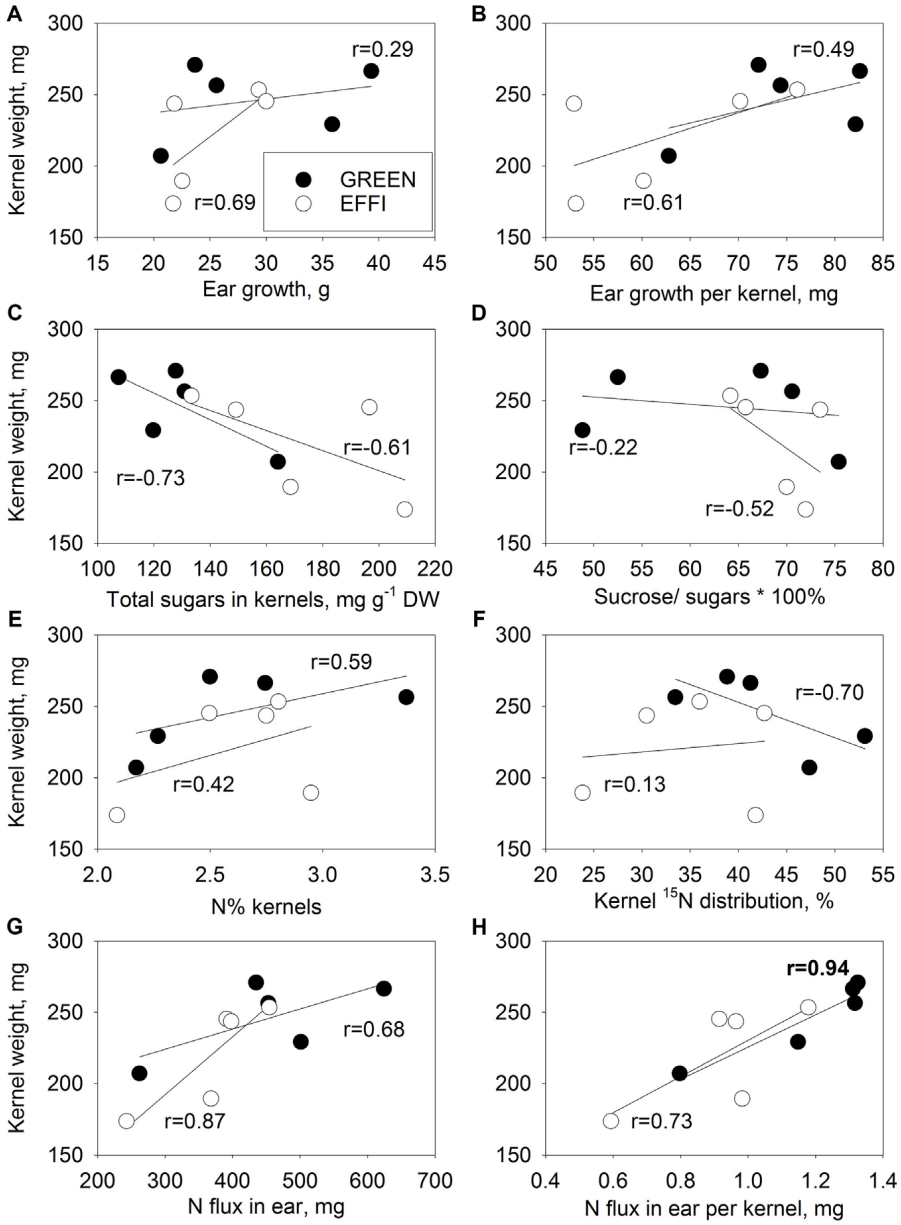

FIGURE 8 | Relationships between kernel weight (KW) of the first ear and parameters describing the supply of the first ear with N and carbohydrate during the lag phase for two genotypes with different N-use efficiency. Relationships between KW and ear growth **(A)**, ear growth per kernel **(B)**, total soluble sugars in kernel **(C)**, ratio of sucrose to total soluble sugars **(D)**, N% kernel **(E)**, ^{15}N distribution to kernel **(F)**, N flux into ear **(G)**, and N flux into ear per kernel **(H)**. The correlation coefficients (r) in bold are statistically significant at $p < 0.05$.

grown with different levels of N supply showed that N deficiency increased carbohydrate concentration in the cob (Ning et al., 2018). In that study, N deficiency also increased the ratio of sucrose to total soluble sugars in the apical cob section, where kernel abortion usually occurs. The inhibition of carbohydrate utilization in the kernels was ultimately responsible for feedback inhibition of photosynthesis and of sugar export from leaves under low N supply (Ning et al., 2018). Direct evidence for sink limitation under low N conditions was obtained in a study by Peng et al. (2013), who showed that sucrose infusion into stem internodes in N deficient plants did not increase ear growth.

Some evidence indicates that the low sink strength of ears under N deficiency is related to hormonal signals that are transported to or biosynthesized in the ear. Nitrogen deficiency is associated with lower ear concentrations of IAA and GA during the lag phase and low cytokinin levels at the end of the lag phase, as well as increased concentrations of ABA (Yu et al., 2016). Interestingly, shading during the lag phase induced kernel abortion and induced a similar modulation of hormonal

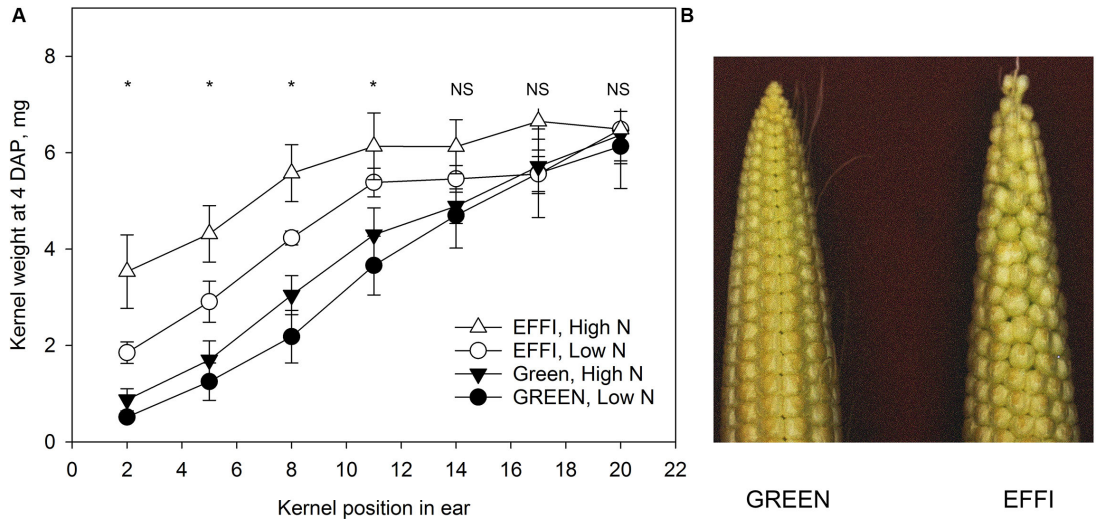

FIGURE 9 | The kernel size four days after pollination for two genotypes with different N-use efficiency grown at high and low level of N supply in a field experiment. **(A)** Kernel dry weight at specific position along the rachis of the ear. Asterisks indicate statistical significant differences among treatments at $p < 0.05$. **(B)** Typical phenotypes of ears of two genotypes at 4 days after pollination.

balance, namely lower concentrations of stimulatory hormones, such as IAA, GA and cytokinins, and higher concentration of the inhibitory hormone ABA (Gao et al., 2018).

Other investigations have indicated that ethylene might play a key role in kernel abortion (Cheng and Lur, 1996). A recent investigation on transgenic maize lines with reduced ethylene biosynthesis showed higher KN under different stresses, including shading and N deficiency (Habben et al., 2014). The observations that different types of stresses induce the same changes in hormonal composition in the ear, and that changes in the same signaling pathway increase the yield under different stresses, suggest the operation of a common mechanism for the regulation of kernel set under stress conditions. In our investigation, the observation that KN was higher in EFFI than in GREEN under low N supply and under shading (**Figure 6A**) further supports the assumption that a common mechanism, involving signaling molecules, might regulate kernel set under different environmental stresses.

In this context, the correlation observed between KN and DM partitioning into the ear (**Figure 7**) might reflect a feedback loop, whereby a decrease in source strength (assimilate availability) under stress conditions modulates hormone transport to, or hormone biosynthesis in, the ear, resulting in synchronization of sink and source activities. A strategy to restrict kernel set under unfavorable conditions can be seen as being advantageous in maize evolution, as it ensures a sufficient weight and thus amount of reserves in the remaining kernels to support seedling establishment in the following generation. However, this strategy brings no advantages to agriculturally cultivated crops, because a restriction of KN, and thus, sink capacity under unfavorable environmental conditions during the lag phase will strongly decrease final yields.

In this respect, the EFFI genotype is interesting because it was able to maintain a high KN in the first ear even under unfavorable conditions. In this genotype, KN was not related to ear or kernel traits related to assimilate supply to the ear (ear growth during the lag phase, **Figure 7A**), to assimilate supply to the individual kernels (ear growth per kernel, **Figure 7B**; total sugar concentrations in kernels, **Figure 7C**), or to assimilate utilization within the kernels (ratio of sucrose to total sugars in kernels, **Figure 7D**). The higher KN in the nitrogen use efficient EFFI genotype in comparison to the control GREEN genotype under stress conditions was therefore not related to a higher assimilate supply or to better assimilate utilization by the kernels during the lag phase but was controlled by other plant traits.

Differences Between Genotypes in Kernel Set Under N Deficiency Are Related to Ear Morphology

The greater ability of EFFI than GREEN to maintain constant KN under low N or shading (**Figure 6A**) might be related to the differences observed in ear morphology at the beginning of the lag phase (**Figure 9**). The ears of EFFI contained bigger kernels at the apical part of the ear, resulting in a lower gradient of kernel size along the rachis of the ear. This bigger kernel size at the apical part of the ear might be related with lower dominance of the basal kernels and increase the survival rate of the apical kernels. A smaller kernel size shortly after pollination is associated with a higher probability of kernel abortion in the apical areas (Tollenaar and Daynard, 1978). Moreover, the EFFI genotype, having a shorter ear, might have a more synchronous pollination among silks, which could also contribute to differences in dominance between the basal and apical kernels. Indeed, a reduction in the number of florets per ear should lead to a more uniform development within an ear row and less abortion of apical kernels, as suggested previously (Lafitte and Edmeades, 1995). Recently, genotypic differences

were shown in the number of florets and the growth dynamic of kernels at the early stages of cob development in maize, and these differences were related to the capacity of different genotypes to resist abiotic stresses by modulation of kernel abortion (Yan et al., 2018). In that study, the genotype with a higher floret number had a higher rate of kernel loss from the apical position, especially under environmental stress (Yan et al., 2018). Thus, genotypes with a moderate number of florets, but ones of equivalent size, might have the advantages shown the EFFI genotype in our investigation, and this trait could be considered a promising plant characteristic for the selection of genotypes resistant to stress conditions.

The lower kernel size gradient within the cob between apical and basal kernel positions in EFFI in comparison to GREEN was not related to carbohydrate supply to the kernels or to utilization within the kernels (**Figures 7A–D**). Instead, the larger kernels at the ear apex at the beginning of the lag phase (**Figure 9**) were more resistant to abortion. Although no advantages were found for carbohydrate utilization in kernels at the end of the lag phase, EFFI had a higher carbohydrate utilization efficiency at the plant level, as indicated by the lower concentration of carbohydrates in the stalk (**Figure 3** and **Supplementary Table S2**). This finding indicates that genotypic differences that lead to more efficient carbohydrate utilization in the stalk can also contribute to the carbohydrate utilization efficiency at the plant level.

The data on N concentrations of different organs in the two genotypes (**Figure 4**) did not indicate a greater ability of EFFI than GREEN to utilize or redistribute accumulated N. Differences between genotypes in N concentration were found only in the stalk under high N (**Table 3**), indicating that GREEN might have a higher capacity to accumulate N in the pre-silking stage. This might be advantageous in buffering grain yield under post-silking stress conditions (Nasielski et al., 2019). At the end of the lag phase, EFFI had a lower N concentration in the roots (**Figure 4D** and **Supplementary Table S3**), suggesting that the N costs for root growth were lower in EFFI than in GREEN. The lower N concentration in the roots was associated with a higher DM partitioning to the roots, indicating that the more efficient utilization of N for root growth might be an important trait that contributes to the higher NUE of EFFI.

Applying ^{15}N 4 days before silking also allowed us to address the question of whether the allocation to various plant organs of the N taken up during the critical period might contribute to more efficient N use. When compared to GREEN, EFFI incorporated more of the ^{15}N into the roots and allocated less ^{15}N to other vegetative organs, leaves, and the stalk, as well as to the first ear (**Table 4**). The partitioning of N shortly before silking should be considered in the context of resource competition between the generative organs and roots (Triboi and Triboi-Blondel, 2002). Thus, a higher N investment into the roots might be an important trait of EFFI, as it might contribute to greater root growth, as indicated by the higher DM partitioning into the roots at the end of the lag phase. It might be related to or associated with an alteration in hormone synthesis (Takei et al., 2001), which, in turn, could affect physiological responses in the aboveground plant organs.

Ear Formation Is Induced by an Unknown Signal

The other indication that unknown signaling molecules might be involved in the regulation of KN per plant is the formation of the second ear in the EFFI genotype following an abrupt increase in N supply at silking (**Figure 6A**). We found that this abrupt increase in N supply did not significantly modulate plant growth during the lag phase (**Figure 2A**), indicating that the formation of the second ear was not due to a greater availability of photoassimilates. Interestingly, the formation of the second ear was not typical for the same genotype in the field (Paponov et al., 2005b) and might be related to the low plant density and better N supply used in our hydroponic experiment. The strong increase in sink capacity of the second ear in the EFFI genotype was not associated with genotypic differences in carbohydrate or N concentrations in this genotype when compared with the GREEN genotype. Therefore, we assume that the formation of a second ear was induced by application of nitrate to the roots, which, in turn, stimulated the biosynthesis of phytohormones affecting ear development. The role of hormones in ear initiation has received almost no attention and requires further investigation.

The positive response of the EFFI genotype to high N supply during the lag phase makes this a promising genotype for agronomic management with late N application, which could substantially reduce the losses of applied N occurring through leaching or denitrification, especially in agricultural areas with excessive spring precipitation (Wang et al., 2016). Previous research has generally found that late N application near the critical stage had neither negative nor positive impacts on yield when compared with early season application (Mueller et al., 2017; Mueller and Vyn, 2018b). Interestingly, comparison of modern and 20-year-old genotypes did not show any differences between these two groups in terms of their efficiency at using late applied N fertilizer or with respect to other physiological differences, such as N allocation or DM distribution, among the different organs during the critical period of kernel set establishment (Mueller and Vyn, 2018a). Thus, the differences found here between our two genotypes might be specifically related to the focus of the breeding program, which aimed at breeding genotypes capable of high yield under low N supply conditions.

Potential KW Is Defined by N Flux per Kernel

The potential KW is fixed at the end of the lag phase, when the number of endosperm cells and the number of starch granules per kernel is established (Jones et al., 1996). However, whether the number of endosperm cells or the number of starch granules is the more important trait that determines the final KW is genotype dependent (Jones et al., 1996). Later, kernel water dynamics have been used as an alternative and easier way than determining endosperm cell number or number of starch granules for estimating potential KW (Borras and Westgate, 2006). The kernel water content at the end of the lag phase provides an indirect estimate of kernel sink capacity

(Borras and Gambin, 2010). The evidence that kernel water content at the end of the lag phase is a good predictor of potential KW has been validated by comparing kernel water content with the final KW under optimal conditions during grain filling for a wide range of genotypes and environmental conditions (Borras and Westgate, 2006). Interestingly, for maize, in most cases, the final KW is closely related with the potential size established during the lag phase (Capitano et al., 1983; Reddy and Daynard, 1983; Jones et al., 1996; Borras and Westgate, 2006), so that further optimization of the growth environment (for example, by reduction of plant density) did not increase the final KW. Thus, if no stress conditions occurred during grain filling, the potential kernel weight was usually implemented as the final kernel weight during the grain filling stage.

We cultivated our plants during the effective grain filling stage under luxury conditions (nutrient solution culture with non-limiting supplies of water and nutrients and low numbers of plants m^{-2} ground area to ensure little mutual shading between plants); therefore, we assume that no limitations for effective grain filling existed and that the KW measured at the end of the grain filling stage was very near to the potential KW. Methods involving measurements at the end of the lag phase do not directly measure potential KW; however, they are good predictors of potential KW, as shown previous investigation (Jones et al., 1985; Borras and Westgate, 2006). Nevertheless, the cultivation of plants under luxury conditions during effective grain filling provides a direct way to measure the potential KW, and a direct method can be considered a more robust method for potential KW evaluation.

The GREEN genotype represents an ideal model to study the direct effect of N supply during the lag phase on potential KW because this genotype does not change its KN in the first ear (**Figure 6A**) in response to changes in N supply. This allows a direct estimation of the effect of N on potential KW in intact plants. Our hydroponic experiment with the abrupt change in N supply showed that N could directly increase the potential KW independent of carbohydrate availability. The evidence for a direct regulation of potential KW by N fluxes is that the abrupt increase in N supply during the lag phase significantly increased the potential KW (**Figure 6B** and **Supplementary Table S5**). We assume that this effect is directly related to N and not to carbohydrate availability to the kernels, because a 16-day abrupt change in the N supply did not significantly change the plant biomass (**Figure 2A**) but strongly increased the N concentration in plant tissues (**Figure 4**). The close correlation between KW and the amount of N flux per kernel further supports this assumption for both genotypes (**Figure 8**).

Evidence for direct N effects on the potential KW was also derived from an *in vitro* experiment with kernel explants cultivated in media with varying combinations of N and sucrose (Cazetta et al., 1999). The authors showed that external N, but not sucrose, increased the kernel sink capacity, as indicated by an increased number of cells and starch granules in the endosperm. Numerous field experiments have also shown that both KN and potential KW depend on assimilate availability per kernel during the lag phase (Borras and Westgate, 2006; Gambin et al., 2006, 2008; Severini et al., 2011). However, because of the close link between N and carbohydrate metabolism, the specific effect of N on sink capacity was not resolved. The abrupt change in N availability in our experiment by cultivating plants in hydroponics and shading during the lag phase allowed us to partially dissect the N and carbohydrate fluxes in the plants and to obtain additional indications that N can directly contribute to the potential KW. These results are also supported by the recent observation that a high rate of N increases the number of endosperm cells realized during the lag phase and is associated with the final kernel weights at maturity (Olmedo Pico et al., 2019). This effect was stronger than the increase in carbohydrate availability due to reduced plant density (Olmedo Pico et al., 2019).

Compared to GREEN, EFFI had almost twice the number of kernels per plant after the application of N to the nutrient solution; this difference increases the challenge to elucidate the direct effect of N on potential KW in this genotype. Interestingly, for EFFI, the level of N supplied before silking contributed to the potential KW (**Figure 6B**). This finding that conditions before silking might affect KW agrees with the consensus that the period 15 days before silking is important for establishing the potential KW (Ordonez et al., 2018). Suboptimal conditions before flowering affect the size of the ovary in wheat, and the size of the ovary affects the final KW (Calderini et al., 1999). However, in maize, the effects of suboptimal conditions before silking require more attention in the future.

CONCLUSION

The main finding of this work is that KN and potential KW are regulated by different resources, despite their simultaneous establishment. KN is regulated differently in genotypes that differ in their ability to build grain yield at a low level of N supply. For the standard GREEN genotype, transient shading or a low pre-silking N supply significantly reduced KN, thereby showing a close positive relationship between KN and carbohydrate flux to the ear during the lag phase. The regulation of KN would ensure that the kernels actually established are adequately supplied with organic and inorganic nutrients during grain filling. This growth strategy includes kernel abortion, which leads to fewer kernels but produces kernels that have a better ability to support next-generation seedlings with kernel-derived resources. By contrast, the EFFI genotype, which was selected for its high NUE in a breeding program (Presterl et al., 2002), was characterized by its maintenance of a high KN in the first ear, even under unfavorable N supply or shading conditions, indicating no association between KN and carbohydrate flux to the ear during the lag phase in this genotype. Moreover, under high N supply during the lag phase, the EFFI genotype was able to build the second ear, thereby almost doubling the KN. We assume that this genotype has several advantages for sustainable agriculture as it can build higher sink capacity under both favorable

and unfavorable conditions during the lag phase; however, the cultivation of this genotype increases the risk of ending up with small reserves per kernel if growing conditions during grain filling are unfavorable for sufficient resource supply. These different genotypic responses to low N supply and shading during critical kernel formation stages were related to genotypic differences in ear morphology, as the efficient genotype had bigger apical kernels, indicating a reduction in the usual dominance of basal over apical kernels in the control genotype. In contrast to KN, the regulation of potential KW appeared to operate similarly in both contrasting genotypes, as KW was related to the amount of N flux per kernel during the lag phase.

DATA AVAILABILITY STATEMENT

All datasets generated for this study are included in the article/**Supplementary Material**.

AUTHOR CONTRIBUTIONS

IP and CE conceived and designed the study. IP, MP, and CE wrote the manuscript. IP, MP, and PS performed the experiment. IP and MP performed the analyses.

FUNDING

This work was supported by the Deutsche Forschungsgemein schaft (DFG EN342).

SUPPLEMENTARY MATERIAL

The Supplementary Material for this article can be found online at: https://www.frontiersin.org/articles/10.3389/fpls.2020.00586/full#supplementary-material

REFERENCES

Andrade, F. H., Echarte, L., Rizzalli, R., Della Maggiora, A., and Casanovas, M. (2002). Kernel number prediction in maize under nitrogen or water stress. *Crop Sci.* 42, 1173–1179. doi: 10.2135/cropsci2002.1173

Bihmidine, S., Hunter, C. T., Johns, C. E., Koch, K. E., and Braun, D. M. (2013). Regulation of assimilate import into sink organs: update on molecular drivers of sink strength. *Front. Plant Sci.* 4:177. doi: 10.3389/fpls.2013.00177

Blakeney, A. B., and Mutton, L. L. (1980). A simple colorimetric method for the determination of sugars in fruit and vegetables. *J. Sci. Food Agr.* 31, 889–897. doi: 10.1002/jsfa.2740310905

Borras, L., and Gambin, B. L. (2010). Trait dissection of maize kernel weight: Towards integrating hierarchical scales using a plant growth approach. *Field Crop. Res.* 118, 1–12. doi: 10.1016/j.fcr.2010.04.010

Borras, L., and Vitantonio-Mazzini, L. N. (2018). Maize reproductive development and kernel set under limited plant growth environments. *J. Exp. Bot.* 69, 3235–3243. doi: 10.1093/jxb/erx452

Borras, L., and Westgate, M. E. (2006). Predicting maize kernel sink capacity early in development. *Field Crop. Res.* 95, 223–233. doi: 10.1016/j.fcr.2005.03.001

Calderini, D. F., Abeledo, L. G., Savin, R., and Slafer, G. A. (1999). Effect of temperature and carpel size during pre-anthesis on potential grain weight in wheat. *J. Agr. Sci.* 132, 453–459. doi: 10.1017/s0021859699006504

Cameron, K. C., Di, H. J., and Moir, J. L. (2013). Nitrogen losses from the soil/plant system: a review. *Ann. Appli. Biol.* 162, 145–173. doi: 10.1111/aab.12014

Capitano, R., Gentinetta, E., and Motto, M. (1983). Grain weight and its components in maize inbred lines. *Maydica* 28, 365–379.

Cazetta, J. O., Seebauer, J. R., and Below, F. E. (1999). Sucrose and nitrogen supplies regulate growth of maize kernels. *Ann. Bot.* 84, 747–754. doi: 10.1006/anbo.1999.0976

Cheng, C. Y., and Lur, H. S. (1996). Ethylene may be involved in abortion of the maize caryopsis. *Physiol. Plant.* 98, 245–252. doi: 10.1034/j.1399-3054.1996.980205.x

Ciampitti, I. A., and Vyn, T. J. (2013). Grain nitrogen source changes over time in maize: a review. *Crop Sci.* 53, 366–377. doi: 10.2135/cropsci2012.07.0439

D'Andrea, K. E., Otegui, M. E., and Cirilo, A. G. (2008). Kernel number determination differs among maize hybrids in response to nitrogen. *Field Crop. Res.* 105, 228–239. doi: 10.1016/j.fcr.2007.10.007

D'Andrea, K. E., Otegui, M. E., Cirilo, A. G., and Eyherabide, G. H. (2009). Ecophysiological traits in maize hybrids and their parental inbred lines: phenotyping of responses to contrasting nitrogen supply levels. *Field Crop. Res.* 114, 147–158. doi: 10.1016/j.fcr.2009.07.016

DeBruin, J. L., Hemphill, B., and Schussler, J. R. (2018). Silk development and kernel set in maize as related to nitrogen stress. *Crop Sci.* 58, 2581–2592. doi: 10.2135/cropsci2018.03.0160

Erisman, J. W., Sutton, M. A., Galloway, J., Klimont, Z., and Winiwarter, W. (2008). How a century of ammonia synthesis changed the world. *Nat. Geosci.* 1:636. doi: 10.1038/ngeo325

Gambin, B. L., Borras, L., and Otegui, M. E. (2006). Source-sink relations and kernel weight differences in maize temperate hybrids. *Field Crop. Res.* 95, 316–326. doi: 10.1016/j.fcr.2005.04.002

Gambin, B. L., Borras, L., and Otegui, M. E. (2008). Kernel weight dependence upon plant growth at different grain-filling stages in maize and sorghum. *Aust. J. Agr. Res.* 59, 280–290. doi: 10.1071/ar07275

Gao, J., Shi, J. G., Dong, S. T., Liu, P., Zhao, B., and Zhang, J. W. (2018). Grain development and endogenous hormones in summer maize (Zea mays L.) submitted to different light conditions. *Int. J. Biometeorol.* 62, 2131–2138. doi: 10.1007/s00484-018-1613-4

Gonzalez, V. H., Lee, E. A., Lukens, L. L., and Swanton, C. J. (2019). The relationship between floret number and plant dry matter accumulation varies with early season stress in maize (Zea mays L.). *Field Crop. Res.* 238, 129–138. doi: 10.1016/j.fcr.2019.05.003

Guo, H. C., and York, L. M. (2019). Maize with fewer nodal roots allocates mass to more lateral and deep roots that improve nitrogen uptake and shoot growth. *J. Exp. Bot.* 70, 5299–5309. doi: 10.1093/jxb/erz258

Habben, J. E., Bao, X. M., Bate, N. J., DeBruin, J. L., Dolan, D., Hasegawa, D., et al. (2014). Transgenic alteration of ethylene biosynthesis increases grain yield in maize under field drought-stress conditions. *Plant Biotechnol. J.* 12, 685–693. doi: 10.1111/pbi.12172

Hanft, J. M., Jones, R. J., and Stumme, A. B. (1986). Dry-matter accumulation and carbohydrate concentration patterns of field-grown and invitro cultured maize kernels from the tip and middle-ear positions. *Crop Sci.* 26, 568–572. doi: 10.2135/cropsci1986.0011183X002600030029x

Hisse, I. R., D'Andrea, K. E., and Otegui, M. E. (2019). Source-sink relations and kernel weight in maize inbred lines and hybrids: responses to contrasting nitrogen supply levels. *Field Crop. Res.* 230, 151–159. doi: 10.1016/j.fcr.2018.10.011

Imsande, J., and Touraine, B. (1994). N-demand and the regulation of nitrate uptake. *Plant Phys.* 105, 3–7. doi: 10.1104/pp.105.1.3

Ingestad, T., and Lund, A. B. (1986). Theory and techniques for steady state mineral nutrition and growth of plants. *Scand. J. Forest Res.* 1, 439–453. doi: 10.1080/02827588609382436

Jones, R. J., Roessler, J., and Ouattar, S. (1985). Thermal environment during endosperm cell-division in maize: effects on number of endosperm cells and starch granules. *Crop Sci.* 25, 830–834. doi: 10.2135/cropsci1985.0011183X002500050025x

Jones, R. J., Schreiber, B. M. N., and Roessler, J. A. (1996). Kernel sink capacity in maize: genotypic and maternal regulation. *Crop Sci.* 36, 301–306. doi: 10.2135/cropsci1996.0011183X003600020015x

Lafitte, H. R., and Edmeades, G. O. (1995). Stress tolerance in tropical maize is linked to constitutive changes in ear growth characteristics. *Crop Sci.* 35, 820–826. doi: 10.2135/cropsci1995.0011183X003500030031x

Lemcoff, J. H., and Loomis, R. S. (1986). Nitrogen influences on yield determination in maize. *Crop Sci.* 26, 1017–1022. doi: 10.2135/cropsci1986.0011183X002600050036x

Lemcoff, J. H., and Loomis, R. S. (1994). Nitrogen and density influences on silk emergence, endosperm development, and grain-yield in maize (*Zea mays* L.). *Field Crop. Res.* 38, 63–72. doi: 10.1016/0378-4290(94)90001-90009

Macduff, J. H., Jarvis, S. C., Larsson, C. M., and Oscarson, P. (1993). Plant growth in relation to the supply and uptake of NO3-: a comparison between relative addition rate and external concentration as driving variables. *J. Exp. Bot.* 44, 1475–1484. doi: 10.1093/jxb/44.9.1475

McLaughlin, J. E., and Boyer, J. S. (2004). Sugar-responsive gene expression, invertase activity, and senescence in aborting maize ovaries at low water potentials. *Ann. Bot.* 94, 675–689. doi: 10.1093/aob/mch193

Moll, R. H., Kamprath, E. J., and Jackson, W. A. (1982). Analysis and interpretation of factors which contribute to efficiency of nitrogen-utilization. *Agr. J.* 74, 562–564.

Monneveux, P., Zaidi, P. H., and Sanchez, C. (2005). Population density and low nitrogen affects yield-associated traits in tropical maize. *Crop Sci.* 45, 535–545. doi: 10.2135/cropsci2005.0535

Mueller, S. M., Camberato, J. J., Messina, C., Shanahan, J., Zhang, H., and Vyn, T. J. (2017). Late-split nitrogen applications increased maize plant nitrogen recovery but not yield under moderate to high nitrogen rates. *Agr. J.* 109, 2689–2699. doi: 10.2134/agronj2017.05.0282

Mueller, S. M., and Vyn, T. J. (2018a). Can late-split nitrogen application increase ear nitrogen accumulation rate during the critical period in maize? *Crop Sci.* 58, 1717–1728. doi: 10.2135/cropsci2018.02.0118

Mueller, S. M., and Vyn, T. J. (2018b). Physiological constraints to realizing maize grain yield recovery with silking-stage nitrogen fertilizer applications. *Field Crop. Res.* 228, 102–109. doi: 10.1016/j.fcr.2018.08.025

Nasielski, J., Earl, H., and Deen, B. (2019). Luxury vegetative nitrogen uptake in maize buffers grain yield under post-silking water and nitrogen stress: a mechanistic understanding. *Front. Plant Sci.* 10:318. doi: 10.3389/fpls.2019.00318

Ning, P., Yang, L., Li, C. J., and Fritschi, F. B. (2018). Post-silking carbon partitioning under nitrogen deficiency revealed sink limitation of grain yield in maize. *J. Exp. Bot.* 69, 1707–1719. doi: 10.1093/jxb/erx496

Olmedo Pico, L. B., Zhang, C., and Vyn, T. J. (2019). "Nitrogen management consequences on endosperm cell number formation in maize kernels," in *Proceedings of the ASA-CSSA-SSSA International Annual Meeting, 2019 Nov 10-13*, San Antonio, TX.

Ordonez, R. A., Savin, R., Cossani, C. M., and Slafer, G. A. (2018). Maize grain weight sensitivity to source-sink manipulations under a wide range of field conditions. *Crop Sci.* 58, 2542–2557. doi: 10.2135/cropsci2017.11.0676

Oscarson, P. (2000). The strategy of the wheat plant in acclimating growth and grain production to nitrogen availability. *J. Exp. Bot.* 51, 1921–1929. doi: 10.1093/jexbot/51.352.1921

Paponov, I. A., and Engels, C. (2005). Effect of nitrogen supply on carbon and nitrogen partitioning after flowering in maize. *J. Plant Nutr. Soil Sci.* 168, 447–453. doi: 10.1002/jpln.200520505

Paponov, I. A., Sambo, P., Erley, G. S. A., Presterl, T., Geiger, H. H., and Engels, C. (2005b). Kernel set in maize genotypes differing in nitrogen use efficiency in response to resource availability around flowering. *Plant Soil* 272, 101–110. doi: 10.1007/s11104-004-4210-4218

Paponov, I. A., Sambo, P., Erley, G. S. A., Presterl, T., Geiger, H. H., and Engels, C. (2005a). Grain yield and kernel weight of two maize genotypes differing in nitrogen use efficiency at various levels of nitrogen and carbohydrate availability during flowering and grain filling. *Plant Soil* 272, 111–123. doi: 10.1007/s11104-004-4211-4217

Peng, Y. F., Li, C. J., and Fritschi, F. B. (2013). Apoplastic infusion of sucrose into stem internodes during female flowering does not increase grain yield in maize plants grown under nitrogen-limiting conditions. *Physiol. Plant.* 148, 470–480. doi: 10.1111/j.1399-3054.2012.01711.x

Perez, C. M., Palmiano, E. P., Baun, L. C., and Juliano, B. O. (1971). Starch metabolism in leaf sheaths and culm of rice. *Plant Physiol.* 47, 404–408. doi: 10.1104/pp.47.3.404

Poorter, H., Niklas, K. J., Reich, P. B., Oleksyn, J., Poot, P., and Mommer, L. (2012). Biomass allocation to leaves, stems and roots: meta-analyses of interspecific variation and environmental control. *New Phytol.* 193, 30–50. doi: 10.1111/j.1469-8137.2011.03952.x

Presterl, T., Groh, S., Landbeck, M., Seitz, G., Schmidt, W., and Geiger, H. H. (2002). Nitrogen uptake and utilization efficiency of European maize hybrids developed under conditions of low and high nitrogen input. *Plant Breed.* 121, 480–486. doi: 10.1046/j.1439-0523.2002.00770.x

Reddy, V. M., and Daynard, T. B. (1983). Endosperm characteristics associated with rate of grain filling and kernel size in corn. *Maydica* 28, 339–355.

Sattelmacher, B., Horst, W. J., and Becker, H. C. (1994). Factors that contribute to genetic variation for nutrient efficiency of crop plants. *Z. Pflanz. Bodenkunde* 157, 215–224. doi: 10.1002/jpln.19941570309

Severini, A. D., Borras, L., Westgate, M. E., and Cirilo, A. G. (2011). Kernel number and kernel weight determination in dent and popcorn maize. *Field Crop. Res.* 120, 360–369. doi: 10.1016/j.fcr.2010.11.013

Shannon, J. C. (1972). Movement of 14C-labeled assimilates into kernels of *Zea mays* L: I. Pattern and rate of sugar movement. *Plant Physiol.* 49, 198–202. doi: 10.1104/pp.49.2.198

Takei, K., Sakakibara, H., Taniguchi, M., and Sugiyama, T. (2001). Nitrogen-dependent accumulation of cytokinins in root and the translocation to leaf: implication of cytokinin species that induces gene expression of maize response regulator. *Plant Cell Physiol.* 42, 85–93. doi: 10.1093/pcp/pce009

Tollenaar, M. (1977). Sink-source relationships during reproductive development in maize. A review. *Maydica* 22, 49–75.

Tollenaar, M., and Daynard, T. B. (1978). Dry weight, soluble sugar content, and starch content of maize kernels during early postsilking period. *Can. J. Plant Sci.* 58, 199–206. doi: 10.4141/cjps78-029

Triboi, E., and Triboi-Blondel, A. M. (2002). Productivity and grain or seed composition: a new approach to an old problem - invited paper. *Eur. J. Agron.* 16, 163–186. doi: 10.1016/s1161-0301(01)00146-140

Uhart, S. A., and Andrade, F. H. (1995). Nitrogen deficiency in maize: I. Effects on crop growth, development, dry matter partitioning, and kernel set. *Crop Sci.* 35, 1376–1383. doi: 10.2135/cropsci1995.0011183X003500050020x

Wang, R. Y., Bowling, L. C., and Cherkauer, K. A. (2016). Estimation of the effects of climate variability on crop yield in the Midwest USA. *Agr. Forest Meteorol.* 216, 141–156. doi: 10.1016/j.agrformet.2015.10.001

Yan, P., Chen, Y. Q. A., Sui, P., Vogel, A., and Zhang, X. P. (2018). Effect of maize plant morphology on the formation of apical kernels at different sowing dates and under different plant densities. *Field Crops Res.* 223, 83–92. doi: 10.1016/j.fcr.2018.04.008

Yu, J. J., Han, J. N., Wang, R. F., and Li, X. X. (2016). Down-regulation of nitrogen/carbon metabolism coupled with coordinative hormone modulation contributes to developmental inhibition of the maize ear under nitrogen limitation. *Planta* 244, 111–124. doi: 10.1007/s00425-016-2499-2491

Zinselmeier, C., Jeong, B. R., and Boyer, J. S. (1999). Starch and the control of kernel number in maize at low water potentials. *Plant Physiol.* 121, 25–35. doi: 10.1104/pp.121.1.25

Conflict of Interest: The authors declare that the research was conducted in the absence of any commercial or financial relationships that could be construed as a potential conflict of interest.

frontiers in Plant Science

ORIGINAL RESEARCH
published: 26 May 2020
doi: 10.3389/fpls.2020.00442

Chloride Improves Nitrate Utilization and NUE in Plants

Miguel A. Rosales[1,2†], Juan D. Franco-Navarro[1,3†], Procopio Peinado-Torrubia[1], Pablo Díaz-Rueda[1], Rosario Álvarez[4] and José M. Colmenero-Flores[1,2*]*

[1] Grupo Regulación Iónica e Hídrica en Plantas, Instituto de Recursos Naturales y Agrobiología, Consejo Superior de Investigaciones Científicas (CSIC), Seville, Spain, [2] Laboratorio Interdepartamental de Ecofisiología Molecular de Plantas, Instituto de Recursos Naturales y Agrobiología, Consejo Superior de Investigaciones Científicas (CSIC), Seville, Spain, [3] BioScripts – Centro de Investigación y Desarrollo de Recursos Científicos, Seville, Spain, [4] Departamento de Biología Vegetal y Ecología, Facultad de Biología, Universidad de Sevilla, Seville, Spain

Chloride (Cl^-) has traditionally been considered harmful to agriculture because of its toxic effects in saline soils and its antagonistic interaction with nitrate (NO_3^-), which impairs NO_3^- nutrition. It has been largely believed that Cl^- antagonizes NO_3^- uptake and accumulation in higher plants, reducing crop yield. However, we have recently uncovered that Cl^- has new beneficial macronutrient functions that improve plant growth, tissue water balance, plant water relations, photosynthetic performance, and water-use efficiency. The increased plant biomass indicates in turn that Cl^- may also improve nitrogen use efficiency (NUE). Considering that N availability is a bottleneck for the growth of land plants excessive NO_3^- fertilization frequently used in agriculture becomes a major environmental concern worldwide, causing excessive leaf NO_3^- accumulation in crops such as vegetables, which poses a potential risk to human health. New farming practices aimed to enhance plant NUE by reducing NO_3^- fertilization should promote a healthier and more sustainable agriculture. Given the strong interaction between Cl^- and NO_3^- homeostasis in plants, we have verified if indeed Cl^- affects NO_3^- accumulation and NUE in plants. For the first time to our knowledge, we provide a direct demonstration which shows that Cl^-, contrary to impairing NO_3^- nutrition, facilitates NO_3^- utilization and improves NUE in plants. This is largely due to Cl^- improvement of the N–NO_3^- utilization efficiency (NU_TE), having little or moderate effect on N–NO_3^- uptake efficiency (NU_PE) when NO_3^- is used as the sole N source. Clear positive correlations between leaf Cl^- content vs. NUE/NU_TE or plant growth have been established at both intra- and interspecies levels. Optimal NO_3^- vs. Cl^- ratios become a useful tool to increase crop yield and quality, agricultural sustainability and to reduce the negative ecological impact of NO_3^- on the environment and on human health.

Keywords: chloride, nitrate, nitrogen use efficiency, crop yield, fertilizer, tobacco, leafy vegetables, nutritional quality

OPEN ACCESS

Edited by:
Guillermo Esteban Santa María, National University of General San Martín, Argentina

Reviewed by:
Maria Gonnella, Institute of Food Production Sciences, Italian National Research Council, Italy
Silvia Quaggiotti, University of Padova, Italy

***Correspondence:**
Miguel A. Rosales
mrosales@irnas.csic.es
José M. Colmenero-Flores
chemacf@irnase.csic.es

† These authors have contributed equally to this work

Specialty section:
This article was submitted to Plant Nutrition, a section of the journal Frontiers in Plant Science

Received: *20 December 2019*
Accepted: *25 March 2020*
Published: *26 May 2020*

Citation:
Rosales MA, Franco-Navarro JD, Peinado-Torrubia P, Díaz-Rueda P, Álvarez R and Colmenero-Flores JM (2020) Chloride Improves Nitrate Utilization and NUE in Plants. Front. Plant Sci. 11:442. doi: 10.3389/fpls.2020.00442

INTRODUCTION

Nitrogen (N) is the main limiting nutrient for land plants and, therefore, has been classified as an essential macronutrient. Nitrate (NO_3^-) represents the major N source and a signal molecule involved in the control of many physiological and developmental processes, strongly improving crop yield (Frink et al., 1999; Wang et al., 2012; Krapp et al., 2014; Guan, 2017). The decisive role of N in crop yield has led to excessive use of NO_3^- in agriculture over decades

generating serious environmental problems like water pollution, which is harmful to people and nature (Nitrates Directive, 1991; Kant et al., 2011). In addition, when the application rate of NO_3^- exceeds the plant growth needs, overaccumulation of NO_3^- in leaves reduces the nutritional quality of crops (Prasad and Chetty, 2008; Xing et al., 2019). Many large-leaved plants such as beets, cabbage, celery, lettuce, or spinach tend to store huge amounts of NO_3^- (MAFF, 1998), posing a serious risk to human health. When ingested, NO_3^- is rapidly converted to nitrite and N-nitrous compounds as nitrosamines or nitric oxide causing *methemoglobinemia* or "blue baby syndrome" in infants and gastric cancer among other pathological disorders (Comly, 1945; Santamaria et al., 1999; Mensinga et al., 2003).

Considering that the growing world population is predicted to reach 9.8 billion in 2050, global efforts are being made to increase food resources by improving crop or agronomic practices (Tilman et al., 2002; Godfray et al., 2010). Since only 30–40% of the N applied to soil is used by plants, a greater N use efficiency (NUE) could improve the yield and quality of crops, reducing economic costs as well as decreasing environmental degradation (Baligar et al., 2001). NUE can be defined as the vegetative or reproductive biomass yield per unit of N available in the soil (Moll et al., 1982; Woodend and Glass, 1993; Ríos et al., 2010). This concept has many variants that can be split into two main elements: (i) N uptake efficiency (NU_PE), defined as the capacity of plant roots to take N from soil, and (ii) N utilization efficiency (NU_TE), defined as the fraction of plant-acquired N to be converted to total biomass or grain yield (Xu et al., 2012). Both are considered important traits in agriculture to reduce the abusive use of N fertilizers or when low N availability constrains plant growth, with substantial benefits for farmers and to the environment (Baligar et al., 2001; Han et al., 2016). Crops with higher NUE promote greater yields under limited N in soil, or require lower N to produce the same yield as those with lower NUE capacity (Ruiz et al., 2006; Kant et al., 2011; Rubio-Wilhelmi et al., 2012). Therefore, when NUE is increased, both crop-production costs and the harmful input of NO_3^- into ecosystems are reduced.

Traditionally, chloride (Cl^-) has been considered an essential micronutrient for plants (White and Broadley, 2001; Broadley et al., 2012). But recently, Cl^- has been uncovered as beneficial when accumulated to macronutrient levels in plant tissues (Franco-Navarro et al., 2016; Raven, 2017; Wege et al., 2017; Colmenero-Flores et al., 2019), with new biological functions that improve tissue water balance, whole-plant water relations, photosynthesis performance, and water-use efficiency (Franco-Navarro et al., 2016, 2019; Nieves-Cordones et al., 2019). Chloride represents the dominant inorganic anion in the vacuole, with leaf contents that can be similar to those of the macronutrient K^+, promoting cell osmoregulation, turgor-driven processes, leaf cell elongation, and a reduction in stomatal conductance (g_s; Franco-Navarro et al., 2016). In addition, Cl^- specifically increases mesophyll diffusion conductance to CO_2 (g_m) as a consequence of the greater surface area of chloroplasts exposed to the intercellular airspace of mesophyll cells, which in turn points towards Cl^- playing a role in chloroplast performance (Franco-Navarro et al., 2019). Thus, Cl^- specifically reduces g_s and water loss through transpiration without affecting the photosynthetic capacity due to g_m stimulation, resulting in overall higher water-use efficiency (Franco-Navarro et al., 2016, 2019; Maron, 2019). Nitrate and Cl^- are the most abundant inorganic anions, having similar physical and osmoregulatory properties and sharing transport mechanisms (Colmenero-Flores et al., 2019). This is probably the reason why NO_3^- and Cl^- show strong dynamic interactions in plants (Wege et al., 2017), a phenomenon that has been described as a competitive interaction between these two monovalent anions. Different studies have reported a negative effect of Cl^- on root NO_3^- uptake and accumulation (Siddiqi et al., 1990; Cerezo et al., 1997; Xu et al., 2000). For this reason and because of the toxicity generated by excessive Cl^- accumulation in sensitive crops under salt–stress conditions (Li et al., 2017; Geilfus, 2018), Cl^- has been considered detrimental to agriculture. Overall, Cl^- is believed to reduce NUE by limiting NO_3^- uptake and accumulation in plant tissues, reducing in turn its availability for plant metabolism (Xu et al., 2000; Anjana and Iqbal, 2007; Wege et al., 2017). However, Cl^- is a non-metabolized anion readily accumulated in plant tissues, whose vacuolar sequestration requires a lower energy cost than the accumulation of NO_3^- (Wege et al., 2017). Thus, considering the close interactions between these two anions, it has been hypothesized that preferential Cl^- compartmentalization may reduce vacuolar NO_3^- storage in leaves (Flowers, 1988), allowing higher NO_3^- availability for plant metabolism and, consequently, promoting more efficient use of this N source, meaning higher NUE (Colmenero-Flores et al., 2019). Therefore, the goal of this study was to verify whether Cl^- reduces leaf NO_3^- accumulation while promoting more efficient use of N–NO_3^-. In order to prove this, different plant species with contrasting Cl^--accumulating abilities have been used in this work: three leafy herbaceous species with strong Cl^--including capacity (chard, spinach, and lettuce), two herbaceous Cl^--including *Solanaceae* species (tobacco and tomato), and two Cl^--excluding woody species (olive and the salt-tolerant citrus rootstock Cleopatra mandarin). To directly ascertain the effect of Cl^- on NO_3^- nutrition, plant growth and different NUE parameters have been quantified, using NO_3^- as the sole N source.

MATERIALS AND METHODS

Plant Species and Nutritional Treatments

Tobacco (*Nicotiana tabacum* L. var. habana) plants were grown under experimental greenhouse conditions at 25 ± 3°C/17 ± 2°C (day/night), relative humidity of 60 ± 10% (EL-1-USB Data-logger, Lascar Electronics Inc., Erie, PA, United States), a 14 h/10 h photoperiod with a photosynthetic photon flux density [average photosynthetically active radiation (PAR)] of 300–350 μmol m^{-2} s^{-1} (quantum sensor, LI-6400; Li-COR, Lincoln, NE, United States), and a luminous emittance of 9,000–10,000 lx (Digital Lux Meter, LX1010B; Carson Electronics, Valemount, Canada). Seeds were sown in flat trays (cell size, 4 cm × 4 cm × 10 cm) containing peat previously washed with the corresponding nutrient solutions. After 2 days of vernalization in a cold chamber (4°C), seedbeds were

transferred to a greenhouse. 21 days after sowing (DAS), seedlings were transplanted to 7.5 L pots (with a pot size of 20 cm × 17 cm × 25 cm) that contained a mix of perlite/vermiculite (4:6). Plants were watered with a basal nutrient solution supplemented with three salt solutions containing the same cationic balance: 5 mM Cl^--based treatment (CL; with 5.075 mM Cl^- and 5.25 mM NO_3^-), 5 mM NO_3^--based treatment (N; with 75 μM Cl^- and 10.25 mM NO_3^-) and sulfate + phosphate (SO_4^{2-} + PO_4^{3-})-based treatment (SP; with 75 μM Cl^- and 5.25 mM NO_3^-). The composition of the basal solution (BS) was as follows: 1.25 mM KNO_3, 0.725 mM KH_2PO_4, 0.073 mM K_2HPO_4, 2 mM $Ca(NO_3)_2$, 1 mM $MgSO_4$, 0.1 mM FeNa–ethylenediaminetetraacetic acid (EDTA), 0.1 mM H_3BO_3, 0.1 mM $MnSO_4$, 29 μM $ZnSO_4$, 0.1 μM $CuSO_4$, 1 μM Na_2MoO_4, and 5 μM KI. A detailed description of the nutritional treatments is given in the **Supplementary Table S1**. Considering that 50 μM Cl^- was reported to ensure Cl^- micronutrient requirements in different plant species (Johnson et al., 1957), 75 μM Cl^- (added as 11 μM $CoCl_2$ and 53 μM KCl, including water traces) was present in the basal nutrient solution to fulfill micronutrient Cl^- functions in low Cl^- treatments (Franco-Navarro et al., 2016, 2019). In these previous works, we showed that the SP supplement did not modify the parameters analyzed with respect to the baseline treatment (BS). For this reason, and because the SP treatment only modifies the anionic content with respect to the CL treatment (while the BS solution differs in both anionic and cationic content), the BS treatment was not included in this work. Furthermore, previous experiments showed no significant differences in NUE parameters between BS and SP treatments (results not shown). A second set of experiments with increasing concentrations of anions was used in CL treatments: 0 mM Cl^- (basal solution containing 0.075 mM Cl^-), 0.151 mM Cl^-, 0.301 mM Cl^-, 1.075 mM Cl^-, 2.575 mM Cl^-, and 5.075 mM Cl^-. As a control condition, equivalent SP treatments were used to ensure similar cationic balance as in the different CL treatments (**Supplementary Table S1**). All experimental solutions were adjusted to pH 5.7 with KOH. Pots were irrigated up to field capacity (3.5 mL g^{-1} substrate) along with the experiments. Tobacco plants were harvested at 64 DAS, and different plant tissues were preserved for subsequent analyses.

To find out the ratio of Cl^- vs. NO_3^- that promotes more efficient use of N, tobacco plants were subjected to varying ratios of Cl^-, NO_3^-, and SO_4^{2-} + PO_4^{3-} as follows (**Supplementary Table S2**): (i) constant 8 mM NO_3^- combined with increasing Cl^- concentrations and decreasing SO_4^{2-} + PO_4^{3-} concentrations (mM; NO_3^-/SO_4^{2-} + PO_4^{3-}: 0.075:8, 0.575:7.5, 2.075:6, 4.075:4, and 6.075:2) and (ii) constant 6.075 mM Cl^- combined with increasing SO_4^{2-} + PO_4^{3-} concentrations and decreasing NO_3^- concentrations (mM; Cl^-/SO_4^{2-} + PO_4^{3-}: 6:4, 4:6). The minimum content of Cl^- was maintained at 75 μM to ensure the minimal micronutrient requirement (Franco-Navarro et al., 2016), which was estimated up to 50 μM in the nutrient solution as reported in Johnson et al. (1957) and Whitehead (1985), and salt combinations contained the same cationic balance.

SP and CL treatments (5 mM) were applied at 21 DAS under similar experimental conditions (as described above) in: (i) woody species like olive (*Olea europaea* L. ssp. *europaea* var. *sylvestris* Brot.) and the citrus rootstock Cleopatra mandarin (*Citrus reshni* Hort. ex Tan.); and (ii) herbaceous species like cherry tomato (*Solanum lycopersicum* L. cv *zarina*), Taglio chard (*Beta vulgaris* L. ssp. *vulgaris* convar. *cicla* var. *flavescens* Dc.), America spinach (*Spinacia oleracea* L. var. *america*), and lettuce romaine (*Lactuca sativa* ssp. *longifolia* Lam.). For olive plants, *in vitro* germination of zygotic embryos was required. Seeds were sterilized and germinated under sterile conditions in tubes containing 10 mL of olive culture medium (Rugini, 1984) supplemented with 1 mg L^{-1} zeatin, 20 g L^{-1} mannitol, and 6 g L^{-1} agar. Medium pH was adjusted to 5.7 before autoclaving at 121°C for 20 min. After placing the embryos in the agar medium, they were incubated in the growth chamber for 60 days. Growing conditions were 23 ± 2°C, 16 h light/8 h dark photoperiod, and 70%/30% Red/Blue with a photosynthetic photon flux (PPF) of 34 μE. Seedlings were placed in rooting medium for 21 days before being acclimatized in pots for 21 days and then harvested at 200 DAS. The other plant species were harvested at different times as follows: at 67 DAS in tomato, 84 DAS in mandarin, 106 DAS in spinach, and 147 DAS in chard and lettuce.

Plant samples harvested in all experiments were dried in a forced-air oven at 75°C to obtain the dry weight (DW) and dry preserved for subsequent determinations. All experiments were performed in at least three independent trials.

Nutrient Content and NUE Parameters

For the determination of nutrient content, fully photosynthetic and expanded mature leaves (non-senescent) were used. Oven-dried leaf tissue was ground into powder using a grinder, and the concentration of Cl^-, NO_3^-, SO_4^{2-}, and PO_4^{3-} was determined as previously reported in Franco-Navarro et al. (2016). NH_4^+ was determined from an aqueous extraction by using the colorimetric method described by Krom (1980), and was measured with the absorbance microplate reader "Omega SPECTROstar" (BMG LABTECH GmbH, Germany). Organic N was determined by the Kjeldahl method (Bradstreet, 1954). Total N content (TNC) was expressed as mg g^{-1} DW and represents the sum of organic N, NH_4^+, and NO_3^- (Ríos et al., 2010). Total N accumulation (TNA) was calculated as the result of TNC divided by total DW as described in Sorgona et al. (2006), and results were expressed as mg of N. NUE is commonly defined as vegetative yield per unit of N available to the crop (g DW g^{-1} N; Moll et al., 1982; Woodend and Glass, 1993; Rubio-Wilhelmi et al., 2012) and can be subdivided into two types: (i) N utilization efficiency (NU_TE) calculated as total DW divided by TNC (g^2 DW mg^{-1} N; Siddiqi and Glass, 1981) and (ii) N uptake efficiency (NU_PE) calculated as TNA divided by root DW (mg N g^{-1} root DW; Elliott and Læuchli, 1985).

Statistical Analysis

Statistical analysis was performed using the STATGRAPHICS Centurion XVI software (StatPoint Technologies, Warrenton, VA, United States). The Shapiro–Wilk (*W*) test was used to verify the normality of the datasets. Both one-way analysis of variance (ANOVA) and multivariate analysis of variance

(MANOVA) were done to determine significant differences between groups of samples, and levels of significance were described by asterisks: $P \leq 0.05$ (*), $P \leq 0.01$ (**), and $P \leq 0.001$ (***). No significant (NS) differences were indicated when $P > 0.05$. Multiple comparisons of means were determined by the Tukey's honestly significant difference (HSD) and multiple range test (MRT) tests included in the afore-mentioned software. Correlations between NUE parameters and Cl^- concentrations were calculated through Pearson's product-moment correlation coefficient (r^2). Values represent the mean of at least five tobacco plants in each treatment, which were reproducible in at least two independent experiments.

RESULTS

Effect of Cl^- on Leaf Ion Content, Growth, and NUE Parameters in Tobacco Plants

The three nutritional treatments assayed (SP, N, and CL) showed leaf ionic contents consistent with the nutritional supplements applied (**Supplementary Table S3**). Thus, CL plants accumulated Cl^- at levels that are typical of a macronutrient such as K^+ (55.1 mg Cl^- g^{-1} DW and 49.5 mg K^+ g^{-1} DW, respectively). Leaf Cl^- content in CL plants was higher than the contents of NO_3^- and $SO_4^{2-} + PO_4^{3-}$ in N and SP plants, respectively (**Supplementary Table S3**). It is important to notice that the leaf Cl^- content in tobacco plants treated with low Cl^- levels (SP and N treatments) exceeded the critical deficiency threshold reported for Cl^- in non-halophytic plants (<0.2 mg g^{-1} shoot DW; Flowers, 1988; Xu et al., 2000; White and Broadley, 2001). Therefore, N and SP treatments satisfied plant Cl^- requirements as essential micronutrient, and no symptoms of Cl^- deficiency like wilting, chlorosis, bronzing, or necrosis were observed. As a demonstration of this fact, we noted that N plants, containing low Cl^- content, exhibited the highest plant growth (Franco-Navarro et al., 2016; **Figure 1A**). As previously observed, Cl^- supplementation stimulated plant growth (when compared to the SP treatment) (**Figures 1A**, **2A**). Interestingly, the beneficial effect of Cl^- nutrition on plant dry biomass was only evident in response to treatments higher than 1 mM Cl^-, within the macronutrient-content range (**Figure 2A**). Therefore, these results show that Cl^- stimulates plant growth when it is supplied at macronutrient levels and ruled out the occurrence of Cl^- deficiency in plants subjected to low Cl^- treatments (SP and N treatments).

In tobacco plants, the N treatment (10.25 mM NO_3^-) duplicated the NO_3^- concentration in comparison with SP and CL treatments (5.25 mM NO_3^-), resulting in strong stimulation of plant growth (**Supplementary Table S1** and **Figure 1A**) and confirming the well-known fact that N availability bottlenecks plant growth (Glass, 2003; Hawkesford et al., 2012; Wang et al., 2012; Krapp et al., 2014; Guan, 2017). However, the most efficient use of N occurred in CL plants, which showed the highest NUE values (**Figure 1B**) despite presenting the lowest NO_3^- content (**Supplementary Table S3**). NUE defines the total biomass production per unit of N (NO_3^-) available in the soil (Moll et al., 1982). Two different components of NUE can be in turn distinguished: (i) how efficiently is this nutrient transported into the plant, defined by the N uptake efficiency (NU_PE), and (ii) how efficiently the transported N is used by the plant, defined by the N utilization efficiency (NU_TE), which takes into account the plant yield component (Siddiqi and Glass, 1981). As a result of the greater NO_3^- availability, the N treatment resulted in a strong increase in NU_PE (**Figure 1C**), giving rise to higher TNC (**Figure 1D**) and TNA (**Figure 1E**) in comparison to the SP and CL treatments. However, such high tissue content of N determined the lowest NU_TE value in N plants (**Figure 1E**), which was 70% lower than that of CL plants. Interestingly, while both CL and SP treatments contained the same NO_3^- concentration, the CL treatment determined 41% higher NU_TE than the SP treatment.

To better define the interaction between Cl^- and NUE, the plant response to increasing Cl^- concentrations was compared to equivalent gradients of $SO_4^{2-} + PO_4^{3-}$ concentrations. A clear positive response to Cl^- treatments was observed beyond 1 mM Cl^-, significantly improving plant growth (**Figure 2A**) and NUE (**Figure 2B**) in comparison to SP treatments. These CL treatments determined leaf tissue contents of about 40–110 mM Cl^-, confirming the beneficial effect of Cl^- at macronutrient levels. Interestingly, no significant differences were observed in the NU_PE between the CL and SP treatments (both containing the same concentration of 5.25 mM NO_3^-; **Figure 2C**), whereas NU_TE values were higher in CL plants subjected to treatments $\geq$ 1 mM Cl^- (**Figure 2D**). This confirmed that the NUE component improved by Cl^- is the utilization rather than the uptake efficiency of NO_3^-. Thus, a positive and statistically significant correlation between NU_TE and leaf Cl^- content was confirmed ($r^2 = 0.99$; **Figure 2F**), which could not be established with the NU_PE (**Figure 2E**) in tobacco plants.

Effect of Different Cl^-/NO_3^- and $Cl^-/SO_4^{2-} + PO_4^{3-}$ Ratios on Anion Content, Growth, and NUE Parameters of Tobacco Plants

To better understand whether Cl^- has a direct antagonistic effect on NO_3^- nutrition, and therefore on plant performance, tobacco plants treated with the same NO_3^- concentration (8 mM NO_3^-) were supplemented with growing Cl^- concentrations (0, 0.5, 2, 4, and 6 mM Cl^-). To maintain a similar cationic and osmotic balance in all treatments, Cl^- salts were compensated with $SO_4^{2-} + PO_4^{3-}$ salts according to the experimental design presented in **Supplementary Table S2**. Increasing Cl^- concentrations gave rise to increasing leaf Cl^- contents, which in turn produced significant reductions in NO_3^- content in the 4 and 6 mM Cl^- treatments (53 and 71% reduction in NO_3^- content, respectively; **Figure 3A**). Interestingly, these strong reductions in leaf NO_3^- content did not result in a worsening of plant performance, and contrary to what is traditionally belief, Cl^- treatments significantly increased plant biomass (**Figure 3B**) and NUE (**Figure 3C**). The results clearly suggest that a reduction in NO_3^- content by Cl^- application

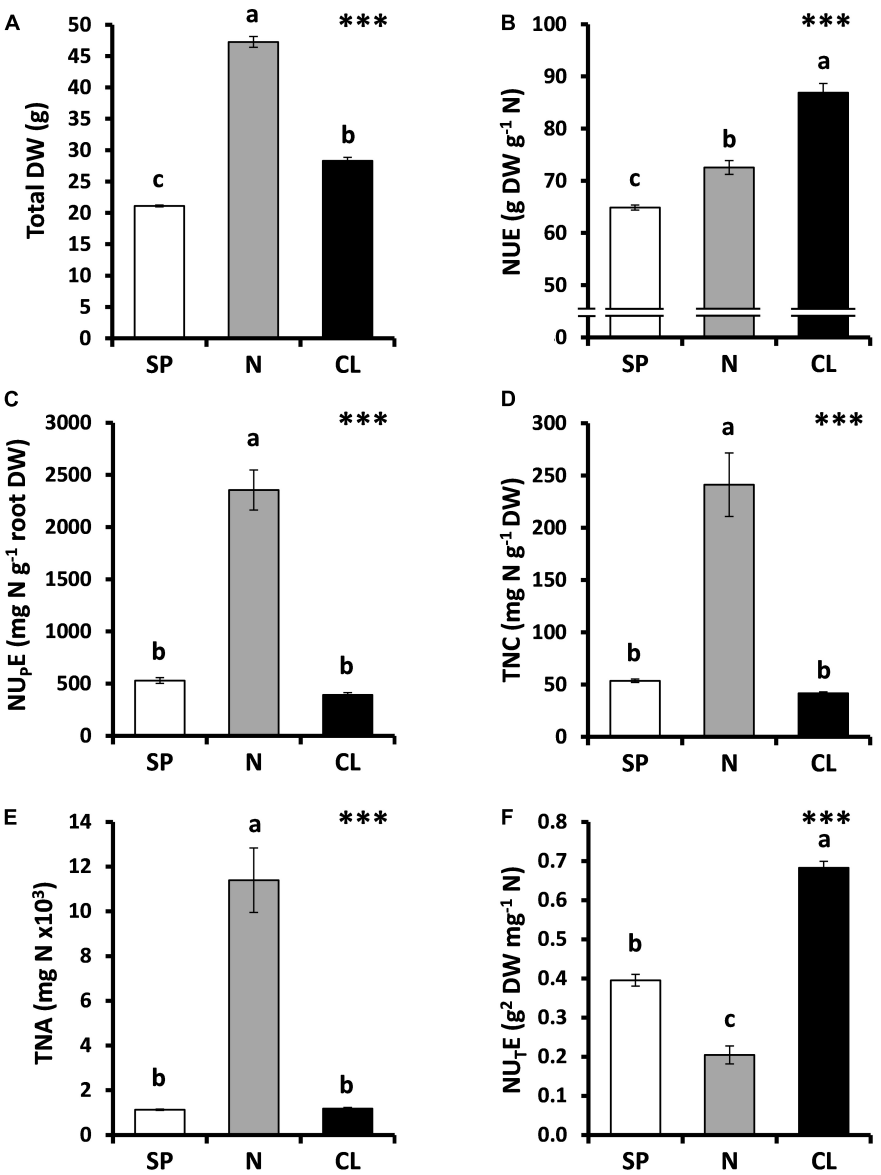

FIGURE 1 | Effect of Cl^- nutrition on tobacco biomass and nitrogen use efficiency (NUE) parameters. Treatments consisted of the application of the basal nutrient solution supplemented with 5 mM Cl^- (CL), 5 mM NO_3^- (N), or the SO_4^{2-} + PO_4^{3-} (SP) salt mixture, containing the same cationic balance in all treatments. **(A)** Total dry weight (DW). **(B)** NUE. **(C)** Nitrogen-uptake efficiency (NU_PE). **(D)** Total nitrogen content (TNC). **(E)** Total nitrogen assimilated (TNA). **(F)** Nitrogen-utilization efficiency (NU_TE). Mean values ± SE, n = 4-6. Levels of significance: $^{***}P \leq 0.001$; and "homogeneous group" statistics was calculated through ANOVA tests, where mean values with different letters are significantly different according toTukey's test.

is not due to a reduction in NO_3^- availability within the plant but to a greater NO_3^- assimilation, which results in increased NUE and plant biomass. Additionally, we applied decreasing NO_3^- treatments (from 8 to 6 and 4 mM NO_3^-) while maintaining the 6 mM Cl^- treatment (by replacing NO_3^- by equivalent concentrations of SO_4^{2-} + PO_4^{3-} salts). Although leaf NO_3^- contents were only slightly reduced after reducing 25 and 50% the NO_3^- concentration in the nutrient solution, total plant biomass strongly dropped up to 45% of the dry weight, coinciding with a slight reduction in NUE (**Figures 3D–F**). This is a consequence of the lower availability of NO_3^- for the plant, causing a strong reduction in plant biomass.

Effect of Cl^- on NUE Parameters in Different Plant Species

Considering these results, we hypothesized that a positive interaction between Cl^- nutrition and NUE is a widespread phenomenon in land plants. In order to answer this important question, herbaceous and woody plant species from different families with contrasting capacities to transport and accumulate Cl^- were tested in response to the 5 mM Cl^- treatment (**Table 1**).

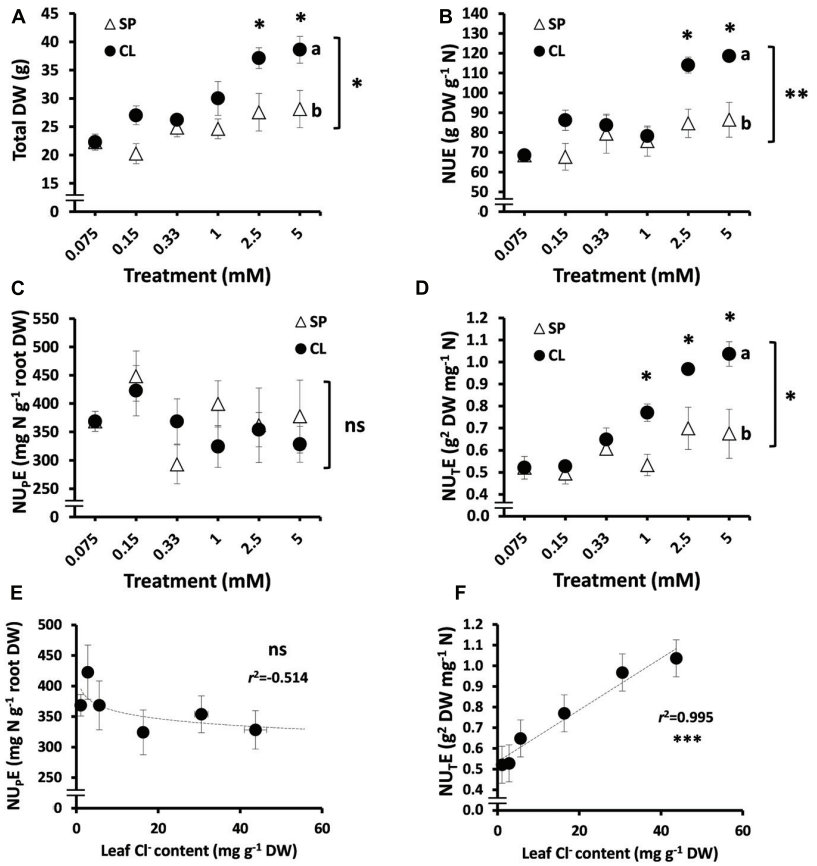

FIGURE 2 | Effect of Cl^- nutrition on tobacco plant biomass and nitrogen use efficiency (NUE) parameters. Treatments consisted of increasing concentrations of Cl^- (CL) or SO_4^{2-} + PO_4^{3-} (SP) salts maintaining the same cationic balance. **(A)** Effect on total dry weight (DW). **(B)** NUE. **(C)** Nitrogen-uptake efficiency (NU_PE). **(D)** Nitrogen-utilization efficiency (NU_TE); **(E)** Pearson correlation (r^2) between NU_PE and leaf anion content in tobacco plants. **(F)** Pearson correlation (r^2) between NU_TE and leaf anion content in tobacco plants. Mean values ± SE, n = 4–6. Levels of significance: $P > 0.05$ (ns, not significant), $^*P \leq 0.05$, $^{**}P \leq 0.01$, and $^{***}P \leq 0.001$; and "homogeneous group" statistics was calculated through ANOVA and multivariate (MANOVA) tests, where mean values with different letters are significantly different according toTukey's test. Correlations between NU_TE or NU_PE and leaf anion content were calculated through the Pearson's product-moment correlation coefficient (r^2).

This study included several herbaceous and woody species of agricultural interest: leafy vegetables with strong Cl^--including capacity from the *Amaranthaceae* (chard) and the *Asteraceae* (lettuce) families; Cl^--including species from the *Solanaceae* family (tobacco and tomato); and two Cl^--excluding woody perennial species from the *Oleaceae* (olive) and the *Rutaceae* families (the salt-tolerant citrus rootstock Cleopatra mandarin; Brumós et al., 2010).

When treated with 5 mM Cl^-, the Cl^--excluding species *O. europaea* and Cleopatra mandarin accumulated 7.36 and 18.23 mg Cl^- g^{-1} DW in leaf tissues, respectively; the Cl^--including tomato and tobacco plants accumulated 32.33 and 55.10 mg Cl^- g^{-1} DW in leaf tissues, respectively; and the strong Cl^--including leafy vegetables lettuce, spinach, and chard accumulated 76.71, 80.86, and 107.12 mg Cl^- g^{-1} DW in leaf tissues, respectively. It is noteworthy that Cl^- improved biomass and NU_TE in all the species tested (**Figure 4**), with the exception of olive, which was the species with the lowest Cl^- accumulation ability (**Table 1**). Thus, Cl^- stimulated plant biomass (**Figure 4A**), reduced leaf NO_3^- content (**Figure 4B** and **Supplementary Table S4**) and NU_PE (**Figure 4C**), and stimulated NU_TE (**Figure 4D**). These responses showed a clear correlation with the content of Cl^- accumulated in the leaves of the different plant species, up to a value of ∼50 mg Cl^- g^{-1} DW in tobacco leaves. Species accumulating higher Cl^- contents showed a saturation response (**Figure 4**).

It is worth mentioning that, as previously described in tobacco plants (Franco-Navarro et al., 2016), Cl^- nutrition significantly increased water content of all the tested plant species except for the Cl^- excluders olive and Cleopatra mandarin (**Supplementary Table S4**). Notably, NO_3^- content significantly decreased by the application of Cl^- in all species tested (**Figure 4B** and **Supplementary Table S4**). Regarding TNC, we observed that, in comparison to the SP treatment, the Cl^- treatment did not induce significant changes in olive, lettuce, and spinach (as in tobacco plants; **Figure 1D**), whereas a slight decrease was found in other species like tomato, Cleopatra mandarin, and chard (**Table 1**). Interestingly, NU_PE was unaffected in the poor Cl^-

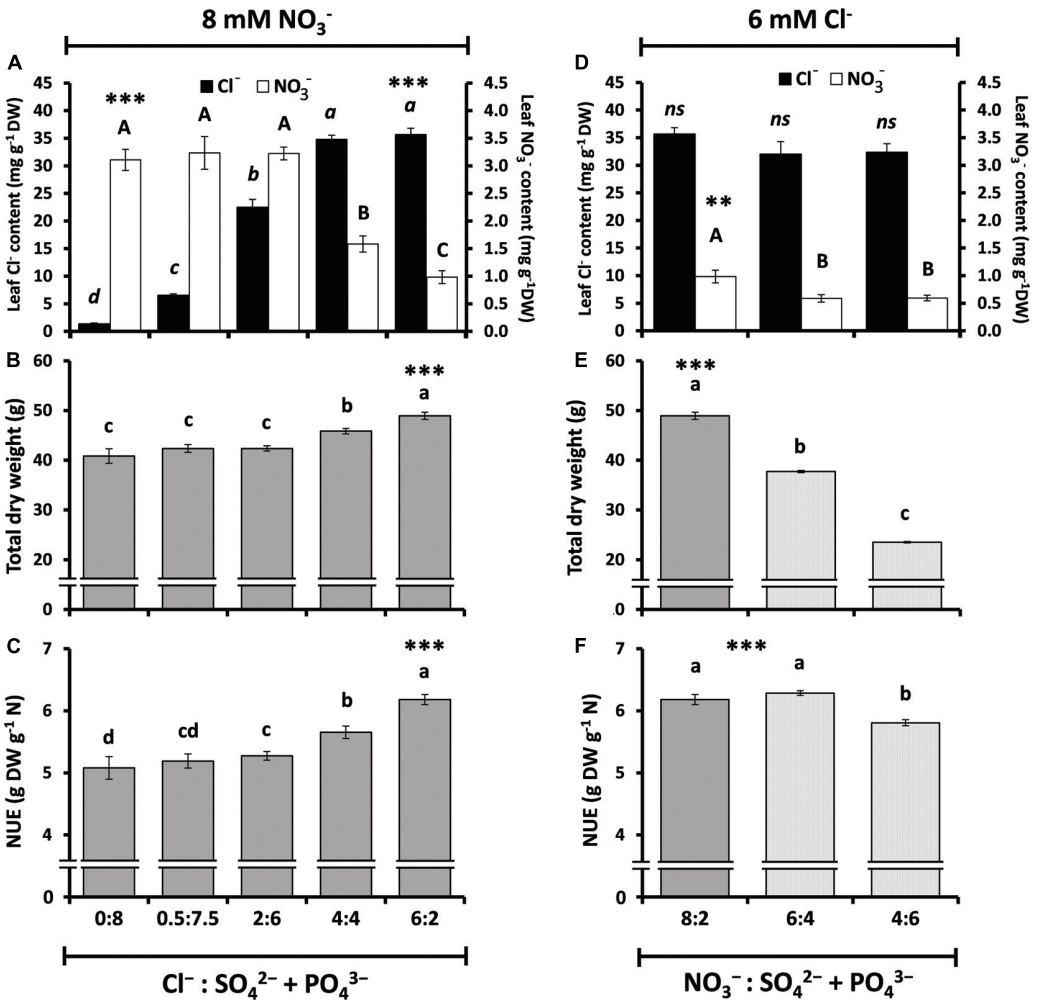

FIGURE 3 | Effect of different ratios of Cl^- nutrition on anion content, plant growth, and nitrogen use efficiency (NUE) in tobacco plants. Treatments consisted of the application of: (**A–C**; $\uparrow Cl^-/\downarrow SO_4^{2-} + PO_4^{3-}$) increasing concentrations of Cl^- (from 0.075 to 6 mM) and decreasing concentrations of $SO_4^{2-} + PO_4^{3-}$ (from 8 to 2 mM) while keeping constant the concentration of NO_3^- (8 mM); and (**D–F**; $\downarrow NO_3^-/\uparrow SO_4^{2-} + PO_4^{3-}$) decreasing concentrations of NO_3^- (from 8 to 4 mM) and increasing concentrations of $SO_4^{2-} + PO_4^{3-}$ (from 2 to 6 mM) while keeping constant the concentration of Cl^- (6 mM). **(A,D)** Effect on leaf anion contents (NO_3^- and Cl^-). **(B,E)** Effect on total dry weight (DW). **(C,F)** Effect on nitrogen-use efficiency (NUE). Mean values ± SE, $n = 6$. Levels of significance: $P > 0.05$ (ns, not significant differences); $^{***}P \leq 0.001$; and "homogeneous group" statistics was calculated through ANOVA tests, where mean values with different letters are significantly different according toTukey's test.

including species (olive and Cleopatra mandarin), whereas it was moderately reduced (∼20%) in the Cl^--including species (**Figure 4C**). Thus, the increase in leaf Cl^- accumulation showed positive correlations with biomass and NU_TE among the species (**Figures 4A,D**). These results indicate that the beneficial effect of Cl^- as a macronutrient on plant growth and NUE is a highly relevant phenomenon that could be extended to cultivated plants.

DISCUSSION

NO_3^-, an essential source of N, and Cl^-, an important osmoregulatory molecule and beneficial macronutrient, are the most abundant inorganic anions in plants, and both must be coordinately incorporated during the active growth of plants (Cubero-Font et al., 2016; Colmenero-Flores et al., 2019). Both anions play important roles in charge balance and turgor regulation, showing strong dynamic interactions in land plants (Wege et al., 2017; Geilfus, 2018; Colmenero-Flores et al., 2019). Since NO_3^- and Cl^- also present similar physical properties in solution, they share ion transport mechanisms with uncertain selectivities for both anions. NO_3^-, as a source of the essential macronutrient N, is assimilated during anabolic metabolism, while Cl^-, which is not metabolized, becomes accumulated in plant tissues. Interaction between NO_3^- and Cl^- has been traditionally understood as antagonistic. For instance, a high tissue content of Cl^- is believed to reduce the content of NO_3^- and *vice versa* (Xu et al., 2000; Umar and Iqbal, 2007). The presence of external NO_3^- has been shown to inhibit root Cl^- uptake (Glass and Siddiqi, 1985;

TABLE 1 | Effect of Cl^- nutrition on biomass, anion content and NUE parameters in different species of agronomic interest.

Family	Species	N.T.	Total plant biomass (g DW)	Anion content and NUE parameters					
				Cl^- (mg g^{-1} DW)	NO_3^- (mg g^{-1} DW)	TNC (mg g^{-1} DW)	NU_PE (mg N g^{-1} root DW)	NU_TE (g^2 DW mg^{-1} N)	NUE (g DW mg^{-1} N)
Solanaceae	Tomato	SP	34.20 ± 0.66	0.73 ± 0.02	4.10 ± 0.35	36.86 ± 0.54	707.9 ± 29.1	0.93 ± 0.02	105.05 ± 2.04
		CL	47.81 ± 0.79	32.33 ± 1.12	2.20 ± 0.41	31.85 ± 0.61	555.3 ± 31.2	1.51 ± 0.05	146.86 ± 2.42
		P-value	***	***	**	***	**	***	***
Oleaceae	Olive	SP	0.44 ± 0.03	1.67 ± 0.31	2.40 ± 0.09	27.70 ± 1.57	258.8 ± 14.6	0.016 ± 0.001	1.36 ± 0.10
		CL	0.40 ± 0.08	7.36 ± 0.79	1.71 ± 0.20	28.06 ± 1.28	257.1 ± 11.7	0.014 ± 0.003	1.24 ± 0.24
		P-value	**ns**	***	*	**ns**	**ns**	**ns**	**ns**
Rutaceae	Mandarin	SP	9.68 ± 0.13	1.03 ± 0.09	3.46 ± 0.52	26.07 ± 1.04	444.7 ± 14.3	0.37 ± 0.02	28.67 ± 0.33
		CL	11.02 ± 0.28	18.23 ± 0.36	2.11 ± 0.11	23.52 ± 0.48	452.6 ± 2.88	0.47 ± 0.01	32.29 ± 0.59
		P-value	**	***	*	*	**ns**	**	*
Asteraceae	Lettuce	SP	18.42 ± 0.91	16.47 ± 2.02	9.04 ± 0.20	23.94 ± 1.02	221.4 ± 9.47	0.78 ± 0.07	56.58 ± 2.80
		CL	27.95 ± 3.19	76.71 ± 2.13	7.56 ± 0.50	23.39 ± 1.48	175.9 ± 11.1	1.20 ± 0.14	85.86 ± 9.79
		P-value	*	***	*	**ns**	*	*	*
Amaranthaceae	Spinach	SP	7.23 ± 0.36	12.29 ± 1.07	4.79 ± 0.26	26.79 ± 1.39	247.7 ± 12.8	0.27 ± 0.02	45.25 ± 1.21
		CL	9.07 ± 0.37	80.86 ± 4.14	4.45 ± 0.05	25.22 ± 0.68	189.6 ± 5.14	0.36 ± 0.02	55.13 ± 2.97
		P-value	*	***	**ns**	**ns**	*	*	*
	Chard	SP	14.73 ± 0.39	10.82 ± 0.54	7.41 ± 0.34	21.48 ± 0.50	198.6 ± 4.60	0.69 ± 0.01	56.58 ± 2.80
		CL	17.95 ± 0.97	107.1 ± 3.35	5.57 ± 0.26	18.99 ± 0.59	142.8 ± 4.40	0.95 ± 0.07	85.86 ± 9.79
		P-value	*	***	**	*	***	*	*

*Nutritional Treatment (N.T.) consisted of a basal nutrient solution supplemented with 5 mM Cl^- (CL) or the SO_4^{2-} + PO_4^{3-} (SP) salt mixture containing the same cationic balance in all treatments. Tomato (Solanum lycopersicum L.); Olive (Olea europaea L. ssp. europaea); Mandarin (Citrus reshni Hort. ex Tan.); Lettuce (Lactuca sativa L.); Spinach (Spinacia oleracea L.), and Chard (Beta vulgaris L. ssp. vulgaris convar. cicla). TNC (Total Nitrogen Content); NU_PE (Nitrogen-Uptake Efficiency); NU_TE (Nitrogen-Utilization Efficiency); NUE (Nitrogen-Use Efficiency). Mean values ± SE, n = 4–6. Levels of significance: P > 0.05 ("ns," not significant differences);*P ≤ 0.05. **P ≤ 0.01. ***P ≤ 0.001. "Homogeneous group" statistics was calculated through ANOVA test. DW, dry weight.*

Iglesias et al., 2004), and on the contrary, high Cl^- content reduces NO_3^- accumulation in plants, suggesting that common transport mechanisms could facilitate the influx of both anions (Xu et al., 2000; Teakle and Tyerman, 2010). This antagonism between NO_3^- and Cl^- has been widely reported for many crops, pointing to a clear detrimental effect of Cl^- on NO_3^- nutrition (transport, accumulation, and/or assimilation; Buwalda and Smith, 1991; Cerezo et al., 1997; Xu et al., 2000). As a result, Cl^- is considered harmful to crop productivity, to the extent that its presence in some types of plant fertilizers is considered as a negative indicator of their quality (EU Regulation 2019/1009). However, Cl^- has been recently defined as a beneficial macronutrient that improves plant development, water relations, CO_2 assimilation, and water-use efficiency when supplemented at concentrations higher than those necessary to satisfy micronutrient requirements but insufficient to cause toxicity (e.g., in the beneficial range of 1–5 mM Cl^-; Colmenero-Flores et al., 2019; Franco-Navarro et al., 2019). The fact that Cl^- specifically promotes plant biomass due to these beneficial effects (Franco-Navarro et al., 2016) is difficult to reconcile with a detrimental effect on NO_3^- nutrition.

Consistent with our previous findings (Franco-Navarro et al., 2016, 2019), tobacco plants accumulated Cl^- at levels that are typical of a macronutrient, stimulating plant growth when applied at concentrations above 1 mM Cl^- (**Figures 1A**, **2A**). Furthermore, although leaf Cl^- content was ∼120 times lower in SP and N plants in comparison to CL, it remained over the critical threshold of Cl^- deficiency reported for non-halophytic plants (<0.2 mg g^{-1} shoot DW; Flowers, 1988; Xu et al., 2000; White and Broadley, 2001; Franco-Navarro et al., 2016), which ruled out the occurrence of Cl^- deficiency in SP and N treatments. Moreover, the higher growth of N plants (**Figure 1A**) confirmed this point and strengthens the well-known fact that NO_3^- has a strong impact on plant growth and development (Glass, 2003; Hawkesford et al., 2012; Wang et al., 2012; Krapp et al., 2014; Guan, 2017).

NUE is an important crop trait described as a useful tool to improve agricultural systems (Fageria et al., 2008). This work clearly states that, contrary to what was previously believed, Cl^- improves NUE in plants, at least when NO_3^- is used as the sole N source. The decline in leaf biomass has been directly correlated to N deficiency particularly in tobacco plants (Balachandran et al., 1997), since this crop requires high quantities of NO_3^- for maximum vegetative yield (Ruiz et al., 2006). Considering that N is not only an essential nutrient for optimal crop yield but also an environmental concern, adequate management of N fertilization regimes to enhance NUE remains critical for crop breeding. Our results confirm that Cl^- significantly increases NUE, not only in tobacco plants (**Figures 1**, **2**) but also in different crop species (**Figure 4**), when accumulated at macronutrient levels. NUE improvement in tobacco plants was a consequence of more efficient use of the NO_3^- taken up by the plant (NU_TE; **Figures 2D**, **3C**), meaning that Cl^-

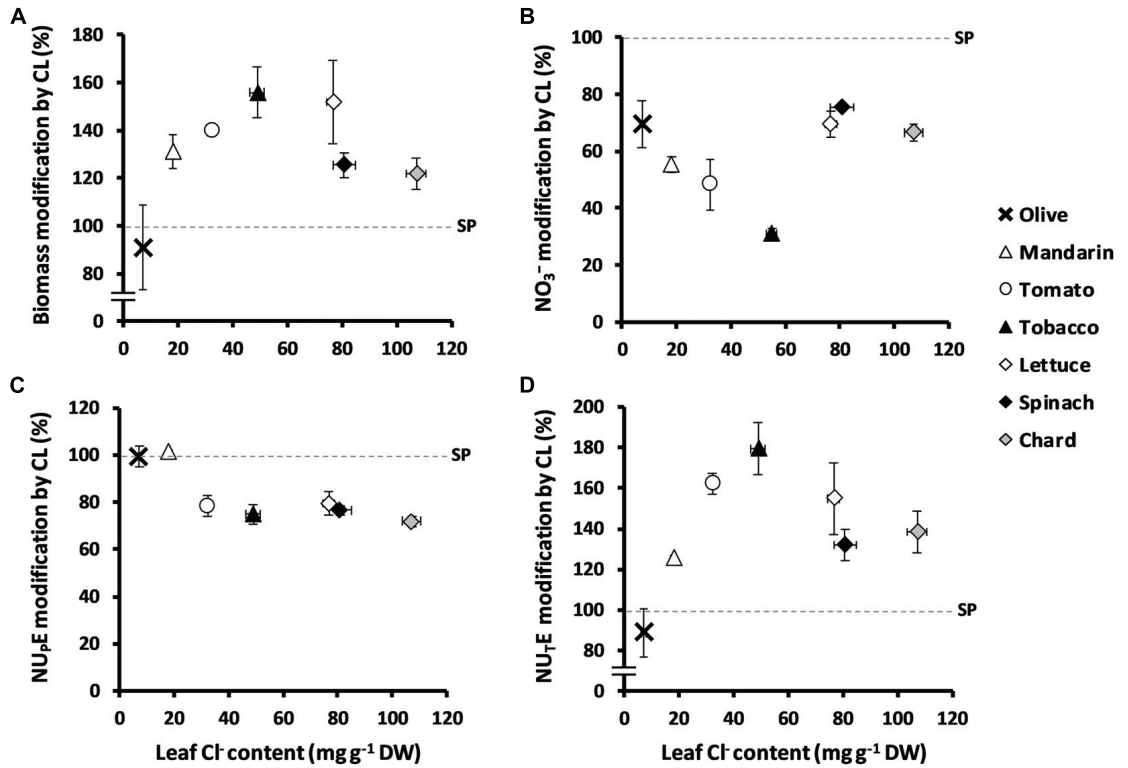

FIGURE 4 | Effect of Cl^- nutrition on plant growth, NO_3^- content, N uptake efficiency (NU_PE), and N utilization efficiency (NU_TE) in several species of agronomic interest. Plants were treated with two nutritional treatments: 5 mM Cl^- salts (CL) and a mixture of SO_4^{2-} + PO_4^{3-} salts (SP) containing the same cationic balance as in the CL treatment. Ratios of total biomass **(A)**, NO_3^- content expressed as mg kg^{-1} of fresh weight **(B)**, NU_PE **(C)**, and NU_TE **(D)** are presented considering the % of CL in relation to SP treatment and in contrast to leaf anion content in several species. Olive (*Olea europaea* L. ssp. *europaea*; bold cross), mandarin (*Citrus reshni* Hort. ex Tan; open triangles), tomato (*Solanum lycopersicum* L.; open circles), tobacco (*Nicotiana tabacum* L.; filled triangles), lettuce (*Lactuca sativa* L.; open diamonds); spinach (*Spinacia oleracea* L.; filled diamonds), and chard (*Beta vulgaris* L. ssp. *vulgaris*; gray-colored diamonds); mean values ± SE, $n = 6$.

improves NO_3^- assimilation, as observed in other crop species (**Figure 4D**). A significant positive correlation (r^2 = 0.995) between leaf Cl^- content and NU_TE was established in tobacco plants (**Figure 2F**). Interestingly, this positive correlation was also observed in different plant species with contrasting abilities to accumulate Cl^- (**Figure 4D**). Thus, NU_TE gain by Cl^- application was minimal in Cl^- excluding species (0–22% NU_TE increment in olive and the citrus rootstock Cleopatra mandarin plants, respectively) and maximal in Cl^- including ones (60–80% NU_TE increment in tomato and tobacco plants, respectively), indicating a positive ecophysiological correlation between leaf Cl^- accumulation and NU_TE. However, this correlation was lost in strong Cl^- including vegetables (30–55% NU_TE increment in the large-leaved spinach, chard, and lettuce plants), suggesting the occurrence of a saturable response, possibly as a consequence of excessive Cl^- accumulation. This positive correlation between Cl^- content and NU_TE can be a selection criterion to identify new cultivars or genotypes obtained from breeding programs, with potentially improved NUE capacity. Thus, genotypes that, in the presence of 5 mM Cl^-, show leaf Cl^- contents between 20 and 50 mg g^{-1} DW (**Table 1**), within the positive linear response range shown in **Figure 4D**, could be good candidates not only for improved NUE but also for higher efficiency in the use of water and CO_2 (Colmenero-Flores et al., 2019).

These results were obtained comparing SP and CL treatments, both containing the same NO_3^- concentration (5 mM NO_3^-). However, NU_TE stimulation by Cl^- was much higher when the CL treatment was compared with the N treatment (10.25 mM NO_3^-). The increase in NU_TE in CL vs. N tobacco plants was ∼250% (**Figure 1F**), suggesting that NO_3^- fertilization in the field can be efficiently regulated if optimal supplies of NO_3^-/Cl^- ratios are used. Thus, increasing the Cl^-/NO_3^- ratio showed two positive effects on plants: reduction in leaf NO_3^- content (**Figure 3A**) while at the same time increasing plant biomass (**Figure 3B**). Different studies have proposed a negative effect of Cl^- on NO_3^- uptake and accumulation (Siddiqi et al., 1990; Cerezo et al., 1997; Li et al., 2017), which is supposed to reduce NUE. Nevertheless, our results ruled out the possibility that Cl^- impairs N use because the CL treatment increased plant biomass (**Figure 3B**), while the effective reduction in NO_3^- in the nutrient solution produced a strong reduction in plant biomass (**Figure 3E**). This clearly indicates that the loss of leaf NO_3^- content through Cl^- application is not a consequence of lower root NO_3^- uptake (e.g., lower NO_3^- availability as a consequence of Cl^- antagonism; **Figure 2C**)

but of a greater NO_3^- assimilation capacity. The NO_3^- vs. Cl^- antagonism must be understood in terms of the selectivity of anion transporters. Given the great relevance of N for plant nutrition, plants prioritize NO_3^- uptake over Cl^- uptake when NO_3^- is available in the soil. This means that active transport mechanisms are normally more selective for NO_3^- than for Cl^- (Glass and Siddiqi, 1985; Wege et al., 2017; Wen et al., 2017). Consequently, increasing the NO_3^- concentration in the nutrient solution reduces Cl^- content in plants (Glass and Siddiqi, 1985; Iglesias et al., 2004). However, the opposite situation is not necessarily true. Although widely reported (Xu et al., 2000; and references therein), Cl^- application in the low millimolar range should not impair NO_3^- uptake given the high selectivity for NO_3^- over Cl^-. Thus, total N content of plants does not decrease in response to Cl^- application (**Figure 1D**; Ourry et al., 1992; Liu and Shelp, 1996; Inal et al., 1998). However, in **Figure 4C**, a moderate reduction in NU_PE can be observed in different plant species in response to Cl^- application. Rather than an effective reduction in NO_3^- uptake transport through transmembrane transporters at the soil–root interface, NU_PE reduction can be a consequence of the calculation procedure. The NU_PE formula computes the NO_3^- content in plant tissues, which is lower in plants treated with Cl^- because NO_3^- is more efficiently assimilated, as is also proposed by Liu and Shelp (1996). It is very likely, however, that under salinity stress conditions, Cl^- antagonizes NO_3^- influx in plant cells, significantly reducing root NO_3^- uptake (Cerezo et al., 1997; Li et al., 2017).

Therefore, our results strongly support the previously suggested role of Cl^- as preferred plant osmoregulatory molecule in plants (Flowers, 1988; Franco-Navarro et al., 2016; Colmenero-Flores et al., 2019). Thus, we propose that, on the one hand, Cl^- is preferably compartmentalized in the vacuole. On the other hand, NO_3^-, an essential N source for land plants, is preferentially assimilated, which is not possible when this molecule is sequestered in the vacuole to carrry out an osmotic function. Only when Cl^- is not sufficiently available in the soil, or as a result of excessive NO_3^- availability, NO_3^- could be preferentially compartmentalized (Siddiqi et al., 1991; Radcliffe et al., 2005). Therefore, macronutrient accumulation of Cl^- reduces NO_3^- compartmentalization in the vacuole, facilitating its assimilation, which increases NUE and plant biomass. Under the same premise, Cl^- should also play an adaptive role to improve plant growth under conditions of low N availability, which is also explained in terms of differential transport selectivity. When little NO_3^- is available, root Cl^- uptake through active anion transporters is less inhibited (Wen et al., 2017), increasing cell Cl^- content and replacing NO_3^- in the vacuole, which facilitates NO_3^- assimilation and NUE. A clear demonstration that the relationship between Cl^- and NO_3^- homeostasis in higher plants is not limited to an antagonistic interaction has been recently shown by Cubero-Font et al. (2016). This work describes a molecular mechanism that determines the rate of NO_3^-/Cl^- accumulation in aerial organs of *Arabidopsis thaliana* based on the Cl^- conductance of the AtSLAH3 channel, which is in turn regulated by environmental cues.

Agronomic and scientific communities have traditionally believed that little amounts of Cl^- are required to achieve suitable crop yields (Geilfus, 2018). Nevertheless, some studies have shown that the application of Cl^--enriched fertilizers to the soil increases the vegetative yield in different crops (Christensen et al., 1981; Timm et al., 1986; Inal et al., 1998; Xu et al., 2000). However, it was not clear to what extent plant yield improvement was due to the accompanying cations or whether other anions could replace Cl^- in the reported growth-promoting effects. In accordance with the recently revealed functions of Cl^- as a beneficial macronutrient (Franco-Navarro et al., 2016; Colmenero-Flores et al., 2019), it has been proven that a number of physiological perturbations impairing the growth and yield of durum wheat under field conditions are specifically due to soil Cl^- deficiency (Schwenke et al., 2015). Hence, we investigated how crops could benefit from certain levels of Cl^- fertilization. In the herbaceous species studied (i.e., tomato, lettuce, spinach, and chard), the 5 mM Cl^- treatment determined plant biomass gains in accordance with the leaf Cl^- content within the beneficial macronutrient range (40–110 mg g^{-1} DW; Colmenero-Flores et al., 2019; **Figure 3B**). These Cl^- content values are up to an order of magnitude above what was classically considered toxic concentrations in plants (Xu et al., 2000), largely dismantling this view of Cl^- as detrimental to agriculture (Colmenero-Flores et al., 2019).

Given the high NO_3^- content in fertilizers and its often abusive use in agriculture, NO_3^- can be excessively accumulated in the leaves of most horticultural crops, resulting in food safety problems (e.g., methemoglobinemia and cancer) because of its transformation into nitrites and nitrosamines (Colla et al., 2018). This is particularly harmful in leafy vegetables, for which the European Commission has developed severe regulations (1881/2006 and 1258/2011) to reduce the excessive dietary intake of NO_3^-, especially that of vulnerable people such as infants, the elderly, and vegetarians. As previously stressed, increasing the Cl^-/NO_3^- ratios reduced the leaf NO_3^- content (**Figure 3A**) without impairing, or even increasing, plant biomass (**Figure 3B**). In our study, the NO_3^- content in leafy species (lettuce, spinach, and chard) treated with SP ranged between 577 and 1,035 mg NO_3^- kg^{-1} FW (**Supplementary Table S4**), proving to be much lower than the maximum permitted levels, which are set at 3,500 and 2,500 mg NO_3^- kg^{-1} FW in spinach and iceberg lettuce, respectively. It should be noted, however, that the SP treatment contains 5 mM NO_3^-, probably well below the levels applied in the field by farmers. Chloride reduced about 25–70% the NO_3^- content in the plant species assayed (compared to SP plants; **Figure 4B**). These results are in accordance with those reported by Urrestarazu et al. (1998) in lettuce, Inal et al. (1998) in carrot, and Borgognone et al. (2016) in cardoon. Therefore, Cl^- nutrition is expected to considerably improve the nutritional quality of vegetables and brings to light the important benefits of using Cl^--enriched fertilizers in human health. Interestingly, Cl^--treated tobacco plants showed the strongest decrease in NO_3^- content (∼70% compared to SP plants; **Figure 4B**). Considering that NO_3^- is the main inducer

of nitrogen oxides and nitrosamines in flue-cured tobacco during smoking (Hoffmann and Hecht, 1985), Cl^- nutrition could also help to reduce the nitrosamine levels in cigarettes, improving the quality of this crop.

CONCLUSION

We provide for the first time a direct demonstration which shows that Cl^-, contrary to impairing NO_3^- nutrition, facilitates NO_3^- utilization and improves NUE in plants. This is largely due to Cl^- improvement of NU_TE, having a little or moderate effect on NU_PE when NO_3^- is used as the sole N source in the nutrient solution. Clear positive correlations between leaf Cl^- content vs. NU_TE or vs. plant growth have been established at both intra- and interspecies levels: in tobacco plants treated with growing Cl^- concentrations and comparing different species with contrasting abilities to accumulate Cl^-. Our results strongly suggest that macronutrient Cl^- nutrition reduces NO_3^- sequestration in plant leaf tissues (e.g., vacuolar compartmentalization), making this valuable N source available for assimilation and biosynthesis of organic N. Our results give light to a brand-new interpretation of Cl^- properties as a beneficial macronutrient for higher plants that promote more efficient use of water, carbon, and nitrogen, becoming a potential resource to improve agricultural production and quality, reducing NO_3^- inputs in the field and unhealthy leaf NO_3^- content in vegetables.

DATA AVAILABILITY STATEMENT

The datasets generated for this study are available on request to the corresponding author.

AUTHOR CONTRIBUTIONS

JF-N performed the experiments, analyzed the data, and participated in the writing of the manuscript. PP-T and PD-R participated in the experiments. RÁ participated in the conception of research plans. MR and JC-F conceived research plans, supervised the experiments, and wrote the manuscript.

FUNDING

This work was supported by the Spanish Ministry of Science Innovation and Universities-FEDER grants AGL2015-71386-R and RTI2018-094460-B-I00, and by the Spanish National Research Council grants CSIC-201840E132, CSIC-201940E039, and CSIC-201940E077.

ACKNOWLEDGMENTS

We acknowledge support of the publication fee by the CSIC Open Access Publication Support Initiative through its Unit of Information Resources for Research (URICI). Help, expertise, and technical assistance of A. Vázquez-Rodríguez, F. J. Durán, and E. Gutiérrez-González are gratefully acknowledged.

SUPPLEMENTARY MATERIAL

The Supplementary Material for this article can be found online at: https://www.frontiersin.org/articles/10.3389/fpls.2020.00442/full#supplementary-material

REFERENCES

Anjana, S. U., and Iqbal, M. (2007). Nitrate accumulation in plants, factors affecting the process, and human health implications: a review. *Agron. Sustain. Dev.* 27, 45–57.

Balachandran, S., Hull, R. J., Martins, R. A., Vaadia, Y., and Lucas, W. F. (1997). Influence of environmental stress on biomass partitioning in transgenic tobacco plants expressing the movement protein of tobacco mosaic virus. *Plant Physiol.* 114, 475–481. doi: 10.1104/pp.114.2.475

Baligar, V. C., Fageria, N. K., and He, Z. L. (2001). Nutrient use efficiency in plants. *Commun. Soil Sci. Plant Anal.* 32, 921–950.

Borgognone, D., Rouphael, Y., Cardarelli, M., Licini, L., and Colla, G. (2016). Changes in biomass, mineral composition, and quality of cardoon in response to NO_3^-:Cl^- ratio and nitrate deprivation from the nutrient solution. *Front. Plant Sci.* 7:978. doi: 10.3389/fpls.2016.00978

Bradstreet, R. B. (1954). Kjeldahl method for organic nitrogen. *Anal. Chem.* 26, 185–187.

Broadley, M., Brown, P., Cakmak, I., Rengel, Z., and Zhao, F. (2012). "Chapter 7 – function of nutrients: micronutrients," in *Marschner's Mineral Nutrition of Higher Plants (Third Edition)*, ed. P. Marschner (San Diego: Academic Press), 191–248.

Brumós, J., Talón, M., Bouhlal, R. Y. M., and Colmenero-Flores, J. M. (2010). Cl^- homeostasis in includer and excluder citrus rootstocks: transport mechanisms and identification of candidate genes. *Plant Cell Environ.* 33, 2012–2027.

Buwalda, J. G., and Smith, G. S. (1991). Influence of anions on the potassium status and productivity of kiwifruit (*Actinidia deliciosa*) vines. *Plant Soil* 133, 209–218.

Cerezo, M., Garcia-Agustin, P., Serna, M. D., and Primo-Millo, E. (1997). Kinetics of nitrate uptake by citrus seedlings and inhibitory effects of salinity. *Plant Sci.* 126, 105–112.

Christensen, N. W., Taylor, R. G., Jackson, T. L., and Mitchell, B. L. (1981). Chloride effects on water potentials and yield of winter wheat infected with take-all root rot. *Agron. J.* 73, 1053–1058.

Colla, G., Kim, H.-J., Kyriacou, M. C., and Rouphael, Y. (2018). Nitrate in fruits and vegetables. *Sci. Hortic.* 237, 221–238.

Colmenero-Flores, J. M., Franco−Navarro, J. D., Cubero−Font, P., Peinado-Torrubia, P., and Rosales, M. A. (2019). Chloride as a beneficial macronutrient in higher plants: new roles and regulation. *Int. J. Mol.* 20:4686. doi: 10.3390/ijms20194686

Comly, H. H. (1945). Cyanosis in infants caused by nitrates in well water. *JAMA-J. Am. Med. Assoc.* 129, 112–116.

Cubero-Font, P., Maierhofer, T., Jaslan, J., Rosales Miguel, A., Espartero, J., Díaz-Rueda, P., et al. (2016). Silent S-type anion channel subunit SLAH1 gates SLAH3 open for chloride root-to-shoot translocation. *Curr. Biol.* 26, 2213–2220. doi: 10.1016/j.cub.2016.06.045

Elliott, G. C., and Læuchli, A. (1985). Phosphorus efficiency and phosphate-iron interaction in maize 1. *Agron. J.* 77, 399–403.

Fageria, N. K., Baligar, V. C., and Li, Y. C. (2008). The role of nutrient efficient plants in improving crop yields in the twenty-first century. *J. Plant Nutr.* 31, 1121–1157.

Flowers, T. J. (1988). "Chloride as a nutrient and as an osmoticum," in *Advances. in Plant. Nutrition*, Vol. 3, eds P. B. Tinker and A. Laüchli (New York, NY: Praeger), 55–78.

Franco-Navarro, J. D., Brumós, J., Rosales, M. A., Cubero-Font, P., Talón, M., and Colmenero-Flores, J. M. (2016). Chloride regulates leaf cell size and water relations in tobacco plants. *J. Exp. Bot.* 67, 873–891. doi: 10.1093/jxb/erv502

Franco-Navarro, J. D., Rosales, M. A., Cubero-Font, P., Calvo, P., Álvarez, R., Díaz-Espejo, A., et al. (2019). Chloride as macronutrient increases water use efficiency by anatomically-driven reduced stomatal conductance and increased mesophyll diffusion to CO2. *Plant J.* 99, 815–831. doi: 10.1111/tpj.14423

Frink, C. R., Waggoner, P. E., and Ausubel, J. H. (1999). Nitrogen fertilizer: retrospect and prospect. *Proc. Natl. Acad. Sci. U.S.A.* 96, 1175–1180.

Geilfus, C. M. (2018). Chloride: from nutrient to toxicant. *Plant Cell Physiol.* 59, 877–886. doi: 10.1093/pcp/pcy071

Glass, A. D. (2003). Nitrogen use efficiency of crop plants: physiological constraints upon nitrogen absorption. *Crit. Rev. Plant Sci.* 22, 453–470.

Glass, A. D. M., and Siddiqi, M. Y. (1985). Nitrate inhibition of chloride influx in barley: implications for a proposed chloride homeostat. *J. Exp. Bot.* 36, 556–566.

Godfray, H. C. J., Beddington, J. R., Crute, I. R., Haddad, L., Lawrence, D., Muir, J. F., et al. (2010). Food security: the challenge of feeding 9 billion people. *Science* 327, 812–818. doi: 10.1126/science.1185383

Guan, P. (2017). Dancing with hormones: a current perspective of nitrate signaling and regulation in *Arabidopsis*. *Front. Plant Sci.* 8:1697. doi: 10.3389/fpls.2017.01697

Han, Y. L., Song, H. X., Liao, Q., Yu, Y., Jian, S. F., Lepo, J. E., et al. (2016). Nitrogen use efficiency is mediated by vacuolar nitrate sequestration capacity in roots of *Brassica napus*. *Plant Physiol.* 170, 1684–1698. doi: 10.1104/pp.15.01377

Hawkesford, M., Horst, W., Kichey, T., Lambers, H., Schjoerring, J., Møller, I. S., et al. (2012). "Functions of macronutrients," in *Marschner's Mineral Nutrition of Higher Plants*, (Cambridge, MA: Academic Press), 135–189.

Hoffmann, D., and Hecht, S. S. (1985). Nicotine-derived N-Nitrosamines and tobacco-related cancer: current status and future directions. *Cancer Res.* 45, 935–944.

Iglesias, D. J., Levy, Y., Gómez-Cadenas, A., Tadeo, F. R., Primo-Millo, E., and Talon, M. (2004). Nitrate improves growth in salt-stressed citrus seedlings through effects on photosynthetic activity and chloride accumulation. *Tree Physiol.* 24, 1027–1034.

Inal, A., Gunes, A., Alpaslan, M., and Demir, K. (1998). Nitrate versus chloride nutrition effects in a soil-plant system on the growth, nitrate accumulation, and nitrogen, potassium, sodium, calcium, and chloride content of carrot. *J. Plant Nutr.* 21, 2001–2011.

Johnson, C. M., Stout, P. R., Broyer, T. C., and Carlton, A. B. (1957). Comparative chlorine requirements of different plant species. *Plant Soil* 8, 337–353.

Kant, S., Bi, Y. M., and Rothstein, S. J. (2011). Understanding plant response to nitrogen limitation for the improvement of crop nitrogen use efficiency. *J. Exp. Bot.* 62, 1499–1509. doi: 10.1093/jxb/erq297

Krapp, A., David, L. C., Chardin, C., Girin, T., Marmagne, A., Leprince, A. S., et al. (2014). Nitrate transport and signalling in *Arabidopsis*. *J. Exp. Bot.* 65, 789–798. doi: 10.1093/jxb/eru001

Krom, M. D. (1980). Spectrophotometric determination of ammonia: study of a modified Berthelot reaction using salicylate and dichloroisocianurate. *Analyst* 105, 305–316.

Li, B., Tester, M., and Gilliham, M. (2017). Chloride on the move. *Trends Plant Sci.* 22, 236–248. doi: 10.1016/j.tplants.2016.12.004

Liu, L., and Shelp, B. J. (1996). Impact of chloride on nitrate absorption and accumulation by broccoli (*Brassica oleracea* var. *italica*). *Can. J. Plant Sci.* 76, 367–377.

MAFF (1998). *1997/8 UK monitoring programme of nitrate in lettuce and spinach, food surveillance information sheet n8 154*. London: MAFF.

Maron, L. G. (2019). From foe to friend: the role of chloride as a beneficial macronutrient. *Plant J.* 99, 813–814. doi: 10.1111/tpj.14498

Mensinga, T. T., Speijers, J. G. A., and Meulenbelt, J. (2003). Health implications of exposure to environmental nitrogenous compounds. *Toxicol. Rev.* 14:576584.

Moll, R. H., Kamprath, E. J., and Jackson, W. A. (1982). Analysis and interpretation of factors which contribute to efficiency of nitrogen utilization 1. *Agron. J.* 74, 562–564.

Nieves-Cordones, M., García-Sánchez, F., Pérez-Pérez, J. G., Colmenero-Flores, J. M., Rubio, F., and Rosales, M. A. (2019). Coping with water shortage: an update on the role of K+, Cl^-, and water transport mechanisms on drought resistance. *Front. Plant Sci.* 10:1619. doi: 10.3389/fpls.2019.01619

Nitrates Directive (1991). *Council Directive 91/676/EEC concerning the protection of waters against pollution*. Available online at: https://ec.europa.eu/environment/water/water-nitrates/index_en.html (accessed September 15, 2019).

Ourry, A., Mesle, S., and Boucaud, J. (1992). Effects of osmotic-stress (NaCl and polyethylene-glycol) on nitrate uptake, translocation, storage and reduction in ryegrass (*Lolium-perenne* L). *New Phytol.* 120, 275–280.

Prasad, S., and Chetty, A. A. (2008). Nitrate-N determination in leafy vegetables: study of the effects of cooking and freezing. *Food Chem.* 106, 772–780.

Radcliffe, S. A., Miller, A. J., and Ratcliffe, R. G. (2005). Microelectrode and 133Cs nuclear magnetic resonance evidence for variable cytosolic and cytoplasmic nitrate pools in maize root tips. *Plant Cell Environ.* 28, 1379–1387.

Raven, J. A. (2017). Chloride: essential micronutrient and multifunctional beneficial ion. *J. Exp. Bot.* 68, 359–367. doi: 10.1093/jxb/erw421

Ríos, J. J., Blasco, B., Cervilla, L. M., Rubio-Wilhelmi, M. M., Rosales, M. A., Sanchez-Rodriguez, E., et al. (2010). Nitrogen-use efficiency in relation to different forms and application rates of Se in lettuce plants. *J. Plant Growth Regul.* 29, 164–170.

Rubio-Wilhelmi, M. M., Sanchez-Rodriguez, E., Rosales, M. A., Blasco, B., Rios, J. J., Romero, L., et al. (2012). Ammonium formation and assimilation in PSARK:: IPT tobacco transgenic plants under low N. *J. Plant Physiol.* 169, 157–162. doi: 10.1016/j.jplph.2011.09.011

Rugini, E. (1984). *In vitro*-propagation of some olive (*Olea europaea spp. sativa* L) cultivars with different root-ability, and medium development using analytical data from developing shoots and embryos. *Sci. Hort.* 24, 123–134.

Ruiz, J. M., Rivero, R. M., Cervilla, L. M., Castellano, R., and Romero, L. (2006). Grafting to improve nitrogen-use efficiency traits in tobacco plants. *J. Sci. Food Agr.* 86, 1014–1021.

Santamaria, P., Elia, A., Serio, F., and Todaro, E. (1999). A survey of nitrate and oxalate content in fresh vegetables. *J. Sci. Food Agr.* 79, 1882–1888.

Schwenke, G. D., Simpfendorfer, S. R., and Collard, B. C. Y. (2015). Confirmation of chloride deficiency as the cause of leaf spotting in durum wheat grown in the Australian northern grains region. *Crop Pasture Sci.* 66, 122–134.

Siddiqi, M. Y., and Glass, A. D. (1981). Utilization index: a modified approach to the estimation and comparison of nutrient utilization efficiency in plants. *J. Plant Nutr.* 4, 289–302.

Siddiqi, M. Y., Glass, A. D., and Ruth, T. J. (1991). Studies of the uptake of nitrate in barley: III. Compartmentation of NO3-. *J. Exp. Bot.* 42, 1455–1463.

Siddiqi, M. Y., Glass, A. D., Ruth, T. J., and Rufty, T. W. (1990). Studies of the uptake of nitrate in barley: I. Kinetics of 13NO3- influx. *Plant Physiol.* 93, 1426–1432.

Sorgona, A., Abenavoli, M. A., Gringeri, P. G., and Cacco, G. (2006). A comparison of nitrogen use efficiency definitions in citrus rootstocks. *Sci. Hort.* 109, 389–393.

Teakle, N. L., and Tyerman, S. D. (2010). Mechanisms of Cl^- transport contributing to salt tolerance. *Plant Cell Environ.* 33, 566–589. doi: 10.1111/j.1365-3040.2009.02060.x

Tilman, D., Cassman, K. G., Matson, P. A., Naylor, R., and Polasky, S. (2002). Agricultural sustainability and intensive production practices. *Nature* 418, 671–677.

Timm, C. A., Goos, R. J., Johnson, B. E., Sobolik, F. J., and Stack, R. W. (1986). Effect of potassium fertilizers on malting barley infected with common root rot. *Agron. J.* 782, 197–200.

Umar, A. S., and Iqbal, M. (2007). Nitrate accumulation in plants, factors affecting the process, and human health implications: a review. *Agron. Sustain. Dev.* 27, 45–57.

Urrestarazu, M., Postigo, A., Salas, M., Sánchez, A., and Carrasco, G. (1998). Nitrate accumulation reduction using chloride in the nutrient solution on lettuce growing by NFT in semiarid climate conditions. *J. Plant Nutr.* 21, 1705–1714.

Wang, Y. Y., Hsu, P. K., and Tsay, Y. F. (2012). Uptake, allocation and signaling of nitrate. *Trends Plant Sci.* 17, 458–467. doi: 10.1016/j.tplants.2012.04.006

Wege, S., Gilliham, M., and Henderson, S. W. (2017). Chloride: not simply a 'cheap osmoticum', but a beneficial plant macronutrient. *J. Exp. Bot.* 68, 3057–3069. doi: 10.1093/jxb/erx050

Wen, Z., Tyerman, S. D., Dechorgnat, J., Ovchinnikova, E., Dhugga, K. S., and Kaiser, B. N. (2017). Maize NPF6 proteins are homologs of *Arabidopsis* CHL1 that are selective for both nitrate and chloride. *Plant Cell* 29, 2581–2596. doi: 10.1105/tpc.16.00724

White, P. J., and Broadley, M. R. (2001). Chloride in soils and its uptake and movement within the plant: a review. *Ann. Bot.* 88, 967–988. doi: 10.1016/j.tplants.2012.04.006

Whitehead, D. C. (1985). Chlorine deficiency in red-clover grown in solution culture. *J. Plant Nutr.* 8, 193–198.

Woodend, J. J., and Glass, A. D. M. (1993). Genotype-environment interaction and correlation between vegetative and grain production measures of potassium use-efficiency in wheat (*T. aestivum* L.) grown under potassium stress. *Plant Soil* 151, 39–44.

Xing, Y., Jiang, W., He, X., Fiaz, S., Ahmad, S., Lei, X., et al. (2019). A review of nitrogen translocation and nitrogen-use efficiency. *J. Plant Nutr.* 42, 2624–2641.

Xu, G., Fan, X., and Miller, A. J. (2012). Plant nitrogen assimilation and use efficiency. *Annu. Rev. Plant Biol.* 63, 153–182. doi: 10.1146/annurev-arplant-042811-105532

Xu, G., Magen, H., Tarchitzky, J., and Kafkafi, U. (2000). Advances in chloride nutrition of plants. *Adv. Agron.* 68, 97–150.

Conflict of Interest: The authors declare that the research was conducted in the absence of any commercial or financial relationships that could be construed as a potential conflict of interest.

frontiers in Plant Science

ORIGINAL RESEARCH
published: 04 June 2020
doi: 10.3389/fpls.2020.00588

A Rice Autophagy Gene *OsATG8b* Is Involved in Nitrogen Remobilization and Control of Grain Quality

Tian Fan[1,2†], Wu Yang[2†], Xuan Zeng[2], Xinlan Xu[2], Yanling Xu[3], Xiaorong Fan[3], Ming Luo[2], Changen Tian[1], Kuaifei Xia[2,4] and Mingyong Zhang[2,4]*

[1] School of Life Sciences, Guangzhou University, Guangzhou, China, [2] Innovation Academy for Seed Design, Guangdong Provincial Key Laboratory of Applied Botany, Key Laboratory of South China Agricultural Plant Molecular Analysis and Genetic Improvement, South China Botanical Garden, Chinese Academy of Sciences, Guangzhou, China, [3] State Key Laboratory of Crop Genetics and Germplasm Enhancement, Nanjing Agricultural University, Nanjing, China, [4] Center of Economic Botany, Core Botanical Gardens, Chinese Academy of Sciences, Guangzhou, China

OPEN ACCESS

Edited by:
Guillermo Esteban Santa María, National University of General San Martín, Argentina

Reviewed by:
Caiji Gao, South China Normal University, China
Juan Guiamet, National University of La Plata, Argentina

***Correspondence:**
Mingyong Zhang
zhangmy@scbg.ac.cn

[†] These authors have contributed equally to this work

Specialty section:
This article was submitted to Plant Nutrition, a section of the journal Frontiers in Plant Science

Received: 10 December 2019
Accepted: 20 April 2020
Published: 04 June 2020

Citation:
Fan T, Yang W, Zeng X, Xu X, Xu Y, Fan X, Luo M, Tian C, Xia K and Zhang M (2020) A Rice Autophagy Gene OsATG8b Is Involved in Nitrogen Remobilization and Control of Grain Quality. Front. Plant Sci. 11:588. doi: 10.3389/fpls.2020.00588

Enhancing nitrogen (N) use efficiency is a potential way to reduce excessive nitrogen application and increase yield. Autophagy is a conserved degradation system in the evolution of eukaryotic cells and plays an important role in plant development and stress response. Autophagic cores have two conjugation pathways that attach the product of autophagy-related gene 8 (ATG8) to phosphatidylethanolamine (PE) and ATG5 to ATG12, respectively, which then help with vesicle elongation and enclosure. Rice has six *ATG8* genes, which have not been functionally confirmed so far. We identified the rice gene *OsATG8b* and characterized its role in N remobilization to affect grain quality by generating transgenic plants with its over-expression and knockdown. Our study confirmed the autophagy activity of OsATG8b through the complementation of the yeast autophagy-defective mutant *scatg8* and by observation of autophagosome formation in rice. The autophagy activity is higher in *OsATG8b*-OE lines and lower in *OsATG8b*-RNAi than that in wild type (ZH11). ^{15}N pulse-chase analysis revealed that *OsATG8b*-OE plants conferred higher N recycling efficiency to grains, while *OsATG8b*-RNAi transgenic plants exhibited lower N recycling efficiency and poorer grain quality. The autophagic role of *OsATG8b* was experimentally confirmed, and it was concluded that OsATG8b-mediated autophagy is involved in N recycling to grains and contributes to the grain quality, indicating that OsATG8b may be a potential gene for molecular breeding and cultivation of rice.

Keywords: autophagy, *OsATG8b*, nitrogen recycling, rice, seed quality

Abbreviations: APE1, aminopeptidase 1; CVT, cytoplasm-to-vacuole targeting; DAG, days after germination; DW, dry weight; HI, harvest index; IRRI, International Rice Research Institute; LSCM, laser-scanning confocal microscopy; mAPE1, mature APE1; N, nitrogen; NHI, nitrogen harvest index; NUE, nitrogen use efficiency; NRE, nitrogen recycling efficiency; OE, over-expression; ORF, open reading frame; *OsATG8b*, *Oryza sativa* autophagic-related gene 8b; PE, phosphatidylethanolamine; qRT-PCR, quantitative real-time PCR; RNAi, RNA interference.

INTRODUCTION

Nitrogen (N) is one of the most limiting nutrients for crop yield. Increasing N utilization efficiency (NUE) is not only important for increasing yield and reducing production cost but also for avoiding environmental pollution and keeping agriculture sustainable (Good et al., 2004; Masclaux-Daubresse et al., 2010). Therefore, it is very important to find effective genes to improve NUE and yield. Plant N utilization involves complex mechanisms of absorption, translocation, assimilation, and remobilization. Of those steps, N remobilization plays an important role during seed filling (Masclaux-Daubresse et al., 2008, 2010). At the vegetative stages, most N uptake is directed to leaves, in which most proteins are synthesized. During the reproductive stage, leaf proteins degrade rapidly to amino acids and small peptides, which are transported to seeds (Masclaux-Daubresse et al., 2008). N remobilization of cereals in senescent leaves has been shown to account for 50–90% of the grain N content (Kichey et al., 2007). The 26S proteasome/ubiquitin system and autophagy are the two main pathways of protein degradation (Wada et al., 2009; Roberts et al., 2012). Autophagy can degrade proteins, bulk organelles and cytosolic macromolecules with low selectivity and high throughput (Suzuki and Ohsumi, 2007).

Autophagy is a conserved degradation system in the evolution of eukaryotic cells. In the process of autophagy, the cytoplasm and organelles are separated by bilayer vesicles called autophagosomes and transported to vacuoles of yeast and plant cells or lysosomes of animal cells for degradation and recycling (Nakatogawa et al., 2009; Li and Vierstra, 2012; Yoshimoto, 2012). More than 30 autophagy-related genes (ATGs) have been identified in yeast, and 17 of them are necessary for autophagosome formation (Xie and Klionsky, 2007; Yoshimoto, 2012). Recently, orthologs of most yeast core *ATG* genes have been found in *Arabidopsis* and rice (Doelling et al., 2002; Hanaoka et al., 2002; Yoshimoto et al., 2004; Bassham et al., 2006; Xia et al., 2011). ATG8 is one of the core proteins for forming autophagosome. It covalently binds to membrane lipid phosphatidylethanolamine (PE) through a ubiquitin-related binding system (Xie and Klionsky, 2007). ATG8 is a scaffold for membrane expansion and elongation during autophagosome formation (Nakatogawa et al., 2007; Xie et al., 2008). Yeast *ATG8* also participates in the cytoplasm-to-vacuole targeting (CVT) pathway. Vacuole hydrolases, such as the precursor of aminopeptidase 1 (APE1), are selectively transported into the vacuole to produce mature APE1 (Yamaguchi et al., 2010). Unlike yeast, which has a single copy of the *ATG8* gene, plants usually have an *ATG8* family, comprising nine genes in *Arabidopsis* (Yoshimoto et al., 2004), five in maize (Chung et al., 2009), and six in rice (Xia et al., 2011). The different expression patterns of *Arabidopsis ATG8*s suggest that some *ATG8*s possess functional diversity besides possible redundancy (Slavikova et al., 2005).

Like yeast and animals, plant autophagy plays an important role in nutrient recycling under N- and C-starvation conditions (Li and Vierstra, 2012; Ohsumi, 2014). Currently, research on autophagy often focuses on the remobilization of N (Guiboileau et al., 2012, 2013; Xia et al., 2012; Li et al., 2015). Most *Arabidopsis ATG* genes are up-regulated by N-starvation and during leaf senescence (Doelling et al., 2002; Rose et al., 2006). Loss of function of *Arabidopsis* autophagy (*atg5*, *atg7*, *atg10*, and *atg13a atg13b*) caused hypersensitivity to N-limiting conditions in *Arabidopsis* and accelerated senescence even under N-rich conditions (Hanaoka et al., 2002; Phillips et al., 2008; Suttangkakul et al., 2011). Overexpression of *AtATG8f* and *GmATG8c* made *Arabidopsis* more tolerant to both N- and C-starvation (Slavikova et al., 2008; Xia et al., 2012). Autophagy mutants of *Arabidopsis* and maize (*atg5* and *atg7* in *Arabidopsis* and *atg12* in maize) showed reduced seed yield, seed N content, and N remobilization efficiency (NRE) (Guiboileau et al., 2012, 2013; Li et al., 2015). About 50% of the remobilized N of *Arabidopsis* is proven to come from autophagy (Guiboileau et al., 2012). These studies showed that autophagy plays a central role in N remobilization.

Since evidence for the contribution of autophagy to plant physiology largely comes from the study of *Arabidopsis*, little is known about crop autophagy except for maize. Rice is an important cereal crop for the world population, especially in Asia. Currently, little is known about the contribution of autophagy to rice seed quality. Rice *OsATG7* plays a role in NUE at the vegetative stage (Wada et al., 2015), and overexpression of rice gene *osatg8b* confers tolerance to nitrogen starvation and increases yield and nitrogen use efficiency in *Arabidopsis* (Zhen et al., 2019). However, the male sterility of *osatg7* limits research on autophagy-mediated N recycling to grains in rice.

In our study, we functionally analyzed *OsATG8b* in rice. Complementation of a yeast *atg* mutant and subcellular localization analysis demonstrated the role of *OsATG8b* in the autophagy process. In addition, we characterized the role of *OsATG8b* in N remobilization and seed quality by generating transgenic plants with over-expression and knockdown of *OsATG8b*. The phenotypic and ^{15}N-partitioning analysis showed that *OsATG8b* plays a role in N remobilization and grain quality. This result may provide strategic guidance for N application in molecular breeding and production of rice.

MATERIALS AND METHODS

Plant Materials and Growth Conditions

From spring to autumn, the *japonica* rice cultivar Zhonghua11 (ZH11) and transgenic plants were grown in a controlled paddy with normal planting. In winter, they were grown in a greenhouse at 28°C with 14-h light and 10-h dark per day. For hydroponic experiments, we used the modified rice nutrient solution of the International Rice Research Institute (IRRI, 1.43 mM NH_4NO_3, 0.32 mM NaH_2PO_4, 0.51 mM K_2SO_4, 1 mM $CaCl_2$, 1.65 mM $MgSO_4$, 8.9 mM $MnSO_4$, 0.5 mM Na_2MoO_4, 18.4 mM H_3BO_3, 0.14 mM $ZnSO_4$, 0.16 mM $CuSO_4$, 40 mM $FeSO_4$) in a growth room with a 30°C, 14 h light/10 h dark photoperiod (Yoshida et al., 1976). The solution was refreshed every 3-day. For nitrogen treatments, after the plants were germinated in water, they were grown on the IRRI solution for 7 days, and then plants were grown in the IRRI solution supplemented with high nitrogen (HN, 5 mM NH_4NO_3) and low nitrogen (LN, 0.2 mM NH_4NO_3) for different times.

Quantitative Real-Time RT-PCR (qRT-PCR)

Total RNA isolation, cDNA synthesis, and qRT-PCR of the rice were performed as previously described (Xia et al., 2011). Relative gene expression was normalized to the expression level of *e-EF-1a* with triplicate repeat. All primers are listed in **Supplementary Table S1**. qRT-PCR was repeated with three biological replicates, and each sample was assayed in triplicate by PCR.

Complementation of Yeast *scatg8* Mutants

OsATG8b ORF was cloned downstream of promoter *GAL1* of the yeast vector pYES260. Wild-type yeast KVY55 and the *scatg8* mutant KVY5 (MATa *leu2 ura3 trp1 lys2 his3 suc2-*△*9*△*atg8::HIS3*) were gifts from Dr. Yoshinori Ohsumi (Tokyo Institute of Technology, Japan). The vector was transformed into *scatg8* according to the LiAc/SS-DNA/PEG TRAFO protocol (Clontech). Yeast were cultured and shaken at 30°C in SC medium supplemented with 0.67% (w/v) YNB (yeast N base without NH_4SO_4 and amino acids), 2% (w/v) galactose, 0.5% (w/v) NH_4SO_4, and Ura DO Supplement. When the yeast grew to the logarithmic metaphase of growth (OD_{600} = 1), yeast cells were collected by centrifugation, washed, and incubated for another 5 h in 0.67% YNB medium without amino acids, galactose and NH_4SO_4 for nutrient deprivation to induce autophagy. The collected cells were used for immunoblotting with anti-APE1 antibody (Santa Cruz); the immunoblot analysis process used was as previously described (Hamasaki et al., 2005).

Scanning Electron Microscopy

Rice seeds were used for scanning electron microscopy (SEM) analysis. Samples were fixed overnight with 3% glutaraldehyde-sodium phosphate buffer (0.1M) at room temperature and rinsed three times with 0.1M sodium phosphate buffer. The samples were dehydrated through an ethanol series and infiltrated with an isoamyl acetate series. Seeds were then sputter-coated with gold/palladium in six different 30 s pulses (Hitachi JEE-420) and analyzed by scanning electron microscope (Hitachi S-3000N).

Subcellular Localization of *OsATG8b* Protein Fused With Green Fluorescent Protein Derivatives

GFP-OsATG8b and *sGFP-OsATG8b* were constructed to analyze the subcellular localization of OsATG8b in yeast and rice, respectively. For yeast subcellular localization, the fused construct was inserted downstream of promoter *GAL1* in pYES260 vector. For rice subcellular localization, the fused construct was inserted downstream of *35S* promoter (Okano et al., 2008). For root imaging, 7-day seedlings were treated with 1 μM concanamycin A for 6 h at 28°C in darkness, and 5 mm of root from the root tip was cut off for observation. The green fluorescent protein (GFP) fusion protein was analyzed by confocal laser scanning microscope (ZEISS-710 Meta) with a 488-nm exciting wavelength. The thickness of the optical sections (pinhole) was 2.1 μm. The images presented are average projections of 8–20 optical sections.

Generation of *OsATG8b*-Overexpression and -RNAi Transgenic Plants

To overexpress *OsATG8b*, the full-length CDS of *OsATG8b* was amplified by PCR and was inserted into the intermediate vector pUC18-sGFP. The whole cassette was finally PCR-amplified and inserted into the binary vector pCAMBIA1301 to replace the *GUS* via *Nco* I and *BstE* II. For the construction of the RNAi vector, a 230-bp fragment of the non-conserved 5′ end of *OsATG8b* was amplified with primers OsATG8b-Ri-F and OsATG8b-Ri-R and inserted in vector pTCK303 by *Bam*H I and *Kpn* I for the sense strand and by *Spe* I and *Sac* I for the antisense strand (Wang et al., 2004). These vectors were transformed into *A. tumefaciens* EHA105 and then transformed into ZH11 with the Agrobacterium-mediated transformation method (Hiei et al., 1997).

Antibodies

Antibodies of OsATG8b were made with 6 × His-OsATG8b proteins as the antigen; these were purified using a Ni column (Novagen) and injected directly into rabbits by Beijing ComWin Biotech Co., Ltd.

Protein Extraction and Immunoblot Analysis

Two-week old seedlings were used for total cell extracts and were ground in liquid N. The powders were extracted with the lysis buffer (25 mM Tris-HCl pH7.5, 1 mM EDTA, 1% Triton X-100, 150 mM NaCl, and Complete Protease Inhibitor Cocktail from Roche). The solution was then centrifuged at 13,000*g* for 20 min at 4°C, and the supernatant was used as total protein. The supernatant was run by SDS-PAGE with or without 6M urea and then transferred to nitrocellulose filter membranes for immunoblot analysis. The membranes were blocked and then incubated with mouse GFP antibodies (Santa Cruz) at a dilution of 1:1,000, while rabbit serum of OsATG8b was diluted by 1:500. All results came from three independent plant materials.

^{15}N-Labeling and Determination of ^{15}N Content

Rice plants were grown in IRRI solution in a greenhouse with 16-h light/8-h dark cycling. At 40 days after germination (DAG), plants were labeled with ^{15}N for 5-day by adding 10 atom% excess $Na^{15}NO_3$ to the IRRI solution. The plants were then washed thoroughly with distilled H_2O and transferred in the field for further growth. For ^{15}N uptake measurements, thirteen plants of each genotype were harvested 2-day after ^{15}N labeling. The ^{15}N-labeled plants were further grown in the field to maturity, and grains and remains were separated for N recycling assessment. A dry weight (DW) of each sample was assayed for ^{15}N and total N content using an isotope ratio mass spectrometer coupled with an N elemental analyzer (IsoPrime100, Elemental Scientific, United States). The ^{15}N content of each sample was calculated as a % of total N, which was calculated as atom% or $A\%_{sample} = 100 \times (^{15}N)/(^{15}N + ^{14}N)$ (Li et al., 2015).

NUE and N Recycling Efficiency (NRE) Calculations

Factors of calculation for NUE and NRE were estimated through the procedure provided by Guiboileau et al. (2012) and Li et al. (2015). The HI (harvest index) for yield evaluation was defined as the $DW_{grain}/(DW_{remain} + DW_{grain})$. The N harvest index (NHI) for assessing grain filling with N was calculated as $N\%_{grain} \times DW_{grain}/(N\%_{remain} \times DW_{remain} + N\%_{grain} \times DW_{grain})$. NUE was then calculated as the NHI/HI ratio, and NUE values of different genotypes were compared. The efficiency of N recycling to grains was shown by ^{15}NHI (^{15}N harvest index), which was calculated by $(A\%_{grains} \times N\%_{grains} \times DW_{grains})/[(A\%_{remain} \times N\%_{remain} \times DW_{remain}) + (A\%_{grains} \times N\%_{grains} \times DW_{grains})]$. The ^{15}NHI:HI ratio was used to compare the NRE of different transgenic plants. ^{15}N-labeling data were compiled from three biological replicates involving five plants for each genotype.

Quantification of Soluble Proteins and Starch

Total protein concentration and starch content were determined as described previously (Masclaux-Daubresse et al., 2002; Carlsson et al., 2011). Quantification data were compiled from three biological replicates involving 40 seeds from five plants for each genotype.

RESULTS

OsATG8b Restores Autophagy Activity in Yeast *scatg8* Mutant

Six *OsATG8*s have been identified in the rice genome (Xia et al., 2011). The ATG8 phylogenetic tree generated from amino acid sequences showed that plant ATG8s are clustered into two main subgroups. Subgroup I covers most of the plant *ATG8* family members, comprising *OsATG8a*, *b*, and *c*. Subgroup II covers 1–3 plant *ATG8* family members from each species, containing *OsATG8d*, *e*, and *f* (**Supplementary Figure S1**). The existence of two subgroups may imply specific functions to each, besides possible redundancy. To explore the relationship between N remobilization derived by autophagy and rice grain quality, we analyzed the expression of *OsATG8s* in developing endosperm by searching the Rice Expression Profile Database (RiceXpro)[1] and found that only *OsATG8b* expression increased with endosperm development compared with *OsATG8a* and *OsATG8c* (**Supplementary Figure S8**). These data indicated that the *OsATG8b* may be a potential rice ATG8 gene in grain filling, and it was chosen for further analyses. OsATG8b is encoded by a single gene (Os04g0642400) in rice. It is a soluble protein of 119 amino acids, with a predicted molecular mass of 13.7 kD and pI of 8.78. OsATG8b shares 81.8% amino acid identity with yeast ScATG8, 71.4% identity with human HsGABARAP, and 86.9% identity with *Arabidopsis* AtATG8a (**Supplementary Figure S2A**). Like other ATG8 proteins, OsATG8b has a conserved Gly residue at the C-terminus for PE conjugation (**Supplementary Figure S2A**). The result of 3D model prediction revealed that OsATG8b protein contains an N-terminal helical domain, two hydrophobic pockets named the W-site and the L-site, and a C-terminal ubiquitin-like domain, similar to yeast ScATG8 (**Supplementary Figures S2A,B**) (Noda et al., 2010). This implies that OsATG8b may have the autophagic function, similar to yeast ScATG8.

To verify the autophagic function of *OsATG8b*, we investigated whether *OsATG8b* rescues defects of *ATG8*-deficient (*scatg8*) yeast KVY5 (Kirisako et al., 1999). *OsATG8b* cDNA containing the entire ORF was driven by the yeast *GAL1* promoter in a plasmid (pYES260) and expressed in *scatg8* yeast. *OsATG8b* can rescue the abnormal cell morphology of the *scatg8* yeast under N starvation (**Figure 1A**). In yeast, the precursor aminopeptidase1 (prAPE1) was delivered to the vacuole for processing into mature APE1 (mAPE1) through the Cvt/autophagy pathway (Yamaguchi et al., 2010). Thus, we monitored the protein levels of both prAPE1 and mAPE1 after 5 h of starvation. Both wild-type yeast and *scatg8* cells complemented with *OsATG8b* accumulated mAPE1. In contrast, mAPE1 was detected in neither *scatg8* cells nor the *scatg8* cells transformed with the empty vector (**Figure 1B**). This suggests that prAPE1 was delivered to the vacuole and processed to mAPE1 in *scatg8b* yeast when *OsATG8b* was expressed in these cells. These results confirmed

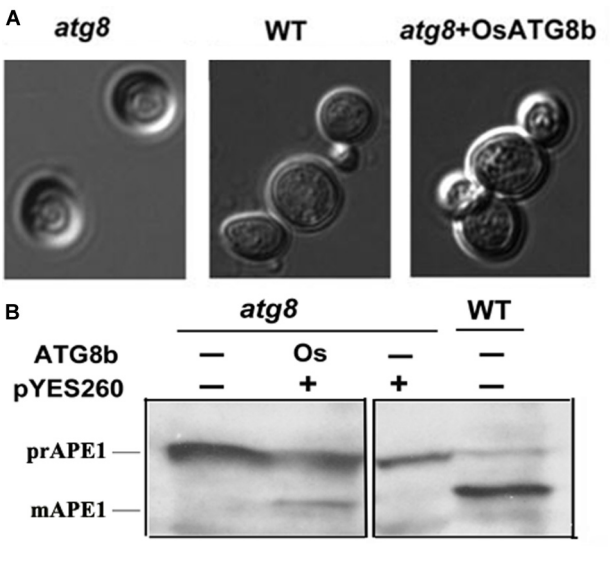

FIGURE 1 | Functional complementation of yeast *atg8* mutant by *OsATG8b*. *OsATG8b* cDNA was cloned into the plasmid pYES260 and expressed in yeast *atg8* mutant KVY5 strain. **(A)** *OsATG8b* restores normal cell morphology of the yeast *scatg8* mutant under N starvation. Abnormal morphology of *scatg8* yeast cell (left), compared with normal cell of wild-type (WT) yeast (middle), and *scatg8* yeast transformed with *OsATG8b* (right). **(B)** API protein identification by Western blot. Yeast cells were grown to mid-log phase to be collected and washed, incubated in the presence of 2% galactose to induce *OsATG8b* expression, and then incubated for another 5 h in nutrient deprivation medium and harvested for protein extraction. Proteins were then resolved by SDS-PAGE followed by immunoblotting with anti-APE1 antibody. prAPE1, precursor of aminopeptidase 1; mAPE1, mature aminopeptidase 1.

[1]https://ricexpro.dna.affrc.go.jp/

the autophagic activity of OsATG8b and showed that OsATG8b is a functional homolog of yeast ScATG8.

OsATG8b Expression Is Induced by N- and C-Starvation

To determine the spatial and temporal expression pattern of *OsATG8b*, we employed qRT-PCR to examine *OsATG8b* expression. qRT-PCR analysis showed that *OsATG8b* transcripts accumulated in all studied organs, including roots, stems, leaves, leaf sheaths, and panicles at different growth stages (**Figure 2A**). The results showed that *OsATG8b* transcript levels were higher in roots of plants at 45 days after germination (DAG) than in those of plants at other growth stages. At 60 DAG, *OsATG8b* transcript was relatively abundant in stems, leaf, and panicle (**Figure 2A**). The expression level of *OsATG8b* was also examined under N deficiency and darkness treatment for C starvation, respectively (**Figures 2B,C**). *OsATG8b* transcript level increased in response to both N deficiency and darkness treatment. When rice seedlings were subjected to the N-free treatment, the expression level of *OsATG8b* gradually increased, peaking at 10-day after treatment application. Similarly, darkness treatment rapidly induced a roughly three-fold increase in *OsATG8b* expression within 2-day after treatment. Taken together, these results suggest that *OsATG8b* may play a crucial role in regulating multiple developmental processes and in response to nutrient stresses.

GFP-OsATG8b Is Localized to Autophagosomes

To determine whether OsATG8b is conjugated onto the autophagosome membrane and completed or delivered into the vacuole, GFP was fused to its N-terminus and transformed into *scatg8* yeast cells. Under control conditions, GFP-OsATG8b was mainly localized in the cytosol with punctate distribution, whereas after starvation, it accumulated within the vacuole of

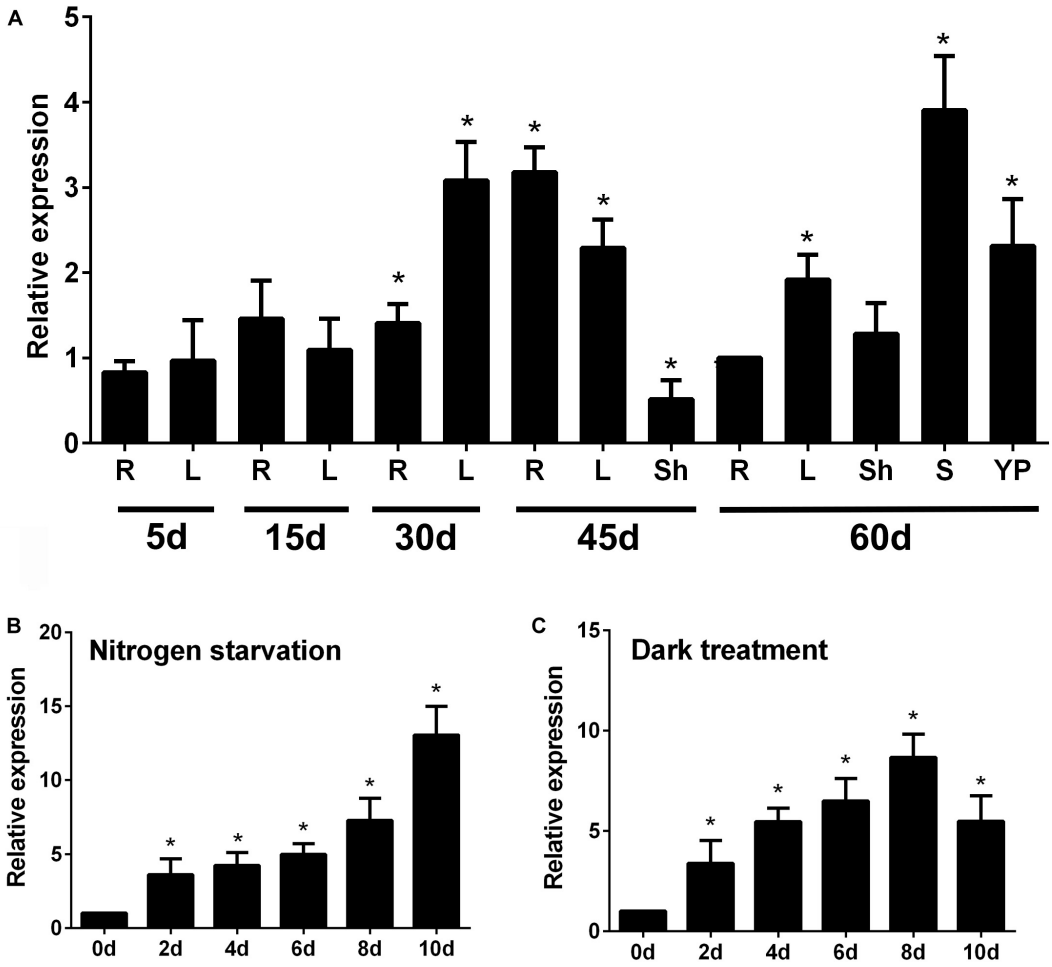

FIGURE 2 | Expression patterns of *OsATG8b* in developing tissues of rice by qRT-PCR analysis. **(A)** Expression of *OsATG8b* in developing tissues. Total RNA was isolated from roots €, sheaths (Sh), young panicles (YP), stems (S), and leaves (L) at different growth stages. *OseEF-1a* was used as an internal reference. **(B,C)** Expression profiles of *OsATG8b* in an N-starvation solution **(B)** and in darkness **(C)**. Total RNA was isolated from 5-leaf seedlings treated for 2, 4, 6, 8, and 10-day with N-starvation and darkness. Error bars indicate standard deviations of independent biological replicates ($n = 3$). One asterisk (*$p < 0.05$, *t*-test) represents significant difference.

yeast (**Figure 3A**). These data suggest that OsATG8b may be localized to the autophagosomes of cytosol under the control conditions and translocate from the cytosol to the vacuole in an autophagy-dependent manner after starvation in yeast. To further verify the above result in rice, *sGFP-OsATG8b* was also transiently expressed in rice protoplasts, but the data showed that the sGFP-OsATG8b fusion protein was localized to the membrane, cytoplasm, and nucleus (**Supplementary Figure S3**), similar to the free sGFP control. To further confirm subcellular localization, transgenic rice expressing s*GFP-OsATG8b* were generated under the control of *35S* promoter (**Figure 3B**). The 5 mm of the roots from the tip were cut off and immediately observed by LSCM. In *sGFP-OsATG8b*, GFP fluorescence was detected in the cytoplasm and nucleus; however, after 6 h of incubation in darkness with concanamycin A (an inhibitor of vacuolar H^+-ATPase) to help in the observation of autophagic bodies through increasing vacuolar pH (Ishida et al., 2008; Izumi et al., 2015), many vesicles with a strong GFP signal and the spread of a faint GFP signal were observed (**Figure 3B**). These results indicate that the sGFP-OsATG8b-labeled puncta located in autophagosomes and the sGFP-OsATG8b can be used to visualize the progression of autophagy in rice, and overexpression of *OsATG8b* could increase the autophagic activity. Immunoblot analysis using proteins isolated from either ZH11 or transgenic *sGFP* and *sGFP-OsATG8b* rice plants showed that the OsATG8b antibodies recognized the endogenous as well as the GFP fusion proteins (**Supplementary Figures S4A,B**). Meanwhile, we performed an sGFP-ATG8 processing assay by the levels of free GFP moiety in anti-GFP immunoblots. After entering into the vacuole, sGFP-ATG8 is digested and releases free GFP, which is in a soluble and relatively stable form during autophagic body turnover (Suttangkakul et al., 2011). This free vacuolar GFP accumulates to a higher level when autophagy accelerates, so it represents the transport of ATG8 to vacuoles. Since OsATG8b antibody can also recognize OsATG8a and c (**Supplementary Figure S9**), the endogenous OsATG8(a/b/c) band of ZH11 and G1 (**Supplementary Figure S4B**) is very weak, but in *OsATG8b*-OE, the OsATG8(a/b/c) band is very strong, indicating that OsATG8b is overexpressed. These results indicated that the OsATG8 has already conjugated onto the autophagosome membrane and is able to be completed or delivered into the vacuole (**Supplementary Figure S4A**), which further confirms the autophagic activity of OsATG8b.

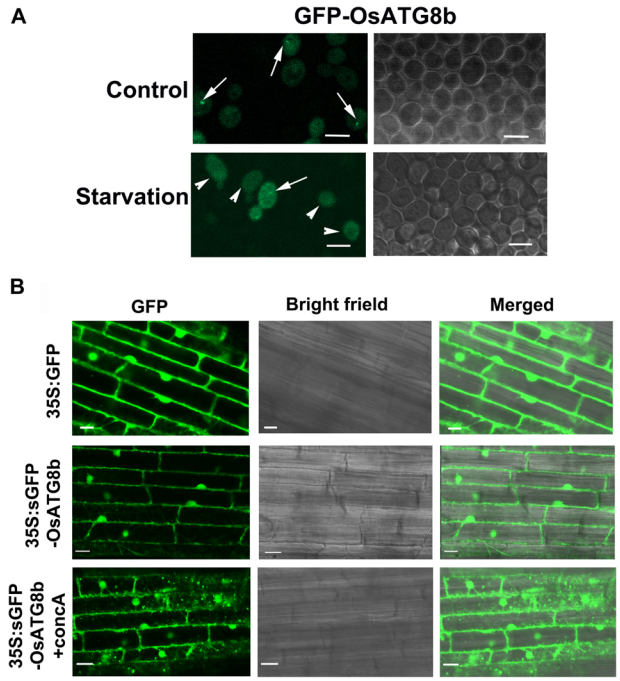

FIGURE 3 | Subcellular localization of OsATG8b. **(A)** Subcellular localization of GFP-OsATG8b in yeast cells. Yeast cells were grown to mid-exponential phase and then incubated in the presence of 2% galactose to induce *GFP-OsATG8b* expression. Cells grown in both the control and starvation media were visualized by confocal laser scanning microscope. Arrows indicate the pre-autophagosomal structure (PAS), and arrowheads indicate GFP within vacuoles. Bars = 5 μm. **(B)** Subcellular localization of sGFP-OsATG8b in roots of transgenic rice. Fresh root samples of transgenic rice plants expressing *35S:sGFP-OsATG8b* were excised and observed immediately (0 h) and after 6-h treatment with 1 μM concanamycin A. The region at approximately 5 mm from the root tip was observed in a laser scanning confocal microscope. Simultaneously obtained sGFP fluorescence images and DIC images are shown. Bars = 10 μm.

Knockdown of *OsATG8b* Expression Affects Root Growth at Grain Germination Stage

To investigate the function of *OsATG8b*, *OsATG8b* overexpression (*OsATG8b*-OE), and RNA-interference (*OsATG8b*-RNAi), transgenic lines were generated. RT-PCR analysis showed that *OsATG8b* expression increased in flag leaves of *OsATG8b*-OE lines and decreased in flag leaves of *OsATG8b*-RNAi lines (**Figures 4A,B**). The *OsATG8b*-RNAi construct was targeted specifically to the non-conserved 5′ end (**Supplementary Figure S5A**) of *OsATG8b* outside the ubiquitin domain to avoid interference with other OsATG8 proteins. Three of the *OsATG8b*-RNAi lines (Ri20, Ri24, and Ri25) and three of the *OsATG8*-OE lines (OE3, OE4, and OE6) were selected for subsequent analysis. In order to observe the effect of altered *OsATG8b* expression on *OsATG8a* and *OsATG8c*, we detected the expression of *OsATG8a* and *OsATG8c* in the shoots and roots of the transgenic rice seedling at four-leaf stage (**Supplementary Figures S5B,C**). The results showed that there is no significant difference in *OsATG8a* or *OsATG8c* transcript level among ZH11, the *OsATG8*-OE lines, and the *OsATG8b*-RNAi lines.

To confirm whether autophagic activities are altered in the *OsATG8b*-RNAi and *OsATG8b*-OE lines, we examined the ATG8a/b/c autophagic activities in 14 days-after-germination shoots of *OsATG8b*-RNAi, *OsATG8b*-OE, and ZH11 lines using OsATG8b antibodies (**Figure 4C**). The bands of ATG8 and ATG8-PE respectively represent the sum of OsATG8a/b/c or OsATG8a/b/c-PE (**Figure 4C**), since OsATG8b antibody can also recognize OsATG8a and OsATG8c (**Supplementary Figure S9**). The immunoblot analysis showed that the levels of OsATG8a/b/c-PE (representing the forming or completed autophagosomes) and cytosolic OsATG8a/b/c form were

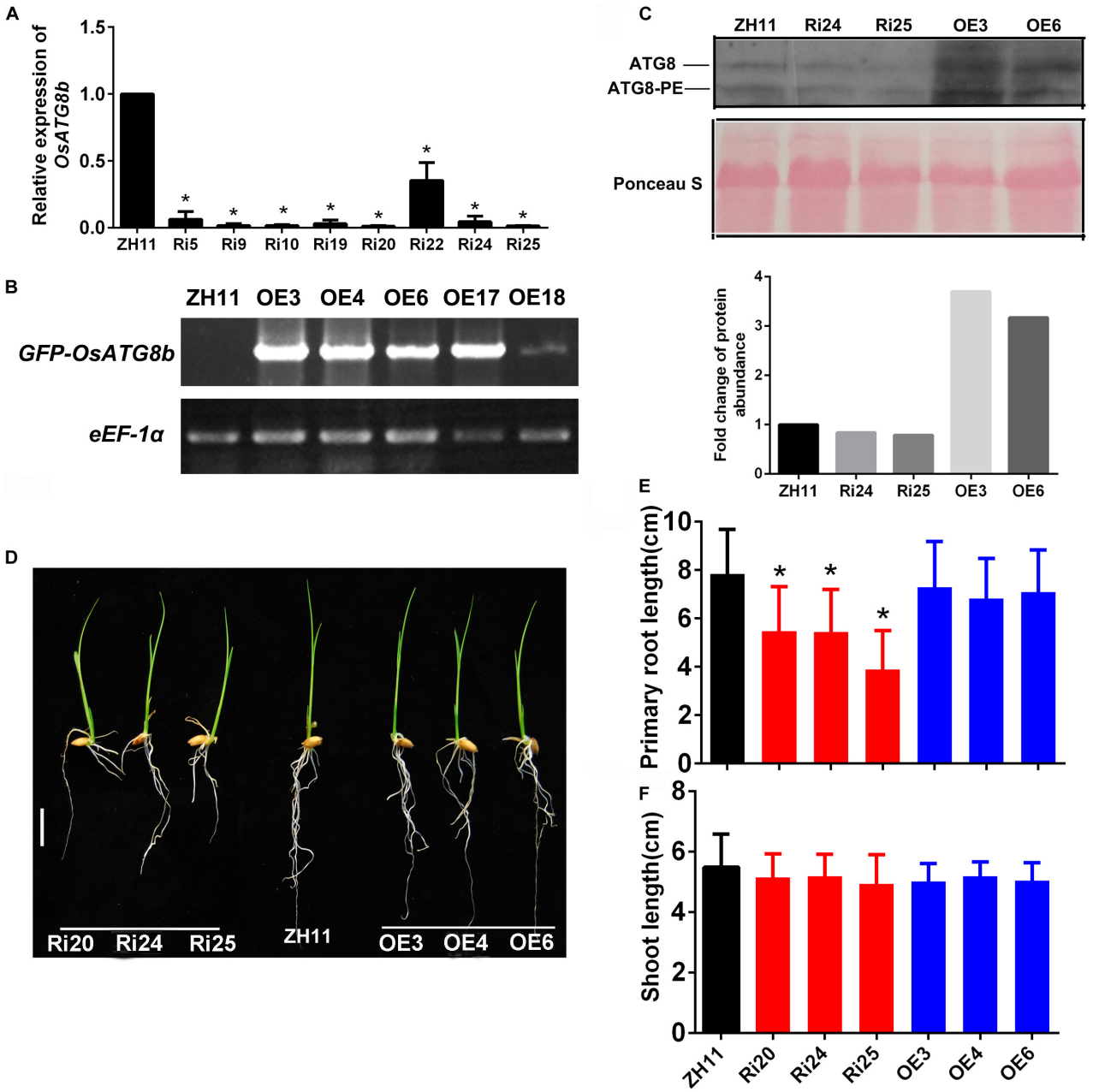

FIGURE 4 | *OsATG8b* affects root growth at seed germination stage. **(A,B)** Expression levels of *OsATG8b* in flag leaves of *OsATG8b*-RNAi (Ri) **(A)** and *OsATG8b*-overexpression (OE) lines **(B)**, measured by qRT-PCR and semi-qRT-PCR analyses, respectively. *OseEF-1a* was used as an internal reference. Error bars indicate standard deviations of independent biological replicates ($n = 3$). One asterisk (*$p < 0.05$, *t*-test) represents significant difference. **(C)** Immunoblot detection of the OsATG8a/b/c and OsATG8a/b/c lipidation level in 14 days-after-germination shoots of ZH11, *OsATG8b*-RNAi, and *OsATG8b*-OE lines. Total protein extracts were subjected to SDS-PAGE in the presence of 6M urea and immunoblotted with OsATG8b antibody. The fold change of ATG8a/b/c-PE was quantified using Image J software v1.45. **(D–F)** Seedlings **(D)** and statistical analysis of root **(E)** and shoot length **(F)** of *OsATG8b*-RNAi and *OsATG8b*-OE lines and ZH11 at 7-day after germination in water. Bar = 1 cm. Three biological replicates, each containing 80 plants, were used for data analysis. Results are the mean ± SD from 80 plants. *$p < 0.05$ (*t*-test): significantly different from ZH11. No asterisks mean no significant difference.

remarkably increased in *OsATG8b*-OE lines compared with ZH11 lines, and the quantified results showed that there is a slight decrease (about 17–20%) in them in *OsATG8b*-RNAi compared with in ZH11. Because *OsATG8a/c* expression does not change in these transgenic rice (**Supplementary Figures S5B,C**), these changes to the immunoblot bands should represent the changes of OsATG8b and OsATG8b-PE in *OsATG8b*-OE and *OsATG8b*-RNAi (**Figure 4C**). These results indicated that the autophagic activity is higher in *OsATG8b*-OE lines and may be a little lower in *OsATG8b*-RNAi than that in ZH11.

When the role of OsATG8b in growth at the vegetative stage was analyzed, we observed that the roots of 7-day-old *OsATG8b*-RNAi seedlings were much shorter than those of ZH11 and *OsATG8b*-OE lines (**Figures 4D,E**) when germinated in water. To reveal how the N level affects autophagy in rice, growth of *OsATG8b*-RNAi and *OsATG8b*-OE lines was measured under low nitrogen (LN, 0.2 mM NH_4NO_3) and high nitrogen (HN, 5 mM NH_4NO_3) for 30- or 60-day. Under LN and HN levels, the *OsATG8b*-RNAi and *OsATG8b*-OE lines exhibited a relatively normal phenotype and a similar growth rate when compared with ZH11 at 30 (**Supplementary Figures S6A–D**) or 60 DAG (**Supplementary Figures S6E–H**). Neither root nor shoot length showed any significant difference among these lines (**Supplementary Figures S6C,D,G,H**). These data may indicate that knocking down *OsATG8b* affects root growth at the stage of seed germination.

OsATG8b Affects Grain Yield and Grain Quality in Rice

The phenotypes of *OsATG8b*-RNAi and *OsATG8b*-OE rice at the reproductive stage were investigated in the paddy field under normal N conditions. Previous studies have shown that the autophagy-defective rice mutant *osatg7* displayed complete sporophytic male sterility. However, *OsATG8b*-RNAi and *OsATG8b*-OE plants produced healthy pollen grains and could be fertilized normally. The statistical results showed that grain number and grain yield per plant increased in *OsATG8b*-OE plants but decreased in *OsATG8b*-RNAi ones compared with ZH11 plants (**Figure 5**). These data indicate that *OsATG8b* may be involved in grain development and yield.

The grains of *OsATG8b*-RNAi have a brown-spotted hull and contain chalky endosperm (**Figures 6A,B**). This showed that it produced poor quality seeds. The percentage of hulled rice with chalkiness was higher in *OsATG8b*-RNAi lines than in ZH11 (**Figure 6C**). SEM revealed that there are many loosely packed and small starch granules in the endosperm of *OsATG8b*-RNAi, which differed from the large and tightly packed starch granules in ZH11 (**Figure 6D**). Conversely, endosperm starch granules of *OsATG8b*-OE and ZH11 grains seemed larger and tighter (**Figure 6D**). Compared with ZH11, soluble protein content in *OsATG8b*-RNAi lines was lower, while that in *OsATG8b*-OE lines was higher (**Figure 6E**). However, starch content showed no significant difference among those lines (**Figure 6F**).

OsATG8b Affects N Recycling to Grains

To investigate whether *OsATG8b* plays a role in N recycling to grains in rice, we performed a pulse-chase assay with $^{15}NO_3^-$, as previously conducted with *Arabidopsis* (Masclaux-Daubresse and Chardon, 2011; Guiboileau et al., 2012). ^{15}N and the $^{14}N/^{15}N$ ratio were measured (**Figure 7A**). Plant dry weight (DW) was higher in *OsATG8b*-OE lines and lower in *OsATG8b*-RNAi lines than in ZH11 (**Figure 7B**). This is similar to what was observed in *Arabidopsis* mutants (*atg5*, *atg7*) (Doelling et al., 2002; Guiboileau et al., 2012). HI, an important productivity indicator (Yang and Zhang, 2010), was lower in *OsATG8b*-RNAi lines but higher in *OsATG8b*-OE lines than in ZH11 (**Figure 7C**), which shows that autophagy plays an important role at the grain-filling stage.

NHI is the main index of the efficiency of N distribution to grains and N grain filling (Guiboileau et al., 2012). The NHI of *OsATG8b*-RNAi was lower than that of ZH11, while that in *OsATG8b*-OE was higher (**Figure 7D**). As the NHI/HI ratio is considered a good indicator of NUE in plants (Masclaux-Daubresse and Chardon, 2011), we then measured the NHI/HI ratio of *OsATG8b*-RNAi, *OsATG8b*-OE, and ZH11. The results showed that the NHI/HI ratio increased dramatically in *OsATG8b*-OE lines but decreased in *OsATG8b*-RNAi lines when compared to ZH11 (**Figure 7E**). These data indicate that *OsATG8b*-mediated autophagy plays a role in grain NUE.

On the seventh day after $^{15}NO_3^-$ labeling, the ^{15}N contents of *OsATG8b*-RNAi, *OsATG8b*-OE, and ZH11 showed no significant differences. This is consistent with the normal growth of the *OsATG8b*-RNAi and *OsATG8b*-OE lines under N-rich conditions (**Supplementary Figure S7**). The abundances of ^{15}N in grains and remains were determined using isotopic ratio mass spectrometry, which enabled us to calculate the partitioning of ^{15}N in grains (^{15}NHI) by combining these values with DW and N% data. ^{15}NHI and the ^{15}NHI:HI ratio, an indicator for NRE, were lower in *OsATG8b*-RNAi lines and higher in *OsATG8b*-OE lines than in ZH11 (**Figures 7F,G**). Taken together, these ^{15}N partitioning results show that *OsATG8b*-mediated autophagy significantly affects NRE during the grain-filling stage.

DISCUSSION

Plant autophagy plays important roles in growth and development, grain filling, response to pathogen infection and to abiotic and biotic stresses, and N recycling (Wada et al., 2009; Yoshimoto et al., 2009; Guiboileau et al., 2012). All of these functions have major agricultural relevance, and most *ATG* orthologs in crops have been identified in maize and rice (Chung et al., 2009; Xia et al., 2011). Here, we report that rice *OsATG8b* is involved in N recycling and thus affects rice yield and seed quality.

OsATG8b Is a Functional Homologue of Yeast ScATG8 and a Useful Autophagosome Marker for Rice

Evolutionarily, autophagy is a highly conserved intracellular mechanism of degradation of cellular components in eukaryotic cells (Michaeli et al., 2016). At the elongation and final enclosure stages of the autophagosome, the linkage of ATG8 to PE anchors the former to both inner and outer membranes of the phagophore (Zientara-Rytter and Sirko, 2016). Therefore, the ATG8 protein is a useful molecular marker of autophagosomes, allowing for their distinction from other cellular vesicles and intracellular membranes (Yoshimoto et al., 2004; Zientara-Rytter and Sirko, 2016). Unlike yeast, which has a single *ATG8*, higher eukaryotes usually have an *ATG8* family. Rice has six *ATG8*s (Xia et al., 2011), and five of their proteins have the conservative glycine in the C-terminal for PE conjugation except for OsATG8f. OsATG8a, b, and c belong to subgroup I of the plant ATG8 phylogenetic

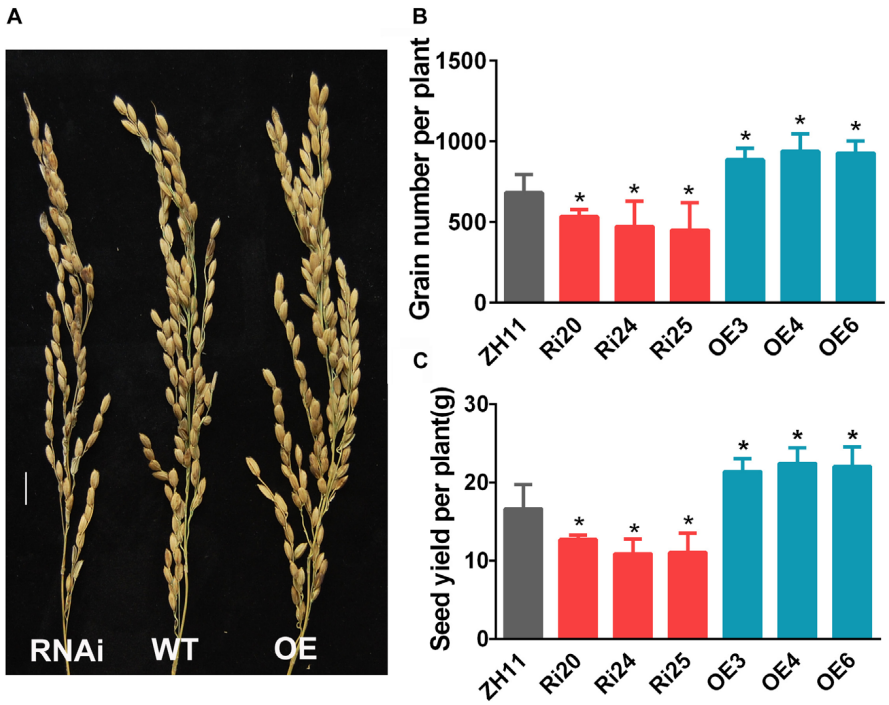

FIGURE 5 | *OsATG8b* affects rice grain yield. *OsATG8b*-RNAi (Ri) and *OsATG8b*-OE (OE) lines and ZH11 were grown in the paddy field with normal fertilizer. **(A–C)** Panicle architecture **(A)**, grain number **(B)**, and grain yield **(C)** per plant of *OsATG8b*-RNAi and *OsATG8b*-OE lines and ZH11. Bar = 1 cm. Three biological replicates, each containing 80 plants, were used for data analysis. Results are the mean ± SD from 80 plants. *$p < 0.05$ (*t*-test): significantly different from ZH11.

tree (**Supplementary Figure S1**), as all three proteins have extra amino acids behind the conserved Gly residue and need cleavage by ATG4 to expose the Gly residue (**Supplementary Figure S2**). On the other hand, OsATG8d and e belong to subgroup II (**Supplementary Figure S1**), as both have an innate C-terminal-exposed Gly residue, which makes OsATG8 quickly proceed conjugate with PE without ATG4 processing (**Supplementary Figure S2**). Expression of nine *AtATG8* genes showed different patterns (Slavikova et al., 2005), which indicates that different *ATG8* members may have multiple non-redundant functions and that individual *ATG8*s may have specific functions.

Plant *ATG8s* can functionally complement yeast *atg8* mutants, such as those in *Arabidopsis* (Slavikova et al., 2005), soybean (Xia et al., 2012), and wheat (Pei et al., 2014). In our study, *OsATG8b* expression restored autophagy defects in the corresponding yeast *atg8* mutant (**Figure 1**). This indicated that OsATG8b has an autophagic function similar to yeast ATG8. At present, observation of GFP-ATG8 puncta has been shown to be the best and most convenient detection method for autophagic activity (Kliosnky, 2016). However, it is showed that GFP-ATG8 signal foci in cytoplasm might not be the true autophagosomes in the cytoplasm of *atg4a-1atg4b-1* double mutants (Yoshimoto et al., 2004) and *atg7-2* mutants (Suttangkakul et al., 2011) since the foci may be GFP-ATG8 aggregates (Kuma et al., 2007; Kim et al., 2012). However, in the presence of concanamycin A, the mutants (*atg7-2*, *atg5*, *atg10*, and *atg4a-1atg4b-1* in *Arabidopsis* and *atg7* in rice) always lack GFP-ATG8 labeled autophagic foci in the vacuole (Yoshimoto et al., 2004; Thompson et al., 2005; Phillips et al., 2008; Izumi et al., 2015). This indicates that vacuolar GFP-ATG8 spots should be utilized as an autophagy indicator instead of GFP-ATG8 dots (Chung, 2011). The sGFP-OsATG8b puncta in vacuoles of rice root cells in the presence of concanamycin A were observed (**Figure 3B**); therefore, sGFP-OsATG8b is considered to be a marker for measuring the autophagic activity of rice cells. We also detected autophagosomes in vacuoles of sGFP-ATG8b transgenic rice (**Figure 3B**). Free GFP released from fused sGFP-ATG8b also supports this transfer and accumulates in vacuoles (**Supplementary Figure S4B**). Therefore, the sGFP-ATG8b test is a biochemical way to monitor the autophagic flux of rice cells.

OsATG8b Affects Grain Number and Grain Quality

Arabidopsis and maize *atg* mutants are sensitive to nutrient-limiting conditions (Hanaoka et al., 2002; Slavikova et al., 2005; Li et al., 2015). However, the *OsATG8b*-RNAi and *OsATG8b*-OE lines showed a relatively normal phenotype. In rice, there are six *ATG8s*, of which *OsATG8a*, *OsATG8b*, and *OsATG8c* have high homology. Data from RiceXpro (**Supplementary Figure S8**) showed that these three genes have similar expression patterns at vegetative stage. However, there are some different patterns during grain development; in particular, only *OsATG8b* expression increases with endosperm development (**Supplementary Figure S8B**). These data indicate that *OsATG8s* function redundantly in response to nutrient stress

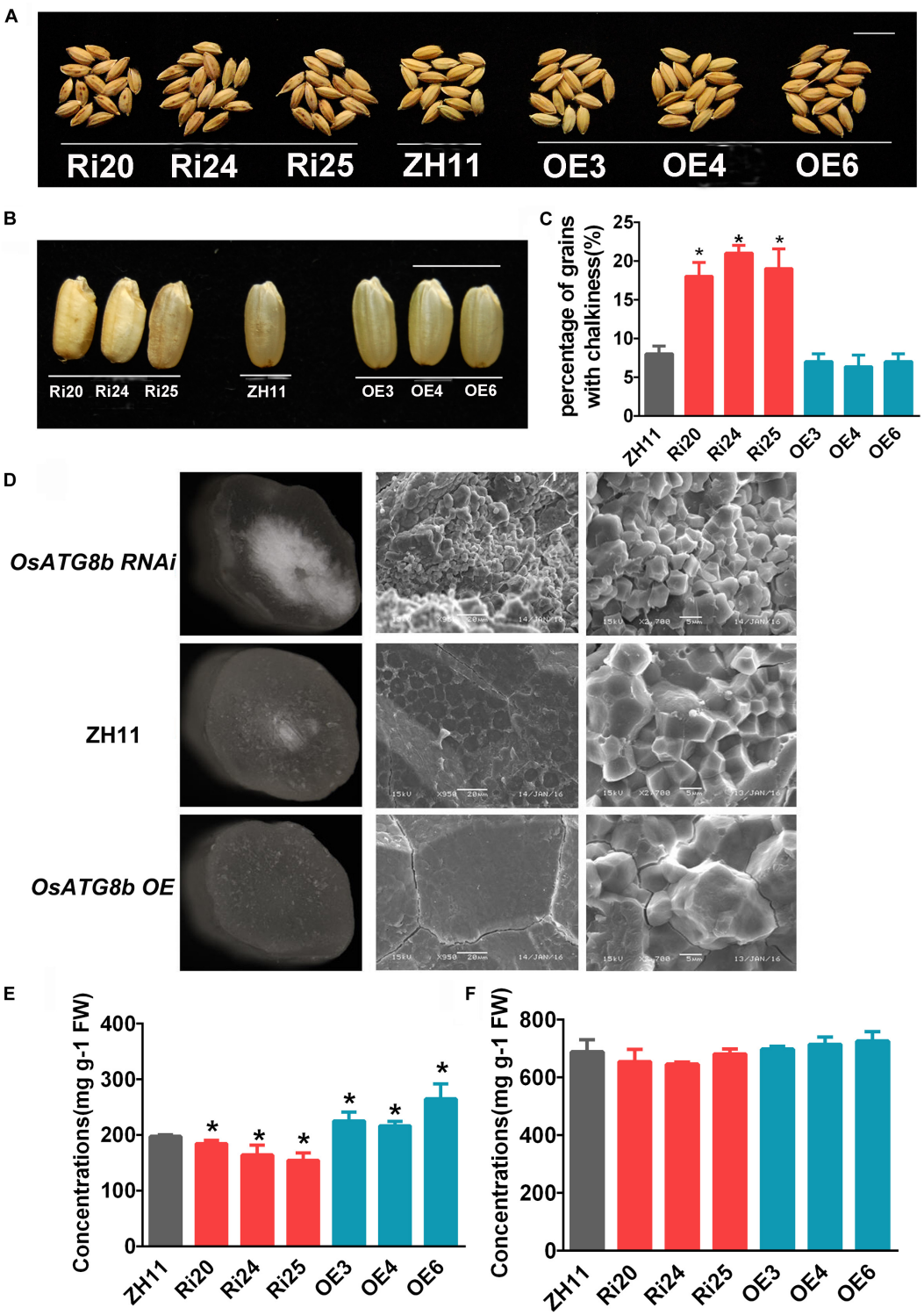

FIGURE 6 | *OsATG8b*-mediated autophagy affects grain quality in rice. *OsATG8b*-RNAi (Ri) and *OsATG8b*-OE (OE) lines and ZH11 were grown in a paddy field under normal growth conditions. **(A)** Seed grains. *OsATG8b*-RNAi lines produced grains with brown spotted hulls. Bar = 1 cm. **(B)** Hulled *OsATG8b*-RNAi rice lines showed a chalky endosperm phenotype. Bar = 1 cm. **(C)** Percentage of hulled rice with chalkiness. **(D)** Scanning electron micrographs of cracked mature caryopses of rice grains under different magnifications. Endosperms of *OsATG8b*-RNAi lines had small, loosely packed starch granules, which differed markedly from the large, tightly packed starch granules of ZH11 and *OsATG8b*-OE lines. **(E)** Soluble protein concentration in grains. **(F)** Starch concentration in grains. Three biological replicates, each containing 40 seeds from five plants, were used for data analysis. Results are the mean ± SD from five plants. $^{*}p < 0.05$ (*t*-test): significantly different from ZH11 **(C,E,F)**.

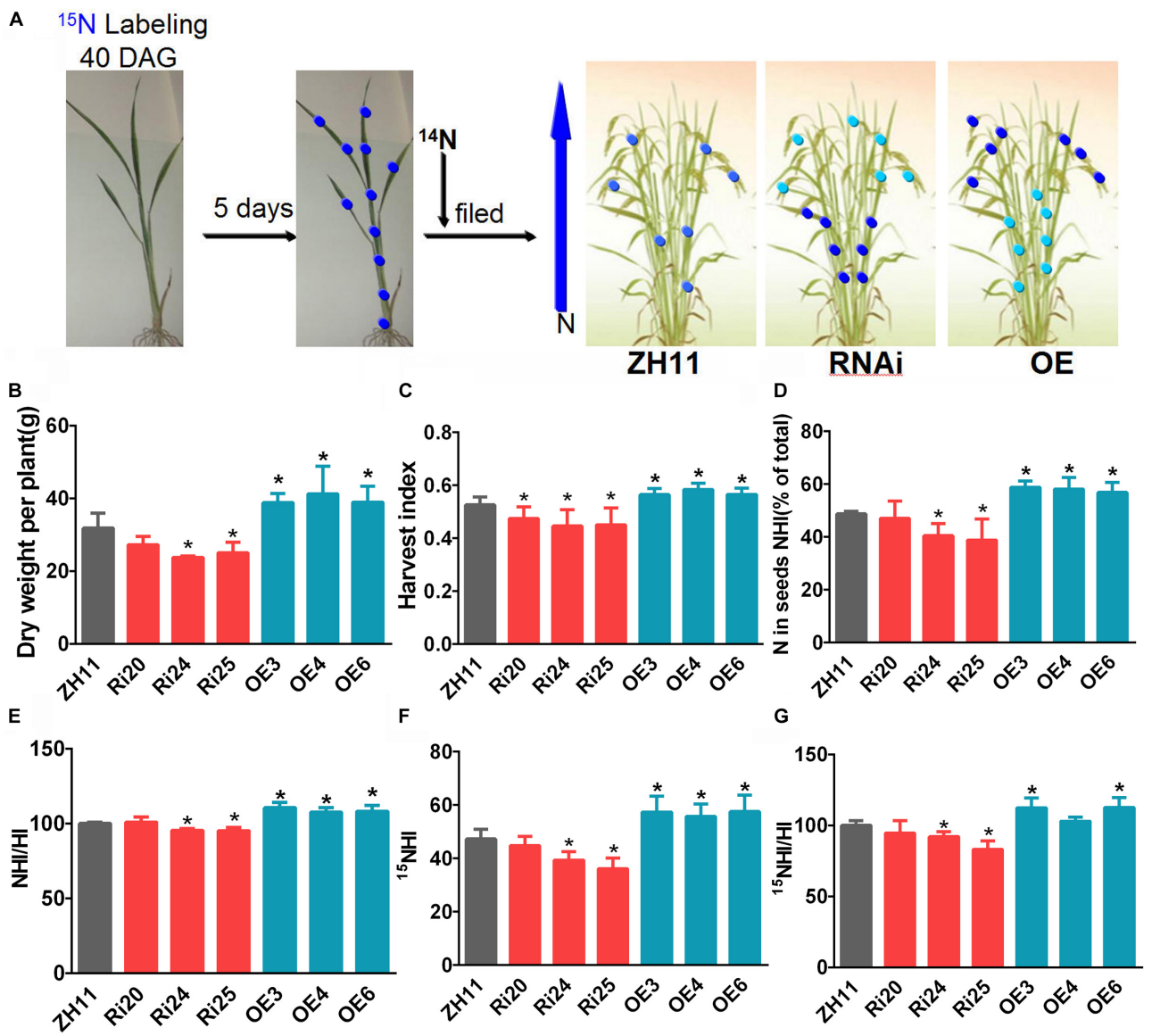

FIGURE 7 | *OsATG8b*-mediated autophagy significantly affects N recycling efficiency (NRE). *OsATG8b*-RNAi (Ri) and *OsATG8b*-OE (OE) lines and ZH11 were grown in IRRI solution with $^{14}NO_3^-$ supplementation until 40-day after germination and then labeled by a 5-day pulse of $^{15}NO_3^-$ and subsequently grown in normal conditions to mature stage. After grain filling, ^{15}N and the $^{14}N/^{15}N$ ratio were analyzed by isotopic ratio mass spectrometry. **(A)** Overview of ^{15}N labeling and subsequent N partitioning. The deeper the blue of the dot, the higher the N content. **(B)** Biomass accumulation as measured by dry weight (DW) per plant. **(C)** Harvest index (HI) as measured by ratio of DW of grains to DW of the aboveground plant parts. **(D)** Nitrogen harvest index (NHI) as measured by the partitioning of total plant N in grains. **(E)** NHI:HI ratio as an estimate of N use efficiency. **(F)** Partitioning of total ^{15}N in grains. **(G)** ^{15}NHI:HI ratio as an indicator of N recycling efficiency. Three biological replicates, each containing five plants, were used for data analysis. Results are the mean ± SD from five plants. *$p < 0.05$ (*t*-test): significantly different from ZH11.

at the vegetative stages, but individual *ATG8*s may have specific functions in grain development. Indeed, in our study, *OsATG8b*-RNAi lines showed a chalky endosperm phenotype and carried small, loosely packed starch granules (**Figures 6B,D**), while in *OsATG8b*-OE lines endosperm, starch granules seemed larger and tighter (**Figure 6D**). Many genes and environmental factors control the grain endosperm chalkiness of rice (Siebenmorgen et al., 2013). Starch is the main storage material in rice grains, accounting for nearly 90% of the total dry weight, while protein accounts for about 8% of the endosperm weight of rice, filling the area between starch grains (Lin et al., 2014). Previous studies have shown that incomplete accumulation of starch and inadequate accumulation of proteins cannot fully fill the gap between starch granules, which may lead to the formation of chalk (Delrosario et al., 1968; Lin et al., 2014).

Starch and protein of rice grain are products of C and N, which are transported from source organs to produce starch and protein in precise quantities and proportions (Duan and Sun, 2005).

C and N statuses are affected in *Arabidopsis atg* (*atg5* and *atg7*) mutants (Guiboileau et al., 2013; Masclaux-Daubresse, 2016). We showed that soluble protein content decreased in *OsATG8b*-RNAi lines and increased in *OsATG8b*-OE lines, while starch content showed no difference between these lines (**Figures 6E,F**). In *OsATG8b*-RNAi lines, autophagic activity was slightly inhibited, and grain yield and quality were reduced (**Figures 4A,C**). The root shortening phenotype in 7-day-old *OsATG8b*-RNAi seedling (**Figures 4D,E**) may be caused by this impaired grain, since there are no obvious morphological differences between *OsATG8b*-RNAi and ZH11 at other vegetative stages (**Supplementary Figure S6**). We deduced that knocking-down *OsATG8b* in grains may cause decreased degradation of stored proteins in the germinating grains and then attenuate the growth rate of roots at the grain germination stage. These results suggest that *OsATG8b*-RNAi lines produced chalky endosperm mainly by breaking the balance between C and N in rice grains.

During early reproductive stage, panicle primordia and spikelets differentiate and develop in the shoot apical meristems, and the top four leaves and their respective internodes are developed on the mature dwarf stem and leaves. All of these events are mainly maintained by the N storage in the epiphylls of the dwarf stem and supply of new N from soil (Yoneyama et al., 2016). Therefore, spikelet number is determined by the N obtained from both recycling from leaves and root uptake. Our data showed that grain number per plant in *OsATG8b*-OE lines increased while that in *OsATG8b*-RNAi lines decreased compared with that in ZH11 in the field, indicating that *OsATG8b*-mediated autophagy affects grain number mainly by influencing N recycling from the dwarf stem-attached leaves to spikelet development.

OsATG8b-Mediated Autophagy Is Involved in N Recycling to Grains

Grain yield is affected by both soil N and remobilized N during reproductive stage (Kichey et al., 2007). To increase the NUE and crop yield, traditional methods focus on the operation of basic genes for N uptake and assimilation, such as *NRT*, *NR*, etc. (Pathak et al., 2008). In the grain-filling process, leaf organic N supply is more important because it contributes to plant N economy and limits the demand for exogenous N after flowering (Hanaoka et al., 2002). That is to say, the available N of grain was obtained from existing organic storage through recycling rather than from soil sources. Recently, studies on *Arabidopsis* and maize have shown that autophagy is the main factor affecting N recycling from senescent leaves to seeds (Guiboileau et al., 2012; Li et al., 2015). N recycling in senescent leaves was suppressed in *osatg7* at the vegetative stage, but the male sterility of *osatg7* limited evaluation of autophagy on both N economy and grain yield (Kurusu et al., 2014). Thus, we inferred that N recycling contributed by autophagy from the plant remains to grains in rice by over-expression and RNA interference of *OsATG8b*. Immunoblotting analysis results showed that autophagy activity is higher in *OsATG8b*-OE lines and a little lower in *OsATG8b*-RNAi than that in ZH11. Previous studies showed that OsATG8b antibody can also recognize OsATG8a and OsATG8c (**Supplementary Figure S9**). In *OsATG8b* RNAi lines, the band recognized by OsATG8b antibody represents the total OsATG8s, including OsATG8a, OsATG8b, and OsATG8c, so it is difficult to observe obvious differences in OsATG8b protein level with this method. Therefore, in our study, *OsATG8b*-RNAi lines showed slightly inhibited autophagic activity, which leads to reduced NRE from vegetative tissues to developing grains and finally results in reduced grain yield and quality. Meanwhile, reduced grain quality may cause decreased degradation of stored proteins in the germinating grains and then slow down the root growth at the grain germination stage. Conversely, *OsATG8b*-OE plants have higher yield and increased NRE (**Figures 6**, **7**), and higher autophagic activity (**Figure 4C**). Thus, higher autophagic activity causes increased NRE, which leads to better grain yield. These results confirm that autophagy plays a crucial role in the N recycling process in rice. Therefore, improving N recycling by operating autophagy may be a useful strategy for increasing rice yield.

DATA AVAILABILITY STATEMENT

Data of this study are included in this article and its additional files. The material that supports the findings of this study is available from the corresponding author on request.

AUTHOR CONTRIBUTIONS

MZ and TF designed the research. TF, WY, XZ, XX, YX, and ML performed experiments. TF, MZ, XF, KX, and CT analyzed data. TF and MZ wrote the manuscript. All authors read and approved the final manuscript.

FUNDING

This work was supported by the National Key Research and Development Program of China (2017YFD0100100), the National Natural Science Foundation of China (31772384/31601817), STS of the Chinese Academy of Sciences (KFJ-STS-QYZX-032) and Outstanding youth of Jiangsu Province (BK20160030), the Strategic Priority Research Program, and the Guangdong Provincial Key Laboratory of Applied Botany of the Chinese Academy of Sciences (AB2018007).

ACKNOWLEDGMENTS

We thank Prof. Yoshinori Ohsumi of Tokyo Institute of Technology for providing the *atg8* yeast strain.

SUPPLEMENTARY MATERIAL

The Supplementary Material for this article can be found online at: https://www.frontiersin.org/articles/10.3389/fpls.2020.00588/full#supplementary-material

FIGURE S1 | Phylogenetic tree of ATG8s by amino sequence alignment of different species. *Glycine max* (Gm), *Arabidopsis thaliana* (At), *Saccharomyces cerevisiae* (Sc), *Selaginella moellendorffii* (Sm), *Oryza sativa* (Os), *Homo sapiens* (Hs), *Solanum lycopersicum* (Sly), *Triticum aestivum* (Ta), and *Brachypodium distachyon* (Bd). Deduced amino acid sequences were aligned by CLUSTALX; the phylogenetic tree was generated by the neighbor-joining method and constructed using MEGA4.

FIGURE S2 | Alignment of ATG8 amino acid sequence and 3D model of OsATG8b. **(A)** Alignment of ATG8 amino acid sequences from rice, *Arabidopsis*, human, and yeast. Arrows indicate the C-terminal glycine residue, which is processed by ATG4 cysteine protease. Residues constituting W- and L-sites are colored red and green, respectively. Sc, *S. cerevisiae*; Hs, *Homo sapiens*; At, *Arabidopsis thaliana*; Os, *Oryza sativa*. **(B)** 3D models of OsATG8b. Two hydrophobic pockets responsible for the recognition of Trp and Leu are labeled W-site and L-site, respectively, and circled.

FIGURE S3 | Subcellular localization of sGFP-OsATG8b in rice protoplasts. Bars = 1 μm.

FIGURE S4 | Immunoblot detection of the vacuolar delivery of GFP in *GFP-OsATG8b* lines and immunoblot analysis with OsATG8b antibodies. Total proteins extracted from shoots of 14-day-old-seedlings in *GFP-OsATG8b* (OE) and *GFP* (G1) transgenic lines and ZH11. **(A)** Total proteins were subjected to immunoblot analysis with GFP antibody. **(B)** OsATG8b antibodies recognize the endogenous proteins OsATG8(a/b/c) as well as the GFP fusion proteins in ZH11 and *GFP-OsATG8b* transgenic lines.

FIGURE S5 | The expression of *OsATG8a* and *OsATG8c* in ZH11, *OsATG8b*-OE, and *OsATG8b*-RNAi lines. **(A)** Sequence comparison with other homologous genes for construction of *OsATG8b* RNAi. The RNAi fragment is demarcated by the box. **(B,C)** qRT-PCR analysis of *OsATG8a* and *OsATG8c* expression. The seedlings of ZH11, *OsATG8b*-OE, and *OsATG8b*-RNAi at four-leaf stage were divided into the shoots and roots. *OseEF-1a* was used as an internal reference. Error bars indicate standard deviations of independent biological replicates ($n = 3$). No asterisks mean no significant difference (*t*-test).

FIGURE S6 | *OsATG8b*-RNAi (Ri) and *OsATG8b*-OE (OE) lines exhibited a relatively normal phenotype and a similar growth rate when compared with ZH11 at 30 and 60-day after germination (DAG). **(A,B)** Phenotype of *OsATG8b*-RNAi and *OsATG8b*-OE plants grown under low (LN, 0.2 mM NH_4NO_3) **(A)** and high N contents (HN, 5 mM NH_4NO_3) **(B)** at 30 DAG. **(C,D)** Statistical analysis of root **(C)** and shoot **(D)** length of *OsATG8b*-RNAi and *OsATG8b*-OE plants grown under both LN and HN conditions at 30 DAG. **(E,F)** Phenotype of *OsATG8b*-RNAi and *OsATG8b*-OE plants grown under LN **(E)** and HN **(F)** conditions at 60 DAG. **(G,H)** Statistical analysis of root **(G)** and shoot **(H)** length of *OsATG8b*-RNAi and *OsATG8b*-OE plants grown under both LN and HN conditions, at 60 DAG. Three biological replicates, each containing thirty plants, were used for data analysis. Error bars indicate standard deviations of independent biological replicates. No asterisks mean no significant difference (*t*-test).

FIGURE S7 | ^{15}N-labeling efficiency of ZH11, *OsATG8b*-RNAi (Ri), and *OsATG8b*-OE (OE) lines. Plants at 40-day after germination were labeled for 5-day with $^{15}NO_3^-$, harvested 7-day later, and then assayed for ^{15}N content in seedlings. Results are the mean ± SD from three plants. Three biological replicates, each containing three plants, were used for data analysis.

FIGURE S8 | Spatio-temporal expression of *OsATG8a* **(A)**, *OsATG8b* **(B)**, and *OsATG8c* **(C)** in various tissues/organs throughout the entire plant growth in the field. Data were obtained from RiceXpro (http://ricexpro.dna.affrc.go.jp/).

FIGURE S9 | OsATG8b antibody cannot distinguish OsATG8a, OsATG8b, and OsATG8c. The proteins of OsATG8a, OsATG8b, and OsATG8c were expressed in *E. coli*, and detected by the anti-OsATG8b antibody.

TABLE S1 | All primers used in this study.

REFERENCES

Bassham, D. C., Laporte, M., Marty, F., Moriyasu, Y., Ohsumi, Y., Olsen, L. J., et al. (2006). Autophagy in development and stress responses of plants. *Autophagy* 2, 2–11. doi: 10.4161/auto.2092

Carlsson, N., Borde, A., Wolfel, S., Akerman, B., and Larsson, A. (2011). Quantification of protein concentration by the Bradford method in the presence of pharmaceutical polymers. *Anal. Biochem.* 411, 116–121. doi: 10.1016/j.ab.2010.12.026

Chung, T. (2011). See how I eat my greens-autophagy in plant cells. *J. Plant Biol.* 54, 339–350. doi: 10.1007/s12374-011-9176-5

Chung, T., Suttangkakul, A., and Vierstra, R. D. (2009). The ATG autophagic conjugation system in maize: ATG transcripts and abundance of the ATG8-Lipid adduct are regulated by development and nutrient availability. *Plant Physiol.* 149, 220–234. doi: 10.1104/pp.108.126714

Delrosario, A. R., Briones, V. P., Vidal, A. J., and Juliano, B. O. (1968). Composition and endosperm structure of developing and mature rice kernel. *Cereal Chem.* 45, 225–235.

Doelling, J. H., Walker, J. M., Friedman, E. M., Thompson, A. R., and Vierstra, R. D. (2002). The APG8/12-activating enzyme APG7 is required for proper nutrient recycling and senescence in *Arabidopsis thaliana*. *J. Biol. Chem.* 277, 33105–33114. doi: 10.1074/jbc.M204630200

Duan, M. J., and Sun, S. S. M. (2005). Profiling the expression of genes controlling rice grain quality. *Plant Mol. Biol.* 59, 165–178. doi: 10.1007/s11103-004-7507-3

Good, A. G., Shrawat, A. K., and Muench, D. G. (2004). Can less yield more? Is reducing nutrient input into the environment compatible with maintaining crop production? *Trends Plant Sci.* 9, 597–605. doi: 10.1016/j.tplants.2004.10.008

Guiboileau, A., Avila-Ospina, L., Yoshimoto, K., Soulay, F., Azzopardi, M., Marmagne, A., et al. (2013). Physiological and metabolic consequences of autophagy deficiency for the management of nitrogen and protein resources in *Arabidopsis* leaves depending on nitrate availability. *New Phytol.* 199, 683–694. doi: 10.1111/nph.12307

Guiboileau, A., Yoshimoto, K., Soulay, F., Bataille, M. P., Avice, J. C., and Masclaux-Daubresse, C. (2012). Autophagy machinery controls nitrogen remobilization at the whole-plant level under both limiting and ample nitrate conditions in *Arabidopsis*. *New Phytol.* 194, 732–740. doi: 10.1111/j.1469-8137.2012.04084.x

Hamasaki, M., Noda, T., Baba, M., and Ohsumi, Y. (2005). Starvation triggers the delivery of the endoplasmic reticulum to the vacuole via autophagy in yeast. *Traffic* 6, 56–65. doi: 10.1111/j.1600-0854.2004.00245.x

Hanaoka, H., Noda, T., Shirano, Y., Kato, T., Hayashi, H., Shibata, D., et al. (2002). Leaf senescence and starvation-induced chlorosis are accelerated by the disruption of an *Arabidopsis* autophagy gene. *Plant Physiol.* 129, 1181–1193. doi: 10.1104/pp.011024

Hiei, Y., Komari, T., and Kubo, T. (1997). Transformation of rice mediated by Agrobacterium tumefaciens. *Plant Mol. Biol.* 35, 205–218.

Ishida, H., Yoshimoto, K., Izumi, M., Reisen, D., Yano, Y., Makino, A., et al. (2008). Mobilization of rubisco and stroma-localized fluorescent proteins of chloroplasts to the vacuole by an ATG gene-dependent autophagic process. *Plant Physiol.* 148, 142–155. doi: 10.1104/pp.108.122770

Izumi, M., Hidema, J., Wada, S., Kondo, E., Kurusu, T., Kuchitsu, K., et al. (2015). Establishment of monitoring methods for autophagy in rice reveals autophagic recycling of chloroplasts and root plastids during energy limitation. *Plant Physiol.* 167, 1307–1316. doi: 10.1104/pp.114.254078

Kichey, T., Hirel, B., Heumez, E., Dubois, F., and Le Gouis, J. (2007). In winter wheat (*Triticum aestivum* L.), post-anthesis nitrogen uptake and remobilisation to the grain correlates with agronomic traits and nitrogen physiological markers. *Field Crop. Res.* 102, 22–32. doi: 10.1016/j.fcr.2007.01.002

Kim, S. H., Kwon, C., Lee, J. H., and Chung, T. (2012). Genes for plant autophagy: functions and interactions. *Mol. Cells* 34, 413–423. doi: 10.1007/s10059-012-0098-y

Kirisako, T., Baba, M., Ishihara, N., Miyazawa, K., Ohsumi, M., Yoshimori, T., et al. (1999). Formation process of autophagosome is traced with Apg8/Aut7p in yeast. *J. Cell Biol.* 147, 435–446. doi: 10.1083/jcb.147.2.435

Kliosnky, D. (2016). Guidelines for the use and interpretation of assays for monitoring autophagy (3rd edition). *Autophagy* 12, 1–222. doi: 10.1080/15548627.2015.1100356

Kuma, A., Matsui, M., and Mizushima, N. (2007). LC3, an autophagosome marker, can be incorporated into protein aggregates independent of autophagy. *Autophagy* 3, 323–328. doi: 10.4161/auto.4012

Kurusu, T., Koyano, T., Hanamata, S., Kubo, T., Noguchi, Y., Yagi, C., et al. (2014). *OsATG7* is required for autophagy-dependent lipid metabolism in rice postmeiotic anther development. *Autophagy* 10, 878–888. doi: 10.4161/auto.28279

Li, F. Q., Chung, T., Pennington, J. G., Federico, M. L., Kaeppler, H. F., Kaeppler, S. M., et al. (2015). Autophagic recycling plays a central role in maize nitrogen remobilization. *Plant Cell.* 27, 1389–1408. doi: 10.1105/tpc.15.00158

Li, F. Q., and Vierstra, R. D. (2012). Autophagy: a multifaceted intracellular system for bulk and selective recycling. *Trends Plant Sci.* 17, 526–537. doi: 10.1016/j.tplants.2012.05.006

Lin, Z. M., Zhang, X. C., Yang, X. Y., Li, G. H., Tang, S., Wang, S. H., et al. (2014). Proteomic analysis of proteins related to rice grain chalkiness using iTRAQ and a novel comparison system based on a notched-belly mutant with white-belly. *BMC Plant Biol.* 14:163. doi: 10.1186/1471-2229-14-163

Masclaux-Daubresse, C. (2016). Autophagy controls carbon, nitrogen, and redox homeostasis in plants. *Autophagy* 12, 896–897. doi: 10.4161/auto.36261

Masclaux-Daubresse, C., and Chardon, F. (2011). Exploring nitrogen remobilization for seed filling using natural variation in *Arabidopsis thaliana*. *J. Exp. Bot.* 62, 2131–2142. doi: 10.1093/jxb/erq405

Masclaux-Daubresse, C., Daniel-Vedele, F., Dechorgnat, J., Chardon, F., Gaufichon, L., and Suzuki, A. (2010). Nitrogen uptake, assimilation and remobilization in plants: challenges for sustainable and productive agriculture. *Ann. Bot. Lond.* 105, 1141–1157. doi: 10.1093/aob/mcq028

Masclaux-Daubresse, C., Reisdorf-Cren, M., and Orsel, M. (2008). Leaf nitrogen remobilisation for plant development and grain filling. *Plant Biol.* 10, 23–36. doi: 10.1111/j.1438-8677.2008.00097.x

Masclaux-Daubresse, C., Valadier, M. H., Carrayol, E., Reisdorf-Cren, M., and Hirel, B. (2002). Diurnal changes in the expression of glutamate dehydrogenase andnitrate reductase are involved in the C/N balance of tobacco source leaves. *Plant Cell Environ.* 25, 1451–1462. doi: 10.1046/j.1365-3040.2002.00925.x

Michaeli, S., Galili, G., Genschik, P., Fernie, A. R., and Avin-Wittenberg, T. (2016). Autophagy in plants – What's new on the menu? *Trends Plant Sci.* 21, 134–144. doi: 10.1016/j.tplants.2015.10.008

Nakatogawa, H., Ichimura, Y., and Ohsumi, Y. (2007). Atg8, a ubiquitin-like protein required for autophagosome formation, mediates membrane tethering and hemifusion. *Cell* 130, 165–178. doi: 10.1016/j.cell.2007.05.021

Nakatogawa, H., Suzuki, K., Kamada, Y., and Ohsumi, Y. (2009). Dynamics and diversity in autophagy mechanisms: lessons from yeast. *Nat. Rev. Mol. Cell Biol.* 10, 458–467. doi: 10.1038/nrm2708

Noda, N. N., Ohsumi, Y., and Inagaki, F. (2010). Atg8-family interacting motif crucial for selective autophagy. *FEBS Lett.* 584, 1379–1385. doi: 10.1016/j.febslet.2010.01.018

Ohsumi, Y. (2014). Historical landmarks of autophagy research. *Cell Res.* 24, 9–23. doi: 10.1038/cr.2013.169

Okano, Y., Miki, D., and Shimamoto, K. (2008). Small interfering RNA (siRNA) targeting of endogenous promoters induces DNA methylation, but not necessarily gene silencing, in rice. *Plant J.* 53, 65–77. doi: 10.1111/j.1365-313X.2007.03313.x

Pathak, R. R., Ahmad, A., Lochab, S., and Raghuram, N. (2008). Molecular physiology of plant nitrogen use efficiency and biotechnological options for its enhancement. *Curr. Sci. India* 94, 1394–1403.

Pei, D., Zhang, W., Sun, H., Wei, X. J., Yue, J. Y., and Wang, H. Z. (2014). Identification of autophagy-related genes ATG4 and ATG8 from wheat (*Triticum aestivum* L.) and profiling of their expression patterns responding to biotic and abiotic stresses. *Plant Cell Rep.* 33, 1697–1710. doi: 10.1007/s00299-014-1648-x

Phillips, A. R., Suttangkakul, A., and Vierstra, R. D. (2008). The ATG12-conjugating enzyme ATG10 is essential for autophagic vesicle formation in *Arabidopsis thaliana*. *Genetics* 178, 1339–1353. doi: 10.1534/genetics.107.086199

Roberts, I. N., Caputo, C., Criado, M. V., and Funk, C. (2012). Senescence-associated proteases in plants. *Physiol. Plantarum.* 145, 130–139. doi: 10.1111/j.1399-3054.2012.01574.x

Rose, T. L., Bonneau, L., Der, C., Marty-Mazars, D., and Marty, F. (2006). Starvation-induced expression of autophagy-related genes in *Arabidopsis*. *Biol. Cell.* 98, 53–67. doi: 10.1042/BC20040516

Siebenmorgen, T. J., Grigg, B. C., and Lanning, S. B. (2013). Impacts of preharvest factors during kernel development on rice quality and functionality. *Annu. Rev. Food Sci. T* 4, 101–115. doi: 10.1146/annurev-food-030212-182644

Slavikova, S., Shy, G., Yao, Y. L., Giozman, R., Levanony, H., Pietrokovski, S., et al. (2005). The autophagy-associated *Atg8* gene family operates both under favourable growth conditions and under starvation stresses in *Arabidopsis* plants. *J. Exp. Bot.* 56, 2839–2849. doi: 10.1093/jxb/eri276

Slavikova, S., Ufaz, S., Avin-Wittenberg, T., Levanony, H., and Galili, G. (2008). An autophagy-associated Atg8 protein is involved in the responses of *Arabidopsis* seedlings to hormonal controls and abiotic stresses. *J. Exp. Bot.* 59, 4029–4043. doi: 10.1093/jxb/ern244

Suttangkakul, A., Li, F. Q., Chung, T., and Vierstra, R. D. (2011). The ATG1/ATG13 protein kinase complex is both a regulator and a target of autophagic recycling in *Arabidopsis*. *Plant Cell.* 23, 3761–3779. doi: 10.1105/tpc.111.090993

Suzuki, K., and Ohsumi, Y. (2007). Molecular machinery of autophagosome formation in yeast, *Saccharomyces cerevisiae*. *FEBS Lett.* 581, 2156–2161. doi: 10.1016/j.febslet.2007.01.096

Thompson, A. R., Doelling, J. H., Suttangkakul, A., and Vierstra, R. D. (2005). Autophagic nutrient recycling in *Arabidopsis* directed by the ATG8 and ATG12 conjugation pathways. *Plant Physiol.* 138, 2097–2110. doi: 10.1104/pp.105.060673

Wada, S., Hayashida, Y., Izumi, M., Kurusu, T., Hanamata, S., Kanno, K., et al. (2015). Autophagy supports biomass production and nitrogen use efficiency at the vegetative stage in rice. *Plant Physiol.* 168, 60–73. doi: 10.1104/pp.15.00242

Wada, S., Ishida, H., Izumi, M., Yoshimoto, K., Ohsumi, Y., Mae, T., et al. (2009). Autophagy plays a role in chloroplast degradation during senescence in individually darkened leaves. *Plant Physiol.* 149, 885–893. doi: 10.1104/pp.108.130013

Wang, M., Chen, C., Xu, Y. Y., Jiang, R. X., Han, Y., Xu, Z. H., et al. (2004). A practical vector for efficient knockdown of gene expression in rice (*Oryza sativa* L.). *Plant Mol. Biol. Rep.* 22, 409–417. doi: 10.1007/bf02772683

Xia, K. F., Liu, T., Ouyang, J., Wang, R., Fan, T., and Zhang, M. Y. (2011). Genome-wide identification, classification, and expression analysis of autophagy-associated gene homologues in rice (*Oryza sativa* L.). *DNA Res.* 18, 363–377. doi: 10.1093/dnares/dsr024

Xia, T. M., Xiao, D., Liu, D., Chai, W. T., Gong, Q. Q., and Wang, N. N. (2012). Heterologous expression of *ATG8c* from Soybean confers tolerance to nitrogen deficiency and increases yield in *Arabidopsis*. *PLoS One* 7:e37217. doi: 10.1371/journal.pone.0037217

Xie, Z. P., and Klionsky, D. J. (2007). Autophagosome formation: core machinery and adaptations. *Nat. Cell Biol.* 9, 1102–1109. doi: 10.1038/ncb1007-1102

Xie, Z. P., Nair, U., and Klionsky, D. J. (2008). Atg8 controls phagophore expansion during autophagosome formation. *Mol. Biol. Cell.* 19, 3290–3298. doi: 10.1091/mbc.e07-12-1292

Yamaguchi, M., Noda, N. N., Nakatogawa, H., Kumeta, H., Ohsumi, Y., and Inagaki, F. (2010). Autophagy-related protein 8 (Atg8) family inte racting motif in Atg3 mediates the Atg3-Atg8 interaction and is crucial for the cytoplasm-to-vacuole targeting pathway. *J. Biol. Chem.* 285, 29599–29607. doi: 10.1074/jbc.m110.113670

Yang, J. C., and Zhang, J. H. (2010). Crop management techniques to enhance harvest index in rice. *J. Exp. Bot.* 61, 3177–3189. doi: 10.1093/jxb/erq112

Yoneyama, T., Tanno, F., Tatsumi, J., and Mae, T. (2016). Whole-plant dynamic system of nitrogen use for vegetative growth and grain filling in rice plants (*Oryza sativa* L.) as revealed through the production of 350 grains from a germinated seed over 150 days: a review and synthesis. *Front. Plant Sci.* 7:1151. doi: 10.3389/fpls.2016.01151

Yoshida, S., Forno, D. A., Cook, J. H., and Gomez, K. A. (eds) (1976). "Routine procedures for growing rice plants in culture solution", in *Laboratory Manual for Physiological Studies of Rice* (Los Banos, Philippines: International Rice Research Institute), 61–66.

Yoshimoto, K. (2012). Beginning to understand autophagy, an intracellular self-degradation system in plants. *Plant Cell Physiol.* 53, 1355–1365. doi: 10.1093/pcp/pcs099

Yoshimoto, K., Hanaoka, H., Sato, S., Kato, T., Tabata, S., Noda, T., et al. (2004). Processing of ATG8s, ubiquitin-like proteins, and their deconjugation by ATG4s are essential for plant autophagy. *Plant Cell.* 16, 2967–2983. doi: 10.1105/tpc.104.025395

Yoshimoto, K., Jikumaru, Y., Kamiya, Y., Kusano, M., Consonni, C., Panstruga, R., et al. (2009). Autophagy negatively regulates cell death by controlling NPR1-dependent salicylic acid signaling during senescence and the innate immune response in *Arabidopsis*. *Plant Cell.* 21, 2914–2927. doi: 10.1105/tpc.109.068635

Zhen, X., Xu, F., Zhang, W., and Li, X. (2019). Overexpression of rice gene OsATG8b confers tolerance to nitrogen starvation and increases yield and nitrogen use efficiency (NUE) in *Arabidopsis*. *PLoS One* 14:e0223011. doi: 10.1371/journal.pone.0223011

Zientara-Rytter, K., and Sirko, A. (2016). To deliver or to degrade – an interplay of the ubiquitin-proteasome system, autophagy and vesicular transport in plants. *FEBS J.* 283, 3534–3555. doi: 10.1111/febs.13712

Conflict of Interest: The authors declare that the research was conducted in the absence of any commercial or financial relationships that could be construed as a potential conflict of interest.

frontiers in Plant Science

ORIGINAL RESEARCH
published: 04 June 2020
doi: 10.3389/fpls.2020.00563

Short-Term Magnesium Deficiency Triggers Nutrient Retranslocation in *Arabidopsis thaliana*

*Takaaki Ogura[1], Natsuko I. Kobayashi[1], Christian Hermans[2], Yasunori Ichihashi[3], Arisa Shibata[4], Ken Shirasu[4], Naohiro Aoki[1], Ryohei Sugita[1], Takahiro Ogawa[1], Hisashi Suzuki[5], Ren Iwata[6], Tomoko M. Nakanishi[1,7] and Keitaro Tanoi[1,8]**

[1] Graduate School of Agricultural and Life Sciences, The University of Tokyo, Tokyo, Japan, [2] Crop Production and Biostimulation Laboratory, Interfacultary School of Bioengineers, Université libre de Bruxelles, Brussels, Belgium, [3] RIKEN BioResource Research Center, Tsukuba, Japan, [4] RIKEN Center for Sustainable Resource Science, Yokohama, Japan, [5] National Institute of Radiological Sciences, National Institutes for Quantum and Radiological Science and Technology, Chiba, Japan, [6] Cyclotron and Radioisotope Center, Tohoku University, Sendai, Japan, [7] Hoshi University, Tokyo, Japan, [8] PRESTO, Japan Science and Technology Agency, Kawaguchi, Japan

OPEN ACCESS

Edited by:
Francisco Rubio,
Spanish National Research Council, Spain

Reviewed by:
Ioannis E. Papadakis,
Agricultural University of Athens, Greece
R.J. Tang,
University of California, Berkeley, United States
Mokded Rabhi,
Center of Biotechnology of Borj Cedria (CBBC), Tunisia

***Correspondence:**
Keitaro Tanoi
uktanoi@g.ecc.u-tokyo.ac.jp

Specialty section:
This article was submitted to Plant Nutrition, a section of the journal Frontiers in Plant Science

Received: 05 December 2019
Accepted: 15 April 2020
Published: 04 June 2020

Citation:
Ogura T, Kobayashi NI, Hermans C, Ichihashi Y, Shibata A, Shirasu K, Aoki N, Sugita R, Ogawa T, Suzuki H, Iwata R, Nakanishi TM and Tanoi K (2020) Short-Term Magnesium Deficiency Triggers Nutrient Retranslocation in Arabidopsis thaliana. Front. Plant Sci. 11:563. doi: 10.3389/fpls.2020.00563

Magnesium (Mg) is essential for many biological processes in plant cells, and its deficiency causes yield reduction in crop systems. Low Mg status reportedly affects photosynthesis, sucrose partitioning and biomass allocation. However, earlier physiological responses to Mg deficiency are scarcely described. Here, we report that Mg deficiency in *Arabidopsis thaliana* first modified the mineral profile in mature leaves within 1 or 2 days, then affected sucrose partitioning after 4 days, and net photosynthesis and biomass production after 6 days. The short-term Mg deficiency reduced the contents of phosphorus (P), potassium, manganese, zinc and molybdenum in mature but not in expanding (young) leaves. While P content decreased in mature leaves, P transport from roots to mature leaves was not affected, indicating that Mg deficiency triggered retranslocation of the mineral nutrients from mature leaves. A global transcriptome analysis revealed that Mg deficiency triggered the expression of genes involved in defence response in young leaves.

Keywords: defense response, magnesium transporter, mineral profile, nutrient deficiency, photosynthesis, sucrose partitioning, translocation

INTRODUCTION

The magnesium ion (Mg^{2+}) is the second most abundant cation in plant cells after potassium (Marschner, 1995) and is engaged in crucial biological functions for plants, such as stabilisation of chlorophyll (Strouse, 1974) and ribosome (Akanuma et al., 2014) structures and the regulation of enzymatic activities (Clarkson and Hanson, 1980; Cowan, 2002). Crop fertilisation most often focuses on nitrogen (N), phosphorus (P) and potassium (K), but ignores Mg (Fageria et al., 2008). Nonetheless, Mg deficiency affects the productivity of various crops (cereals, potatoes, sugar beets, etc.) and fruits (Gerendás and Führs, 2013).

The apparent symptom of Mg deficiency is interveinal chlorosis as a result of chlorophyll degradation (Marschner, 1995; Tanoi and Kobayashi, 2015). However, chlorophyll degradation is a late-stage symptom, because Mg bound to chlorophyll is not readily lost (Marschner, 1995). One of the earliest reported physiological symptoms is accumulation of sucrose and starch

(Fischer and Bremer, 1993; Fischer et al., 1998; Hermans et al., 2004, 2005; Hermans and Verbruggen, 2005), due to impaired sucrose phloem loading from leaves (King and Zeevaart, 1974; Fischer and Bremer, 1993; Cakmak et al., 1994a,b; Hermans et al., 2005). Hermans and Verbruggen (2005) suggested that sucrose accumulation leads to the reduction in chlorophyll content through the repression of *CHLOROPHYLL A/B BINDING PROTEIN 2* (*CAB2*) gene. Cakmak and Kirkby (2008) proposed that sugar accumulation leads to chlorophyll degradation through the generation of reactive oxygen species (ROS); high sugar levels exert a negative feedback on photosynthesis (Sheen, 1994; Oswald et al., 2001), and the use of light energy for the photosynthetic electron transport chain decreases. This results in surplus light energy, which provides reducing equivalents with molecular oxygen to form ROS. Meanwhile, recent studies suggest that sugar accumulation is not the only cause of ROS generation, as the oxidative damage is detected in leaves of Mg-deficient rice before sugars accumulate (Kobayashi et al., 2013b, 2018) and roots of Mg-deficient sweet orange (Cai et al., 2019). Apart from that, a decrease in leaf transpiration is reported in Mg-deficient rice (Kobayashi et al., 2013b) and maize (Jezek et al., 2015), and this is suggested to be responsible for chlorosis development (Kobayashi et al., 2013b). To further clarify the mechanisms whereby Mg deficiency leads to chlorosis, it is important to identify early responses.

To cope with mineral deficiency, higher plants have strategies to optimise use and acquisition of deficient minerals. Retranslocation of minerals is the first strategy for plants to maintain growth during deficiency. This strategy requires mostly phloem transport of minerals from mature leaves. The mobility of Mg is highly variable among plant species, with retranslocation found in barley, bread wheat, rapeseed (Maillard et al., 2015), European ash (Hagen-Thorn et al., 2006) and Pedunculated oak (Hagen-Thorn et al., 2006; Maillard et al., 2015) but not in Arabidopsis (Himelblau and Amasino, 2001), maize, pea, black alder, black poplar (Maillard et al., 2015), silver birch or small-leaved lime (Hagen-Thorn et al., 2006). Mineral retranslocation is also induced during leaf senescence, and retranslocation of essential minerals during leaf senescence has been described in various plant species (Himelblau and Amasino, 2001; Waters and Grusak, 2008; Moreira and Fageria, 2009; Maillard et al., 2015). Meanwhile, studies on mineral deficiency mainly focus on retranslocation of the deficient mineral and rarely describe the profile of other minerals.

The second strategy is for roots to increase the uptake of deficient minerals. This strategy either induces the expression of root transporters (Gojon et al., 2009), stimulates the root growth (De Pessemier et al., 2013; Gruber et al., 2013) or exudes organic compounds that mobilise some minerals (Dakora and Phillips, 2002). The induction of root Mg^{2+} uptake is characterised in Arabidopsis (Ogura et al., 2018) and rice (Tanoi et al., 2014), and Mg^{2+} transporter family MITOCHONDRIA RNA SPLICING 2/MAGNESIUM TRANSPORTER (MRS2/MGT; Schock et al., 2000; Li et al., 2001) is indicated to be putatively responsible (Mao et al., 2014; Ogura et al., 2018). However, there is uncertainty regarding the root transcriptional regulation of *MRS2/MGT* genes with some reports suggesting that Mg deficiency induces root transcript levels of *MRS2/MGT* (Mao et al., 2014; Li et al., 2017; Liu et al., 2019) and others suggesting no transcriptional induction of *MRS2/MGT* (Gebert et al., 2009; Hermans et al., 2010a,b; Ogura et al., 2018).

The aims of the current study were firstly to identify the physiological and transcriptional responses to Mg deficiency prior to the reported physiological symptoms such as sugar accumulation. Since the symptoms of mineral deficiency usually appear on leaves at a specific age, leaf-specific responses were investigated in Arabidopsis. Secondly, the mineral profile of Mg-deficient plants was investigated for possible retranslocation of Mg and other minerals. Finally, the effects of Mg deficiency on root Mg^{2+} uptake and the expression of putative Mg^{2+} transporters in roots were re-examined.

MATERIALS AND METHODS

Hydroponic Culture System

For all measurements, with the exception of root morphology analysis, *Arabidopsis thaliana* ecotype Columbia-0 (Inplanta Innovations Inc., Yokohama, Japan) was grown hydroponically. Three to four seeds were placed on a piece of soaked polyurethane sponge (KP-1300, Hikari, Osaka, Japan) 5 mm in thickness. Up to 32 sponges were set into a float and placed in a container with 2 L of a hydroponic solution. The containers were covered with plastic wrap to make a high humidity environment for germination and placed in a growth room at 22°C and under a photoperiod of 16 h light (100 μmol m^{-2} s^{-1})/8 h darkness. After 1 week, the plastic wrap was removed, and the seedlings were thinned to leave one seedling per sponge. Ten days after germination, half of the plants were subjected to Mg deficiency treatment. At this point (day 0), the size of the first two rosette leaves was similar to that of the cotyledons, and the third and fourth rosette leaves had just appeared. We refer to the first two rosette leaves and the next two rosette leaves as mature leaves and expanding leaves, respectively (**Figure 1**). After the onset of Mg deficiency treatment, the fresh shoots and roots were separately weighed for four plants every 2 days, and the shoot-to-root fresh

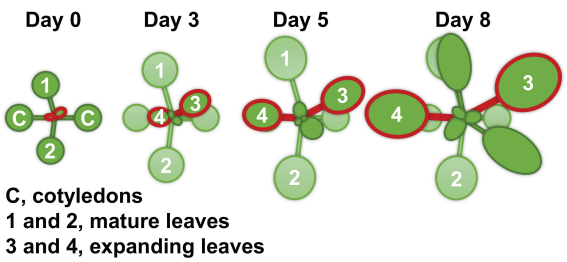

FIGURE 1 | A schematic diagram of the shoot growth of *Arabidopsis thaliana* under the control condition (magnesium 1.5 mM). The Columbia-0 accession was grown hydroponically at 22°C and under a photoperiod of 16 h light (100 μmol m^{-2} s^{-1})/8 h darkness. Ten days after germination (day 0 of treatment), half of the plants were subjected to Mg deficiency (no Mg added). Mature leaves are identified as the first two leaves 1 and 2, and expanding leaves as 3 and 4.

weight ratio was calculated. The two expanding leaves of each plant were weighed for eight plants every day from day 2. For the hydroponic solution, we used the MGRL solution (Fujiwara et al., 1992), which contained 1.5 mM $MgSO_4$, 3.0 mM KNO_3, 2.0 mM $Ca(NO_3)_2$, 1.5 mM NaH_2PO_4, 0.25 mM Na_2HPO_4, 30 μM H_3BO_3, 10 μM $MnSO_4$, 8.6 μM $FeSO_4$, 0.13 μM $CoCl_2$, 1.0 μM $CuSO_4$, 1.0 μM $ZnSO_4$, 0.024 μM $(NH_4)_6Mo_7O_{24}$ and 67 μM EDTA-2Na (pH 5.8). For the Mg deficiency treatment, 1.5 mM $MgSO_4$ in the original MGRL solution was substituted with 1.5 mM Na_2SO_4 to compensate for the lack of sulphate. All the hydroponic solutions were renewed every 2 days.

Chlorophyll Content Analysis

Chlorophyll content in expanding leaves was determined for eight plants. Leaves were flash-frozen with liquid nitrogen, and chlorophyll was extracted with 250 μL of 80% (v/v) acetone using a bead homogeniser (BMS-A20TP, Bio Medical Science, Tokyo, Japan). The extract was left overnight at 4°C and centrifuged at 14,000 *g* for 10 min. The supernatant was analysed for its optical densities by a UV-Vis spectrophotometer (NanoDrop, Thermo Fisher Scientific, Waltham, MA, United States) at 647 and 664 nm. The total content of chlorophylls *a* and *b* in the extract was determined by including two optical density values in the equations described by Porra et al. (1989).

Determination of Carbon Assimilation and Photosynthate Partitioning

The carbon dioxide (CO_2) assimilation in leaves and subsequent photosynthate partitioning were evaluated radiometrically using radiolabelled CO_2 ($^{14}CO_2$), as previously described by Sugita et al. (2018). The $^{14}CO_2$ molecules (0.2 MBq) were generated in a vial by the chemical reaction between ^{14}C-sodium bicarbonate (200 kBq, PerkinElmer, Waltham, MA, United States) and lactic acid. At 12 h into the light period, four plants from each treatment were supplied with $^{14}CO_2$ for 15 min at 22°C by sending air from the vial to an airtight polypropylene bag containing all plants. Immediately after the $^{14}CO_2$ introduction, all leaves and roots were separated and contacted to an Imaging Plate (BAS-IP MS, GE Healthcare, Buckinghamshire, United Kingdom) at 4°C. The Imaging Plate was scanned by a laser scanner (FLA-5000, GE Healthcare, Buckinghamshire, United Kingdom), and ^{14}C in each part of the plant was quantified with an image analysis software (Image Gauge, Fujifilm, Tokyo, Japan). The CO_2 assimilation rate was determined after dividing the amount of ^{14}C assimilated in leaves for 15 min by the leaf area.

Sugar Quantification

The sucrose and glucose contents in expanding leaves were determined enzymatically according to Okamura et al. (2016). Expanding leaves were harvested and composited from two to five plants (ca. 10 mg fresh weight) at 3 h into the light period. The composited sample was flash-frozen with liquid nitrogen and powdered with a bead homogeniser (BMS-A20TP, Bio Medical Science, Tokyo, Japan). Soluble sugars were successively extracted by double extraction using 500 and 200 μL of 80% (v/v) ethanol at 80°C for 10 min each time. After evaporation, samples were resuspended in 250 μL of distilled water using an ultrasonic bath (Branson 1200, Yamato Scientific, Tokyo, Japan). The contents of sucrose and glucose in solution were quantified with the F-kit #716260 (J. K. International, Tokyo, Japan).

Elemental Analysis

The contents of mineral elements were determined in mature leaves, expanding leaves and roots. The fresh tissue samples were harvested from four plants, weighed separately and dried overnight at 60°C. The dried sample was digested with 2 mL of 30% (v/v) HNO_3 (Kanto Chemical, Tokyo, Japan) at 90°C for 1 h. The digested solution was diluted 30× with Milli-Q water (Merck Millipore, Burlington, MA, United States) and filtered before the elemental analysis. The inductively coupled plasma-mass spectrometer NexION 350S (PerkinElmer, Waltham, MA, United States) was used to determine the contents of Mg, P, K, calcium (Ca), boron (B), manganese (Mn), copper (Cu), zinc (Zn) and molybdenum (Mo) in the digested solution.

Determination of Phosphorus Transport

The process of P transport from roots to leaves was evaluated radiometrically with radiolabelled phosphate (^{32}P-phosphate), as previously described by Sugita et al. (2017). The ^{32}P-phosphate (PerkinElmer, Waltham, MA, United States) was added to each treatment solution (6 MBq L^{-1}; phosphate, 1.75 mM) and introduced into four plants by soaking their roots for 30 min at 22°C under light conditions (100 μmol m^{-2} s^{-1}). Roots were subsequently rinsed for 10 min with an ice-cold MGRL solution to wash out ^{32}P from the apoplast. Phosphorus transported into mature and expanding leaves was separately quantified using an Imaging Plate (BAS-IP MS, GE Healthcare, Buckinghamshire, United Kingdom), as previously described by Kobayashi et al. (2013a).

Global Transcriptome Analysis

The transcriptome was analysed with RNA sequencing (RNA-seq, Ozsolak and Milos, 2011). Mature leaves, expanding leaves and roots were separated, and tissues from two or three plants (ca. 5–30 mg fresh weight) were composited. A protocol of Breath Adapter Directional sequencing (BrAD-seq; Townsley et al., 2015; Ichihashi et al., 2018) was used to construct a strand-specific RNA-seq library, with which the entire transcriptome can be analysed including vital non-processed RNAs (Mills et al., 2013). Briefly, six tissue samples were lysed with a lysis/binding buffer and mRNA was extracted from the lysate. The quality of RNA was assessed with an Agilent 2100 Bioanalyzer and at least three biological replicates were selected for further analysis. After mRNA was fragmented and primed with 3′ adapter, cDNA was synthesised and strand-specific 5′ adapter sequence was added and incorporated. The average fragment length of the constructed library was approximately 400 bp. All the libraries were pooled and subjected to 50 bp single-end sequencing with Illumina HiSeq 2500 by Macrogen Japan (Kyoto, Japan).

The obtained reads were analysed according to Ichihashi et al. (2018). Briefly, the reads were mapped to the TAIR10 Arabidopsis reference genome sequence after removing low-quality reads. The mapped reads were counted, and the count data were normalised.

The raw reads and normalised count data have been deposited in NCBI's Gene Expression Omnibus (Edgar et al., 2002) and are accessible through GEO Series accession number GSE140070. Changes in gene expression by Mg deficiency were determined as the logarithm of A/B to the base two, with A and B a normalised count of Mg-deficient plants and that of control plants, respectively. Thereafter, the statistical analysis identified the differentially expressed genes (DEGs) during deficiency by using the Exact Test ($p < 0.01$, Robinson and Smyth, 2008) incorporated in edgeR Bioconductor package (Robinson et al., 2010). The up- and down-regulated genes were subjected to gene ontology (GO) enrichment analysis. The GO enrichment was determined by PANTHER Overrepresentation Test, using GO Ontology database released on the 6th of September 2018 for the annotation version, GO biological process complete for the annotation dataset, and the Fisher's exact test with a false discovery rate (FDR) correction ($p < 0.05$) for the test type.

Determination of Root Magnesium Uptake

The root Mg^{2+} uptake rate was determined radiometrically, as previously described by Tanoi et al. (2013). The radioisotope ^{28}Mg was produced with $^{27}Al(\alpha, 3p)^{28}Mg$ reaction in a cyclotron and was purified following the procedure of Iwata et al. (1992). Four plants from each treatment were fed with 1/30-strength MGRL solution containing ^{28}Mg (6 MBq L^{-1}; Mg^{2+}, 50 μM) for 1 h at 22°C under light conditions (100 μmol m^{-2} s^{-1}). Roots were subsequently rinsed for 10 min with an ice-cold MGRL solution to wash out ^{28}Mg from the apoplast. After harvest, the whole plant tissue was solubilised with 0.5 mL of Soluene® - 350 (PerkinElmer, Waltham, MA, United States) and mixed with 3 mL of liquid scintillation cocktail (Hionic-Fluor, PerkinElmer, Waltham, MA, United States). Magnesium taken up by each plant was quantified using a liquid scintillation counter (LSC-6100, Aloka, Tokyo, Japan), as previously described by Sugita et al. (2013). Since the ^{28}Mg half-life is ca. 21 h and its radioactivity decreased while all the samples were analysed, the activity at the same time point was calculated for all the samples.

Root Morphology Analysis

The morphology of the root system was examined for the wild type Columbia-0 and the following transfer DNA (T-DNA) insertion lines of *MRS2*/*MGT* genes: single mutant lines of *MRS2-4*/*MGT6*, *MRS2-1*/*MGT2* and *MRS2-10*/*MGT1*, and the three double and one triple mutant lines of *MRS2* genes that belong to the MRS2 subclade B (Gebert et al., 2009), namely *MRS2-1*/*MGT2*, *MRS2-5*/*MGT3* and *MRS2-10*/*MGT1*. Seeds of *mrs2-4* (SALK_145997) were provided by Dr. T. Kamiya (Oda et al., 2016), and seeds of *mrs2-1* (SALK_006797C), *mrs2-10* (SALK_100361C), *mrs2-1* × *mrs2-5*, *mrs2-1* × *mrs2-10*, *mrs2-5* × *mrs2-10* and *mrs2-1* × *mrs2-5* × *mrs2-10* lines were provided by Dr. V. Knoop (Gebert et al., 2009; Lenz et al., 2013). Seeds were surface sterilised with 70% (v/v) ethanol for 10 min and 20% (v/v) HClO solution for 5 min, and rinsed twice with sterile water. Plant growth conditions were as described in Xiao et al. (2015). Briefly, seeds were plated on 1× strength Murashige and Skoog medium (Murashige and Skoog, 1962) modified to contain a single source and lower concentration of nitrogen (10 mM KNO_3), 1% (w/v) sucrose, 0.8% (w/v) agar (high gel strength agar, A9799, Sigma-Aldrich, St. Louis, MO, United States) and a final pH of 5.7. Control or low Mg plates contained 1,500 μM $MgSO_4$ or 5 μM $MgSO_4$ + 1,495 μM Na_2SO_4, respectively. Seeds were stratified at 4°C for 2 days and incubated in a growth chamber at 22°C and under a photoperiod of 16 h light (100 μmol m^{-2} s^{-1})/8 h darkness. Ten days after germination, root morphology parameters were measured for 13–38 seedlings, as described in Xiao et al. (2015), and fresh root and shoot organs were separately weighed.

Statistical Analysis

The Student's *t*-test was carried out using Microsoft Excel version 1909 to compare differences in the measured variables between control and Mg-deficient plants. A factorial analysis of variance (ANOVA) was used to test differences of the measured variables in the root morphology analysis. When a difference was found, the Tukey-Kramer test was carried out using R software version 3.6.0 to compare the values of different lines and to test in which comparison the difference was significant. Significance was set at the 5% level.

RESULTS

Growth and Leaf Chlorophyll Content Were Affected After Six Days of Magnesium Deficiency

To characterise early responses to Mg deficiency, we cultivated wild-type Arabidopsis plants hydroponically for 10 days with a Mg-replete solution (1.5 mM) and then fed half of the plants with a Mg-deplete (0 mM) solution. Fresh biomass production of the whole shoot, expanding leaves and root was measured during 8 days of treatment. In control plants, the fresh weight of the whole shoot and expanding leaves gradually increased (**Figure 2A**). In Mg-deficient plants, the biomass production was affected on day 6, when the fresh weight of the whole shoot and expanding leaves were 13% ($p < 0.05$) and 44% ($p < 0.01$) lower, respectively, compared to the control plants (**Figure 2A**). However, there was no difference in the root fresh weight between Mg conditions until day 8 (**Figure 2B**). Therefore, the shoot-to-root fresh weight ratio was lower ($p < 0.05$) in Mg-deficient plants from day 6 (**Figure 2C**).

Chlorophyll content was measured in expanding leaves between days 4 and 8, when the plants exhibited strong growth inhibition due to Mg deficiency. The chlorophyll content was unaffected until day 5 and decreased thereafter during Mg deficiency compared to the control plants (**Figure 2D**). On day 6, the chlorophyll content in Mg-deficient leaves was 52% lower ($p < 0.01$) compared to the control leaves (**Figure 2D**). Therefore, the time window of chlorophyll reduction overlapped with the reduction in shoot fresh weight.

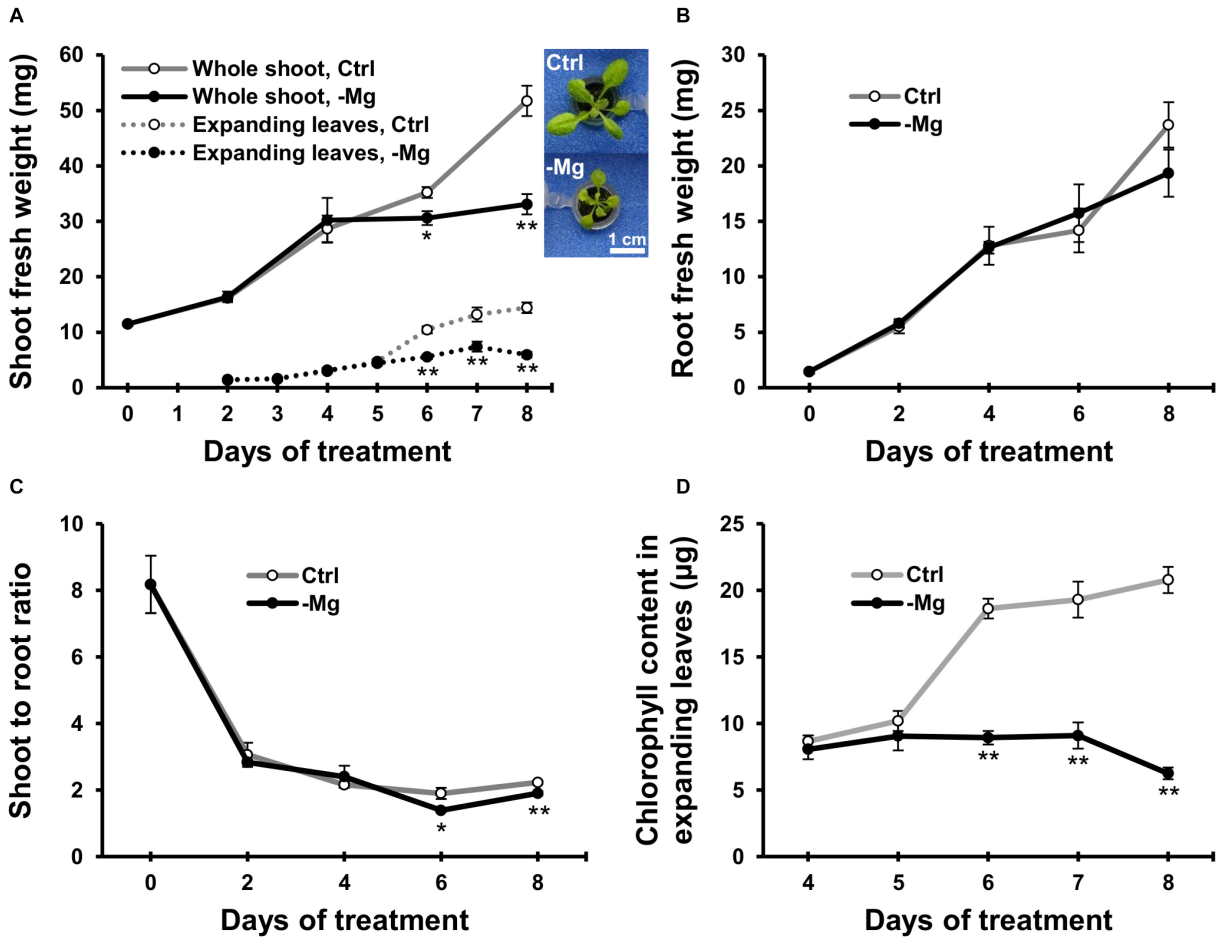

FIGURE 2 | Effect of magnesium deficiency on biomass production and chlorophyll content. **(A)** Evolution of the fresh weight of the whole shoot (solid lines, $n = 4$) and expanding leaves (dotted lines, $n = 8$). The inserted images are the representative plant phenotypes on day 8 of control and Mg deficiency treatment. Scale bar: 1 cm. **(B)** Evolution of the fresh weight of root organs ($n = 4$). **(C)** The shoot-to-root ratio on the basis of fresh weight ($n = 4$). **(D)** The chlorophyll content in expanding leaves ($n = 8$). Data represent means with standard error. Ctrl, control; -Mg, magnesium deficiency. Asterisks indicate significant differences in measured variables between control and Mg-deficient plants (Student's *t*-test, $^{*}p < 0.05$, $^{**}p < 0.01$).

Carbon Assimilation and Photosynthate Partitioning Were Affected After Four to Five Days of Magnesium Deficiency

We used ^{14}C-labelled CO_2 as a tracer to determine the CO_2 assimilation rate in leaves between days 3 and 6, when the chlorophyll content started to decrease due to Mg deficiency. In mature leaves, the CO_2 assimilation rate was greater ($p < 0.01$) in Mg-deficient than in control plants on days 3, and then it was similar between control and Mg-deficient plants until day 6 (**Figure 3A**). In expanding leaves, the CO_2 assimilation rate was lower in Mg-deficient plants from day 5 (**Figure 3A**), which is before the reduction in fresh weight and chlorophyll content. On day 5, the CO_2 assimilation rate in expanding leaves was 12% lower ($p < 0.05$) compared to the control plants (**Figure 3A**).

To evaluate photosynthate partitioning from source leaves to roots, we determined the ratio of ^{14}C partitioned into the root to the total ^{14}C in the plant. The ratio was similar between control and Mg-deficient plants on day 3 (**Figure 3B**). After day 3, the ratio gradually increased in control plants, whereas it was constant in Mg-deficient plants (**Figure 3B**). On day 4, the ratio was 47% lower ($p < 0.05$) in Mg-deficient than in control plants (**Figure 3B**). The disruption in photosynthate partitioning was detected at an early stage of Mg deficiency (day 4) when the CO_2 assimilation was not inhibited yet. Consistently, the contents of sucrose and glucose in expanding leaves were higher in Mg-deficient than in control plants from day 4 (**Figures 3C,D**). On day 4, the sucrose and glucose contents were 3.0 ($p < 0.01$) and 2.3 ($p < 0.01$) times greater, respectively, in Mg-deficient plants (**Figures 3C,D**).

Mineral Contents Were Reduced in Mature Leaves Within Two Days of Magnesium Deficiency

To examine changes in the mineral profile, mineral contents in mature leaves and root were determined on days 0, 1, 2, 4 and 6, and contents in expanding leaves were determined on

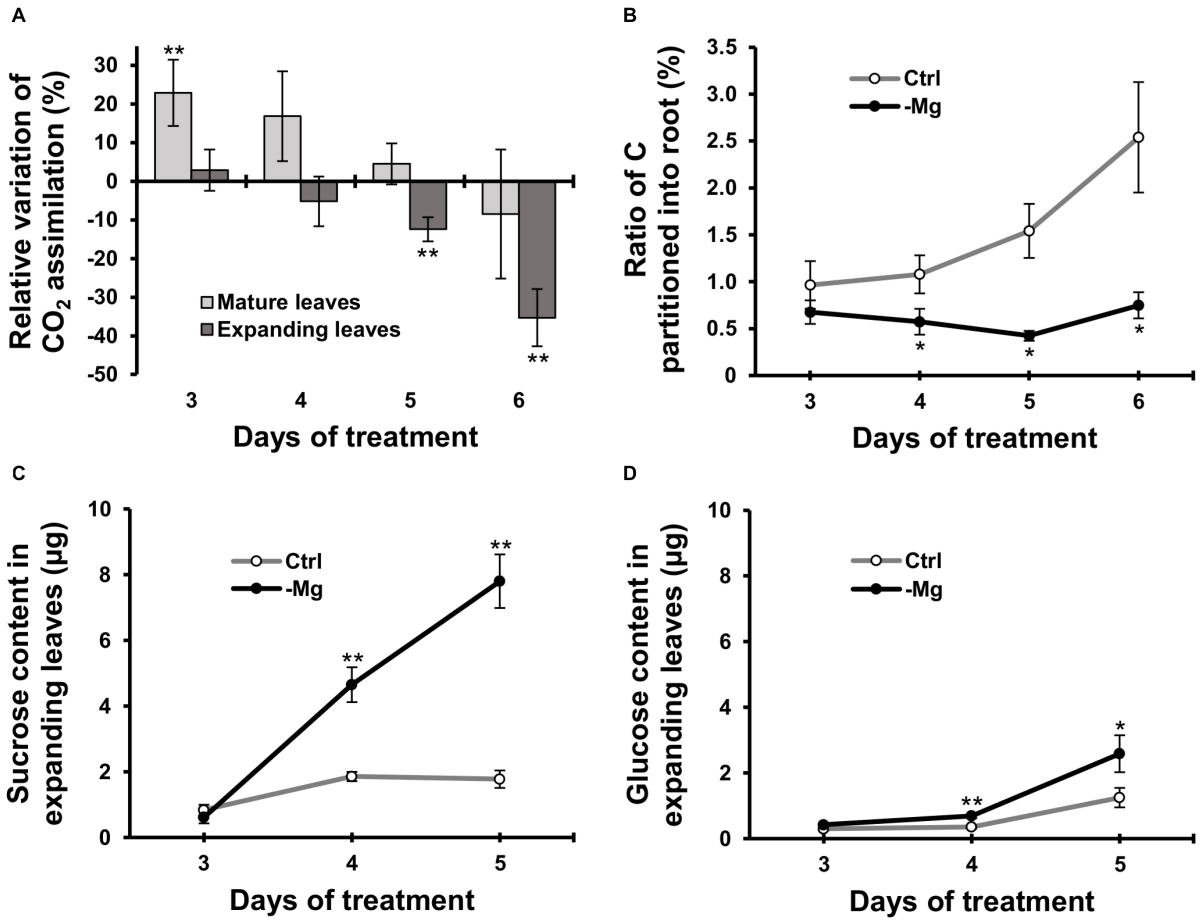

FIGURE 3 | Effect of magnesium deficiency on carbon assimilation and photosynthate partitioning ($^{14}CO_2$ tracer study). **(A)** Relative variation of carbon assimilation rate by magnesium deficiency (^{14}C tracer study, $n = 4$). The relative variation was determined after dividing the difference in the amount of ^{14}C assimilated in mature leaves (pale grey) or expanding leaves (dark grey) between control and Mg-deficient plants by the amount of assimilated ^{14}C in control plants. **(B)** The ratio of photosynthate partitioned into roots (^{14}C tracer study, $n = 4$). The ratio was determined after dividing the amount of ^{14}C in roots by the amount of ^{14}C in the whole plant. **(C,D)** The contents of sucrose **(C)** and glucose **(D)** in expanding leaves determined enzymatically ($n = 6$). Data represent means with standard error. Ctrl: control, -Mg: magnesium deficiency. Asterisks indicate significant differences in measured variables between control and Mg-deficient plants (Student's *t*-test, $^*p < 0.05$, $^{**}p < 0.01$).

days 2, 4 and 6. The Mg content increased in control plants along with the growth in all organs analysed (**Figures 4A–C**). By contrast in Mg-deficient plants, the Mg content in mature leaves gradually decreased, the content in expanding leaves remained constant, and the content in root slowly increased (**Figures 4A–C**). Compared to the control plants, the Mg content was 41% ($p < 0.01$) and 6.8% ($p < 0.05$) lower in mature leaves and root on day 1, respectively, and 58% ($p < 0.01$), 45% ($p < 0.01$) and 17% ($p < 0.05$) lower in mature leaves, expanding leaves and root on day 2, respectively (**Figures 4A–F**), which indicates that the loss of Mg was more severe in the shoot than in the root.

For the other minerals, with the exception of Ca, the general tendency showed the relative decrease in mineral contents in mature leaves and no change in contents in expanding leaves and root, compared to the control plants. For instance, the P content in mature leaves was lower ($p < 0.05$) in Mg-deficient than in control plants between days 1 and 6 (**Figure 4D**), while the content in expanding leaves was maintained until day 4 (**Figure 4E**), and the content in root was sometimes even higher ($p < 0.05$) in Mg-deficient plants (**Figure 4F**). The relative decrease in mineral contents in mature leaves within 2 days of Mg deficiency was observed for P, K, B, Mn, Cu, Zn and Mo (**Figure 4D**). Some of these minerals (P, K, Mn, Zn and Mo) showed no change or an increase in contents in expanding leaves and root before day 6 (**Figures 4E,F**). On day 6, contents of P, K, Ca and Mo in expanding leaves were lower ($p < 0.05$) in Mg-deficient than in control plants (**Figure 4E**), which corresponds to the relative decrease in biomass (**Figure 2A**).

Phosphorus Transport From Roots to Mature Leaves Was Not Affected During Six Days of Magnesium Deficiency

The relative decrease in mineral contents in mature leaves could be attributed to an inhibition of root uptake and xylem transport from roots to mature leaves during Mg deficiency. To test

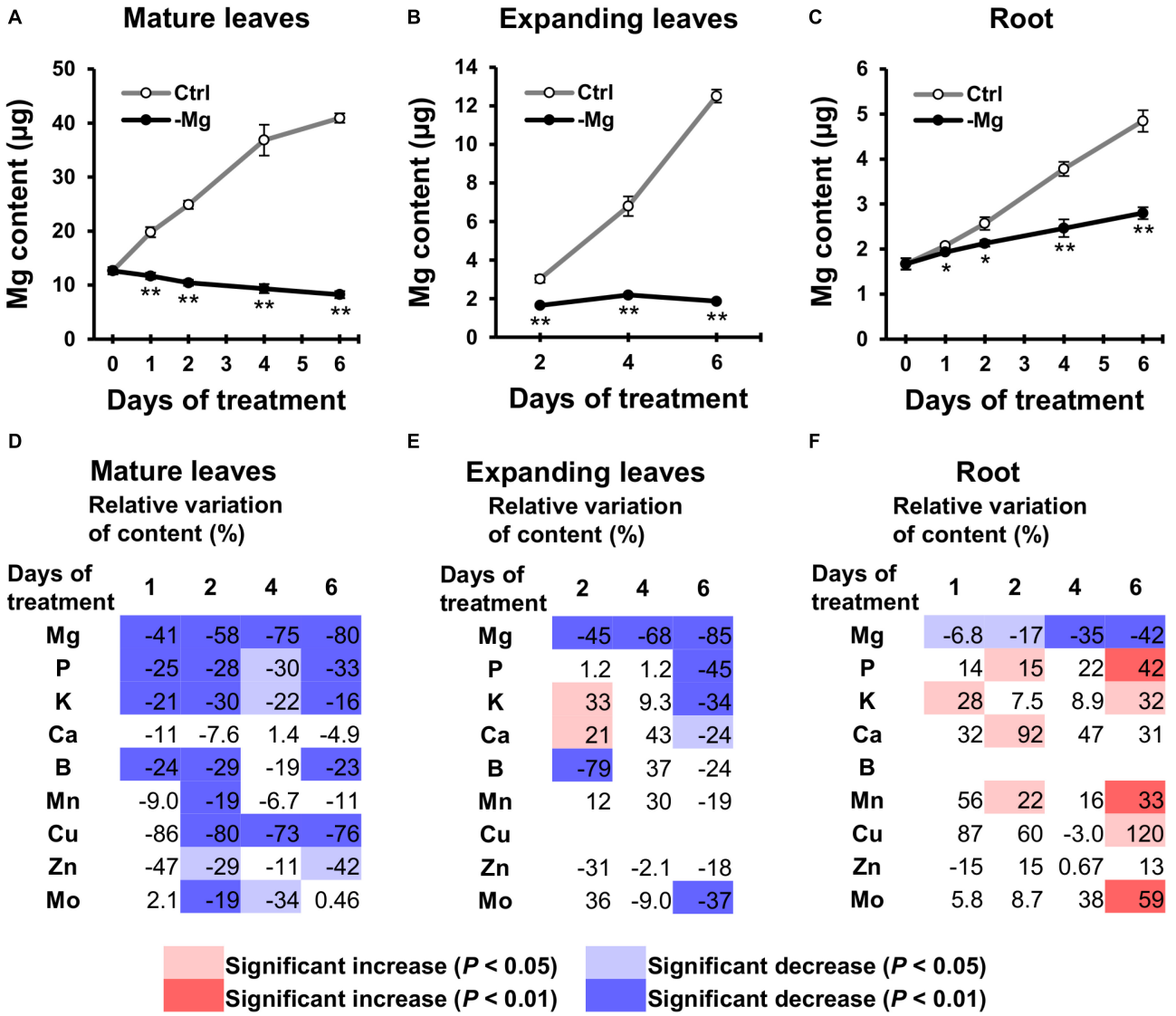

FIGURE 4 | Effect of magnesium deficiency on the plant mineral profile. **(A–C)** The magnesium content in mature leaves **(A)**, expanding leaves **(B)** and roots **(C)** during magnesium deficiency. Data represent means (n = 4) with standard error. Ctrl, control; -Mg, magnesium deficiency. Asterisks indicate significant differences in the Mg content between control and Mg-deficient plants (Student's t-test, $^{*}p < 0.05$, $^{**}p < 0.01$). **(D–F)** Relative variation of mineral content in mature leaves **(D)**, expanding leaves **(E)** and roots **(F)** during magnesium deficiency. The relative variation was determined after dividing the difference in mineral contents between control and Mg-deficient plants by the mineral content in control plants. The contents of copper (Cu) in expanding leaves and boron (B) in roots are not represented, because they were below the detection limit of ICP-MS measurement. Data represent means (n = 4). The cell colours indicate significant differences in the mineral contents between control and Mg-deficient plants (Student's t-test, pale colours, $p < 0.05$; dark colours, $p < 0.01$).

that possibility, we determined the short-term transport of P from roots to leaves between days 3 and 6 using ^{32}P-labelled phosphate as a radiotracer. Between days 3 and 6, the short-term P transport into mature leaves was not affected significantly ($p \geq 0.05$) by Mg deficiency, but there was a numerical decrease ($p < 0.05$) in P transport into mature leaves between days 4 and 6 (**Figure 5**), which can be partly responsible for the reduced P content in mature leaves. On day 3, however, the P transport into mature leaves was slightly (but not significantly) more active in Mg-deficient plants (**Figure 5**). This excludes the possibility that the inhibition of root uptake and xylem transport is the cause of reduced P content in mature leaves within 2 days of Mg deficiency.

The P transport into expanding leaves was unaffected on day 3 and decreased thereafter during Mg deficiency compared to the control plants (**Figure 5**). The P transport into expanding leaves of Mg-deficient plants was 54% lower ($p < 0.05$) compared to that of control plants on day 4 (**Figure 5**), when the P content in expanding leaves was similar between control and Mg-deficient plants (**Figure 4E**). This suggests that the reduced P transport from roots to expanding leaves was balanced by retranslocation from other plant parts.

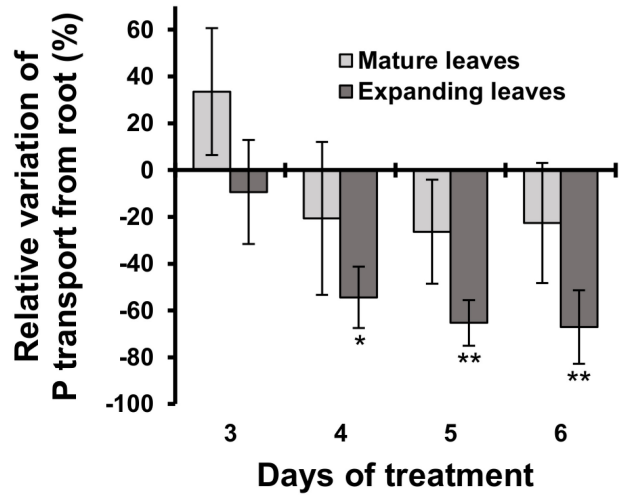

FIGURE 5 | Effect of magnesium deficiency on short-term phosphorus transport (^{32}P tracer study). Relative variation of P transport from roots by Mg deficiency was determined after dividing the difference in the amount of P transported into mature leaves (pale grey) or expanding leaves (dark grey) between control and Mg-deficient plants by the amount of transported P in control plants. Data represent means (n = 4) with standard error. Asterisks indicate significant differences in the amount of transported P between control and Mg-deficient plants (Student's t-test, *$p < 0.05$, **$p < 0.01$).

Transcriptome Analysis Revealed Leaf Position-Specific and Time-Dependent Gene Expression Profile During Magnesium Deficiency

In search of responsive genes to Mg deficiency, we performed a global transcriptome analysis in mature and expanding leaves on days 3, 5 and 8, and in roots on day 3 after withdrawing Mg from the nutrient solution. Although the shoot growth was inhibited earlier than the root growth (**Figures 2A–C**), the number of differentially expressed genes (DEGs; $p < 0.01$) on day 3 was larger in roots than in both types of leaves (**Table 1**). The number of DEGs was larger in expanding than in mature leaves (**Table 1**), as mirrored by more severe physiological impacts. In expanding leaves, the set of DEGs was not necessarily consistent on different days of treatment; for instance, among the set of up-regulated genes on day 3, only half were also up-regulated on day 5 (**Figure 6**). This suggests that the gene expression pattern in response to Mg deficiency is unique to the stage of deficiency.

The DEGs are listed in **Supplementary Data S1**, and the gene ontology (GO) terms enriched in each DEG set in **Supplementary Data S2**. On day 3, the GO terms enriched in the set of down-regulated genes in expanding leaves included the light harvesting of photosynthesis (**Supplementary Data S2**). The down-regulated genes annotated to this term were *CAB2*, *LIGHT-HARVESTING CHLOROPHYLL-PROTEIN COMPLEX I SUBUNIT A4* (*LHCA4*) and *B2.1*, *B6* (*LHCB2.1, B6*) (**Supplementary Table S1**). The repression of *CAB2* expression was previously reported in Mg-deficient Arabidopsis and proposed to be partly responsible for the chlorophyll degradation (Hermans and Verbruggen, 2005). Besides the repression of *CAB2* expression, the down-regulation of Mg chelatase-encoding genes (Neuhaus et al., 2013) and the up-regulation of genes involved in chlorophyll catabolism (Hermans et al., 2010b; Verbruggen and Hermans, 2013) have also been proposed to be responsible for the chlorophyll degradation. Consistently, both the down-regulation of *MAGNESIUM CHELATASE I1*, *I2* (*CHLI1*, *I2*) and the up-regulation of *NON-YELLOWING 1* (*NYE1*) and *MULTIDRUG RESISTANCE ASSOCIATED PROTEIN 3* (*MRP3*) were detected in expanding leaves on day 5 (**Supplementary Table S1**), which was before the chlorophyll content decreased (**Figure 2D**). Besides, we found the down-regulation of a gene involved in chlorophyll synthase (*CHLG*) in expanding leaves on day 5 (**Supplementary Table S1**). For enzymes involved in carbon fixation, two genes encoding ribulose-1,5-bisphosphate carboxylase/oxygenase small subunit (*RBCS1B* and *RBCS2B*) and a gene encoding phosphoenolpyruvate carboxylase (*PPC2*) were down-regulated in expanding leaves on day 5 (**Supplementary Table S1**), which may be partly responsible for the reduction in the CO_2 assimilation rate. Among sucrose/proton symporters (SUCs), *SUC1* was up-regulated and *SUC2* was down-regulated in expanding leaves on day 3 (**Supplementary Table S1**), when the sucrose content was the same as control (**Figure 3C**).

For the up-regulated genes in expanding leaves on day 3, the enriched GO terms included: the oxidative stress response, glutathione metabolic process and the regulation of systemic acquired resistance (SAR) (**Supplementary Data S2**). Genes encoding glutaredoxin (*GRXS13* and *GRX480*) and glutathione S-transferase tau (*GSTU1*, *4*, *8*, *9*, *10*, *19*, *22*, *24* and *25*) were up-regulated within 5 days of Mg deficiency treatment (**Supplementary Table S2**), suggesting an increase of antioxidative capacity (Hermans et al., 2011). On day 5, genes encoding ferritin (*FER1* and *FER4*) were up-regulated (**Supplementary Table S2**), consistently with the observations in

TABLE 1 | The number of genes differentially expressed (Exact Test, $p < 0.01$) in mature leaves, expanding leaves and roots during magnesium deficiency.

Days of treatment	Mature leaves		Expanding leaves		Roots	
	Up-regulation	Down-regulation	Up-regulation	Down-regulation	Up-regulation	Down-regulation
3	54	32	312	146	340	343
5	149	196	2,492	1,951	ND	ND
8	613	23	4,270	2,355	ND	ND

ND, not determined.

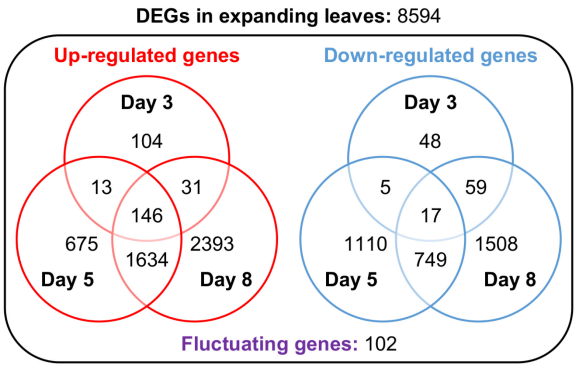

FIGURE 6 | Venn diagrams representing the number of genes up- or down-regulated in expanding leaves after 3, 5 and 8 days of magnesium deficiency. The differentially expressed genes (DEGs) were identified by the Exact Test ($p < 0.01$) and categorised into 15 groups based on the day(s) of treatment on which they were differentially expressed.

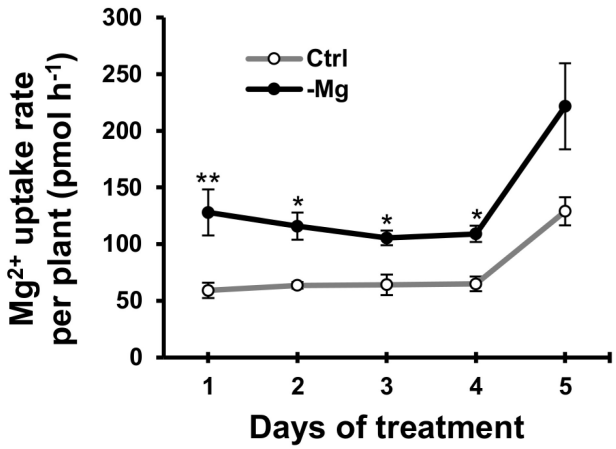

FIGURE 7 | Effect of magnesium deficiency on high-affinity magnesium uptake in roots (^{28}Mg tracer study). The root Mg^{2+} uptake rate was determined as the amount of Mg taken up by one plant in 1 h. Data represent means ($n = 4$) with standard error. Ctrl, control, -Mg, magnesium deficiency. Asterisks indicate significant differences in the Mg^{2+} uptake rate between control and Mg-deficient plants (Student's t-test, $^{*}p < 0.05$, $^{**}p < 0.01$).

Mg-deficient rice (Kobayashi et al., 2018). The up-regulated genes annotated to the regulation of systemic acquired resistance are listed on **Supplementary Table S2** for discussion.

Magnesium Deficiency Induced Root Magnesium Uptake Without Transcriptional Regulation of Magnesium Transporter Genes

To confirm the early root response to Mg deficiency concerning Mg^{2+} acquisition, we determined the root Mg^{2+} uptake rate in the high-affinity range (50 μM Mg^{2+} in the external solution) using ^{28}Mg as a radiotracer. Between days 1 and 4, the high-affinity Mg^{2+} uptake rate was 64–116% ($p < 0.05$) higher in Mg-deficient than in control plant roots (**Figure 7**). However, none of the known and putative Mg^{2+} transporter genes were differentially expressed in Mg-deficient plant roots on day 3, including genes encoding MRS2 (Schock et al., 2000; Li et al., 2001), prokaryotic Mg^{2+} transporter CorA-like proteins (Smith and Maguire, 1995), MAGNESIUM/PROTON EXCHANGER 1 (MHX1; Shaul et al., 1999), mammalian Mg^{2+} transporter NIPA (Quamme, 2010), NIPA homolog ENOR3 and ENOR3-like proteins (Gao et al., 2018; **Supplementary Table S3**), suggesting that root Mg^{2+} uptake is controlled by non-transcriptional regulation. Despite the absence of transcriptional regulation of genes encoding putative Mg^{2+} transporters during Mg deficiency, *MRS2* knockout mutants (*mrs2-1*, *mrs2-1* × *mrs2-5*, *mrs2-1* × *mrs2-10*, *mrs2-1* × *mrs2-5* × *mrs2-10* and *mrs2-4*) grown *in vitro* in a Mg depleted solution had altered root morphology compared to the wild type (**Supplementary Figure S1**).

DISCUSSION

Design of Magnesium Deficiency Treatment

To avoid depleting sulphate from the original MGRL solution while imposing Mg deficiency, we substituted $MgSO_4$ with Na_2SO_4. As the alternative counter cation of SO_4^{2-}, Na^+ was selected over K^+ to permit the examination of the effect of Mg deficiency on the K profile. The Na^+ concentrations in the original and Mg-free MGRL solutions were 2.0 and 5.0 mM, respectively, and the Na content of Mg-deficient plants increased compared to the control plants (data not shown). However, transcript levels of *SALT OVERLY SENSITIVE 1* (*SOS1*), a well-known salt stress marker (Shi et al., 2000) remained unchanged throughout the experiment in leaves and roots (**Supplementary Data S1**). Therefore, the substitution of Na_2SO_4 for $MgSO_4$ was considered valid for a Mg deficiency treatment.

Timeline of Physiological and Transcriptional Responses to Magnesium Deficiency

Sugar accumulation in leaves is regarded as the main cause of chlorophyll degradation observed during Mg deficiency (Tanoi and Kobayashi, 2015). Indeed, many authors documented leaf sugar accumulation before any decline in chlorophyll content or photosynthetic rate in various plant species such as Arabidopsis (Hermans and Verbruggen, 2005), common bean (Fischer and Bremer, 1993; Cakmak et al., 1994a,b), rice (Kobayashi et al., 2013b) and sugar beet (Hermans et al., 2004, 2005). The current study showed that sucrose and glucose accumulate in expanding leaves before any decline in chlorophyll content or CO_2 assimilation rate (**Figures 2D**, **3**). Oswald et al. (2001) found that transcript levels of *CAB2* were low in the presence of sucrose in an Arabidopsis cell suspension culture. Furthermore, Hermans and Verbruggen (2005) reported that sugar accumulation in leaves could lead to chlorophyll degradation through the repression of *CAB2* expression. However, in the current study, we observed lower *CAB2* transcript levels in expanding leaves on day 3, prior to sugar accumulation (**Supplementary Table S1**). Besides *CAB2*, transcript levels of *LHCA4* and *LHCB2.1*, *6* also decreased in

expanding leaves on day 3 (**Supplementary Table S1**). This suggests another regulatory component of the expression of these genes than sugar accumulation. This could be an adaptation strategy that reduces electron transport between photosystems to prevent sugar accumulation (Hermans et al., 2004).

Cakmak and Kirkby (2008) proposed that ROS generation during Mg deficiency is likely due to a decrease in CO_2 assimilation, which causes an over-reduction of the electron transport chain between photosystems. To alleviate the toxicity of ROS, the physiological response to Mg deficiency triggers the activity of antioxidative enzymes and increases the concentration of antioxidant molecules in leaves (Cakmak and Marschner, 1992; Tewari et al., 2006; Hermans et al., 2010b; Kobayashi et al., 2018). The capacity to cope with oxidative stress was recently reported relevant to the tolerance to Mg deficiency in grapevine rootstocks (Livigni et al., 2019). In the current study, the global transcriptome analysis revealed the up-regulation of genes involved in the glutathione metabolic process and the oxidative stress response in expanding leaves (**Supplementary Data S2**). These transcriptional changes were already evident on days 3, when CO_2 assimilation had not yet decreased (**Figure 3A**). Furthermore, genes involved in the reduction process of oxidative stress, such as those encoding thioredoxin superfamily proteins (Arnér and Holmgren, 2000; Marty et al., 2009) and CYP71A23 (Rai et al., 2015) were noticeably up-regulated in roots (**Supplementary Data S1**). These findings suggest that a decline in net photosynthesis is not the only cause of ROS generation. Previously, Kobayashi et al. (2018) proposed that oxidative stress in Mg-deficient rice is caused by iron toxicity. Here, the up-regulation of genes encoding ferritin (*FER1* and *FER4*), which express in response to iron overload (Gaymard et al., 1996; Petit et al., 2001), was confirmed (**Supplementary Table S2**). This supports the possible generation of ROS through iron toxicity.

Induction of Systemic Acquired Resistance in Expanding Leaves During Magnesium Deficiency

The global transcriptome analysis revealed the up-regulation of genes associated with systemic acquired resistance (SAR) in expanding leaves (**Supplementary Table S2**). The SAR is an adaptive response induced at the whole plant level following a localised exposure to a pathogen (Fu and Dong, 2013). It can be induced through the accumulation of the defence hormone salicylic acid (SA) and secretion of PATHOGENESIS-RELATED (PR) proteins (Fu and Dong, 2013). In expanding leaves, three genes encoding PR proteins (*PR1*, *2* and *5*) were up-regulated within 5 days of Mg deficiency treatment (**Supplementary Table S2**). Among the other genes up-regulated within the same time window, *ALD1* and *PAD4* act additively to control *PR1* expression and SA accumulation (Song et al., 2004). The PAD4 protein and its interacting partner ENHANCED DISEASE SUSCEPTIBILITY 1 (EDS1) are important activators of SA signalling (Falk et al., 1999; Wiermer et al., 2005), and six other proteins (AED15, EP1, LLP1, PNP-A, PR2 and 5) display EDS1-dependent accumulation (Breitenbach et al., 2014). The up-regulation of these genes suggests that Mg deficiency induces SAR through the activation of SA signalling.

Nutrient Retranslocation During Short-Term Magnesium Deficiency

During mineral deficiency, plants maintain growth by retranslocating limiting minerals from mature leaves. Maillard et al. (2015) studied the mobility of all essential minerals during leaf senescence in eight crop and tree species and indicated that the mobility of most minerals (P, K, S, Mg, B, Fe, Ni, Cu, Zn, Mo) is variable among plant species. In Arabidopsis, Mg is considered as having limited mobility (Himelblau and Amasino, 2001; Waters and Grusak, 2008). Consistently, symptoms of Mg deficiency tend to appear first in young leaves that develop after deprivation (Hermans and Verbruggen, 2005; Hermans et al., 2010b). In the current study, we found that the Mg content in roots of Mg-deficient plants increased while no additional Mg was available (**Figure 4C**). This indicates that Mg was retranslocated from mature leaves, where the Mg content decreased during deficiency (**Figure 4A**). The molecular mechanisms of Mg retranslocation remain unknown. Although some genes of the Mg^{2+} transporter *MRS2*/*MGT* family are expressed in vascular tissues (Gebert et al., 2009), there was no increase in transcript levels of those genes in mature leaves (**Supplementary Data S1**).

Interestingly, the contents of P, K, B, Mn, Cu, Zn and Mo in mature leaves relatively decreased compared to the control plants within 1 or 2 days following the removal of Mg from the nutrient solution (**Figures 4D–F**). The contents of these minerals, with the exception of B and Cu, were not affected in expanding leaves or root during 4 days of Mg deficiency (**Figures 4D–F**). Although the Cu content in expanding leaves could not be determined, it would have been unaffected or increased, based on the increase in Cu content previously observed in Mg-deficient Arabidopsis leaves (Hermans et al., 2010b, 2011). The decrease in contents of P, K, Mn, Cu, Zn and Mo in mature leaves suggests that Mg deficiency either affects the root uptake and xylem transport of these minerals to mature leaves or triggers the retranslocation from mature leaves. The ^{32}P radiotracer study revealed that Mg deficiency did not disturb P transport from roots to mature leaves within 6 days (**Figure 5**), while it reduced the P content in mature leaves within 1 day (**Figure 4D**). Furthermore, 4 days of Mg deficiency noticeably reduced P transport from roots to expanding leaves (**Figure 5**), while it did not affect the P content in expanding leaves (**Figure 4E**). These findings indicate that the decrease in mineral contents in mature leaves is not attributed to the affected root uptake and xylem transport but to the stimulated retranslocation. Previously, it was shown that P, K, Cu, Zn (Himelblau and Amasino, 2001; Waters and Grusak, 2008) and Mo (Himelblau and Amasino, 2001) were retranslocated from senescing leaves of Arabidopsis. Therefore, the retranslocation of these minerals during Mg deficiency implies the accelerated senescence of mature leaves. Calcium (Biddulph et al., 1958) and Mn (Hocking et al., 1977)

are recognised to have low phloem mobility. There was no evidence of Ca retranslocation from Arabidopsis leaves in either the current or previous studies (Himelblau and Amasino, 2001; Waters and Grusak, 2008). The only contradiction between the current and previous observations is that Mn was retranslocated from Mg-deficient mature leaves (**Figure 4D**) while it was not from senescing leaves of Arabidopsis (Himelblau and Amasino, 2001; Waters and Grusak, 2008). The retranslocation of Mn has been observed in some species such as barley, bread wheat (Maillard et al., 2015), sour orange and sweet orange (Papadakis et al., 2007). For Mn retranslocation, Arabidopsis may have a common mechanism to those species, which is triggered by Mg deficiency but not during leaf senescence.

DATA AVAILABILITY STATEMENT

The raw reads and normalised count data in the global transcriptome analysis can be found in NCBI's Gene Expression Omnibus (https://www.ncbi.nlm.nih.gov/geo/query/acc.cgi?acc=GSE140070).

AUTHOR CONTRIBUTIONS

TO, NK, and KT designed the experiments. TO conducted most of the experiments, analysed the data and wrote the manuscript. CH conducted the root morphology analysis and helped analyse the data. YI, AS, and KS assisted in the global transcriptome analysis. NA assisted in sugar quantification. RS and TOga assisted in the ^{14}C radiotracer study. HS, RI, TN, and KT produced and purified ^{28}Mg. NK, CH, and KT supervised the writing of the manuscript. All the authors approved the final version of the manuscript.

FUNDING

TO is a JSPS research fellow, and CH is an F.R.S.-FNRS research associate. This work was supported by JSPS KAKENHI (Grant Numbers JP19J22719, JP19K05751, and JP17H06172), JST PRESTO (Grant Number JPMJPR15Q7), JSPS and F.R.S.-FNRS Bilateral Joint Research Project, and the Cabinet Office, Government of Japan, Cross-ministerial Strategic Innovation Promotion Program (SIP), "Technologies for Smart Bio-industry and Agriculture" (funding agency: Bio-oriented Technology Research Advancement Institution, NARO).

ACKNOWLEDGMENTS

The authors thank Dr. Volker Knoop and Dr. Takehiro Kamiya for providing seeds of *MRS2* knockout lines, Dr. Kentaro Yoshida for valuable discussion, and Dr. Martin O'Brien for language editing of the manuscript.

SUPPLEMENTARY MATERIAL

The Supplementary Material for this article can be found online at: https://www.frontiersin.org/articles/10.3389/fpls.2020.00563/full#supplementary-material

REFERENCES

Akanuma, G., Kobayashi, A., Suzuki, S., Kawamura, F., Shiwa, Y., Watanabe, S., et al. (2014). Defect in the formation of 70S ribosomes caused by lack of ribosomal protein L34 can be suppressed by magnesium. *J. Bacteriol.* 196, 3820–3830. doi: 10.1128/JB.01896-14

Arnér, E. S. J., and Holmgren, A. (2000). Physiological functions of thioredoxin and thioredoxin reductase. *Eur. J. Biochem.* 267, 6102–6109. doi: 10.1046/j.1432-1327.2000.01701.x

Biddulph, O., Biddulph, S., Cory, R., and Koontz, H. (1958). Circulation patterns for phosphorus, sulfur and calcium in the bean plant. *Plant Physiol.* 33, 293–300. doi: 10.1104/pp.33.4.293

Breitenbach, H. H., Wenig, M., Wittek, F., Jordá, L., Maldonado-Alconada, A. M., Sarioglu, H., et al. (2014). Contrasting roles of the apoplastic aspartyl protease APOPLASTIC, *ENHANCED DISEASE SUSCEPTIBILITY1*-DEPENDENT1 and LEGUME LECTIN-LIKE PROTEIN1 in Arabidopsis systemic acquired resistance. *Plant Physiol.* 165, 791–809. doi: 10.1104/pp.114.239665

Cai, Y., Zhang, H., Qi, Y., Ye, X., Huang, Z., Guo, J., et al. (2019). Responses of reactive oxygen species and methylglyoxal metabolisms to magnesium-deficiency differ greatly among the roots, upper and lower leaves of *Citrus sinensis*. *BMC Plant Biol.* 19:76. doi: 10.1186/s12870-019-1683-4

Cakmak, I., Hengeler, C., and Marschner, H. (1994a). Changes in phloem export of sucrose in leaves in response to phosphorus, potassium and magnesium-deficiency in bean-plants. *J. Exp. Bot.* 45, 1251–1257. doi: 10.1093/jxb/45.9.1251

Cakmak, I., Hengeler, C., and Marschner, H. (1994b). Partitioning of shoot and root dry matter and carbohydrates in bean plants suffering from phosphorus, potassium and magnesium deficiency. *J. Exp. Bot.* 45, 1245–1250. doi: 10.1093/jxb/45.9.1245

Cakmak, I., and Kirkby, E. A. (2008). Role of magnesium in carbon partitioning and alleviating photooxidative damage. *Physiol. Plant.* 133, 692–704. doi: 10.1111/j.1399-3054.2007.01042.x

Cakmak, I., and Marschner, H. (1992). Magnesium deficiency and high light intensity enhance activities of superoxide dismutase, ascorbate peroxidase, and glutathione reductase in bean leaves. *Plant Physiol.* 98, 1222–1227. doi: 10.1104/pp.98.4.1222

Clarkson, D. T., and Hanson, J. B. (1980). The mineral nutrition of higher plants. *Annu. Rev. Plant Physiol.* 31, 239–298. doi: 10.1146/annurev.pp.31.060180.001323

Cowan, J. A. (2002). Structural and catalytic chemistry of magnesium-dependent enzymes. *Biometals* 15, 225–235. doi: 10.1023/A:1016022730880

Dakora, F. D., and Phillips, D. A. (2002). Root exudates as mediators of mineral acquisition in low-nutrient environments. *Plant Soil* 245, 35–47. doi: 10.1023/A:1020809400075

De Pessemier, J., Chardon, F., Juraniec, M., Delaplace, P., and Hermans, C. (2013). Natural variation of the root morphological response to nitrate supply in *Arabidopsis thaliana*. *Mech. Dev.* 130, 45–53. doi: 10.1016/j.mod.2012.05.010

Edgar, R., Domrachev, M., and Lash, A. E. (2002). Gene Expression Omnibus: NCBI gene expression and hybridization array data repository. *Nucleic Acids Res.* 30, 207–210. doi: 10.1093/nar/30.1.207

Fageria, N. K., Baligar, V. C., and Li, Y. C. (2008). The role of nutrient efficient plants in improving crop yields in the twenty first century. *J. Nutr.* 31, 1121–1157. doi: 10.1080/01904160802116068

Falk, A., Feys, B. J., Frost, L. N., Jones, J. D. G., Daniels, M. J., and Parker, J. E. (1999). *EDS1*, an essential component of *R* gene-mediated disease resistance in *Arabidopsis* has homology to eukaryotic lipases. *Proc. Natl. Acad. Sci. U.S.A.* 96, 3292–3297. doi: 10.1073/pnas.96.6.3292

Fischer, E. S., and Bremer, E. (1993). Influence of magnesium-deficiency on rates of leaf expansion, starch and sucrose accumulation, and net assimilation in *Phaseolus Vulgaris*. *Physiol. Plant.* 89, 271–276. doi: 10.1034/j.1399-3054.1993.890204.x

Fischer, E. S., Lohaus, G., Heineke, D., and Heldt, H. W. (1998). Magnesium deficiency results in accumulation of carbohydrates and amino acids in source and sink leaves of spinach. *Physiol. Plant.* 102, 16–20. doi: 10.1034/j.1399-3054.1998.1020103.x

Fu, Z. Q., and Dong, X. (2013). Systemic acquired resistance: turning local infection into global defense. *Annu. Rev. Plant Biol.* 64, 839–863. doi: 10.1146/annurev-arplant-042811-105606

Fujiwara, T., Hirai, M. Y., Chino, M., Komeda, Y., and Naito, S. (1992). Effects of sulfur nutrition on expression of the soybean seed storage protein genes in transgenic petunia. *Plant Physiol.* 99, 263–268. doi: 10.1104/pp.99.1.263

Gao, H., Yang, M., Yang, H., Qin, Y., Zhu, B., Xu, G., et al. (2018). *Arabidopsis ENOR3* regulates RNAi-mediated antiviral defense. *J. Genet. Genomics* 45, 33–40. doi: 10.1016/j.jgg.2017.11.005

Gaymard, F., Boucherez, J., and Briat, J. F. (1996). Characterization of a ferritin mRNA from *Arabidopsis thaliana* accumulated in response to iron through an oxidative pathway independent of abscisic acid. *Biochem. J.* 318, 67–73. doi: 10.1042/bj3180067

Gebert, M., Meschenmoser, K., Svidova, S., Weghuber, J., Schweyen, R., Eifler, K., et al. (2009). A root-expressed magnesium transporter of the *MRS2/MGT* gene family in *Arabidopsis thaliana* allows for growth in low-Mg^{2+} environments. *Plant Cell* 21, 4018–4030. doi: 10.1105/tpc.109.070557

Gerendás, J., and Führs, H. (2013). The significance of magnesium for crop quality. *Plant Soil* 368, 101–128. doi: 10.1007/s11104-012-1555-2

Gojon, A., Nacry, P., and Davidian, J. (2009). Root uptake regulation: a central process for NPS homeostasis in plants. *Curr. Opin. Plant Biol.* 12, 328–338. doi: 10.1016/j.pbi.2009.04.015

Gruber, B. D., Giehl, R. F. H., Friedel, S., and von Wiren, N. (2013). Plasticity of the Arabidopsis root system under nutrient deficiencies. *Plant Physiol.* 163, 161–179. doi: 10.1104/pp.113.218453

Hagen-Thorn, A., Varnagiryte, I., Nihlgård, B., and Armolaitis, K. (2006). Autumn nutrient resorption and losses in four deciduous forest tree species. *For. Ecol. Manage.* 228, 33–39. doi: 10.1016/j.foreco.2006.02.021

Hermans, C., Bourgis, F., Faucher, M., Strasser, R. J., Delrot, S., and Verbruggen, N. (2005). Magnesium deficiency in sugar beets alters sugar partitioning and phloem loading in young mature leaves. *Planta* 220, 541–549. doi: 10.1007/s00425-004-1376-5

Hermans, C., Chen, J., Coppens, F., Inzé, D., and Verbruggen, N. (2011). Low magnesium status in plants enhances tolerance to cadmium exposure. *New Phytol.* 192, 428–436. doi: 10.1111/j.1469-8137.2011.03814.x

Hermans, C., Johnson, G. N., Strasser, R. J., and Verbruggen, N. (2004). Physiological characterisation of magnesium deficiency in sugar beet: acclimation to low magnesium differentially affects photosystems I and II. *Planta* 220, 344–355. doi: 10.1007/s00425-004-1340-4

Hermans, C., and Verbruggen, N. (2005). Physiological characterization of Mg deficiency in *Arabidopsis thaliana*. *J. Exp. Bot.* 56, 2153–2161. doi: 10.1093/jxb/eri215

Hermans, C., Vuylsteke, M., Coppens, F., Craciun, A., Inze, D., and Verbruggen, N. (2010a). Early transcriptomic changes induced by magnesium deficiency in *Arabidopsis thaliana* reveal the alteration of circadian clock gene expression in roots and the triggering of abscisic acid-responsive genes. *New Phytol.* 187, 119–131. doi: 10.1111/j.1469-8137.2010.03258.x

Hermans, C., Vuylsteke, M., Coppens, F., Cristescu, S. M., Harren, F. J. M., Inze, D., et al. (2010b). Systems analysis of the responses to long-term magnesium deficiency and restoration in *Arabidopsis thaliana*. *New Phytol.* 187, 132–144. doi: 10.1111/j.1469-8137.2010.03257.x

Himelblau, E., and Amasino, R. M. (2001). Nutrients mobilized from leaves of *Arabidopsis thaliana* during leaf senescence. *J. Plant Physiol.* 158, 1317–1323. doi: 10.1078/0176-1617-00608

Hocking, P. J., Pate, J. S., Wee, S. C., and McComb, A. J. (1977). Manganese nutrition of *Lupinus* spp. especially in relation to developing seeds. *Ann. Bot.* 41, 677–688. doi: 10.1093/oxfordjournals.aob.a085342

Ichihashi, Y., Fukushima, A., Shibata, A., and Shirasu, K. (2018). "High impact gene discovery: simple strand-specific mRNA library construction and differential regulatory analysis based on gene co-expression network," in *Plant Transcription Factors. Methods in Molecular Biology*, ed. N. Yamaguchi (New York, NY: Humana Press), 163–189. doi: 10.1007/978-1-4939-8657-6_11

Iwata, R., Kawamura, M., Ido, T., and Kimura, S. (1992). Chromatographic purification of no-carrier-added magnesium-28 for biological studies. *J. Radioanal. Nucl. Chem.* 159, 233–237. doi: 10.1007/BF02040716

Jezek, M., Geilfus, C. M., Bayer, A., and Mühling, K. H. (2015). Photosynthetic capacity, nutrient status, and growth of maize (*Zea mays* L.) upon MgSO4 leaf-application. *Front. Plant Sci.* 5:781. doi: 10.3389/fpls.2014.00781

King, R. W., and Zeevaart, J. A. (1974). Enhancement of phloem exudation from cut petioles by chelating-agents. *Plant Physiol.* 53, 96–103. doi: 10.1104/pp.53.1.96

Kobayashi, N. I., Iwata, N., Saito, T., Suzuki, H., Iwata, R., Tanoi, K., et al. (2013a). Application of ^{28}Mg for characterization of Mg uptake in rice seedling under different pH conditions. *J. Radioanal. Nucl. Chem.* 296, 531–534. doi: 10.1007/s10967-012-2010-9

Kobayashi, N. I., Ogura, T., Takagi, K., Sugita, R., Suzuki, H., Iwata, R., et al. (2018). Magnesium deficiency damages the youngest mature leaf in rice through tissue-specific iron toxicity. *Plant Soil* 428, 137–152. doi: 10.1007/s11104-018-3658-x

Kobayashi, N. I., Saito, T., Iwata, N., Ohmae, Y., Iwata, R., Tanoi, K., et al. (2013b). Leaf senescence in rice due to magnesium deficiency mediated defect in transpiration rate before sugar accumulation and chlorosis. *Physiol. Plant.* 148, 490–501. doi: 10.1111/ppl.12003

Lenz, H., Dombinov, V., Dreistein, J., Reinhard, M. R., Gebert, M., and Knoop, V. (2013). Magnesium deficiency phenotypes upon multiple knockout of *Arabidopsis thaliana* MRS2 clade B genes can be ameliorated by concomitantly reduced calcium supply. *Plant Cell Physiol.* 54, 1118–1131. doi: 10.1093/pcp/pct062

Li, H., Wang, N., Ding, J., Liu, C., Du, H., Huang, K., et al. (2017). The maize CorA/MRS2/MGT-type Mg transporter, ZmMGT10, responses to magnesium deficiency and confers low magnesium tolerance in transgenic *Arabidopsis*. *Plant Mol. Biol.* 95, 269–278. doi: 10.1007/s11103-017-0645-1

Li, L., Tutone, A. F., Drummond, R. S. M., Gardner, R. C., and Luan, S. (2001). A novel family of magnesium transport genes in Arabidopsis. *Plant Cell* 13, 2761–2775. doi: 10.1105/tpc.010352

Liu, X., Guo, L., Luo, L., Liu, Y., and Peng, S. (2019). Identification of the magnesium transport (MGT) family in *Poncirus trifoliata* and functional characterization of *PtrMGT5* in magnesium deficiency stress. *Plant Mol. Biol.* 101, 551–560. doi: 10.1007/s11103-019-00924-9

Livigni, S., Lucini, L., Sega, D., Navacchi, O., Pandolfini, T., Zamboni, A., et al. (2019). The different tolerance to magnesium deficiency of two grapevine rootstocks relies on the ability to cope with oxidative stress. *BMC Plant Biol.* 19:148. doi: 10.1186/s12870-019-1726-x

Maillard, A., Diquélou, S., Billard, V., Laîné, P., Garnica, M., Prudent, M., et al. (2015). Leaf mineral nutrient remobilization during leaf senescence and modulation by nutrient deficiency. *Front. Plant Sci.* 6:317. doi: 10.3389/fpls.2015.00317

Mao, D., Chen, J., Tian, L., Liu, Z., Yang, L., Tang, R., et al. (2014). *Arabidopsis* transporter MGT6 mediates magnesium uptake and is required for growth under magnesium limitation. *Plant Cell* 26, 2234–2248. doi: 10.1105/tpc.114.124628

Marschner, H. (1995). *Mineral Nutrition of Higher Plants*, 2nd Edn. London: Academic Press.

Marty, L., Siala, W., Schwarzlander, M., Fricker, M. D., Wirtz, M., Sweetlove, L. J., et al. (2009). The NADPH-dependent thioredoxin system constitutes a functional backup for cytosolic glutathione reductase in *Arabidopsis*. *Proc. Natl. Acad. Sci. U.S.A.* 106, 9109–9114. doi: 10.1073/pnas.0900206106

Mills, J. D., Kawahara, Y., and Janitz, M. (2013). Strand-specific RNA-Seq provides greater resolution of transcriptome profiling. *Curr. Genomics* 14, 173–181. doi: 10.2174/1389202911314030003

Moreira, A., and Fageria, N. K. (2009). Yield, uptake, and retranslocation of nutrients in banana plants cultivated in upland soil of Central Amazonian. *J. Plant Nutr.* 32, 443–457. doi: 10.1080/01904160802660750

Murashige, T., and Skoog, F. (1962). A revised medium for rapid growth and bio assays with tobacco tissue cultures. *Physiol. Plant.* 15, 473–497. doi: 10.1111/j.1399-3054.1962.tb08052.x

Neuhaus, C., Geilfus, C., Zörb, C., and Mühling, K. H. (2013). Transcript expression of Mg-chelatase and H^+-ATPase isogenes in *Vicia faba* leaves as influenced by root and foliar magnesium supply. *Plant Soil* 368, 41–50. doi: 10.1007/s11104-013-1711-3

Oda, K., Kamiya, T., Shikanai, Y., Shigenobu, S., Yamaguchi, K., and Fujiwara, T. (2016). The Arabidopsis Mg transporter, MRS2-4, is essential for Mg homeostasis under both low and high Mg conditions. *Plant Cell Physiol.* 57, 754–763. doi: 10.1093/pcp/pcv196

Ogura, T., Kobayashi, N. I., Suzuki, H., Iwata, R., Nakanishi, T. M., and Tanoi, K. (2018). Magnesium uptake characteristics in Arabidopsis revealed by ^{28}Mg tracer studies. *Planta* 248, 745–750. doi: 10.1007/s00425-018-2936-4

Okamura, M., Hashida, Y., Hirose, T., Ohsugi, R., and Aoki, N. (2016). A simple method for squeezing juice from rice stems and its use in the high-throughput analysis of sugar content in rice stems. *Plant Prod. Sci.* 19, 309–314. doi: 10.1080/1343943X.2015.1128099

Oswald, O., Martin, T., Dominy, P. J., and Graham, I. A. (2001). Plastid redox state and sugars: interactive regulators of nuclear-encoded photosynthetic gene expression. *Proc. Natl. Acad. Sci. U.S.A.* 98, 2047–2052. doi: 10.1073/pnas.021449998

Ozsolak, F., and Milos, P. M. (2011). RNA sequencing: advances, challenges and opportunities. *Nat. Rev. Genet.* 12, 87–98. doi: 10.1038/nrg2934

Papadakis, I. E., Sotiropoulos, T. E., and Therios, I. N. (2007). Mobility of iron and manganese within two citrus genotypes after foliar applications of iron sulfate and manganese sulfate. *J. Plant Nutr.* 30, 1385–1396. doi: 10.1080/01904160701555754

Petit, J. M., Briat, J. F., and Lobréaux, S. (2001). Structure and differential expression of the four members of the *Arabidopsis thaliana* ferritin gene family. *Biochem. J.* 359, 575–582. doi: 10.1042/0264-6021:3590575

Porra, R. J., Thompson, W. A., and Kriedemann, P. E. (1989). Determination of accurate extinction coefficients and simultaneous equations for assaying chlorophylls *a* and *b* extracted with four different solvents: verification of the concentration of chlorophyll standards by atomic absorption spectroscopy. *Biochim. Biophys. Acta* 975, 384–394. doi: 10.1016/S0005-2728(89)80347-0

Quamme, G. A. (2010). Molecular identification of ancient and modern mammalian magnesium transporters. *Am. J. Physiol. Cell Physiol.* 298, C407–C429. doi: 10.1152/ajpcell.00124.2009

Rai, A., Singh, R., Shirke, P. A., Tripathi, R. D., Trivedi, P. K., and Chakrabarty, D. (2015). Expression of rice CYP450-like gene (*Os08g01480*) in *Arabidopsis* modulates regulatory network leading to heavy metal and other abiotic stress tolerance. *PLoS One* 10:e0138574. doi: 10.1371/journal.pone.0138574

Robinson, M. D., McCarthy, D. J., and Smyth, G. K. (2010). edgeR: a Bioconductor package for differential expression analysis of digital gene expression data. *Bioinformatics* 26, 139–140. doi: 10.1093/bioinformatics/btp616

Robinson, M. D., and Smyth, G. K. (2008). Small-sample estimation of negative binomial dispersion, with applications to SAGE data. *Biostatistics* 9, 321–332. doi: 10.1093/biostatistics/kxm030

Schock, I., Gregan, J., Steinhauser, S., Schweyen, R., Brennicke, A., and Knoop, V. (2000). A member of a novel *Arabidopsis thaliana* gene family of candidate Mg^{2+} ion transporters complements a yeast mitochondrial group II intron-splicing mutant. *Plant J.* 24, 489–501. doi: 10.1046/j.1365-313x.2000.00895.x

Shaul, O., Hilgemann, D. W., de-Almeida-Engler, J., Van Montagu, M., Inze, D., and Galili, G. (1999). Cloning and characterization of a novel Mg^{2+}/H^+ exchanger. *EMBO J.* 18, 3973–3980. doi: 10.1093/emboj/18.14.3973

Sheen, J. (1994). Feedback control of gene expression. *Photosynth. Res.* 39, 427–438. doi: 10.1007/BF00014596

Shi, H., Ishitani, M., Kim, C., and Zhu, J. K. (2000). The *Arabidopsis thaliana* salt tolerance gene *SOS1* encodes a putative Na^+/H^+ antiporter. *Proc. Natl. Acad. Sci. U.S.A.* 97, 6896–6901. doi: 10.1073/pnas.120170197

Smith, R. L., and Maguire, M. E. (1995). Distribution of the CorA Mg^{2+} transport-system in gram-negative bacteria. *J. Bacteriol.* 177, 1638–1640. doi: 10.1128/jb.177.6.1638-1640.1995

Song, J. T., Lu, H., McDowell, J. M., and Greenberg, J. T. (2004). A key role for *ALD1* in activation of local and systemic defenses in *Arabidopsis*. *Plant J.* 40, 200–212. doi: 10.1111/j.1365-313X.2004.02200.x

Strouse, C. E. (1974). The crystal and molecular structure of ethyl chlorophyllide *a*·2H2O and its relationship to the structure and aggregation of chlorophyll *a*. *Proc. Natl. Acad. Sci. U.S.A.* 71, 325–328. doi: 10.1073/pnas.71.2.325

Sugita, R., Kobayashi, N. I., Hirose, A., Iwata, R., Suzuki, H., Tanoi, K., et al. (2017). Visualization of how light changes affect ion movement in rice plants using a real-time radioisotope imaging system. *J. Radioanal. Nucl. Chem.* 312, 717–723. doi: 10.1007/s10967-017-5193-2

Sugita, R., Kobayashi, N. I., Hirose, A., Ohmae, Y., Tanoi, K., and Nakanishi, T. M. (2013). Nondestructive real-time radioisotope imaging system for visualizing ^{14}C-labeled chemicals supplied as CO_2 in plants using *Arabidopsis thaliana*. *J. Radioanal. Nucl. Chem.* 298, 1411–1416. doi: 10.1007/s10967-013-2462-6

Sugita, R., Sugahara, K., Kobayashi, N. I., Hirose, A., Nakanishi, T. M., Furuta, E., et al. (2018). Evaluation of plastic scintillators for live imaging of ^{14}C-labeled photosynthate movement in plants. *J. Radioanal. Nucl. Chem.* 318, 579–584. doi: 10.1007/s10967-018-6102-z

Tanoi, K., and Kobayashi, N. I. (2015). Leaf senescence by magnesium deficiency. *Plants* 4, 756–772. doi: 10.3390/plants4040756

Tanoi, K., Kobayashi, N. I., Saito, T., Iwata, N., Hirose, A., Ohmae, Y., et al. (2013). Application of ^{28}Mg to the kinetic study of Mg uptake by rice plants. *J. Radioanal. Nucl. Chem.* 296, 749–751. doi: 10.1007/s10967-012-2219-7

Tanoi, K., Kobayashi, N. I., Saito, T., Iwata, N., Kamada, R., Iwata, R., et al. (2014). Effects of magnesium deficiency on magnesium uptake activity of rice root, evaluated using ^{28}Mg as a tracer. *Plant Soil* 384, 69–77. doi: 10.1007/s11104-014-2197-3

Tewari, R. K., Kumar, P., and Sharma, P. N. (2006). Magnesium deficiency induced oxidative stress and antioxidant responses in mulberry plants. *Sci. Hortic.* 108, 7–14. doi: 10.1016/j.scienta.2005.12.006

Townsley, B. T., Covington, M. F., Ichihashi, Y., Zumstein, K., and Sinha, N. R. (2015). BrAD-seq: breath adapter directional sequencing: a streamlined, ultra-simple and fast library preparation protocol for strand specific mRNA library construction. *Front. Plant Sci.* 6:366. doi: 10.3389/fpls.2015.00366

Verbruggen, N., and Hermans, C. (2013). Physiological and molecular responses to magnesium nutritional imbalance in plants. *Plant Soil* 368, 87–99. doi: 10.1007/s11104-013-1589-0

Waters, B. M., and Grusak, M. A. (2008). Whole-plant mineral partitioning throughout the life cycle in *Arabidopsis thaliana* ecotypes Columbia, Landsberg *erecta*, Cape Verde Islands, and the mutant line *ysl1ysl3*. *New Phytol.* 177, 389–405. doi: 10.1111/j.1469-8137.2007.02288.x

Wiermer, M., Feys, B. J., and Parker, J. E. (2005). Plant immunity: the EDS1 regulatory node. *Curr. Opin. Plant Biol.* 8, 383–389. doi: 10.1016/j.pbi.2005.05.010

Xiao, Q., De Gernier, H., Kupcsik, L., De Pessemier, J., Dittert, K., Fladung, K., et al. (2015). Natural genetic variation of *Arabidopsis thaliana* root morphological response to magnesium supply. *Crop Past. Sci.* 66, 1249–1258. doi: 10.1071/CP15108

Conflict of Interest: The authors declare that the research was conducted in the absence of any commercial or financial relationships that could be construed as a potential conflict of interest.

frontiers in Plant Science

ORIGINAL RESEARCH
published: 25 June 2020
doi: 10.3389/fpls.2020.00955

Short-Term Response of Cytosolic NO_3^- to Inorganic Carbon Increase in *Posidonia oceanica* Leaf Cells

Lourdes Rubio[1]*, *Delia García-Pérez*[1], *Julia M. Davies*[2] and *José A. Fernández*[1]

[1] Departamento de Botánica y Fisiología Vegetal, Facultad de Ciencias, Universidad de Málaga, Málaga, Spain, [2] Department of Plant Sciences, University of Cambridge, Cambridge, United Kingdom

OPEN ACCESS

Edited by:
Francisco Rubio,
Center for Edaphology and Applied Biology of Segura, Spanish National Research Council, Spain

Reviewed by:
Juan Jose Rios,
Center for Edaphology and Applied Biology of Segura, Spanish National Research Council, Spain
Santiago Alejandro,
Martin Luther University of Halle-Wittenberg, Germany

***Correspondence:**
Lourdes Rubio
Lrubio@uma.es

Specialty section:
This article was submitted to Plant Nutrition, a section of the journal Frontiers in Plant Science

Received: 28 February 2020
Accepted: 10 June 2020
Published: 25 June 2020

Citation:
Rubio L, García-Pérez D, Davies JM and Fernández JA (2020) Short-Term Response of Cytosolic NO_3^- to Inorganic Carbon Increase in Posidonia oceanica Leaf Cells. Front. Plant Sci. 11:955. doi: 10.3389/fpls.2020.00955

The concentration of CO_2 in the atmosphere has increased over the past 200 years and is expected to continue rising in the next 50 years at a rate of 3 ppm·year^{-1}. This increase has led to a decrease in seawater pH that has changed inorganic carbon chemical speciation, increasing the dissolved HCO_3^-. *Posidonia oceanica* is a marine angiosperm that uses HCO_3^- as an inorganic carbon source for photosynthesis. An important side effect of the direct uptake of HCO_3^- is the diminution of cytosolic Cl^- (Cl^-c) in mesophyll leaf cells due to the efflux through anion channels and, probably, to intracellular compartmentalization. Since anion channels are also permeable to NO_3^- we hypothesize that high HCO_3^-, or even CO_2, would also promote a decrease of cytosolic NO_3^- (NO_3^-c). In this work we have used NO_3^-- and Cl^--selective microelectrodes for the continuous monitoring of the cytosolic concentration of both anions in *P. oceanica* leaf cells. Under light conditions, mesophyll leaf cells showed a NO_3^-c of 5.7 ± 0.2 mM, which rose up to 7.2 ± 0.6 mM after 30 min in the dark. The enrichment of natural seawater (NSW) with 3 mM $NaHCO_3$ caused both a NO_3^-c decrease of 1 ± 0.04 mM and a Cl_c^- decrease of 3.5 ± 0.1 mM. The saturation of NSW with 1000 ppm CO_2 also produced a diminution of the NO_3^-c, but lower (0.4 ± 0.07 mM). These results indicate that the rise of dissolved inorganic carbon (HCO_3^- or CO_2) in NSW would have an effect on the cytosolic anion homeostasis mechanisms in *P. oceanica* leaf cells. In the presence of 0.1 mM ethoxyzolamide, the plasma membrane-permeable carbonic anhydrase inhibitor, the CO_2-induced cytosolic NO_3^- diminution was much lower (0.1 ± 0.08 mM), pointing to HCO_3^- as the inorganic carbon species that causes the cytosolic NO_3^- leak. The incubation of *P. oceanica* leaf pieces in 3 mM HCO_3^--enriched NSW triggered a short-term external NO_3^- net concentration increase consistent with the NO_3^-c leak. As a consequence, the cytosolic NO_3^- diminution induced in high inorganic carbon could result in both the decrease of metabolic N flux and the concomitant biomass N impoverishment in *P. oceanica* and, probably, in other aquatic plants.

Keywords: cytosolic NO_3^-, elevated inorganic carbon, NO_3^- efflux, anion channels, intracellular nitrate-selective microelectrodes, seagrasses

INTRODUCTION

Nitrate ion (NO_3^-) is the main source of inorganic nitrogen for plants in aerobic conditions. Compared with the concentrations in soils, the concentration of NO_3^- in seawater is persistently very low, particularly in the oligotrophic Mediterranean Sea (Lepoint et al., 2002; Bethoux et al., 2005). Seagrasses are the unique angiosperms that evolved from land plants to live submerged in the sea, forming the basis of the most productive and widespread coastal ecosystems on the planet (Larkum et al., 2006). For vascular plants, colonizing the sea implicates losses and gains to effect structural and physiological adaptations to complete the submerged life cycle, achieved by a reverse evolutionary trajectory in the seagrass lineage (Williams, 2016). Thus, key land angiosperm innovations were lost in seagrasses including the entire collection of genes involved in stomata differentiation, genes related to the synthesis and sensing of terpenoids and other volatile substances, genes for ultraviolet protection, and phytochromes for far-red sensing (Olsen et al., 2016). However, to survive in the conditions of low NO_3^- availability, seagrasses have evolved high affinity uptake systems to capture NO_3^- through their leaves. These systems have been characterized for *Zostera marina* in which the uptake of NO_3^- and inorganic phosphate (Pi) are driven by the inwardly directed electrochemical gradient for Na^+ (García-Sánchez et al., 2000; Rubio et al., 2005). In the Mediterranean, *Posidonia oceanica* is an endemic coastal species of huge ecological importance (Aires et al., 2011). Similar high-affinity and Na^+-dependent uptake mechanisms also operate in *P. oceanica* for both nutrients and some amino acids (Rubio et al., 2018). In both cases, the low semi-saturation constants observed (2.3 and 8.7 μM NO_3^- for *Z. marina* and *P. oceanica*, respectively: García-Sánchez et al., 2000; Rubio et al., 2018) indicate that those systems are very efficient for NO_3^- uptake at the very low concentrations of NO_3^- in seagrass meadows (Touchette and Burkholder, 2000; Romero et al., 2006). Nevertheless, those systems are energetically expensive because seagrass leaf cells have to keep low homeostatic Na^+ concentrations in the cytosol to maintain the Na^+ motive force (Rubio et al., 2011; Rubio et al., 2018). In this scenario, namely low availability of NO_3^- and the energetically expensive mechanism for its high-affinity uptake, the maintenance of NO_3^- inside the cells appears critical. Therefore, as with other vascular plants, seagrasses must maintain intracellular NO_3^- homeostasis to preserve the N metabolic flux.

In a previous work, besides cytosolic H^+ and Na^+, we also measured cytosolic Cl^- (using intracellular ion-selective microelectrodes) in the mesophyll cells of *P. oceanica* (Rubio et al., 2017). In that work, we demonstrated that this seagrass has a direct plasma membrane symporter to uptake HCO_3^- driven by the H^+ electrochemical potential gradient. A significant increase of photosynthesis in natural seawater supplemented by 3 mM HCO_3^- supported the role of HCO_3^- uptake in the photosynthetic activity of this species (Rubio et al., 2017). Furthermore, the enrichment of seawater with 3 mM HCO_3^- also evoked a delayed, but significant, diminution of the cytosolic Cl^- concentration (Rubio et al., 2017). Similar cytosolic Cl^- efflux has been observed in guard cells of the model land angiosperm *Arabidopsis thaliana* during stomatal closure in response to elevated CO_2 (Xue et al., 2011). This Cl^- efflux from guard cells is described as taking place through the plasma membrane S-type anion channels, whose activation responded to the cytosolic HCO_3^- concentration (Xue et al., 2011). Interestingly, in addition to Cl^- these anion channels have a high permeability to NO_3^- (Schmidt and Schroeder, 1994), which is also released from the guard cells during stomatal closure (Geiger et al., 2011; Demir et al., 2013; Maierhofer et al., 2014).

The release of Cl^- from *P. oceanica* in response to HCO_3^- is driven by the outwardly directed electrochemical potential gradient for Cl^- (Rubio et al., 2017). Considering Cl^--selective microelectrodes are also partially sensitive to NO_3^- (Miller and Zhen, 1991) we hypothesize that the increase of inorganic carbon in seawater could also lead to the decrease of cytosolic NO_3^- in *P. oceanica* leaf cells. Such diminution would affect assimilation (Bloom et al., 2010) and could partially be responsible for the plant biomass nitrogen impoverishment expected under elevated inorganic carbon in vascular plants with non-saturated photosynthesis (Taub and Wang, 2008).

Therefore, the aim of this work was to measure the cytosolic NO_3^- concentration in mesophyll leaf cells of *P. oceanica* to describe the responses to light and dark conditions and to the increase of dissolved inorganic carbon (CO_2 and HCO_3^-) in natural seawater. Ethoxyzolamide, the plasma membrane-permeable carbonic anhydrase inhibitor (Sültemeyer et al., 1993), has been used in combination with CO_2 to test for the effect of limiting any CO_2-dependent HCO_3^- generation. Since the first work in *Chara corallina* (Miller and Zhen, 1991), NO_3^--selective microelectrodes have been used in different plant species, such as barley (Zhen et al., 1991; Van Der Leij et al., 1998), *A. thaliana* (Cookson et al., 2005) and rice (Fan et al., 2007), plus the liverwort *Conocephalum conicum* (Trębacz et al., 1994). However, so far no direct measurement of cytosolic NO_3^- has been reported for marine vascular plants. Furthermore, external NO_3^- has been monitored, and the potential effects of elevated atmospheric CO_2 on the hypothesized diminution on the biomass nitrogen content are also discussed.

MATERIALS AND METHODS

Plant Material

Posidonia oceanica (L.) Delile plants were sampled in Punta de Calaburras (36°30′23.4′′N 4°38′37.6′′W) Málaga, southern Spain, at 2 m depth. Plants with 6 to 12 leaves attached to a piece of the rhizome were collected and transported to the laboratory in a thermos container in less than 30 min. Then, plants were placed in an aquarium filled with continuously aerated natural seawater (NSW). The air used for this purpose was obtained from the compressed air supply of the Faculty of Sciences building. Concentration of CO_2 in the air was regularly monitored (390 ± 10 ppm) using an IRGA, LICOR LI-820, Li, Nebraska (USA). Temperature was held at 15°C, and illumination was at a light intensity of 150 μmol photons·m^{-2}·s^{-1}

with a photoperiod 16L/8D. Renewing the seawater every three days, plants were used for experiments within two weeks after sampling.

Cytosolic NO_3^- and Cl^- Measurements

Cytosolic nitrate and chloride were measured by electrophysiological techniques using double-barreled intracellular microelectrodes. Glass capillary preparation details have been previously described (Fernández et al., 1999). In short, double-barreled capillaries with different diameter (1.5 and 0.75 mm o.d., respectively, Hilgenberg, Germany) were twisted before pulling using a Narishige PD-5 horizontal puller. Then, pulled double-barreled capillaries were heated for 30 min at 180°C and silanized by adding one drop of dichlorodimethylsilane dissolved in benzene (0.05% v/v) to the interior of the blunt end of the larger barrel, while the smaller barrel (that operates as voltage electrode) was not silanized. After that, the silanized double-barrelled capillaries were heated again for 60 min at 180°C. Once cool, the silanized barrel was backfilled with the appropriate chloride or nitrate sensor solution.

For Cl^--microelectrodes, the ionophore I (99408, Fluka), dissolved in a mixture of polyvinylchloride dissolved in tetrahydrofuran (PVC/THF, 4% w/v) was used and backfilled into the silanized barrel. Once THF evaporated, the remainder was filled with 0.5 M KCl (Planes et al., 2015). As described previously (Rubio et al., 2017), Cl^--microelectrodes were calibrated against NaCl solutions (1–100 mM) that contained 5 mM $NaNO_3$, the putative cytosolic NO_3^- concentration (Miller and Smith, 2008), to minimize the interference between Cl^- and NO_3^- in the cytosol (Felle, 1994). Calibration showed a linear relationship of 37 mV/pCl.

NO_3^--microelectrodes were backfilled using a NO_3^- sensor (Fluka 72549) based on the quaternary ammonium compound, methyltridodecylammonium nitrate ($MTDDA.NO_3^-$) containing the PVC/THF solution. These liquid ion-exchange based microelectrodes are highly selective for NO_3^-, maintaining a nitrate detection limit of 0.5 mM in the presence of 100 mM Cl^-, which means any interference will not be important in a physiological situation, as described in Miller and Zhen (1991). Once THF was evaporated from the nitrate-sensor cocktail and before use, the NO_3^--selective barrel was backfilled with 0.1 M $NaNO_3$ and 0.1 M KCl. Then, NO_3^--selective electrodes were calibrated against NO_3K solutions (0.1–20 mM) containing 10 mM KCl, to saturate the presumed interference using the Cl^- concentration reported previously in *P. oceanica* mesophyll leaf cells (Rubio et al., 2017), and KH_2PO_4 (from 15 to 50 mM), to give a constant background ionic strength in the calibration solutions (Miller and Zhen, 1991). NO_3^- calibration showed a linear relationship of 53 mV/pNO_3.

For measurements, the microelectrode voltage barrel was backfilled with 0.5 M KCl (Fernández et al., 1999; Rubio et al., 2005). Then, the NO_3^-- or Cl^--selective microelectrode and the reference electrode (containing agar 0.03% (w/v) in 0.5 M KCl) were fixed to Ag/AgCl electrode holders and connected to a high-impedance differential amplifier (FD223a, WPI, Sarasota, Florida, USA). Amplifier signals were continuously monitored on a double pen chart recorder (Linseis L250E).

Measurements were performed on leaf pieces (≈ 1 cm long), longitudinally peeled to remove part of the epidermis and fixed with paraffin wax on a Plexiglas transparent chamber (1.1 ml volume). A gravity-based flow-through system permitted controlled changes of the assay medium at a rate of 10 $ml{\cdot}min^{-1}$, which renewed chamber volume approximately 10 times every minute. This system kept the temperature, the ionic concentration, and gases constant during the experiments. Measurements were made under a microscope light of 150 $\mu mol\ photons{\cdot}m^{-2}{\cdot}s^{-1}$.

NO_3^- Quantification in Assay Solutions

In order to monitor the net efflux and/or uptake of NO_3^- from assay medium, plants were previously adapted to N-sufficiency by incubation in NSW enriched with 100 μM $NaNO_3$ during 2 days. Then, excised leaves (2–3 g fresh weight) were placed separately in 250 ml flasks and incubated in 100 ml NSW (control) or NSW supplemented with 3 mM $NaHCO_3$. The assay was carried out at 25°C with gentle and constant agitation. For each treatment, samples of assay medium were taken at 0, 1, 2, 3, 5, 7, 10, 15, 20, and 30 min. The highly sensitive method for NO_3^- determination, based on vanadate NO_3^-reduction and the subsequent spectrophotometric determination of NO_2^- (García-Robledo et al., 2014) was used to quantify NO_3^- concentration in each sample. Net efflux and uptake rates were estimated as the slope of the linear phase of NO_3^--concentration time course, as a function of fresh weight (FW). Six replicates were conducted for each assay.

Assay Solutions

Natural seawater (NSW) supplemented with 3 mM HCO_3^- was prepared by adding the appropriate volume of a 0.5 M $NaHCO_3$ stock solution (pH 8.2). CO_2-enriched NSW was obtained by bubbling with artificial air (Air Liquide, Spain, 1000 ppm CO_2-air). A stock solution of the plasma membrane-permeable carbonic anhydrase inhibitor ethoxyzolamide (EZ, 10 mM) was prepared in 0.05 M NaOH. The addition of equivalent volumes of NaOH without the inhibitor had no effect on measurements. All chemicals were analytical grade and were purchased from Sigma-Aldrich.

Data Presentation and Statistical Analyses

Time-course measurements are shown as single traces, representative of a number of equivalent experiments carried out under the same conditions, as stated in the figure legends. Data are presented as means, and error bars are standard deviations. Number of repetitions (n) is indicated in every experiment. Data were analyzed using SPSS Statistics, version 21. The significance level was set at $P < 0.05$.

RESULTS

Effect of Light-Dark Transitions on *P. oceanica* Cytosolic NO_3^-

In NSW, mesophyll leaf cells of *P. oceanica* showed a stable plasma membrane potential of −174 ± 8 mV (as in Rubio et al., 2017) and

a cytosolic NO_3^- concentration of 5.7 ± 0.2 mM (n = 10). The transition from light to darkness evoked a fast depolarization of approximately 14 mV followed by a transient hyperpolarization of 22 mV and a subsequent, more prolonged, depolarization to level of at a lower membrane potential of −140 ± 5 mV (n = 12, P = 0.003, Student t test) after 25 min in the dark. With a delay of a few minutes, light-dark transition promoted the gradual increase of cytosolic NO_3^- concentration that stabilized at a higher value (7.2 ± 0.6 mM NO_3^-; n = 10, P = 0.02, Student t test) after 30 min in the dark (**Figure 1**).

Effect of HCO_3^--Enriched NSW on Cytosolic NO_3^-

We have previously reported that in *P. oceanica* mesophyll leaf cells, incubated in light conditions, the addition of NSW enriched with 3 mM HCO_3^- evoked an initial and transient plasma membrane depolarization that turned into a transient hyperpolarization to stabilize at a depolarized value (Rubio et al., 2017). The simultaneous measurement of cytosolic chloride showed a delayed but significant decrease of the cytosolic concentration of this anion concomitant with the extent of membrane depolarization (Rubio et al., 2017). The partial sensitivity of Cl^--selective microelectrodes to NO_3^- (Miller and Zhen, 1991; Felle, 1994) allows us to hypothesize that HCO_3^- enrichment not only produces the cytosolic Cl^- decrease but could also evoke a cytosolic NO_3^- shift. To test this hypothesis, cytosolic NO_3^- was measured in *P. oceanica* mesophyll leaf cells in the same conditions that we had reported for cytosolic chloride, the monitoring of which was used as a control in this work. **Figure 2** shows the membrane potential response to the enrichment of NSW with 3 mM HCO_3^- (black trace) and the simultaneous measurements of cytosolic Cl^- (green trace) or NO_3^- (blue trace), values and stats are presented in **Table 1**. As found previously (Rubio et al., 2017), the addition of 3 mM HCO_3^- caused an initial and transient membrane depolarization (black trace) of approximately 5 mV, which turned into a transient hyperpolarization (reaching a minimum membrane potential of −181 ± 2 mV, n = 5, P = 0.012, Student t test), followed by a prolonged depolarization that stabilized within approximately 40 min at a membrane potential of −168 ± 3 (n = 5). Also in agreement with the previous study, the addition of 3 mM HCO_3^- evoked a decrease of cytosolic Cl^- (after approximately 4 min) which continued progressively from 9.7 ± 0.2 mM to 6.3 ± 0.3 mM (green trace, n = 5; P = 0.004, Student t test) 20 min after HCO_3^- addition. Supporting the hypothesis of HCO_3^- enrichment's producing a cytosolic NO_3^- shift, *P. oceanica* mesophyll leaf cell cytosolic NO_3^- also decreased in response to the enrichment of NSW with 3 mM HCO_3^- (**Figure 2**, blue trace). In common with the response of cytosolic Cl^-, the diminution of cytosolic NO_3^- started approximately 4 min after HCO_3^- treatment. Cytosolic NO_3^- diminished gradually from 5.7 ± 0.2 mM to a steady lower value of 4.7 ± 0.1 mM after 35 min of HCO_3^- addition, resulting in a significant cytosolic NO_3^- shift of 0.9 ± 0.06 mM (n = 5; P = 0.03, Student t test). In both cases, time courses of cytosolic NO_3^- and cytosolic Cl^- decreases aligned with the recovery of the transient membrane hyperpolarization and profound membrane depolarization, supporting a cytosolic leak of negative charge induced by the HCO_3^- addition.

Effect of CO_2 Increase on Cytosolic NO_3^-

As we have previously reported, in *P. oceanica* mesophyll leaf cells the direct uptake of HCO_3^- and the subsequent use of CO_2 for photosynthesis has consequences for anion homeostasis (Rubio et al., 2017). In this work, we show that HCO_3^- use in this plant has an effect not only on cytosolic Cl^- but also on

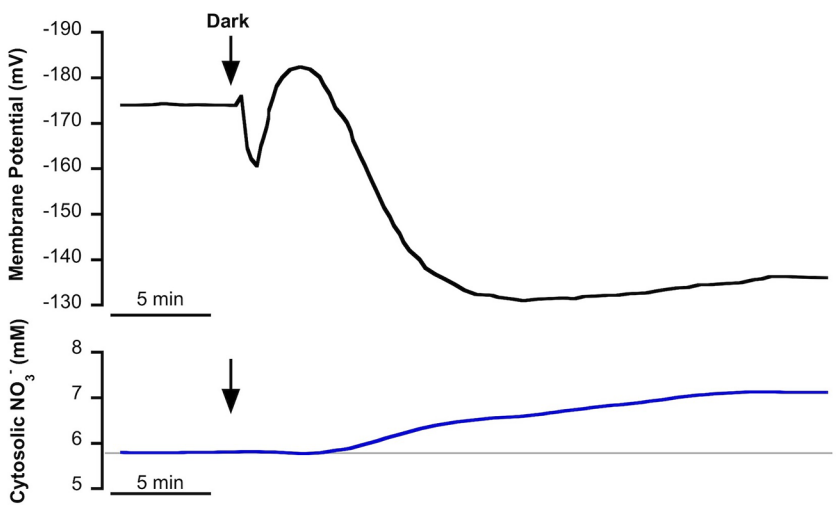

FIGURE 1 | Effect of light-dark transition on plasma membrane potential (*Em*, mV) and cytosolic NO_3^- (mM) in *Posidonia oceanica* mesophyll leaf cells, incubated in natural seawater. Traces are representative examples of intracellular nitrate-selective microelectrode recordings from 10 independent experiments. Arrows indicate the onset of dark treatment. Auxiliary grey line shows the standard cytosolic NO_3^- concentration under light conditions (150 µmol photons m^{-2} s^{-1}). Mean values and statistics are indicated in the text.

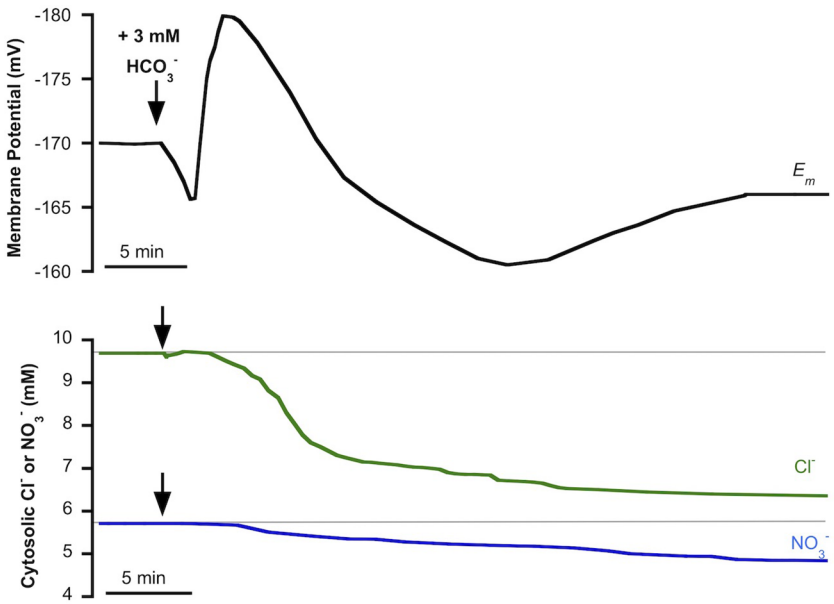

FIGURE 2 | Effect of the addition of 3 mM HCO_3^- on the plasma membrane potential (*Em*, mV), cytosolic chloride (Cl^-, mM) or cytosolic NO_3^- (NO_3^-, mM) measured in mesophyll leaf cells of *Posidonia oceanica*. Assay medium consisted of natural seawater and arrows indicate the addition of 3 mM HCO_3^-. Traces are representative examples from five independent recordings using intracellular Cl^--selective (green trace) or NO_3^--selective (blue trace) microelectrodes, respectively. Auxiliary grey lines indicate the normal cytosolic Cl^- or NO_3^- concentrations before HCO_3^- addition. Mean values and statistics are indicated in the text and in **Table 1**.

TABLE 1 | Membrane potential (mV), cytosolic NO_3^- (mM), and cytosolic Cl^- (mM) measured in mesophyll leaf cells of *P. oceanica* incubated in natural seawater (NSW) supplemented with different inorganic carbon concentrations.

	Membrane Potential (mV)	Cytosolic NO_3^- (mM)	Cytosolic Cl^- (mM)
NSW	−170 ± 8 initial value	5.7 ± 0.2 initial concentration	9.7 ± 0.2 initial concentration
+3 mM HCO_3^-	−181 ± 2* initial hyperpolarization −168 ± 3 final value	4.7 ± 0.1* final concentration	6.3 ± 0.3* final concentration
+1000 ppmCO_2	−174 ± 3 initial hyperpolarization −165 ± 3 final value	5.3 ± 0.6 final concentration	
+1000 ppmCO_2 (0.1 mM EZ)	−178 ± 2 final value	5.6 ± 0.1 final concentration	

EZ is the carbonic anhydrase inhibitor, ethoxyzolamide. Values are mean ± SD of a number of experiments indicated in the text. Asterisks (*) denote significant differences with respect to control conditions (NSW), the statistical values are indicated in the text.

cytosolic NO_3^- (**Figure 2**). The match of membrane depolarization and the onset of cytosolic Cl^- and NO_3^- diminution suggests the involvement of plasma membrane S-type anion channels, which are permeable to both anions and whose activation takes place when cells depolarize (Schmidt et al., 1995; Roelfsema et al., 2004; Roberts, 2006). In terrestrial angiosperm guard cells, these channels are activated when the concentration of HCO_3^- (not CO_2) increases and the cytosolic pH (pHc) is alkaline (Xue et al., 2011). These are similar conditions to those observed in *P. oceanica* in the presence of high HCO_3^- (Rubio et al., 2017). In order to rule out the role of CO_2, cytosolic NO_3^- was measured in mesophyll leaf cells of *P. oceanica* incubated in NSW supplemented with 1000 ppm CO_2, in the absence or in the presence of the plasma membrane-permeable carbon anhydrase inhibitor ethoxyzolamide (0.1 mM EZ; Sültemeyer et al., 1993). As shown in **Figure 3** (data are summarized in **Table 1**), the increase of CO_2 in NSW evoked a gradual plasma membrane hyperpolarization, reaching a value of −174 ± 3 mV (n = 5) after 7 min of 1000 ppm CO_2 treatment. This maximum hyperpolarization was lower and almost 2 min delayed compared to that induced by the treatment with 3 mM HCO_3^-, included in **Figure 3** as control (black trace). Cytosolic NO_3^- also decreased after the addition 1000 ppm CO_2; however, in these conditions cytosolic NO_3^- diminution was lower than that induced by 3 mM HCO_3^- treatment. After 15 min in the presence of 1000 ppm CO_2, cytosolic NO_3^- stabilized at a concentration of 5.3 ± 0.6 mM, a statistically non significant shift (n = 5; P = 0.37, Student t test). Furthermore, in the presence of 0.1 mM EZ, the enrichment of NSW with 1000 ppm CO_2 evoked a marked plasma membrane hyperpolarization that reached a steady maximum value of −178 ± 2 mV after 12 min treatment. In the presence of EZ, cytosolic NO_3^- showed a minimum, statistically non-significant, shift from 5.7 ± 0.2 to 5.6 ± 0.1 mM NO_3^- (n = 4; P = 0.53, Student t test). That neither

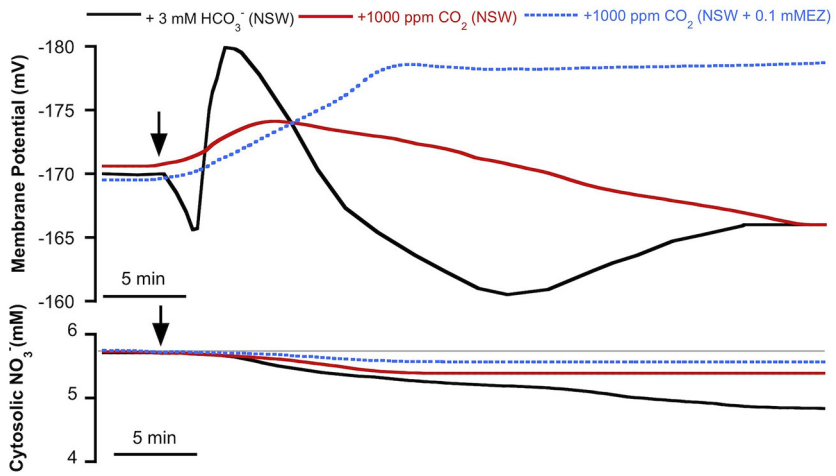

FIGURE 3 | Effect of inorganic carbon increase on the plasma membrane potential (*Em*, mV) and cytosolic NO_3^- (mM) measured in *Posidonia oceanica* mesophyll leaf cells. Arrows indicate the onset of 3 mM HCO_3^- addition to natural seawater (NSW, black traces, control conditions) and the addition of 1,000 ppm CO_2 to NSW (red traces) or to NSW containing 0.1 mM ethoxyzolamide (EZ, dashed blue traces). Traces are representative records of a minimum of four independent experiments using intracellular NO_3^--selective microelectrodes. Mean values and statistics are indicated in the text and **Table 1**. Auxiliary grey line represents the normal cytosolic NO_3^- concentration before the inorganic carbon additions.

the long-term depolarization nor the drop in cytosolic NO_3^- content evoked by HCO_3^- were evident with CO_2 in the presence of EZ (thus restricting HCO_3^- production from the CO_2 source) points to the need for substantial cytosolic HCO_3^- accumulation to effect ionic fluxes. Accordingly, these results strongly indicate that the cytosolic NO_3^- decrease is caused by the HCO_3^- enrichment and point to the S-type anion channel activation by the cytosolic HCO_3^- (not CO_2) increase.

Effect of HCO_3^- Increase on External NO_3^-

The activation of S-type anion channels may allow the efflux of NO_3^- from mesophyll leaf cells; such a phenomenon of NO_3^- efflux should be higher in the case of NO_3^--replete cells. Thus, in order to investigate if the HCO_3^- enrichment of NSW promoted NO_3^- efflux from *P. oceanica* leaves, the time course of external NO_3^- concentration change was monitored in assay medium containing leaves from plants pre-incubated for 2 days in NSW containing 100 μM NO_3^-. NO_3^--supplied leaves were then incubated in NSW containing the standard NO_3^- concentration (10 μM). After the addition of 3 mM HCO_3^-, external NO_3^- concentration increased significantly (10.8 ± 0.04 μM NO_3^-; n = 6; P <0.001, Student t test) within the first minute of incubation. Maximum net efflux rate was 18 ± 2 nmol $NO_3^-{\cdot}g_{FW}^{-1}{\cdot}min^{-1}$. Then, external NO_3^- decreased at a net rate of 8 ± 1 nmol $NO_3^-{\cdot}g_{FW}^{-1}{\cdot}min^{-1}$ until 5 min of incubation to stabilize at a concentration of 9.2 ± 0.1 μM NO_3^- (**Figure 4**). Under control conditions (no HCO_3^- addition), no external NO_3^- increase was detected, but NO_3^- concentration progressively decreased at a net rate of 11 ± 2 nmol $NO_3^-{\cdot}g_{FW}^{-1}{\cdot}min^{-1}$ during the first 10 min of incubation to reach a steady lower value of 7.6 ± 0.2 μM NO_3^- (n = 6;

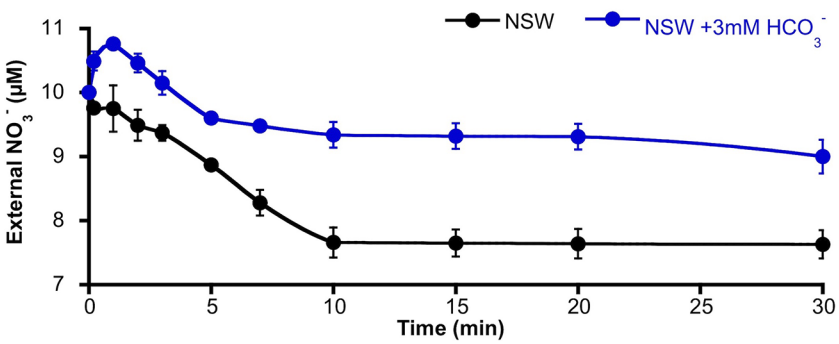

FIGURE 4 | Time course of the external nitrate concentration around *Posidonia oceanica* leaf pieces incubated in NSW. Plants were previously incubated in NSW containing 100 μM NO_3^-, then excised leaves were incubated in NSW (black trace, control condition) or NSW supplemented with 3 mM HCO_3^- (blue trace). At different times within the first 30 min of incubation, samples were taken and used to determinate external NO_3^- concentration. Data are mean ± SD of six independent assays. Mean values, net efflux, and influx NO_3^- rates and statistics are indicated in the text.

P = 0.002, Student t test). External NO_3^- concentrations showed higher values in all samples from leaves incubated in NSW enriched with 3 mM HCO_3^- suggesting a net NO_3^- efflux from *P. oceanica* leaves under these conditions.

DISCUSSION

Cytosolic NO_3^- Changes During Light–Dark Transitions in *P. oceanica* Leaf Cells

The concentration of NO_3^- in the cytosol (NO_3^-c) depends on a series of highly regulated processes at the cellular level that includes sensing and transport at the plasma membrane (uptake and efflux), subcellular compartmentalization and metabolism. Depending on the technique and the plant system used, a wide range of cytosolic NO_3^- values has been reported with also a large degree of variability. Therefore some authors suggest that NO_3^-c would not be subject to homeostasis, as would be the case for cytosolic pH or Ca^{2+} for example (for discussion see Siddiqi and Glass, 2002 or Miller and Smith, 2008). After the development of intracellular NO_3^--selective microelectrodes by Miller and Zhen (1991) it is possible to perform continuous measurements of the cytosolic free ion activity of NO_3^- with the possibility to obtain instantaneous responses to changes in the experimental conditions. This approach has been used here to report the first cytosolic NO_3^- values of a marine vascular plant.

Under light conditions the cytosolic NO_3^- measured using intracellular NO_3^--selective microelectrodes in *P. oceanica* mesophyll leaf cells was 5.7 ± 0.2 mM (n = 10), almost double the value reported for both epidermal and mesophyll leaf cells of *A. thaliana* (2.2 and 2.8 mM NO_3^-c, respectively; Cookson et al., 2005). This cytosolic NO_3^- in mesophyll leaf cells of *P. oceanica* is also much higher than that reported for the intermodal cells of the freshwater alga *C. corallina* (1.6 mM NO_3^-; Miller and Zhen, 1991) or in the liverwort *C. conicum* (0.63 mM NO_3^-; Trębacz et al., 1994), using the same technique. However, the NO_3^-c value found in *P. oceanica* is similar to those observed in root cells of barley (5.4 mM NO_3^-; Zhen et al., 1991) or maize (3.1 mM NO_3^-; Miller and Smith, 1996).

The NO_3^-c value in mesophyll leaf cells of *P. oceanica* is lower than the cytosolic Cl^- concentration (Cl^-c) of 9.7 mM Cl^-, yielding a NO_3^-c/Cl^-c of 0.6. This ratio is higher than that calculated for *C. conicum,* NO_3^-c/Cl^-c ≈ 0.1, taking 7.4 mM as the Cl^-c (Trębacz et al., 1994), but it is in the range of the estimates for root cells of barley (NO_3^-c/Cl^-c ≈ 0.9) or *A. thaliana* mesophyll leaf cells (NO_3^-c/Cl^-c ≈ 0.3). Those values have been calculated considering Cl^-c as 6 mM for barley root cells (Britto et al., 2004) and assuming that the reported cytosolic Cl^- in *A. thaliana* root cells (8.7 mM Cl^-c; Planes et al., 2015) would be the same in mesophyll leaf cells.

Changes in environmental conditions have been related to NO_3^-c alterations, supporting the idea that the cytosol operates a strong ion homeostasis not only for pH, Pi or Ca^{2+}, but also for NO_3^- (reviewed by Miller and Smith, 2008). Light-dark transition triggers a slight increase of NO_3^-c in the liverwort *C. conicum* (Trębacz et al., 1994) and a transient increase, from 2 to 3.5 mM, which peaked after 7 min of darkness in the case of *A. thaliana* leaf cells (Cookson et al., 2005). A similar response has been found here in *P. oceanica* mesophyll leaf cells, in which cytosolic NO_3^- reached a maximum value of 7.2 mM after 25 min of dark treatment. In the case of *A. thaliana*, since the effect was not observed when measurements were performed in the nitrate reductase (NR) mutant (*nia1nia2*) leaf cells, the NO_3^-c increase was explained because the shift to the dark inactivates NR, leading to a transient build-up of NO_3^-c due to a slower reduction rate (Cookson et al., 2005). A higher NO_3^-c in *A. thaliana nia1nia2* mesophyll leaf cells and a similar time course of cytosolic increase to the rate of NR activity change in response to illumination transitions (half-life of 2 to 15 min in spinach; Huber et al., 1992; Kaiser et al., 1992; Riens and Heldt, 1992) support the evidence for the role of NR in regulating NO_3^-c (Cookson et al., 2005). In *P. oceanica*, the NO_3^-c increase observed in the dark could also explain the one-half diminution of the maximum high affinity NO_3^- uptake observed previously in mesophyll leaf cells of this plant (Rubio et al., 2018), due to the apparent substrate inhibition of the transporter.

Inorganic Carbon Increase Triggers Cytosolic NO_3^- Decrease

In a previous work we demonstrated that a plasma membrane nH^+/HCO_3^- symporter mediates the uptake of HCO_3^- in *P. oceanica* mesophyll leaf cells. Further, the direct uptake of HCO_3^- followed by its internal dehydration renders CO_2 (used for photosynthesis) and hydroxyl anions, promoting membrane potential and cytosolic pH and Cl^- variations (Rubio et al., 2017). In the present work, we have also verified that uptake of HCO_3^- promotes the decrease of NO_3^-c in *P. oceanica* mesophyll leaf cells. The increases of cytosolic HCO_3^- and cytosolic pH have been related to promoting the opening of plasma membrane S-type anion channels in guard cells (Xue et al., 2011). A similar pathway seems to explain the NO_3^-c diminution observed in response to HCO_3^- addition in *P. oceanica* mesophyll leaf cells, as was previously proposed in the case of Cl^-c (Rubio et al., 2017), used as a control in this work. In both cases, the onset of NO_3^-c and Cl^-c decreases matched that of the plasma membrane depolarization, and indeed depolarization is a required initial phase to activate S-type anion channels operating at the plasma membrane of guard cells (Schmidt et al., 1995; Roelfsema et al., 2004; Roberts, 2006).

S-type anion channels are encoded by the small *SLAC/SLAH* gene family, that share homology to transport systems found in different kingdoms (Dreyer et al., 2012). In *A. thaliana*, apart from *SLAC1* that is exclusively expressed in guard cells, four additional homologs (*SLAH1-4*) are present (Negi et al., 2008). SLAC1 and SLAH3 channels exhibit a permeability preference for NO_3^- and Cl^- but not for malate (Schmidt and Schroeder, 1994; Geiger et al., 2009; Chen et al., 2010). The SLAH3 channel has the highest permeability for NO_3^- (NO_3^-/Cl^- permeability ratio of 20) and in contrast to SLAC1, SLAH3 also requires extracellular NO_3^- to induce its activity (Geiger et al., 2011).

Furthermore, a role in NO_3^--dependent alleviation of ammonium toxicity in *A. thaliana* roots has been proposed for SLAH3 (Zheng et al., 2015).

Although seagrasses have lost stomata differentiation genes (Olsen et al., 2016) the presence of S-type anion channels cannot be ruled out in those plants since, presumably, these anion channels have evolved as emergency valves, rapidly releasing excess osmolytes under stress conditions (Roelfsema et al., 2012). The *Zostera marina* genome, the first one available from a seagrass (Olsen et al., 2016), contains two homologs for the *A. thaliana SLAC/SLAH* gene family (*Phytozome v12.1*, data base), one *SLAH1* homolog (*Zosma91g00860.1*) and one *SLAC1* homolog (*Zosma76g00610.1*). The presumed homologs of these channels in *P. oceanica* should be good candidates for the proposed channels for the leak of NO_3^- and Cl^- ions from the cytosol, but further molecular analyses are needed to characterize the specific role of these anion channels to mediate anion efflux in response to high HCO_3^-.

In guard cells, stomatal closure in response to high CO_2 is mediated by the activation of S-type (SLAC1/SLAH3) anion channels (reviewed by Hedrich and Geiger, 2017). Interestingly, guard cells do not sense CO_2 themselves, but instead HCO_3^- synthesized from CO_2 within the cytosol by carbonic anhydrases (Xue et al., 2011). The same case could be proposed in *P. oceanica* mesophyll leaf cells, since no significant NO_3^-c decrease was found in response to 1000 ppm CO_2 treatment in either the absence or the presence of the plasma membrane-permeable carbon anhydrase inhibitor ethoxyzolamide, suggesting that HCO_3^-, not CO_2, is the inorganic carbon species that triggers NO_3^-c efflux from *P. oceanica* mesophyll leaf cells (**Figure 5**). Furthermore, probably due to the activation of the H^+-pump in response to the cytosolic accumulation of CO_2, a weak acid, the 1000 ppm CO_2 treatment renders the hyperpolarization of the plasma membrane and the cytosolic acidification (see Rubio et al., 2017). Both responses are prolonged in the presence of ethoxyzolamide, that impairs HCO_3^- production from the CO_2 source, leading to conditions that not support the activation of S-type anion channels described above and could explain the non-significant NO_3^-c diminution observed in response to CO_2 increase.

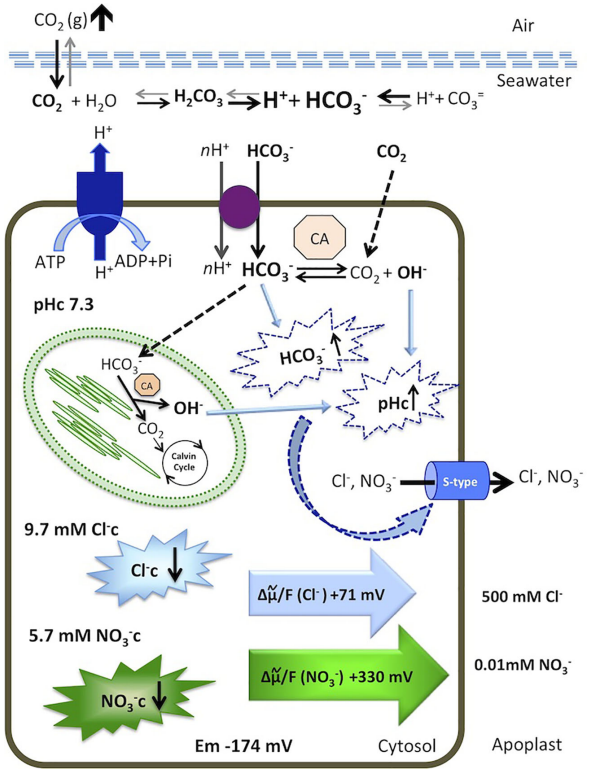

FIGURE 5 | Model for cytosolic NO_3^- and Cl^- responses to an increase of dissolved inorganic carbon in the marine angiosperm *Posidonia oceanica* leaf cells. Elevated atmospheric CO_2 level increases total dissolved inorganic carbon, shifting the equilibrium in favor of HCO_3^- in the seawater. The HCO_3^- is taken up by an H^+-symport and dehydrated in the cytosol or transported to the chloroplast serving as inorganic carbon source for photosynthesis. Internal dehydration, catalyzed by the carbonic anhydrases (CA) renders CO_2, consumed by the Calvin Cycle, and OH^- ions that increase cytosolic pH (pHc). Excess of cytosolic HCO_3^- and elevated pHc activates S-type anion channels, through which Cl^- and NO_3^- leave the cells by an outwardly directed motive force of +71 mV and +330 mV, respectively. Consequently, the cytosolic concentrations of both anions decrease. Membrane potential, ion concentrations, calculations, and discussion are included in the text.

Cytosolic NO_3^- Efflux Under High Inorganic Carbon Could Contribute to Biomass N-Impoverishment in Seagrasses

As we showed previously, direct HCO_3^- uptake has consequences for cytosolic ion homeostasis in *P. oceanica* mesophyll leaf cells (Rubio et al., 2017). The short-term net efflux of NO_3^- and the low NO_3^- net uptake rate observed in the present work also indicate that natural seawater HCO_3^- enrichment may be important not only for cytosolic ion homeostasis but for the metabolic flux of NO_3^- in this seagrass. In natural seawater, containing 500 mM Cl^- and 10 μM NO_3^-, the efflux of Cl^- and NO_3^- from *P. oceanica* mesophyll leaf cells is driven by the outwardly directed anion electrochemical potential gradients for both anions (**Figure 5**). This electrochemical potential gradient (in mV) is almost five-fold higher for NO_3^- (+330 mV) than for Cl^- (+71 mV). However, in response to high HCO_3^- the Cl^-c decrease observed in *P. oceanica* mesophyll leaf cells (ΔCl^-c = 3.4 mM) was much higher than for NO_3^-c (ΔNO_3^-c = 1 mM). This lower NO_3^-c leak than the expected from electrochemical potential gradient comparison with Cl^-c could be explained by a different membrane permeability for both anions and/or different capability of compartmentalization. Nevertheless, even the observed decrease of NO_3^-c, the short-term NO_3^- efflux, and the low NO_3^- uptake rate could impair N-assimilation in *P. oceanica* leaf cells in natural seawater containing high inorganic carbon.

An impaired metabolic flux of N should be relevant in the context of atmospheric CO_2 rise. Oceans have been the sink for 30% of CO_2 released during the industrial era, at a higher rate (3.8 GTons·year^{-1}) than the 1.8 GTons·year^{-1} fixed by photosynthesis or the 2 GTons·year^{-1} removed by abiotic absorption (Behrenfeld et al., 2002). Atmospheric CO_2 is

exchanged into aquatic environments rendering the dissolved inorganic carbon (DIC) equilibrium. Controlled by pH, this equilibrium generates the distribution of DIC species: dissolved CO_2, bicarbonate (HCO_3^-) and carbonate (CO_3^{2-}) ions. Consequently, elevated atmospheric CO_2 concentration increases the total DIC and lowers the pH, shifting the relative proportion of each DIC species. Under current ocean pH (~8.04) and atmospheric CO_2 (~ 410 ppm), the smallest pool of DIC is dissolved CO_2, but this will have the greatest increase (> 250%) among the DIC constituents as the pH drops (~ 0.3–0.4 pH units) under the predicted rise in atmospheric CO_2 (1000 ppm) for 2100. In contrast, the HCO_3^- pool will only increase by 15% at that date (Koch et al., 2013). However, in terms of absolute concentration ($mol{\cdot}kg^{-1}$) HCO_3^- levels will rise more than dissolved CO_2 (Raven et al., 2005). Using the predicted data for 2100, calculations render 2.05 $mmol{\cdot}kg^{-1}$ HCO_3^- and only 0.03 $mmol{\cdot}kg^{-1}$ CO_2 (Koch et al., 2013). Considering such a HCO_3^- rise (1.2 fold higher than actual concentration) and that the addition of 3 mM HCO_3^- corresponds to an increase by 2.3 fold of the HCO_3^- concentration in natural seawater, a NO_3^-c leak of 0.5 mM would be expected in *P. oceanica* mesophyll leaf cells by 2100. However, long-term effect of elevated atmospheric CO_2 concentration on seagrasses N content needs further investigation, since N-deficiency induces high-affinity NO_3^- uptake, which contributes to NO_3^- homeostasis (reviewed by Rubio and Fernández, 2019).

Furthermore, the concomitant natural seawater pH decrease under elevated atmospheric CO_2 could alter N availability in seawater and even the energy cost for nutrient uptake. A pH change from 8.1 to 7.8 evokes a decrease in the amount of NH_3 in the NH_4^+/NH_3 ratio (Raven, 1986), whereas the amount of NO_3^- would not be affected (Zeebe and Wolf-Gladrow, 2001). Instead, the 0.3 external pH unit decrease renders a rise of the proton motive force at the plasma membrane of *P. oceanica* leaf cells of −18 mV, considering −174 mV as membrane potential, 7.3 as the cytosolic pH and constant temperature (Rubio et al., 2017). This amount represents, approximately, a 15% increase of the proton motive force (inwardly directed), which could prompt the activity of H^+-dependent transport systems in this seagrass, including the plasma membrane H^+/HCO_3^- symporter (Rubio et al., 2017). As discussed by Rubio and Fernández (2019), ocean acidification could increase both the H^+ and even the Na^+ motive force due to changes in the activity of the plasma membrane Na^+/H^+ antiporter found in seagrass species (Rubio et al., 2011). The activity of this antiporter generates a lower cytosolic Na^+ concentration at acid external pH and, consequently, a rise of the inwardly directed Na^+ motive force could be also expected, favoring high-affinity NO_3^- uptake based on Na^+-dependent transport systems in seagrasses (reviewed by Rubio and Fernández, 2019). In fact, a recent study in *P. oceanica* beds from the Gulf of Naples (Italy) shows that the long-term exposure (9 months) to acidified seawater (pH 7.82) under constant DIC conditions promotes the diminution of the C/N molar ratio, due to the increase of N content by 21% and 70% in leaves and rhizome, respectively, whereas C content of those organs is not affected by external pH acidification (Scartazza et al., 2017). Those authors suggest that seawater acidification promoted a feed-forward long-term effect on N accumulation in *P. oceanica*, especially at the rhizome, although they recognize the need to specify the effect of acidification on the nutrient availability in their study (Scartazza et al., 2017). Interestingly, long-term nutrient enrichment seems to modulate the effects of ocean acidification on *P. oceanica*. Molecular analysis indicates that after 18 months at low pH (7.78) conditions the expression of nitrate transporter genes in *P. oceanica* leaves is altered; while *NRT1_6.3* and *NRT1_2.13* (involved in NO_3^- sensing and low-affinity transport, respectively) are overexpressed the high-affinity NO_3^- transporter gene *NRT2* shows a down-regulated expression (Ravaglioli et al., 2017). Thus, long-term overexpression of nitrogen transporter genes following nutrient additions at low pH suggests enhanced nutrient uptake and proposes that the effects of ocean acidification on *P. oceanica* depend upon local nutrient concentration (Ravaglioli et al., 2017).

Contrary to the acidification effect in *P. oceanica* meadows, several lines of evidence show that the most common effect of elevated CO_2 is a decrease in the dry mass concentration of N in plant tissue (Cotrufo et al., 1998; Curtis and Wang, 1998; Norby et al., 1999; Jablonski et al., 2002; Ainsworth and Long, 2005; Taub et al., 2008). This suggests that physiological changes leading to decreased biomass N under elevated CO_2 predominate in their effects over factors that would tend to increase N content (reviewed by Taub and Wang, 2008). Consequently, plants with non-saturated photosynthesis at actual atmospheric CO_2, show an ionomic imbalance, with N the main nutrient that decreased at high C assimilation (Loladze, 2014). The physiological mechanisms responsible for this phenomenon have not been well established yet, although different hypotheses are proposed to account for it. In terrestrial vascular plants, the best-supported are the decrease of specific N uptake and assimilation due to a diminution of the transpiration-driven mass flow of N by a decreased stomatal conductance at elevated CO_2 and the biomass dilution of N by increased photosynthetic assimilation of C (reviewed by Taub and Wang, 2008).

Seagrass meadows rank among the most productive ecosystems on Earth (Duarte and Chiscano, 1999), which largely contribute to C uptake in coastal waters and with most species capable of utilizing HCO_3^- as a CO_2 source for photosynthesis (Raven et al., 2014). With the exception of *Cymodocea nodosa* (considered C4), seagrasses show C3 photosynthetic pathways and are not saturated at the current ocean DIC concentration (reviewed by Koch et al., 2013). As occurs in C3 terrestrial plants, a higher C assimilation occurs in seagrasses due to the rise of DIC discussed above (Borum et al., 2016). The unpredicted effect of HCO_3^- enrichment on anion homeostasis in *P. oceanica* mesophyll leaf cells, leading to the short-term efflux of NO_3^- from the cytosol, possibly through the activation of S-type anion channels, supports a new mechanism as a key consideration in understanding the expected biomass N-alteration in seagrasses under elevated DIC, and probably, for terrestrial plants growing in waterlogged alkaline environments.

DATA AVAILABILITY STATEMENT

The datasets generated for this study are available on request to the corresponding author.

AUTHOR CONTRIBUTIONS

LR, DG-P, and JF performed the experiments. DG-P and LR accomplished data analysis. LR, JD, and JF discussed the results, wrote and edited the manuscript. LR and JF conceived the project. All authors contributed to the article and approved the submitted version.

FUNDING

This work was supported by the Spanish Ministerio de Economía y Competitividad (cofinanced by the European Regional Development Fund; grant BFU2017-85117-R) awarded to JF and LR and the University of Cambridge's Central Chest (JD).

ACKNOWLEDGMENTS

This work has been done in the framework of BIO2016-81957-REDT (LR and JF) and Campus de Excelencia Internacional del Mar, CEIMAR (Andalucía Tech).

REFERENCES

Ainsworth, E. A., and Long, S. P. (2005). What have we learned from 15 years of free-air CO_2 enrichment (FACE)? A meta-analytic review of the responses of photosynthesis, canopy properties and plant production to rising CO_2. *New Phytol.* 165, 351– 372. doi: 10.1111/j.1469-8137.2004.01224.x

Aires, T., Marbà, N., Cunha, R. L., Kendrick, G. A., Walker, D. I., Serrão, E. A., et al. (2011). Evolutionary history of the seagrass genus Posidonia. *Mar. Ecol. Prog. Ser.* 421, 117–130. doi: 10.3354/meps08879

Behrenfeld, M. J., Esaias, W. E., and Turpie, K. R. (2002). "Assessment of the primary production at the global scale," in *Phytoplankton Productivity. Carbon Assimilation in Marine and Freshwater Ecosystems*. Eds. P. J. Ie B. Williams, D. N. Thomas and C. S. Reynolds (Oxford, UK: Blackwell Science), 156–186.

Bethoux, J. P., Boukhary, E. 1., Ruiz-Pino, M. S., Porin, D., and Copin-Montégut, P. (2005). "Nutrient, oxygen and carbon ratios, CO_2 sequestration and anthropogenic forcing in the Mediterranean Sea," in *The Mediterranean Sea. The Handbook of Environmental Chemistry*. Ed. A. Saliot (Berlin/Heidelberg, Germany: Springer), 67–87, ISBN: .

Bloom, A. J., Burger, M., Rubio Asensio, J. S., and Cousins, A. B. (2010). Carbon dioxide enrichment inhibits nitrate assimilation in wheat and Arabidopsis. *Science* 328 (5980), 899–903. doi: 10.1126/science.1186440

Borum, J., Pedersen, O., Kotula, L., Fraser, M. W., Statton, J., Colmer, T. D., et al. (2016). Photosynthetic response to globally increasing CO_2 of co-occurring temperate seagrass species. *Plant Cell Environ.* 39 (6), 1240–1250. doi: 10.1111/pce.12658

Britto, D. T., Ruth, T. J., Lapi, S., and Kronzucker, H. J. (2004). Cellular and whole-plant chloride dynamics in barley: Insights into chloride-nitrogen interactions and salinity responses. *Planta* 218 (4), 615–622. doi: 10.1007/s00425-003-1137-x

Chen, Y. H., Hu, L., Punta, M., Bruni, R., Hillerich, B., Kloss, B., et al. (2010). Homologue structure of the SLAC1 anion channel for closing stomata in leaves. *Nature* 467, 1074–1080. doi: 10.1038/nature09487

Cookson, S. J., Williams, L. E., and Miller, A. J. (2005). Light-dark changes in cytosolic nitrate pools depend on nitrate reductase activity in Arabidopsis leaf cells. *Plant Phys.* 138 (2), 1097–1105. doi: 10.1104/pp.105.062349

Cotrufo, M. F., Ineson, P., and Scott, A. (1998). Elevated CO_2 reduces the nitrogen concentration of plant tissues. *Glob. Change Biol.* 4, 43–54. doi: 10.1046/j.1365-2486.1998.00101.x

Curtis, P. S., and Wang, X. (1998). A meta-analysis of elevated CO_2 effects on woody plant mass, form and physiology. *Oecologia* 113, 299–313. doi: 10.1007/s004420050381

Demir, F., Horntrich, C., Blachutzik, J. O., Scherzer, S., Reinders, Y., Kierszniowska, S., et al. (2013). Arabidopsis nanodomain-delimited ABA signaling pathway regulates the anion channel SLAH3. *Proc. Natl. Acad. Sci. U.S.A.* 110, 8296–8301. doi: 10.1073/pnas.1211667110

Dreyer, I., Gomez-Porras, J. L., Riaño-Pachón, D. M., Hedrich, R., and Geiger, D. (2012). Molecular evolution of slow and quick anion channels (SLACs and QUACs/ ALMTs). *Front. Plant Sci.* 3, 263. doi: 10.3389/fpls.2012.00263

Duarte, C. M., and Chiscano, C. L. (1999). Seagrass biomass and production: A reassessment. *Aquat. Bot.* 65, 159–174. doi: 10.1016/S0304-3770(99)00038-8

Fan, X., Jia, L., Li, Y., Smith, S. J., Miller, A. J., and Shen, Q. (2007). Comparing nitrate storage and remobilization in two rice cultivars that differ in their nitrogen use efficiency. *J. Exp. Bot.* 58 (7), 1729–1740. doi: 10.1093/jxb/erm033

Felle, H. (1994). The H^+/Cl^- symporter in root-hair cells of *Sinapis alba*. *Plant Physiol.* 106, 1131–1136. doi: 10.1104/pp.106.3.1131

Fernández, J. A., García-Sánchez, M. J., and Felle, H. (1999). Physiological evidence from a proton pump at the plasma membrane of the marine angiosperm *Zostera marina* L. *J. Exp. Bot.* 50, 1763–1768. doi: 10.1093/jxb/50.341.1763

García-Robledo, E., Corzo, E., and Papaspyrou, S. (2014). A fast and direct spectrophotometric method for the sequential determination of nitrate and nitrite at low concentrations in small volumes. *Mar. Chem.* 162, 30–36. doi: 10.1016/j.marchem.2014.03.002

García-Sánchez, M. J., Jaime, M. P., Ramos, A., Sanders, D., and Fernández, J. A. (2000). Sodium-dependent nitrate transport at the plasma membrane of leaf cells of the marine higher plant *Zostera marina* L. *Plant Phys.* 122 (3), 879–885. doi: 10.1104/pp.122.3.879

Geiger, D., Scherzer, S., Mumm, P., Stange, A., Marten, I., Bauer, H., et al. (2009). Activity of guard cell anion channel SLAC1 is controlled by drought-stress signaling kinase-phosphatase pair. *Proc. Natl. Acad. Sci. U.S.A.* 106, 21425–21430. doi: 10.1073/pnas.0912021106

Geiger, D., Maierhofer, T., Al-Rasheid, K. A., Scherzer, S., Mumm, P., Liese, A., et al. (2011). Stomatal closure by fast abscisic acid signaling is mediated by the guard cell anion channel SLAH3 and the receptor RCAR1. *Sci. Signal.* 4, ra32. doi: 10.1126/scisignal.2001346

Hedrich, R., and Geiger, D. (2017). Biology of SLAC1-type anion channels - from nutrient uptake to stomatal closure. *New Phytol.* 216, 46–61. doi: 10.1111/nph.14685

Huber, J. L., Huber, S. C., Campbell, W. H., and Redinbaugh, M. G. (1992). Reversible light/dark modulation of spinach leaf nitrate reductase activity involves protein phosphorylation. *Arch. Biochem. Biophys.* 296, 58–65. doi: 10.1016/0003-9861(92)90544-7

Jablonski, L. M., Wang, X., and Curtis, P. S. (2002). Plant reproduction under elevated CO_2 conditions: a meta-analysis of reports on 79 crop and wild species. *New Phytol.* 156, 9–26. doi: 10.1046/j.1469-8137.2002.00494.x

Kaiser, W. M., Spill, D., and Brendle-Behnisch, E. (1992). Adenine nucleotides are apparently involved in the light-dark modulation of spinach-leaf nitrate reductase. *Planta* 186, 236–240. doi: 10.1007/BF00196253

Koch, M., Bowes, G., Ross, C., and Zhang, X. H. (2013). Climate change and ocean acidification effects on seagrasses and marine macroalgae. *Glob. Change Biol.* 19 (1), 103–132. doi: 10.1111/j.1365-2486.2012.02791.x

Larkum, W. D., Orth, R. J., and Duarte, C. M. (2006). *Seagrasses: Biology, Ecology and Conservation* (Netherlands: Springer).

Lepoint, G., Millet, S., Dauby, P., Gobert, S., and Bouquegneau, J. M. (2002). Annual nitrogen budget of the seagrass *Posidonia oceanic*a as determined by in situ uptake experiments. *Mar. Ecol. Prog. Ser.* 237, 87–96. doi: 10.3354/meps237087

Loladze, I. (2014). Hidden shift of the ionome of plants exposed to elevated CO_2 depletes minerals at the base of human nutrition. *ELife* 2014 (3), 1–29. doi: 10.7554/eLife.02245

Maierhofer, T., Lind, C., Hüttl, S., Scherzer, S., Papenfuß, M., Simon, J., et al. (2014). A single-pore residue renders the Arabidopsis root anion channel SLAH2 highly nitrate selective. *Plant Cell.* 26 (6), 2554–2567. doi: 10.1105/tpc.114.125849

Miller, A. J., and Smith, S. J. (1996). Nitrate transport and compartmentation in cereal root cells. *J. Exp. Bot.* 47 (7), 843–854. doi: 10.1093/jxb/47.7.843

Miller, A. J., and Smith, S. J. (2008). Cytosolic nitrate ion homeostasis: Could it have a role in sensing nitrogen status? *Ann. Bot.* 101, 485–489. doi: 10.1093/aob/mcm313

Miller, A. J., and Zhen, R. G. (1991). Measurement of intracellular nitrate concentrations in Chara using nitrate-selective microelectrodes. *Planta* 184 (1), 47–52. doi: 10.1007/BF00208235

Negi, J., Matsuda, O., Nagasawa, T., Oba, Y., Takahashi, H., Kawai-Yamada, M., et al. (2008). CO_2 regulator SLAC1 and its homologues are essential for anion homeostasis in plant cells. *Nature* 452, 483–486. doi: 10.1038/nature06720

Norby, R. J., Wullschleger, S. D., Gunderson, C. A., Johnson, D. W., and Ceulemans, R. (1999). Tree responses to rising CO_2 in field experiments: implications for the future forest. *Plant Cell Environ.* 22, 683–714. doi: 10.1046/j.1365-3040.1999.00391.x

Olsen, J. L., Rouzé, P., Verhelst, B., Lin, Y. C., Bayer, T., Collen, J., et al. (2016). The genome of the seagrass Zostera marina reveals angiosperm adaptation to the sea. *Nature* 530 (7590), 331–335. doi: 10.1038/nature16548

Planes, M. D., Niñoles, R., Rubio, L., Bissoli, G., Bueso, E., García-Sánchez, M. J., et al. (2015). A mechanism of growth inhibition by abscisic acid in germinating seeds of Arabidopsis thaliana based on inhibition of plasma membrane H^+-ATPase and decreased cytosolic pH, K^+, and anions. *J. Exp. Bot.* 66 (3), 813–825. doi: 10.1093/jxb/eru442

Ravaglioli, C., Lauritano, C., Buia, M., Balestri, E., Capocchi, A., Fontanini, D., et al. (2017). Nutrient Loading Fosters Seagrass Productivity Under Ocean Acidification. *Sci. Rep.* 7, 13732. doi: 10.1038/s41598-017-14075-8

Raven, J. A., Caldeira, K., Elderfield, H., Hoegh-Guldberg, O., Liss, P., Riebesell, U., et al. (2005). *Ocean Acidification due to Increasing Atmospheric Carbon Dioxide* (London: The Royal Society). Policy Document 12/05.

Raven, J. A., Beardall, J., and Giordano, M. (2014). Energy costs of carbon dioxide concentrating mechanisms in aquatic organisms. *Photosynth. Res.* 121, 111–124. 1. doi: 10.1007/s11120-013-9962-7

Raven, J. A. (1986). "Physiological consequences of extremely small size for autotrophic organisms in the sea," in *Photosynthetic Picoplankton*. Eds. T. Platt and W. K. W. Li (Ottawa, Canada: Canadian Bulletin of Fisheries and Aquatic Sciences), 1–70.

Riens, B., and Heldt, H. W. (1992). Decrease of nitrate reductase activity in spinach leaves during a light-dark transition. *Plant Physiol.* 98, 573–577. doi: 10.1104/pp.98.2.573

Roberts, S. K. (2006). Plasma membrane anion channels in higher plants and their putative functions in roots. *New Phytol.* 169, 647–666. doi: 10.1111/j.1469-8137.2006.01639.x

Roelfsema, M. R. G., Levchenko, V., and Hedrich, R. (2004). ABA depolarizes guard cells in intact plants, through a transient activation of R- and S-type anion channels. *Plant J.* 37, 578–588. doi: 10.1111/j.1365-313x.2003.01985.x

Roelfsema, M. R. G., Hedrich, R., and Geiger, D. (2012). Anion channels: Master switches of stress responses. *Trends Plant Sci.* 17 (4), 221–229. doi: 10.1016/j.tplants.2012.01.009

Romero, J., Lee, K. S., Pérez, M. A., and Alcoverro, T. (2006). "Nutrients dynamics," in *Seagrasses: Biology, Ecology and Conservation*. Eds. A. W. D. Larkum, R. J. Orth and C. M. Duarte (Netherlands: Springer), 227–254.

Rubio, L., and Fernández, J. A. (2019). "Seagrasses, the unique adaptation of angiosperms to the marine environment: effect of high carbon and ocean acidification on energetics and ion homeostasis," in *Halophytes and Climate Change: Adaptive Mechanisms and Potential Uses*. Eds. M. Hasanuzzaman, S. Shabala and M. Fujita (Boston M.A.: CAB International), 89–103.

Rubio, L., Linares-Rueda, A., García-Sánchez, M. J., and Fernández, J. A. (2005). Physiological evidence for a sodium-dependent high-affinity phosphate and nitrate transport at the plasma membrane of leaf and root cells of *Zostera marina* L. *J. Exp. Bot.* 56 (412), 613–622. doi: 10.1093/jxb/eri053

Rubio, L., Belver, A., Venema, K., García-Sánchez, M. J., and Fernández, J. A. (2011). Evidence for a sodium efflux mechanism in the leaf cells of the seagrass *Zostera marina* L. *J. Exp. Mar. Biol. Ecol.* 402, 56–64. doi: 10.1016/j.jembe.2011.03.016

Rubio, L., García, D., García-Sánchez, M. J., Niell, F. X., Felle, H. H., and Fernández, J. A. (2017). Direct uptake of HCO_3^- in the marine angiosperm *Posidonia oceanica* (L.) Delile driven by a plasma membrane H^+ economy. *Plant Cell Environ.* 40, 2820–2830. doi: 10.1111/pce.13057

Rubio, L., García-Pérez, D., García-Sánchez, M. J., and Fernández, J. A. (2018). Na^+-dependent high-affinity nitrate, phosphate and amino acids transport in leaf cells of the seagrass P*osidonia oceanica* (L.) Delile. *Int. J. Mol. Sci.* 19 (6), 1570. doi: 10.3390/ijms19061570

Sültemeyer, D., Schmidt, R., and Heinrich, P. F. (1993). Carbonic anhydrase in higher plants and aquatic microorganisms. *Physiol. Plant* 88, 179–190. doi: 10.1111/j.1399-3054.1993.tb01776.x

Scartazza, A., Moscatello, S., Gavrichkova, O., Buia, M. C., Lauteri, M., Battistelli, A., et al. (2017). Carbon and nitrogen allocation strategy in Posidonia oceanica is altered by seawater acidification. *Sci. Total Environ.* 607–608, 954–964. doi: 10.1016/j.scitotenv.2017.06.084

Schmidt, C., and Schroeder, J. I. (1994). Anion selectivity of slow anion channels in the plasma membrane of guard cells (large nitrate permeability). *Plant Physiol.* 106, 383–391. doi: 10.1104/pp.106.1.383

Schmidt, C., Schelle, I., Liao, Y. J., and Schroeder, J. I. (1995). Strong regulation of slow anion channels and abscisic-acid signaling in guard-cells by phosphorylation and dephosphorylation events. *Proc. Natl. Acad. Sci. U.S.A.* 92, 9535–9539. doi: 10.1073/pnas.92.21.9535

Siddiqi, M. Y., and Glass, A. D. M. (2002). An evaluation of the evidence for, and implications of, cytoplasmic nitrate homeostasis. *Plant Cell Environ.* 25, 1211–1217. doi: 10.1046/j.1365-3040.2002.00927.x

Taub, D. R., and Wang, X. (2008). Why are nitrogen concentrations in plant tissues lower under elevated CO_2? A critical examination of the hypotheses. *J. Integr. Plant Biol.* 50 (11), 1365–1374. doi: 10.1111/j.1744-7909.2008.00754.x

Taub, D. R., Miller, B., and Allen, H. (2008). Effects of elevated CO_2 on the protein concentration of food crops: A meta-analysis. *Glob. Change Biol.* 14 (3), 565–575. doi: 10.1111/j.1365-2486.2007.01511.x

Touchette, B. W., and Burkholder, J. A. M. (2000). Overview of the physiological ecology of carbon metabolism in seagrasses. *J. Exp. Mar. Biol. Ecol.* 250 (1–2), 169–205. doi: 10.1016/S0022-0981(00)00196-9

Trębacz, K., Simonis, W., and Schönknecht, G. (1994). Cytoplasmic Ca^{2+}, K^+, Cl^-, and NO_3^- activities in the liverwort *Conocephalum conicum* L. at rest and during action potentials. *Plant Phys.* 106 (3), 1073–1084. doi: 10.1104/pp.106.3.1073

Van Der Leij, M., Smith, S. J., and Miller, A. J. (1998). Remobilisation of vacuolar stored nitrate in barley root cells. *Planta* 205 (1), 64–72. doi: 10.1007/s004250050297

Williams, S. L. (2016). Genomics: From sea to sea. *Nature* 530, 290–291. doi: 10.1038/nature16869

Xue, S., Hu, H., Ries, A., Merilo, E., Kollist, H., and Schroeder, J. I. (2011). Central functions of bicarbonate in S-type anion channel activation and OST1 protein kinase in CO_2 signal transduction in guard cell. *EMBO J.* 30 (8), 1645–1658. doi: 10.1038/emboj.2011.68

Zeebe, R. E., and Wolf-Gladrow, D. (2001). *CO2vin Seawater: Equilibrium, Kinetics, Isotopes. 1st edn* (Amsterdam: Elsevier).

Zhen, R. G., Koyro, H. W., Leigh, R. A., Tomos, A. D., and Miller, A. J. (1991). Compartmental nitrate concentrations in barley root cells measured with nitrate-selective microelectrodes and by single-cell sap sampling. *Planta* 185 (3), 356–361. doi: 10.1007/BF00201056

Zheng, X., He, K., Kleist, T., Chen, F., and Luan, S. (2015). Anion channel SLAH3 functions in nitrate dependent alleviation of ammonium toxicity in Arabidopsis. *Plant Cell Environ.* 38, 474–486. doi: 10.1111/pce.12389

Conflict of Interest: The authors declare that the research was conducted in the absence of any commercial or financial relationships that could be construed as a potential conflict of interest.

Advantages of publishing in Frontiers

OPEN ACCESS
Articles are free to read for greatest visibility and readership

FAST PUBLICATION
Around 90 days from submission to decision

HIGH QUALITY PEER-REVIEW
Rigorous, collaborative, and constructive peer-review

TRANSPARENT PEER-REVIEW
Editors and reviewers acknowledged by name on published articles

Frontiers
Avenue du Tribunal-Fédéral 34
1005 Lausanne | Switzerland

Visit us: www.frontiersin.org
Contact us: frontiersin.org/about/contact

REPRODUCIBILITY OF RESEARCH
Support open data and methods to enhance research reproducibility

DIGITAL PUBLISHING
Articles designed for optimal readership across devices

FOLLOW US
@frontiersin

IMPACT METRICS
Advanced article metrics track visibility across digital media

EXTENSIVE PROMOTION
Marketing and promotion of impactful research

LOOP RESEARCH NETWORK
Our network increases your article's readership